AD-A093 729 KAMAN AVIDYNE BURLINGTON MA F/G 20/4
MEASUREMENTS OF BLAST PRESSURES ON A RIGID 35 DEG SWEPTBACK WIN--ETC(U)
JAN 80 D A KLEPPIN, J R RUETENIK, R F SMILEY DNA001-79-C-0157
UNCLASSIFIED KA-TR-175 DNA-5211F NL

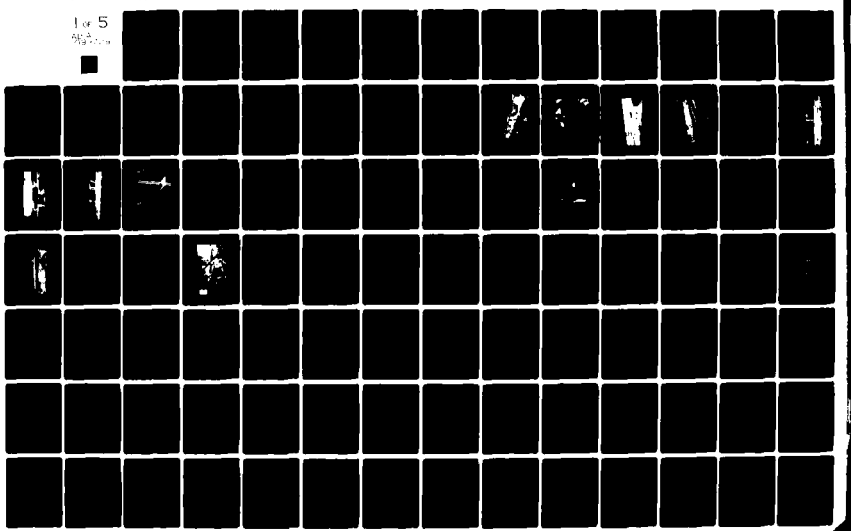

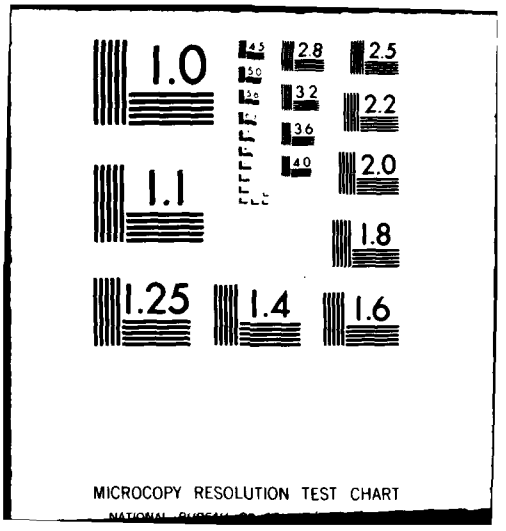
1.0
1.1
1.25
1.4
1.6
1.8
2.0
2.2
2.5
2.8
3.2
3.6
4.0
4.5
5.0
5.6
MICROCOPY RESOLUTION TEST CHART

DNA 5211F

MEASUREMENTS OF BLAST PRESSURES ON A RIGID 35° SWEPTBACK WING AT MACH 0.76 FROM ROCKET PROPELLED SLED TESTS

(12)

Kaman AviDyne
83 Second Avenue
Northwest Industrial Park
Burlington, Massachusetts 01803

LEVEL II

31 January 1980

Final Report for Period 1 February 1979—1 January 1980

CONTRACT No. DNA 001-79-C-0157

APPROVED FOR PUBLIC RELEASE;
DISTRIBUTION UNLIMITED.

THIS WORK SPONSORED BY THE DEFENSE NUCLEAR AGENCY
UNDER RDT&E RMSS CODE B342079464 N99QAXAJ50103 H2590D.

Prepared for
Director
DEFENSE NUCLEAR AGENCY
Washington, D. C. 20305

Destroy this report when it is no longer needed. Do not return to sender.

PLEASE NOTIFY THE DEFENSE NUCLEAR AGENCY, ATTN: STTI, WASHINGTON, D.C. 20305, IF YOUR ADDRESS IS INCORRECT, IF YOU WISH TO BE DELETED FROM THE DISTRIBUTION LIST, OR IF THE ADDRESSEE IS NO LONGER EMPLOYED BY YOUR ORGANIZATION.

UNCLASSIFIED

SECURITY CLASSIFICATION OF THIS PAGE (When Data Entered)

REPORT DOCUMENTATION PAGE

READ INSTRUCTIONS BEFORE COMPLETING FORM

1. REPORT NUMBER	2. GOVT ACCESSION NO.	3. RECIPIENT'S CATALOG NUMBER
DNA 5211F	AD-A093729	

4. TITLE (and Subtitle)
MEASUREMENTS OF BLAST PRESSURES ON A RIGID 35° SWEPTBACK WING AT MACH 0.76 FROM ROCKET PROPELLED SLED TESTS.

5. TYPE OF REPORT & PERIOD COVERED
Final Report for Period 1 Feb 79—1 Jan 80

6. PERFORMING ORG. REPORT NUMBER
KA-TR-175

7. AUTHOR(s)
Dale A. Kleppin
J. Ray Ruetenik
Robert F. Smiley

8. CONTRACT OR GRANT NUMBER(s)
DNA 001-79-C-0157

9. PERFORMING ORGANIZATION NAME AND ADDRESS
Kaman AviDyne
83 Second Avenue, Northwest Industrial Park
Burlington, Massachusetts 01803

10. PROGRAM ELEMENT, PROJECT, TASK AREA & WORK UNIT NUMBERS
Subtask N99QAXAJ0501-03

11. CONTROLLING OFFICE NAME AND ADDRESS
Director
Defense Nuclear Agency
Washington, D.C. 20305

12. REPORT DATE
31 January 1980

13. NUMBER OF PAGES
434

14. MONITORING AGENCY NAME & ADDRESS (if different from Controlling Office)

15. SECURITY CLASS (of this report)
UNCLASSIFIED

15a. DECLASSIFICATION/DOWNGRADING SCHEDULE

16. DISTRIBUTION STATEMENT (of this Report)

Approved for public release; distribution unlimited.

17. DISTRIBUTION STATEMENT (of the abstract entered in Block 20, if different from Report)

18. SUPPLEMENTARY NOTES

This work sponsored by the Defense Nuclear Agency under RDT&E RMSS Code B342079464 N99QAXAJ50103 H2590D.

19. KEY WORDS (Continue on reverse side if necessary and identify by block number)

Blast	Explosive
Shock	Aircraft
Sled Test	Wing
Pressure	Sweptback
Experimental Test	Subsonic

20. ABSTRACT (Continue on reverse side if necessary and identify by block number)

Interaction of a blast wave with a 35°-sweepback wing model was measured in a series of two sled tests performed on the 50,788-ft sled tract at Holloman AFB in September 1979. The model was rigid and had a 5.6 aspect ratio and 0.42 taper ratio. The sled, travelling at Mach 0.76, was intercepted successively by blast waves produced from TNT charges. Blast-induced pressure differentials were measured at 20 locations on the wing. Shock overpressures ranged from 1.3 to 4.1 psi and intercept angles were 45, 90 and 135 degrees from head-on. This report describes the tests and presents the test results.

DD FORM 1 JAN 73 1473 EDITION OF 1 NOV 65 IS OBSOLETE

UNCLASSIFIED

SECURITY CLASSIFICATION OF THIS PAGE (When Data Entered)

194970

20. ABSTRACT (Continued)

Preliminary analysis of the test results indicates the existence of nonlinear blast-induced airloads on the model at the lowest shock overpressure.

PREFACE

This work was performed by the AviDyne Division of the Kaman Sciences Corporation for the Defense Nuclear Agency under Contract DNA001-79-C-0157. MAJ J. Michael Rafferty of the DNA Shock Physics Directorate served as technical monitor. Dr. J. Ray Ruetenik of Kaman AviDyne was the project leader under Dr. Norman P. Hobbs, Technical Director of KA.

Appreciation is expressed to CAPT Rafferty for his continuing interest and significant support of this program. Appreciation is also expressed to the Holloman Air Force Base Test Directorate personnel, particularly Mr. Floyd D. Amburgey of Track Operations for coordination of the test activities, Mr. Daniel J. Krupovage of Track Engineering for mechanical engineering functions, Mr. Joe Haden of Track Instrumentation for electronic and sled-instrumentation support and Mr. Carrol Wood for data processing. Appreciation is also expressed to Army Ballistics Research Laboratories personnel headed by Mr. George Teel for providing the blast-line measurements.

Conversion factors for U.S. customary to metric (SI) units of measurement.

To Convert From	To	Multiply By
angstrom	meters (m)	1.000 000 X E -10
atmosphere (normal)	kilo pascal (kPa)	1.013 25 X E +2
bar	kilo pascal (kPa)	1.000 000 X E +2
barn	meter^2 (m^2)	1.000 000 X E -28
British thermal unit (thermochemical)	joule (J)	1.054 350 X E +3
calorie (thermochemical)	joule (J)	4.184 000
cal (thermochemical)/cm^2	mega joule/m^2 (MJ/m^2)	4.184 000 X E -2
curie	giga becquerel (GBq)*	3.700 000 X E +1
degree (angle)	radian (rad)	1.745 329 X E -2
degree Fahrenheit	degree kelvin (K)	t_k = (t° f + 459.67)/1.8
electron volt	joule (J)	1.602 19 X E -19
erg	joule (J)	1.000 000 X E -7
erg/second	watt (W)	1.000 000 X E -7
foot	meter (m)	3.048 000 X E -1
foot-pound-force	joule (J)	1.355 818
gallon (U.S. liquid)	meter^3 (m^3)	3.785 412 X E -3
inch	meter (m)	2.540 000 X E -2
jerk	joule (J)	1.000 000 X E +9
joule/kilogram (J/kg) (radiation dose absorbed)	Gray (Gy)**	1.000 000
kilotons	terajoules	4.183
kip (1000 lbf)	newton (N)	4.448 222 X E +3
kip/inch^2 (ksi)	kilo pascal (kPa)	6.894 757 X E +3
ktap	newton-second/m^2 (N-s/m^2)	1.000 000 X E +2
micron	meter (m)	1.000 000 X E -6
mil	meter (m)	2.540 000 X E -5
mile (international)	meter (m)	1.609 344 X E +3
ounce	kilogram (kg)	2.834 952 X E -2
pound-force (lbf avoirdupois)	newton (N)	4.448 222
pound-force inch	newton-meter (N·m)	1.129 848 X E -1
pound-force/inch	newton/meter (N/m)	1.751 268 X E +2
pound-force/foot^2	kilo pascal (kPa)	4.788 026 X E -2
pound-force/inch^2 (psi)	kilo pascal (kPa)	6.894 757
pound-mass (lbm avoirdupois)	kilogram (kg)	4.535 924 X E -1
pound-mass-foot^2 (moment of inertia)	kilogram-meter^2 (kg·m^2)	4.214 011 X E -2
pound-mass/foot^3	kilogram/meter^3 (kg/m^3)	1.601 846 X E +1
rad (radiation dose absorbed)	Gray (Gy)**	1.000 000 X E -2
roentgen	coulomb/kilogram (C/kg)	2.579 760 X E -4
shake	second (s)	1.000 000 X E -8
slug	kilogram (kg)	1.459 390 X E +1
torr (mm Hg, 0° C)	kilo pascal (kPa)	1.333 22 X E -1

*The becquerel (Bq) is the SI unit of radioactivity; 1 Bq = 1 event/s.
**The Gray (Gy) is the SI unit of absorbed radiation.

A more complete listing of conversions may be found in "Metric Practice Guide E 380-74," American Society for Testing and Materials.

TABLE OF CONTENTS

LIST OF ILLUSTRATIONS

LIST OF ILLUSTRATIONS (CONTINUED)

LIST OF ILLUSTRATIONS (CONTINUED)

LIST OF ILLUSTRATIONS (CONTINUED)

LIST OF ILLUSTRATIONS (CONCLUDED)

LIST OF TABLES

SECTION 1
INTRODUCTION

Six blast tests conducted at the 50,788-ft high-speed sled track at the Holloman Air Force Base (HAFB), New Mexico, during September 1979 are reported. The test objective was to measure the blast induced airloads on a 35-deg sweepback wing at a high subsonic Mach number.

The program consisted of one calibration shot and two sled runs with five shots. In the calibration test the sled was stationary and the blast wave intercepted the sled laterally (90-deg intercept) for determination of the effects of blast wave interference with the sled and sled track. The nominal shock overpressure was 2.0 psi.

In the two sled runs the nominal shock overpressures were 1.3 psi for a 90-deg intercept from head-on, relative to the sled direction of travel; 2 psi for 45, 90 and 135-deg intercepts; and 4 psi for a 135-deg intercept. The wing had an initial angle of attack of 3.2 degrees with the blast wave oriented to increase the angle of attack. 1000-pound spherical charges of TNT were employed supported on 5-ft high pedestals.

Both sled runs were made at a nominal preintercept Mach number of 0.76 and a Reynolds number of 4.0 million based on the mean chord. The wing span was 60 inches, the aspect ratio 5.6, and the taper ratio 0.42.

The test technique is described in Section 2 and References 1 and 2. The tests are described in Sections 2 to 5. The test results are discussed in Section 6. The graphs of pressure, strain and acceleration time histories are presented in Appendix A.

SECTION 2
TEST EQUIPMENT

2-1 HAFB SLED TRACK.

The 50,788-ft high-speed track and associated general test equipment at HAFB were used for this test program. A general description of these facilities is presented in Reference 3. For these tests a dual-rail sled was launched from south to north starting at approximately the 10,500-ft station and entered the blast test area at about the 12,500-ft station. The sled passed through the test area which ends at about the 13,850-ft station and coasted to a stop near the 40,000-ft station.

2-2 GENERAL TEST ARRANGEMENT.

A sketch of the test area and overall test scheme is shown in Figure 1. As depicted in Figure 1 the sled moves from left to right and encounters three successive blast waves caused by the sequential detonation of 1000-lb TNT charges. Each charge was precisely located and detonated to produce a blast wave which would encounter the sled at a prescribed angle and overpressure.

2-3 TEST AREA.

The test area for this program was 1,350 feet long in the north-south direction and extended 320 feet or more westward from the track between Track Stations 12,500 and 13,850. The surface of this area was prepared as shown in Figure 2.

Special measures were employed to minimize track interference with the blast wave. A sketch of the track cross-section in the test area is shown in Figure 3. The surface of the test area (to the left of track) was level with the mid-height of the rails. Sand bags were inserted in the gap between the built-up asphalt road on the west side and the rail. The trough between the rails was also filled with water to reduce the distortion.

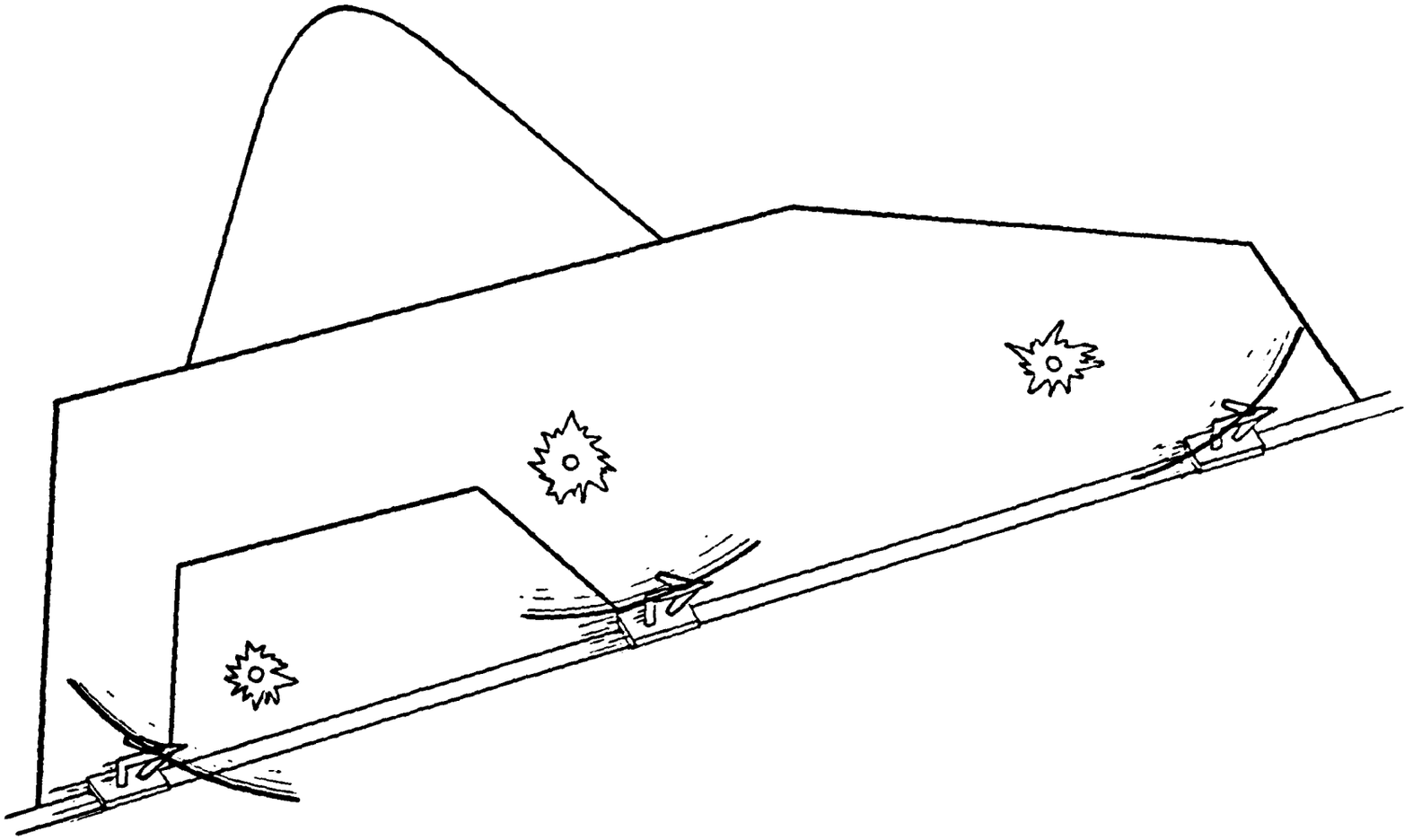

Figure 1. Schematic of Typical HAFB Blast Test Arrangement

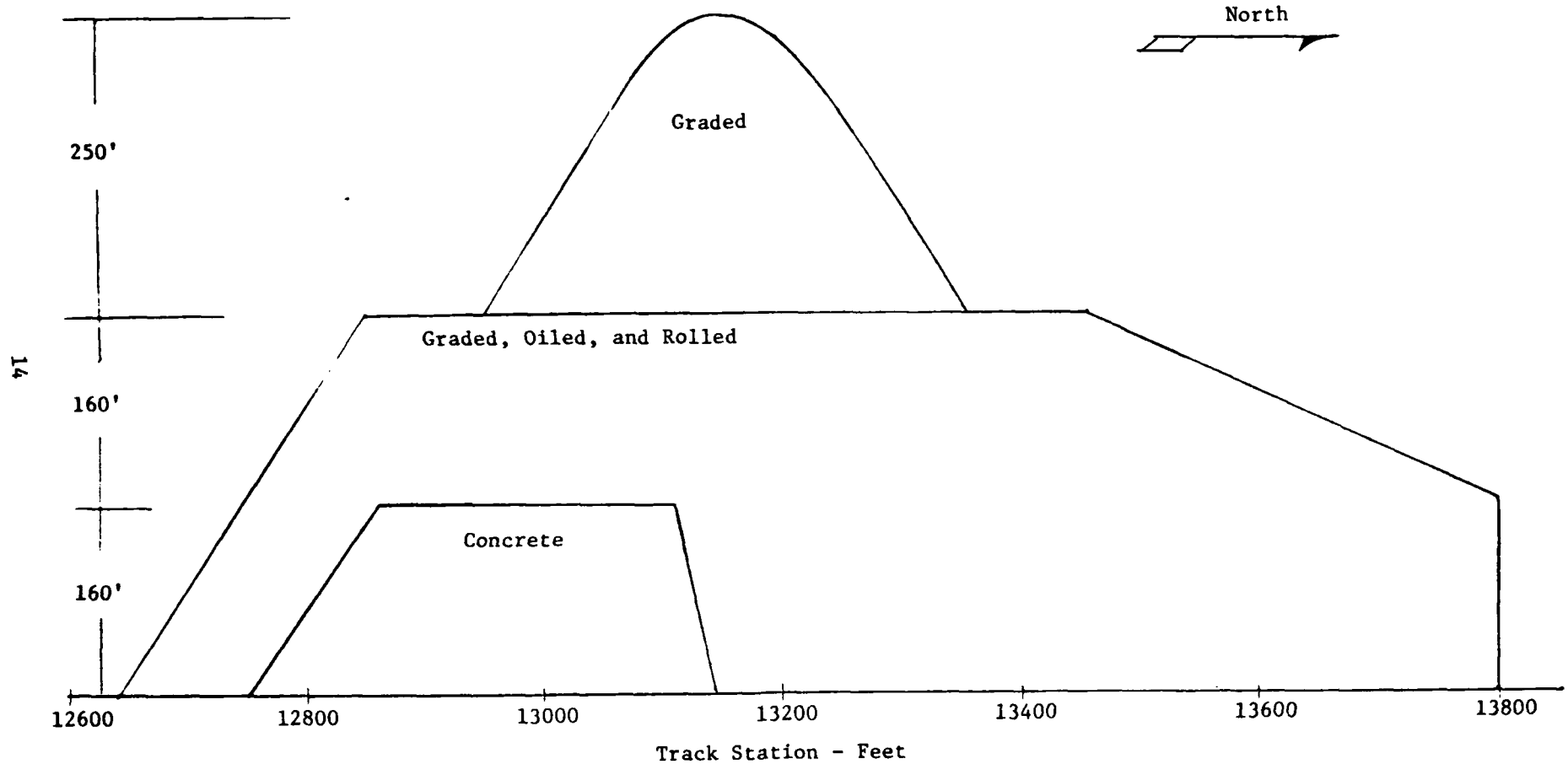

Figure 2. Blast Area Outline

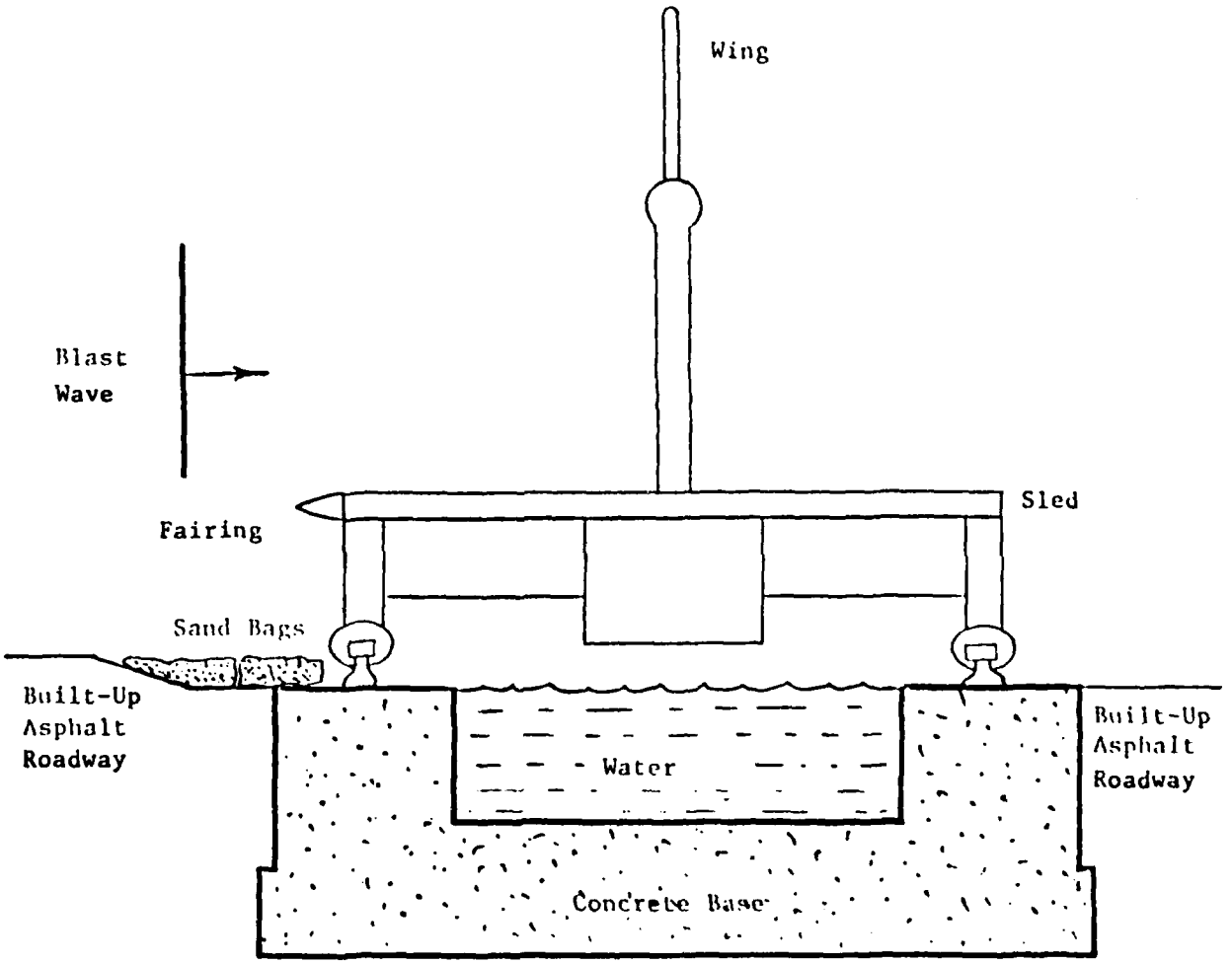

Figure 3. Sketch of Rear View of Sled and Ground Surface Showing Procedures for Reducing Blast Interference Effects

Each of the intercept locations was equipped with four blast-line pressure probes to measure the free-air blast profile. The vertical mounts for these probes were located as shown in Table 1 for the two runs in this program. A typical set of probes is shown in Figure 4. The vertical mounts are set on a line 7.5 feet west of the track center-line. The pressure transducers were mounted in the center of large discs, as shown in Figure 5, which were mounted at the ends of 18-inch arms. The arms extended from the mounts toward the charge so that the transducers were actually about 1 1/2 feet nearer the charge than their mount.

Detonation of the charges and the activation of some of the cameras were controlled by so-called screen boxes. The boxes were located adjacent to the west rail about a foot off the ground at designated locations along the track. The screen boxes held a wire screen in the vertical plane. The wire was positioned to be severed by a knife edge on the side of the sled as it passed. In this way the screen made contact with the knife on the sled. A pair of knives was connected electrically on the sled, so that a circuit including two screen boxes was closed by the knife pair. Therefore two screen boxes served to close one firing circuit. To provide redundancy, two screen-box circuits were employed for each firing unit. A photograph from the rear of a set of four screen boxes is shown in Figure 6. The firing circuit connected a voltage source to the trigger of the firing unit. The 300-volt power supply used for this source is shown in Figure 6 connected to the screen-box set. A post-test photograph of a pair of screen boxes after the contact knives have passed through the screens is shown in Figure 7.

Breakwires placed across the west rail at specified locations were used to provide a common time reference signal for checking time correlation of different recorders. They served as links in circuits which were broken by the leading edge of the front slipper of the sled. The time reference breakwires were located between 7 and 33 feet ahead of the DIP.

TABLE 1

BLAST-LINE STATIONS FOR RUNS

(Location of Blast-Line Probe Mounts)

Intercept No.	Transducer No.	TRACK STATION(1)					
		Test DIP	9B-C1(2) Mounts	Test DIP	9B-B1(3) Mounts	Test DIP	9B-B2 Mounts
1	1	-		-		12742.5	12746.9
	2						12752.6
	3(4)						12758.9
	4						12772.0
2	5(4)	13180.0	13171.9	13180.0	13171.9	13180.0	13171.9
	6		13187.9		13187.9		13187.9
	7		13202.7		13202.7		13202.7
	8		13225.7		13225.7		13225.7
3	9	-		13630.0	13608.1	13630.0	13608.1
	10				13636.4		13636.4
	11				13668.3		13668.3
	12				13712.1		13712.1

DIP = Desired Intercept Point

(1) All mount poles are located 4 feet west of rail (7.5 feet west of track centerline).

(2) Static test - only 1 explosive charge.

(3) Premature detonation of charge 1 only.

(4) Right hand probe; i.e. sensing surface facing south (all others left hand probes).

Figure 4. Set of Blast-Line Pressure Probes Positioned for 45° Intercept

Figure 5. Blast-Line Pressure Transducer and Mounting Disk

Figure 6. Rear View of Screen Boxes with Power Supply

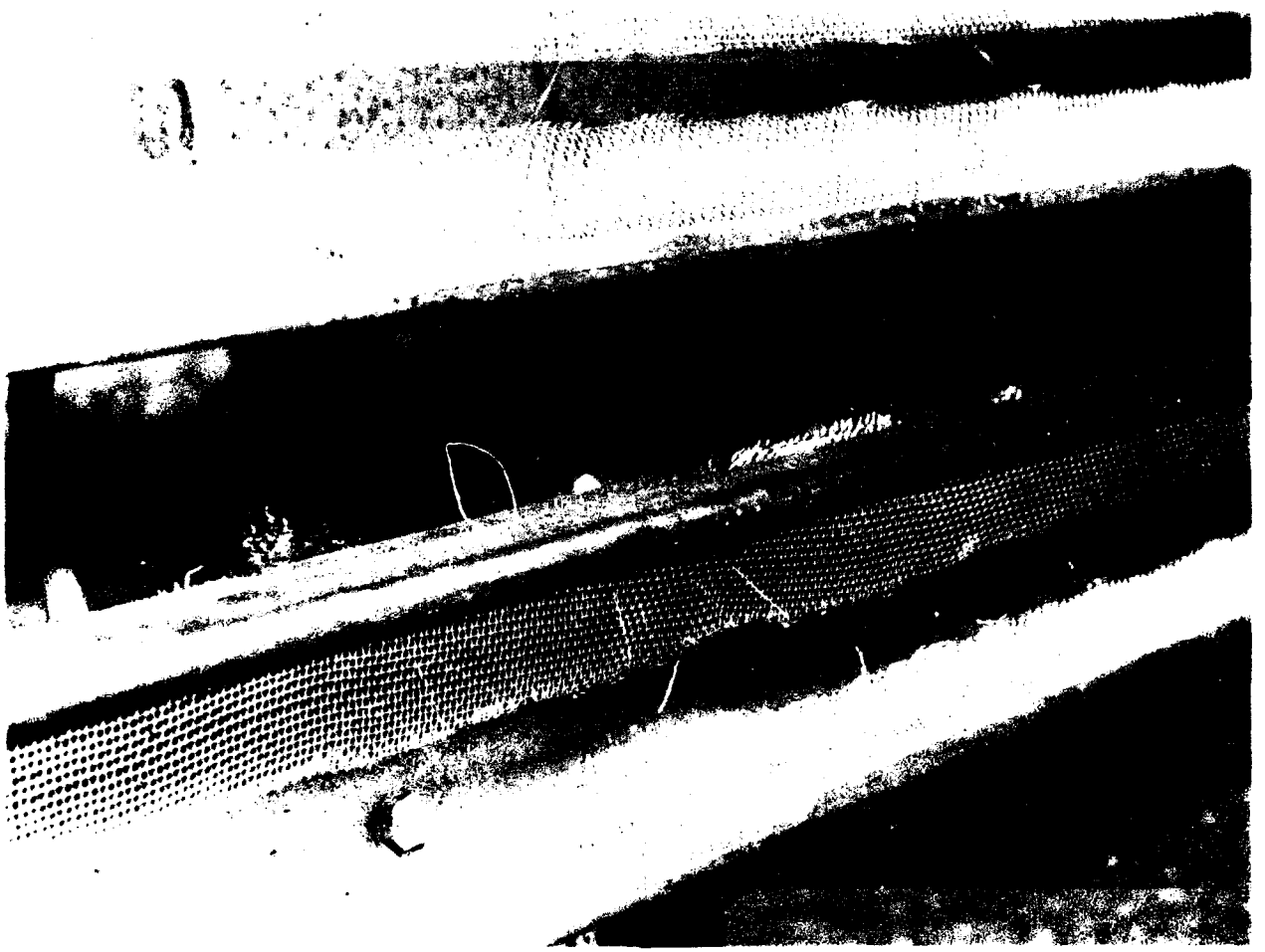

Figure 7. Post-Test Photograph of Severed Screen Box

2-4 SLED.

The HAFB dual rail rocket sled, designated as FDN 6326, was employed in this program. Figure 8 shows the sled and model prior to the first run. As seen the model is mounted toward the front of the sled from a horizontal sting which is attached to a vertical strut. The top surface deck of the sled is basically a thick flat plate. The front and blastward edges of the plate are curled downward to reduce sled drag and minimize distortion of the blast wave as it strikes the model. The onboard camera box on the rear of the sled is also visible in Figure 8.

A view of the sled showing the undercarriage and slippers is presented in Figure 9. The sled structure is basically made up of two longitudinal beams and two horizontal beams. The model strut is supported by a base mounted between the longitudinal beams.

The propulsion systems used to drive the test sled are shown in Figure 10. The two large Nike rockets were mounted on a separate pusher sled and serve as the first stage propulsion unit. They were used to accelerate the sled to approximately Mach 0.6. After burnout of the Nike rockets eighteen of the 23 HVAR rockets on the second propulsion sled were fired to bring the test sled up to the desired velocity. After attaining the test velocity the remaining 5 HVAR rockets were fired to maintain the sled velocity. The data indicates that the sled velocity varied by not more than 4 fps from the intercept value while the model was in the area of interest, which extends in each case from the DIP to approximately 100 feet north along the track.

A pitot probe and two pressure transducers were located together on the upper surface of the sled near the blastward side of the vehicle, as shown in Figures 8 and 11. The pitot probe was located about 6 inches above the surface. Both pressure transducers were mounted flush with the upper surface of the sled about 10 inches ahead of the pitot probe. These transducers were installed to provide a check on the accuracy of the blast pressure measurement obtained from the blast-line probes.

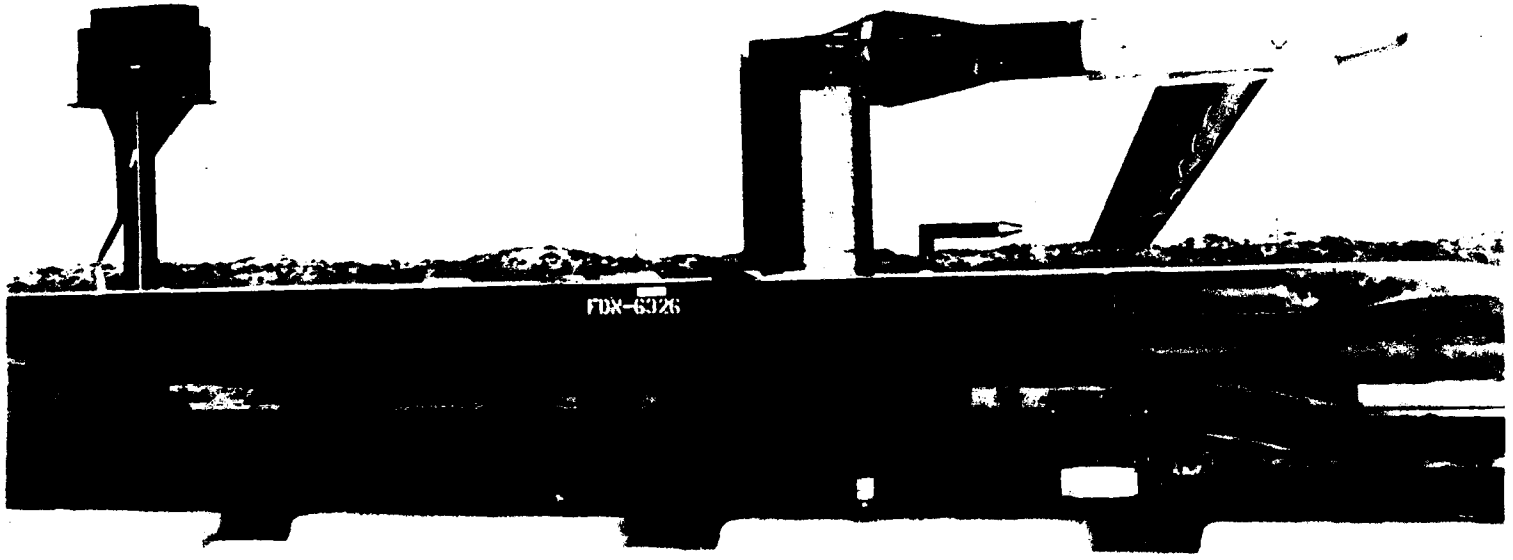

Figure 8. 35-Deg Wing Model Mounted on Dual Rail Rocket Sled FDN6326

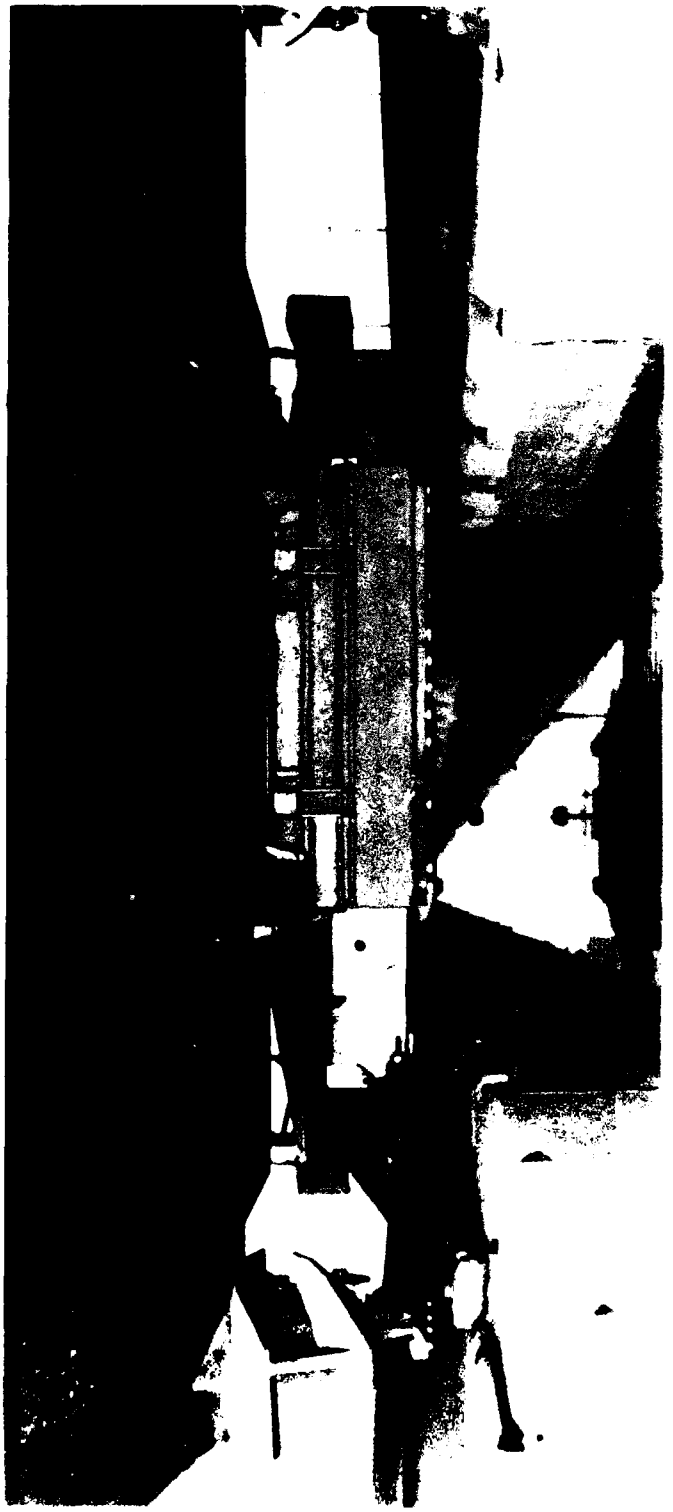

Figure 9. Photograph of Sled Undercarriage

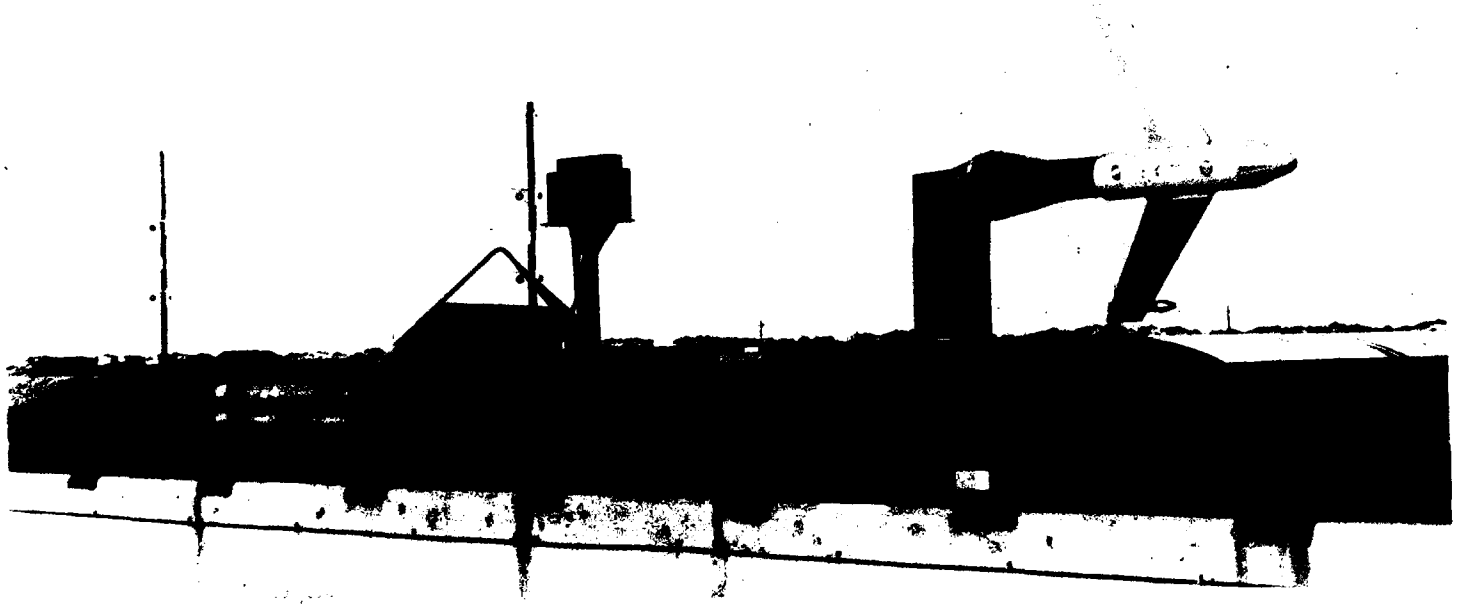

Figure 10. Overall View of Sled and Pushers

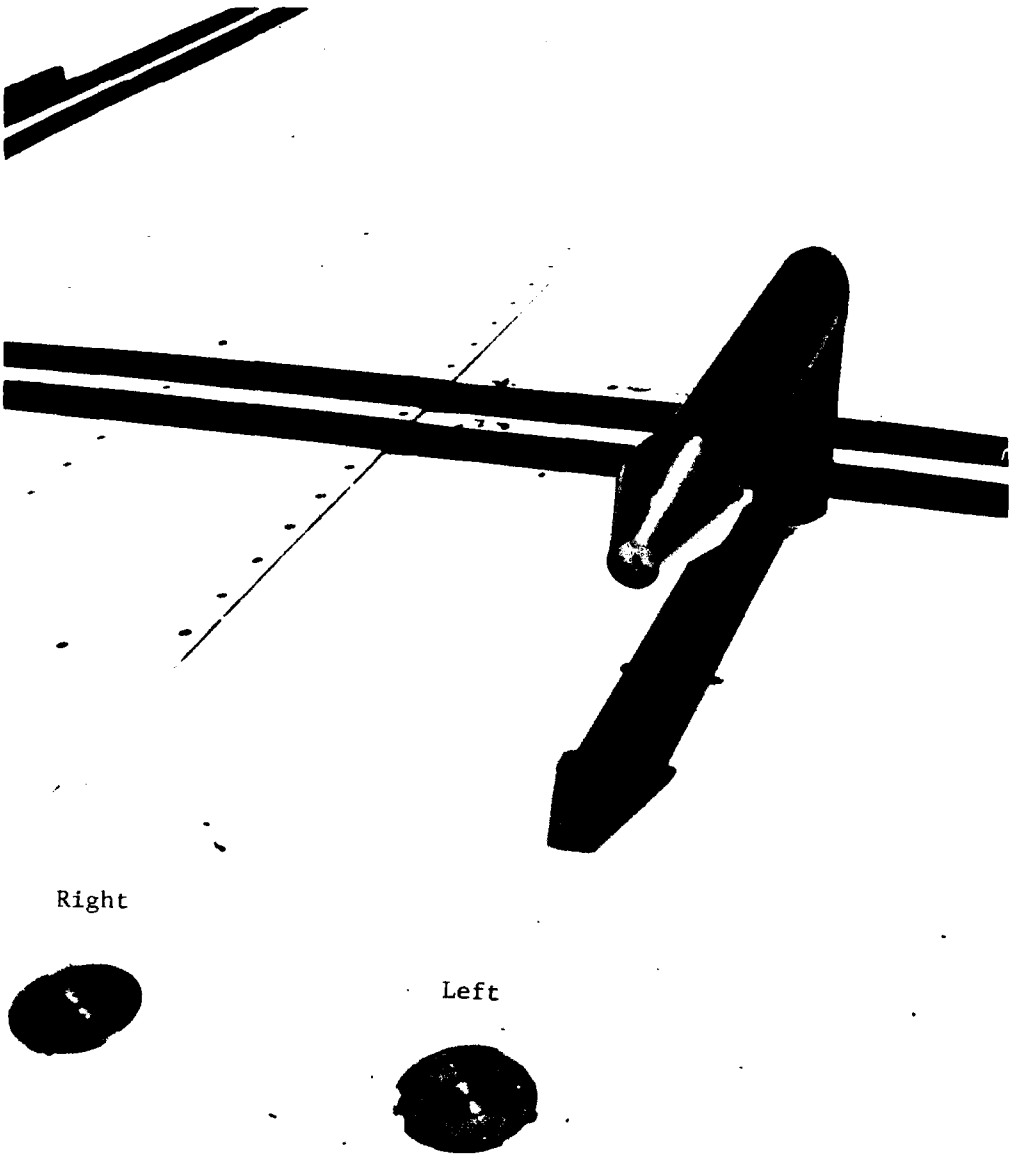

Figure 11. Closeup View of Pressure Transducers on the Sled

2-5 WING MODEL.

The model for this test series was designed to approximate the B-52 in general appearance. It consisted of a wing, partial fuselage and nose mounted on a sting as shown in Figure 8. The streamwise cross section of the wing was contoured as a 64A-xxx symmetric airfoil with a thickness ratio which varied linearly from 17 percent at the body centerline to 10 percent at the tip. The quarter chord sweep angle was 35°. Additional data describing the model are given in Table 2. Details on the model configuration are given in Reference 4.

The left (upper) half of the wing was designed to be instrumented. It was fabricated from a solid piece of 4140 steel. This material was selected to minimize pressure transients associated with elastic structural deformations produced by the blast forces. Each semispan half consisted of two sections, which when bolted together formed the airfoil shape. The aerodynamic contour of each section was formed using a numerically controlled milling machine. The flat or mating side of each section contained holes for the alignment disks as well as channels to accommodate instrumentation leads.

Twenty pairs of pressure transducers were mounted in the upper half of the wing. The locations of the transducers are shown in Figure 12 and listed in Table 3. At each location, transducers were placed on both the blast and leeward wing surfaces to obtain the differential pressures between the two surfaces. An accelerometer was mounted within this half wing near the 57-percent semispan location to measure the wing motion normal to the wing plane.

The right (lower) half of the wing was included mainly to provide reasonable aerodynamic symmetry to the model. Therefore it required no instrumentation and rigidity became less important. Relaxing of these requirements permitted the selection of 7075 aluminum for its cost saving advantages in machining. This half was made in the same manner as the steel half except that the instrumentation holes and lead wire channels were omitted. The outboard five inch tip of the lower (aluminum) wing was removed to provide clearance from the deck of the sled and to reduce ground-effect of the deck while using the existing strut.

TABLE 2

BASIC MODEL DATA

Wing Span, b	60 inches
Wing Planform Area, S	4.46 ft^2
Aspect Ratio	5.6
Taper Ratio	0.42
Leading-Edge Sweepback	37.71°
Quarter-Chord Sweepback	35°
Trailing-Edge Sweepback	25.71°
Mean Chord (S/b)	10.71 inches
Root Chord (at model centerline)	15.091
Wing Section (streamwise)	64A010
Thickness Ratio	
(at model centerline)	17%
(at tip)	10%
Pressure Stations	
(two transducers per station)	20
Fuselage Diameter	8 inches

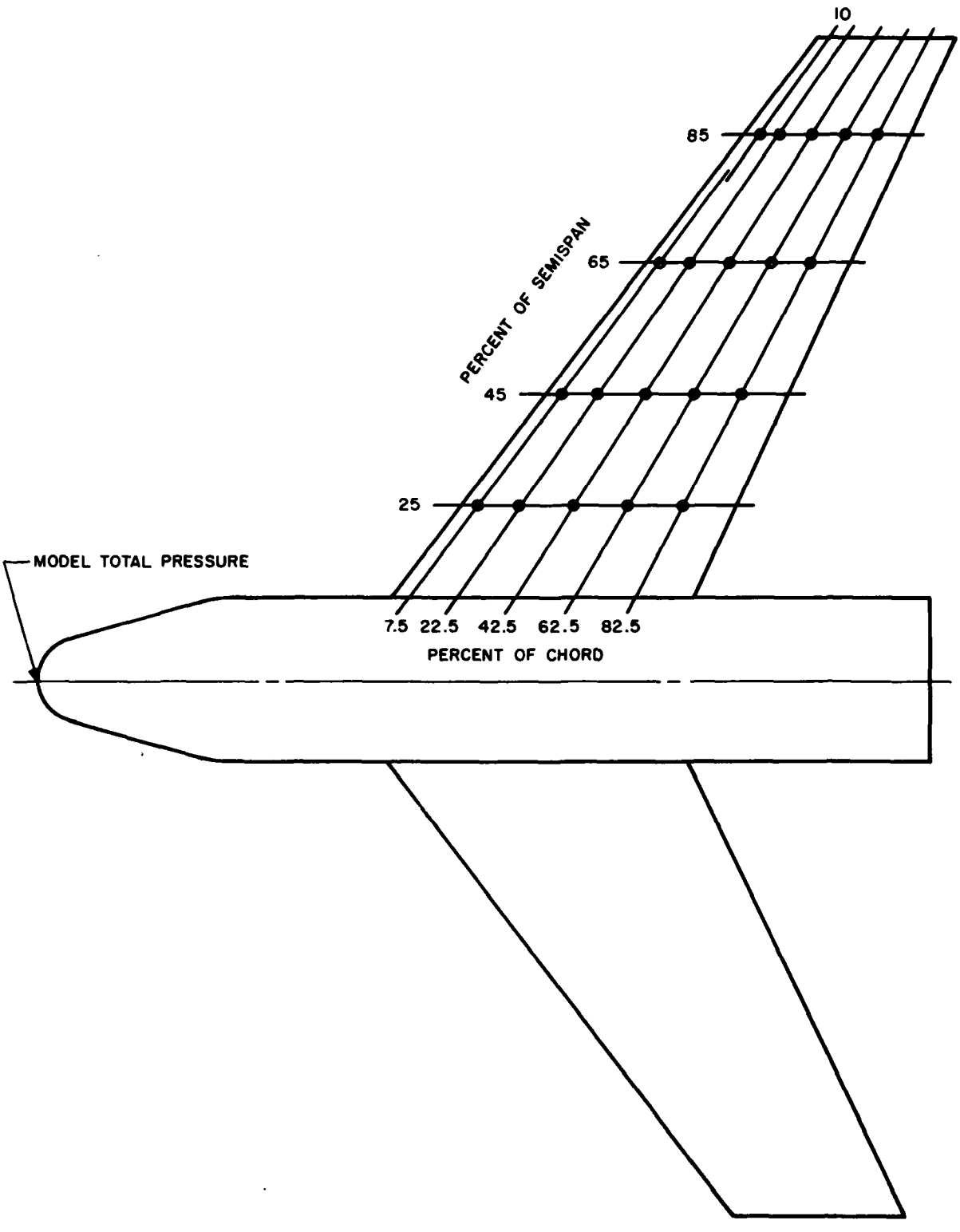

Figure 12. Sketch of Wing and Fuselage Model Showing Pressure Measurement Stations

TABLE 3

MEASUREMENTS ON THE WING

Transducer Location Percent Semispan/ Percent Chord See Figure 12	Type of Measurement[a]	Type of Transducers[b]
25/7.5	D	1
25/22.5	D	1
25/42.5	D	1
25/62.5	D, B, L	1
25/82.5	D	1
45/7.5	D	1
45/22.5	D	1
45/42.5	D	1
45/62.5	D	1
45/82.5	D	1
65/7.5	D	1
65/22.5	D	1
65/42.5	D	1
65/62.5	D	1
65/82.5	D	2
85/10	D	1
85/22.5	D	1
85/42.5	D	1
85/62.5	D	1
85/82.5	D	2

a - D for differential pressure
B for blastward pressure
L for leeward pressure

b - 1 refers to XCQL-41-093-025
2 refers to XF-160
(see Figure 15)

Figure 13 shows the external geometry of the model nose section. It was fabricated from aluminum and the tip was instrumented with a pressure transducer.

The model design and test setup incorporated existing hardware wherever possible. The internal wing attachment (wing box), fuselage fairing, sting and strut from a previous sled test (Reference 1) were used. The wing was mounted at a 3.2° angle of attack with the resulting pre-blast steady-state lift force acting in the same direction as the blast-induced force.

2-6 EXPLOSIVES.

All explosives used in these tests were 1,000-lb charges of TNT. Each charge was cast as a single spherical ball with an integral detonator well. They were mounted on top of 5 ft-high styrofoam pillars as shown in Figure 14 so the charge centers were about 6 feet above the ground. Tie-down straps were used to secure the charges against the possibility of being toppled by preceding detonations.

The explosives were detonated by modified portable Reynolds Industries exploding bridgewire firing sets, using RP-1 detonators. Each firing set was buried about one to two feet below the surface of the test area at a distance of 75 to 100 feet from the respective charge. RG-22 cables, used to trigger the firing sets, were laid on the surface of the test area between the track-side screen boxes and the firing sets. The firing sets were connected to the charge detonators with RG-58 cables laid above ground. The cables were fixed at the charges to prevent pull-away from the detonators.

Arming of the charges was controlled through the panel in the Alpha Blockhouse. RG-22B/u cables connected the control units to the three remote control units which, in turn, were connected to the firing sets. The system was activated by inserting the arming plugs at the control panel.

2-7 BLAST-LINE MEASUREMENTS.

The blast-line probes employed were the standard field instruments used by BRL for the measurement of blast waves. The probes, shown

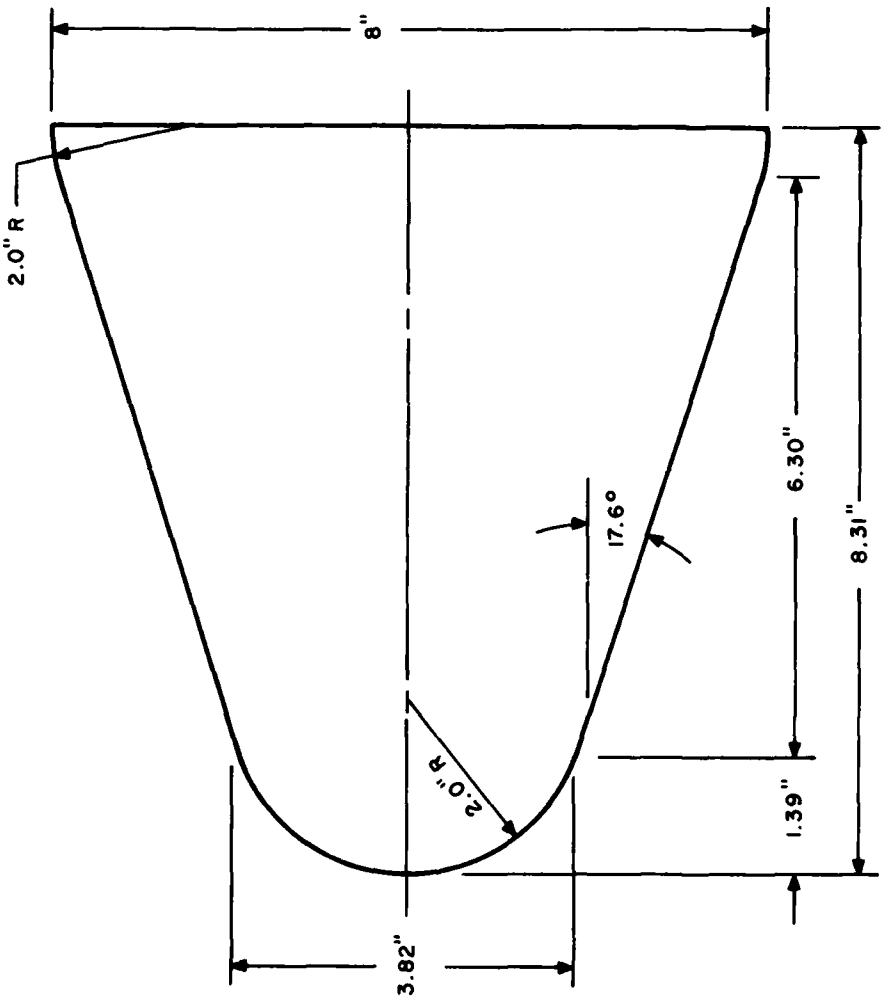

Figure 13. External Geometry of Nose Cap

Figure 14. 1000-lb TNT Charge Mounted on Styrofoam Base

in Figure 5, consist of a transducer mounted flush to the face of an 16 inch diameter disk. Each disk was attached to the end of a 3 inch -OD steel pipe. The steel pipe was welded at a right angle to another steel pipe which was mounted at prescribed locations along the track.

For 10 of the probes, called left-hand (see Table 1), the disks were oriented so that the sensing surface was on the north side of the disc. For the other two probes, called right hand, the disks and piping were oriented so that the sensing surface was on the south side of the disc.

Data from these probes were recorded on tape in a mobile van stationed adjacent to the north side of the test site. The recorders had a frequency response of 4 kHz. For the complete blast-line measurement system the overall response time was about 0.2 milliseconds.

2-8 WING PRESSURE MEASUREMENTS.

Pressures on the wing were measured using Kulite high performance pressure transducers of the XCQL-41-093-025, XCQL-37-093-25D and XF-160-25A series. The external geometries of these instruments are shown in Figure 15. All of these transducers have a 25-psi range and are insensitive to acceleration effects. The first two series mentioned above are 0.093 inches in diameter, 0.25 inches long, and have a 230 kHz natural frequency. The later series is 0.160 inches in diameter, 0.11 long, and has a 100 kHz natural frequency. This transducer was selected for use at the stations on the 82 1/2% chord line at the 65% and 85% semi-span locations. All transducers were mounted flush with the external surface and remained nearly flush through the two sled runs.

The transducer signals were generally connected in pairs electrically through differential amplifiers for measuring the differences in pressures between the blast-side and lee-side of the wing. Before and after each test the transducers were calibrated in this arrangement for matching gains.

The wing was shielded from the sun by polystyrene blocks prior to sled firing to minimize solar heating. The blocks were pulled away from the model as the sled started down the track.

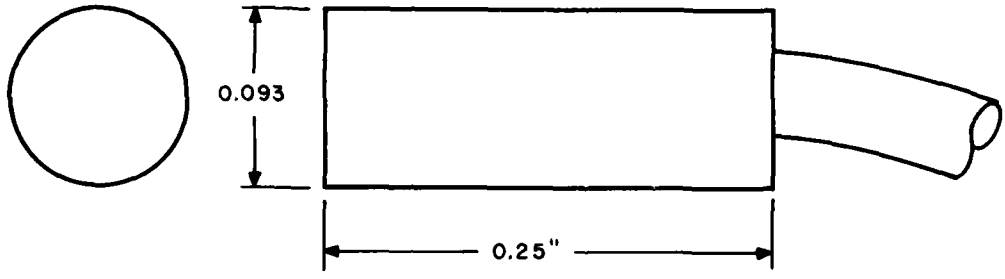

XCQL-41-093-025
XCQL-37-093-250

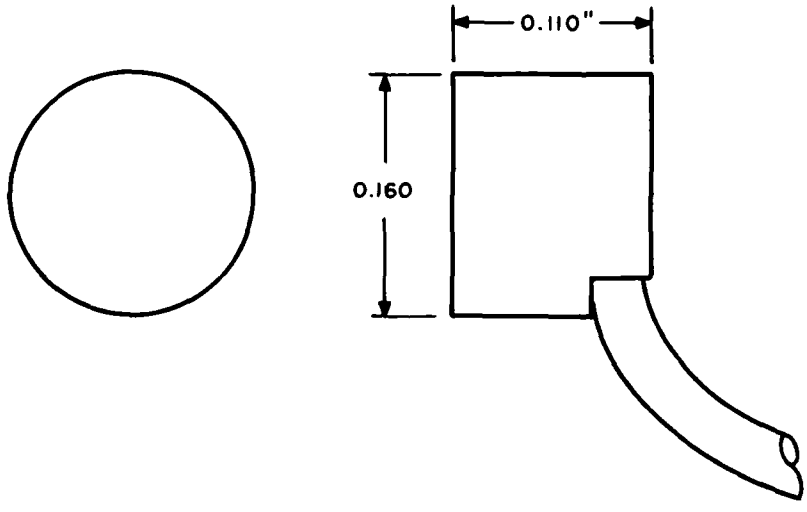

XF-160-25A

Figure 15. Geometry of Kulite Pressure Transducers

2-9 SLED VELOCITY AND POSITION MEASUREMENTS.

Sled position and velocity were measured with the standard HAFB electro-optical velocity measurement system (VMS). This system consists of a sled-borne photocell circuit which is interrupted generally at 13 foot intervals along the track by ground-based bars, each of which produces a signal at the sled which is telemetered to a ground-based recorder station. This basic time-distance record is computer-differenced and smoothed to produce a sled velocity time history. Figure 16 presents these time histories of sled velocity in the test area for the two runs made.

In addition to the above VMS measurements, independent measurements of sled position along the track were obtained for several times from the breakwire signals used to provide firing and timing information (see Section 2.3) and from photographic records by using charge detonation as a time reference.

2-10 HIGH-SPEED PHOTOGRAPHY.

A variety of motion picture data were obtained on this test series. On the preliminary static test, 9B-C1, the coverage was limited to one camera which provided an overall view of the test area. A number of high-speed cameras operating at speeds between 120 and 10,000 frames per second were used for the two sled runs, 9B-B1 and 9B-B2.

For the two sled run tests, 4 x 16-ft grid boards with parallel black and white stripes, Figure 17, were placed west of the track near intercepts 1 and 3 for observation of the blast shock intercept with the sled. A NOVA camera operating at 10,000-fps, was positioned on the east side of the track at each intercept for photographing. Two sled-borne cameras, one set to operate at 600-fps and the other at 1000-fps, were mounted on a pedestal at the aft end of the sled, Figure 8, to monitor lateral deformations of the wing. The 1000-fps camera malfunctioned in both sled runs.

White tufts were mounted on the leeside of the lower wing semispan which was painted black to observe the vortex motion. Two cameras were positioned east of the track to record the tuft motion

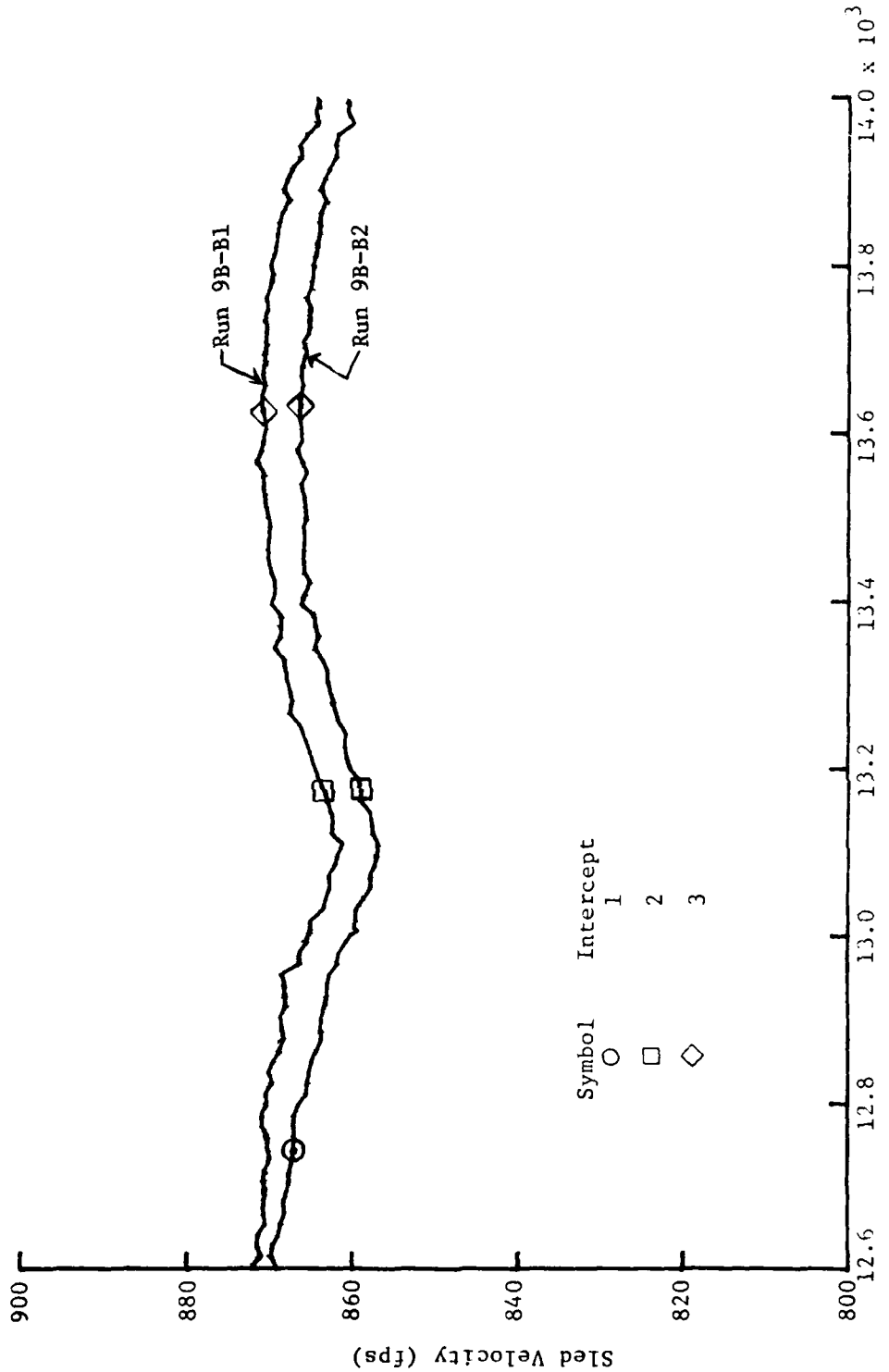

Figure 16. Sled velocity profiles

Figure 17. View of Gridboard at Intercept 1

before, during and after blast intercept. One camera was located about 127 feet from the track in line with the DIP and charge. The other camera was positioned directly north of the first about 17 feet. The field of view on both cameras was set to obtain some overlap in the coverage of the model as it moved through the test area. During Run 9B-B1 auxiliary lighting from flash bulbs was provided to enhance the motion pictures. The lighting was omitted from Run 9B-B2 after it was discovered that it had an effect on some of the pressure transducers (see Section 2-8).

Various lower speed motion picture cameras were used for general surveillance of the run phenomena. Two were mounted over the track at station 14100 looking south while another was positioned on a building about 1/2 mile east of the track.

2-11 TELEMETRY.

All sled-borne transducer signals were telemetered from the sled to a HAFB ground receiving station. Six transmitters were used, operating at carrier RF frequencies near 800 MHz, with 4 transducer signals generally multiplexed in each transmitter at sub-carrier frequencies of 64, 96, 128 and 160 kHz with a frequency deviation of 8 kHz. The signal was played back at a modulation index of two giving a frequency response of 4 kHz. The overall response time of the instrumentation and telemetry system to transient pressures is estimated to be about 0.2 milliseconds.

2-12 MODEL STRENGTH AND STIFFNESS TESTS.

The model was designed strengthwise to meet conservative design specifications of blast airloads. The sting and strut support were the same as used on the previous wing tests (Reference 1) where they were designed and tested for total model loads similar to those predicted for the present model. For stiffness the model and its support were designed to keep the frequencies of the wing modes and the support lateral modes well separated from the frequencies of the

sled lateral modes. In addition the model and its support were designed to keep the model deflections and motion small so the resultant airloads produced by the deflection and motion would be negligible.

Loads and vibration tests were performed on the model, and sled system at HAFB during the period of July 30 to August 1, 1979, prior to the sled test program. A test report was prepared and distributed by HAFB, Reference 5. Critical results of those tests are reviewed here.

2-12.1 Strength.

The wing mounted on the sled as shown in Figure 18 was statically loaded in the laboratory at HAFB. Loads were applied in increments until the design limit load was reached. The wing and support system carried the design-limit load without incident, indicating that the design goals had been met.

2-12.2 Deflection.

Deflections of the wing were measured during the static loading tests. At the design-limit load condition the measured deflections are compared in Figure 19 with the NASTRAN code calculations performed by D.J. Krupovage, Reference 6. The applied load distribution used in the test for the design limit load is indicated in the figure. The deflection at the wing center, Figure 19, is about 73 percent of the NASTRAN prediction, indicating that the stiffness of the support and fuselage combination based on this result is about 37 percent greater than predicted from the design data. The deflections come in closer agreement outboard along the wing semispans, being essentially in agreement at the most outboard positions. This trend outboard indicates that the wing stiffness is somewhat less than predicted, which could be a result of some slippage between the two halves of each wing semispan. The agreement overall is good and essentially confirms the NASTRAN stiffness model.

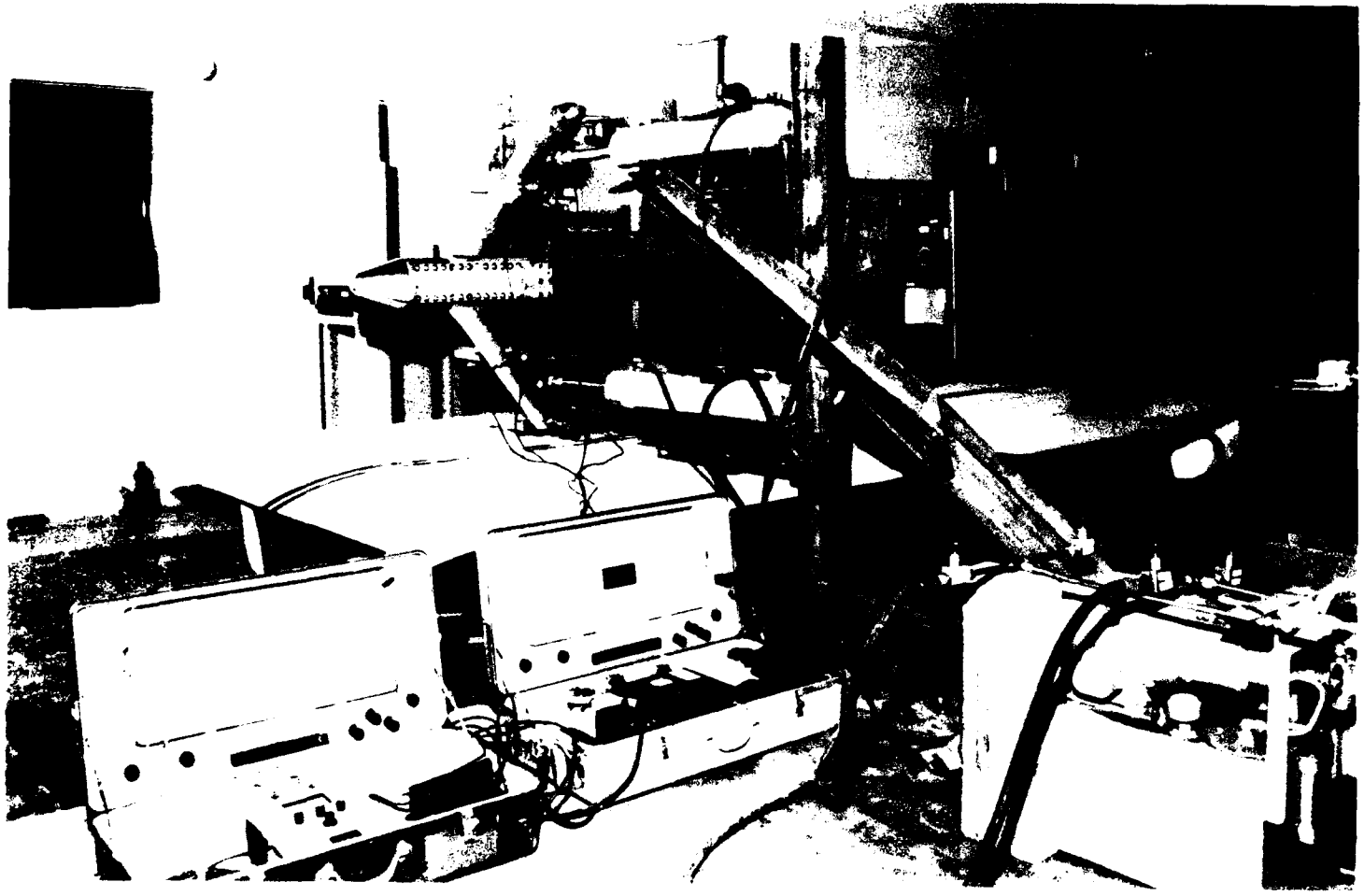

Figure 18. Static Loading Test Setup for Wing Mounted on Sled

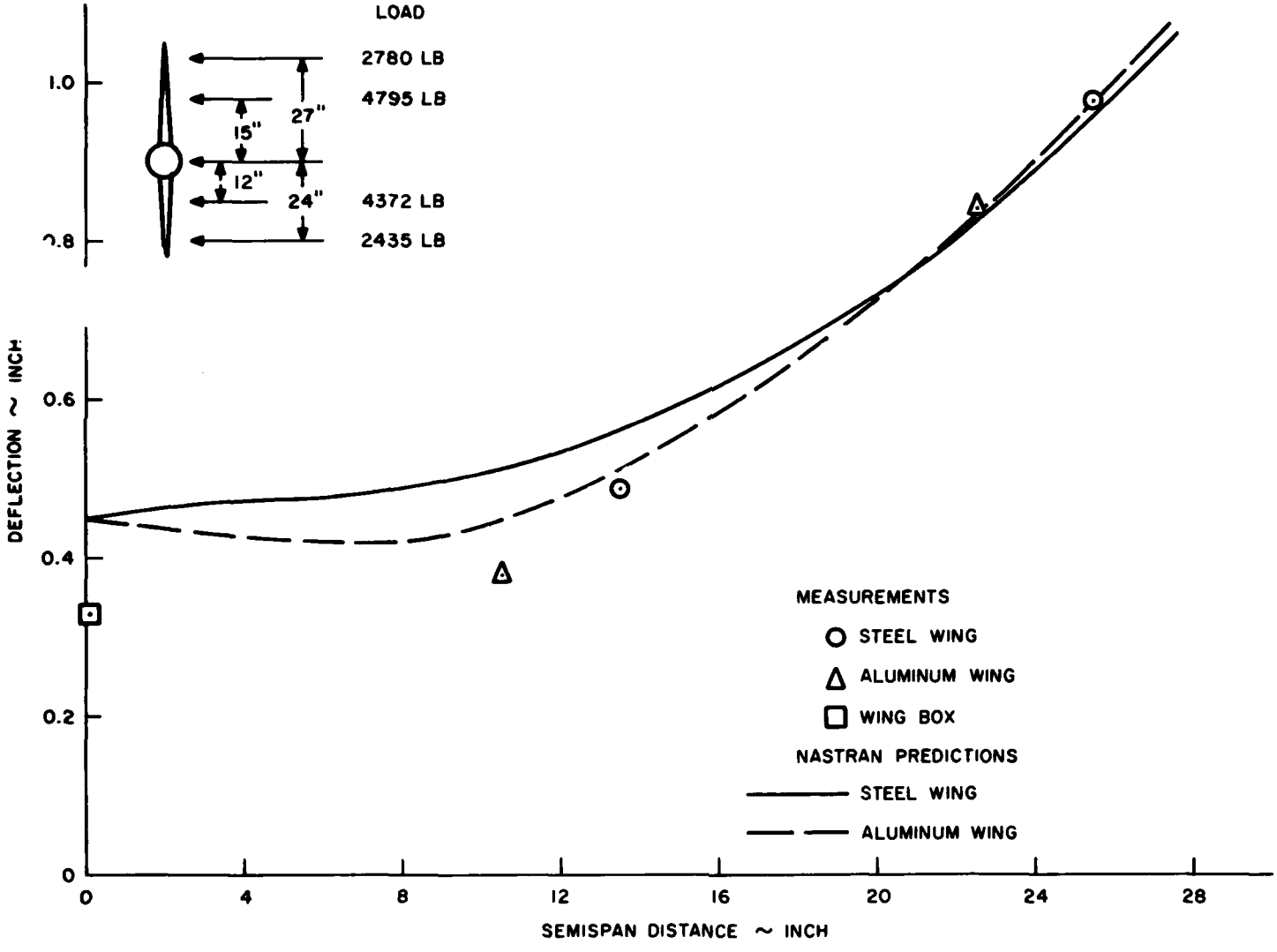

Figure 19. 35° Wing Static Load Test Design Limit Load Condition

2-12.3 Frequencies.

Shake tests were performed with the sled mounted on rails in the laboratory. With a 15-lb shaker force applied in a lateral direction relative to the track, a sine sweep was performed over the frequency range of 15 to 200 Hz. The observed response was similar to that obtained in the program of Reference 1. The lower frequency modes which are related primarily to the sled agreed reasonably well with the NASTRAN predictions. Particular attention was given to the three modes involving the wing. Table 4 lists these modes and shows the NASTRAN predicted frequencies are in reasonable good agreement with the measured frequencies.

TABLE 4

SUPPORT AND MODEL MODES

Mode Shape	Frequency (Hz)	
	Measured	NASTRAN Prediction
Sting Torsion	64.2	65.76
Lateral Wing and Sting Bending	53.5	67.98
Lateral Wing and Sting Bending	71.7	77.49

SECTION 3
TEST SERIES

3-1 INTERCEPT CONDITIONS.

The test conditions for the runs and intercepts are tabulated in Tables 5 and 6. Table 5 gives general sled test conditions for each run, including atmospheric pressure, temperature and wind conditions and the nominal sled speed. Table 6 gives specific charge and blast intercept conditions for each blast intercept, including charge weight, sled intercept velocity, charge-sled intercept geometrical relationships, blast intercept angle (ϕ), incident blast intercept overpressure (Δp_s), and the peak angle of attack produced by the blast wave. The values of incident blast overpressure in Table 6 were obtained for each intercept by scaling the incident blast overpressures for each blast line transducer to the intercept point, using Goodman's empirical curve (Reference 7) scaled to determine the ratio of overpressure at the intercept point to that at the transducer location. The tabulated values of incident overpressure are the average of these scaled values for all blast-line transducers for each intercept.

Sled-borne pressure transducer locations were the same for all runs, as given in Figure 12 and Table 3. For all locations except one only the differential pressures between the two surfaces of the (upper) wing were recorded. For the 25 percent semispan, 62 1/2 percent chord location individual pressures on both the leeward and blastward side of the model were recorded as indicated in Table 3.

The reference point on the wing which is used to define the wing-blast intercept location is defined as that point where the wing 40 percent chordline intersects the centerline of the model fuselage. The corresponding blast intercept time for this point can be easily determined from the observed blast arrival times at the two wing transducers closest to that reference point, which are at the 7.5 and 22.5 percent chord positions at the 25 percent semispan location.

TABLE 5

GENERAL SLED TEST CONDITIONS

Run No.	Date	Ambient Conditions					Nominal Sled Speed		Angle of Attack (deg)
		Pressure		Temp.	Wind				
		(in. Hg)	(psia)	($^{o}_{F}$)	Dir. (deg)	Vel. (Kn)	(fps)	(Mach No.)	
9B-C1	9/12/79	25.85	12.64	82.0	205	8	870	0.76	3.2
9B-B1	9/13/79	25.89	12.66	84.2	180	8	870	0.76	3.2
9B-B2	9/20/79	25.84	12.64	76.8	120	2	870	0.76	3.2

TABLE 6

BLAST INTERCEPT CONDITIONS

Run No.	Intercept No.	Charge Weight (lbs)	Sled Velocity		Distance from Charge Station to Intercept Point (ft)			Intercept Angle (deg. from head-on)	Blast Shock Over-pressure (psi)	Blast[c] Peak Angle of Attack (deg)
			(fps)	(Mach)	Parallel[b] to Track	Perpendicular to Track	Radial Distance			
9B-C1	2	1000	0	0	0.0	258.0	258.0	90.0	1.98	-
9B-B1	1[a]	1000	-	-	-	-	-	-	-	-
	2	1000	864	.755	-4.4	258.8	258.8	89.0	2.12	11.6
	3	1000	871	.762	110.7	116.0	160.3	133.7	4.15	16.8
9B-B2	1	1000	867	.763	-182.2	182.4	257.8	45.0	2.08	8.5
	2	1000	859	.756	-1.7	352.5	352.5	89.7	1.28	8.4
	3	1000	866	.763	185.3	182.4	260.0	135.5	2.00	9.4

[a] Premature detonation

[b] In direction of sled travel.

[c] Includes pre-blast angle of attack.

The track station at blast intercept time for the model reference point was estimated by several independent methods for each intercept, results of which are presented in Table 7.

The first estimate made (A) was based on the sled trajectory measurements described in Reference 1 of DNA 4400F and Section 2.9 and the blast intercept time as determined by the wing pressure transducers (t_1). The second estimate (B) was based on the timing breakwire location, the sled speed, the indicated time of wire breaking and the blast intercept time t_1. The third method (C) was based on the location of the firing screen-box, the sled speed, the time of the detonation, and the blast intercept time t_1. The fourth method (D) was based on the location of the blast line transducer closest to the sled intercept, blast shock velocity, and the times of blast arrival at this blast line transducer and at the sled. The fifth method (E) was based on photographic observations of the intercept of the sled and the blast wave. Values of intercept conditions obtained by these various methods differ somewhat due to the associated experimental uncertainties. It is recommended that the intercept conditions presented in Table 6, based on the average values presented in Table 7, be used for any calculations relevant to the test program.

3-2 RUN 9B-C1.

This test was performed to obtain a blast intercept of 90° at a shock overpressure level of 2 psi with the sled stationary. For this test the sled was set on the track with the model at TS 13180. The charge was located directly west of the model, 258 feet from the centerline of the track. Weather conditions at the time of detonation were good. The temperature was 82°F with an 8 knot wind coming from approximately the 205° direction which is equivalent to a cross wind of about 3 knots. Useful data were obtained from all sled-borne pressure transducers but the blast-line data are of limited value. An opening on the back of each mount which normally is covered was inadvertently left open. Thus the peak pressure is believed to be valid but the response of these gages during the decay period is unreliable.

TABLE 7

COMPARISON OF INTERCEPT LOCATION ESTIMATES

Run No.	Intercept No.	Intercept Station Estimate (ft)[a]					
		A	B	C	D	E	Av.
9B-B1	2	-4.3	-3.9	-4.9	-	-	-4.4
	3	-5.7	-5.0	-5.2	-	-	-5.3
9B-B2	1	0.3	1.0	-0.3	-0.1	-	+0.2
	2	-2.1	-2.6	-1.4	-	-0.7	-1.7
	3	3.0	2.2	3.6	3.0	-	+2.9

[a]Distance ahead of Desired Intercept Point in the direction of sled motion (see text, Sec. 3.1, for meaning of A, B, C, D, E, designations). The Track Station for the DIP is given in Table 1.

This test was also used to determine if loose gravel used to fill in next to the track on the northern portion of the test area would be thrown into the path of the sled by the blast wave. Two shallow pits approximately one foot wide, 2 feet long and 2 inches deep were positioned west of the charge (Figure 20). One was placed where the maximum blast overpressure would be 4 psi and the other where the overpressure would be 8 psi. Both were filled flush with gravel similar in size to that which was used along the track. An examination of both the pit and the adjacent area after the test showed that none of the gravel had been noticeably moved.

3-3 RUN 9B-B1.

This run was performed to obtain 45° and 90° blast intercept data at a 2 psi overpressure and 135° blast intercept data at an overpressure of 4 psi. The weather was clear, the temperature was 84.2°F and the wind was from 180° (south) at 6 knots. Charge 1 detonated shortly after being armed and prior to the command for sled firing. The test was performed after a short delay but with only the last two intercepts. The sled performed as expected and useful data were obtained from all sled-borne transducers at intercepts 2 and 3. Blast-line data were obtained from the probes associated with intercepts 2 and 3 with the exception of probe 10 (the second probe at intercept 3) which malfunctioned. The blast-line data were slightly degraded because the IRIG timing signal was inadvertently omitted from the record during the recording of the data. However, a "dummy" IRIG timing signal was later dubbed on the blast-line records which was correlated with real time with an estimated uncertainty of less than about 1 millisecond.

3-4 RUN 9B-B2.

This run was performed to obtain 45° and 135° blast intercept data at a 2 psi overpressure and 90° blast intercept data at an overpressure of 1.3 psi. The weather conditions were excellent with the temperature at 76.8°F and a slight wind of approximately 2 knots from

Figure 20. Photograph of Gravel Filled Pit

the 120° (southeast) direction. The sled velocity was near the planned value and useful data were obtained from both the blast-line and sled-borne instruments at all three intercepts. The nosetip and leading edges of the wing were slightly rough after the test due to what appeared to be sand adhering to these surfaces.

SECTION 4
TEST DATA

4-1 A/D DATA PROCESSING.

Seven types of event data were obtained as a function of time during a run:

1. Sled position and velocity.
2. Blast-line pressure.
3. Total pressure at the model and at the sled.
4. Static pressure at the sled.
5. Wing pressure.
6. Wing acceleration.
7. Lateral bending moment at the sting root.

All data were processed to digital form by HAFB and were provided to KA as tabular data. In addition Items 2 to 7 were provided in graphical form and on magnetic tapes.

The sled-borne transducer data (Items 2 to 7) were taken from the analog tapes at 0.1 millisecond intervals for about 1,000 times per intercept.

4-2 DATA PRESENTATION.

Graphical time history plots of typical blast-line and sled-borne transducer measurements are presented in Figures 21 to 24. In the figures of sled transducer pressures, the transducer locations are identified by a four-digit code such as 85/10, where the first two digits (85) give the spanwise distance from the model centerline as a percent of the semispan (e.g., 85%) and the last two digits (10) give the percentage of chordwise distance from the leading edge of the wing. The blast-line plots are identified with a number from 1 to 12 and a track station which indicates the location of the mount (see Section 2-7 and Table 1).

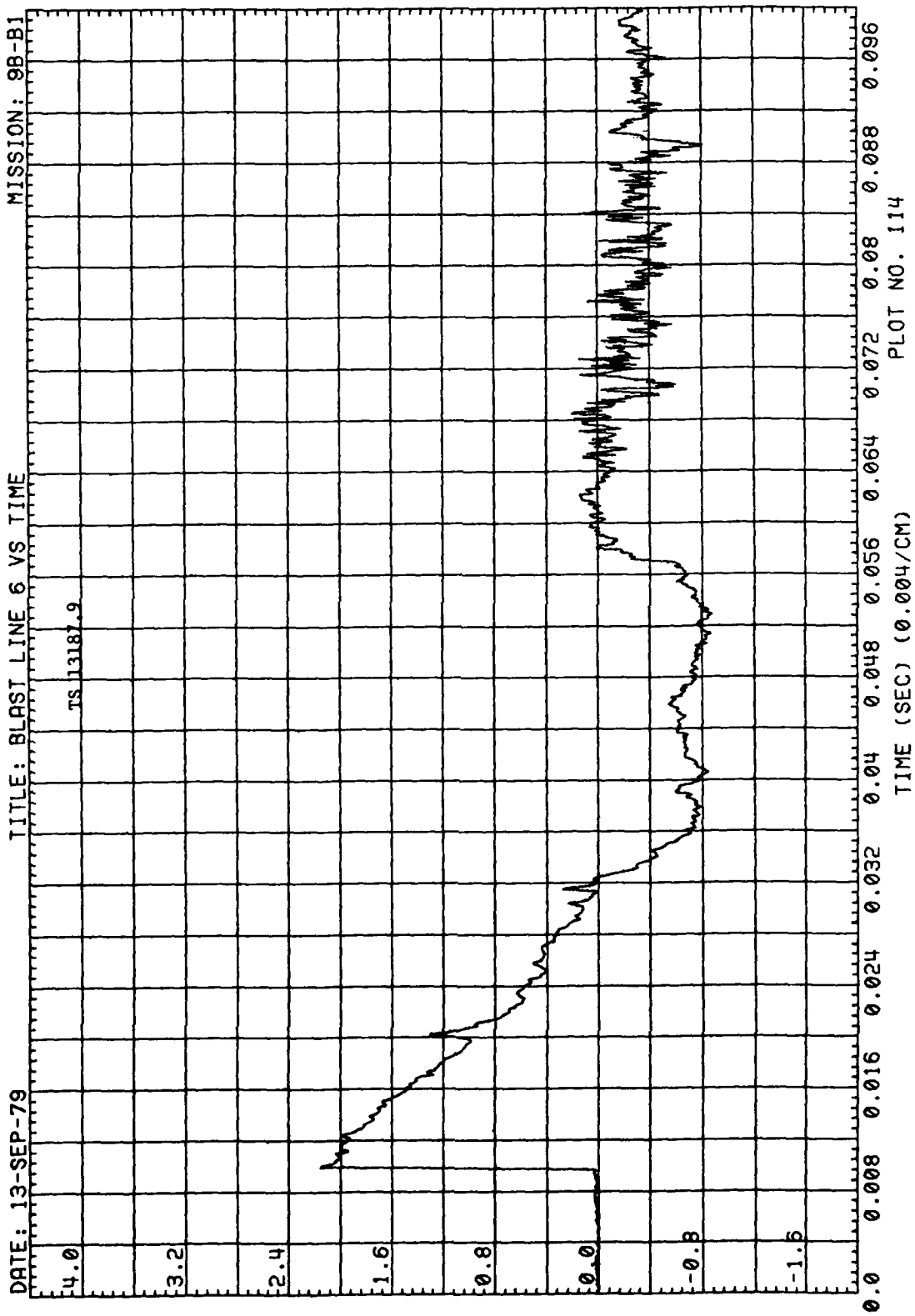

Figure 21. Sample Blast-Line Pressure Time History; Run 9B-B1, Intercept 2

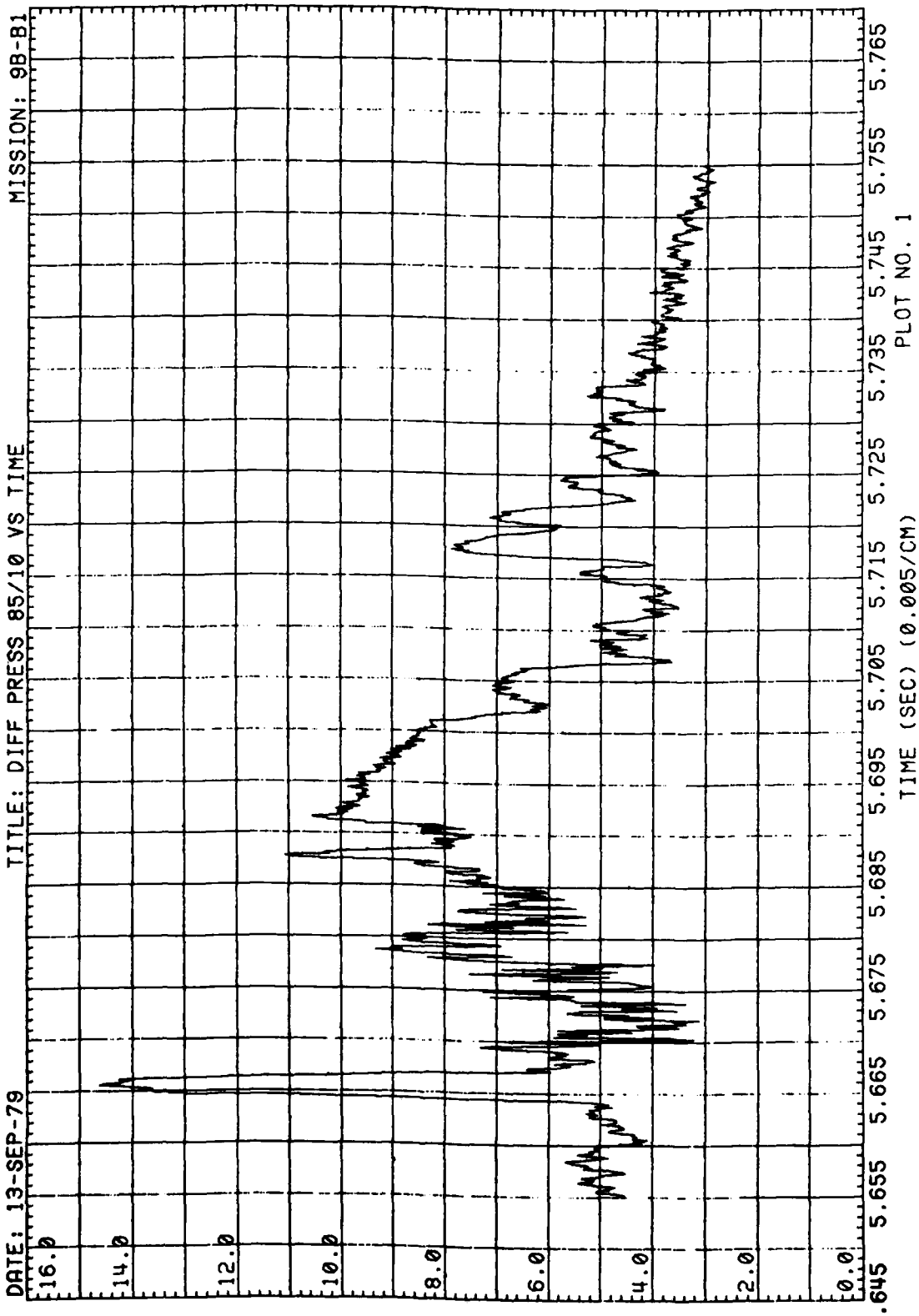

Figure 22. Sample Wing Differential Pressure Time History Run 9B-B1, Intercept 2

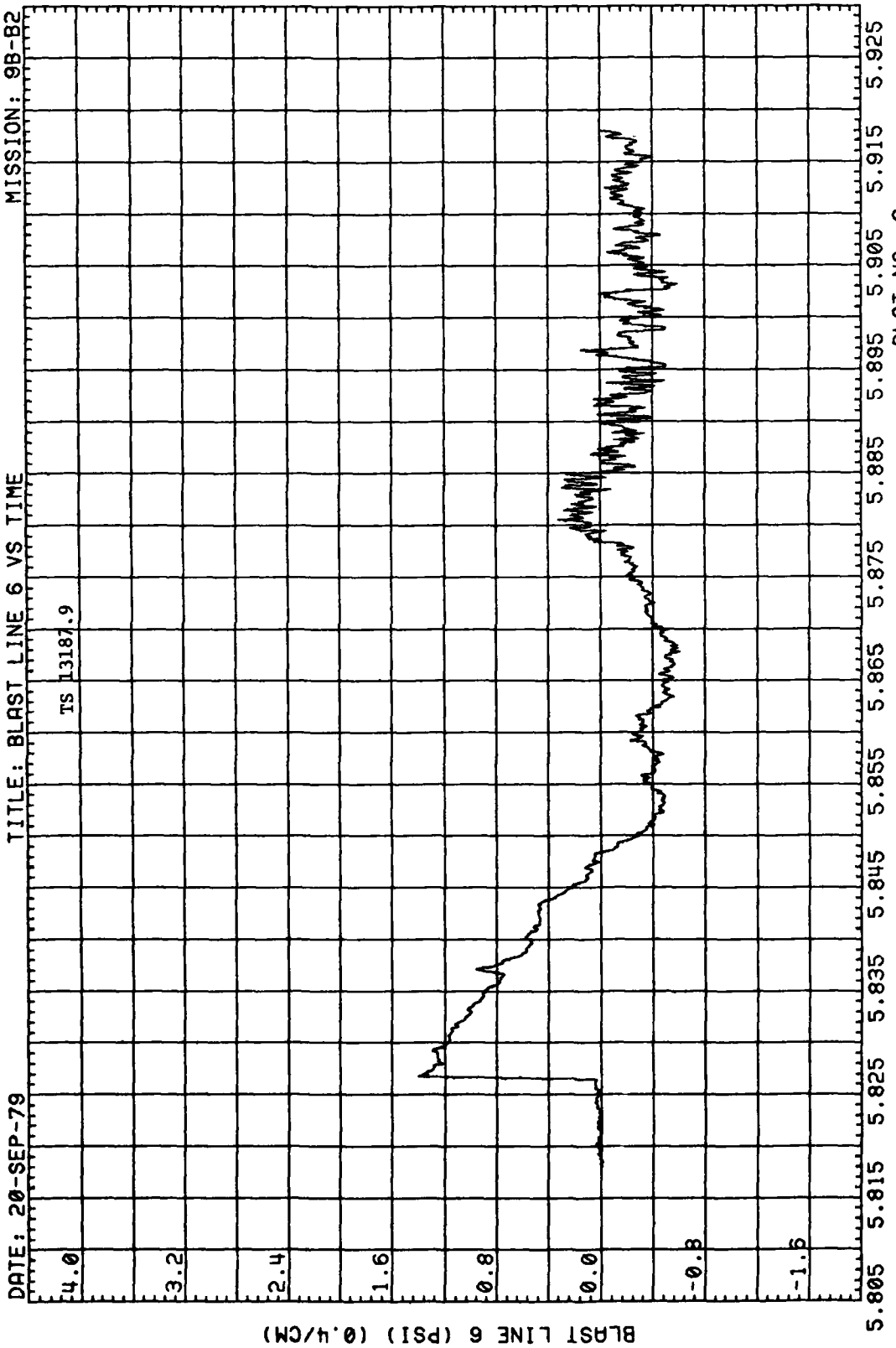

Figure 23. Sample Blast-Line Pressure Time History, Run 9B-B2, Intercept 2

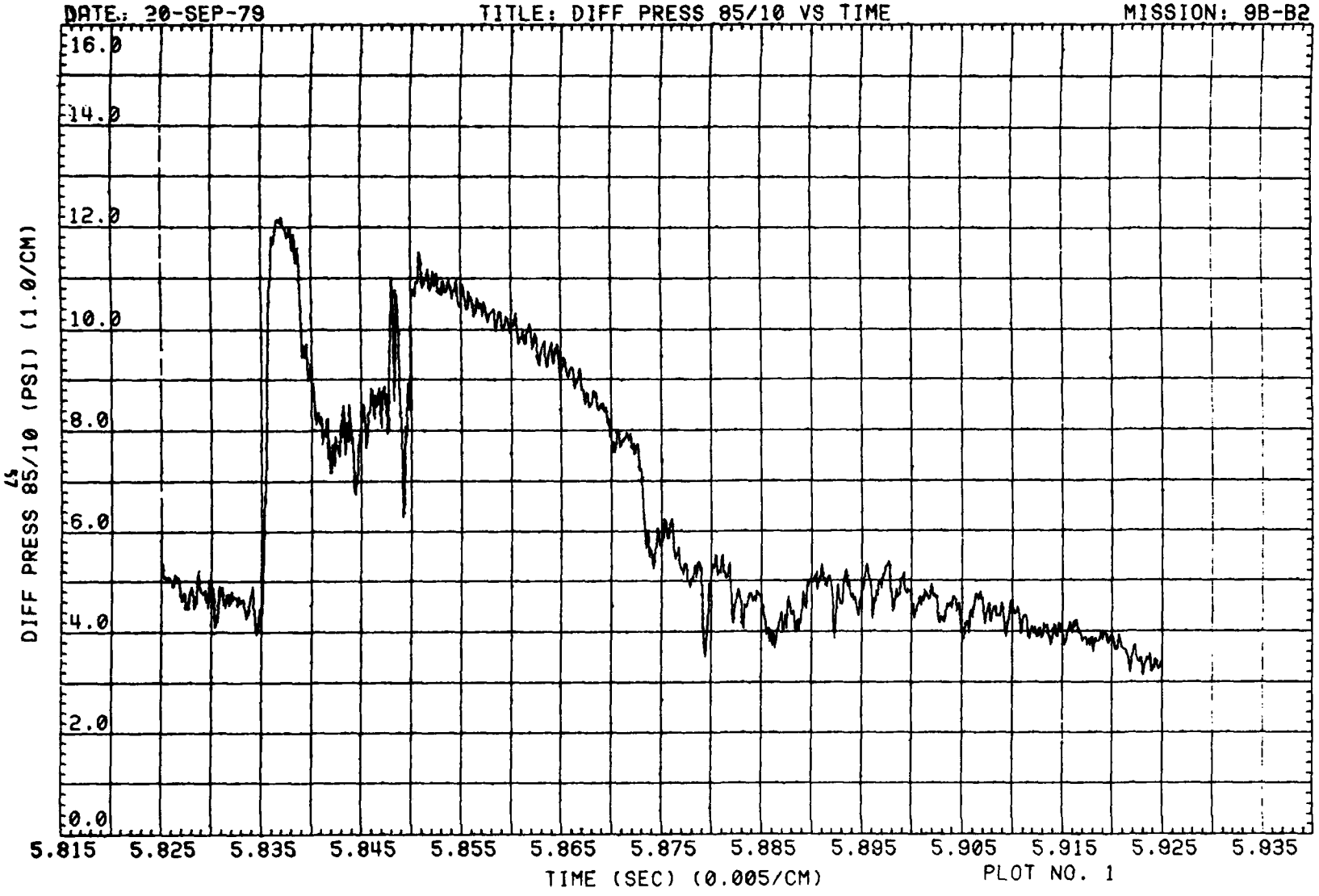

Figure 24. Sample Wing Differential Pressure Time History, Run 9B-B2, Intercept 2

A complete set of measured data, including the blast-line pressures, differential pressures on the wing, blastward and leeward wing pressures at location 25/62.5, total pressure at the model and at the sled, static pressure at the sled, strain on the sting and model acceleration is presented in Appendix A.

4-3 ACCURACY OF DATA.

Data accuracy and interference corrections for the blast-line data are discussed generally in Reference 1.

4-3.1 Blast-Line Transducers.

The general accuracy of the blast-line transducers and required corrections to account for interference pressures produced by passage of the sled past a transducer location are discussed in Reference 1.

4-3.2 Sled-Borne Transducers.

The accuracy of the sled-borne pressure data is discussed in Reference 1. In addition to the sources of data degradation covered there, another cause of erroneous signals was discovered in this test series. It was noted after Run 9B-B1 that 13 of the 20 differential pressure signals displayed an unusual response starting approximately 5 milliseconds prior to the arrival of the shock wave at intercept 2. Instead of the steady state response expected during this period the 13 readings all began to show a marked deviation with some going positive while others went negative. This random behavior was eventually attributed to the flashbulbs used to illuminate the model during the filming of the tufts. Verification of this anamalous response was obtained in an auxiliary test by firing the flash bulbs at the same position relative to the wing but without a blast wave and recording the signal from several pairs of transducers.

To eliminate the spurious signals on Run 9B-B2 the tuft lighting at intercept 2 was removed. Additional information on the problem was obtained by installing a similar set of lights at T.S. 12310, about 430 feet south of the first intercept. The responses of

the differential pressure transducers as they passed the lights was recorded for use in evaluating the 9B-B1 data. These results may not be directly applicable, however, because the road surface on which the lights were placed is further below the track level than in the test area. The results do qualitatively support the effects seen from Run 9B-B1.

4-3.3 Timing.

The relative timing of events on different time history plots in this report can be slightly in error for the following reasons.

a. The process of converting from analog to digital data can introduce irregular time shifts up to about a millisecond.

b. Due to operational problems, the normal IRIG time signal was not available on the blast-line analog tapes for Run 9B-B1. Consequently, it was necessary to impose a dummy IRIG time to the blast-line data and to align the dummy timing with the sled-borne IRIG timing signal by evaluating the time of a common event from both sled-borne and blast-line records. The common event used was the time of blast arrival at the sled for intercept 2. It was estimated that the inaccuracies involved in this process using dummy timing is under one millisecond.

SECTION 5
BLAST VARIABLES AT SLED

In order to utilize the blast-line pressure data presented in Section 4 for the comparison of experimental and theoretical wing pressures, it is necessary to interpolate or extrapolate the experimental blast-line pressures to obtain the blast pressure time history at the sled as a function of time, and to also estimate the corresponding blast density and velocity time histories as well. The blast pressures at the sled were generally obtained as indicated below and the corresponding densities and velocities were obtained by using the method described in Reference 8, as discussed in Appendix B of Reference 1. The resulting time histories of pressure, density and velocity at the sled are presented in Figures 25 to 29 for the sled test runs 9B-B1 and 9B-B2.

For each blast-line transducer time history, a corresponding time history of the blast overpressure at the sled was determined by assuming that the shapes of the overpressure time histories at a blast line transducer location and at the sled location are the same, if the overpressure is expressed as a fraction of the shock overpressure at the location and the time is expressed as a fraction of the positive duration of the blast wave, or

$$\Delta p/\Delta p_s = f(\Delta t/t_{\Delta p+}) \qquad (5\text{-}1)$$

where

Δp_s is the shock overpressure

Δp is the overpressure at time t

Δt is time after shock arrival $(t-t_s)$

t is time

t_s is shock arrival time

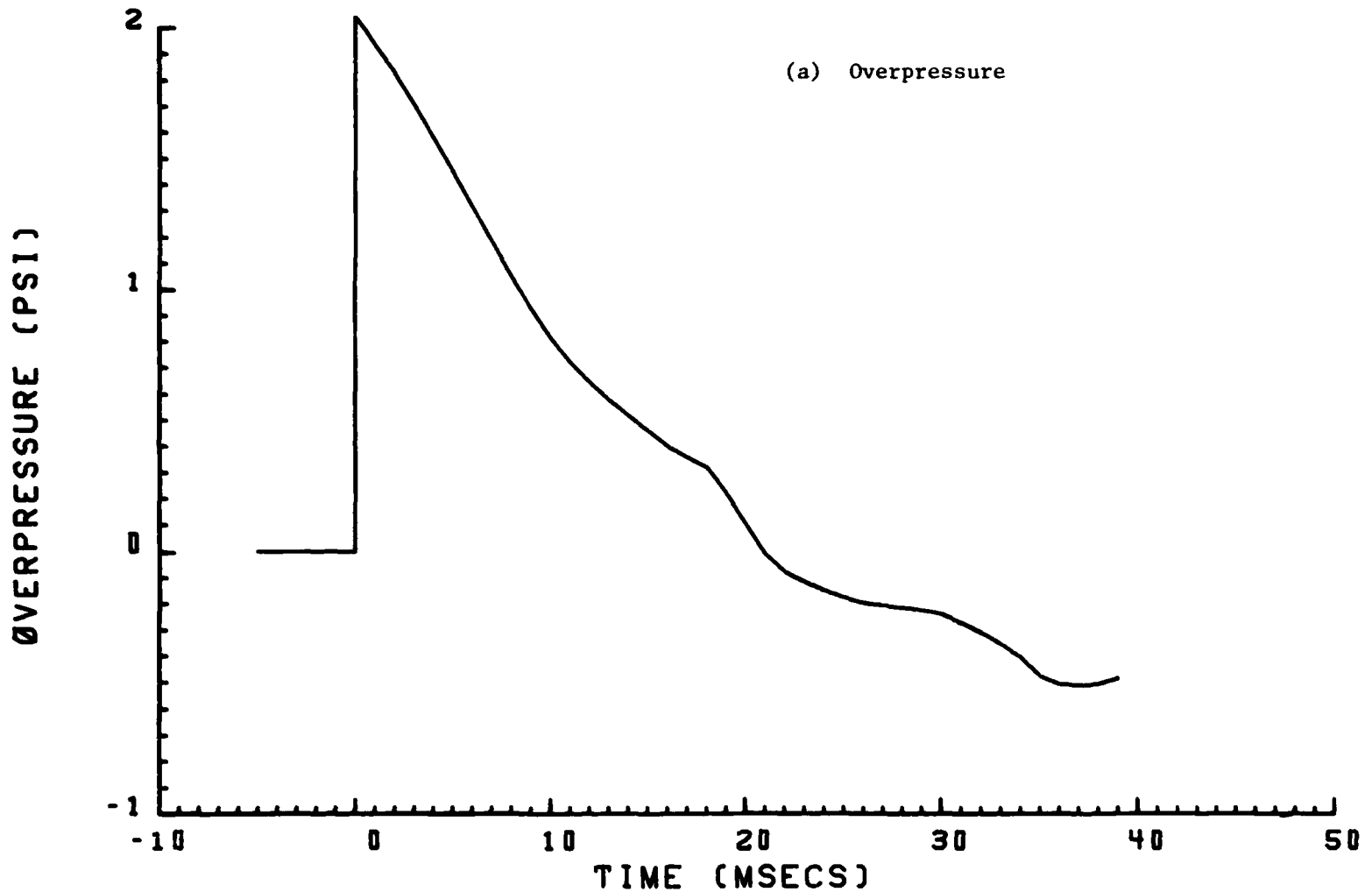

Figure 25. Blast Flow Conditions at the Sled for Run 9B-B1, Intercept 2

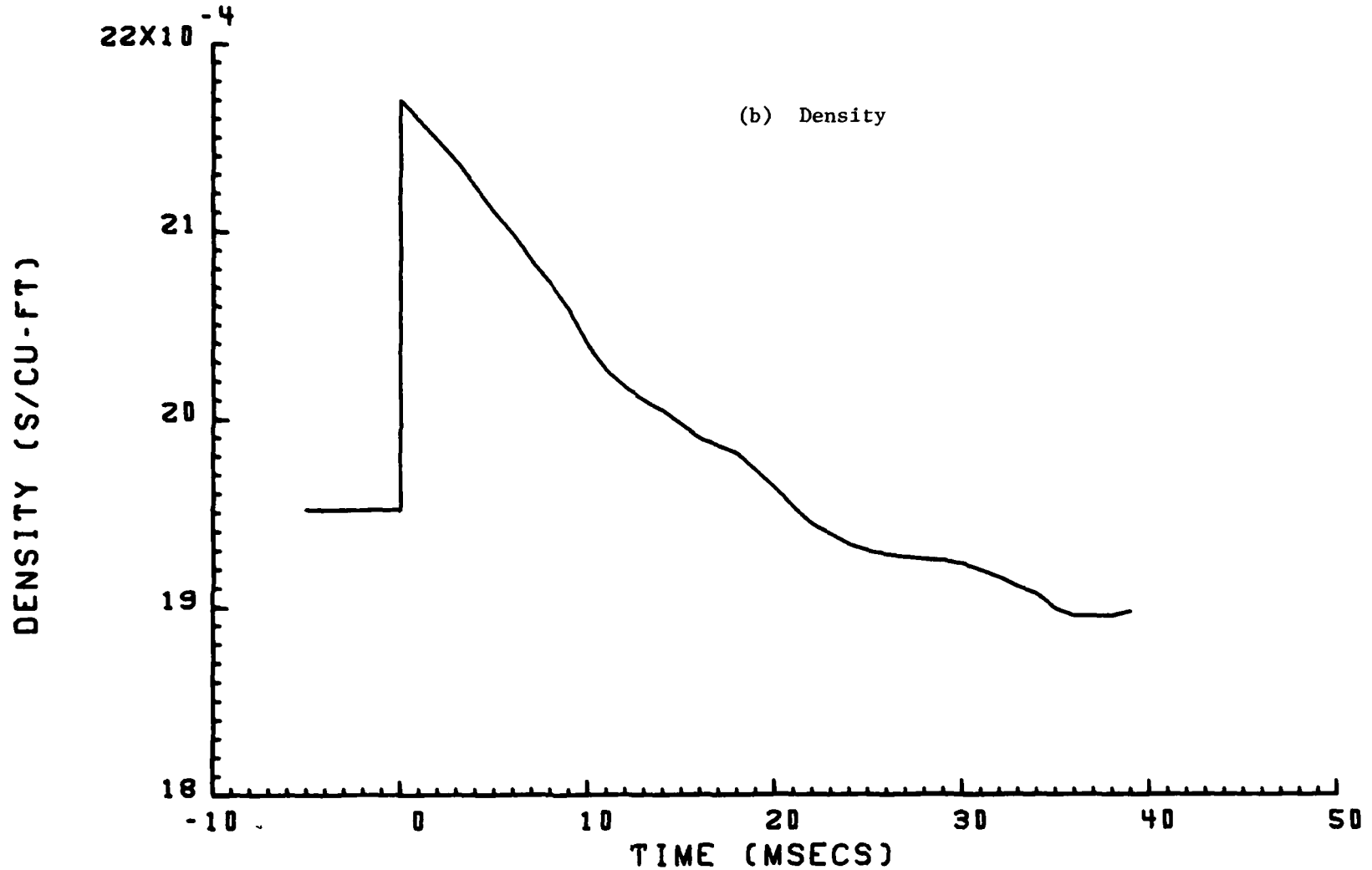

(b) Density

Figure 25. (Continued)

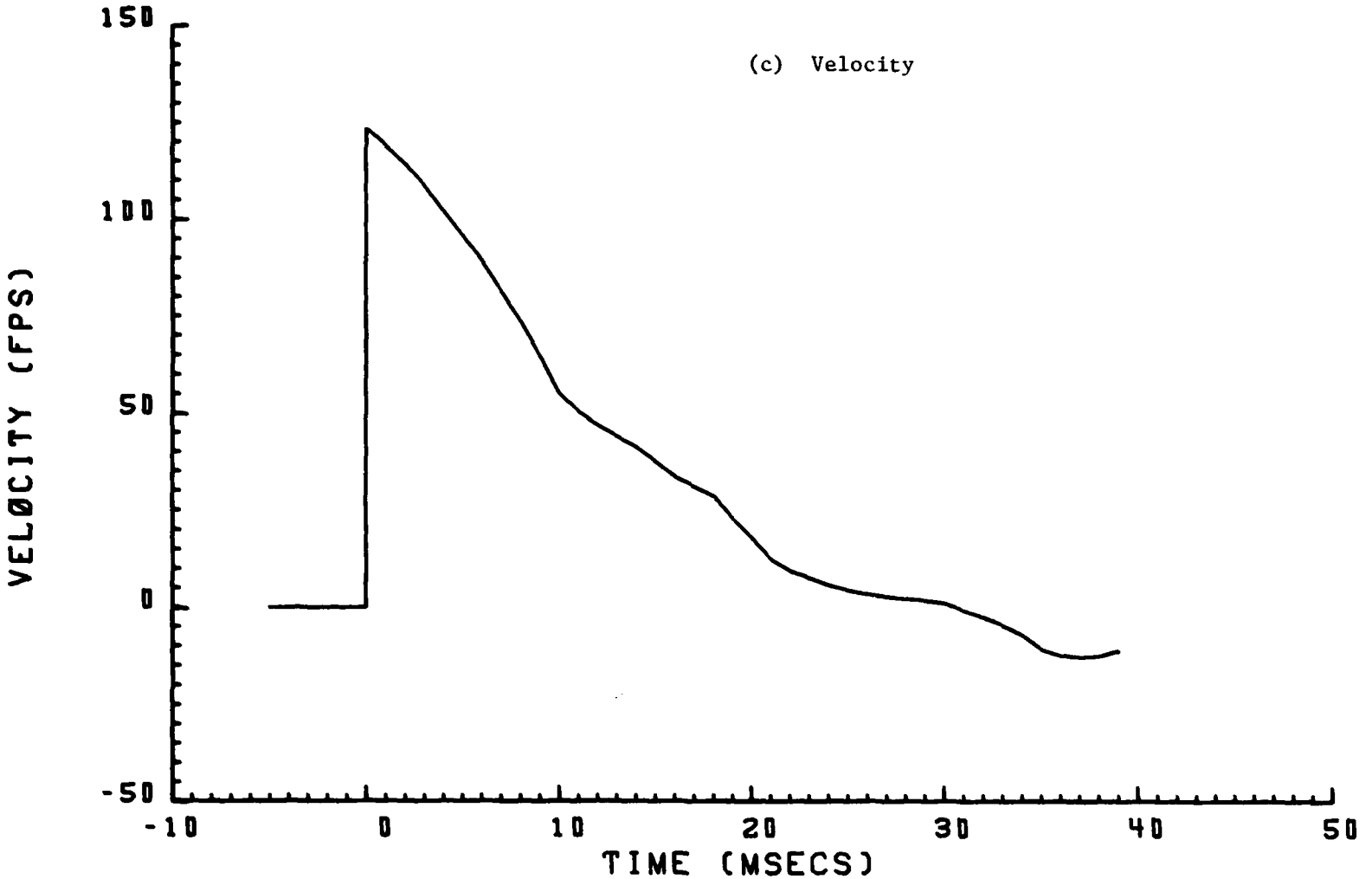

Figure 25. (Concluded)

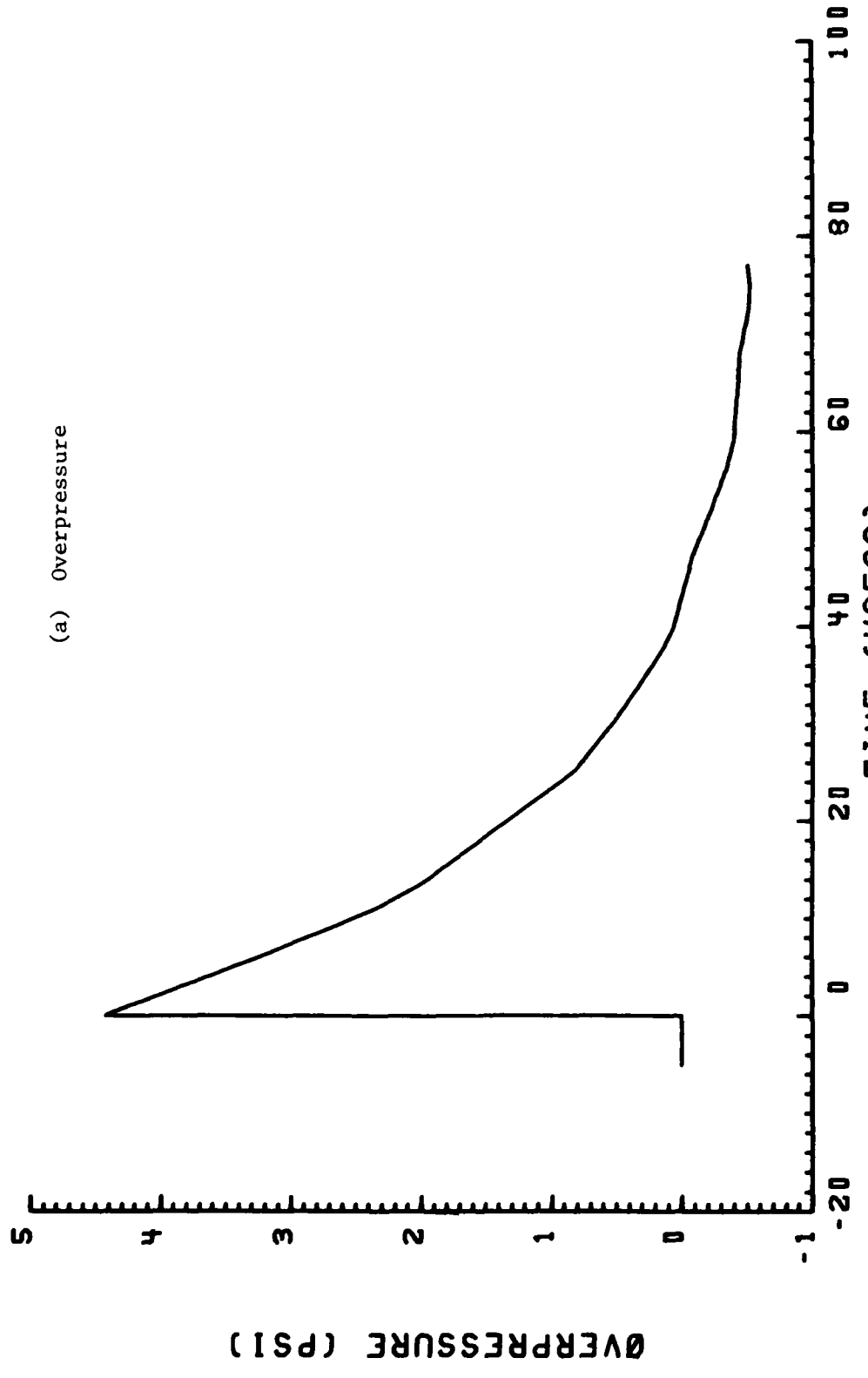

Figure 26. Blast Flow Conditions at the Sled for Run 9B-B1, Intercept 3

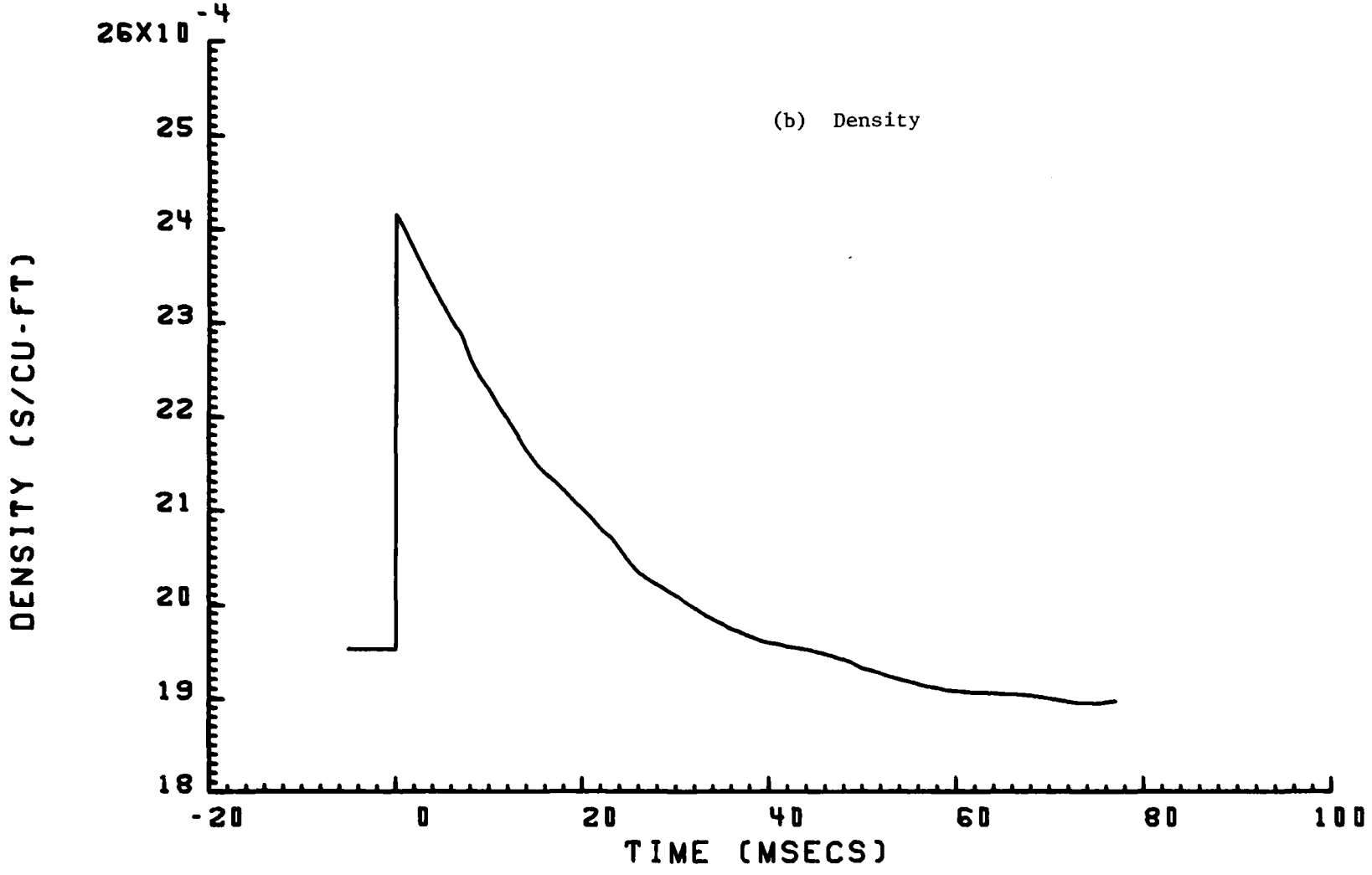

(b) Density

Figure 26. (Continued)

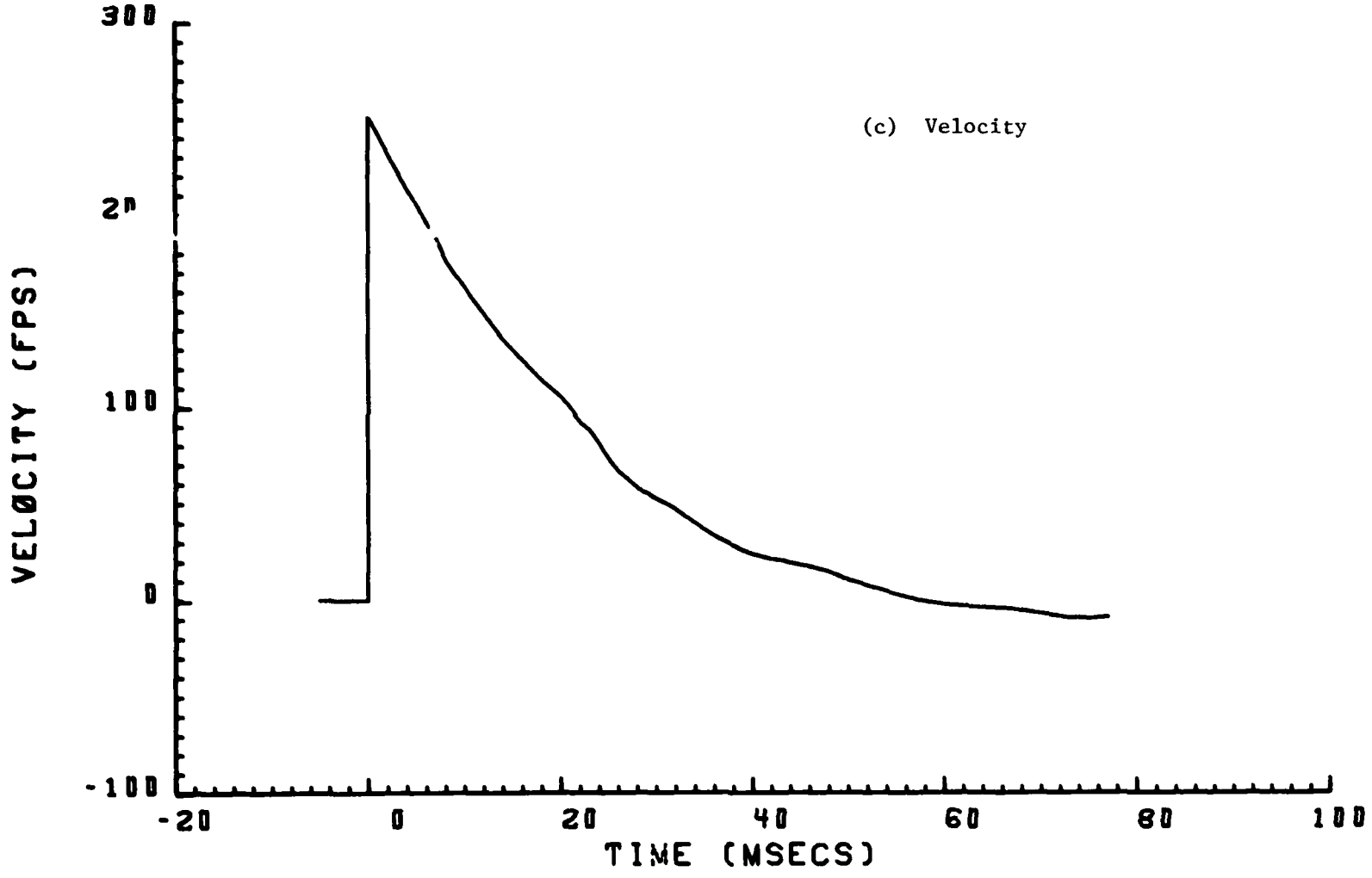

(c) Velocity

Figure 26. (Concluded)

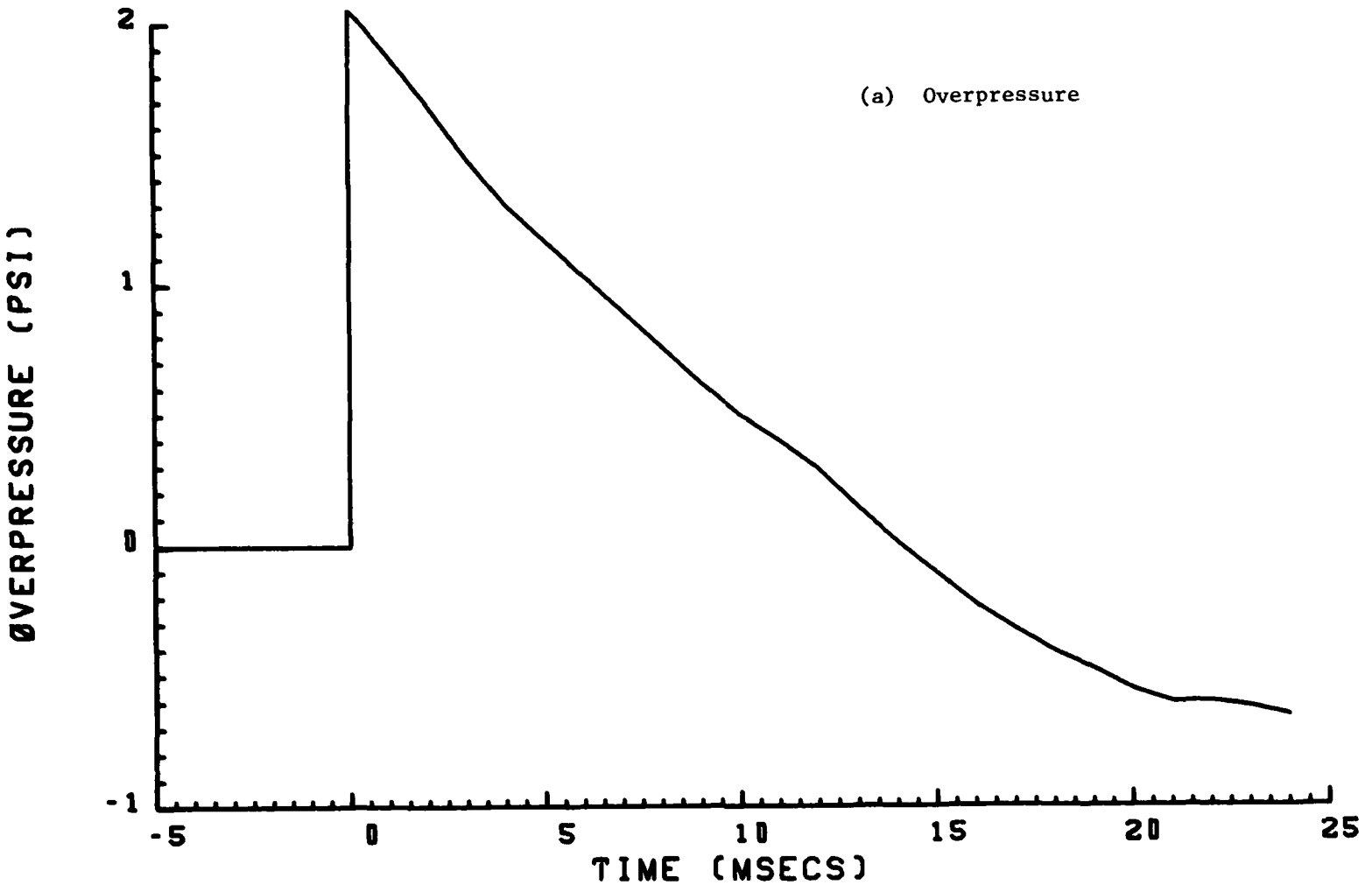

Figure 27. Blast Flow Conditions at the Sled for Run 9B-B2, Intercept 1

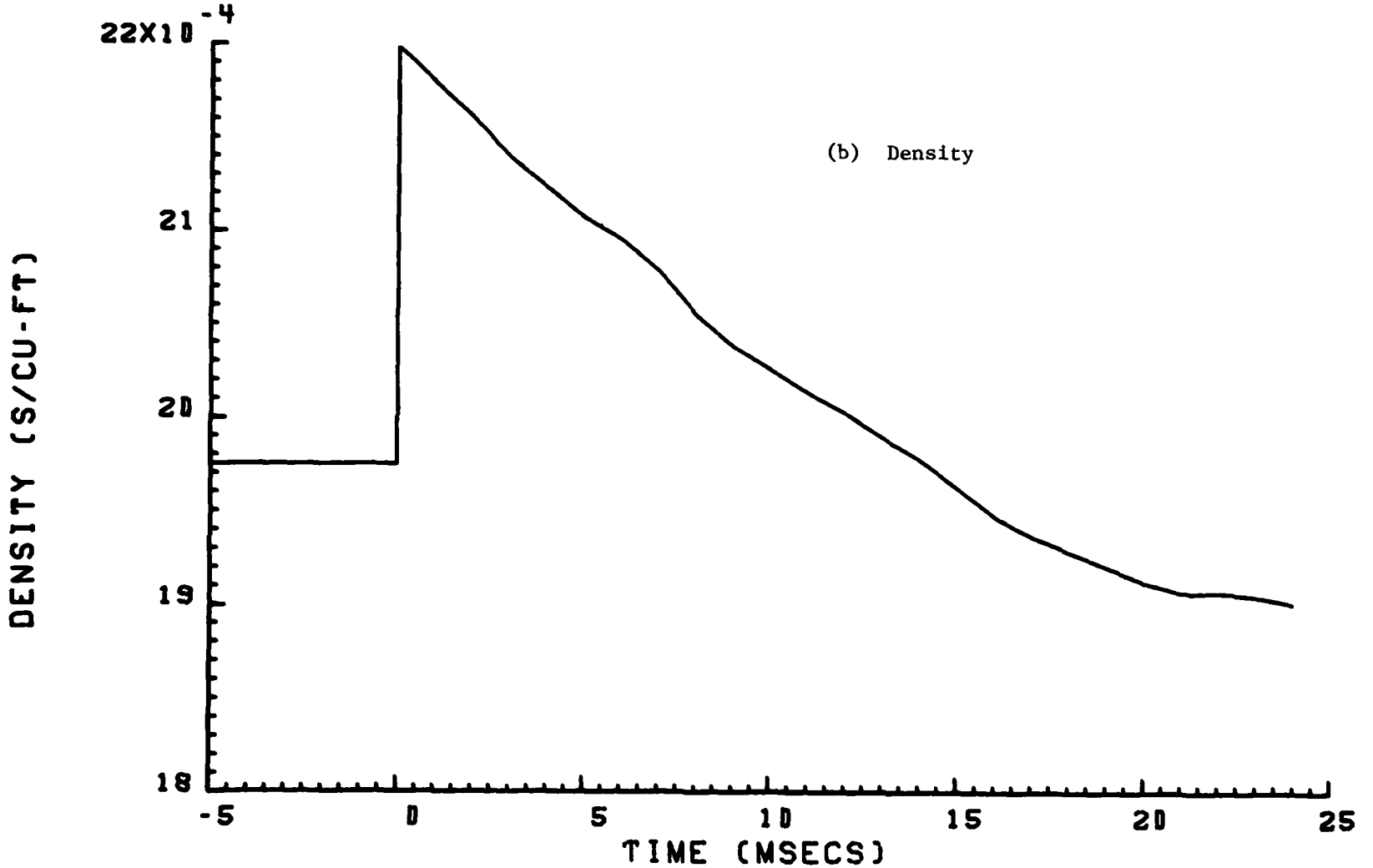

(b) Density

Figure 27. (Continued)

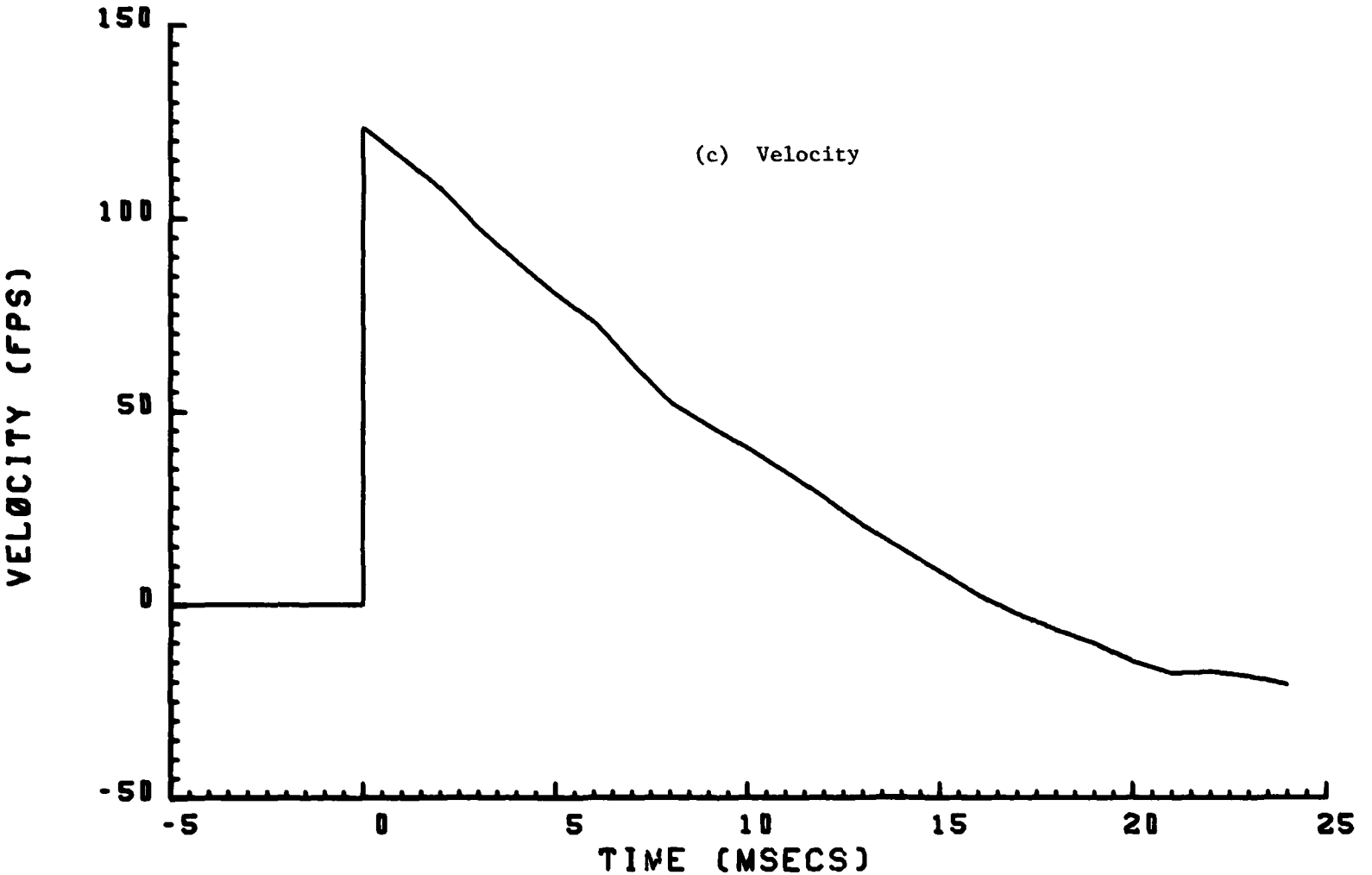

Figure 27. (Concluded)

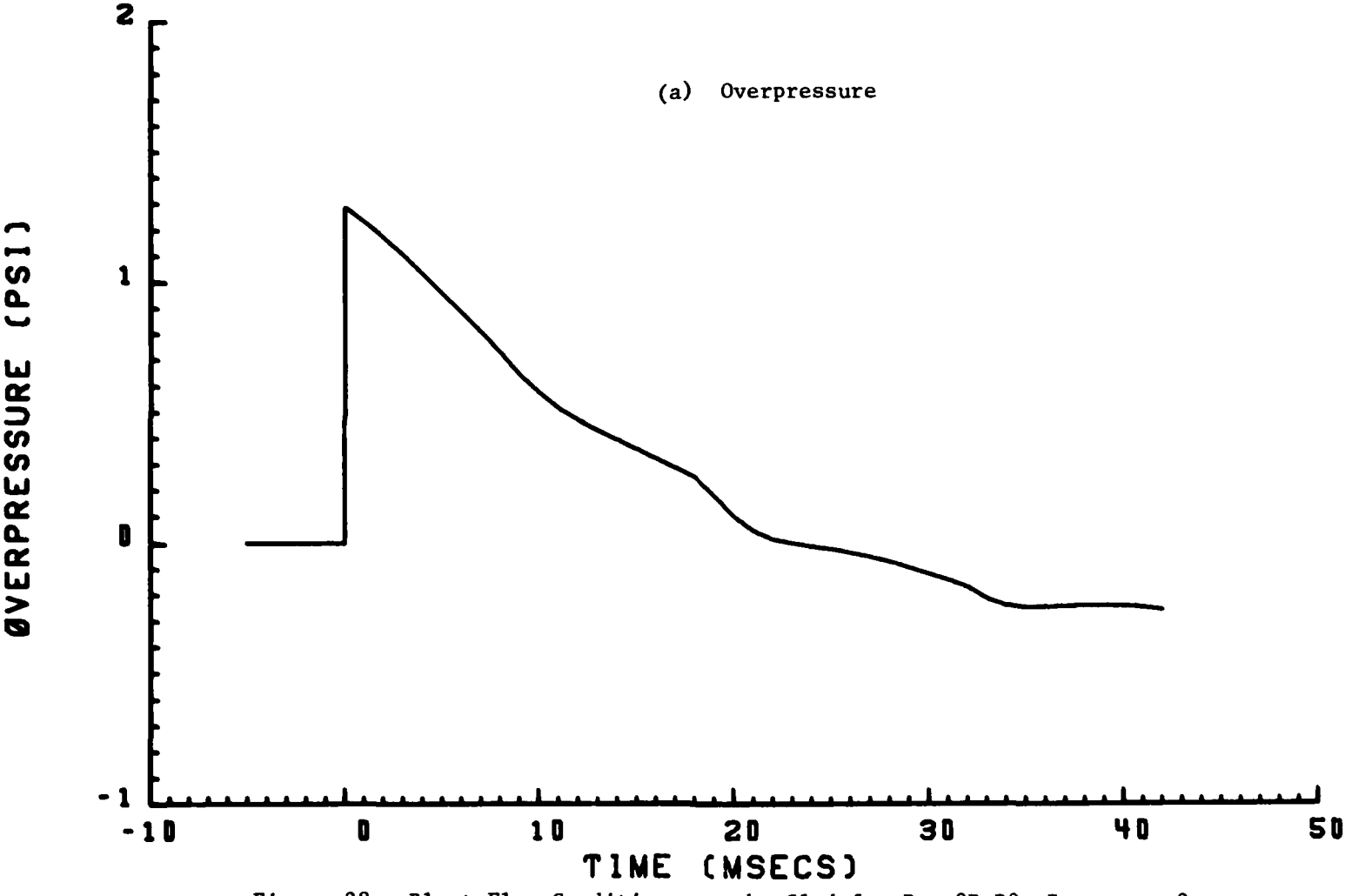

Figure 28. Blast Flow Conditions at the Sled for Run 9B-B2, Intercept 2

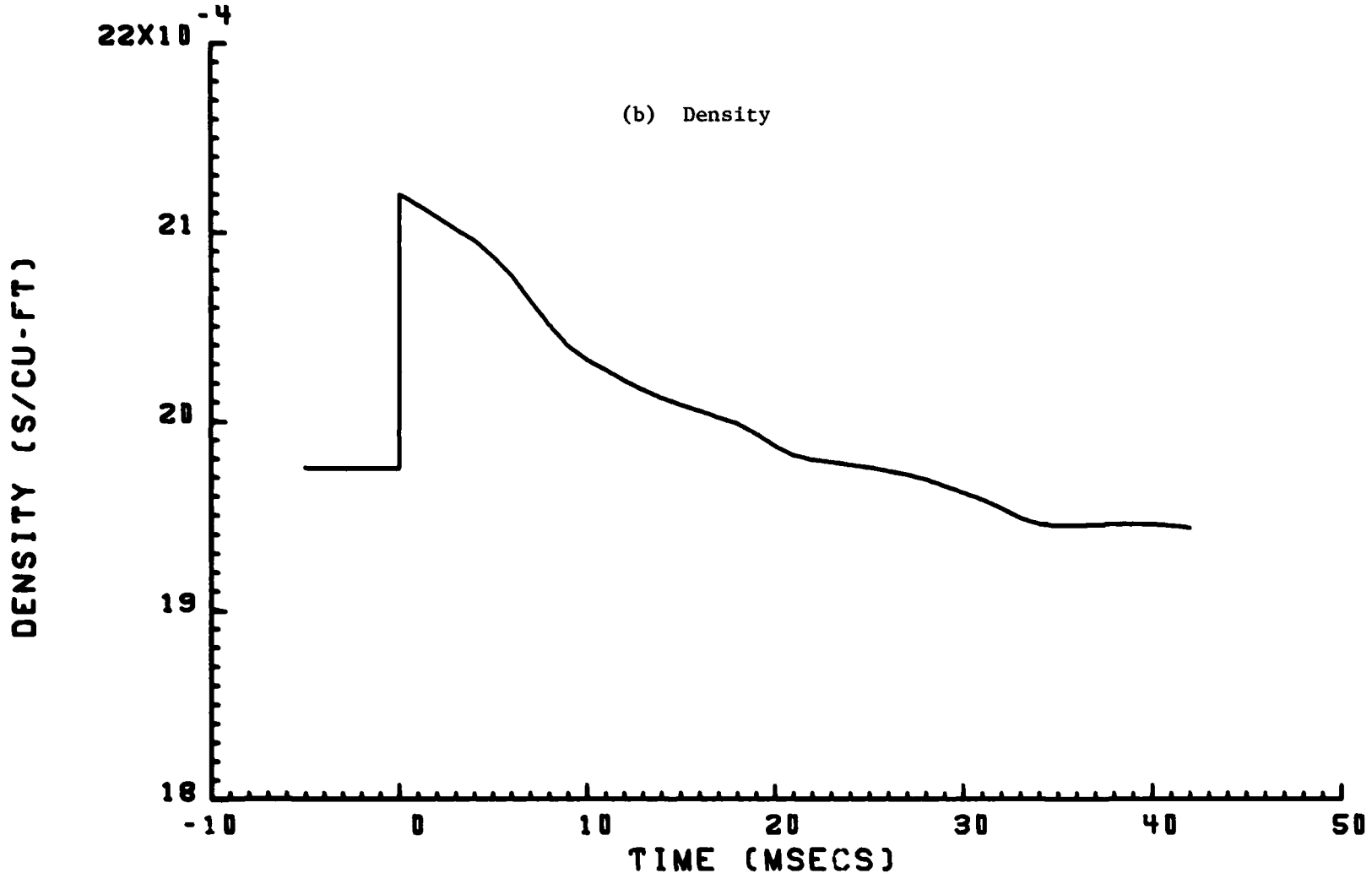

(b) Density

Figure 28. (Continued)

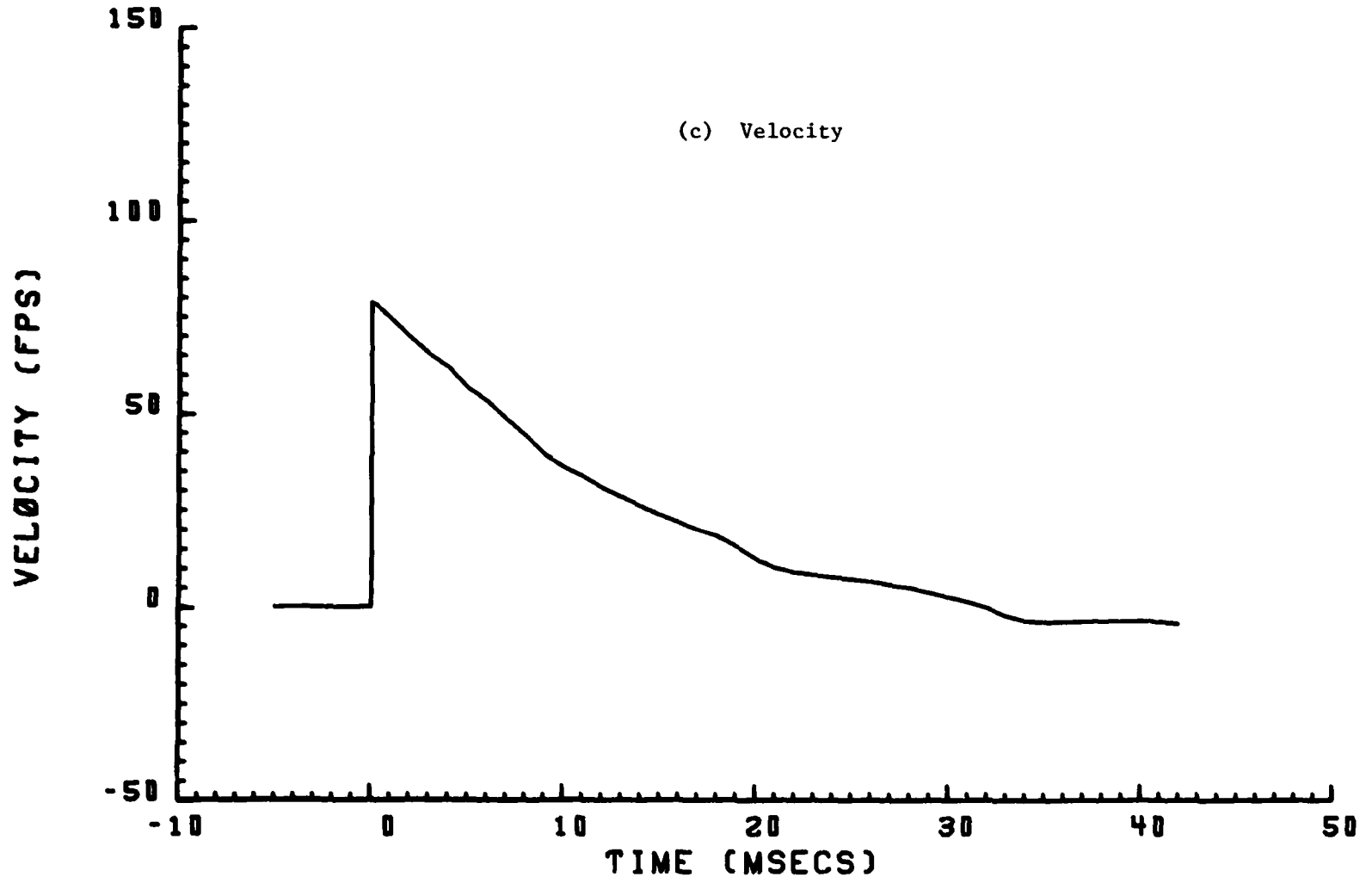

Figure 28. (Concluded)

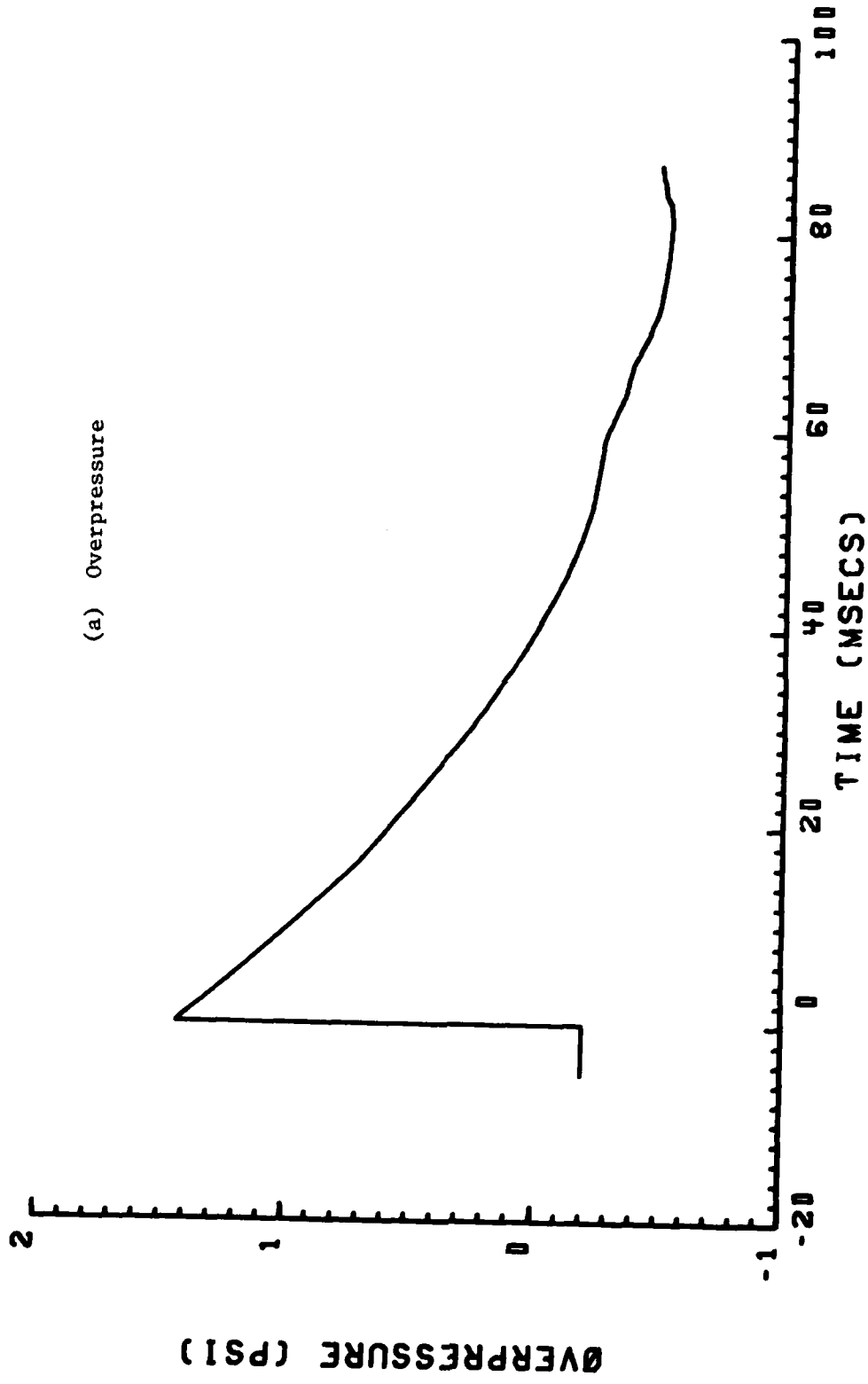

Figure 29. Blast Flow Conditions at the Sled for Run 9B-B2, Intercept 3

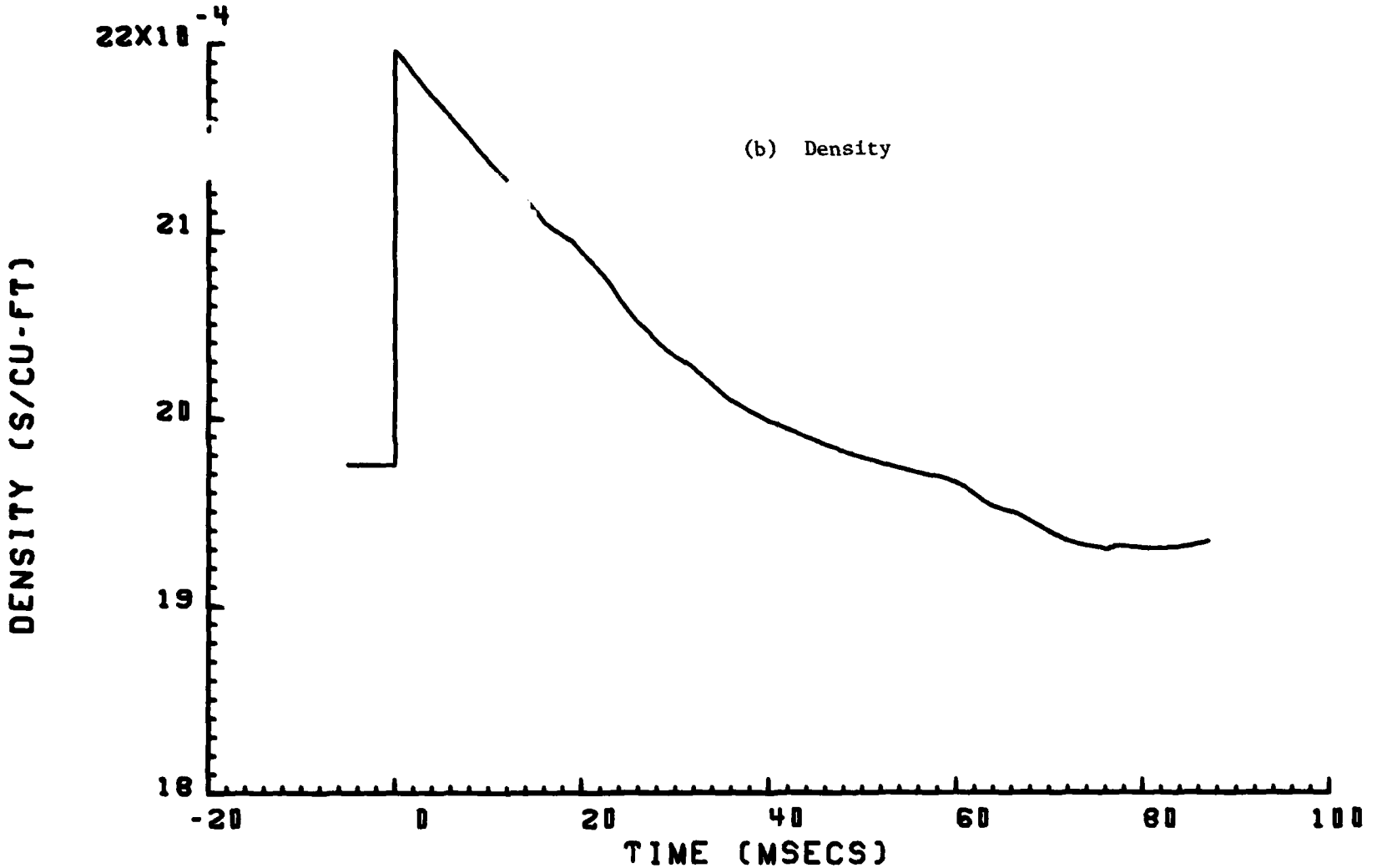

(b) Density

Figure 29. (Continued)

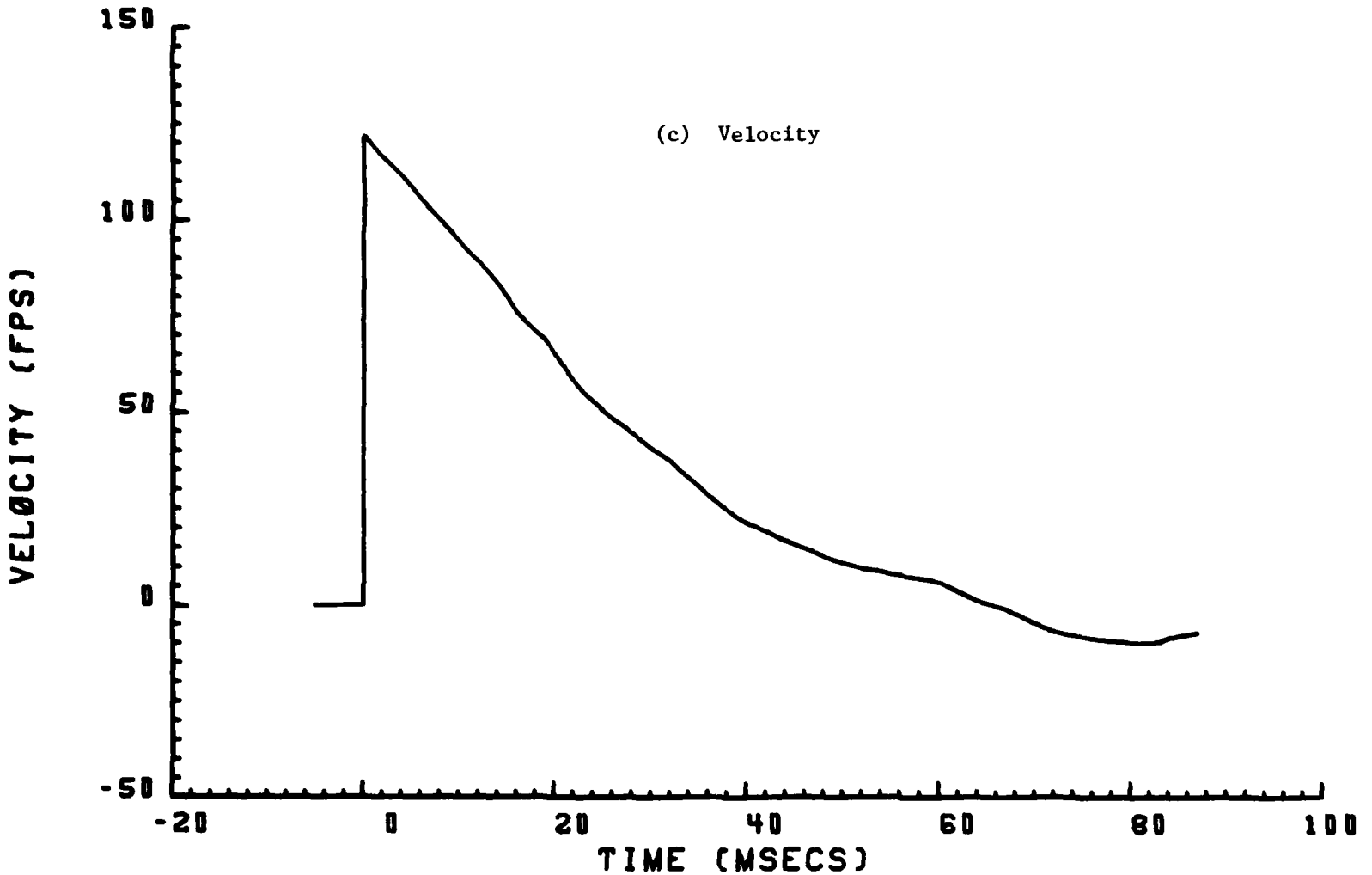

Figure 29. (Concluded)

$t_{\Delta p+}$ is the positive duration time of the overpressure, as determined theoretically from Brode's analysis (Figure 36 of Reference 9).

$t(\Delta t/t_{\Delta p+})$ is the experimental variation of $\Delta p/\Delta p_s$ with $\Delta t/t_{\Delta p+}$ as obtained from a blast-line transducer, after fairing out some obvious interference pulses and noise.

The shock overpressure corresponding to any position of the sled was interpolated or extrapolated from the corresponding blast-line transducer value with the equation

$$\Delta p_s(r_r) = \Delta p_s(r_b)\ [\Delta p_s(r_r)^*/\Delta p_s(r_b)^*] \qquad (5\text{-}2)$$

where

r_b designates the radius from the burst point to the blast-line transducer.

r_r designates the instantaneous radius from the burst point to the model reference point, as determined from the problem geometry and the experimental sled trajectory.

$\Delta p_s(r)$ designates the shock overpressure at a point at a radial distance r from the burst.

$\Delta p_s(r_b)$ is the experimental shock overpressure at the blast-line transducer

and the *'s designate theoretical values as obtained from Brode's theory (Reference 9, using the curves presented in Reference 8).

Using the above equations, overpressure time histories at the sled were calculated for each intercept for all of the blast line transducers for which useful data were obtained. Then all time histories obtained for each intercept were averaged to obtain a best estimate of the true time history for that intercept. The following weighted average equation was used for this purpose.

$$p = \frac{w_1 p_1 + w_2 p_2 + \ldots + w_n p_n}{w_1 + w_2 + \ldots + w_n} \qquad (5\text{-}3)$$

where

p is the weighted average pressure at any time

p_i is the pressure estimate from the i-th transducer

n is the number of transducers

w_i is a weighting factor given by

$$w = \exp\left[-20\left(\Delta p^*_{s,\ \text{sled}} / \Delta p^*_{s,\ \text{blast line}} - 1\right)^2\right] \qquad (5\text{-}4)$$

The factor w gives maximum weight to transducers located at the same radial distance from the blast as the sled. The particular expression for w given above, while somewhat arbitrary, was considered satisfactory since for the data in Reference 1 several other choices of weighting factors gave about the same end results.

As an exception to the above procedure no weight was given to the right hand blast line probe #5 used for intercept 2 in Runs 9B-B1 and 9B-B2. For unknown reasons this probe gave positive blast overpressure durations, after correctings for interference effects, much shorter than for the other blast line and sledborne transducers, about 12 milliseconds for probe #7 compared to 18 to 31 milliseconds for the other probes.

The time histories of the blast overpressures at the sled obtained by the above procedure for all intercepts are shown in the first parts of Figures 25 to 29. These time histories cover the time period from initial shock arrival up to the time of second shock arrival.

The corresponding time histories of blast density and velocity, obtained as described in Appendix B of Reference 1, are also presented in Figures 25 to 29.

SECTION 6
DISCUSSION

6-1 STATIONARY-SLED BLAST TEST, RUN 9B-C1.

Run 9B-C1 was performed with the sled stationary at intercept station No. 2. The test item reference point was positioned at Track Station 13180. A 1000-lb TNT charge was fired normal to the track at the intercept point for a nominal 2-psi intercept at 90 degrees. The objective of the test was to provide data for further validation of the simulation capability of the test method, by testing with sled motion effects eliminated.

6-1.1 Blast-Line Measurements.

The blast-line probe mounts were located at Track Stations 13171.9, 13187.9, 13202.7 and 13225.7. The blast-line overpressure records are shown in Figure 34.* An air leak in the probe mounts was discovered after the tests exposing the reference pressure of the pressure transducers to the blast pressure after several seconds. The way this occurred was that the rear side of each blast-line pressure transducer is connected by a port in the transducer to a reference pressure. The passage inside of the pipes of the probe mounts provided the reference chamber in the tests. The passage is essentially sealed in operation so that it remains at the atmospheric pressure during a test. The leak was discovered at the connection between the horizontal arm and the vertical support post, and its effect was to cause the sensed blast overpressure to drop rapidly beginning about 3 ms after blast arrival. The effect is apparent on the records for blast-line probes No. 5, 6 and 8. The record for probe No. 7 does not show the leak effect and is assumed to have been fairly well sealed.

The shock overpressures measured at the probes, which of course are unaffected by the leak, have been scaled to determine the shock overpressure at the test item by use of Goodman's empirical curve

*Figures numbered 34 and higher are located in the Appendix.

(Reference 7). The shock overpressure of 1.98 psi determined for the test item, given in Table 6, is the average from the four probes; the spread was $\pm$0.1 psi.

The interference effects in the blast wave as measured at the blast-lines probes can be seen in the record for probe No. 7, Figure 34. There is a small, short "blip" with a peak at 0.185 s, about 11 ms after shock arrival, attributed to the reflection of the blast wave from the rail on the blast (west) side of the track. About 11 ms later there is a similar reflection blip associated with the reflection from the exposed portion of the leeside (east) pedestal and rail of the track. These two reflected waves appear to be relatively weak, and they are accounted for in the interference wave corrections applied to the blast-line data for normal sled runs. The interference waves appearing in the record from probe No. 8 are similar.

The records from probes No. 5 and 6 show a somewhat different interference wave pattern due to the reflection of the blast wave from the parked sled and test item. The first interference wave showing up on these two records is the reflected wave from the blast-side rail that peaks in pressure at about 0.185 s, nearly 11 ms after blast arrival. This interference wave is followed by the interference produced by the sled, particularly the undercarriage, and the test item. The quantitative effect of this interference is not readily determinable because of the mount leak in the two probes. The interference of the sled and mount appears to be somewhat greater for probe No. 5 than No. 6 which would be explained by the closer proximity of the large strut base beneath the sled deck. The interference wave reflected from the sled and test item back to the probes would have a somewhat different waveform in a normal test because of the sled motion. This interference is partially corrected in the determination of the properties of the blast wave for normal sled runs in that the rapid interference oscillations are faired out. The effect is further reduced by the averaging of all the probe measurements in the determination. The residual error in the determination would affect only the later pressure history, after the overpressure has fallen to less than one half of the peak value.

The probe records show that the second blast shock arrived at the blast-line probes between 0.221 and 0.223 s, which is well after the period of primary interest.

6-1.2 Sled-Borne Measurements.

The static overpressures measured at the sled are shown in Figures 39 and 40. The shock overpressure measured by the left (blastward) transducer, corrected for decay rate, is 2.20 psi at the test item, and by the right (leeward) transducer is 1.95 psi at the test item, compared with 1.98 psi determined by the blast-line probes, or a spread of about ± 5 percent.

The sled static pressure records show a reflected wave from the test item and support, peaking at 6 to 7 ms after blast wave arrival. The reflected wave has the characteristic N-wave signature of wings and similar bodies. The positive overpressure duration from the left probe is about 26 ms, in agreement with the measurement of blast-line probe No. 7. There is no other significant interference indicated in the measurement of the left sled static pressure probe. The right probe shows some oscillation beginning at about 0.196 s which remains unexplained.

The pitot probe mounted on the sled deck is not a useful measurement of total pressure for the sled at rest with a side-on blast because of the direction of flow. The record, Figure 38, does show the reflected wave from the test item and support which arrives at the probe about 7 ms after blast arrival. It does provide a valid measurement of the duration of positive overpressure which is about 35 ms, or about one-third longer than the 27 ms measured by the sled static-pressure transducers.

The total-pressure signal, Figure 37, from the model nose exhibits some drift prior to blast arrival. There are essentially no apparent interference waves evident in this record.

The record for the strain gage mounted on the sting is shown in Figure 41. It exhibits the predominant 26.65-Hz mode comprising

sting and strut bending coupled with lateral bending of the sled longerons and the 53.5-Hz mode of sting bending and lateral wing motion.

The wing acceleration record shown in Figure 42 is from the accelerometer located near the upper wing tip. The wing loading for the sled at rest is essentially impulsive from the shock diffractive loading having the duration indicated by the width of the -16-g spike. The wing acceleration, except for one 12-g spike, remains mostly within $\pm$6 g's. The sled and support modes are in the range of the predominant modal period of about 50 ms. The higher frequencies of about 125 and 250 Hz are wing modes which are beyond the range of interest.

6-1.3 Test-Item Measurements.

The differential pressures measured at the wing of the test item, Figure 35, have a spike at blast arrival followed by a relatively low level of pressure. The spike results from the shock reflection and diffraction around the wing. The dynamic pressure at the test item for the sled at rest is small in comparison with the shock overpressure, so the differential pressure following the shock diffraction period is relatively small.

The differential pressure during the shock diffraction period would be essentially flat-topped for most locations on the wing until the diffractive waves from the fuselage and wing edges arrive. However the 4-kHz response of the recording system tends to round off the record for the diffraction period because of the signal rise time. Records for locations well away from the fuselage and the wing edges would be expected to rise to the overpressure of the flat top however before the diffractive waves arrive. The peak pressure differentials measured during the shock diffraction period, nominally one millisecond in duration, are presented in Figure 30. For comparison the theoretical value of 4.22 psi for normal reflection of the 1.98 psi incident shock is presented. The peak differentials for the 7 1/2 and 10-percent chord locations are low because of the response time discussed above. Along the 25 percent-semispan chordline they tend to be high because of the fuselage reinforcement of the wave. Between 22 1/2 and 62 1/2 percent of chord for

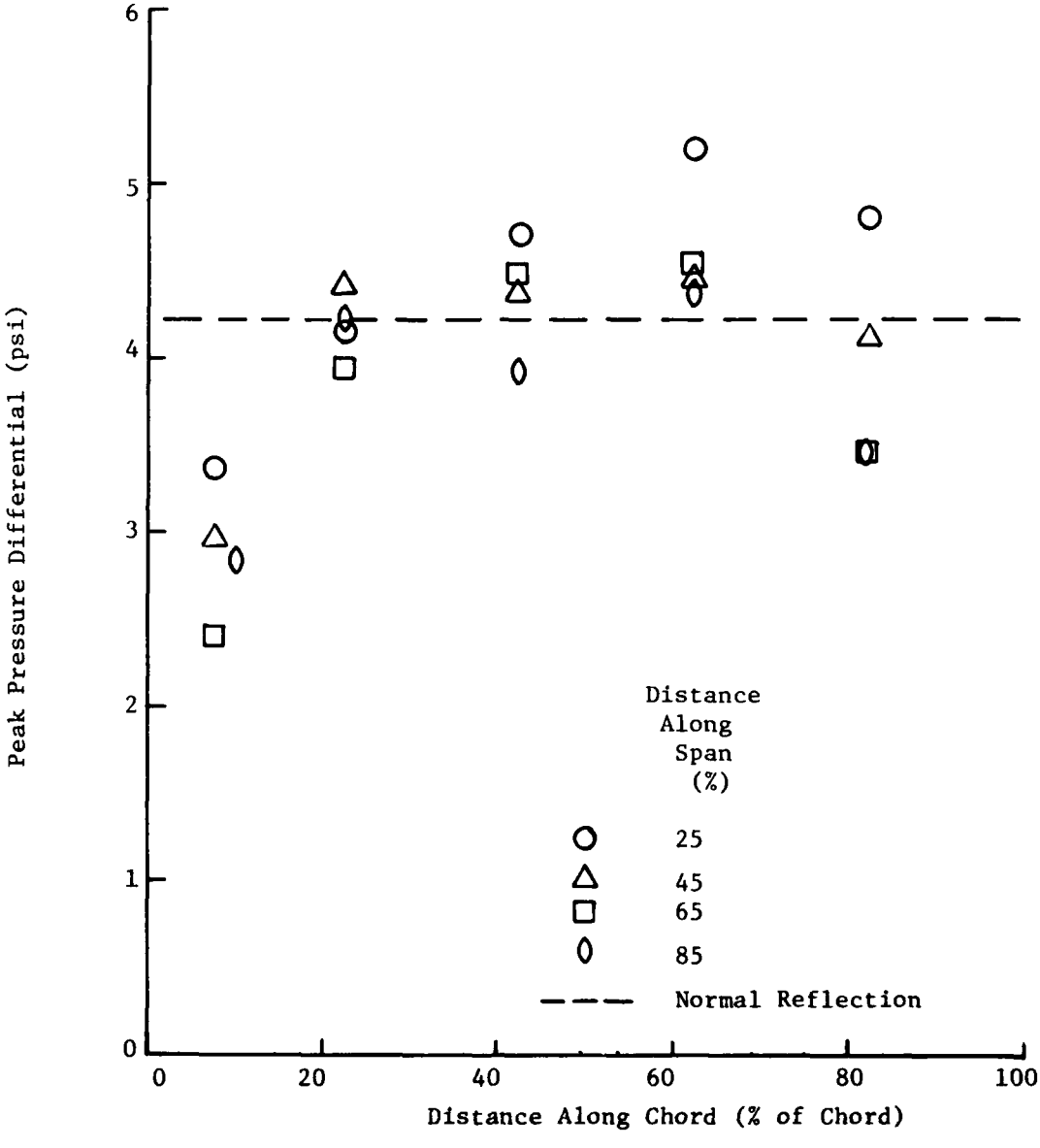

Figure 30. Peak Pressure Differential at the Wing Location Following Blast Arrival for the Stationary Sled Test

the remaining chordlines the peaks all fall within $\pm$0.3 psi or $\pm$7 percent of the theoretical value, which is reasonably good agreement for the 4-kHz system response.

The wing differential-pressure records show no significant indication of interference waves. The strength of the waves reflected from the strut and sting would be comparatively small at the location of the wing. Sled motion in a typical run would reduce this small interference even further. The undercarriage and strut support would produce a sizeable interference wave for the sled at rest except that the sled deck serves to shield the test item from these reflections. It is concluded from this test that there are no significant indications of interference waves reaching the test item from the sled, the support structure or the track. These interferences were a principal problem in the blast tests conducted at Edwards AFB during 1961 to 1963, Reference 10, and the results here indicated that they have been removed by the present test method.

A point of interest, but of no importance to this test, is the indication of vortex formation on the wing in this test. A typical record showing this effect is presented in Figure 35 for Station 85/62.5, where the vortex effect shows up as a slow oscillation.

This vortex effect appears principally in the records of transducers located near the wing edges, where the vortices form. The only importance of this effect to this test is for identification of the effect the vortices produce on the observed signal.

6-2 HIGH-SPEED TESTS, RUNS 9B-B1 AND 9B-B2.

The general features of the transient wing loadings obtained in the intercepts of Runs 9B-B1 and 9B-B2 are illustrated in the selected records shown in Figures 31 and 32. Two records have been selected from each run; an outboard record from Station 85/22.5 (85-percent semispan and 22.5-percent chord from leading edge) and an inboard record from Station 25/42.5.

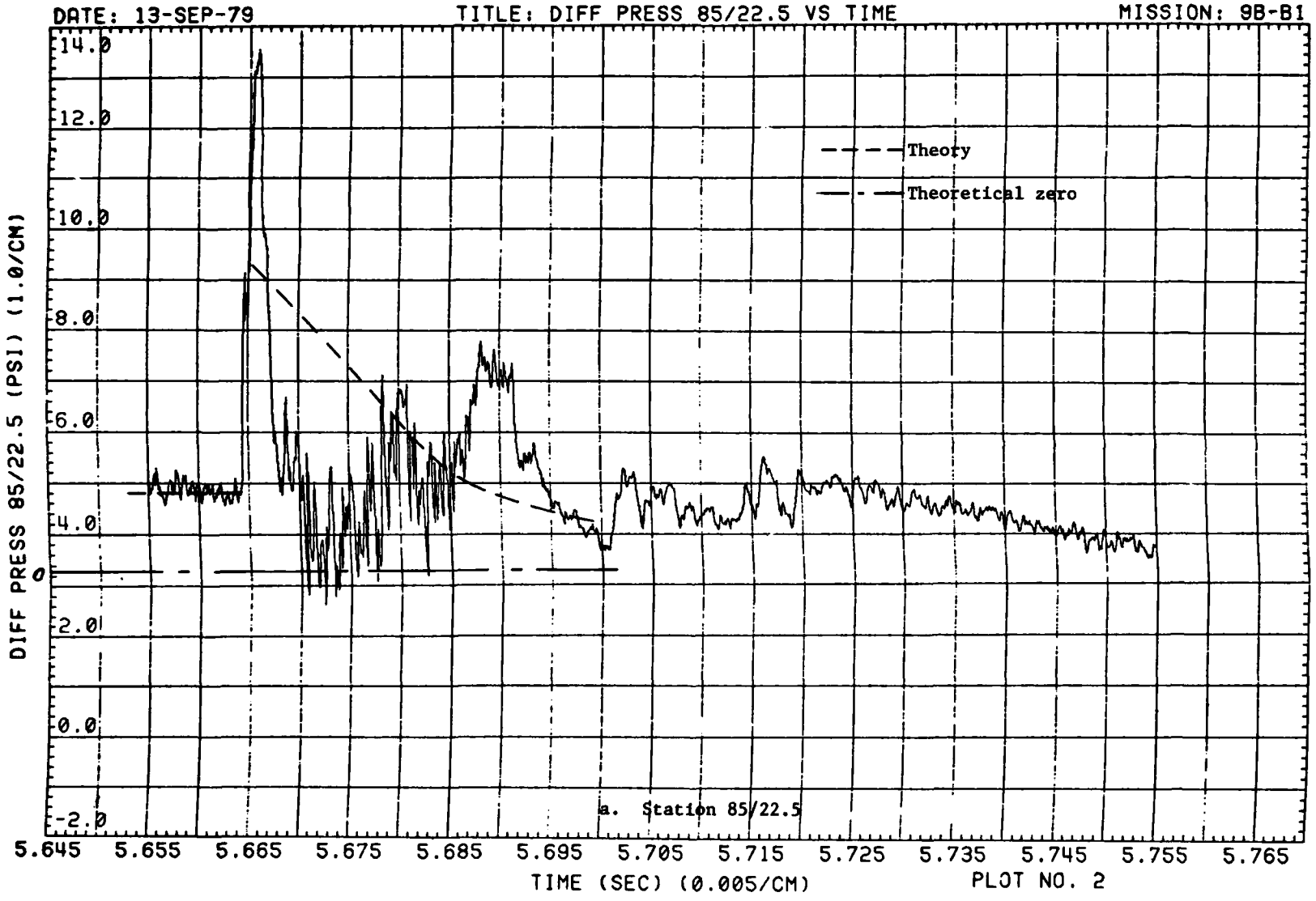

Figure 31. Differential Wing Pressure, Run 9B-B1, Intercept 2, 90-deg Intercept (nom), 2-psi Shock Overpressure (nom).

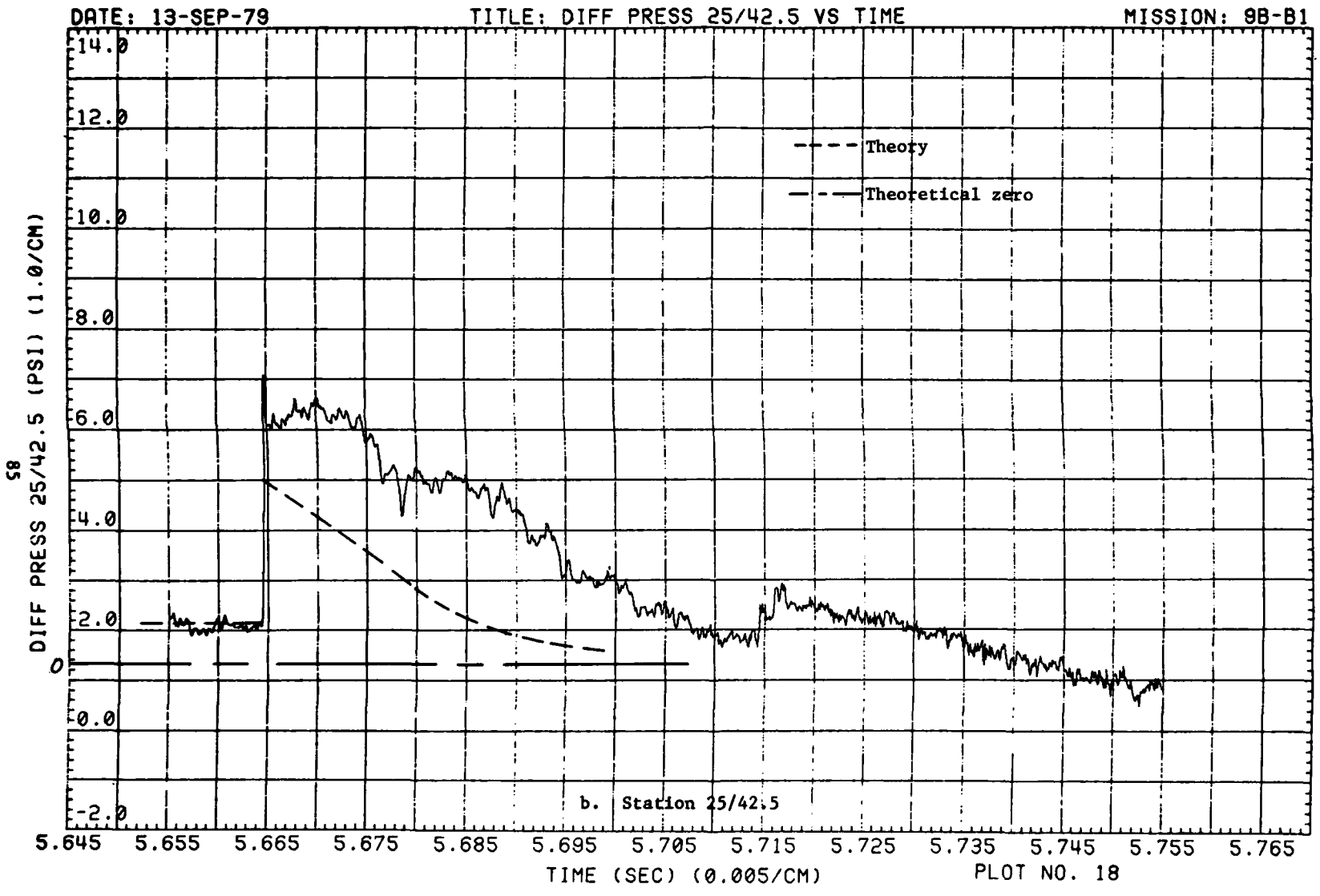

Figure 31. (Concluded)

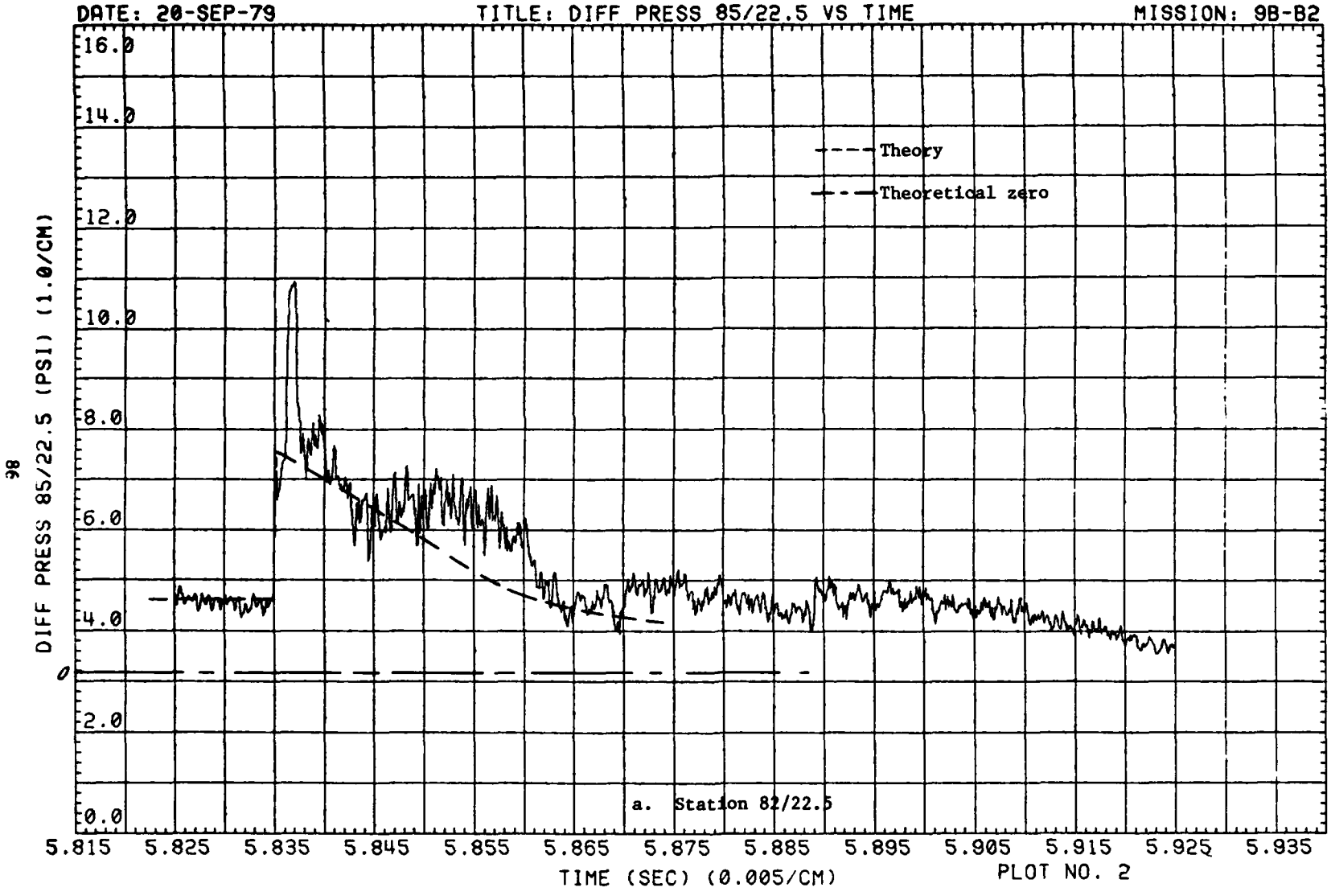

Figure 32. Diffcrential Wing Pressure Run 9B-B2, Intercept 2
90-deg Intercept (nom), 1.3-psi Shock Overpressure (nom).

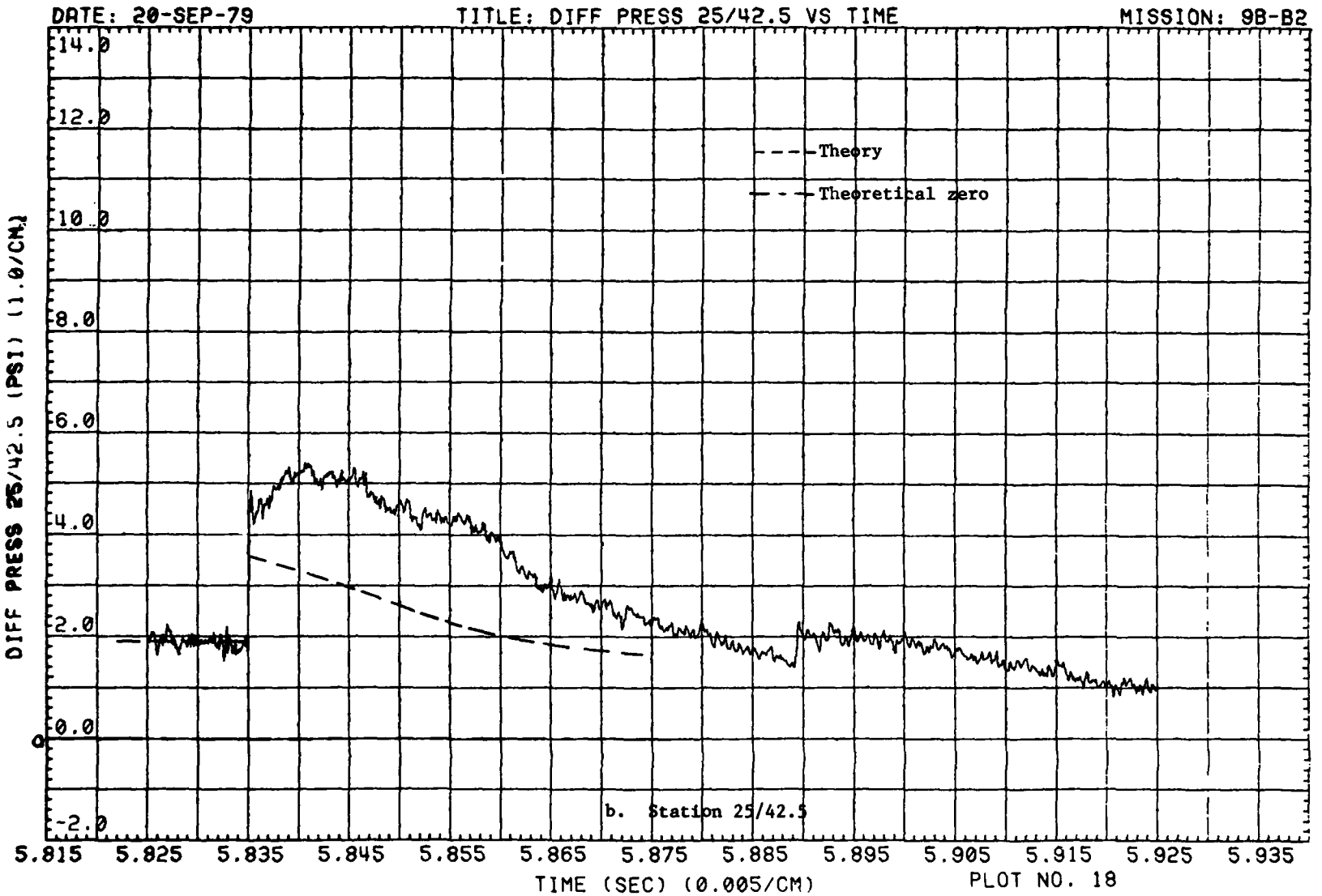

Figure 32. (Concluded)

Also shown as dashed lines on each graph, for comparison, is the quasi-steady pressure differential based on linear theory. This was computed from

$$\delta p = \frac{2\, C_{L_\alpha}\, \bar{c}}{\pi\, c} \left(\frac{c_{L_\alpha}\, c}{C_{L_\alpha}\, \bar{c}} \right) \left(\frac{c-x}{x} \right)^{1/2} q(t) \sin \alpha(t) \qquad (6\text{-}1)$$

where

δp = local pressure differential

c = local chord

x = distance along chord

C_{L_α} = lift curve slope, Reference 11

c = chord

$\bar{c}$ = average chord

$\frac{c_{L_\alpha} c}{C_{L_\alpha} \bar{c}}$ = spanwise loading coefficient, Reference 12

q = instantaneous free-stream dynamic pressure

α = instantaneous angle of attack

The lift curve slope C_{L_α} was determined from the linearized Equation 7-52, page 95, of Reference 11 accounting for Mach number by the Prandtl-Glanert transformation. The spanwise variation $\left(\frac{c_{L_\alpha} c}{C_{L_\alpha} \bar{c}} \right)$ was obtained from the linearized theory result of Reference 12. The chordwise variation $\left(\frac{c-x}{c} \right)^{1/2}$ is from thin airfoil theory. The result is presented in the figure as the quasi-steady linear-theory pressure differential. The purpose of presenting it is to provide a preliminary indication of the trends of the test results.

The measured pressure differentials had an offset from zero due to the preset initial angle of attack of 3.2 degrees and to some drift in the pressure transducer signal principally from aerodynamic heating. The linear-theory curve has been displaced accordingly to match the preintercept measured trace. From this reference level the zero pressure differential level is also indicated based on the linear theory and preset angle of attack.

The test results discussed here were for blast intercepts about 90 degrees from head-on, relative to the direction of travel. The blast shock overpressure for Intercept 2 of Run 9B-B1, Figure 31, was 2.12 psi, and for Intercept 2 of Run 9B-B2, Figure 32, was 1.28 psi. The quasi-steady linear-theory curves were drawn for the nominal shock overpressures of 2.0 and 1.3 psi respectively.

The measured pressure differential in Figure 31 for the 2.12 psi shock overpressure jumps at blast arrival (5.664 sec) to an indicated value of about 8.6 psi due to shock reflection. One millisecond later it jumps further which is attributed to the leading-edge vortex passing over the leeward transducer. The indicated pressure differential reaches 13.5 psi on the scale and then rapidly falls off as the vortex sweeps downstream and separated flow arrives upstream of the vortex. The differential pressure then drops essentially to zero (3.3 psi on the scale).

Meanwhile, the free-field blast flow at the test item decays slowly as indicated by the decrease in the quasi-steady linear-theory differential. The blast-induced angle of attack decreases nearly with the quasi-steady differential. While the angle of attack decreases the measured pressure differential in Figure 31a starts to increase at about 5.67 seconds. The differential pressure reaches a level at about 5.69 seconds nearly equal to the peak quasi-steady value at blast arrival, and this occurs after the angle of attack has decreased below the pre-intercept value. This second peak has been attributed to the return of the leading-edge vortex back toward the leading edge of the wing.

Figure 31b presents the Run 9B-B1 record for Station 25/42.5. Here the nonlinear effects are apparent in another way. The level of the measured pressure differential after blast intercept is nearly double the quasi-steady linear-theory value. By the time that the blast-induced angle of attack returns to the pre-blast value (5.687 seconds), the pressure differential has only decreased by about one third. The measured pressure differential reaches the pre-blast value about 20 ms later.

From this examination of these two records, as well as the other records for this intercept, it is concluded that the airloads are apparently quite nonlinear even for the 1.98 psi shock overpressure. The test was at Mach 0.76. The nonlinear effects would be expected to be more severe at a lower Mach number for the same shock overpressure because the blast-induced angle of attack would be greater. Or, inversely, the same nonlinear effects would be expected to occur at a lower Mach number for a lower shock overpressure.

The comparison needs to be made with predictions of transient linearized theory, such as given by the VIBRA-6 code. But previous comparisons for a 65-deg wing planform, Reference 1, indicate that the tentative conclusions reached here probably would not be changed significantly in a qualitative sense. High-speed cine-photographs taken of the tufts on the lower wing half also show the presence of the vortex and the separated flow on the lee surface.

The records from Run 9B-B2 with the shock overpressure of 1.28 psi are shown in Figure 32 for the same locations on the wing. At Station 85/22.5 the leading-edge vortex still appears (5.837 s) but the measured differential generally agrees better with the quasi-steady linearized-theory curve. At 5.855 s it differs by about one half of the shock jump, but some of that difference may be due to the use of quasi-steady theory instead of transient theory; that remains to be resolved.

The record for the inboard station, Figure 32b, shows that the nonlinear effect there appears to be still marked. Again, comparison with transient linearized theory must be made before an assessment can be made of nonlinear effects, but the results are expected to be qualitatively similar.

To get a preliminary estimate of the possible error in linear theory with respect to loading of the wing, the section normal force has been computed at the four chordwise sections along the semispan where pressure differentials had been measured (5 points per section).

This has been done for the 1.98 psi intercept shown in Figure 31 for the time 10 ms after blast intercept. The results are presented in Figure 33 where a curve has been faired through the four test points to give a spanwise distribution. The comparison shows that the measured section normal force is much lower outboard then given by the quasi-steady linear theory and higher at the 45-percent semispan station.

The normal force and bending moment for the measured and linear-theory distributions have been computed. The ratio of the measured values to the linear-theory values is presented in Table 8. The ratio for the normal force for the full semispan is 0.88 and for the part outboard of the 30 percent-semispan station is 0.83. So the measured normal forces at 10 ms are within 12 and 17 percent respectively of the quasi-steady linear-theory value. The ratio of the moments is 0.72 for the moment at the wing centerline and 0.52 for the 30 percent-semispan station. This means the measured applied moment is 28 and 48 percent less than given by the quasi-steady linear-theory. It must be recognized that this comparison is for only one time and that the wing acts as an integrator. It is presented to illustrate the potential significance of nonlinear airloads on a structure.

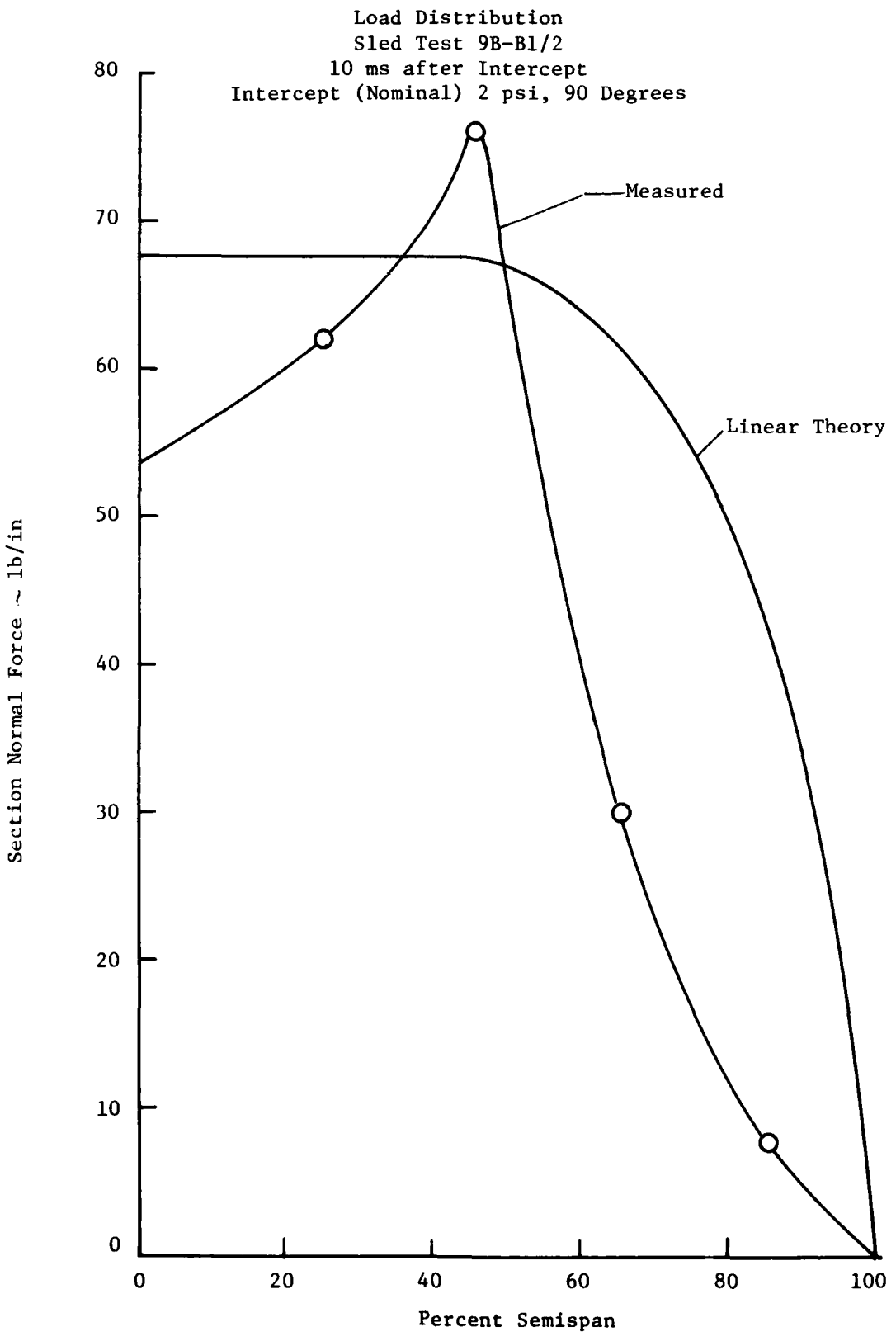

Figure 33. Comparison of Section - Normal Force Distributions from Test Data and Quasi-Steady Linear Theory

TABLE 8

COMPARISON OF MEASURED LOAD AND MOMENT

WITH QUASI-STEADY LINEAR THEORY

AT 10 MILLISECOND AFTER INTERCEPT

SLED TEST 9B-B1

INTERCEPT (NOMINAL) 2 PSI, 90 DEGREES

Wing Station	$\frac{\text{Measured Load}^*}{\text{Linearized Load}}$	$\frac{\text{Measured Moment}^{**}}{\text{Linearized Moment}}$
Centerline	0.88	0.72
30% Semispan	0.83	0.52

*Normal force

**Applied bending moment about wing streamwise station.

AD-A093 729 KAMAN AVIDYNE BURLINGTON MA F/G 20/4
MEASUREMENTS OF BLAST PRESSURES ON A RIGID 35 DEG SWEPTBACK WIN--ETC(U)
JAN 80 D A KLEPPIN, J R RUETENIK, R F SMILEY DNA001-79-C-0157
UNCLASSIFIED KA-TR-175 DNA-5211F NL

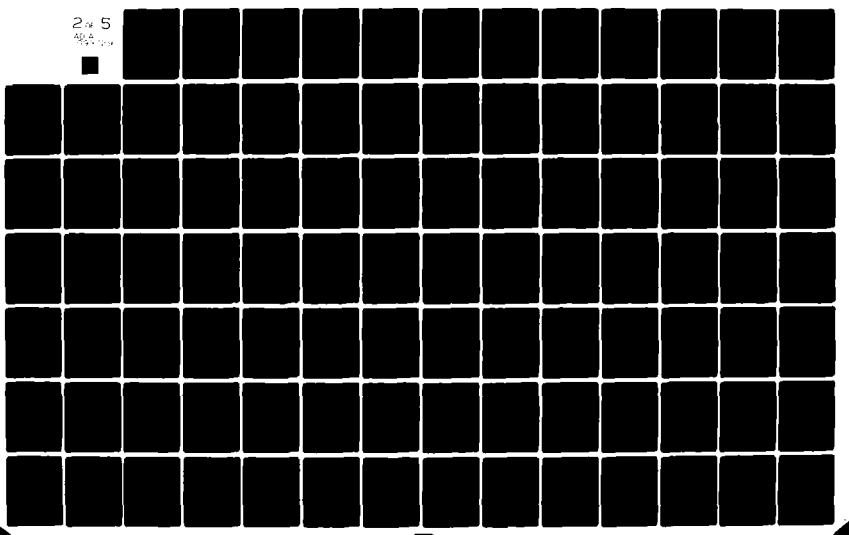

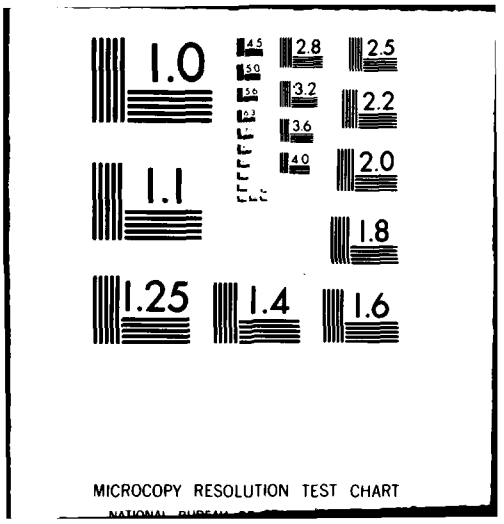
1.0
1.1
1.25
1.4
1.6
1.8
2.0
2.2
2.5
2.8
3.2
3.6
4.0
4.5
5.0
5.6
6.3
MICROCOPY RESOLUTION TEST CHART

SECTION 7
CONCLUDING REMARKS

Blast loadings have been measured on a rigid 35-deg-sweepback wing in three sled runs: one with the sled parked and two at Mach 0.76. Six separate blast intercepts were performed using 1000-lb TNT charges. The nominal intercept overpressures were 1.3, 2 and 4 psi and the nominal intercept angles were 45, 90 and 135 degrees from head-on.

The effect on pressure loading of a vortex formed on the leeward surface following blast intercept at Mach 0.76 was evident at all shock overpressures. High-speed cine-photographs of tufts mounted on the leeward surface verified the presence of a blast-induced vortex and its marked influence on the flow direction at the wing surface.

In this report the test conditions are described and the test data are presented. The data were reduced by the Holloman AFB and independently verified in this work.

It is recommended that similar blast loading tests be conducted with a flexible wing to determine the effects of wing motion upon blast loading. The results from the tests with the rigid and flexible wings are expected to provide a significant data base for validation of methods to be used in prediction of blast airloads on 35-deg-sweepback wings.

REFERENCES

1. Ruetenik, J.R., and Smiley, R.F., Measurements of Blast Pressures on a Rigid 65° Sweptback Wing at Mach 0.76 from Rocket Propelled Sled Tests, Vol. I - Test Documentation, Kaman AviDyne Report TR-137, DNA 4400F-1, 20 June 1977.

2. Ruetenik, J.R., and Smiley, R.F., Measurements of Blast Pressures on a Rigid 65° Sweptback Wing at Mach 0.76 from Rocket Propelled Sled Tests, Phase 2 Test Documentation, Kaman AviDyne Report No. TR-145, DNA 4504F, 24 January 1978.

3. The Holloman Track, Facilities and Capabilities, Test Track Division, 6585th Test Group, AF Special Weapons Center, HAFB, 1974.

4. Engineering Drawings of Wing Construction, Kaman Sciences Corporation Drawings Nos. 710001 Rev. B, and 710002 Rev. B.

5. Valle, Joe, Jr., Test Event Report, Aircraft Blast Interaction Test, Job Order No. 921DST01, 6585 Test Group, Guidance Test Division, Environmental Test Section, HAFB, NM, 20 August 1979.

6. Krupovage, D.J., NASTRAN Code Calculations, HAFB, 3 August 1979, unpublished.

7. Goodman, H.J., Compiled Free-Air Blast Data on Bare Spherical Pentolite, BRL Report 1092, February 1960.

8. Ruetenik, J.R., and Lewis, S.D., Computation of Blast Properties for Spherical TNT or Pentolite from Measured Pressure Histories, AFFDL-TR-66-47, October 1966.

9. Brode, H.J., A Calculation of the Blast Wave from a Spherical Charge of TNT, RAND RM-1965, August 1957.

10. Wolf, I.O., et al., An Experimental Investigation of Blast-Induced Airloads and Response of Lifting Surfaces, AFFDL-TR-64-176, March 1965.

11. High Speed Aerodynamics and Jet Propulsion, Vol. VII, Aerodynamic Components of Aircraft at High Speeds, Princeton University Press, 1957.

12. DeYoung, J., and Harper, C.W., Theoretical Symmetric Span Loading at Subsonic Speeds for Wings Having Arbitrary Planforms, NACA, Report No. 921, 1948.

APPENDIX A
PRESSURE, STRAIN AND ACCELERATION TIME HISTORIES

This appendix presents time histories of all the blast-line and sled-borne transducer measurements obtained during the 9B-C1, 9B-B1 and 9B-B2 sled tests described in this report. The data includes blast-line pressures, differential pressure on the wing, blastward and leeward pressures at station 25/62.5 on the wing, total pressure on the test item nose, total pressure on the sled, sled static pressure, strain in the test item support and wing acceleration. The model instrumentation locations are shown in Figure 12 and Table 3. Table 9 gives the figure numbers for each plot in the appendix.

All of the times shown on the plots (except for 9B-B1 blast-line) are the actual times in seconds. The accompanying date, hour and minute for each test is listed below:

Test	Date	Time
9B-C1	12 Sept. 1979	1246 MDT
9B-B1	13 Sept. 1979	1258 MDT
9B-B2	20 Sept. 1979	1100 MDT

As mentioned in Section 3, the IRIG timing signal was omitted from the 9B-B1 blast-line records. For each of these plots time 0 corresponds to the following:

Blast-line Station	Time ~ seconds
5	5.647
6	5.647
7	5.648
8	5.650
9	6.157
11	6.192
12	6.222

Quasi steady-state predictions were made for three of the intercepts; 9B-B1, Intercepts 2 and 3, and 9B-B2, Intercept 2. A discussion of these analyses is given in Section 6. These predictions have been superimposed on the time histories using dashed lines. The zero reference for the predictions has also been noted.

TABLE 9

INDEX OF TEST DATA

Measurement	Figure Number						
		9B-B1			9B-B2		
	9B-C1[1]	Intercept 1[2]	Intercept 2	Intercept 3	Intercept 1	Intercept 2	Intercept 3
Blast-Line Over-pressure	34	-	43	52	61	70	79
Differential Wing Pressures	35	-	44	53	62	71	80
Blast and Leeward Wing Pressures	36	-	45	54	63	72	81
Total Pressure at Model	37	-	46	55	64	73	82
Total Pressure at Sled	38	-	47	56	65	74	83
Left Side Static Pressure at Sled	39	-	48	57	66	75	84
Right Side Static Pressure at Sled	40	-	49	58	67	76	85
Strain at Model Support	41	-	50	59	68	77	86
Wing Acceleration	42	-	51	60	69	78	87

[1]Sled Stationary at TS 13180

[2]No data - Premature charge detonation

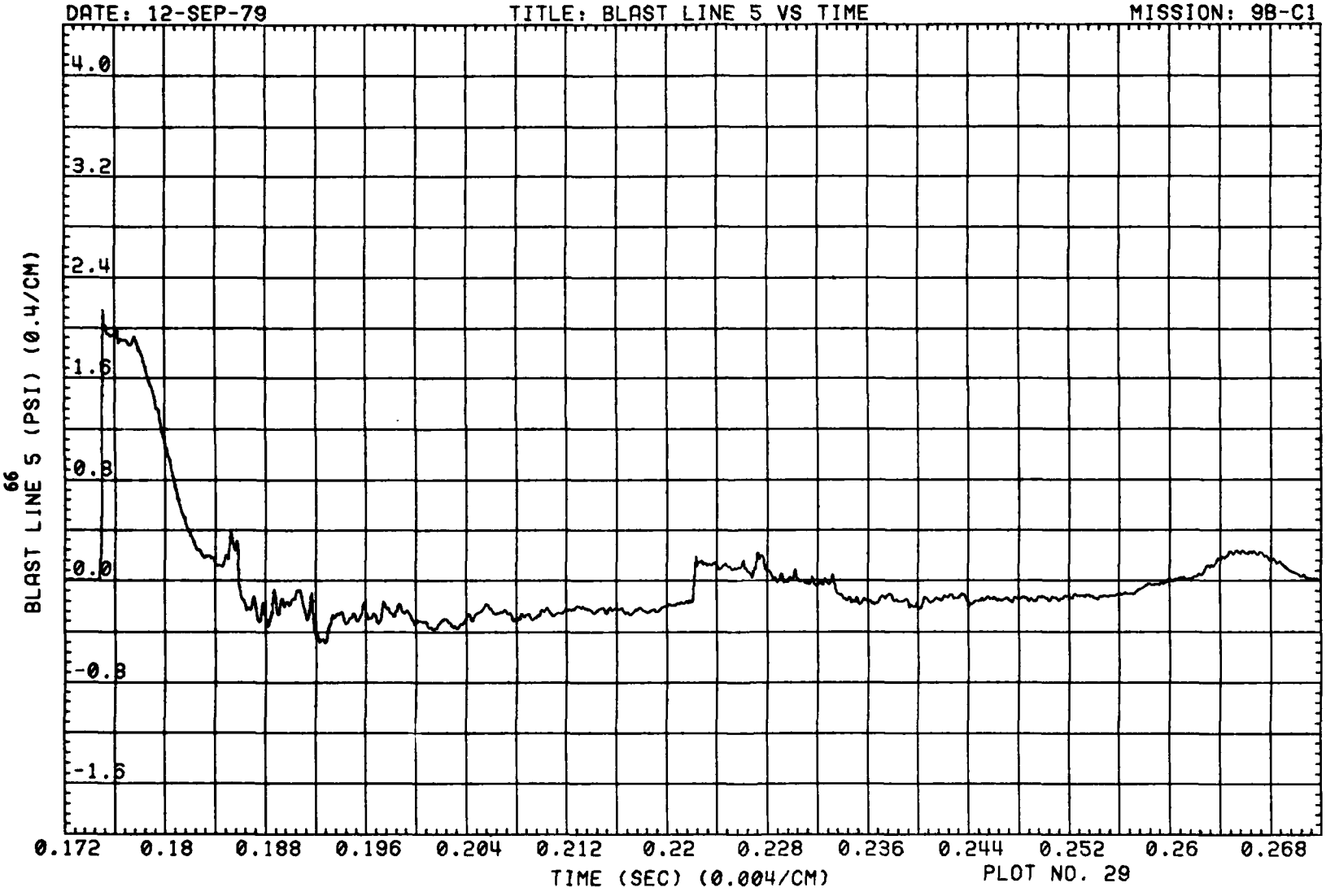

Figure 34. Blast-Line Overpressures, Run 9B-C1, Intercept 2

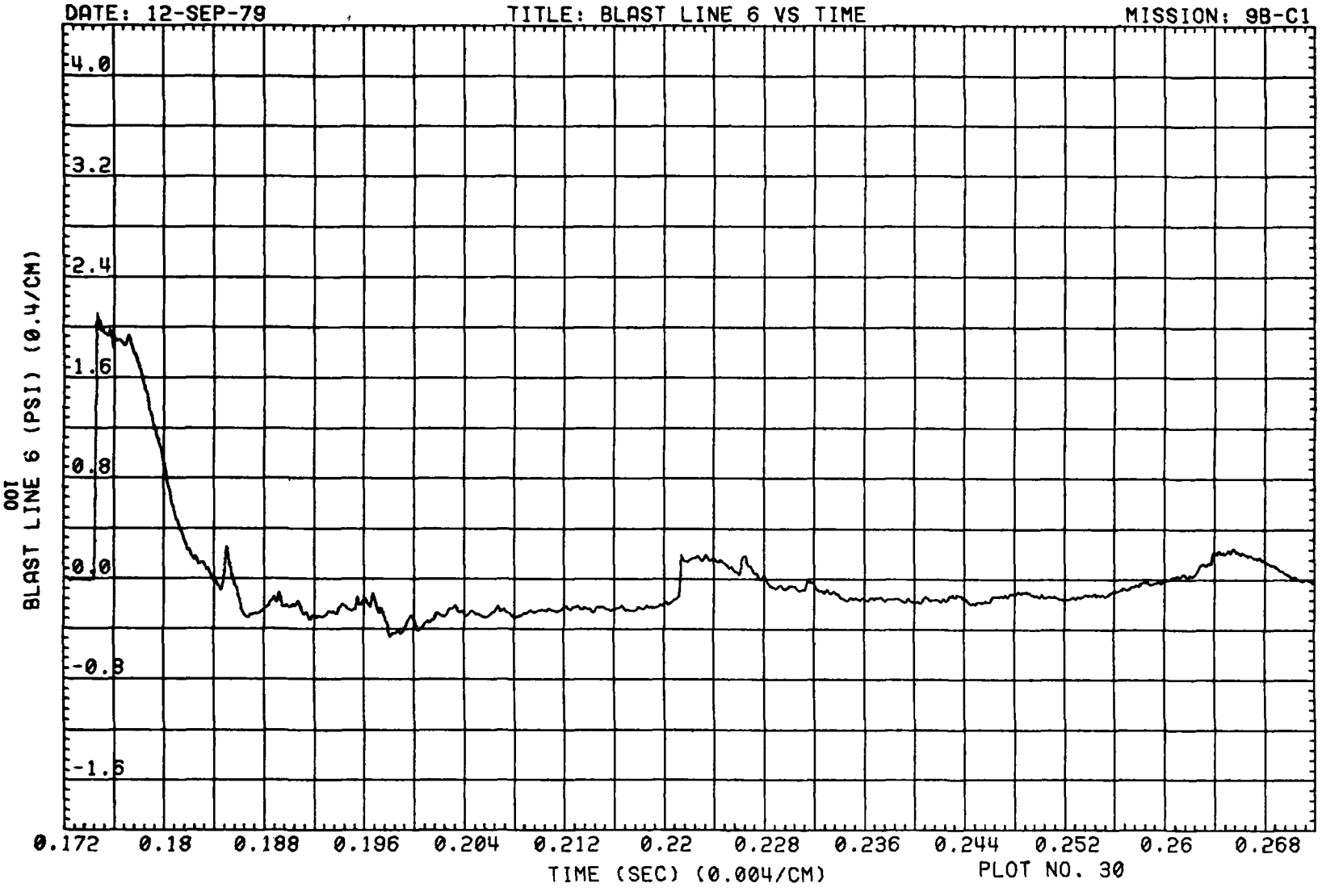

Figure 34. (Contined)

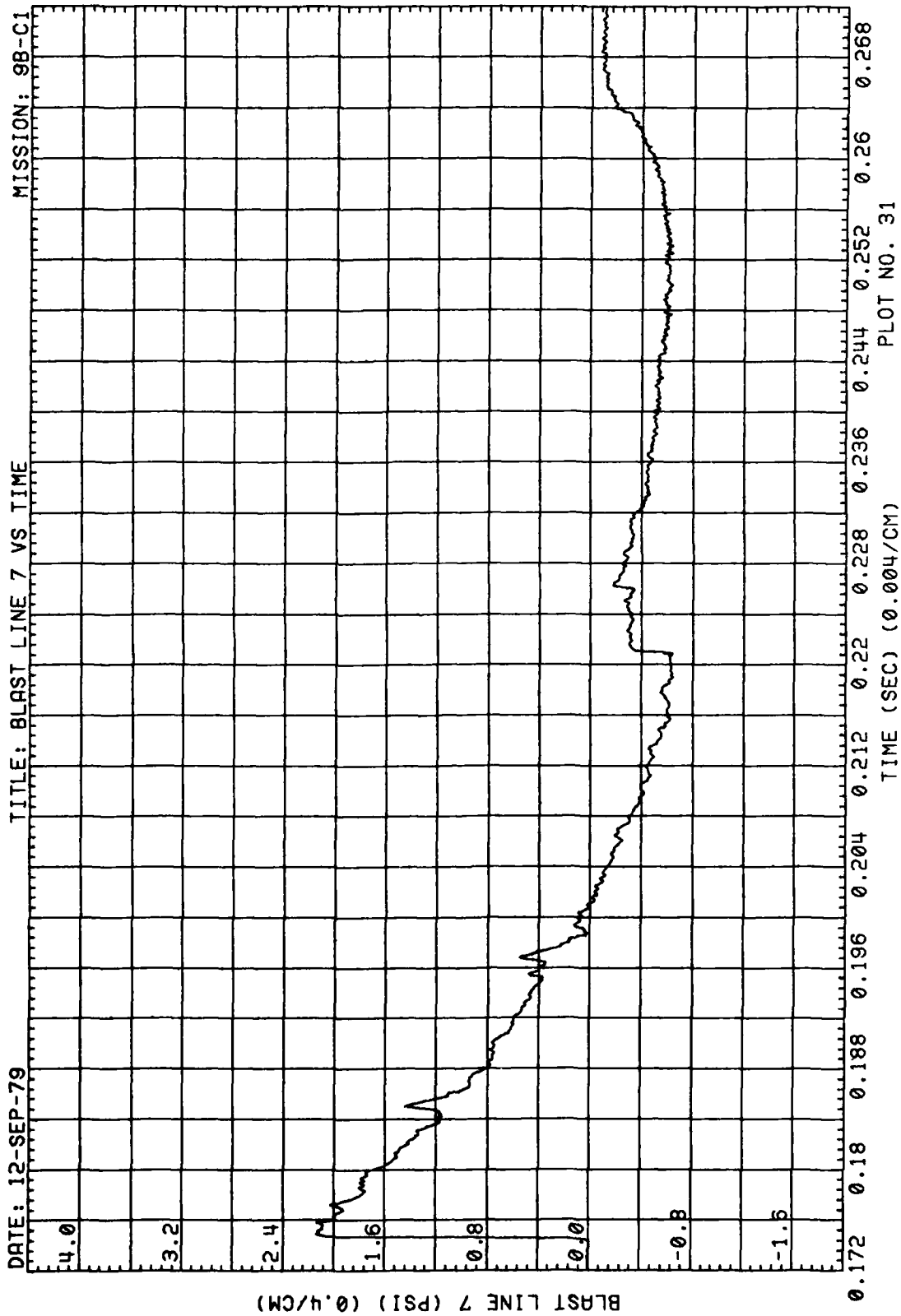

Figure 34. (Continued)

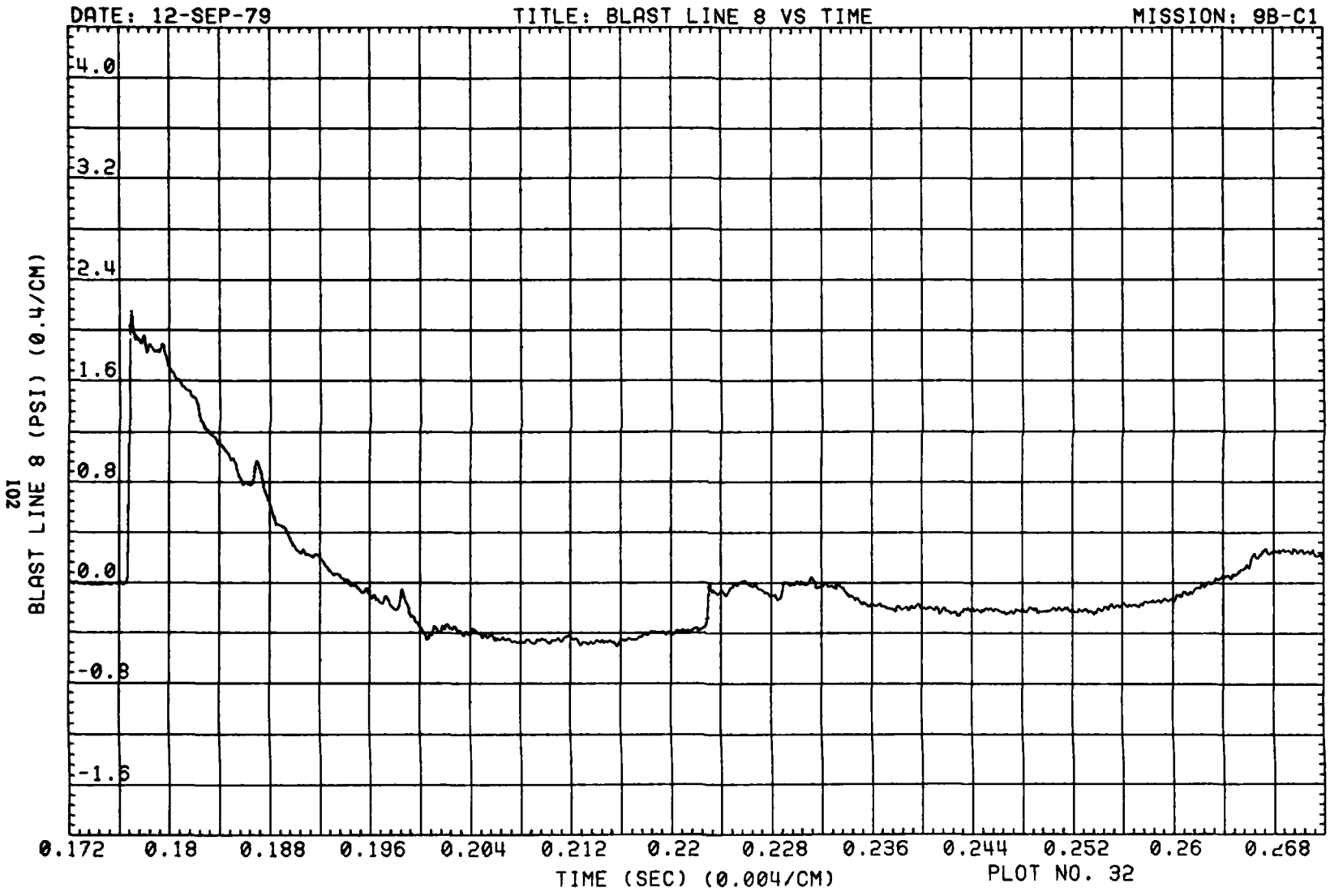

Figure 34. (Concluded)

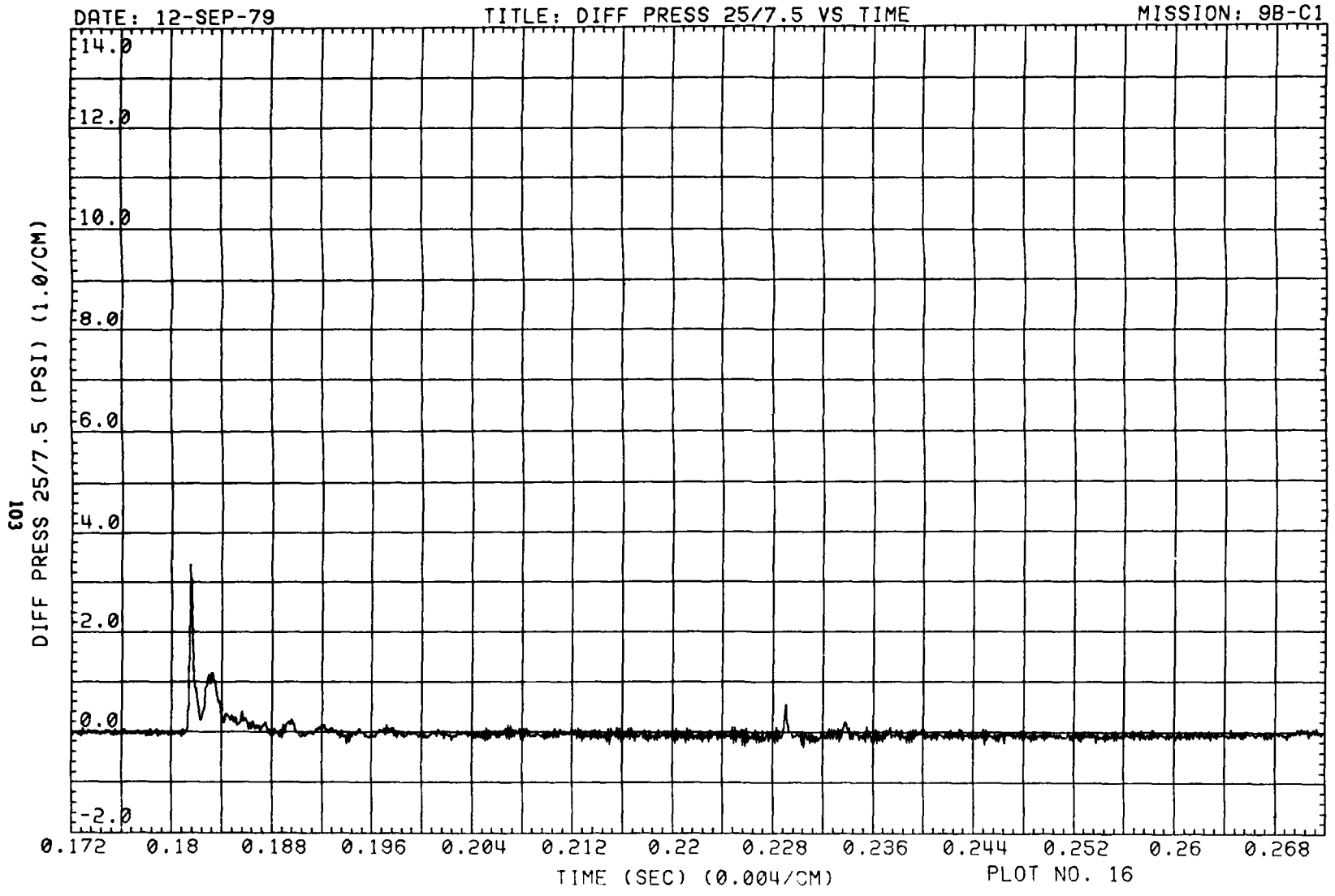

Figure 35. Differential Wing Pressures, Run 9B-C1, Intercept 2

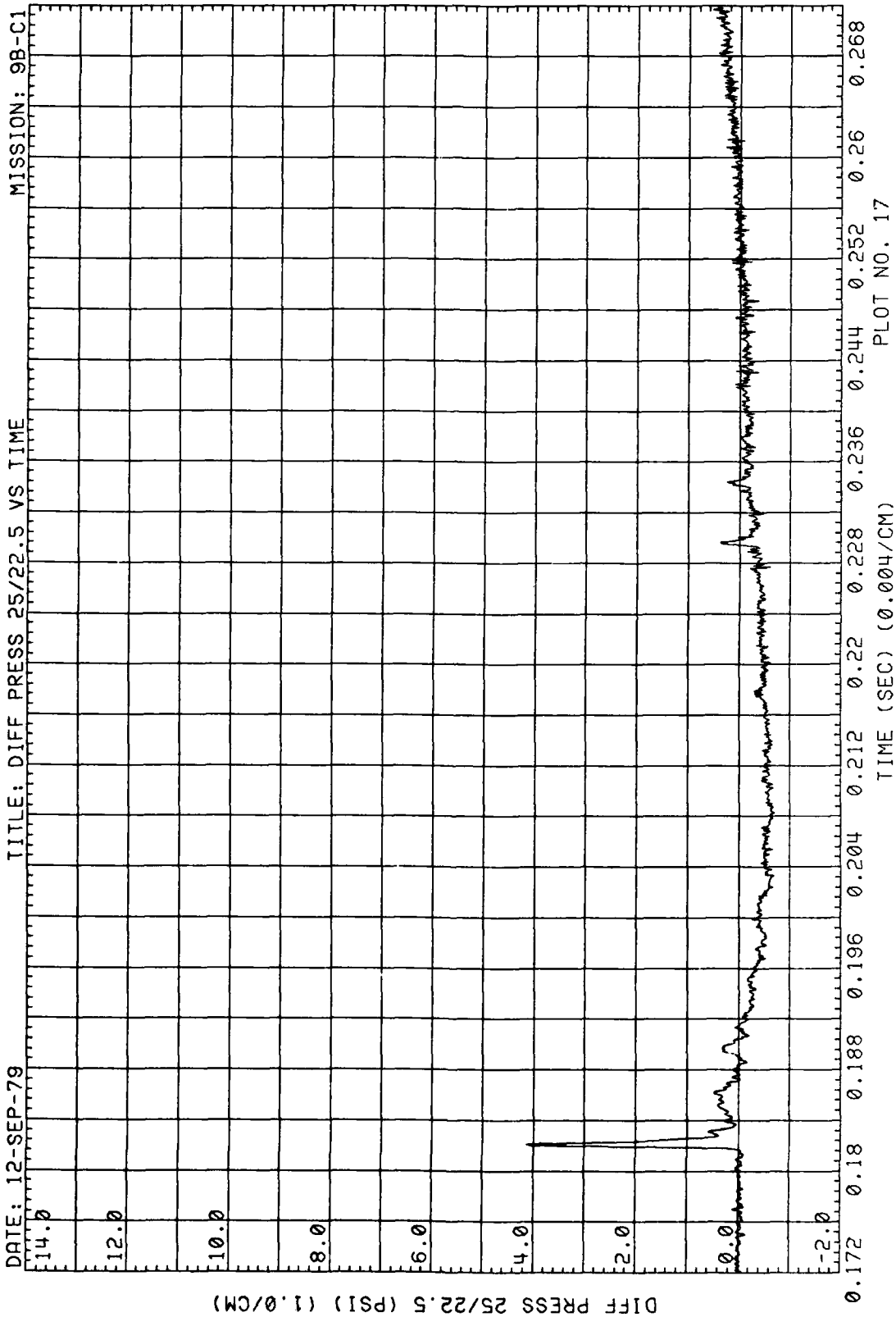

Figure 35. (Continued)

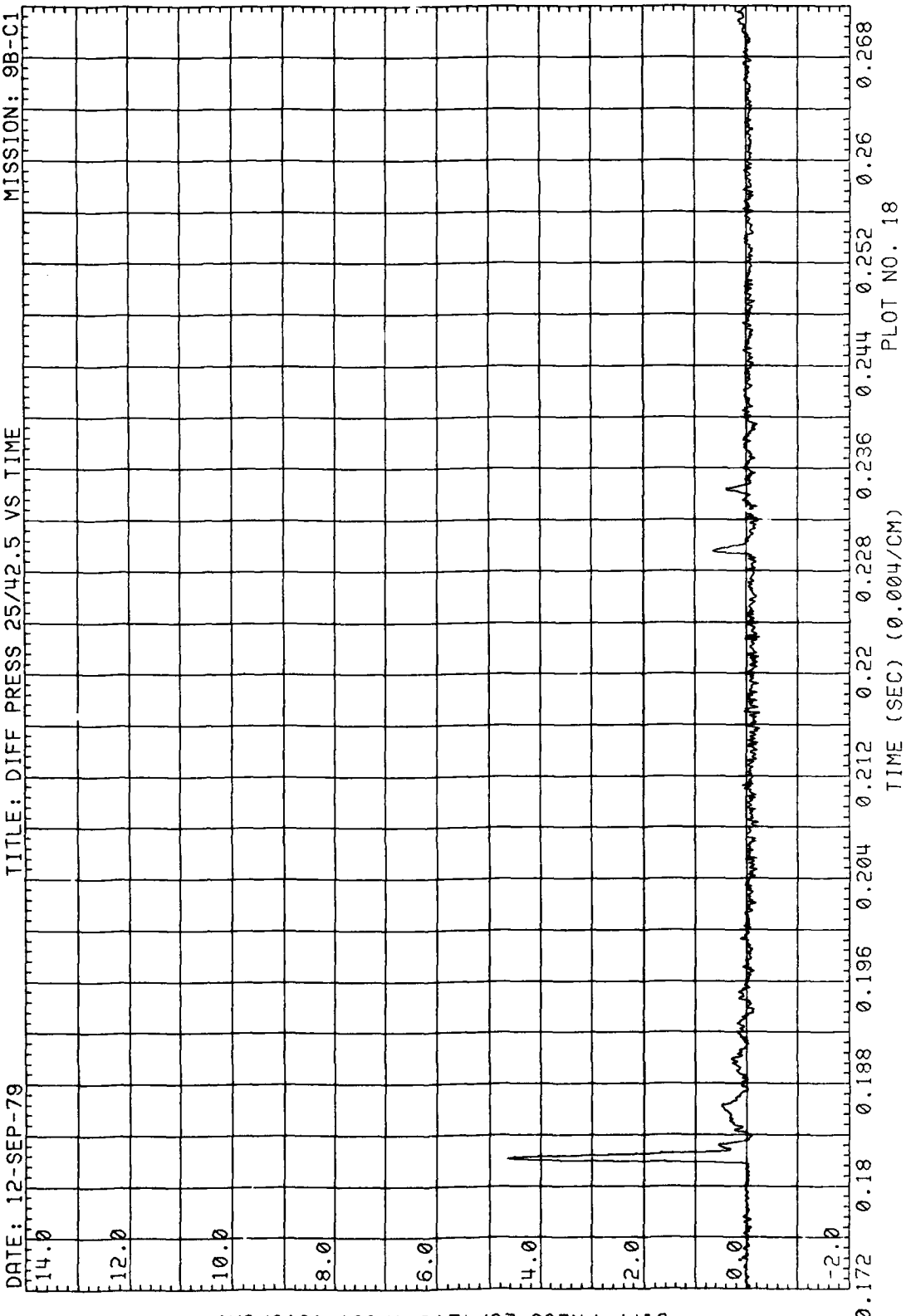

Figure 35. (Continued)

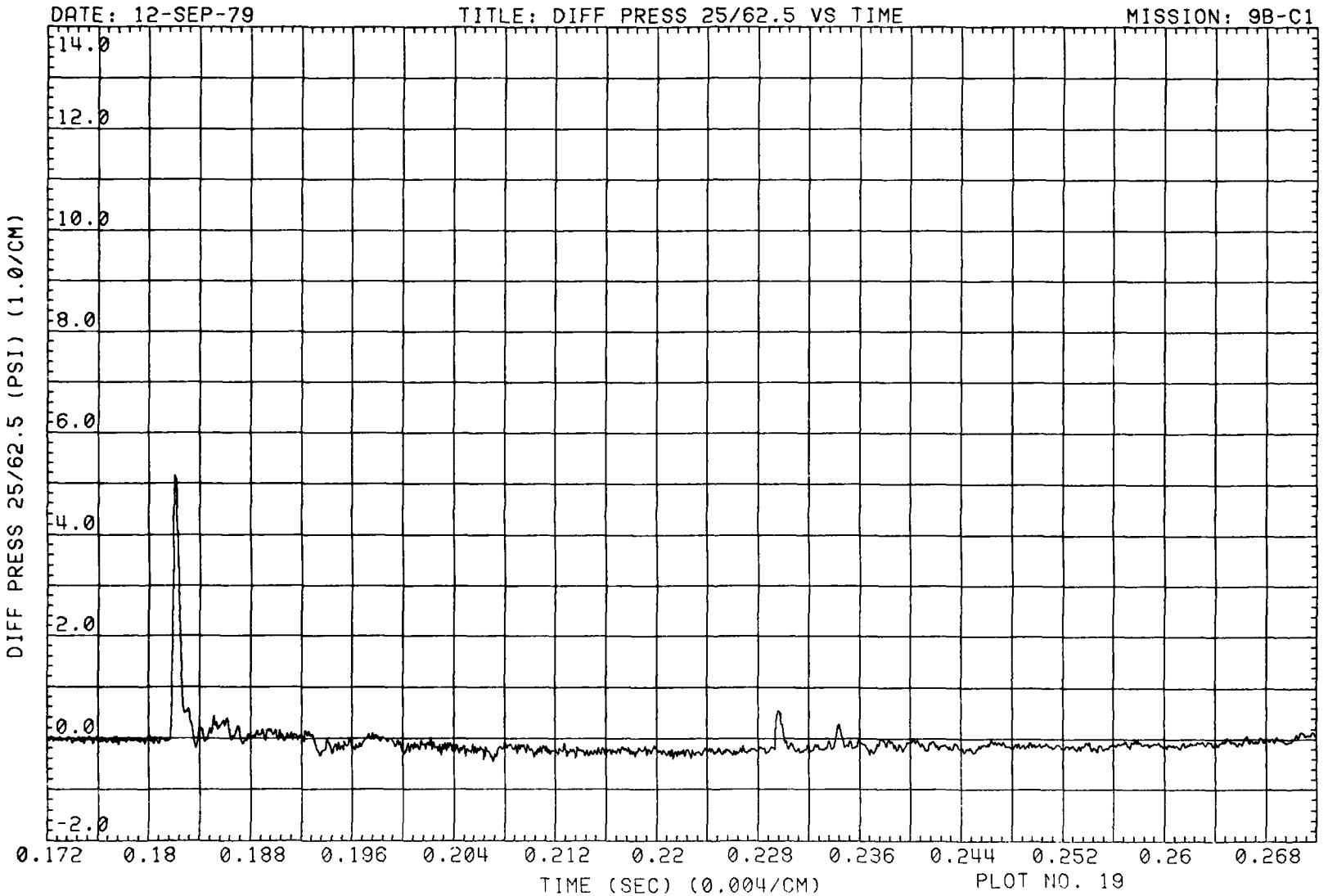

Figure 35. (Continued)

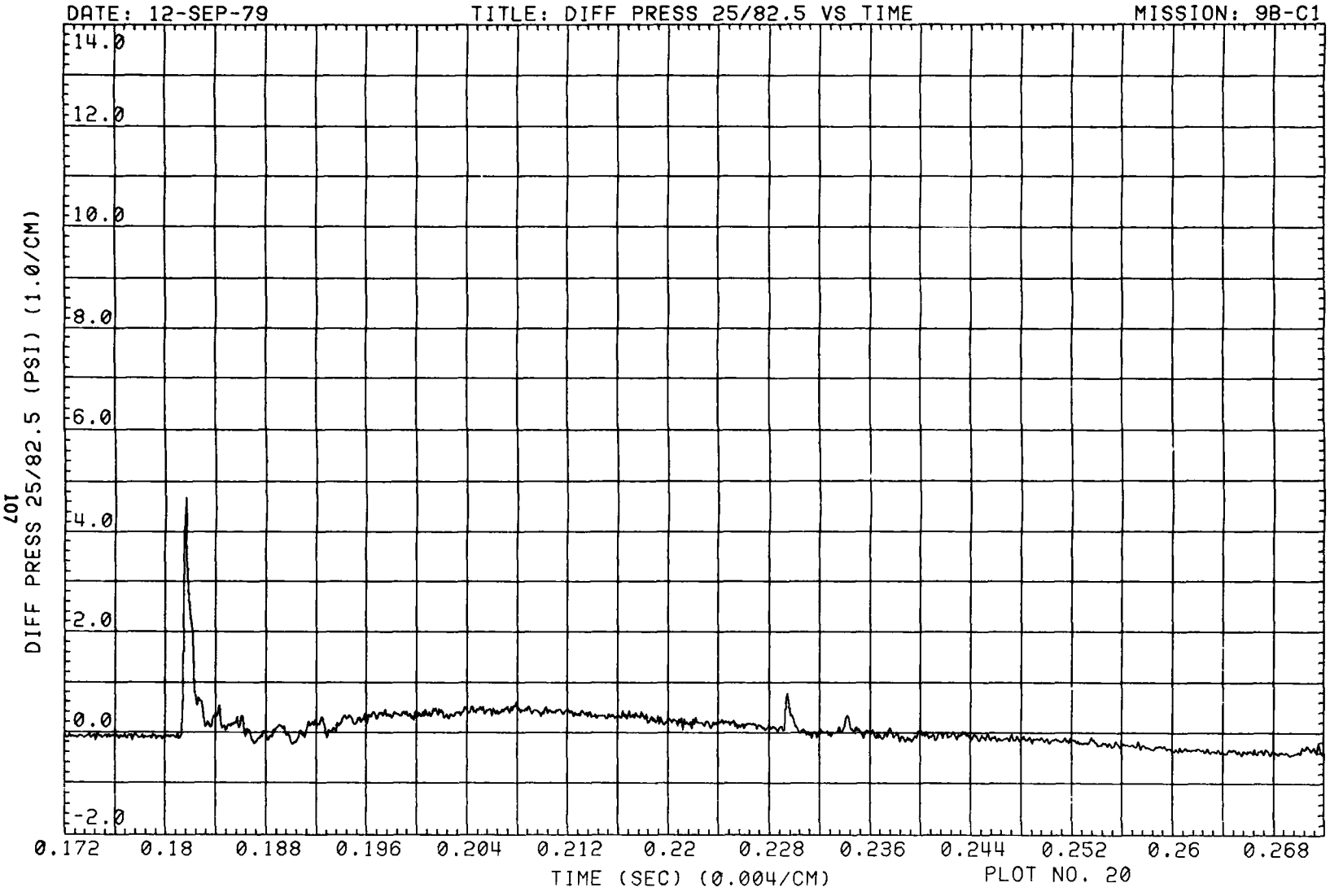

Figure 35. (Continued)

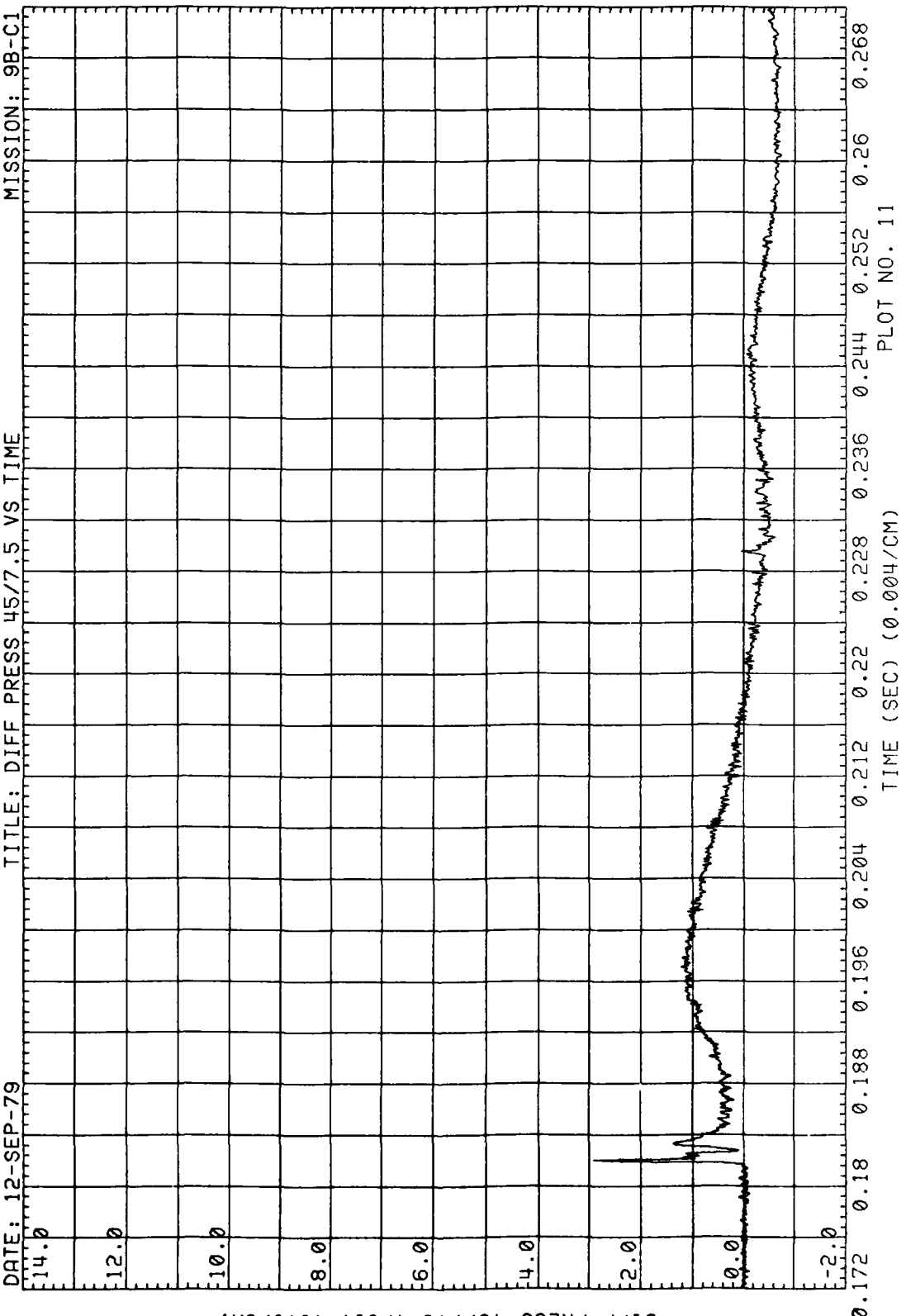

Figure 35. (Continued)

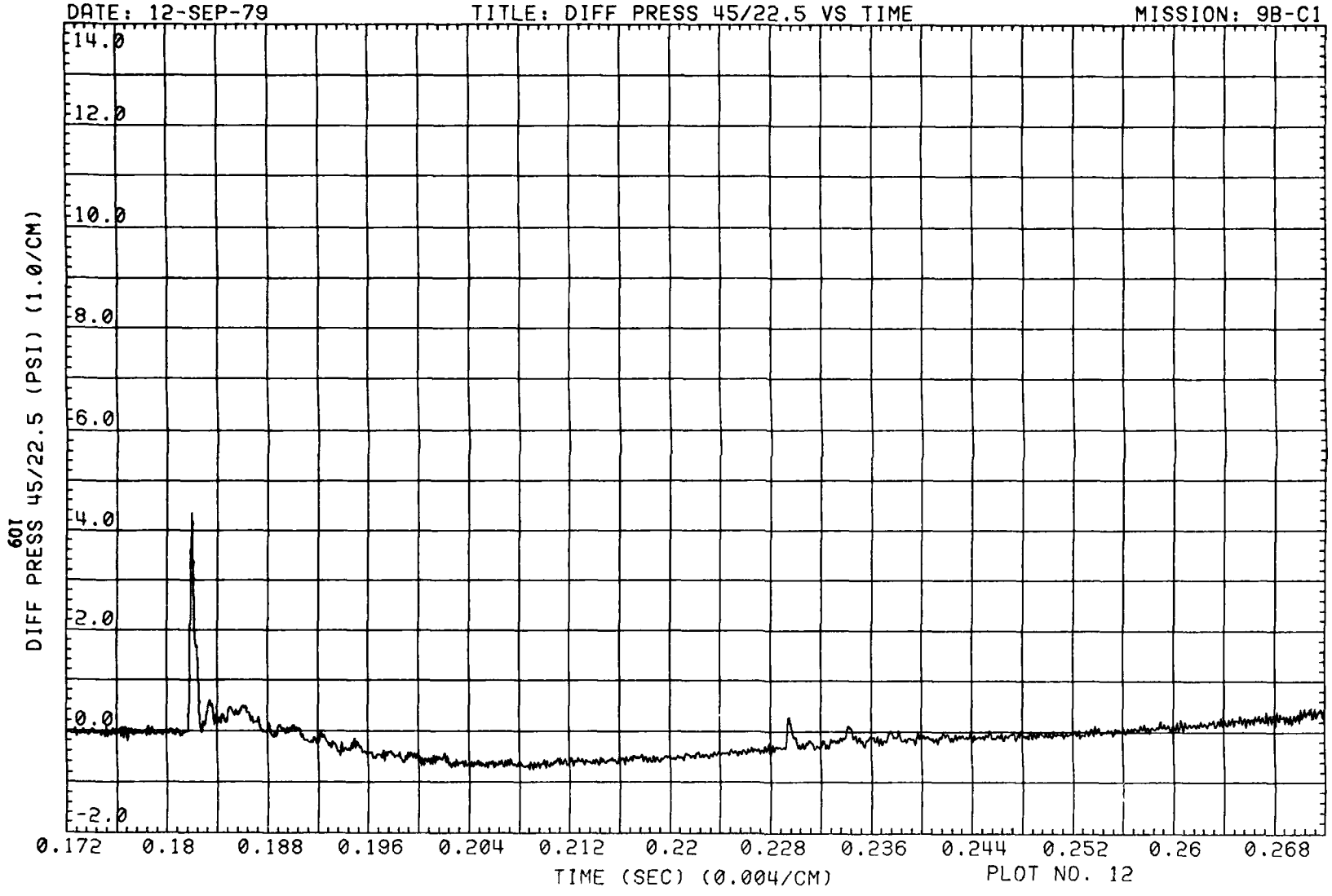

Figure 35. (Continued)

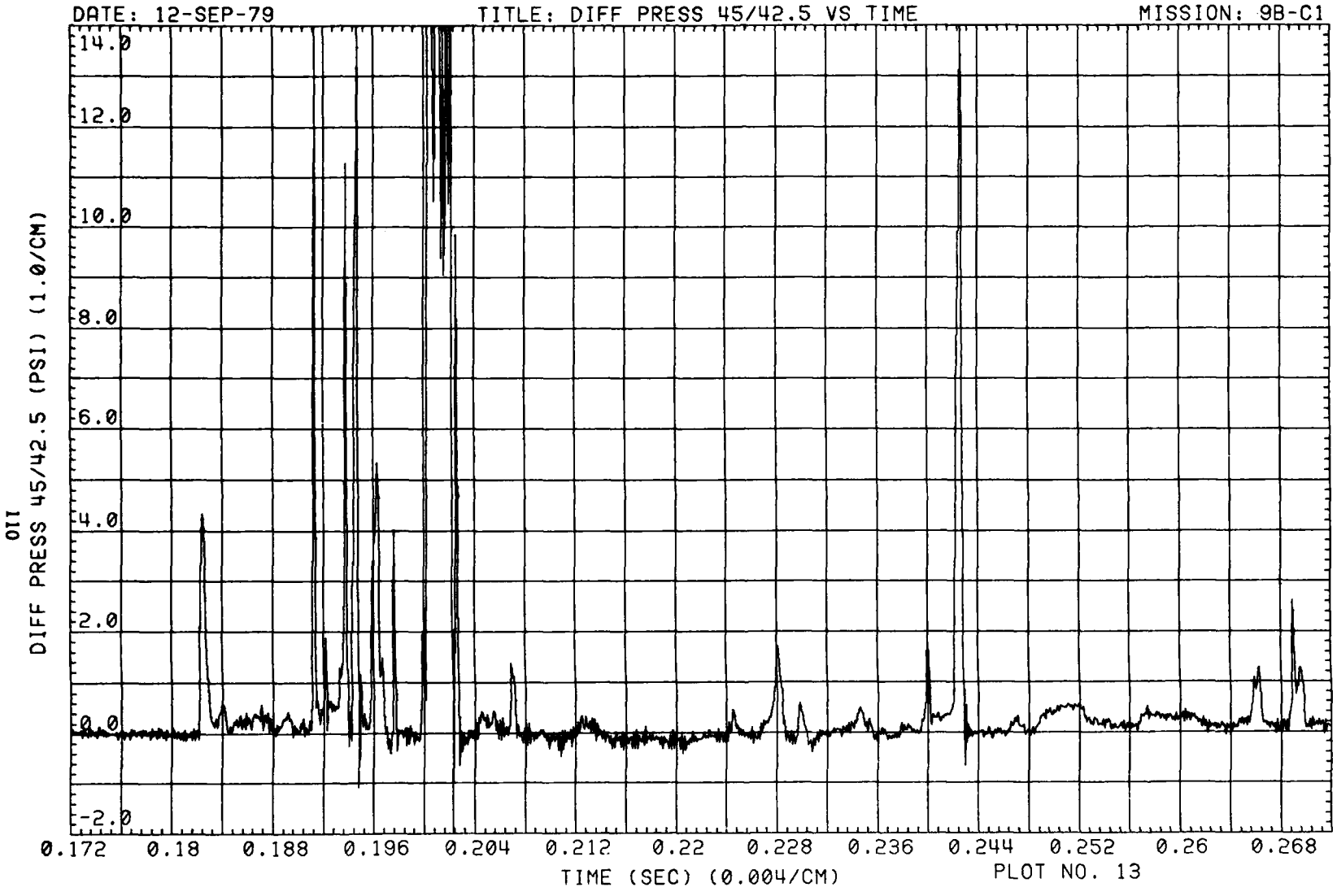

Figure 35. (Continued)

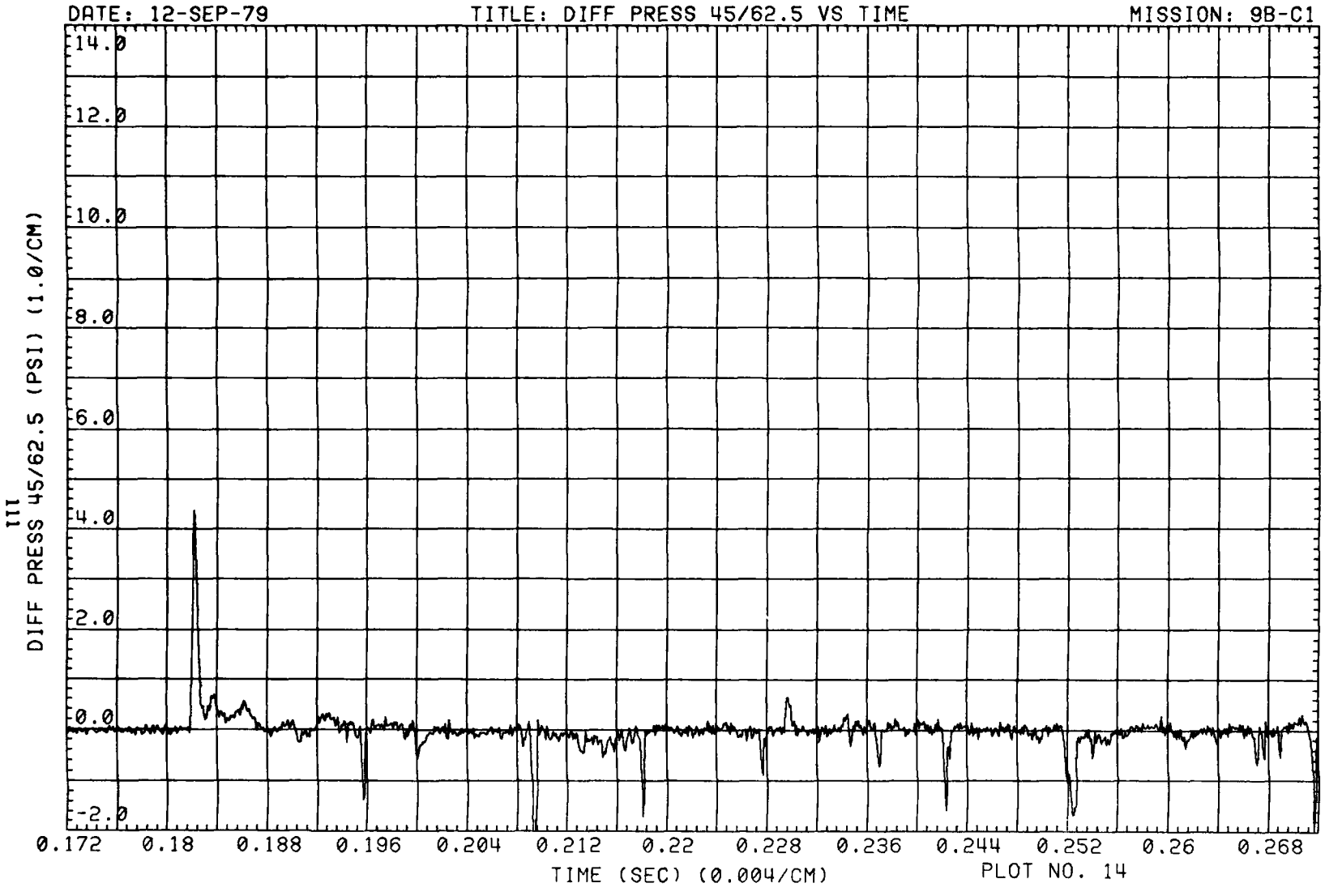

Figure 35. (Continued)

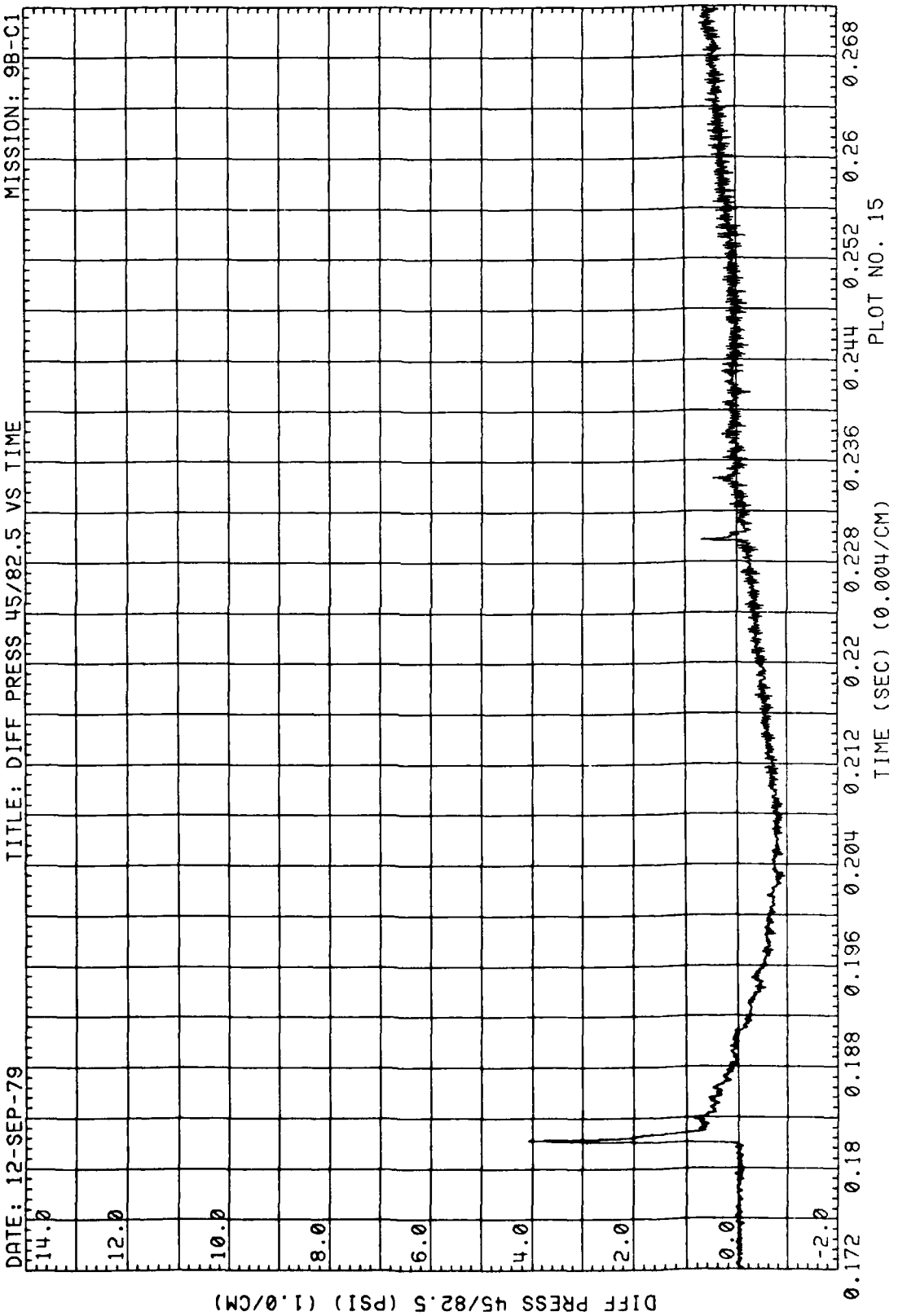

Figure 35. (Continued)

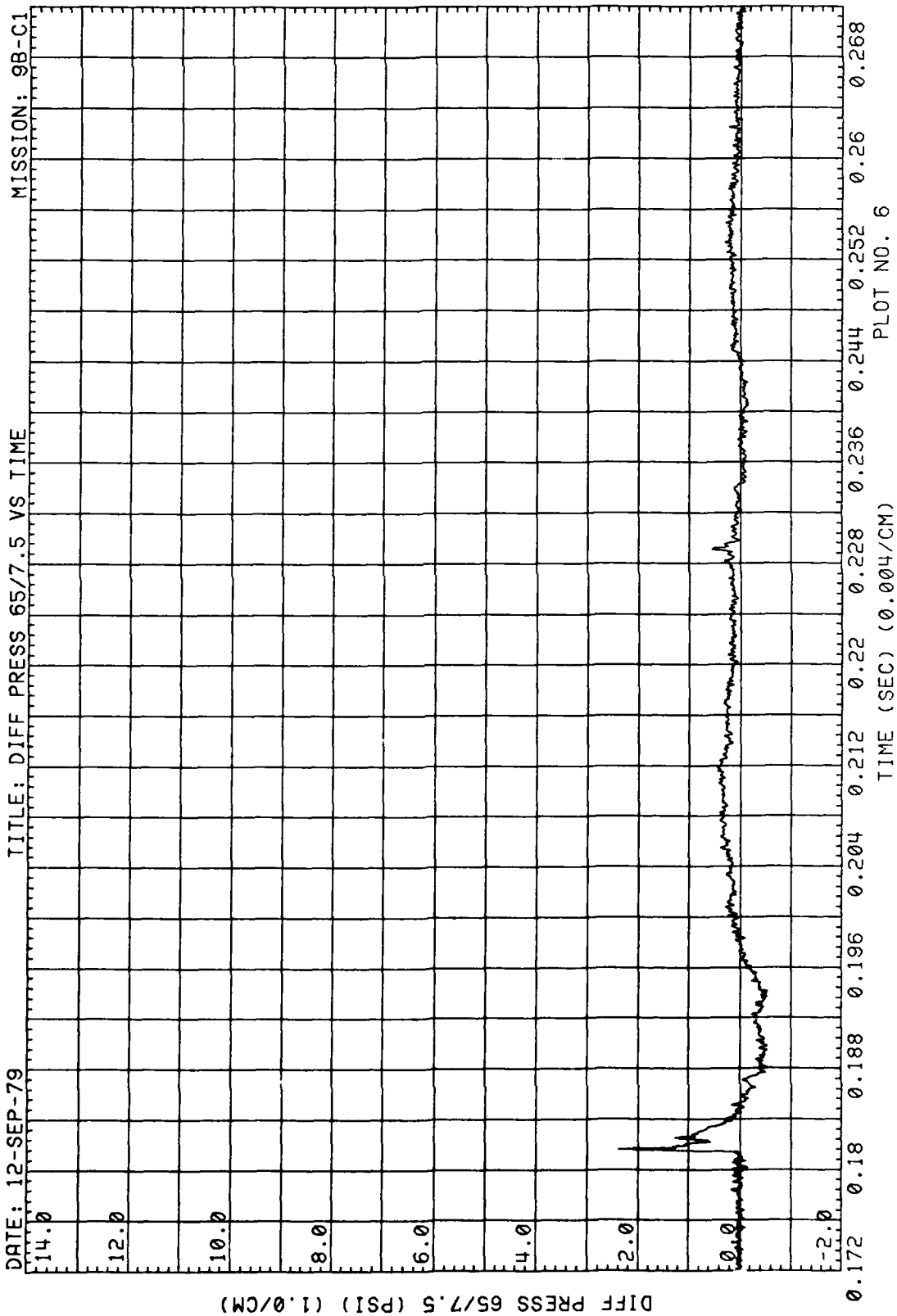

Figure 35. (Continued)

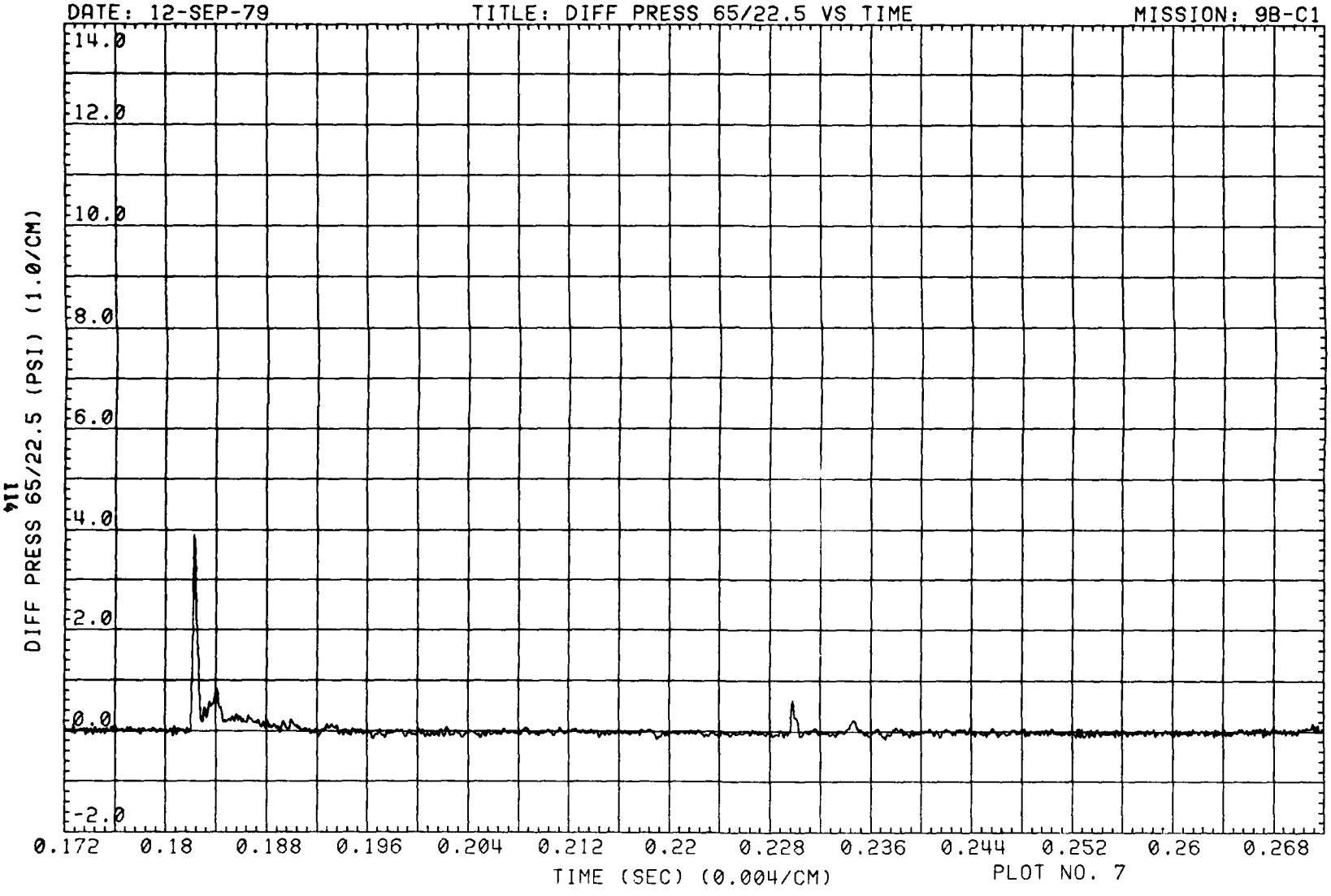

Figure 35. (Continued)

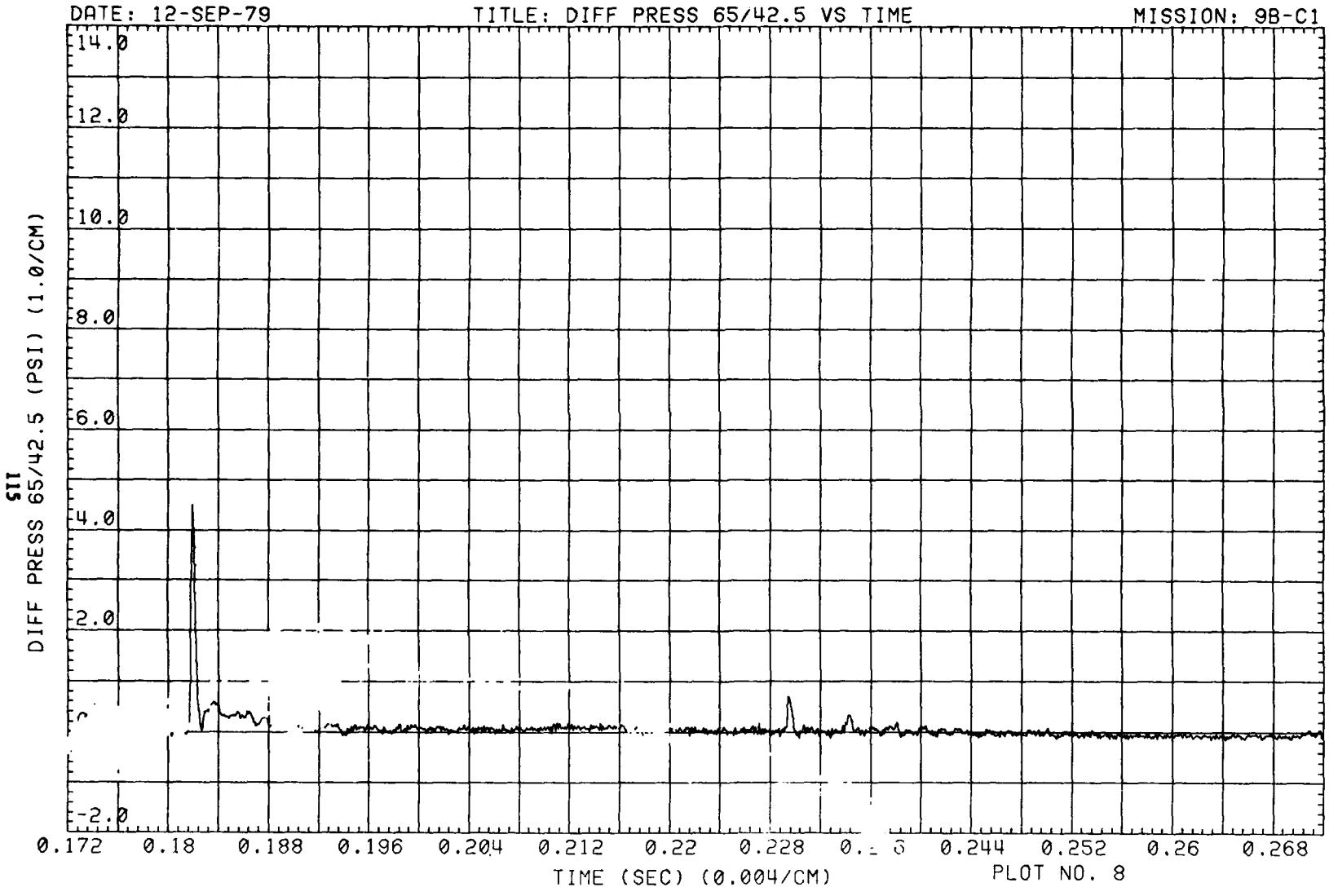

Figure 35. (Continued)

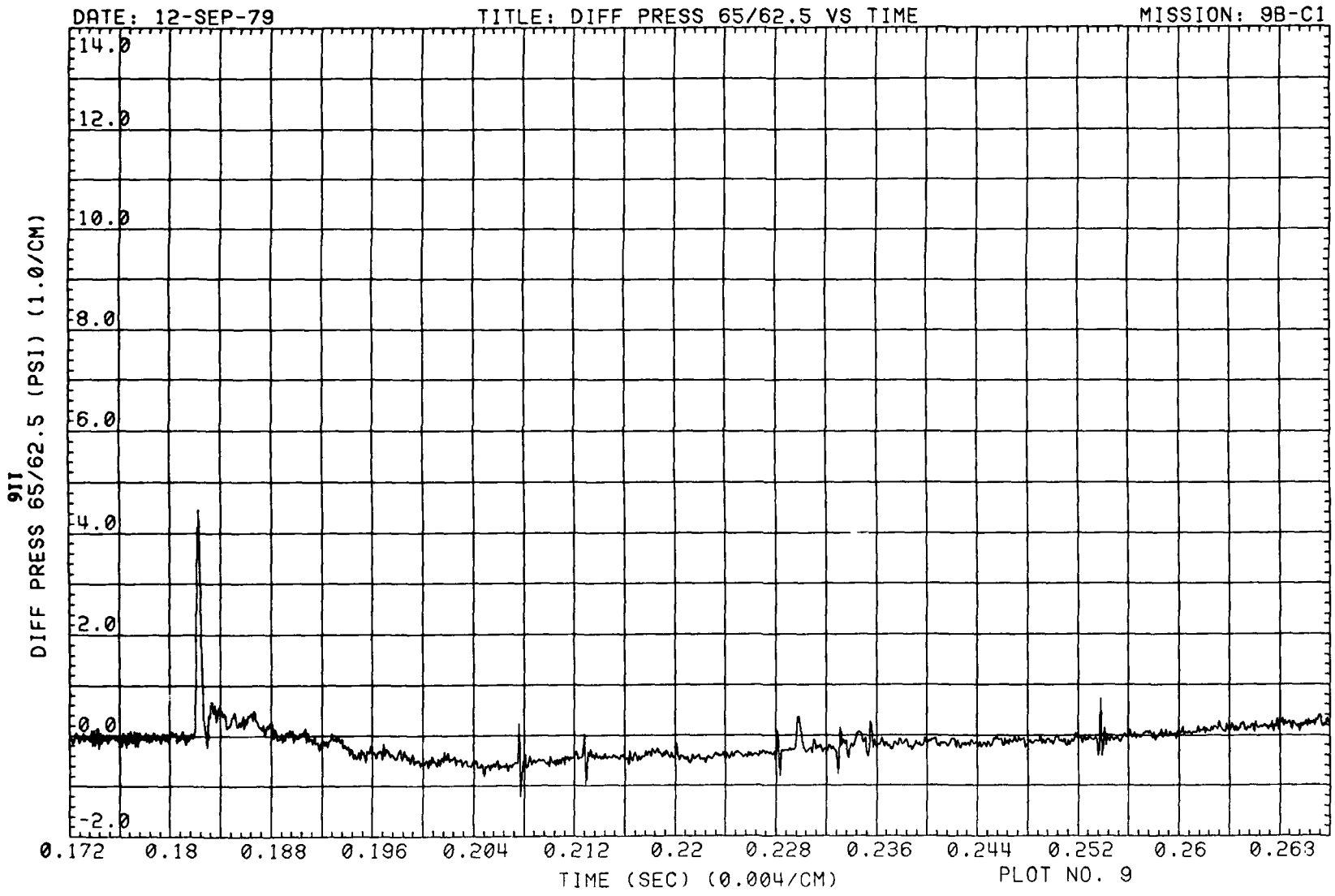

Figure 35. (Continued)

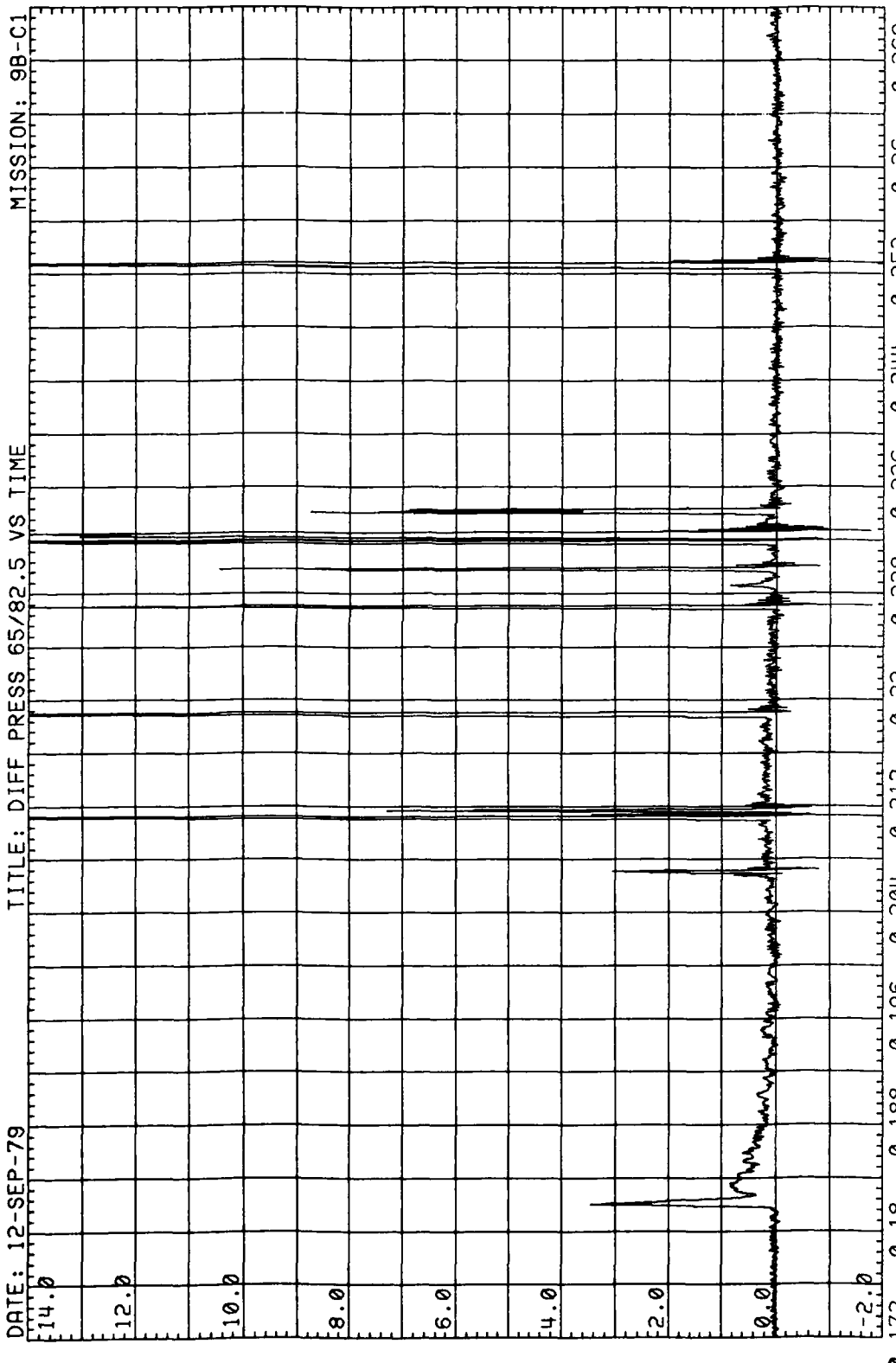

Figure 35. (Continued)

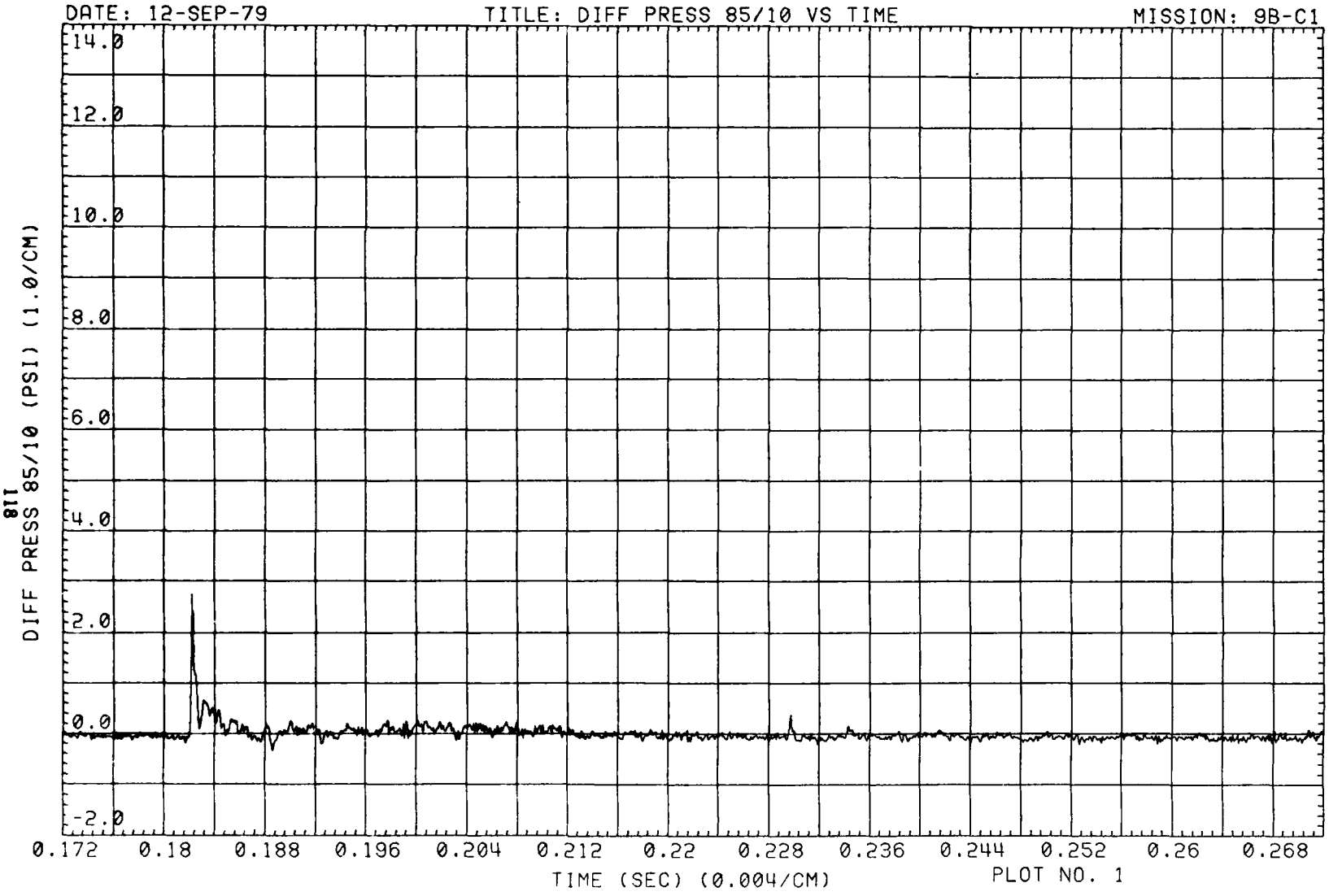

Figure 35. (Continued)

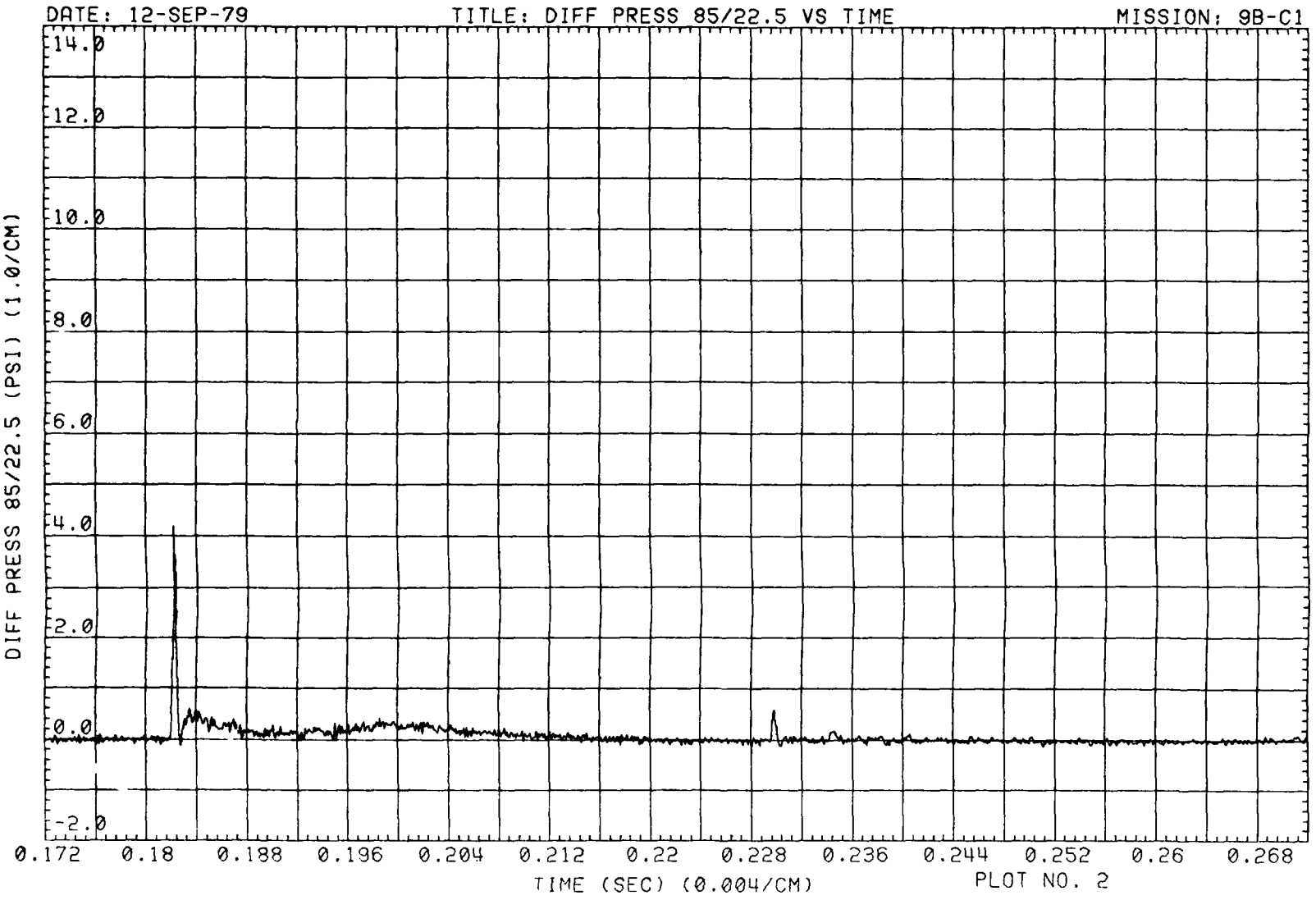

Figure 35. (Continued)

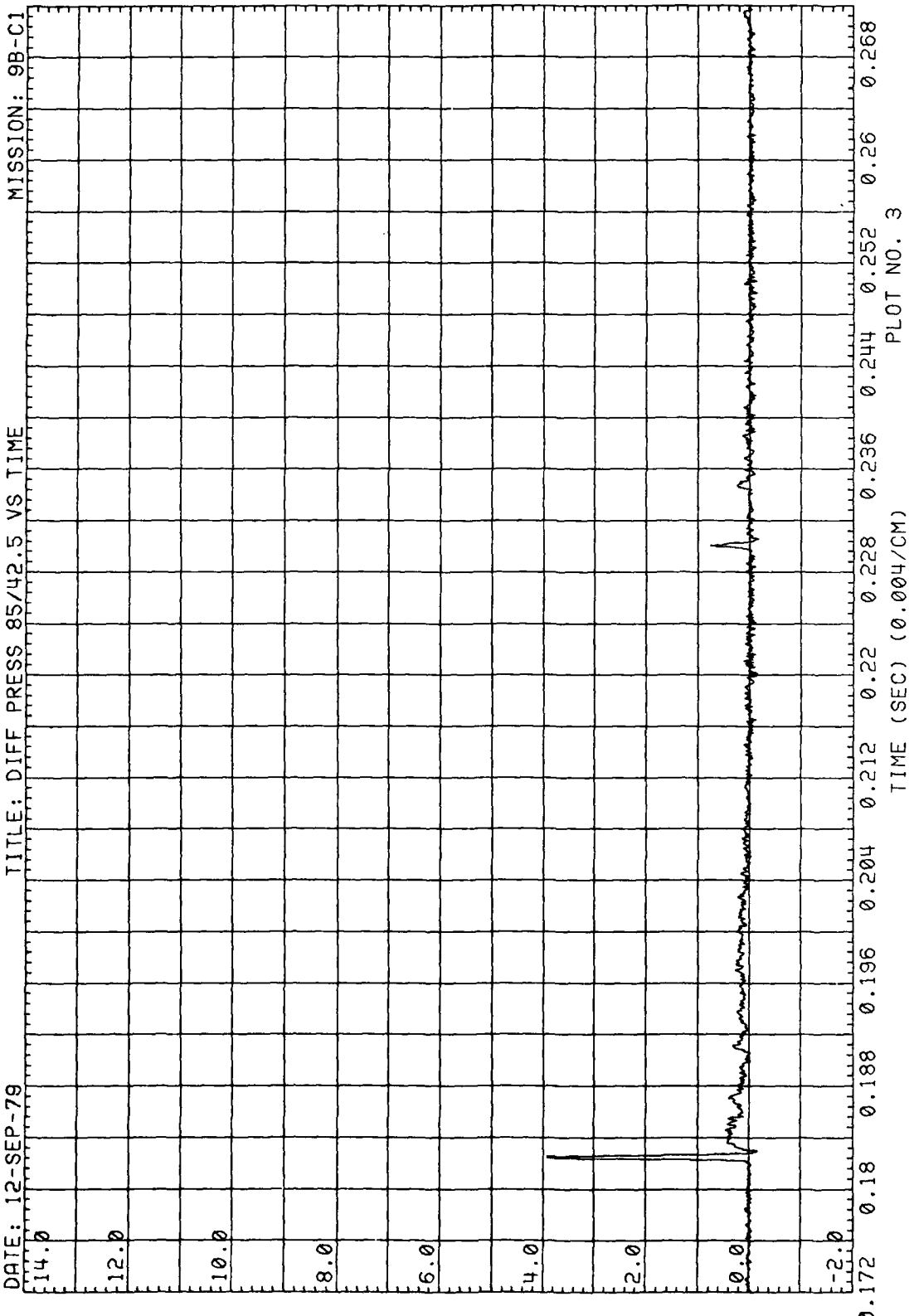

Figure 35. (Continued)

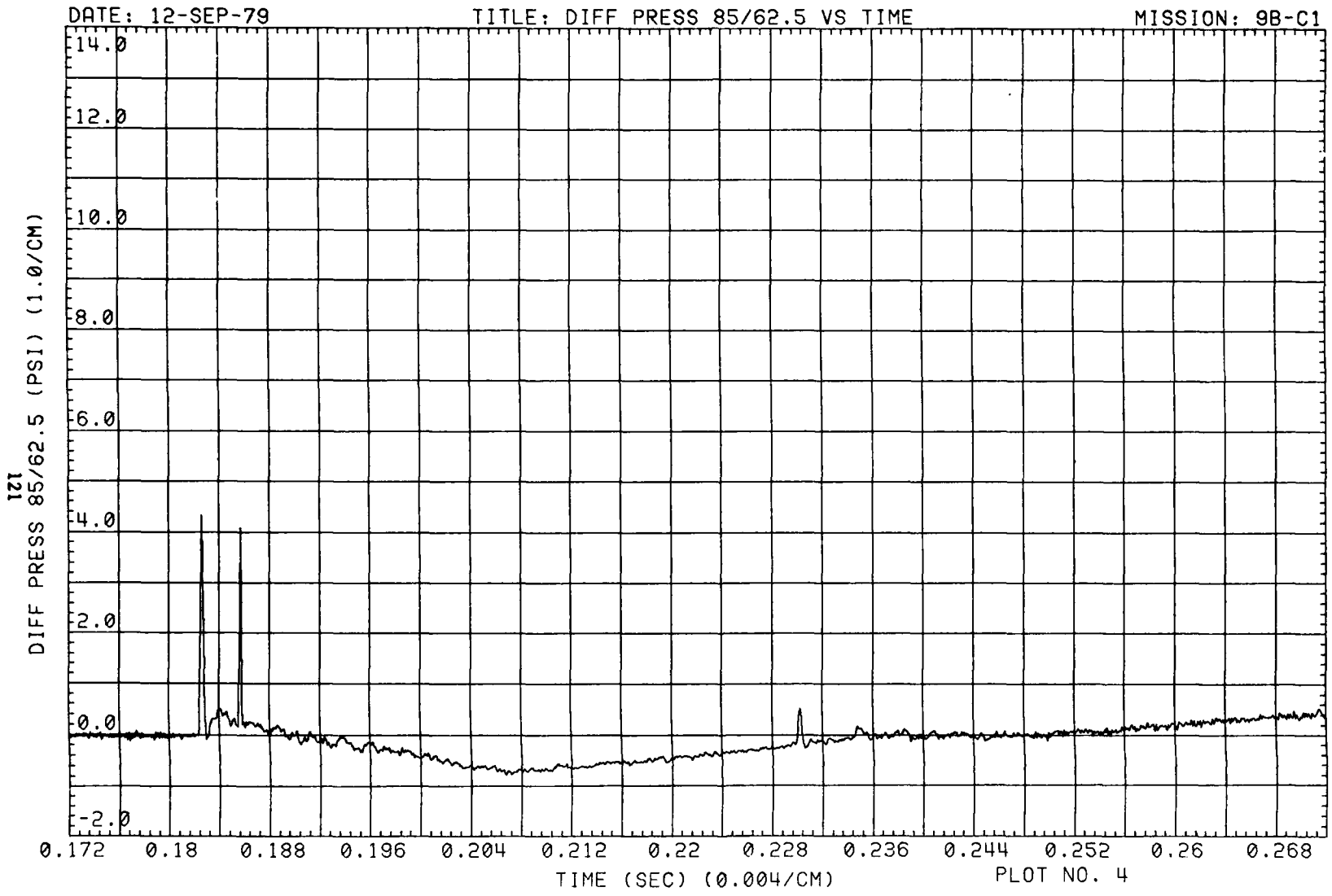

Figure 35. (Continued)

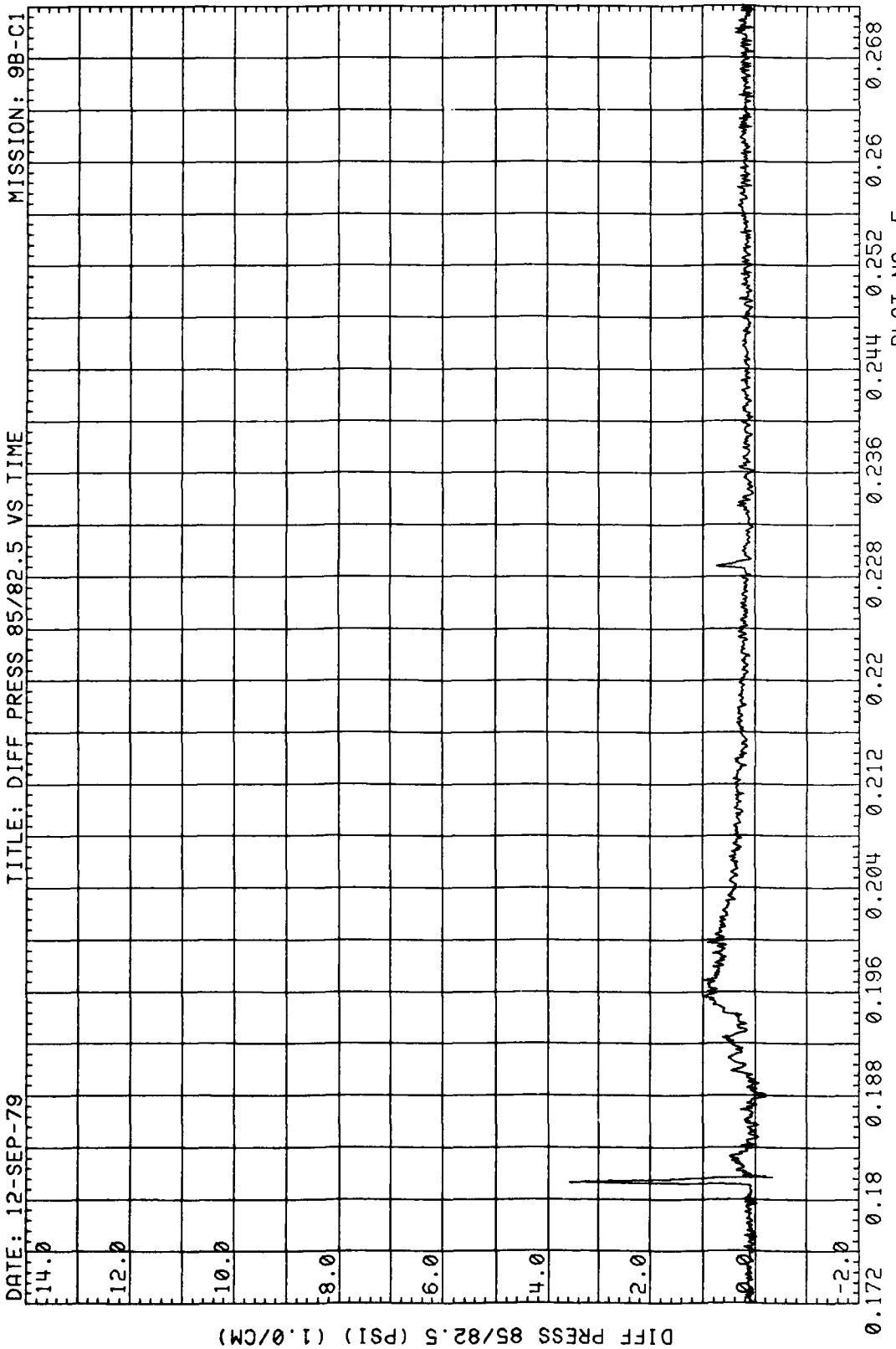

Figure 35. (Concluded)

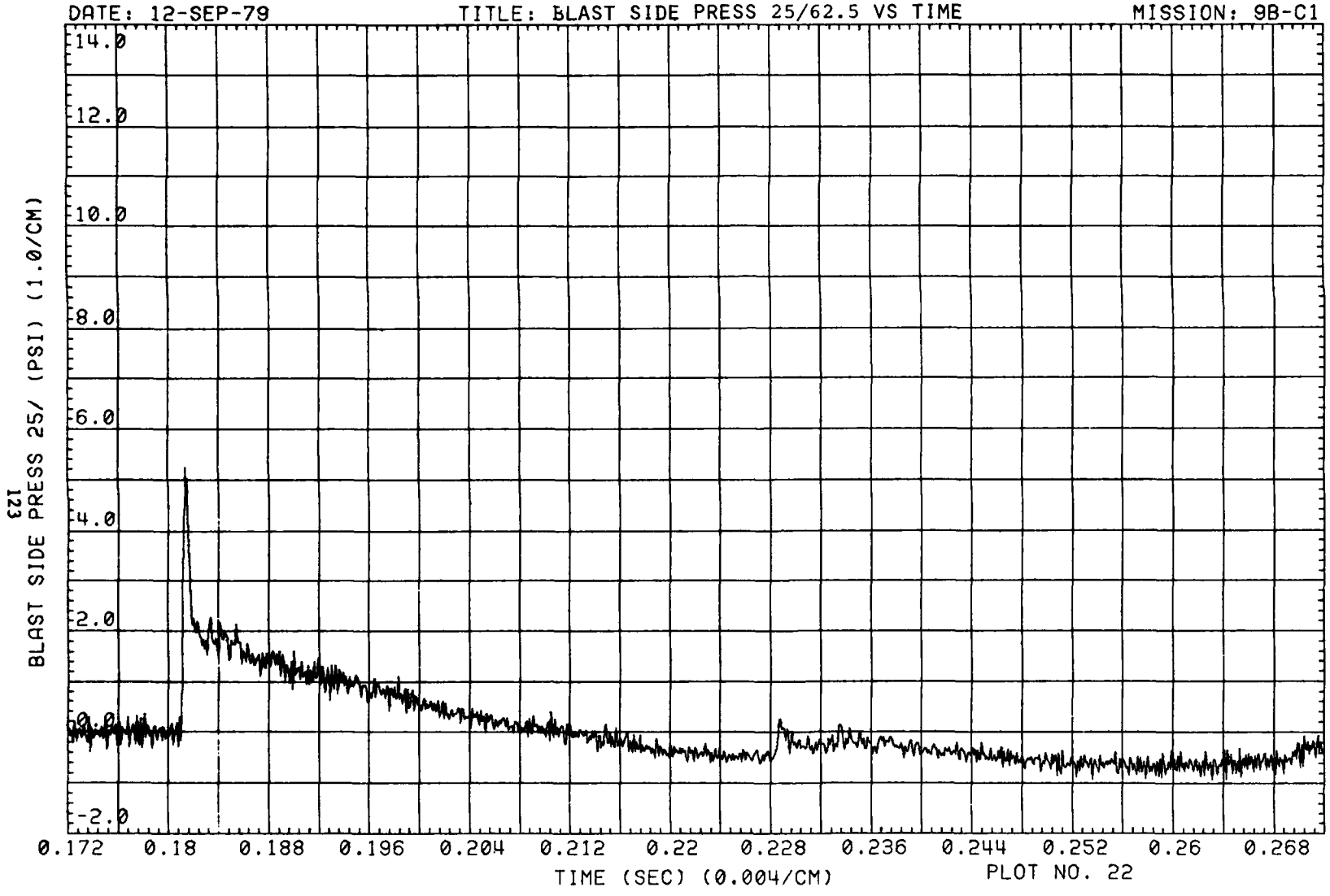

Figure 36. Blastward and Leeward Wind Pressures, Run 9B-C1, Intercept 2

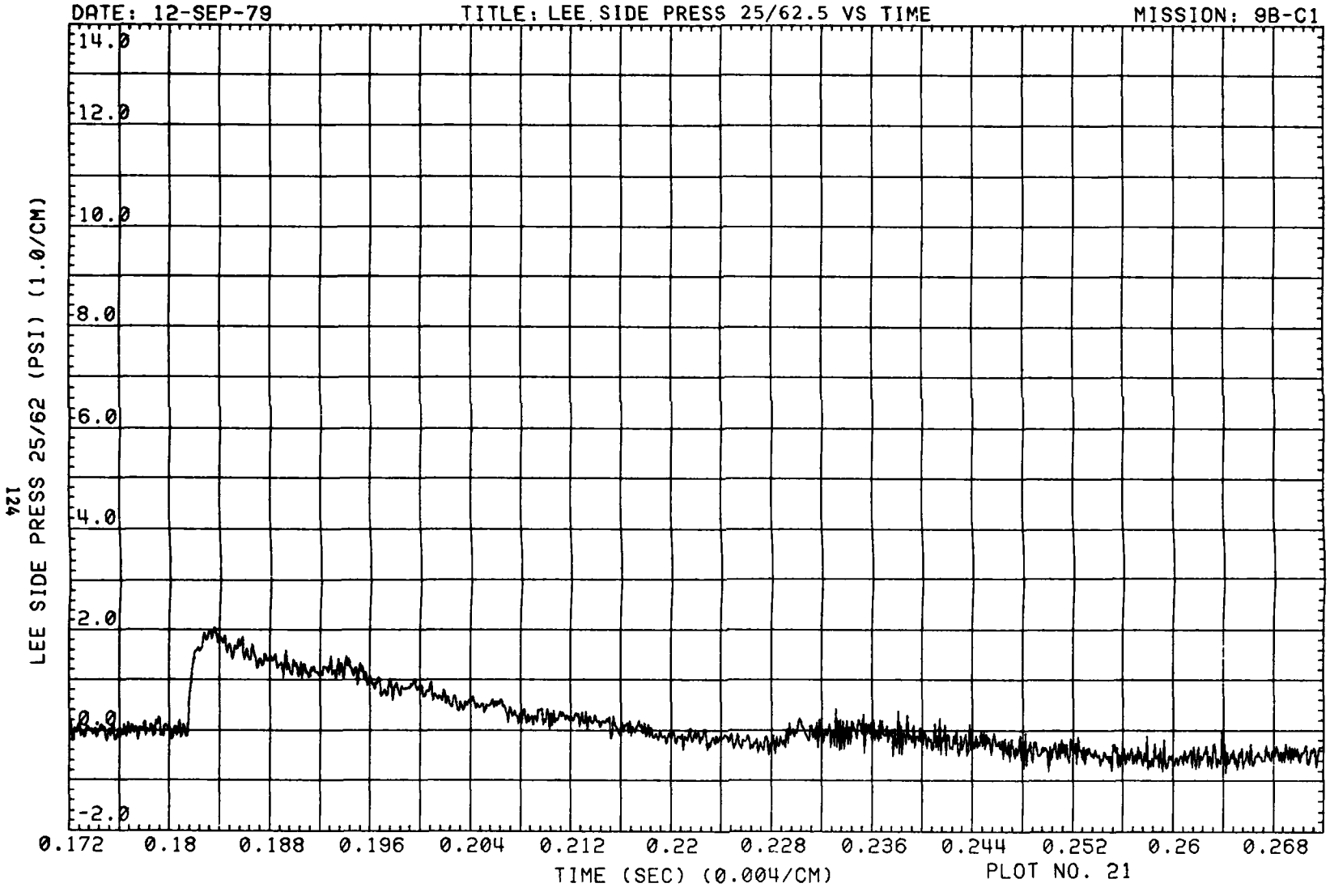

Figure 36. (Concluded)

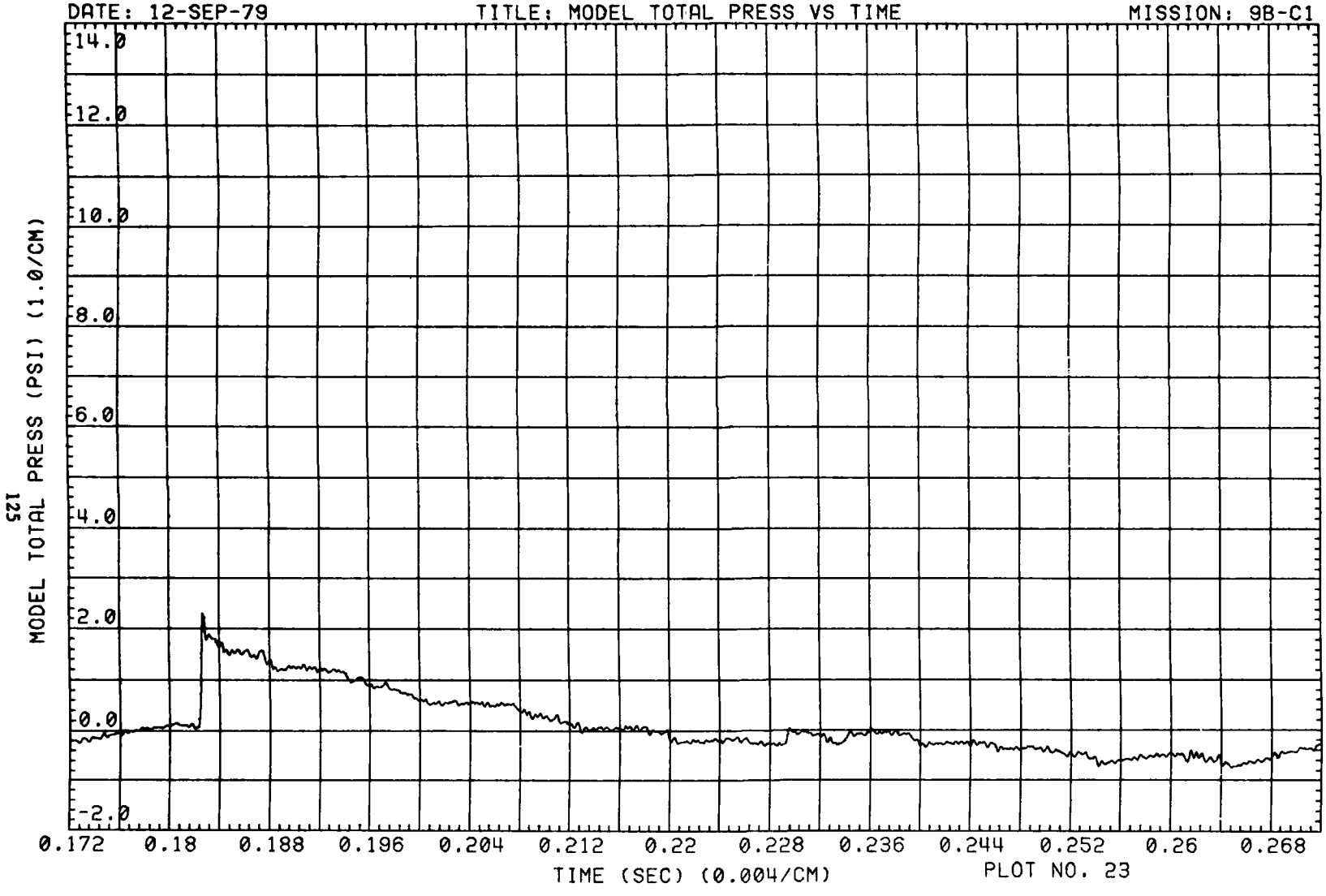

Figure 37. Total Pressure at Model, Run 9B-C1, Intercept 2

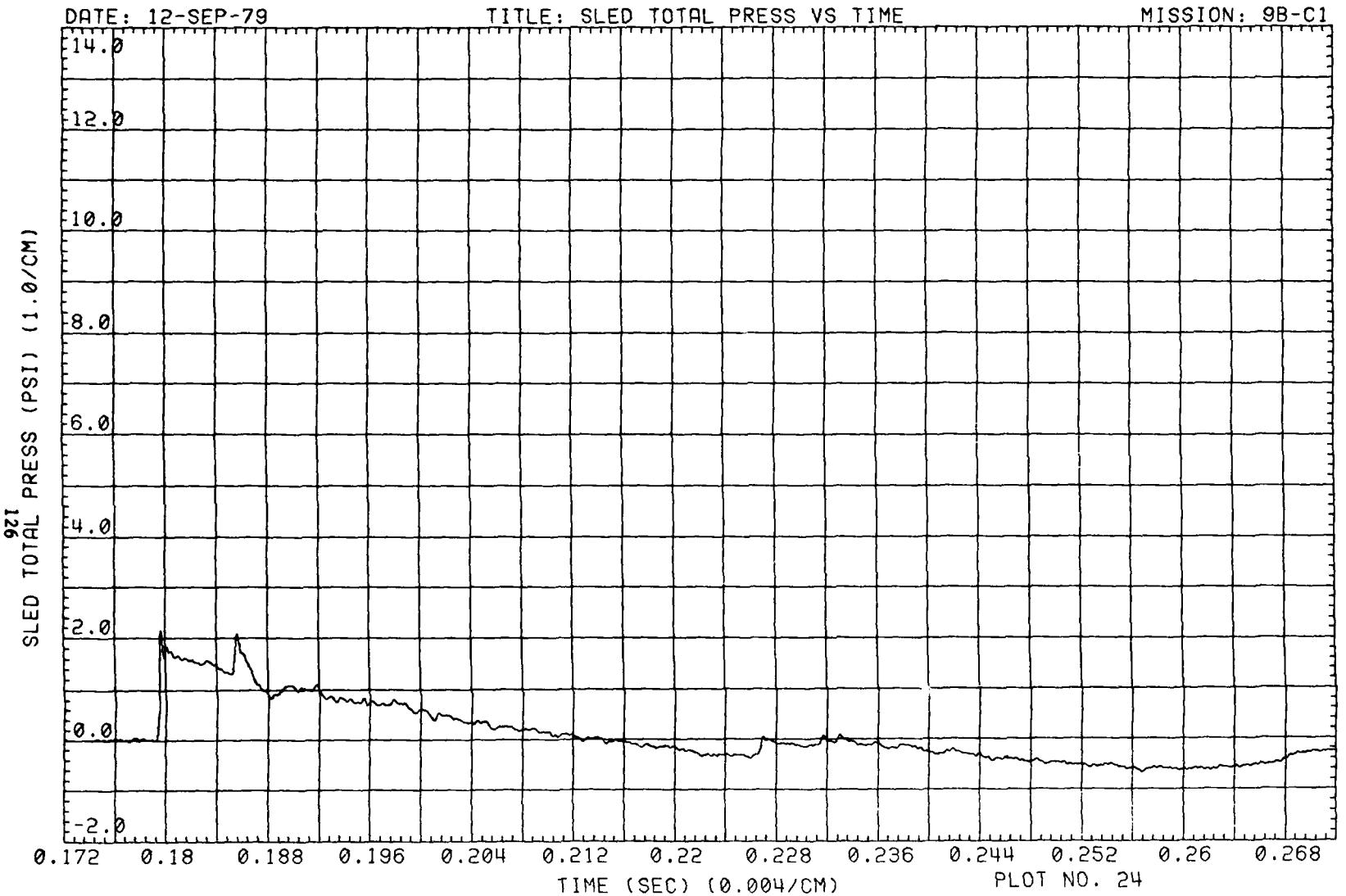

Figure 38. Total Pressure at Sled, Run 9B-C1, Intercept 2

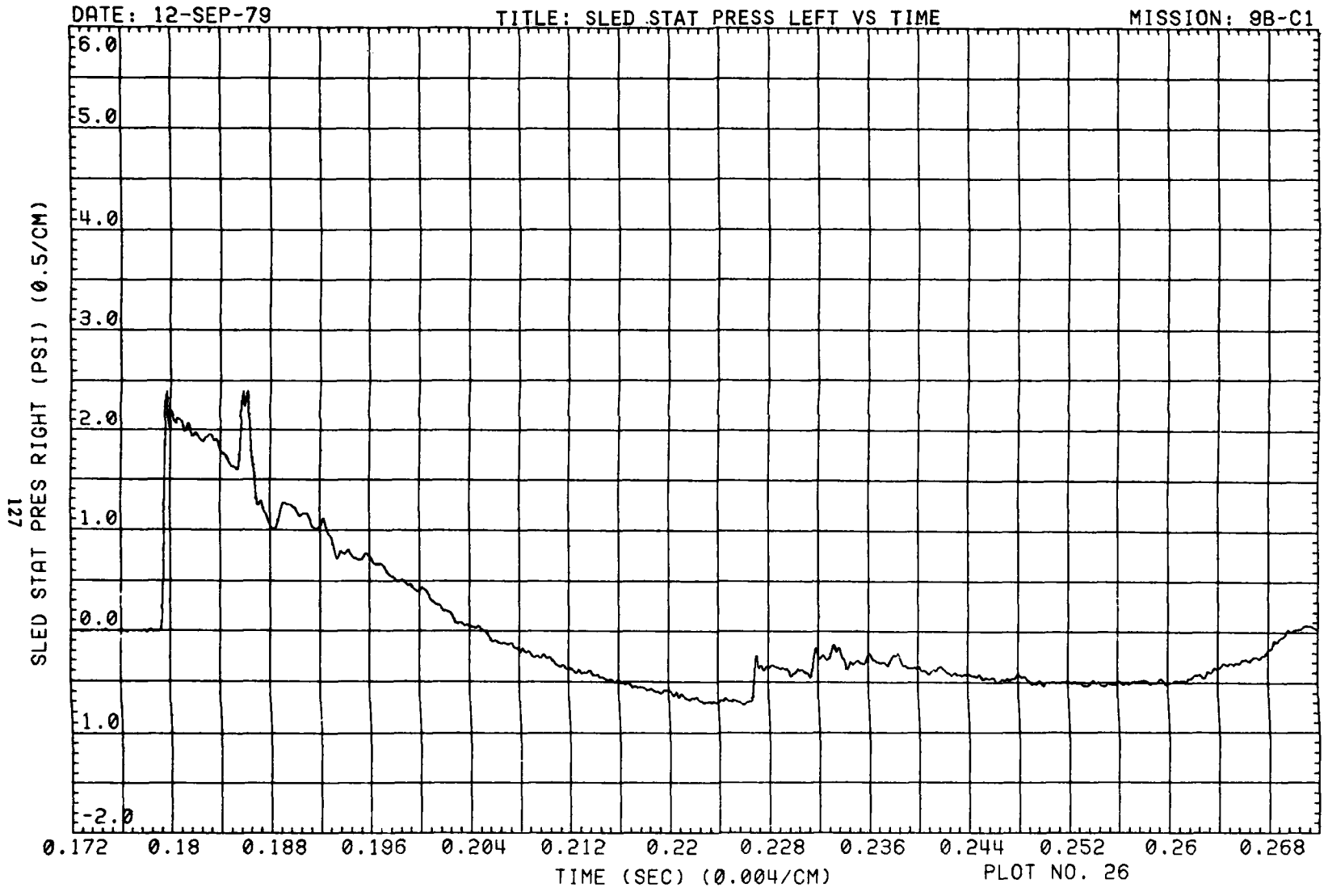

Figure 39. Left Side Static Pressure at Sled, Run 9B-C1, Intercept 2

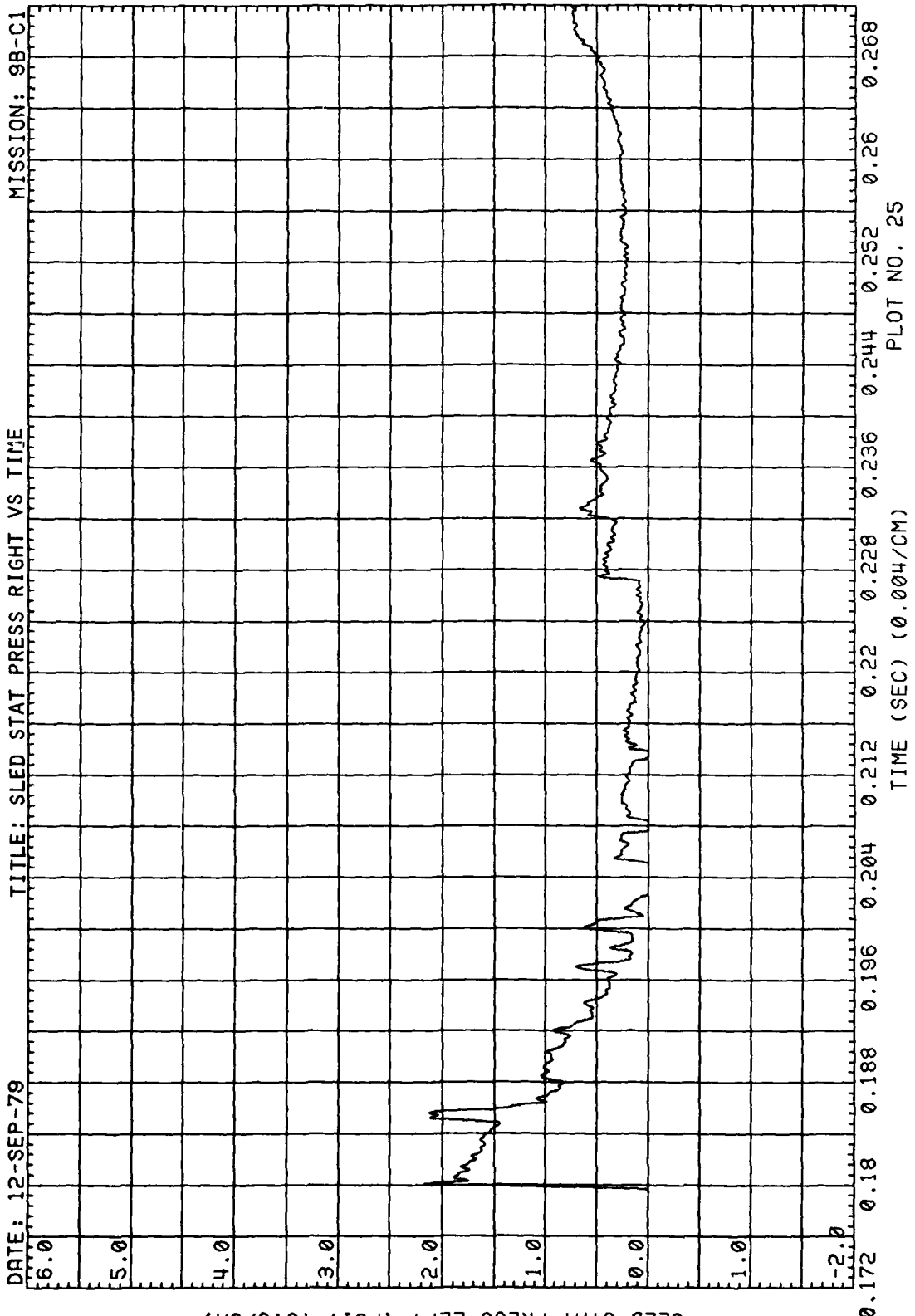

Figure 40. Right Side Static Pressure at Sled, Run 9B-C1, Intercept 2

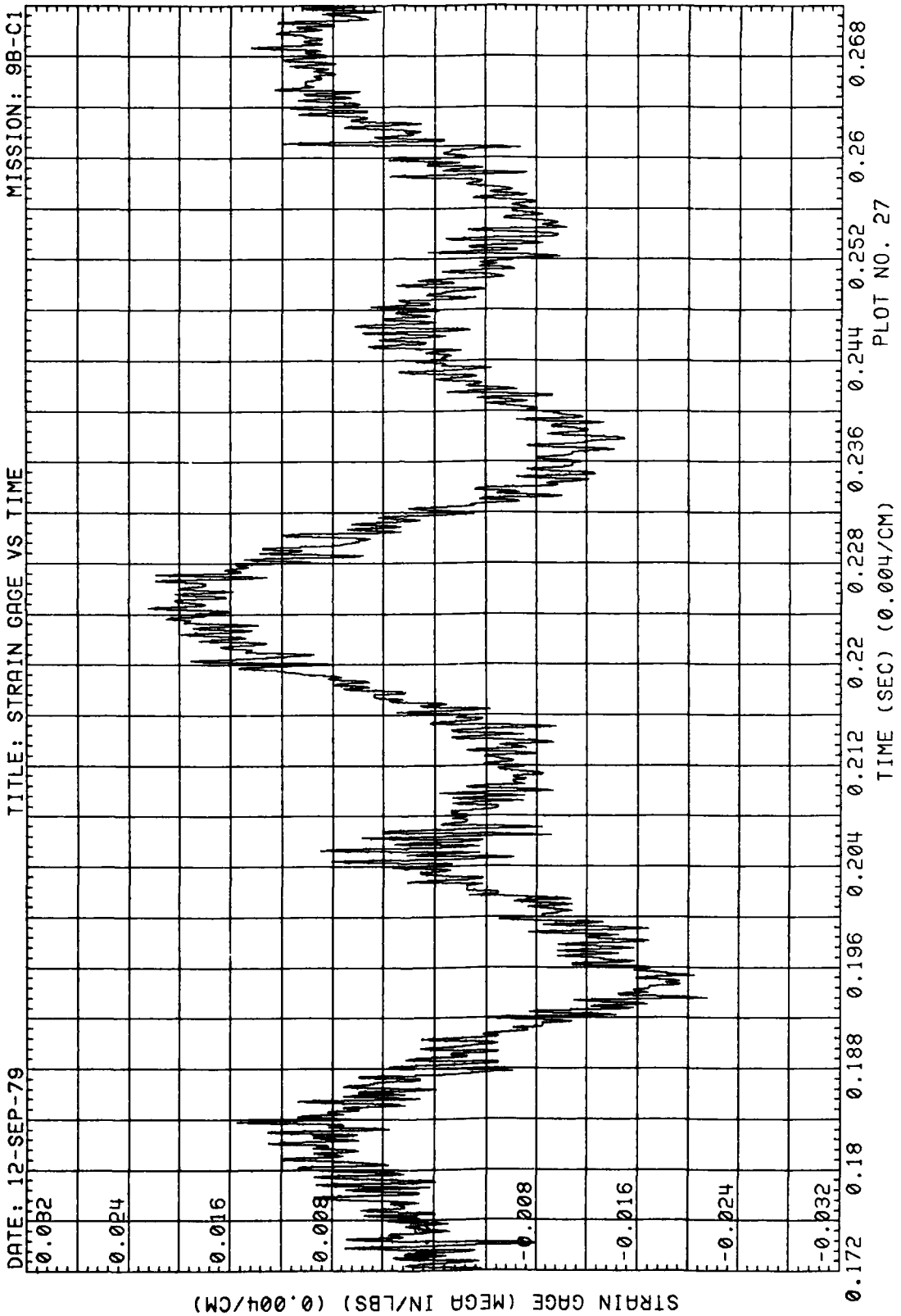

Figure 41. Strain at Model Support, 9B-C1, Intercept 2

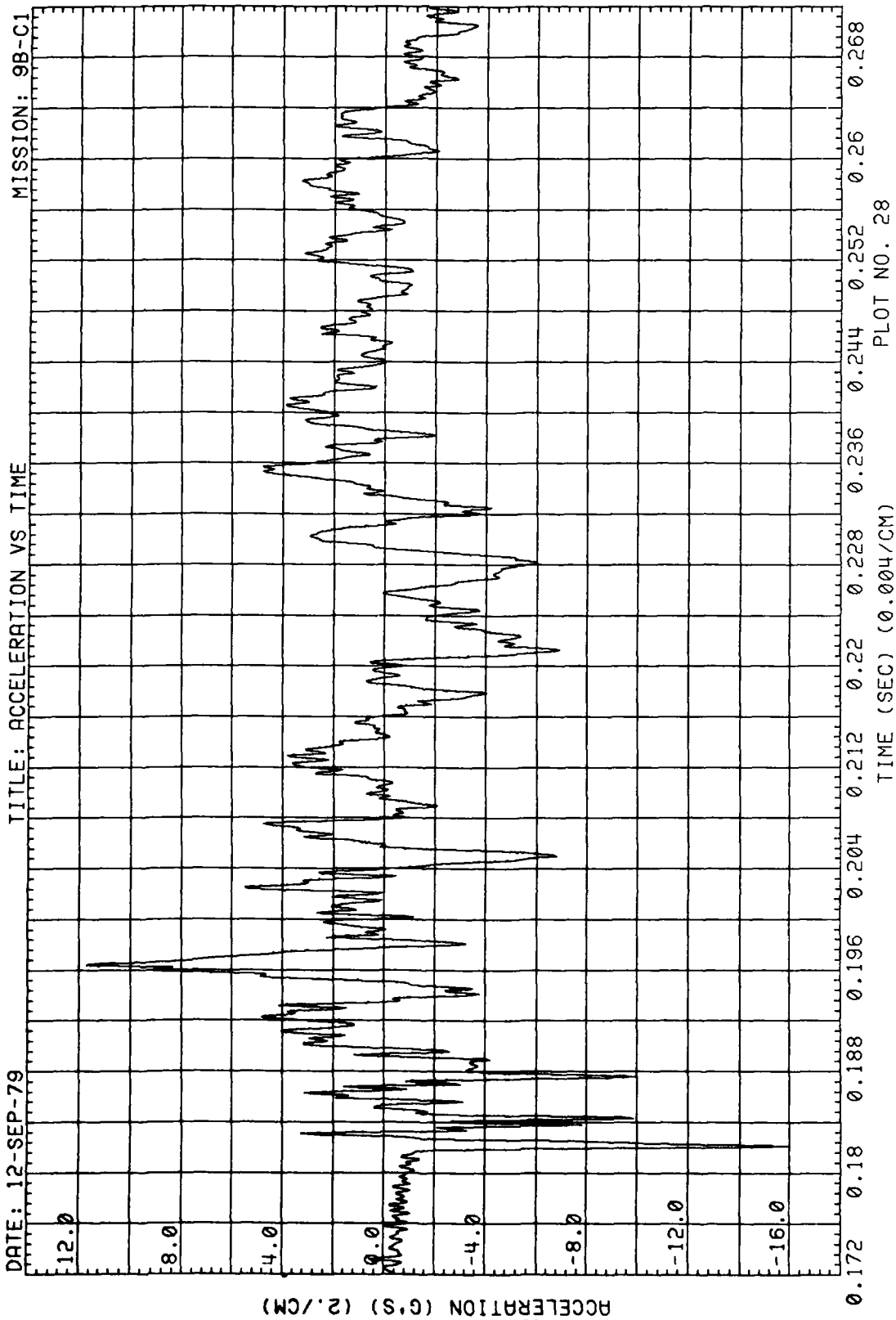

Figure 42. Wing Acceleration, Run 9B-C1, Intercept 2

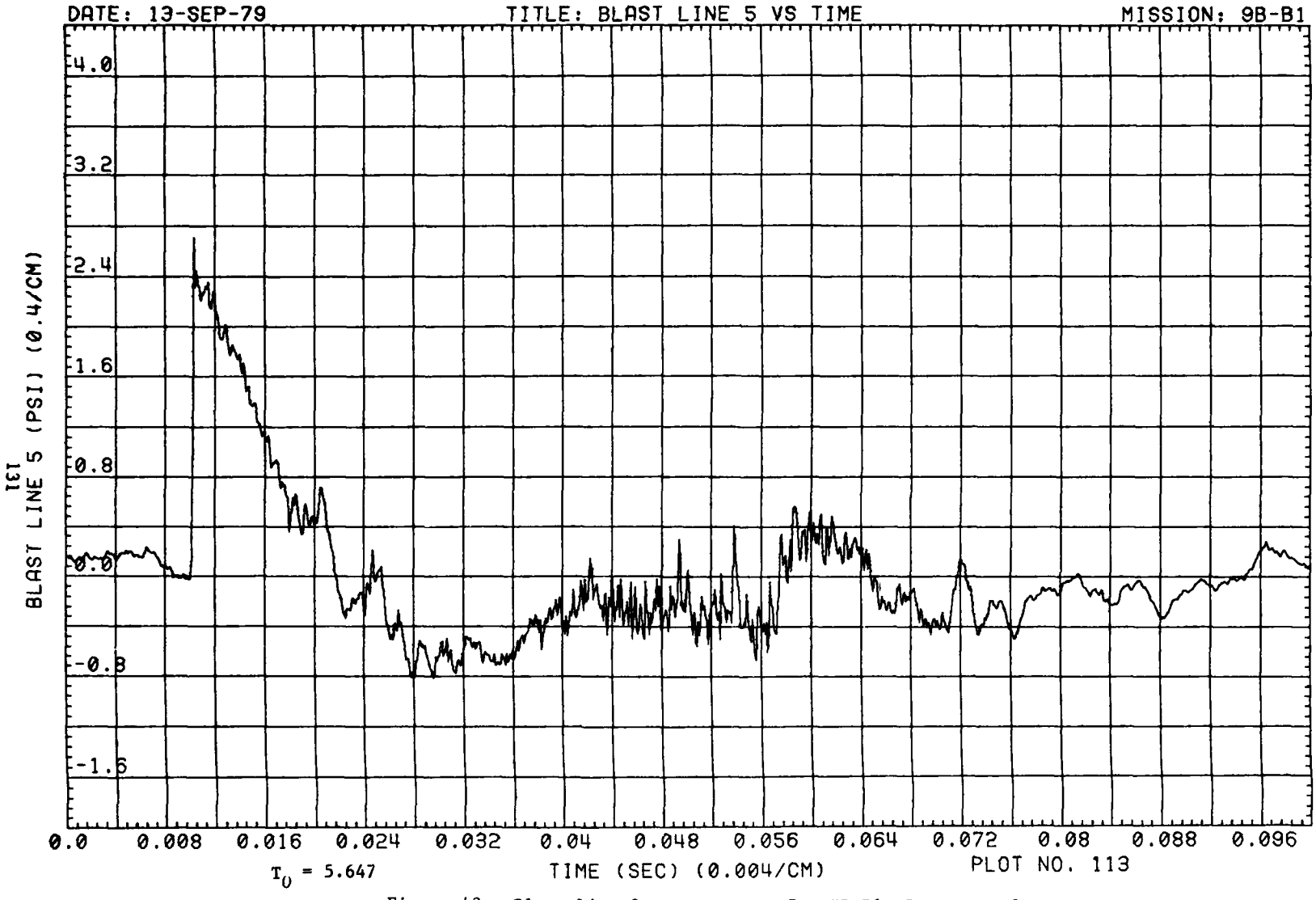

Figure 43. Blast-Line Overpressures, Run 9B-B1, Intercept 2

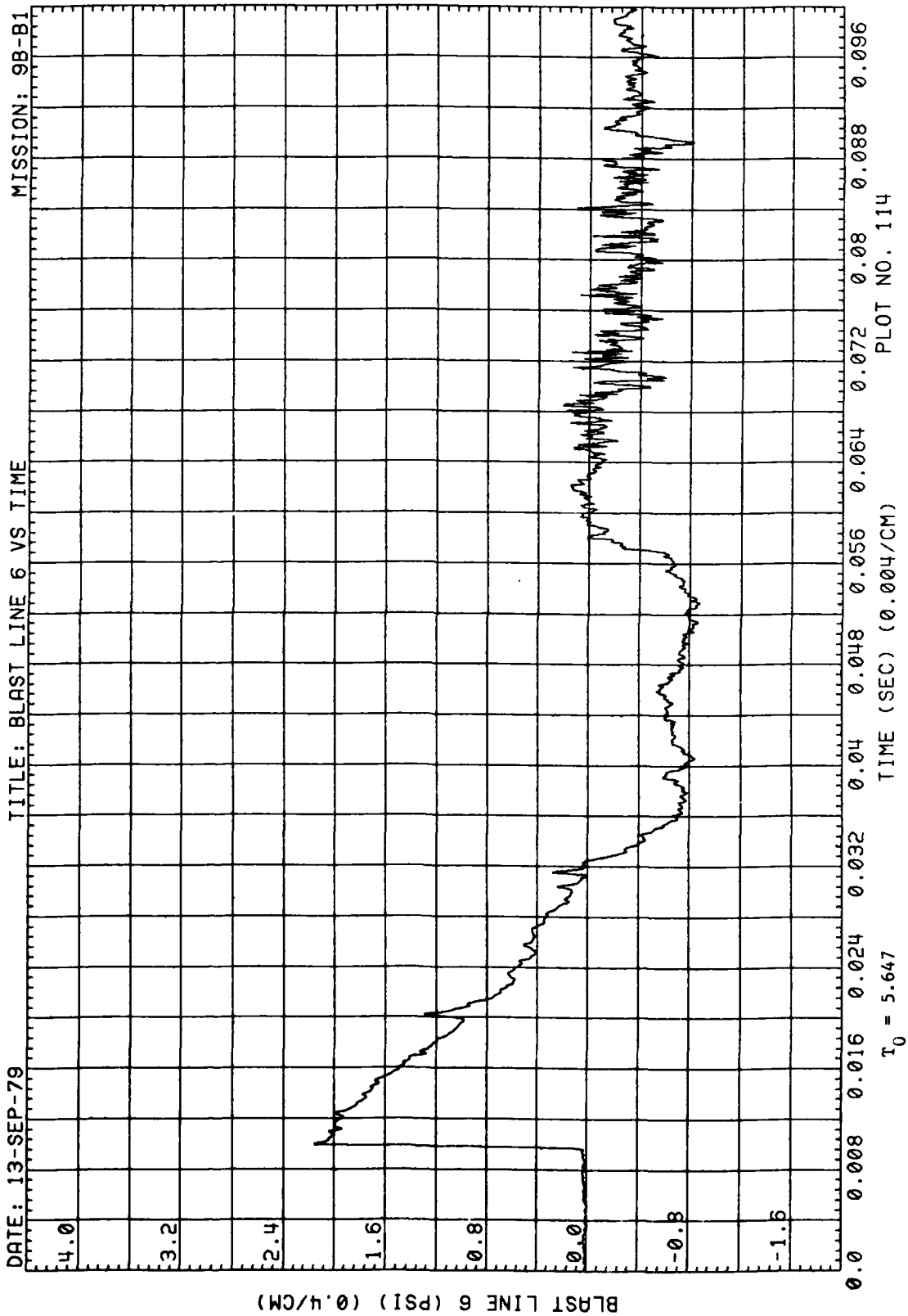

Figure 43. (Continued)

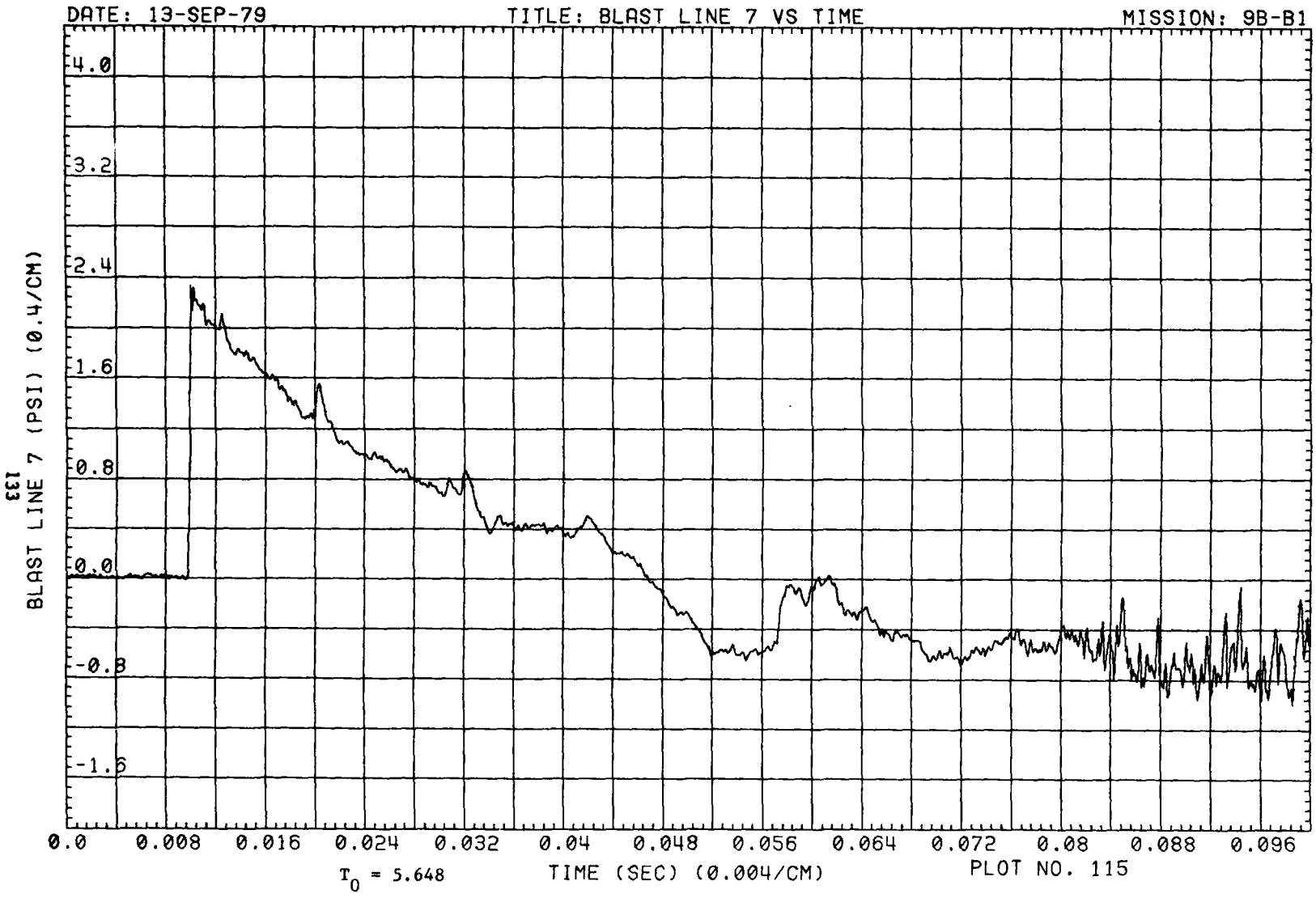

Figure 43. (Continued)

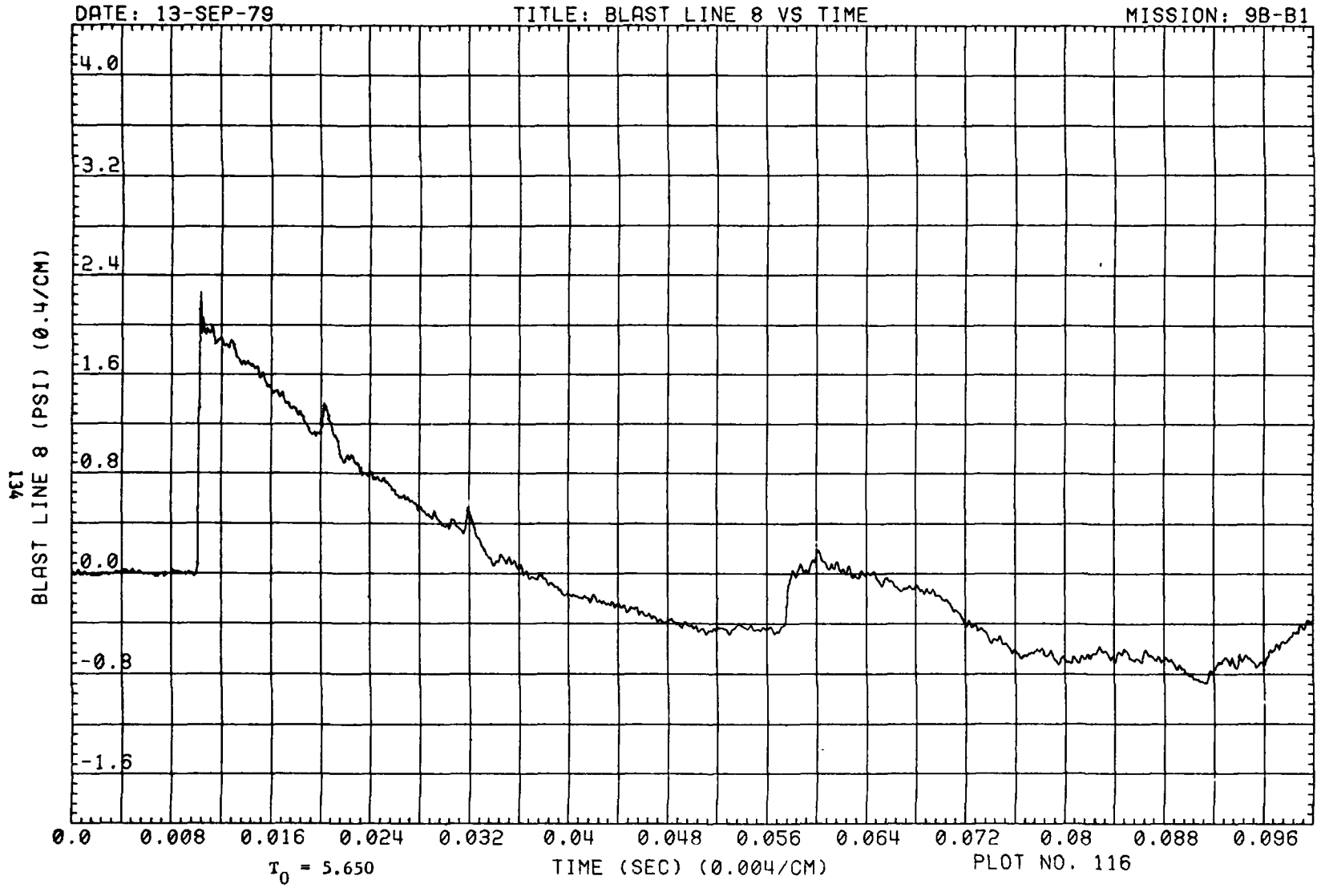

Figure 43. (Concluded)

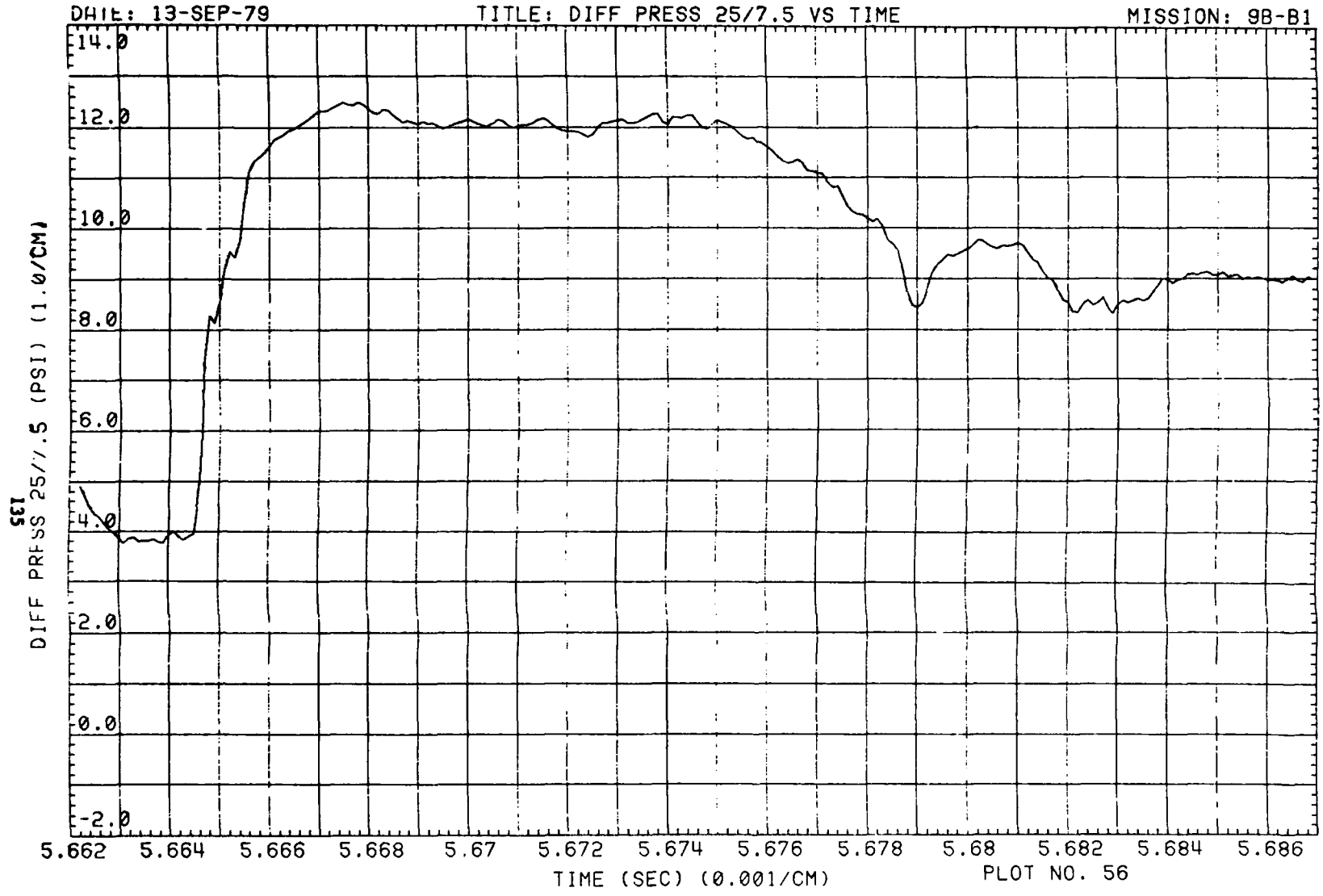

Figure 44. Differential Wing Pressures, Run 9B-B1, Intercept 2

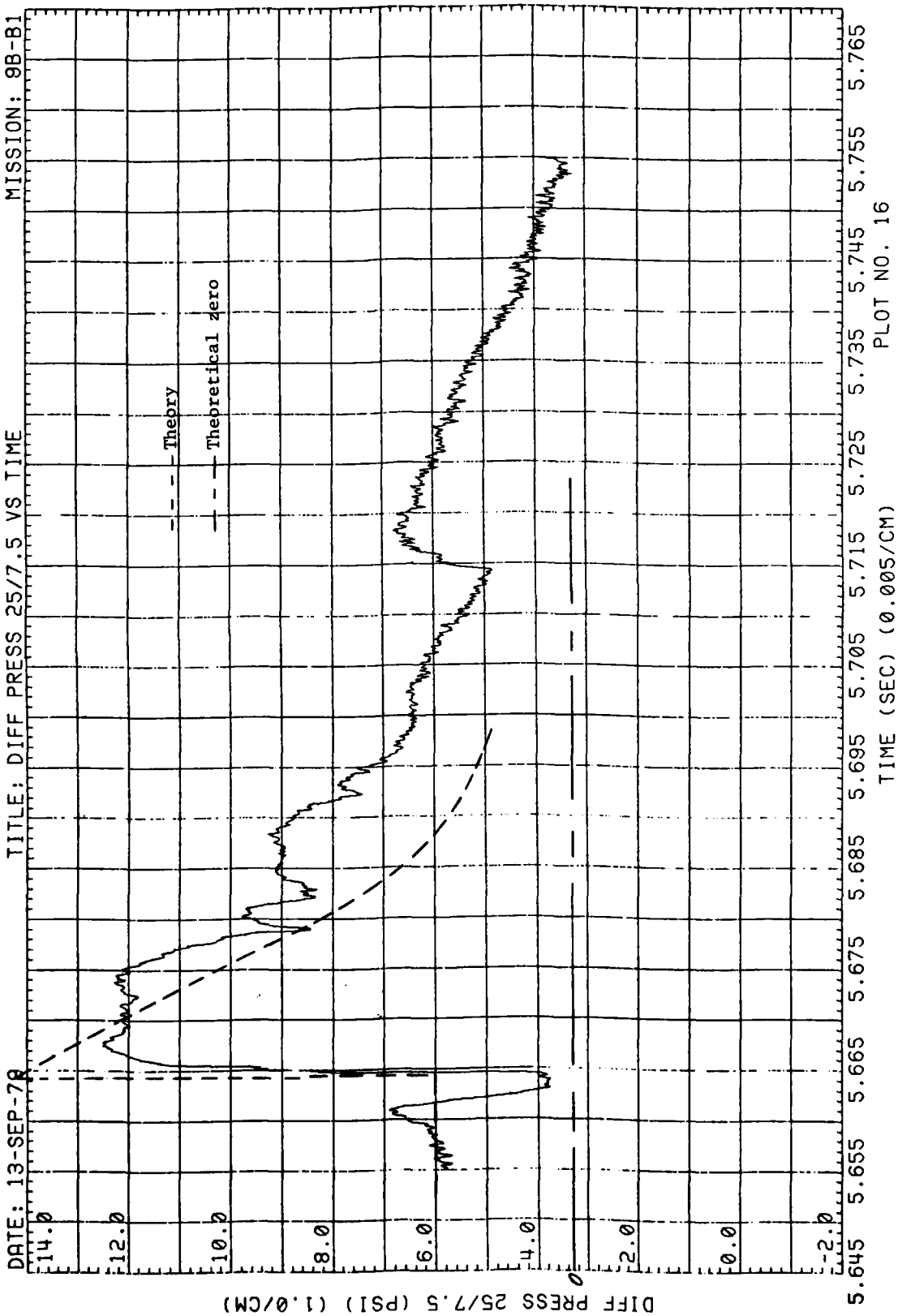

Figure 44. (Continued)

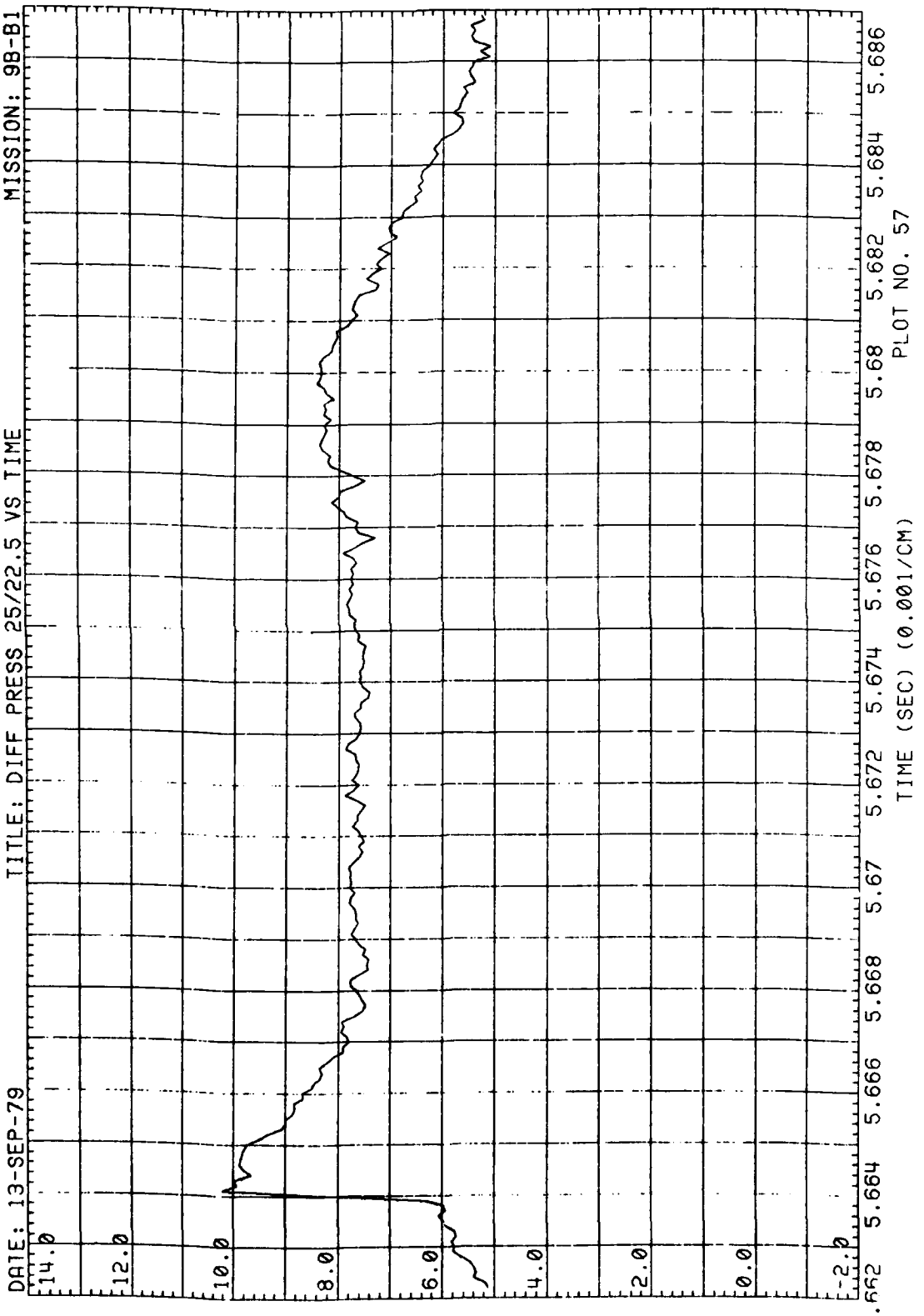

Figure 44. (Continued)

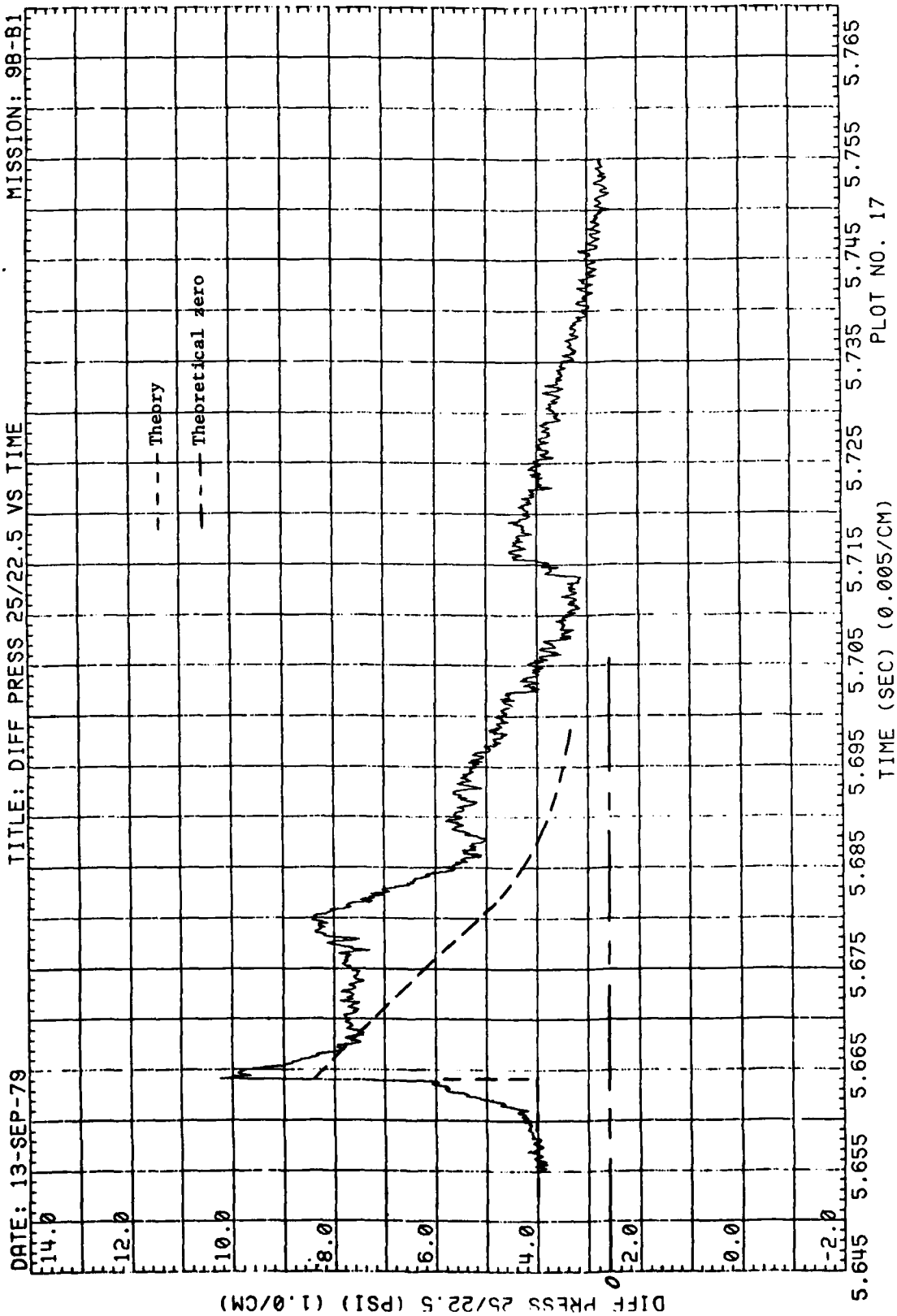

Figure 44. (Continued)

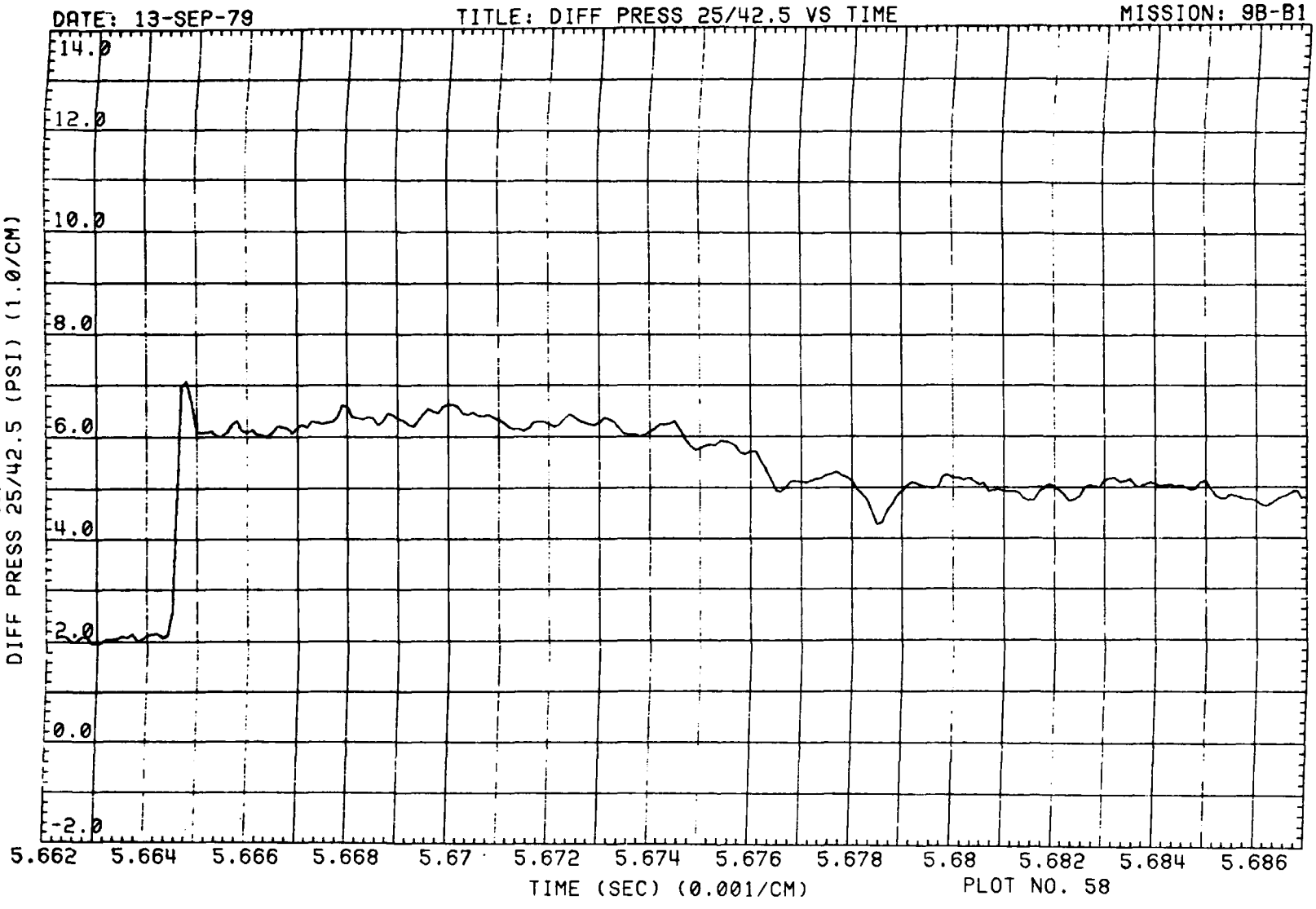

Figure 44. (Continued)

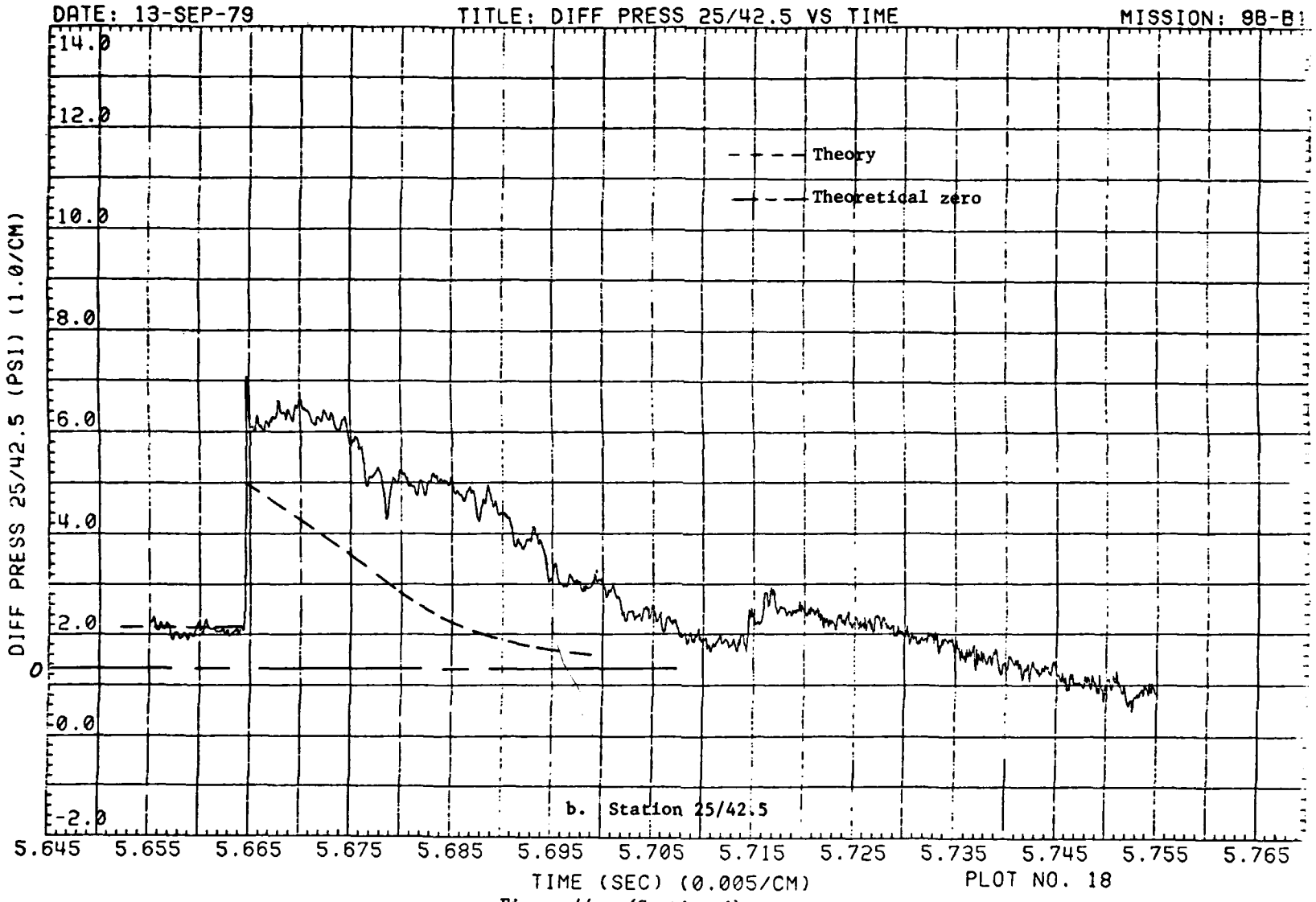

Figure 44. (Continued)

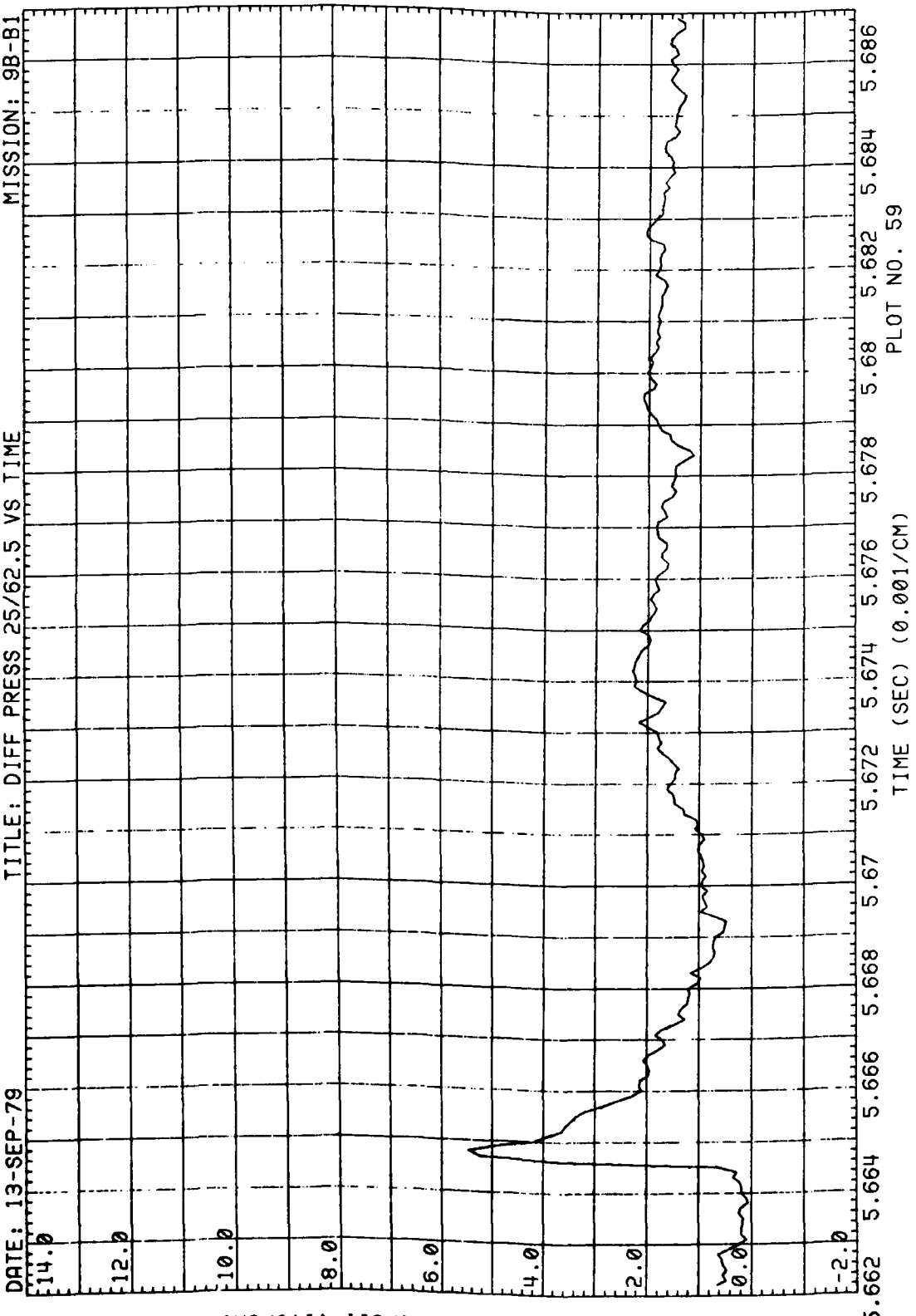

Figure 44. (Continued)

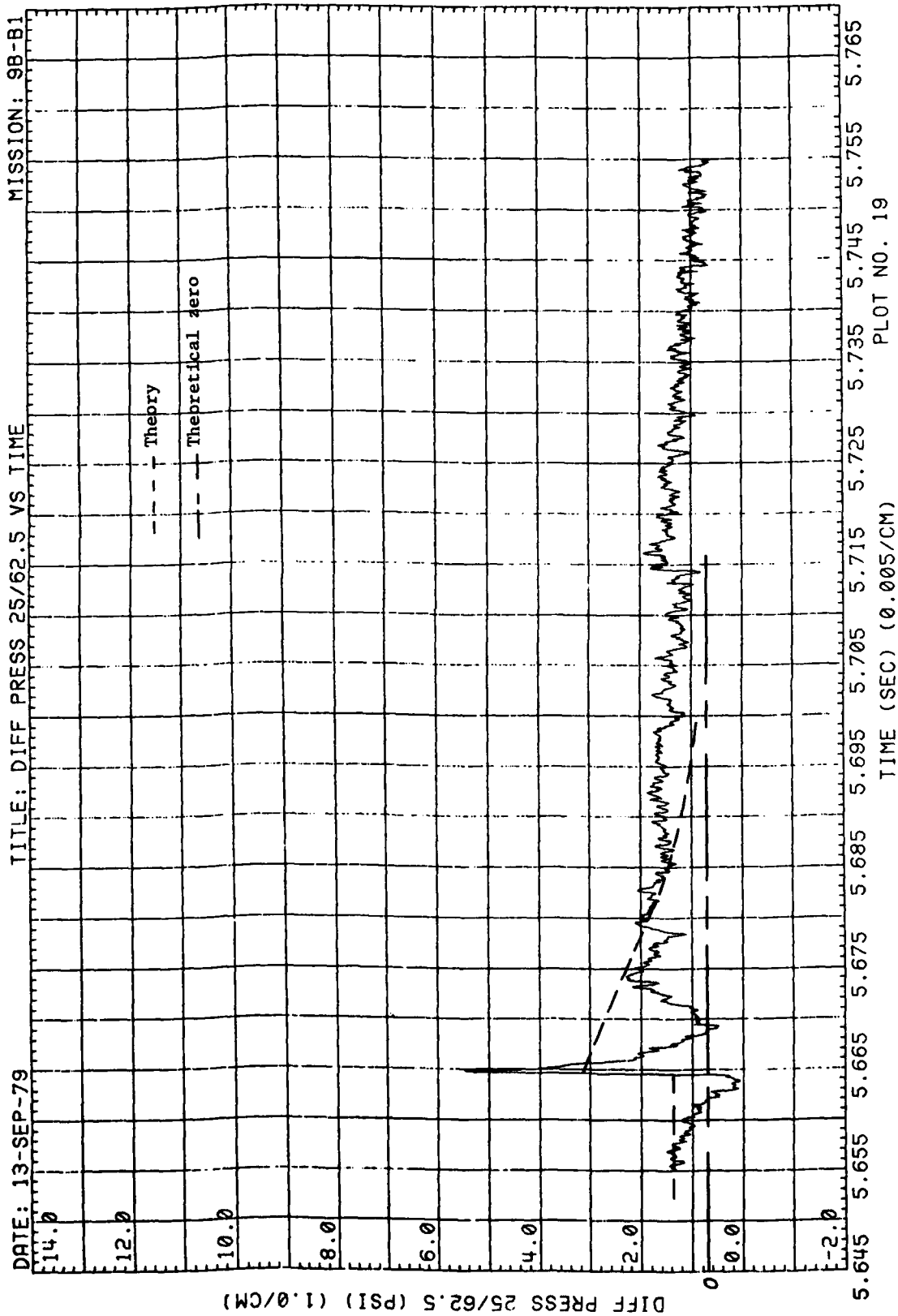

Figure 44. (Continued)

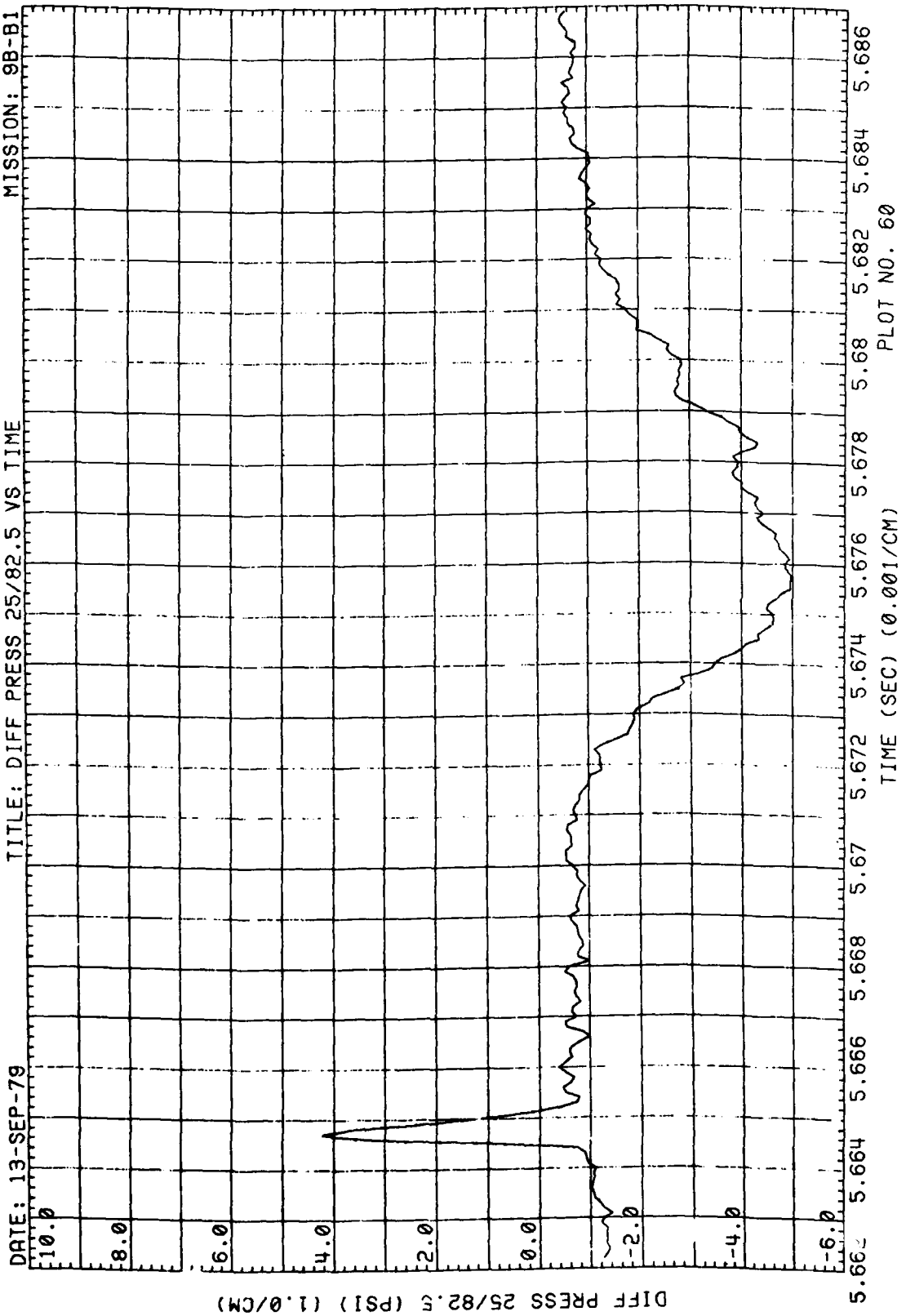

Figure 44. (Continued)

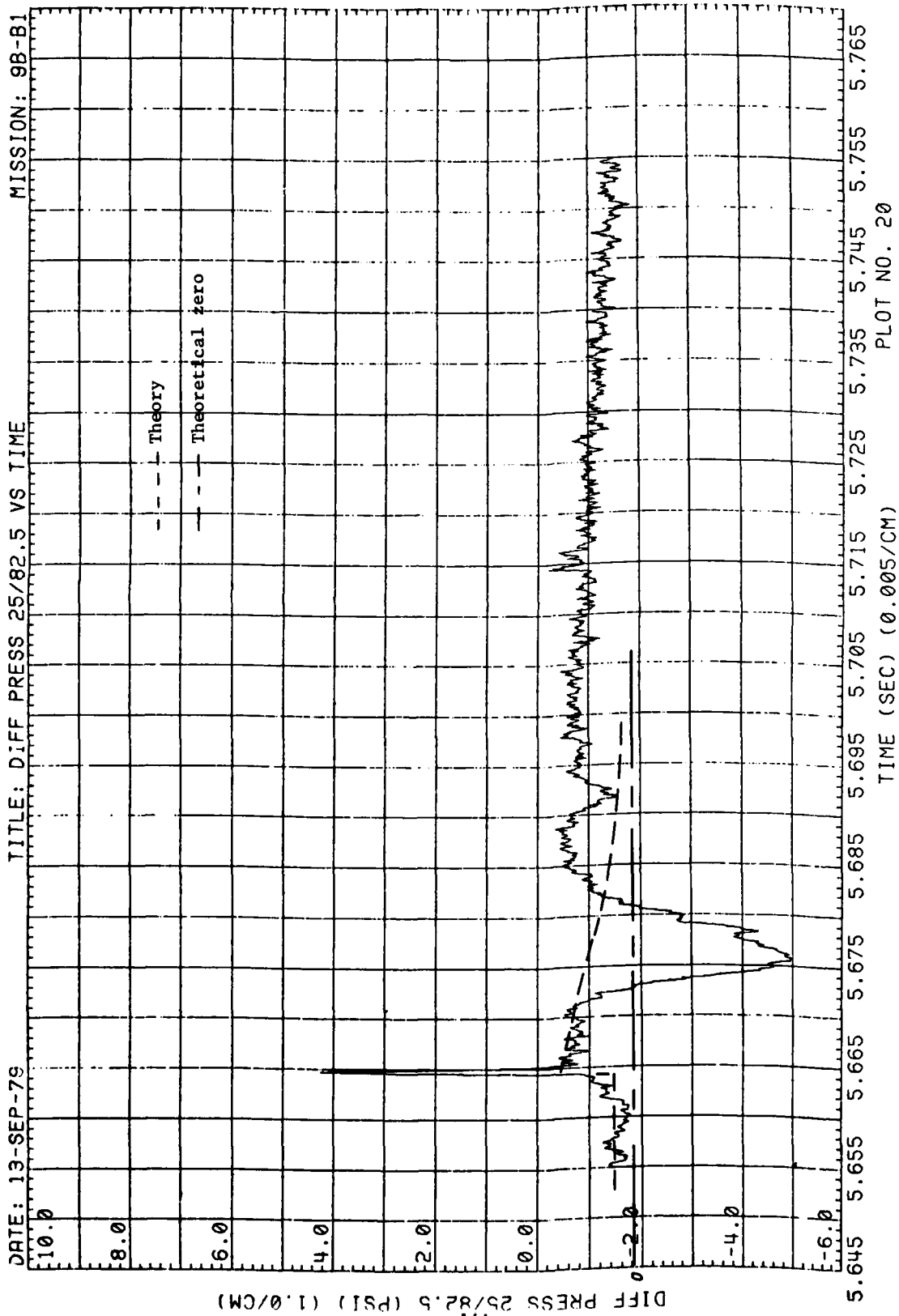

Figure 44. (Continued)

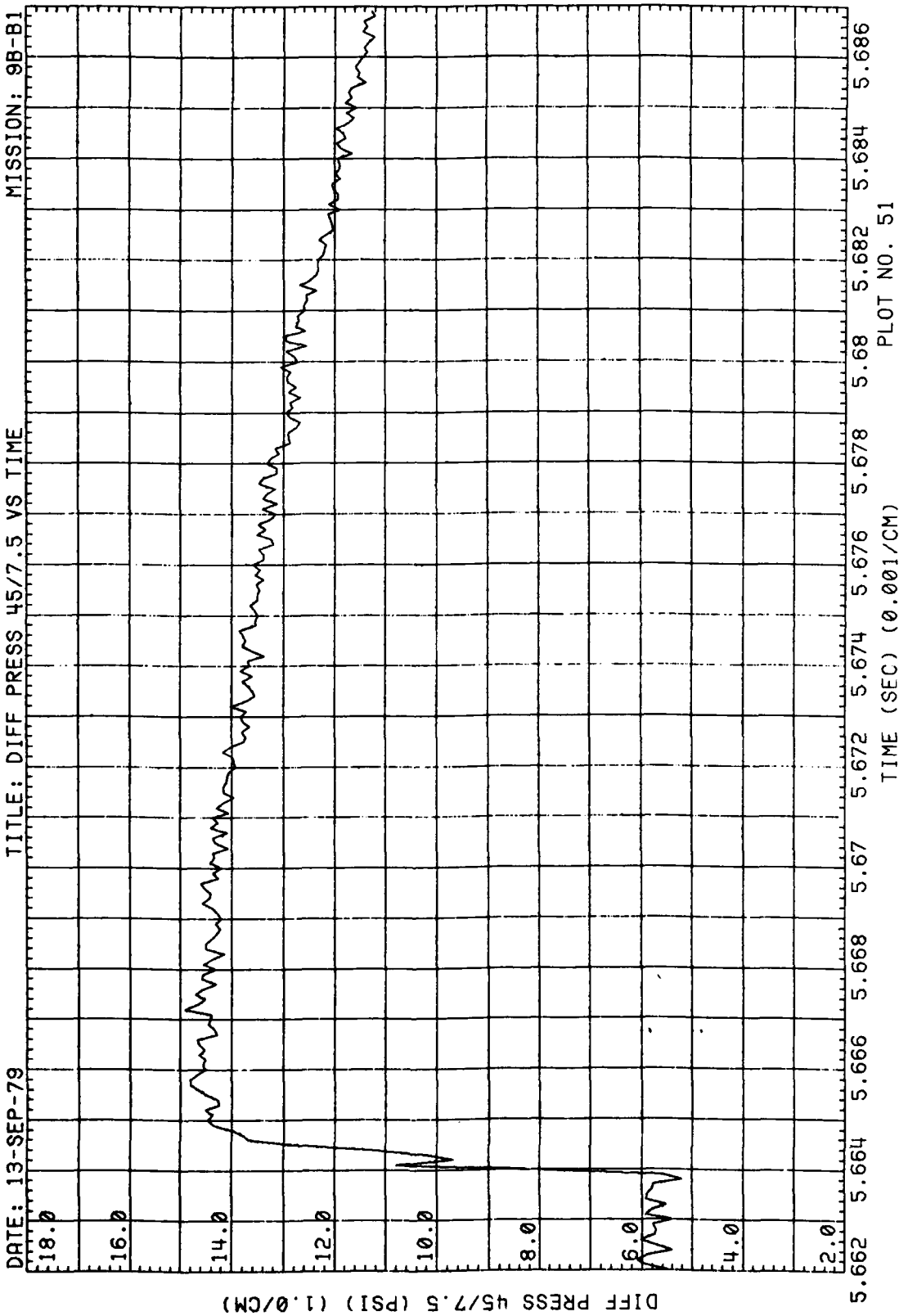

Figure 44. (Continued)

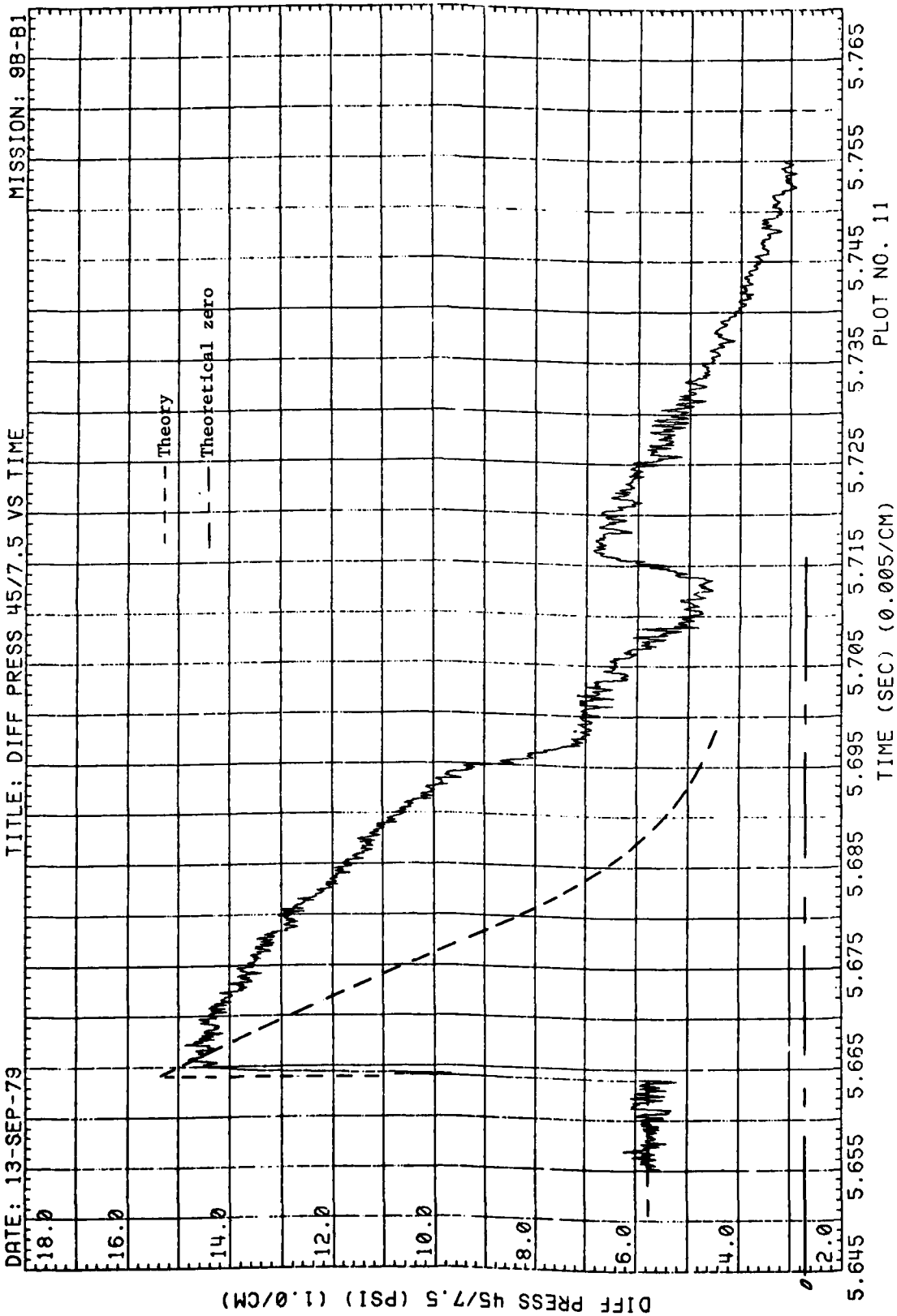

Figure 44. (Continued)

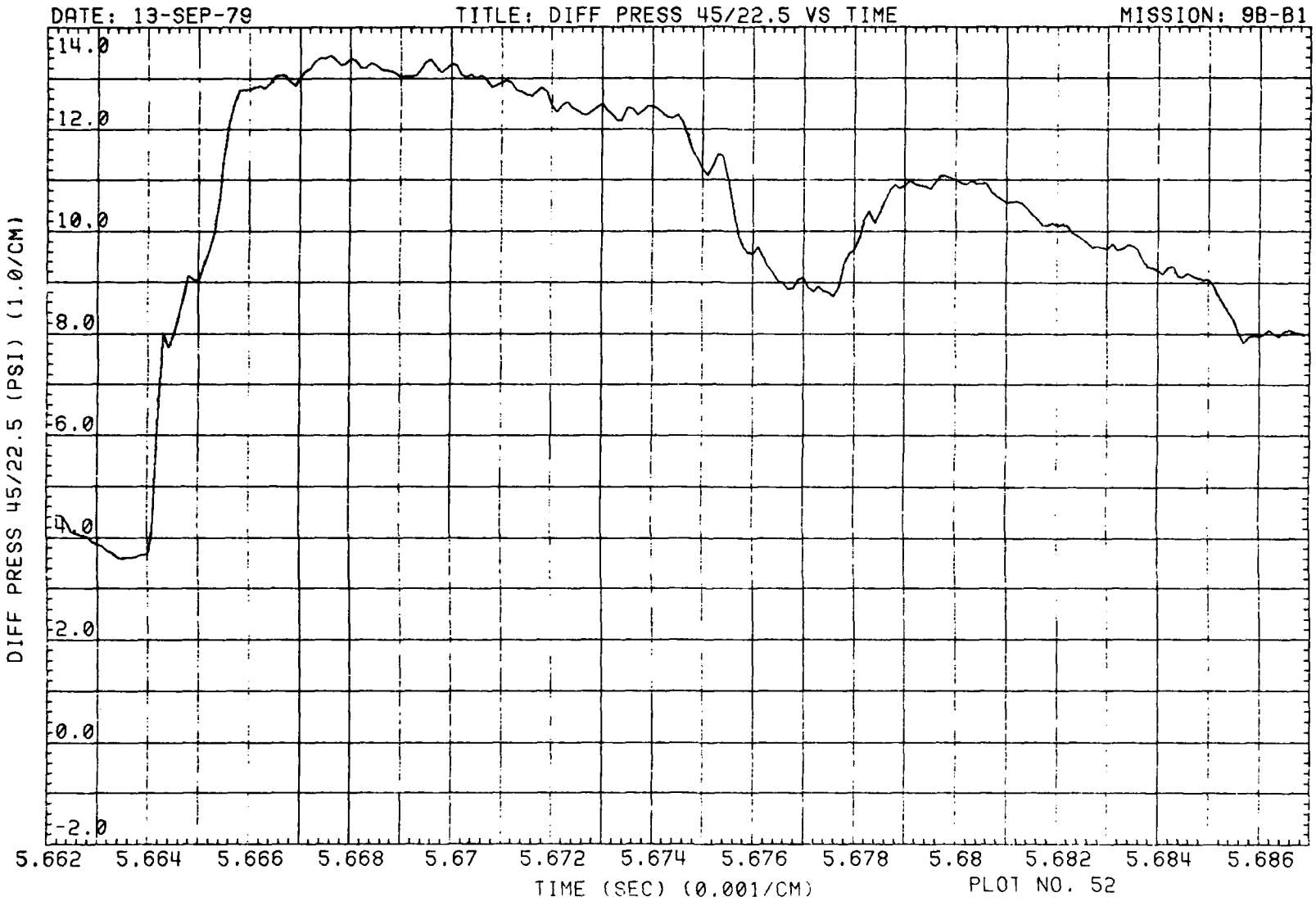

Figure 44. (Continued)

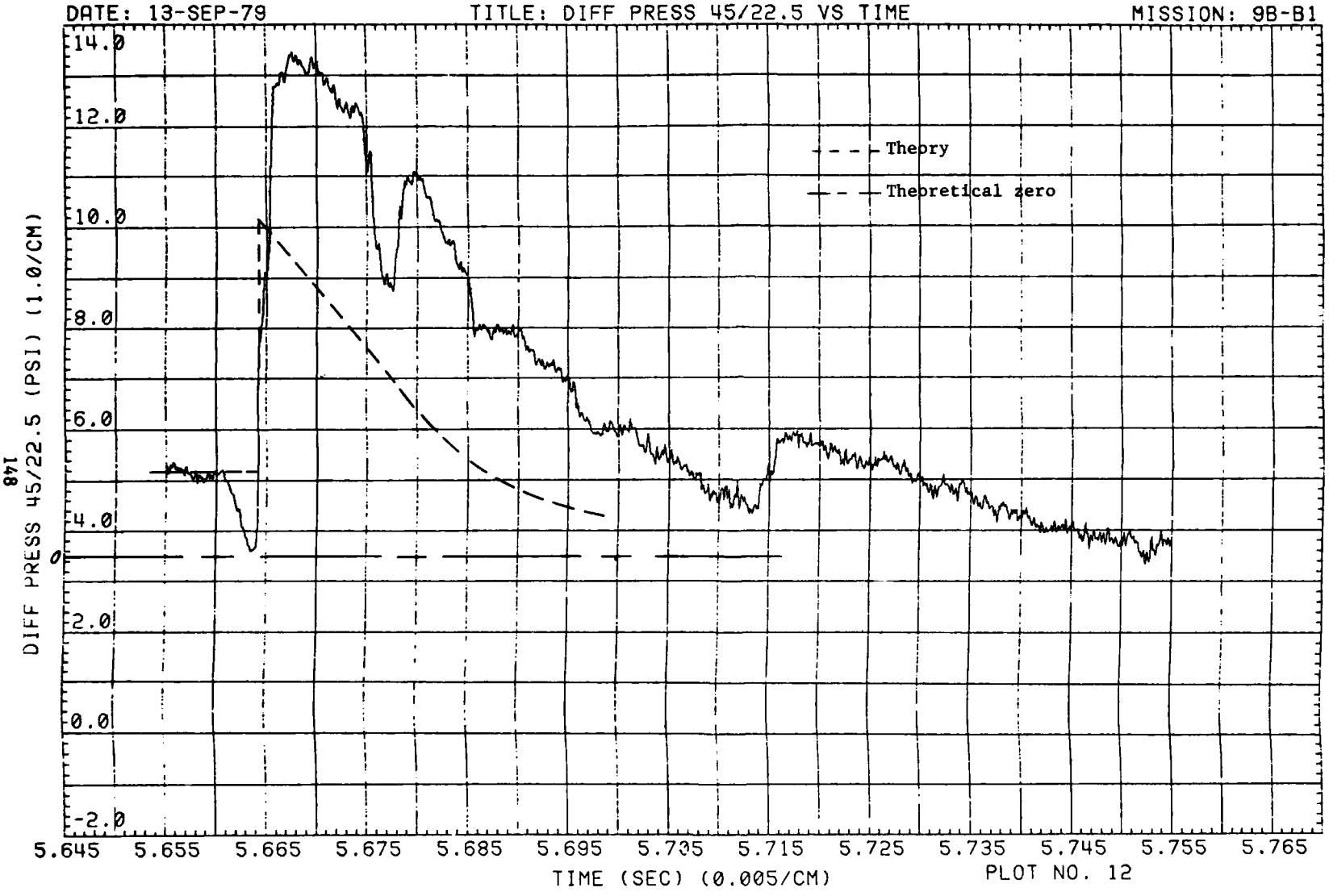

Figure 44. (Continued)

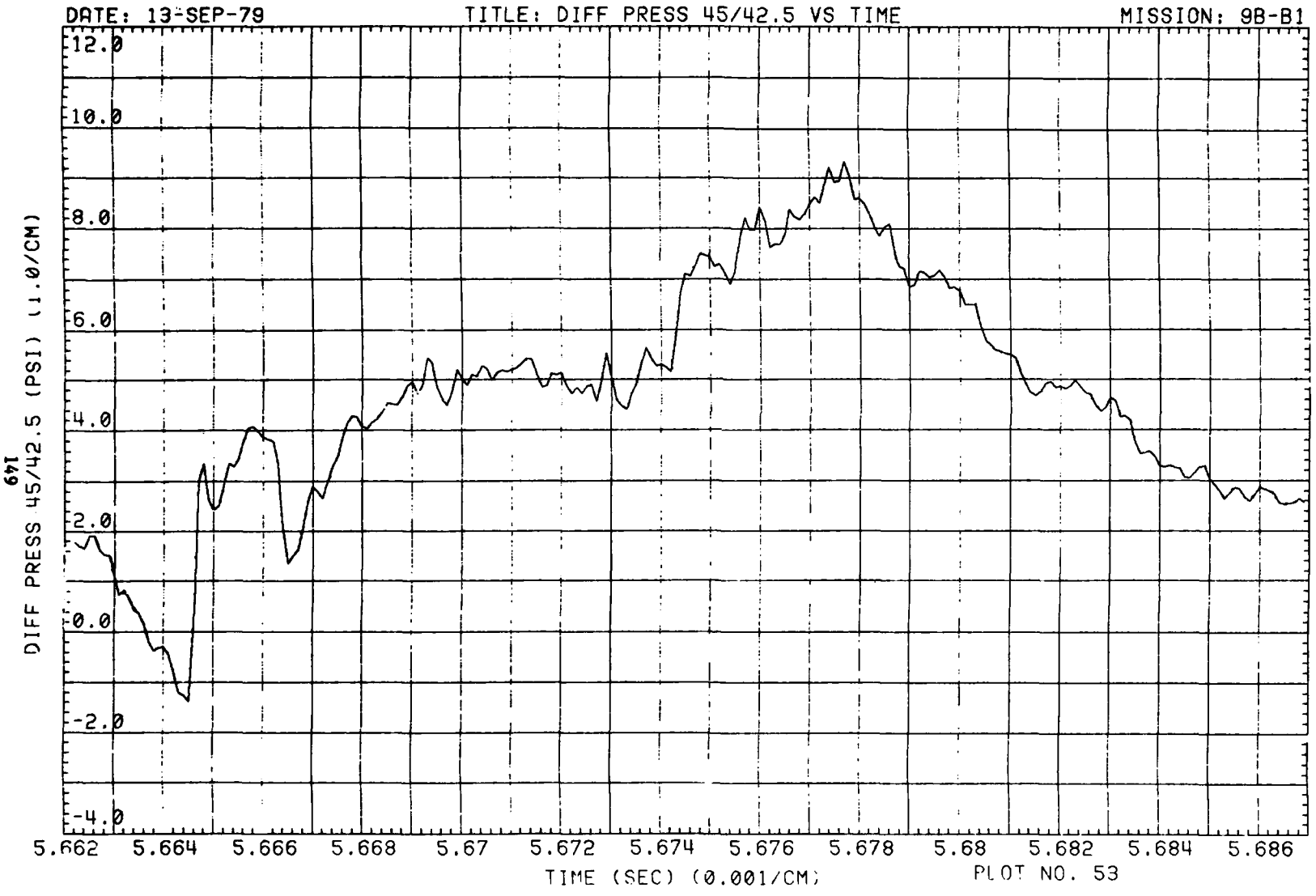

Figure 44. (Continued)

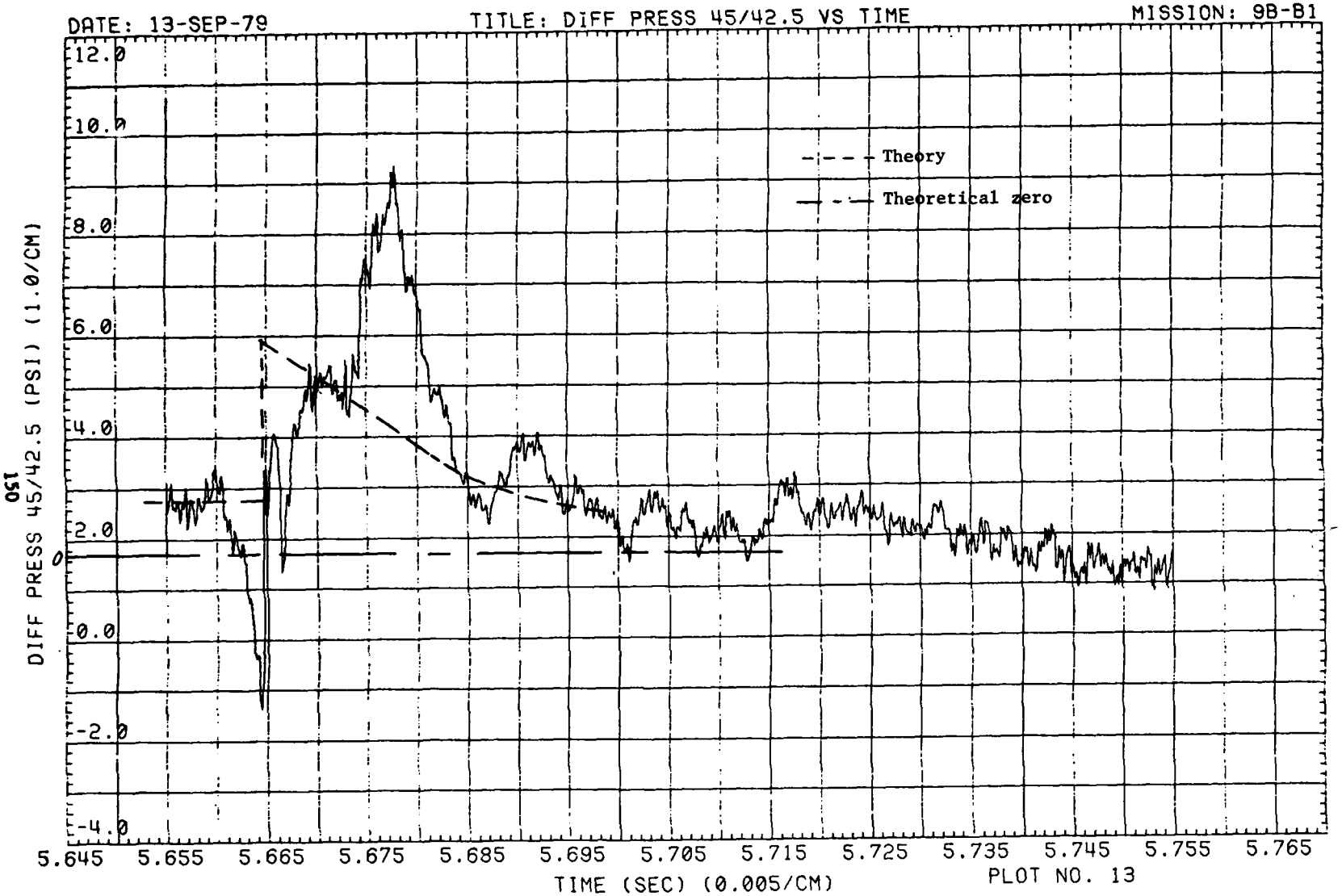

Figure 44. (Continued)

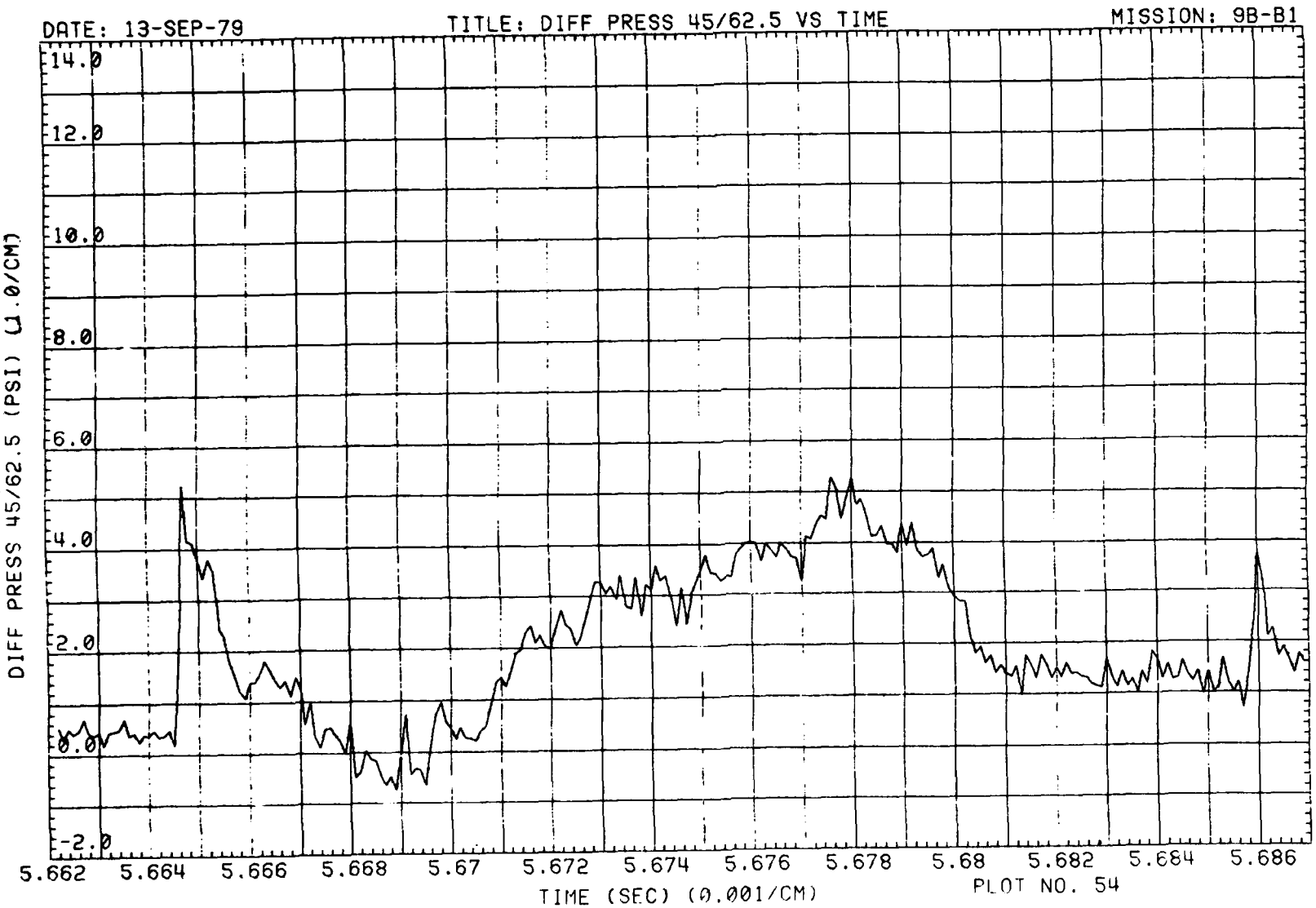

Figure 44. (Continued)

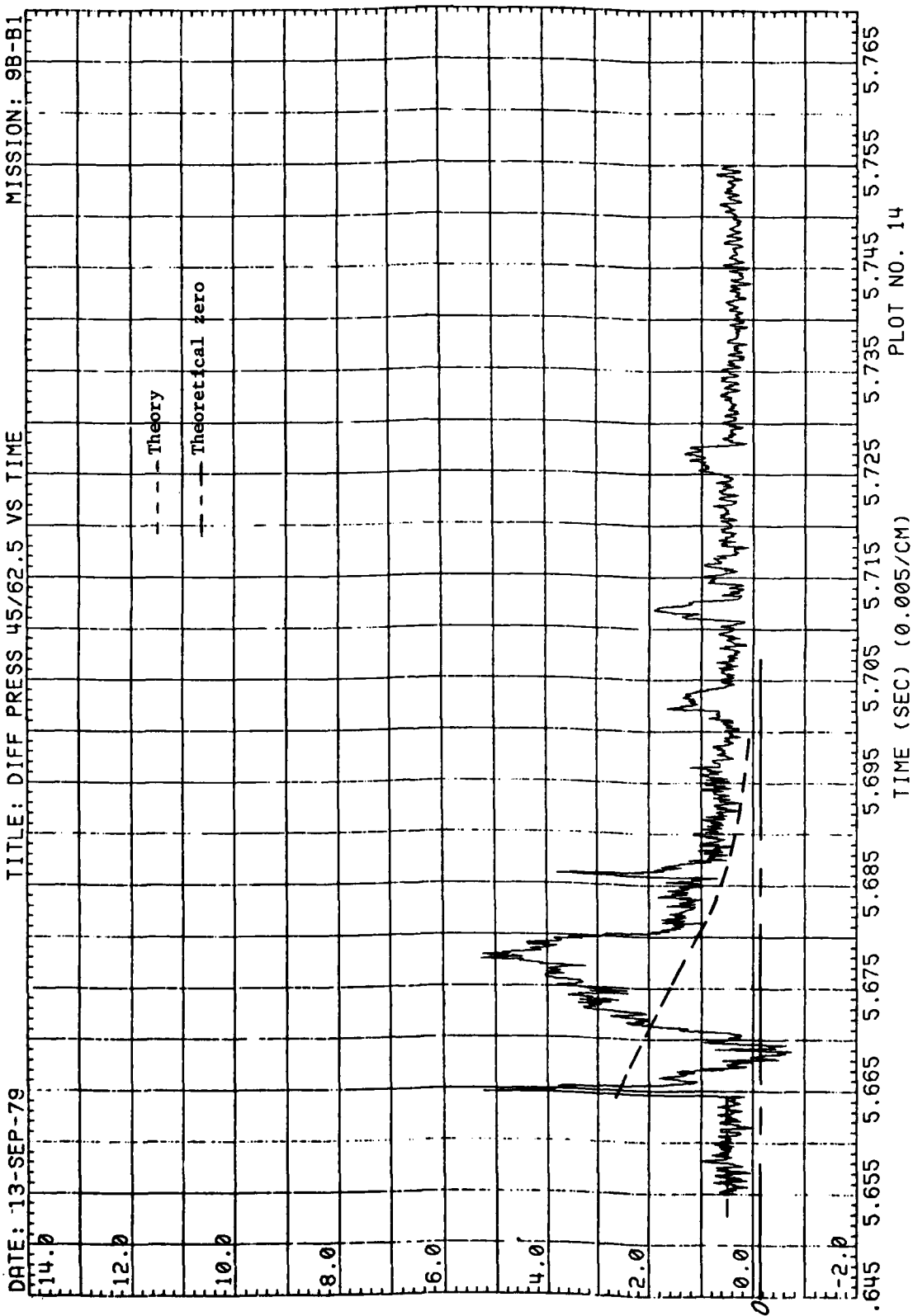

Figure 44. (Continued)

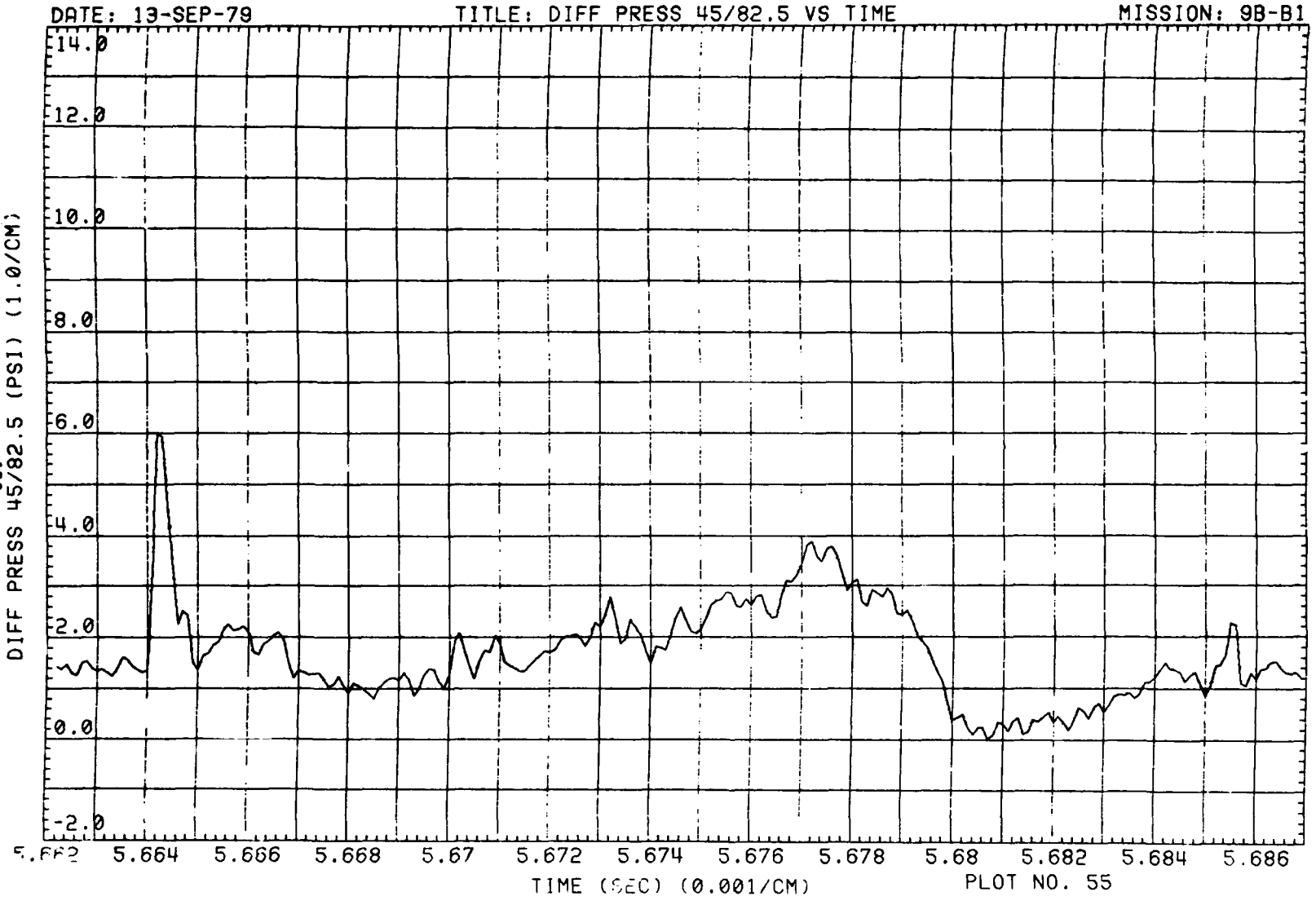

Figure 44. (Continued)

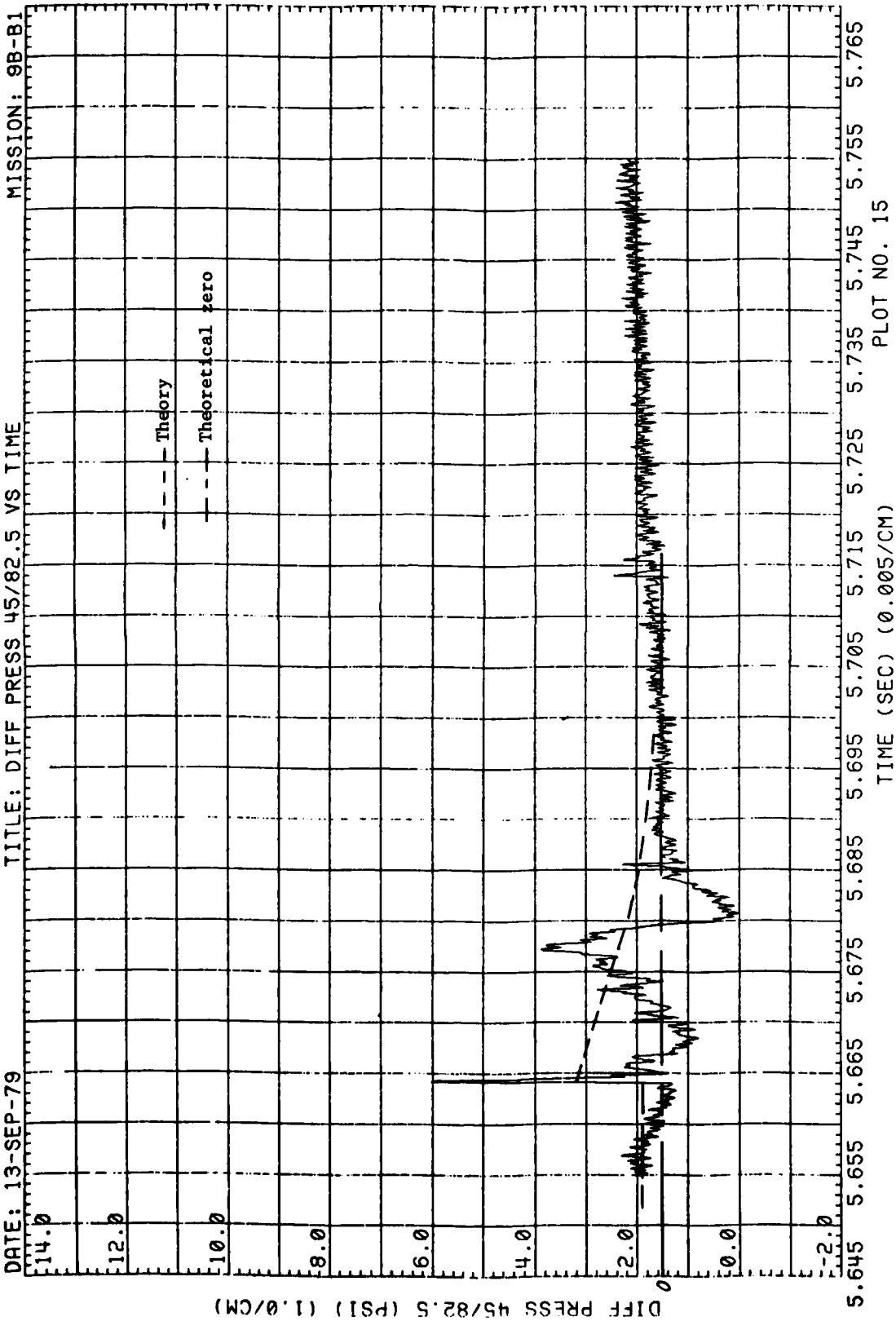

Figure 44. (Continued)

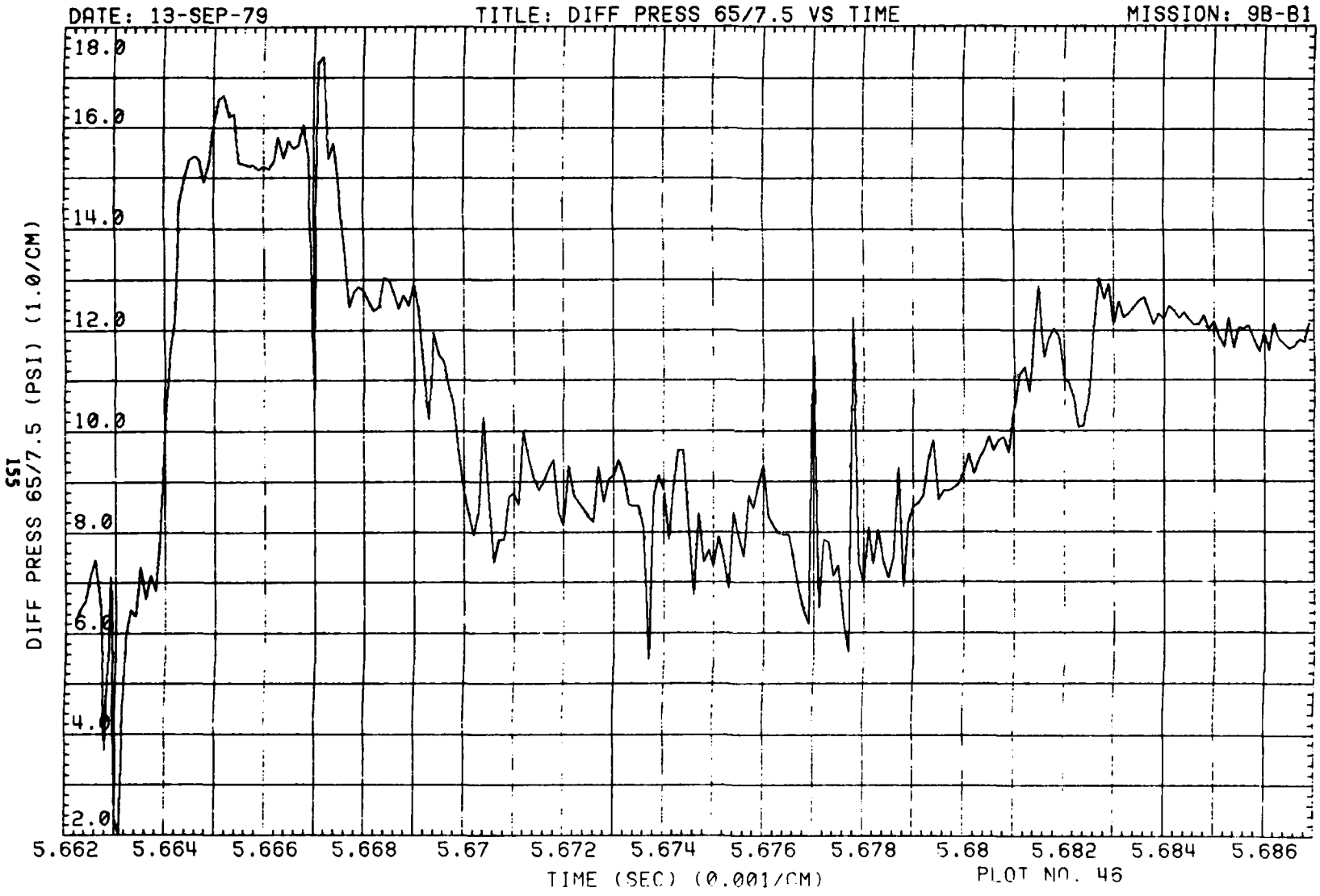

Figure 44. (Continued)

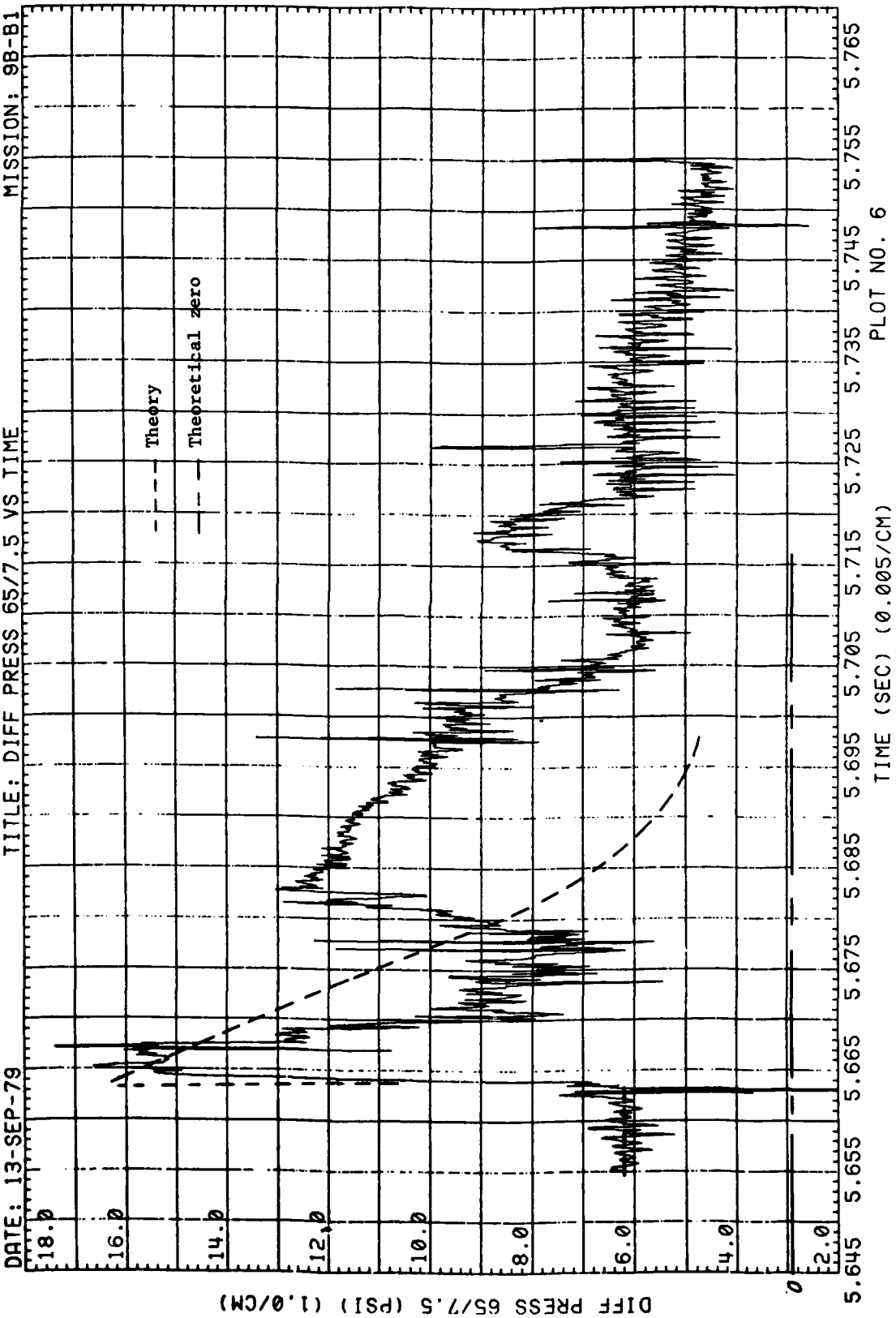

Figure 44. (Continued)

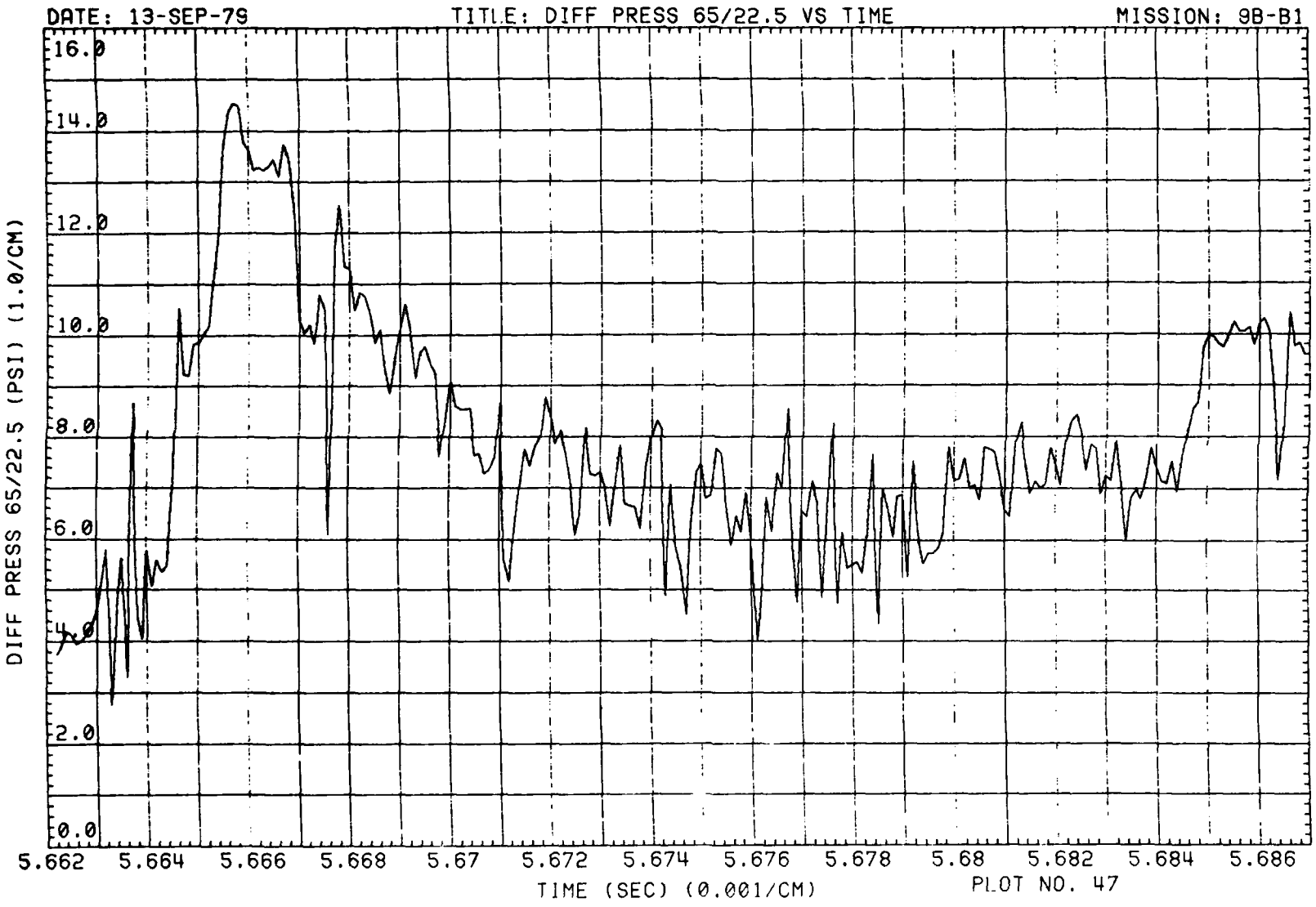

Figure 44. (Continued)

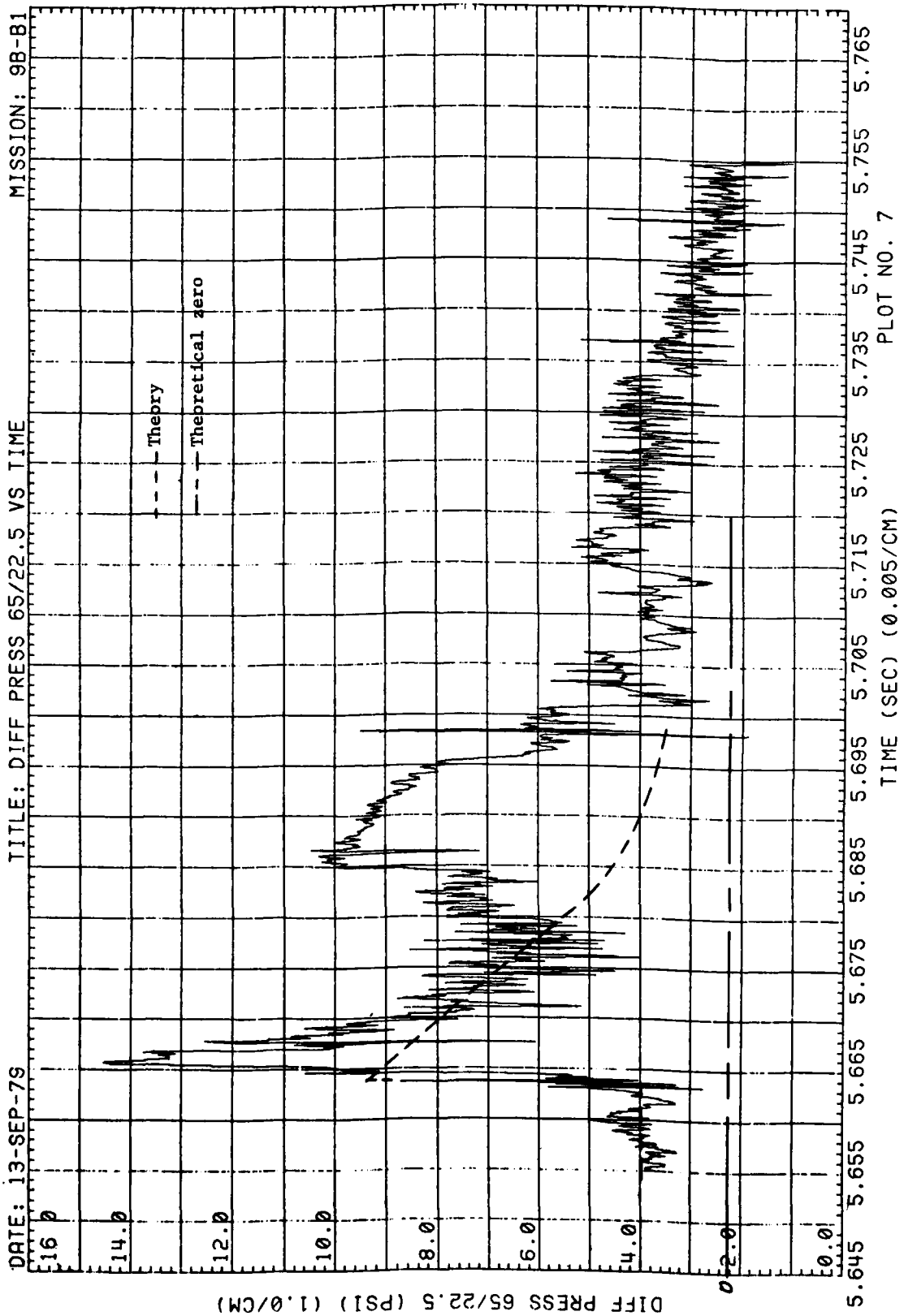

Figure 44. (Continued)

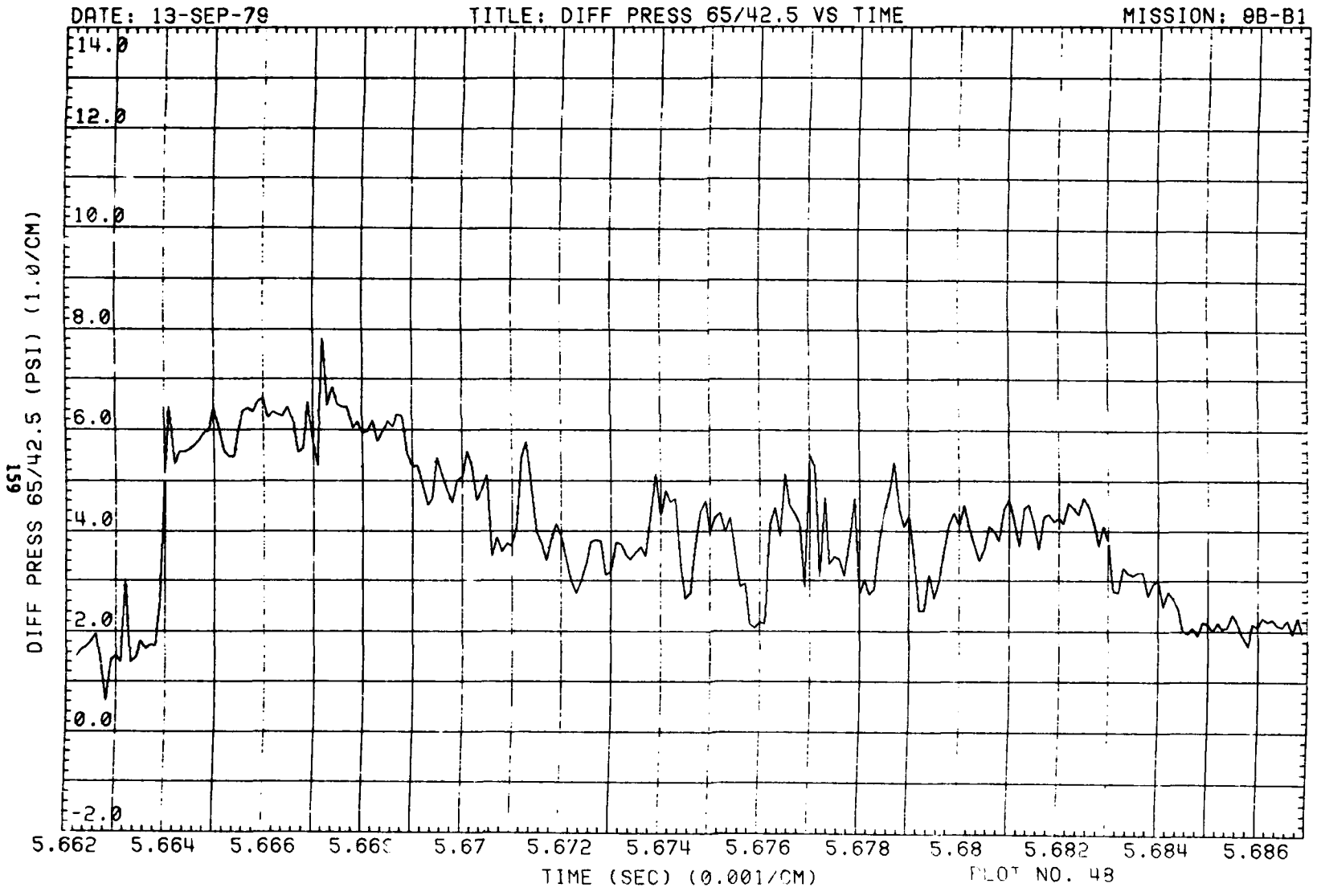

Figure 44. (Continued)

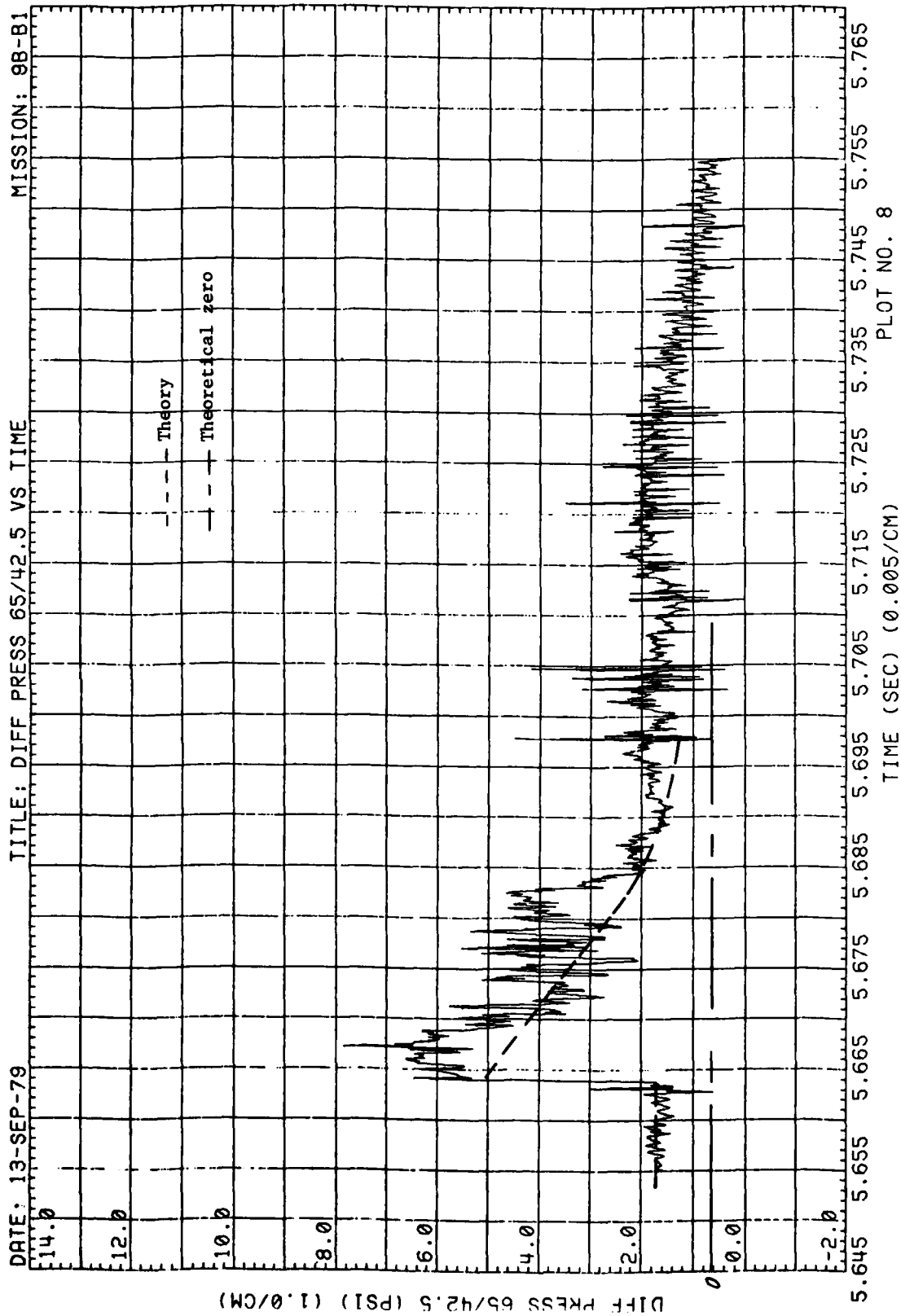

Figure 44. (Continued)

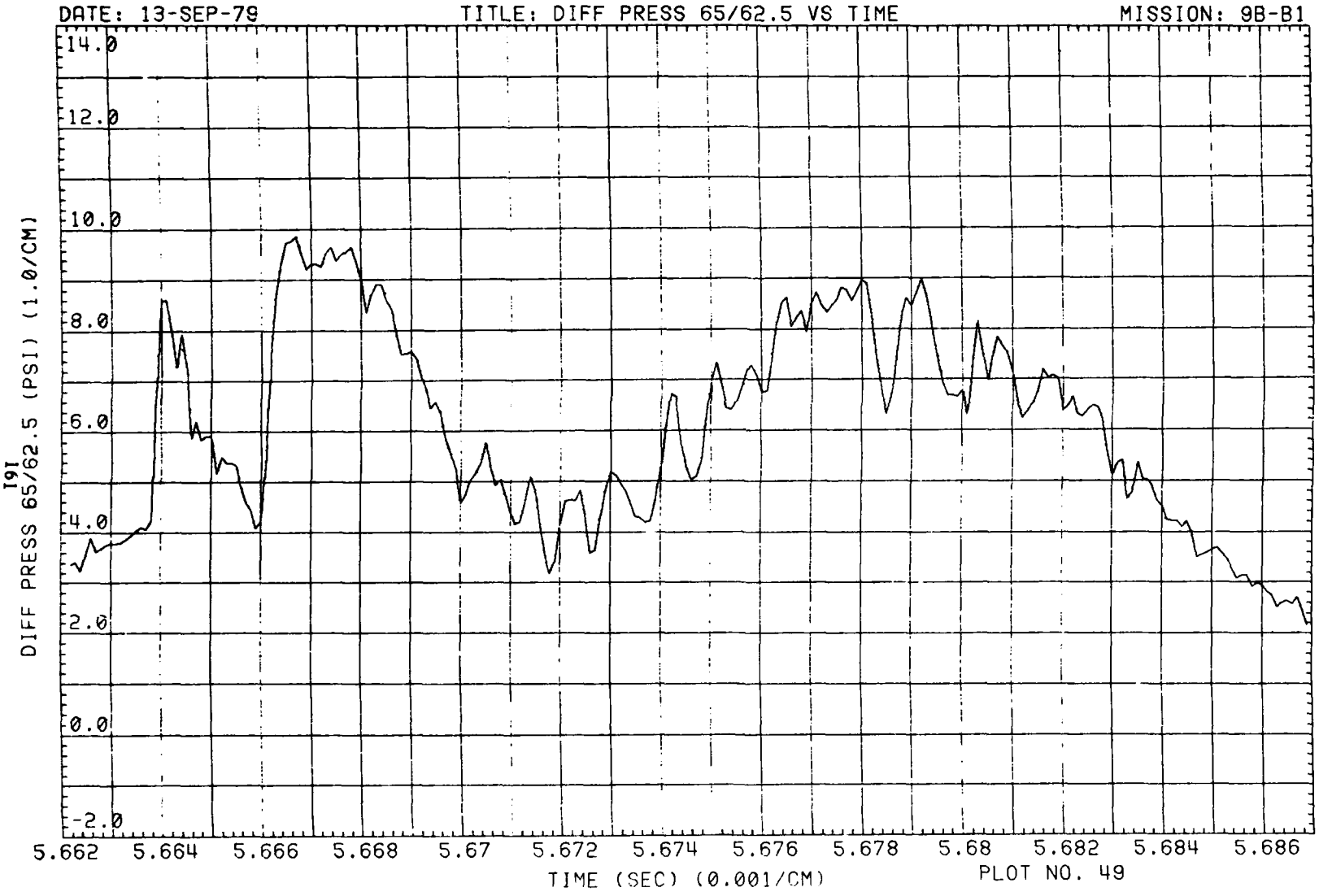

Figure 44. (Continued)

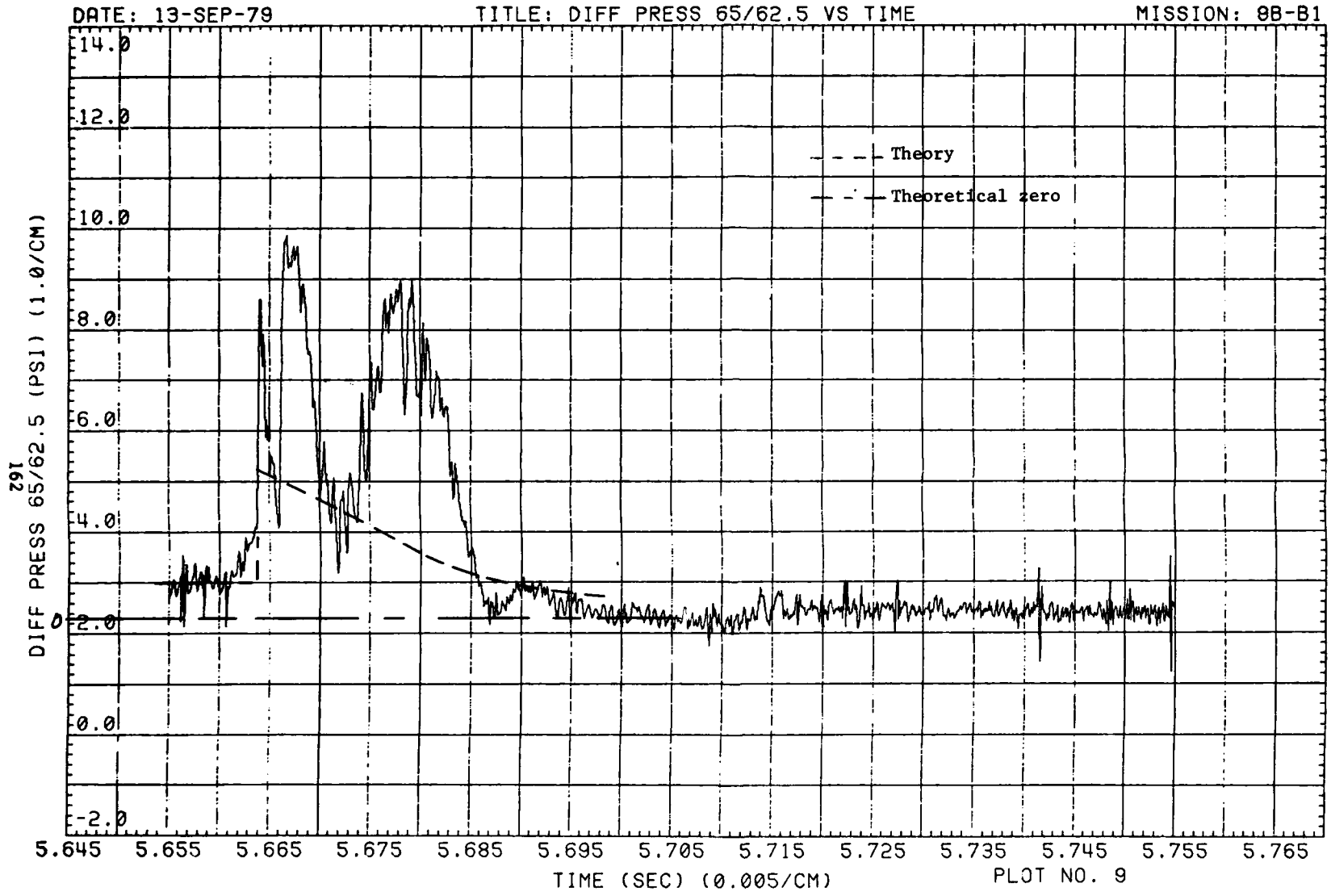

Figure 44. (Continued)

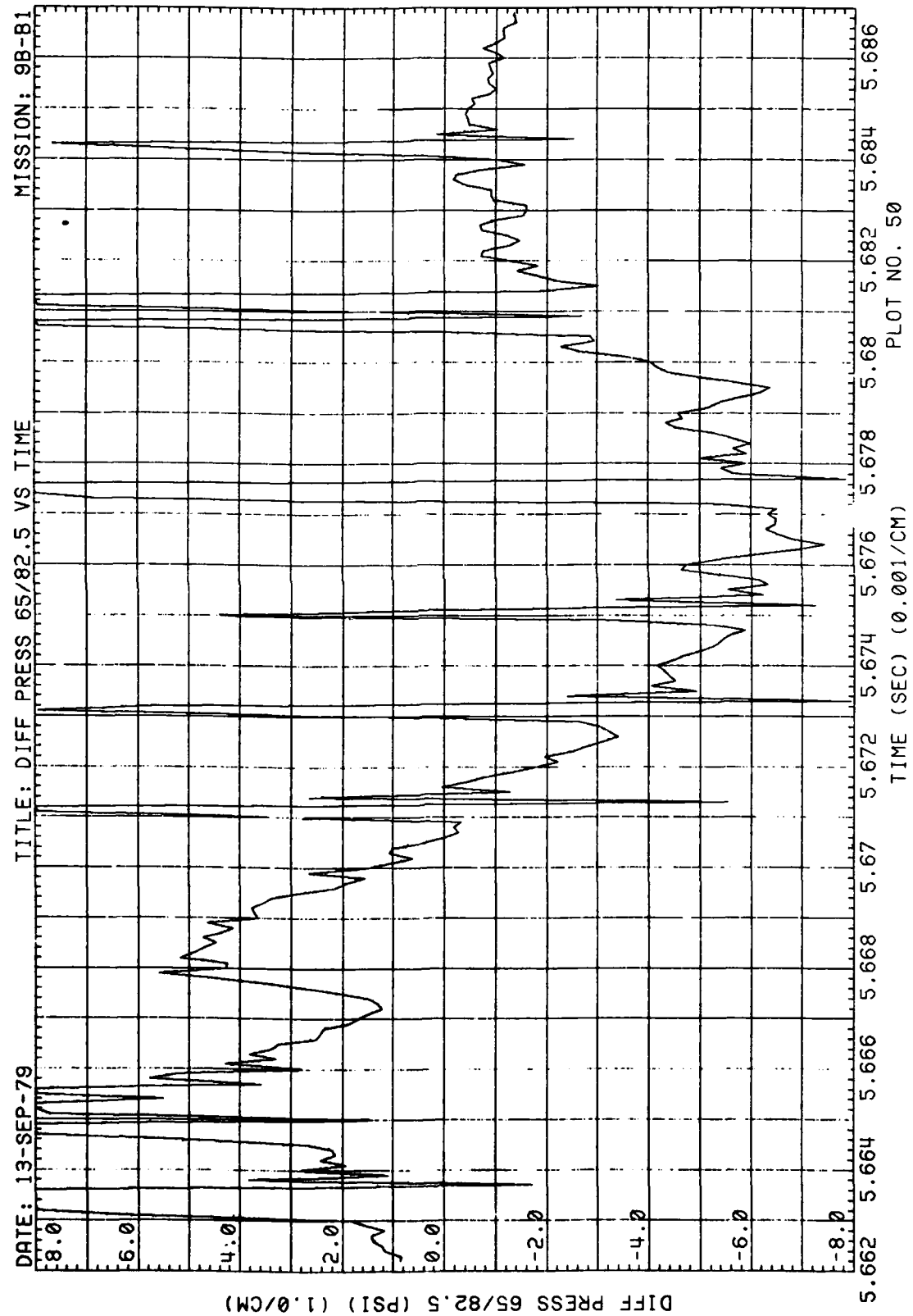

Figure 44. (Continued)

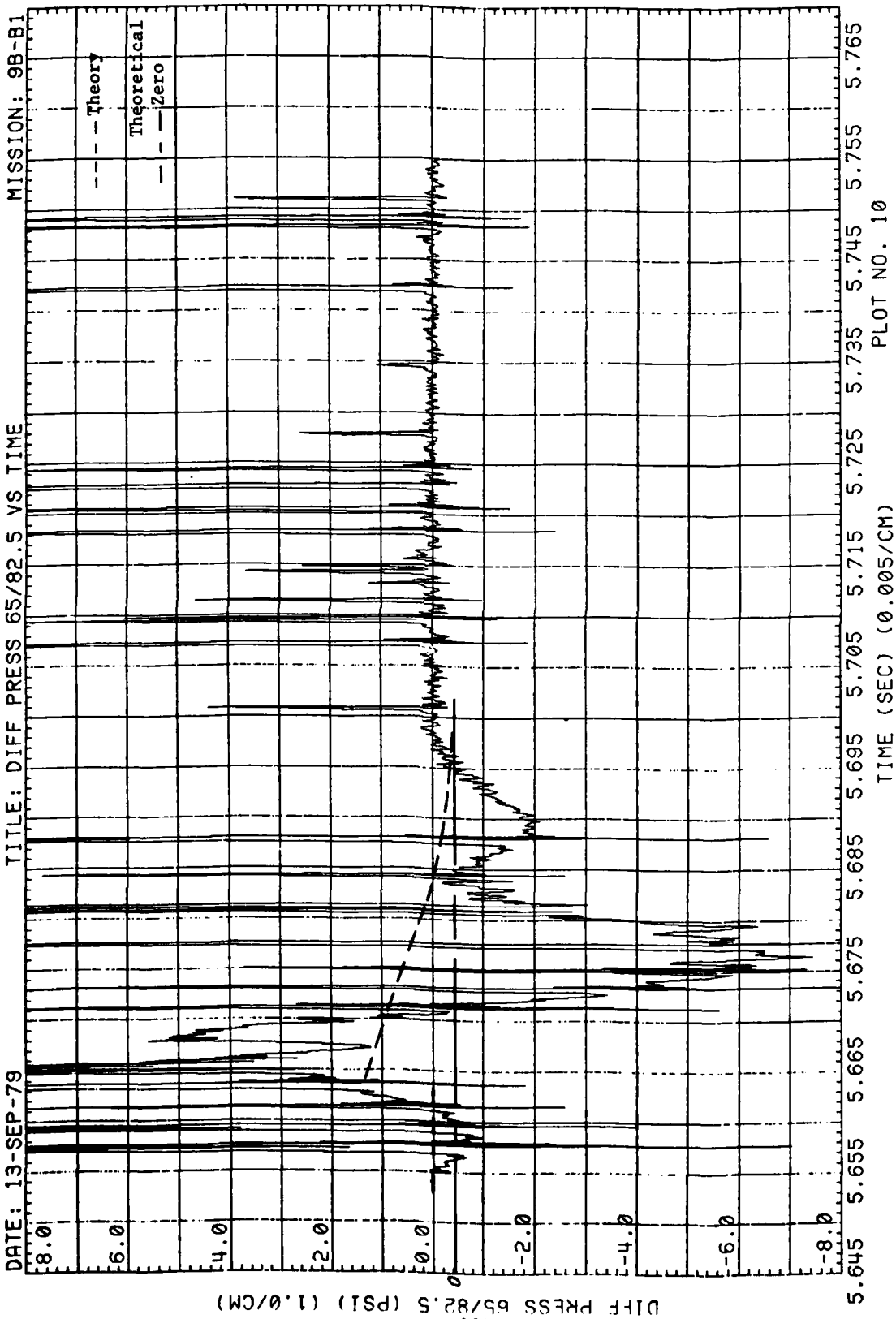

Figure 44. (Continued)

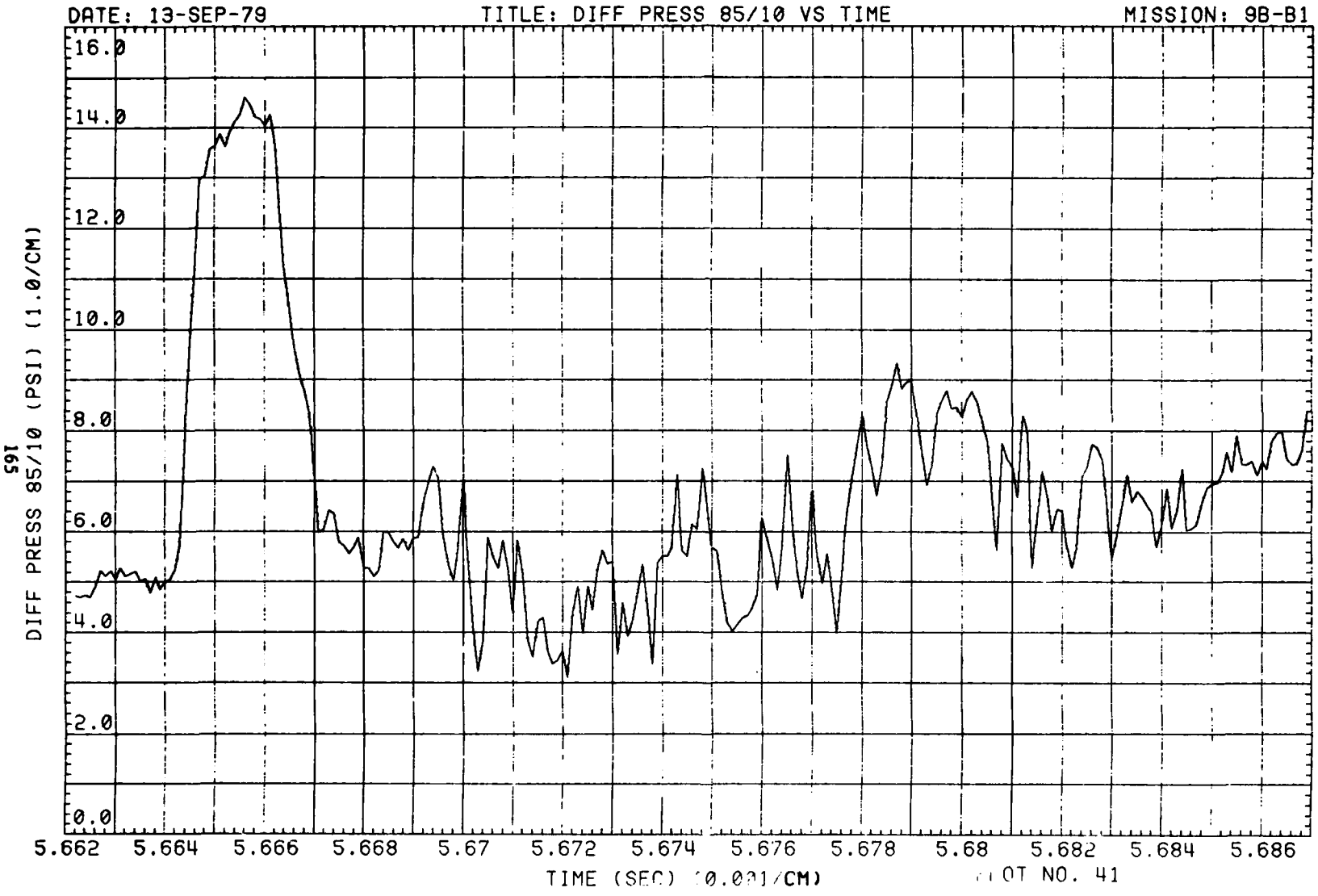

Figure 44. (Continued)

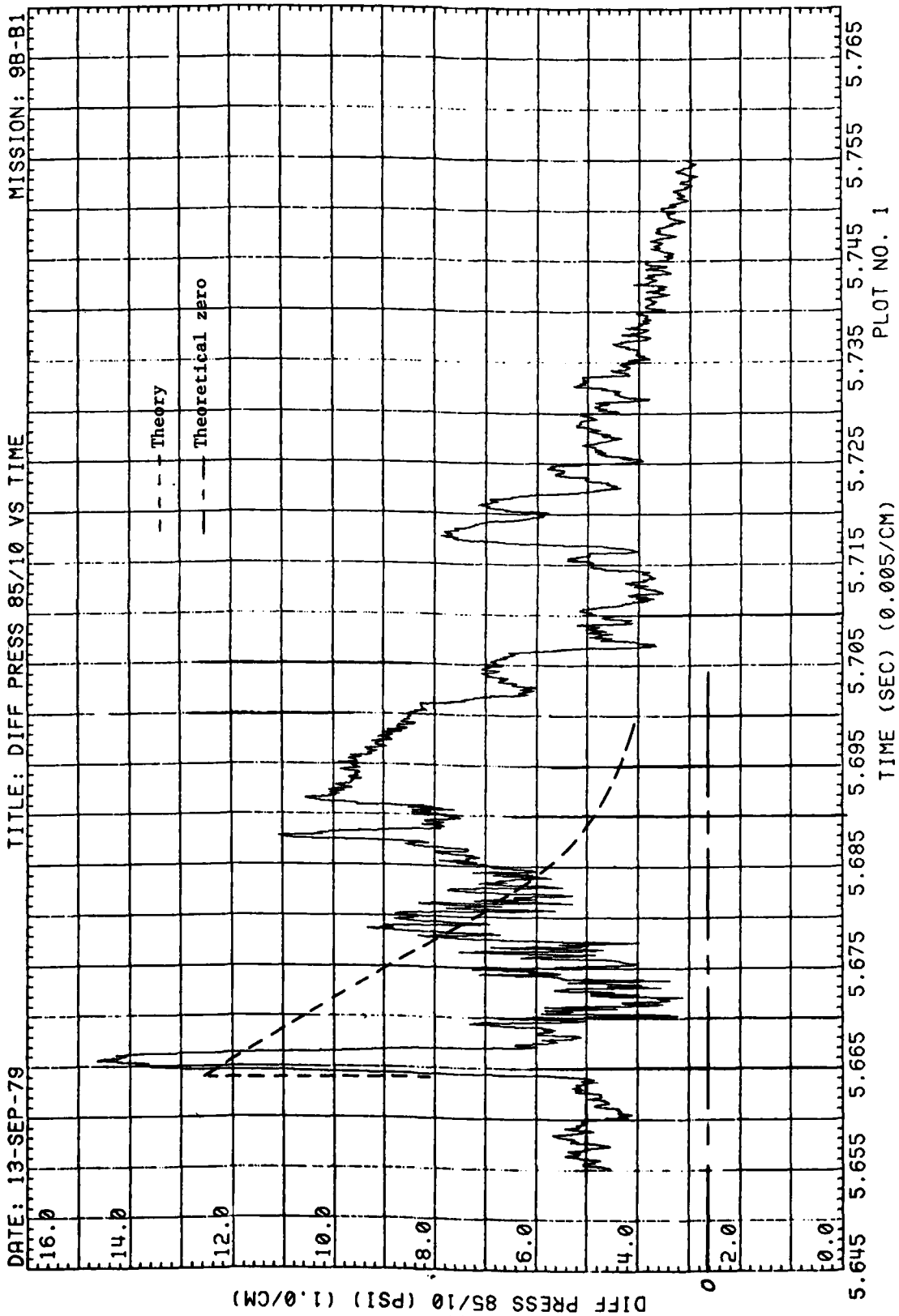

Figure 44. (Continued)

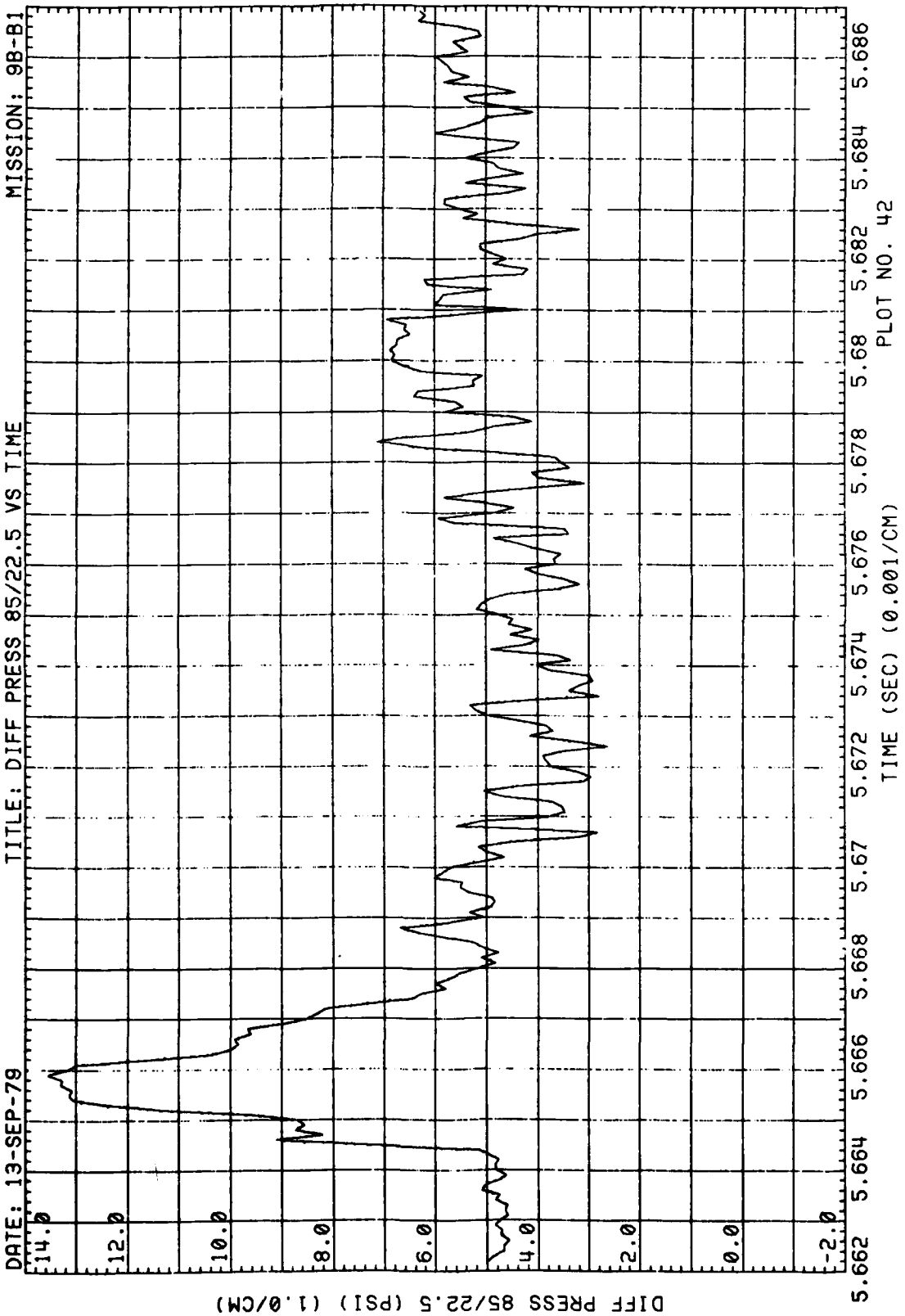

Figure 44. (Continued)

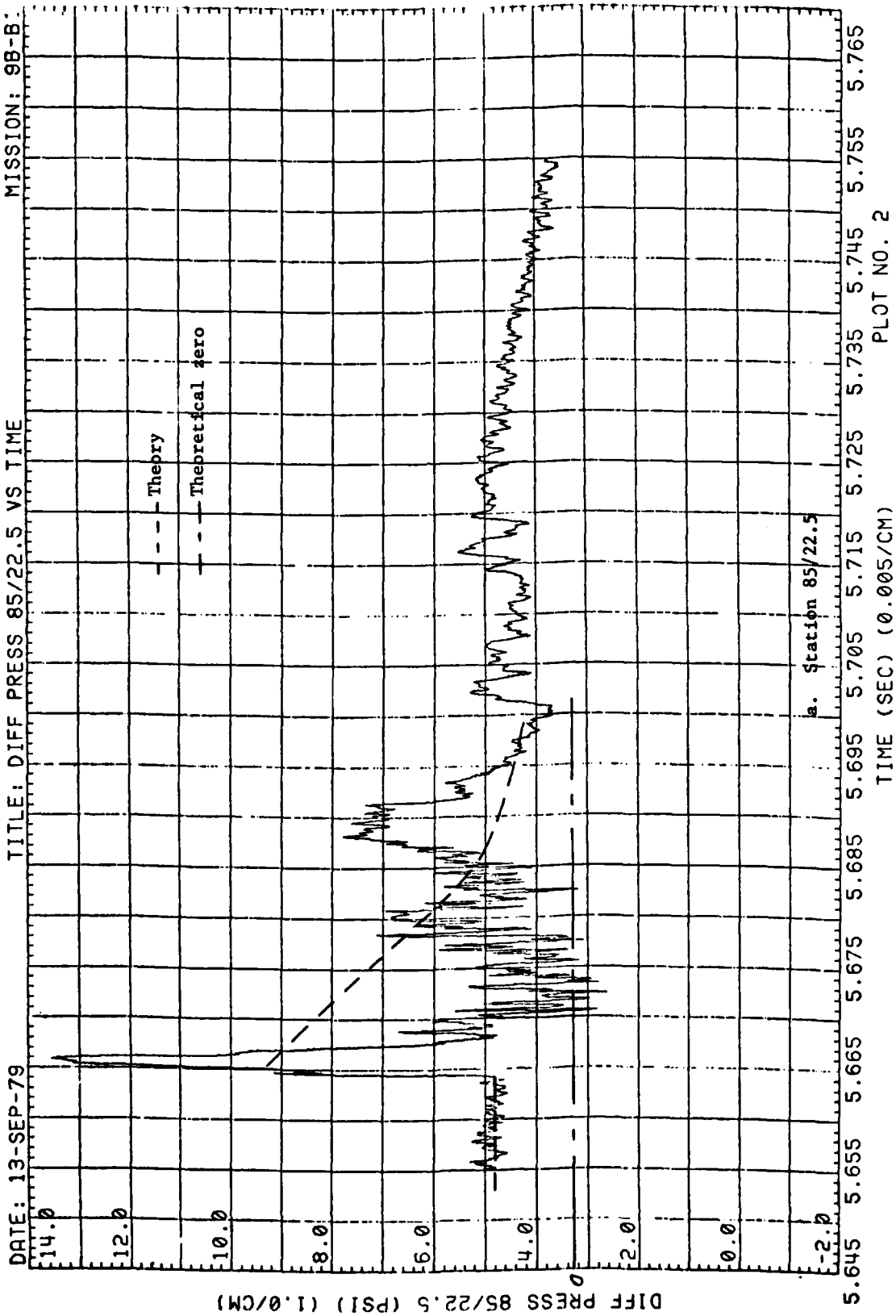

Figure 44. (Continued)

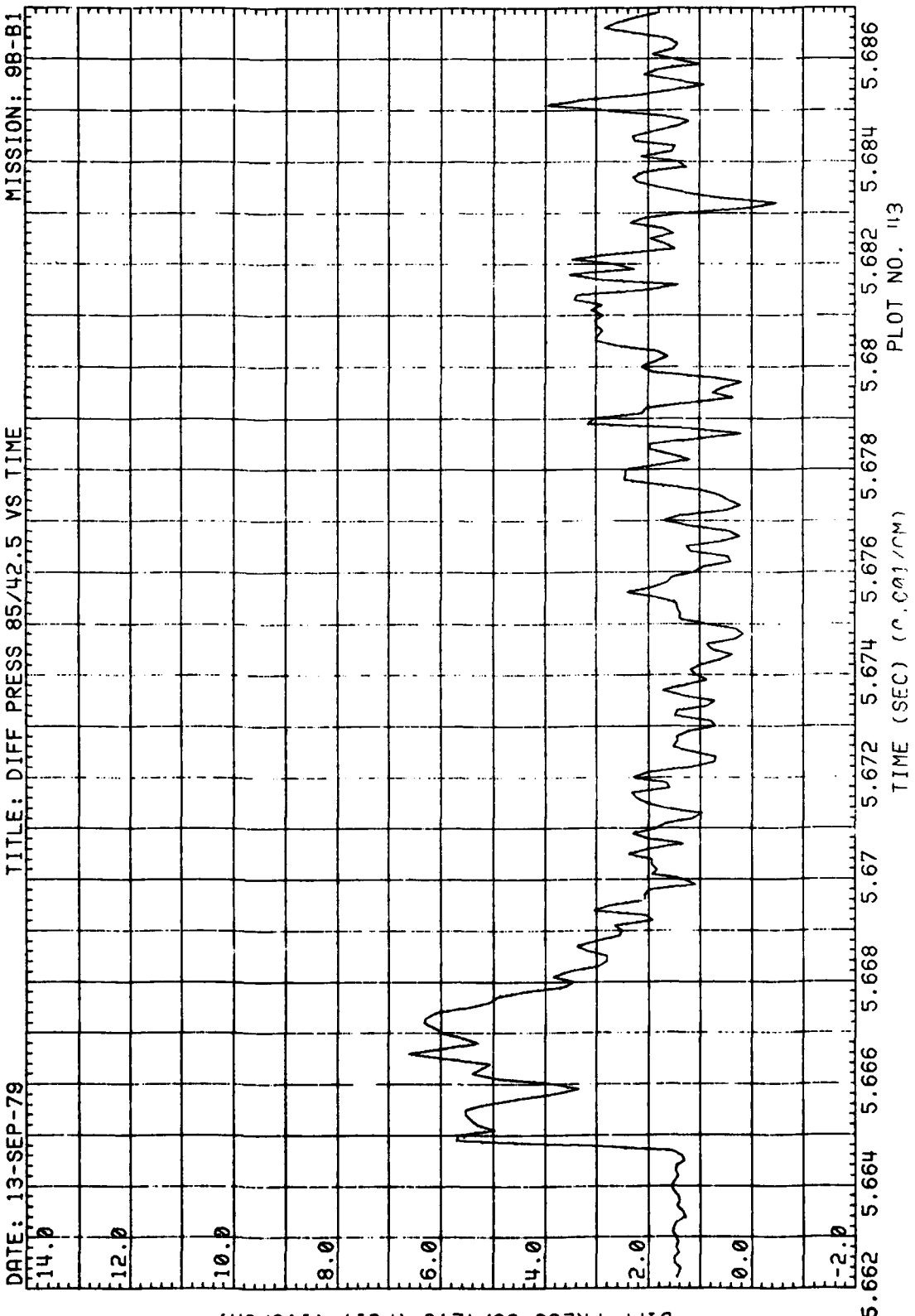

Figure 44. (Continued)

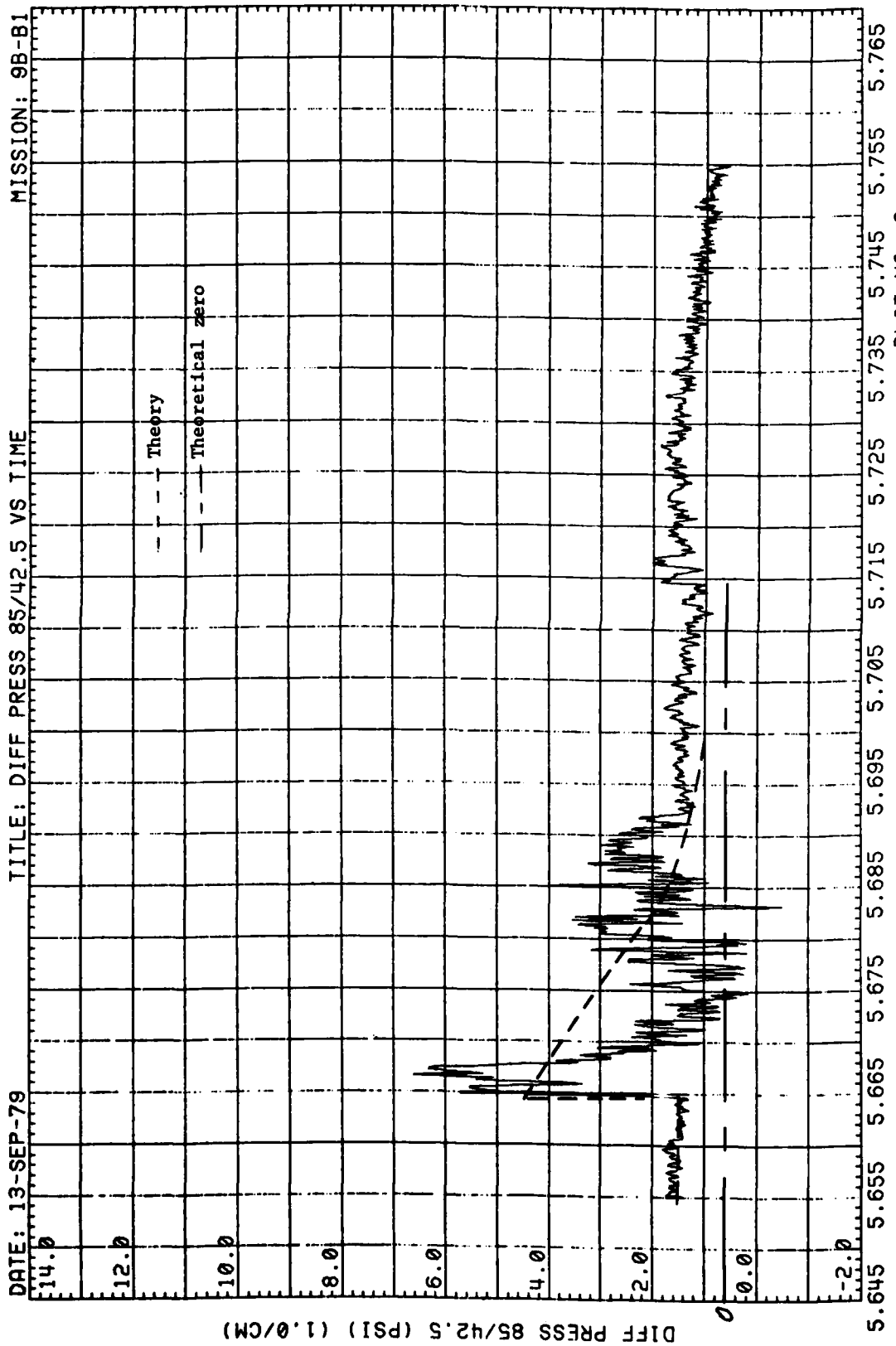

Figure 44. (Continued)

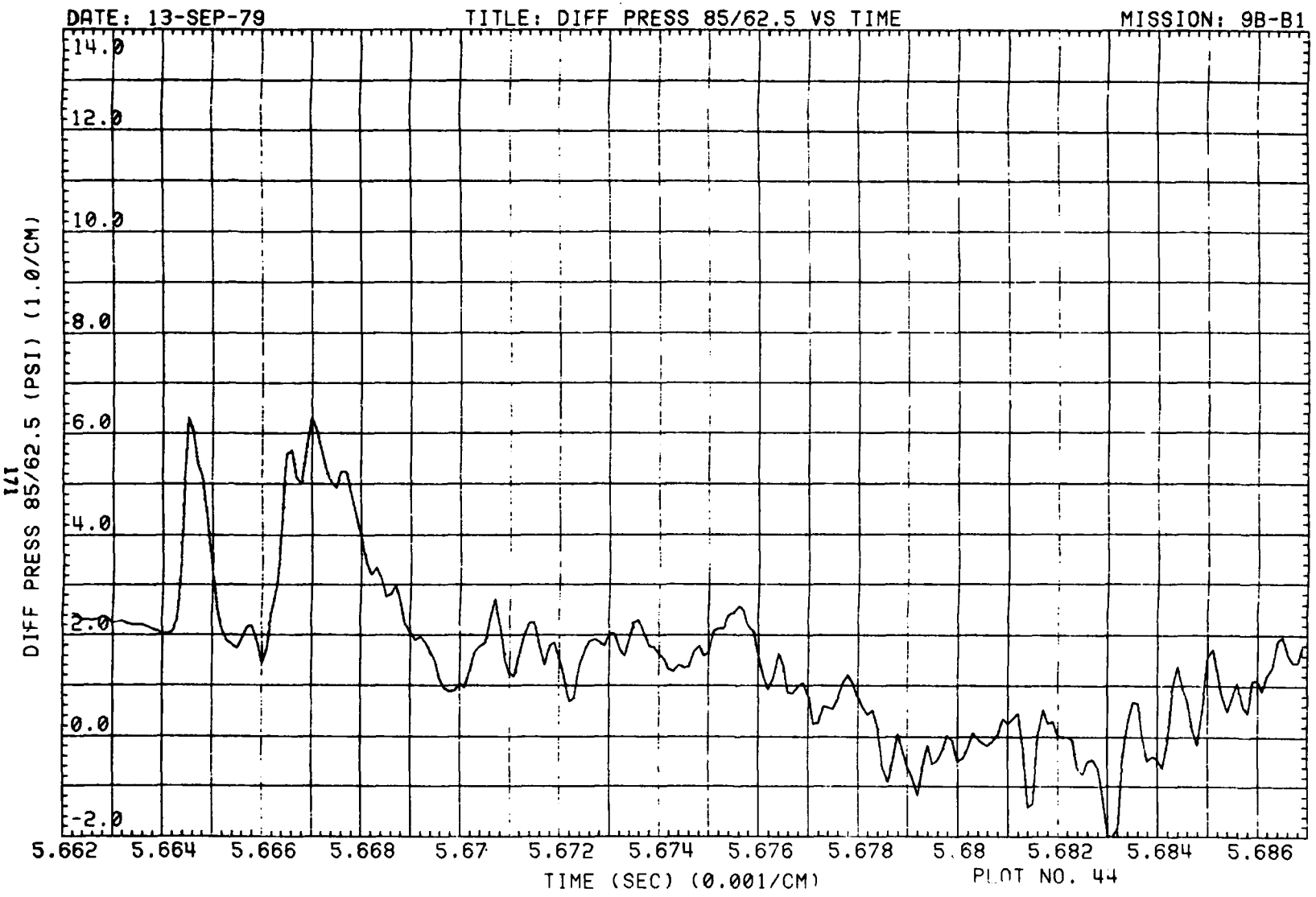

Figure 44. (Continued)

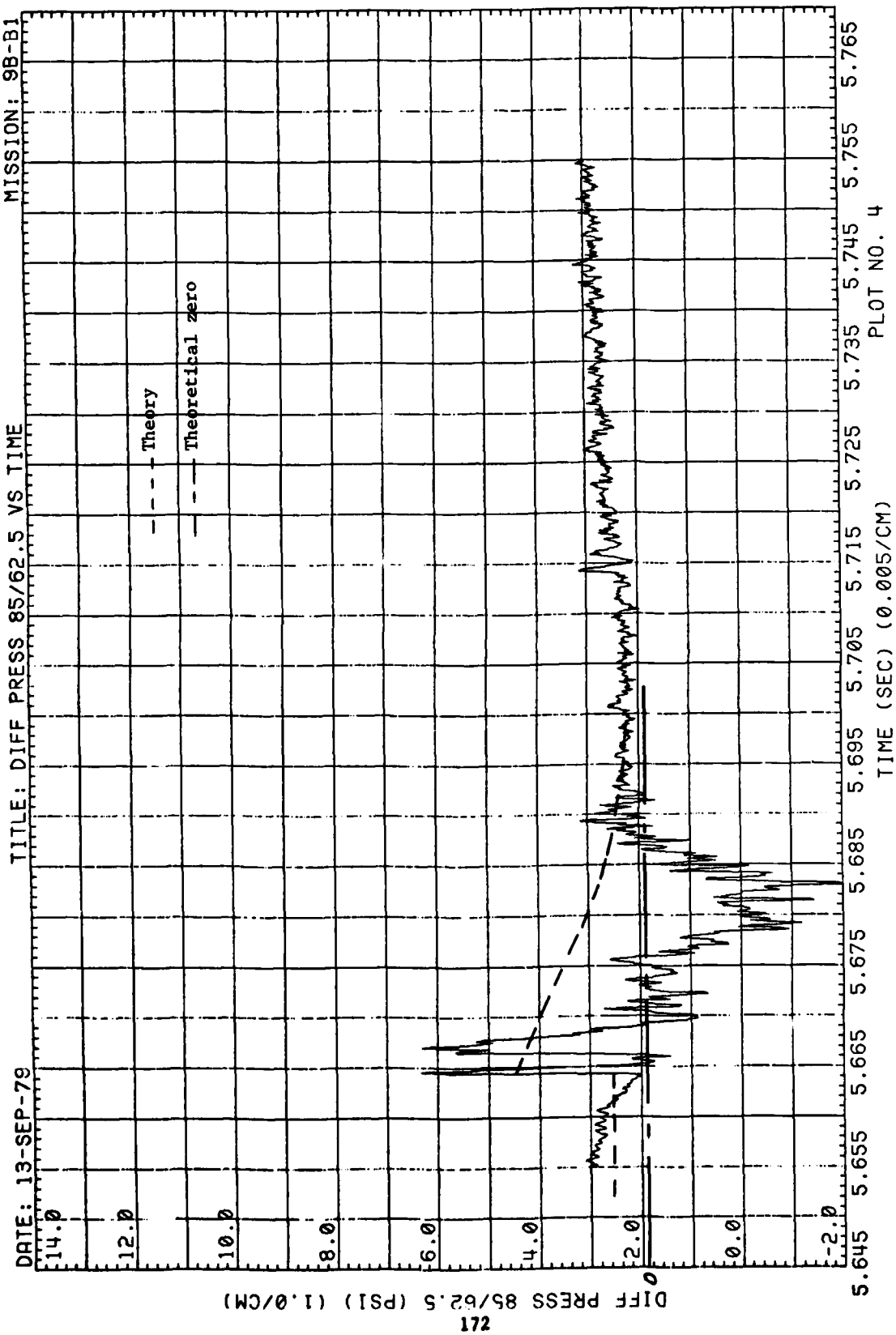

Figure 44. (Continued)

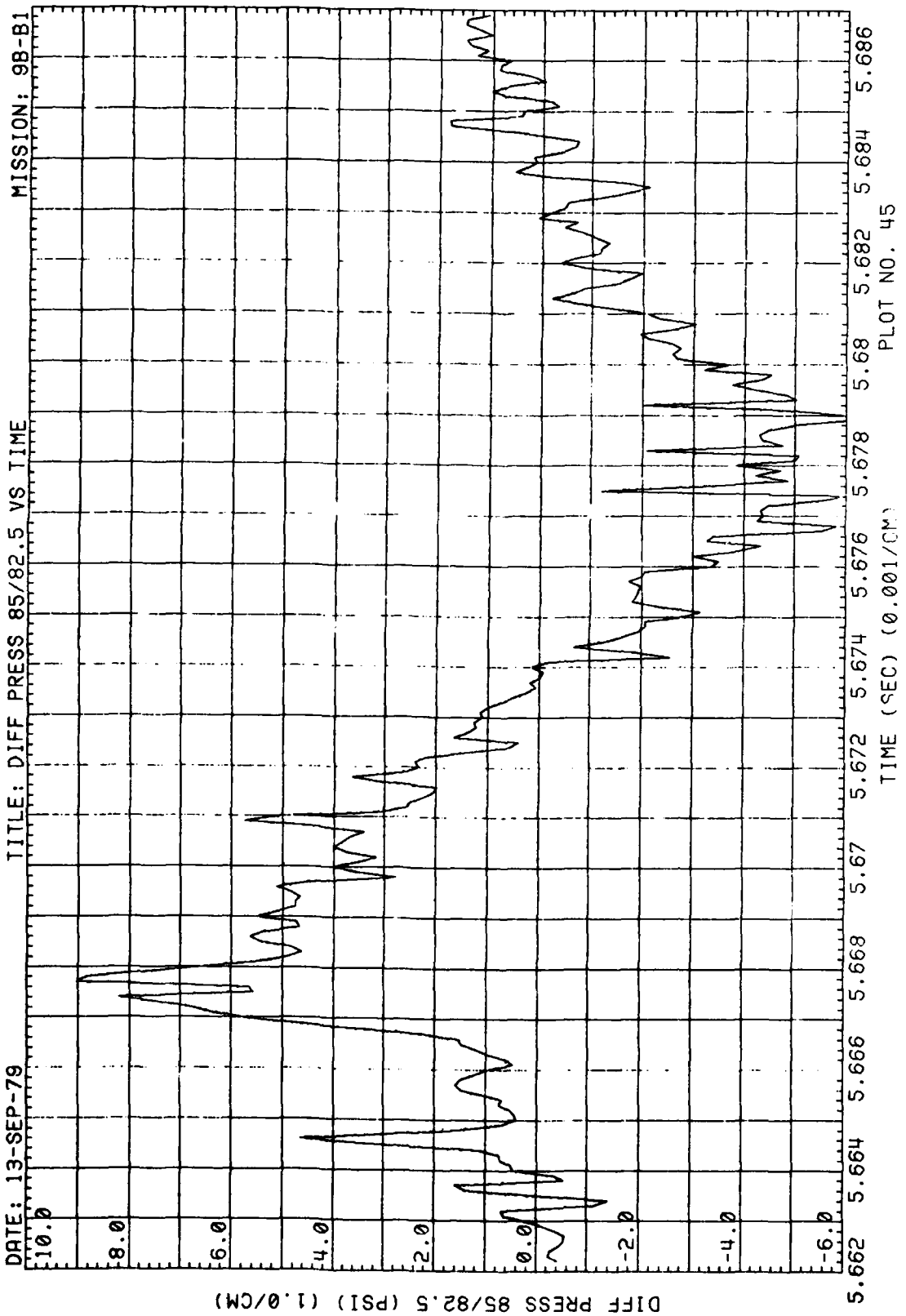

Figure 44. (Continued)

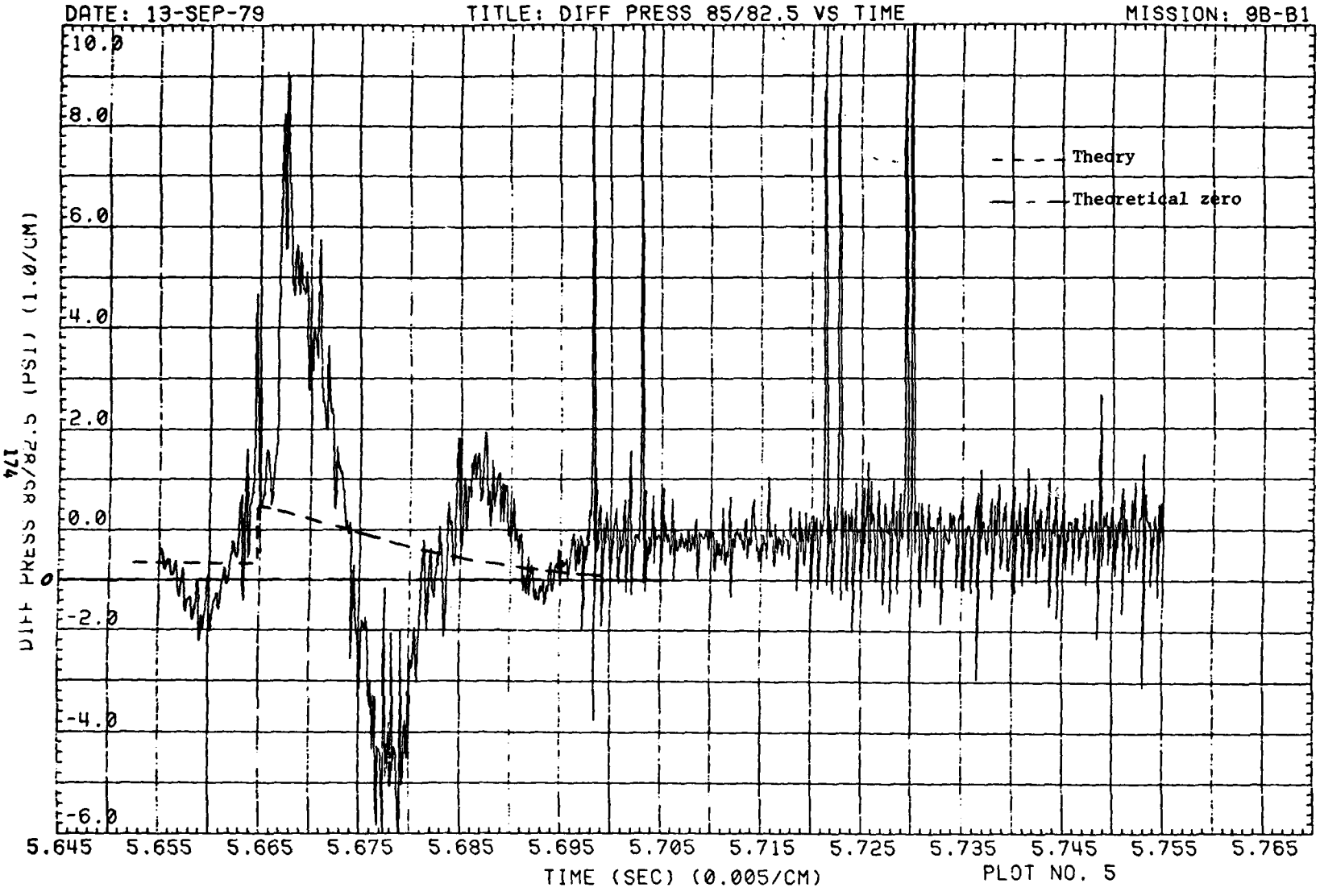

Figure 44. (Concluded)

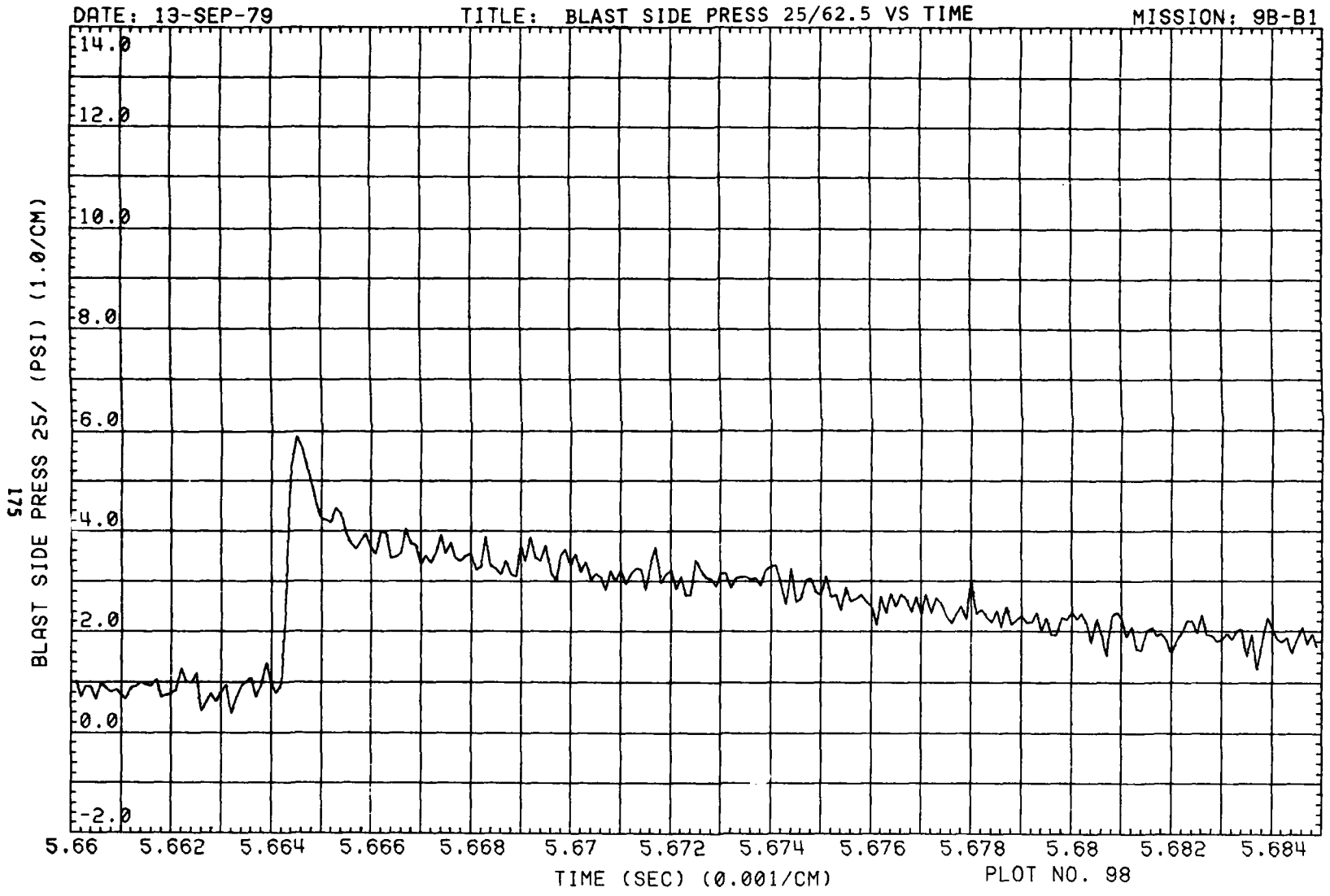

Figure 45. Blastward and Leeward Wing Pressures, Run 9B-B1, Intercept 2

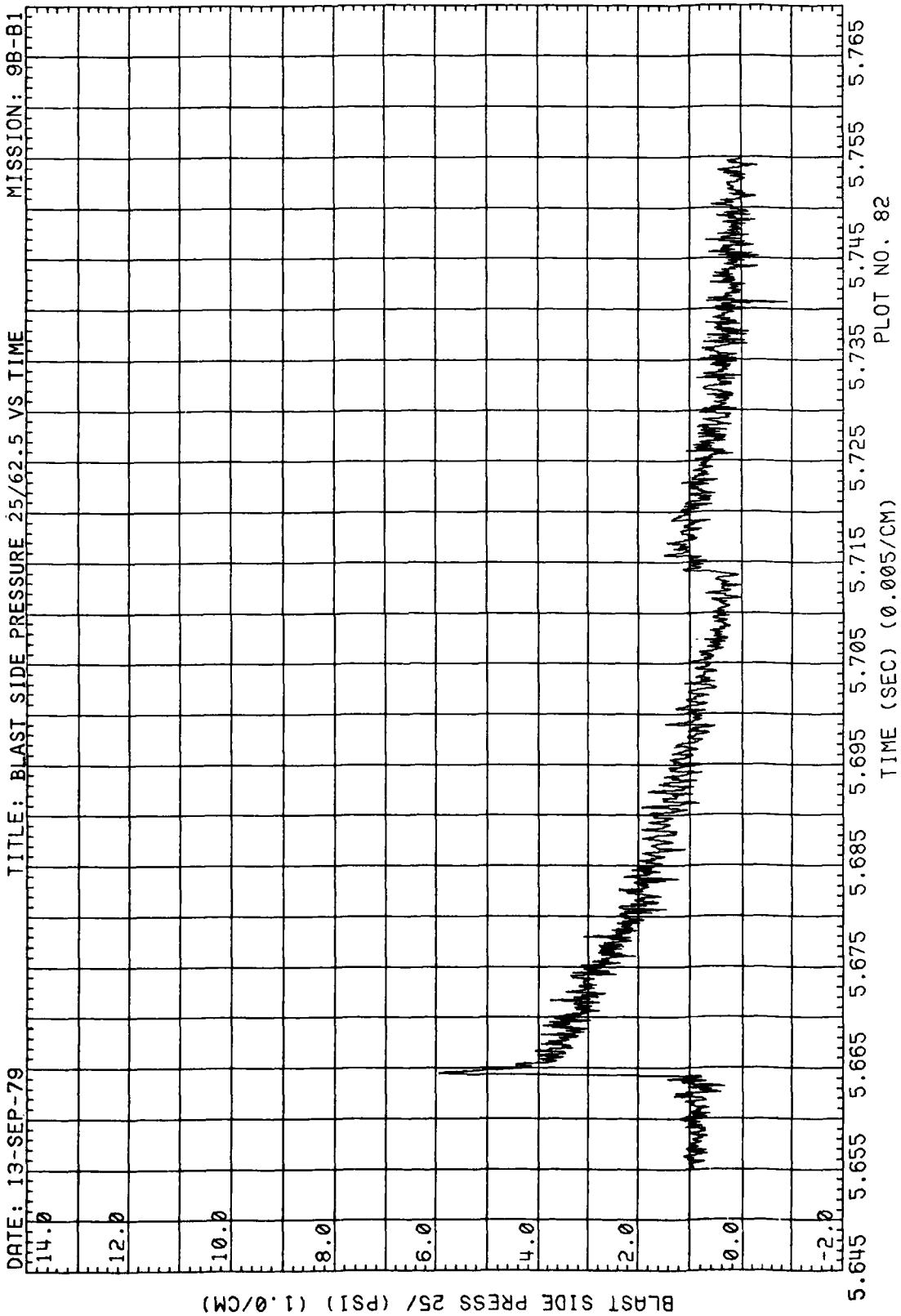

Figure 45. (Continued)

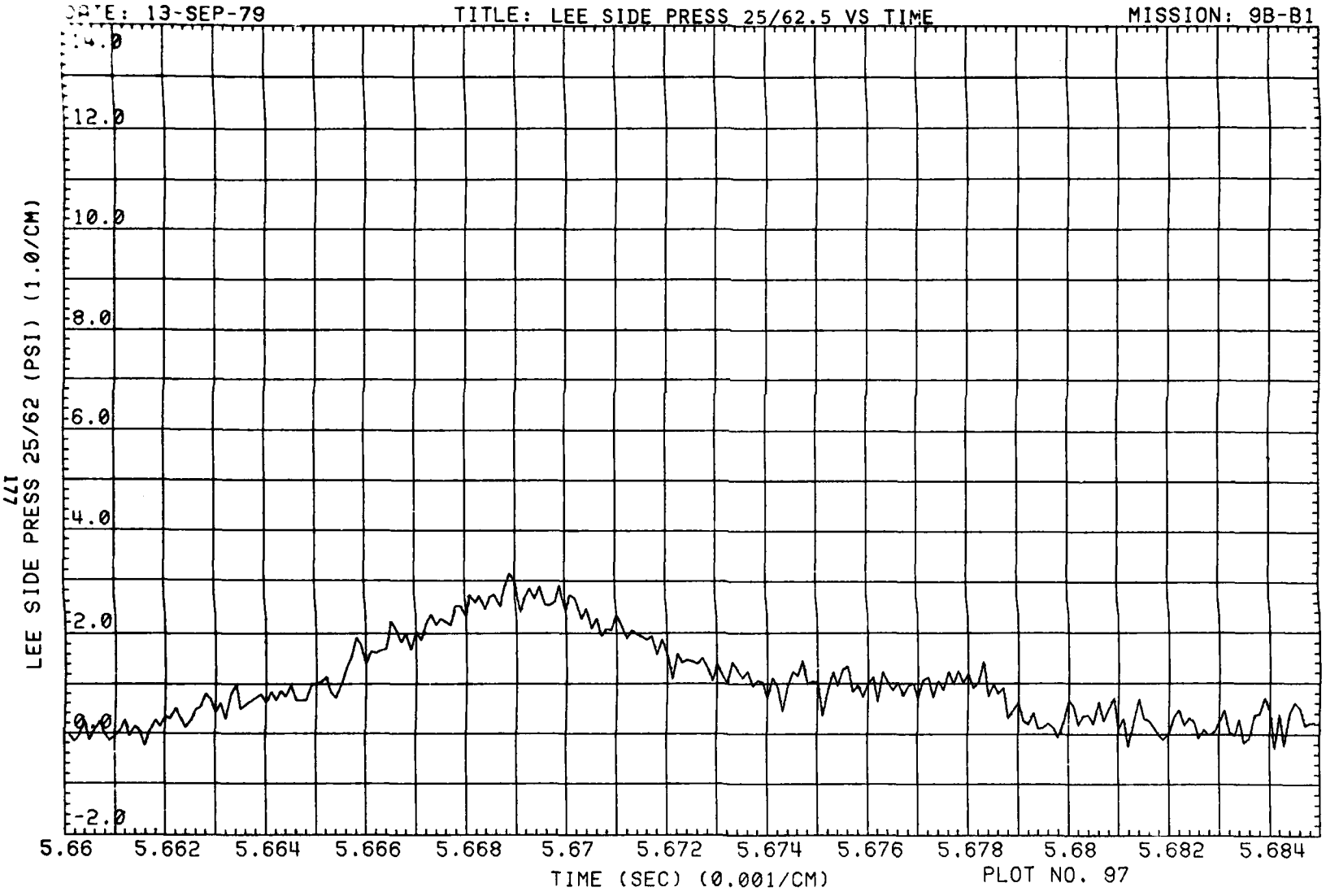

Figure 45. (Continued)

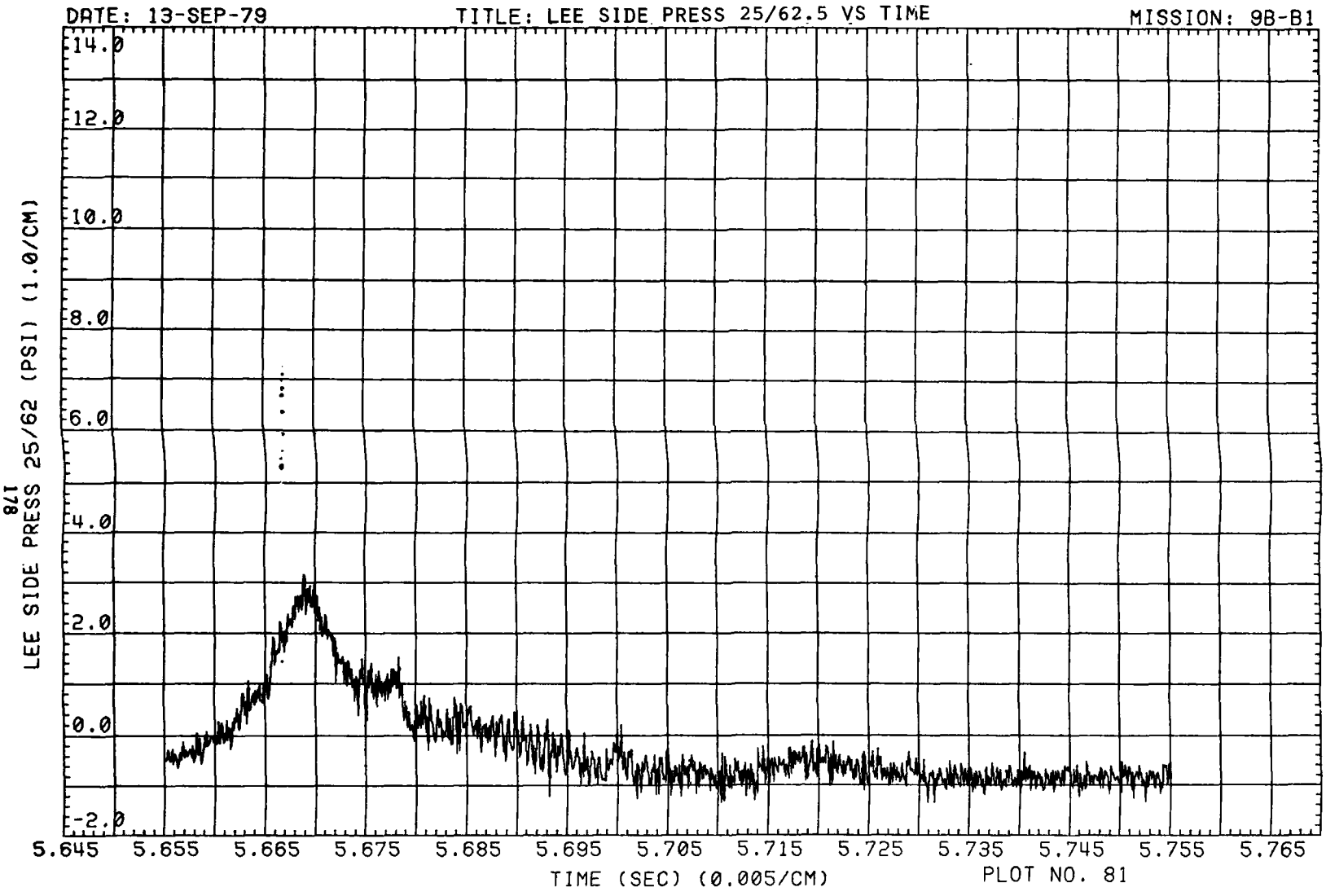

Figure 45. (Concluded)

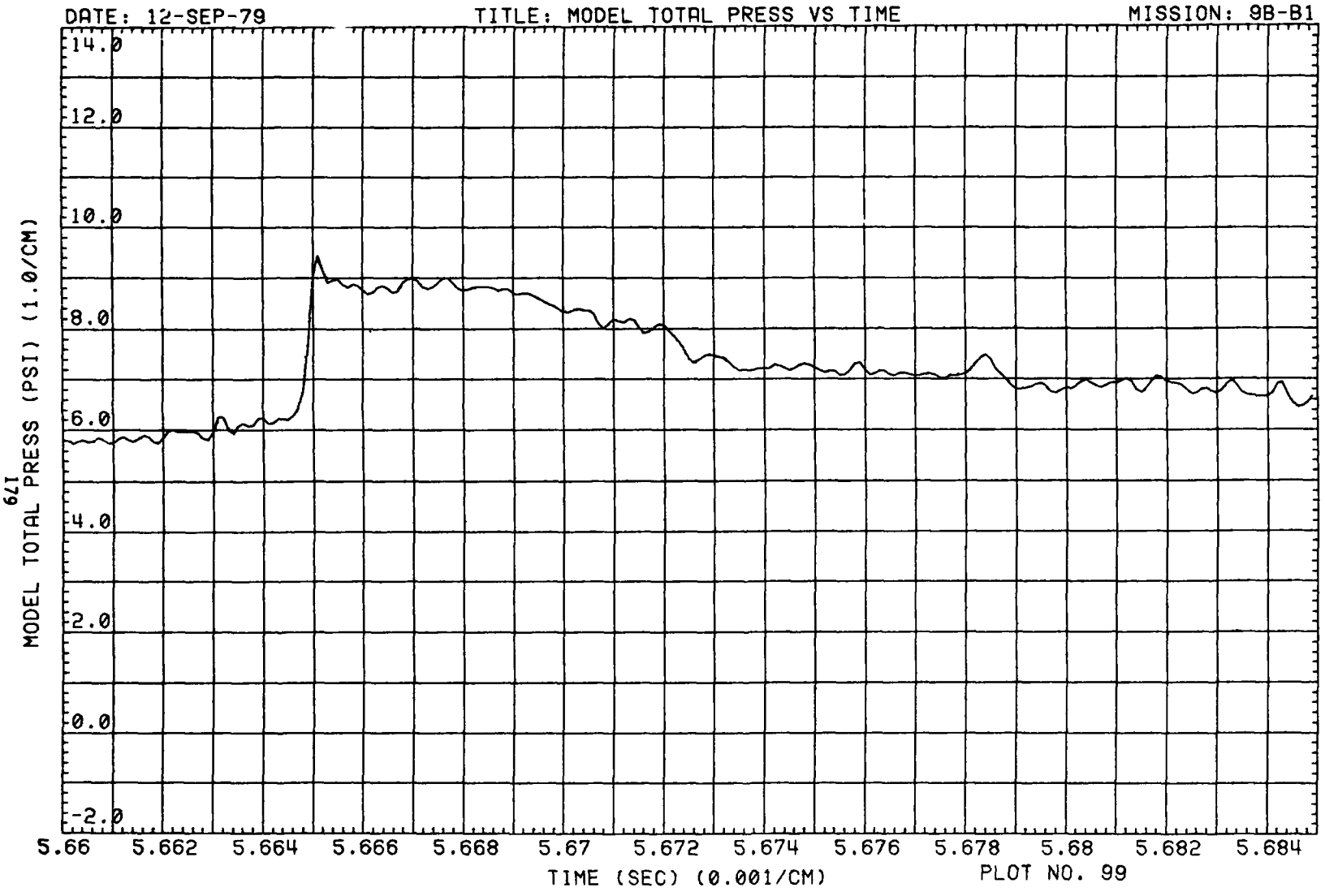

Figure 46. Total Pressure at Model, Run 9B-B1, Intercept 2

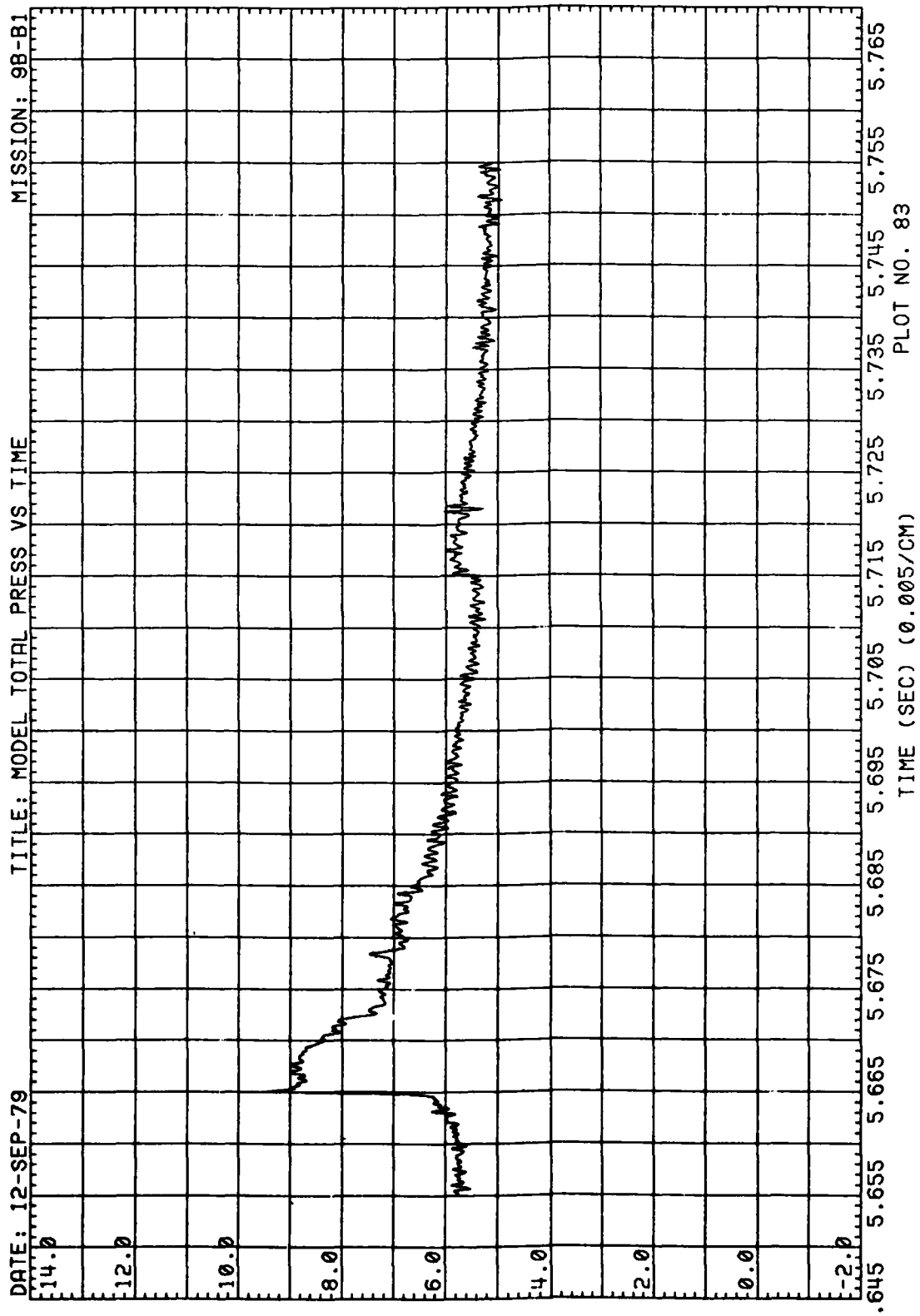

Figure 46. (Concluded)

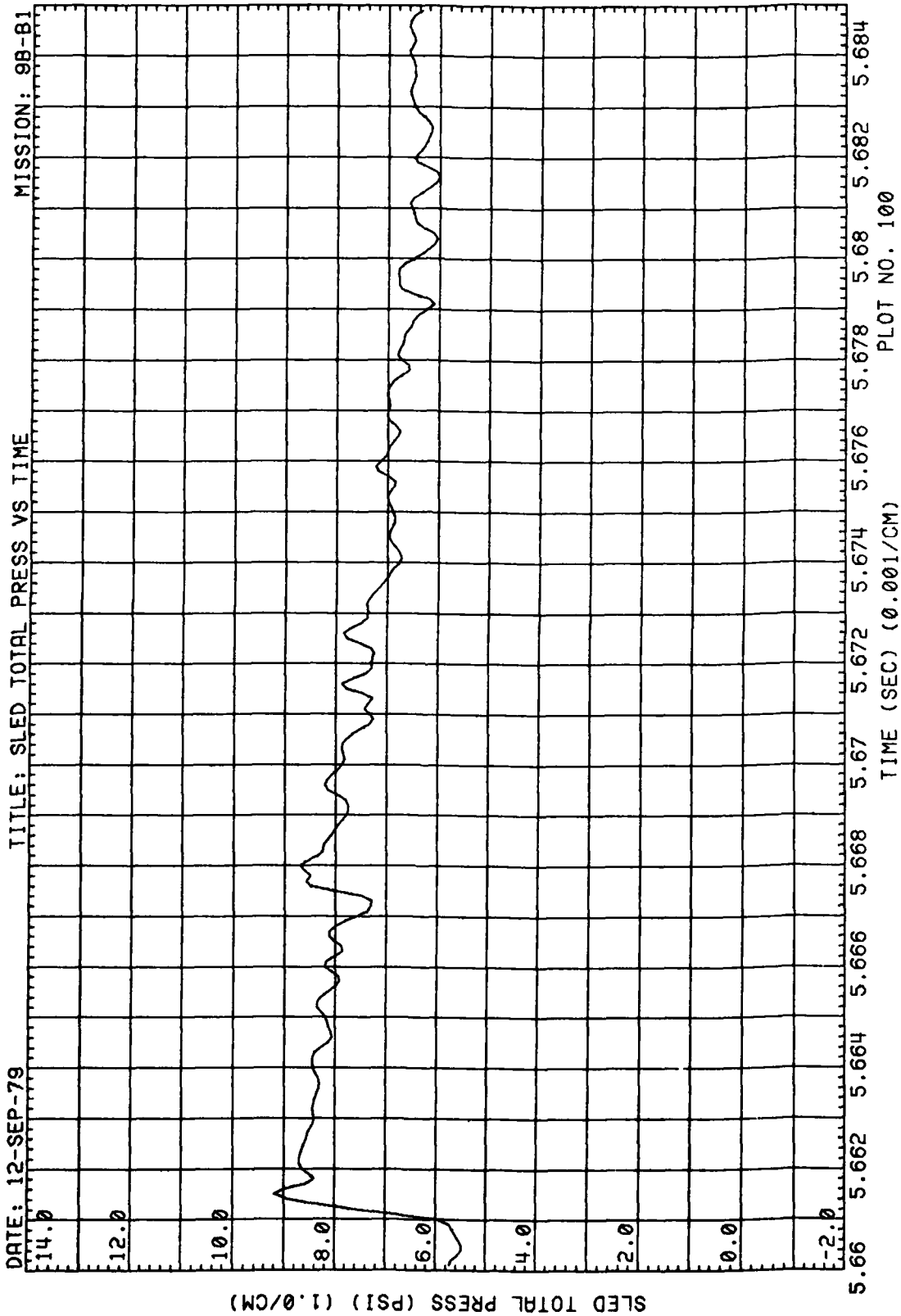

Figure 47. Total Pressure at Sled, Run 9B-B1, Intercept 2

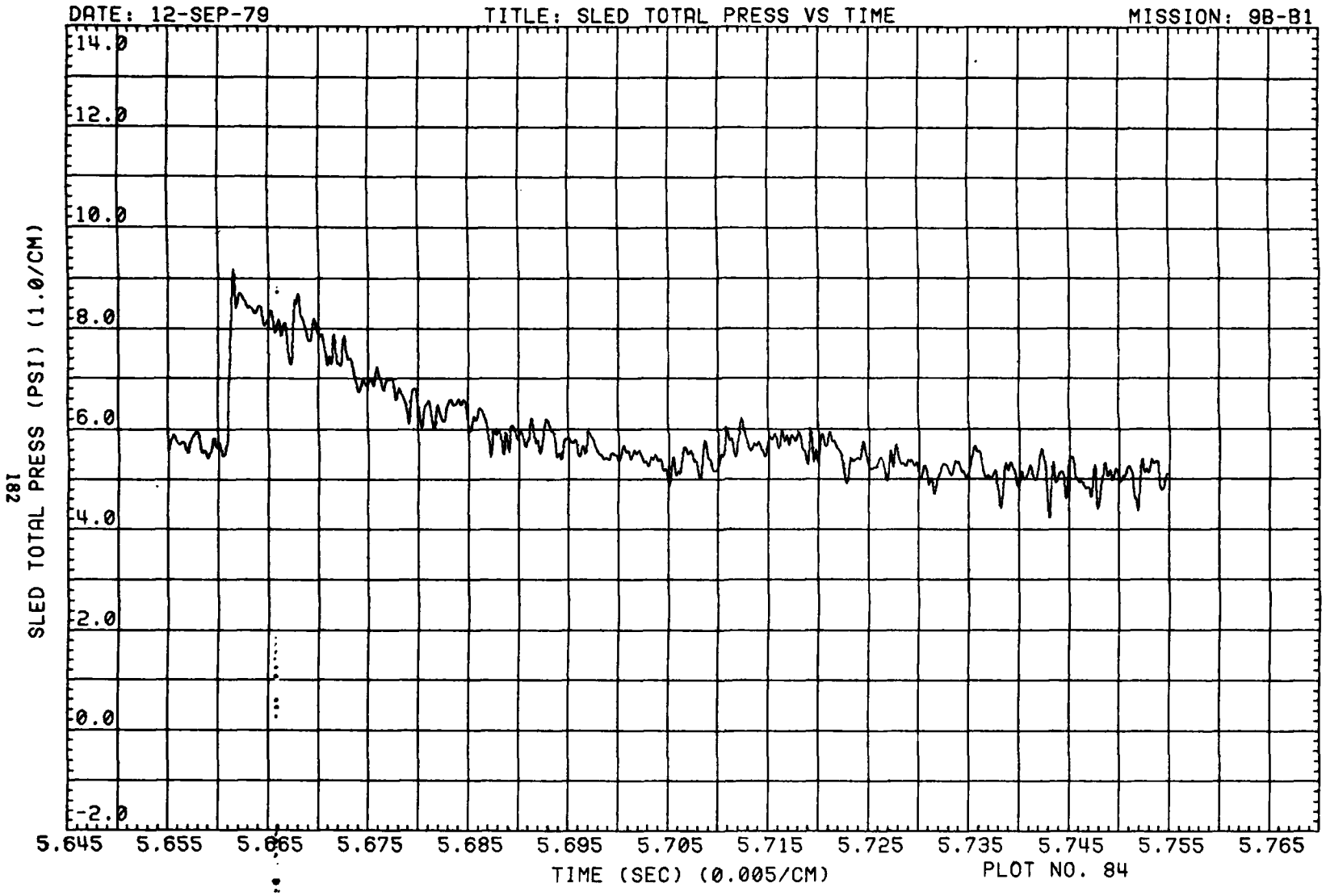

Figure 47. (Concluded)

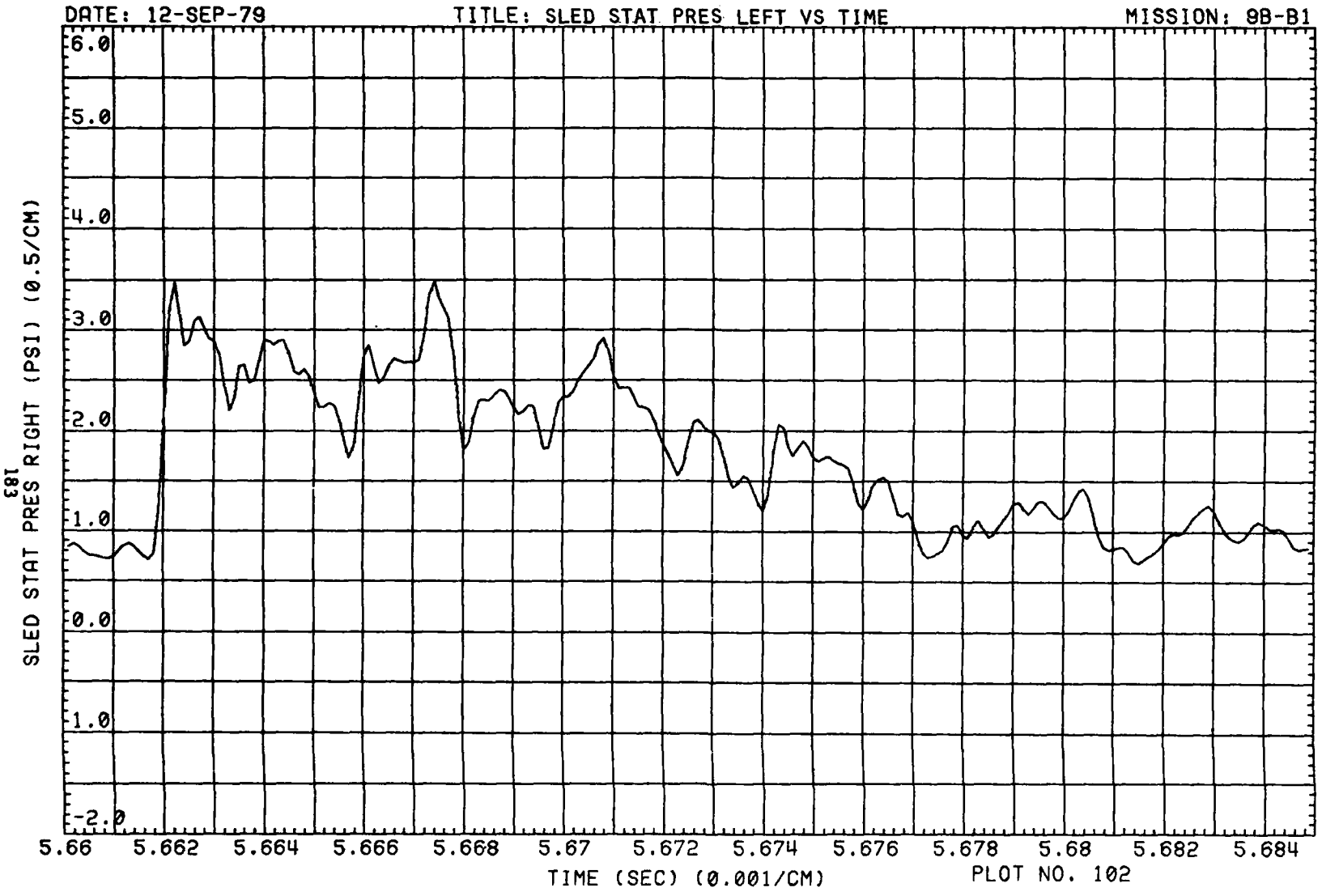

Figure 48. Left Side Static Pressure at Sled, Run 9B-B1, Intercept 2

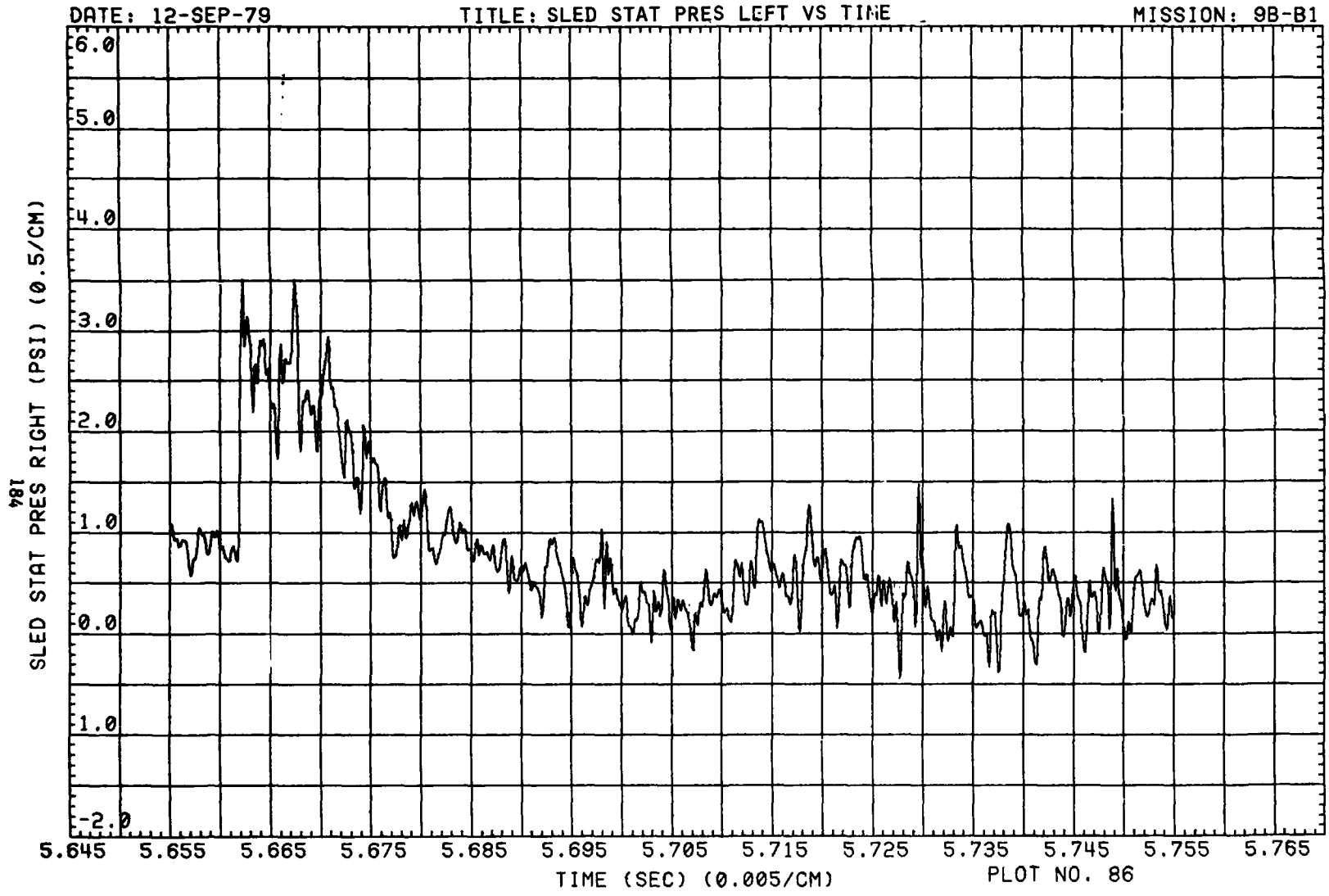

Figure 48. (Concluded)

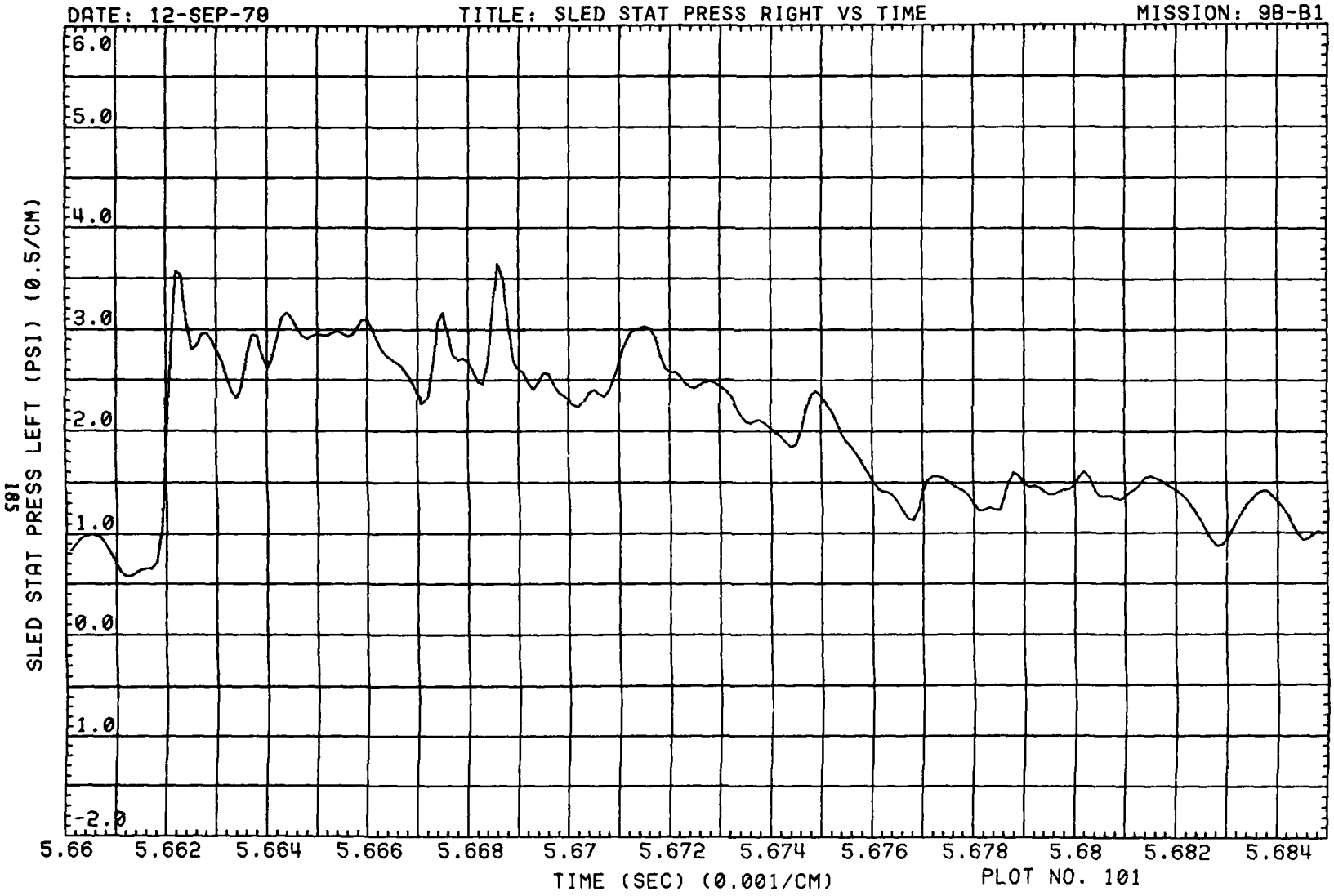

Figure 49. Right Side Static Pressure at Sled, Run 9B-B1, Intercept 2

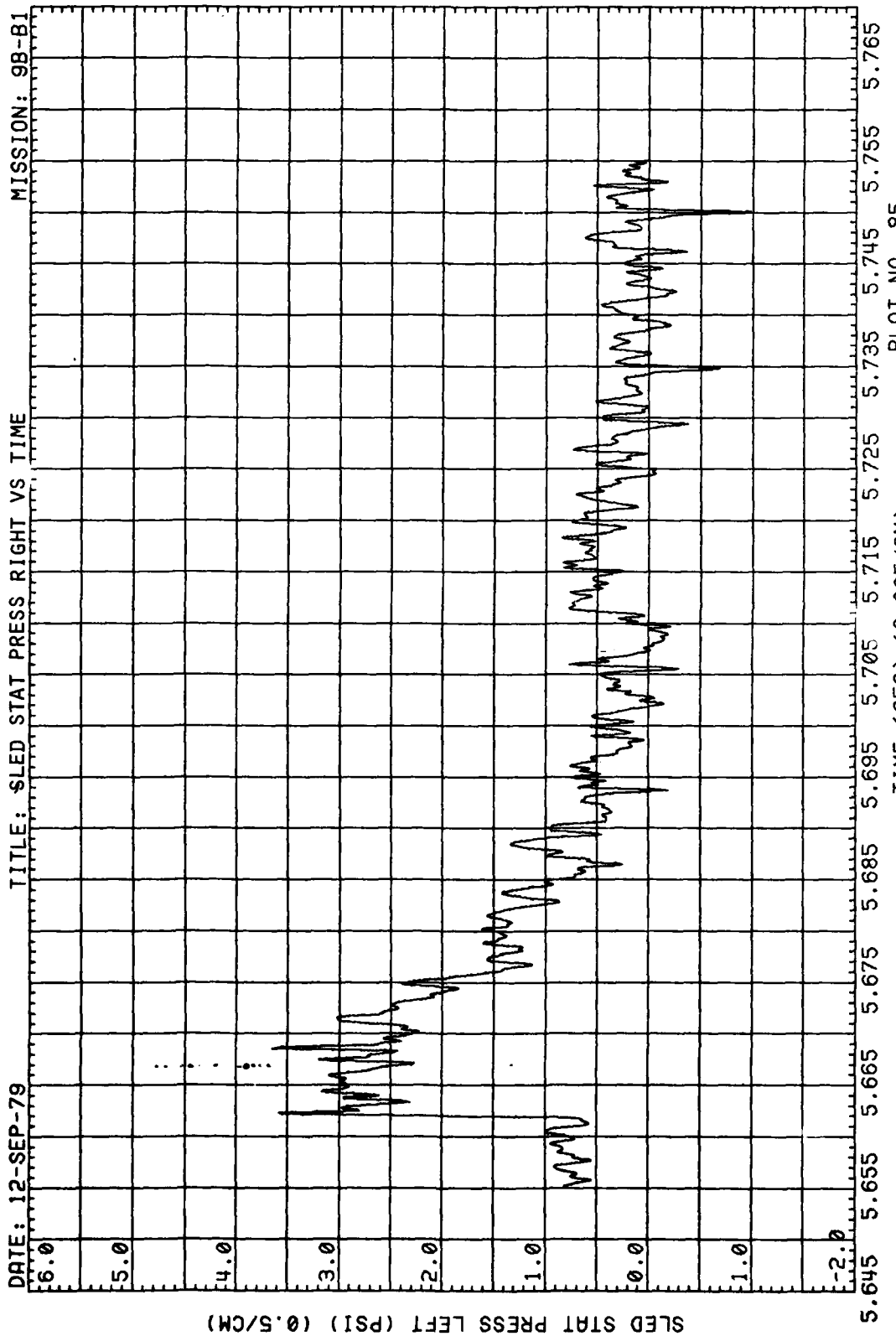

Figure 49. (Concluded)

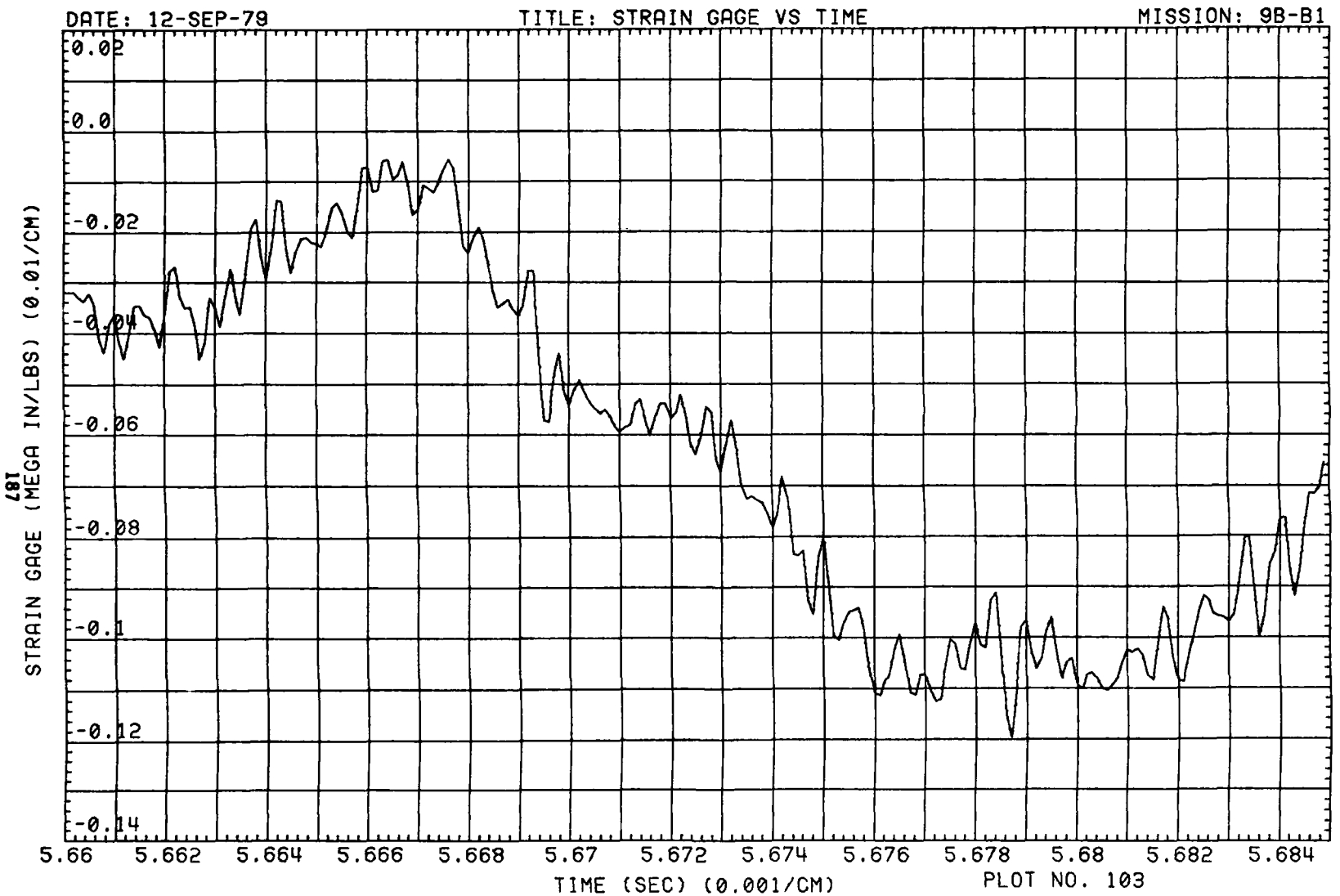

Figure 50. Strain at Model Support, Run 9B-B1, Intercept 2

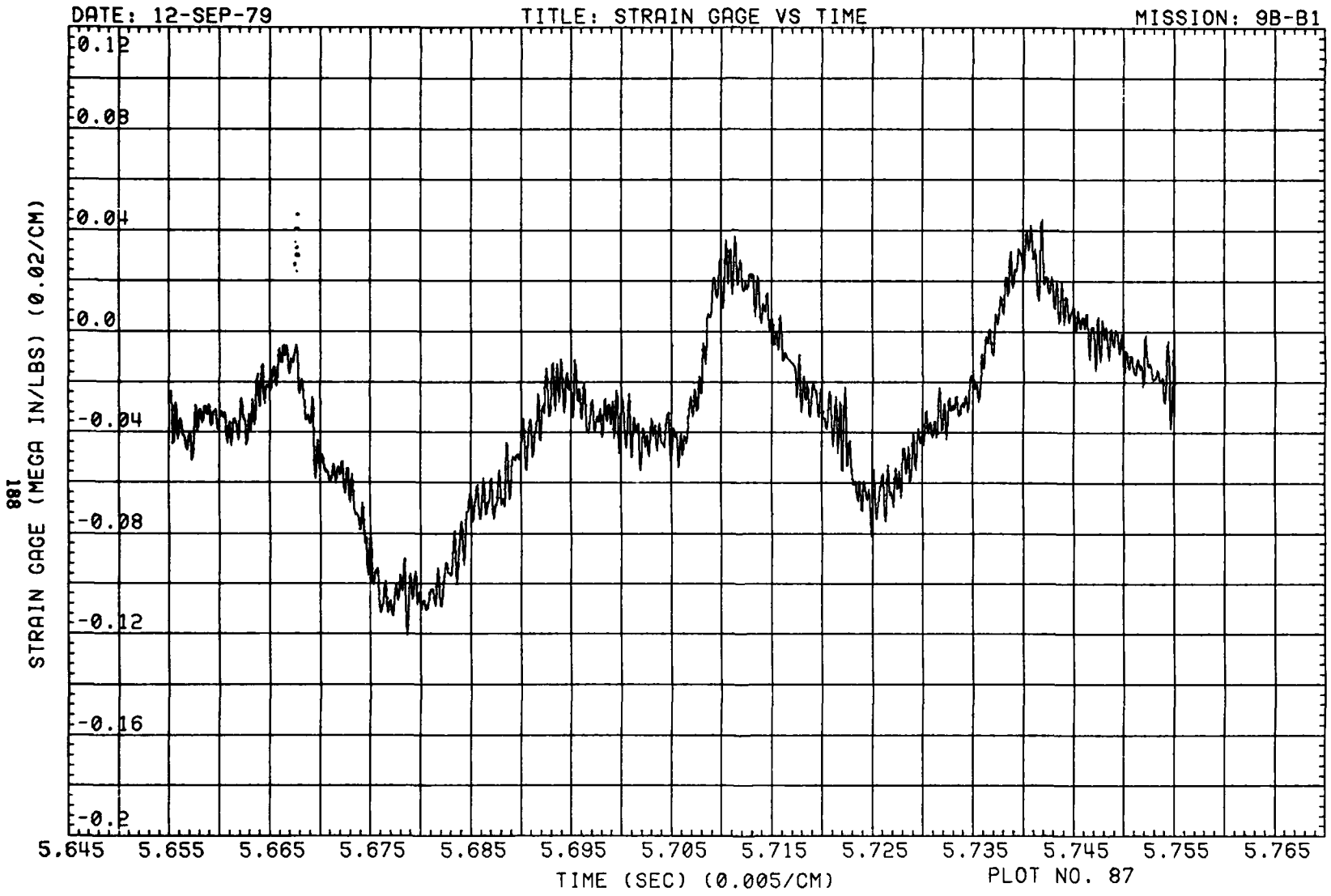

Figure 50. (Concluded)

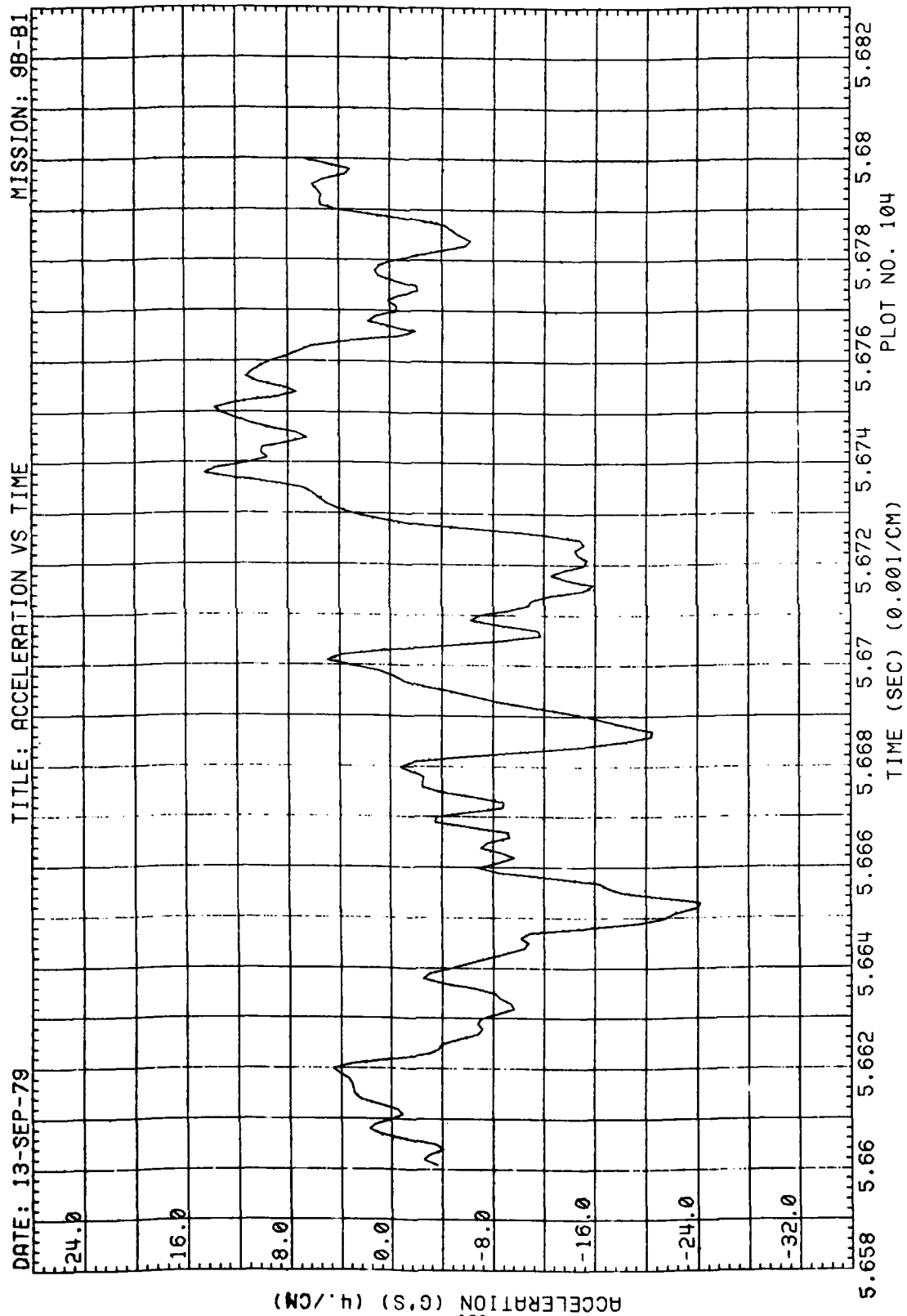

Figure 51. Wing Acceleration, Run 9B-B1, Intercept 2

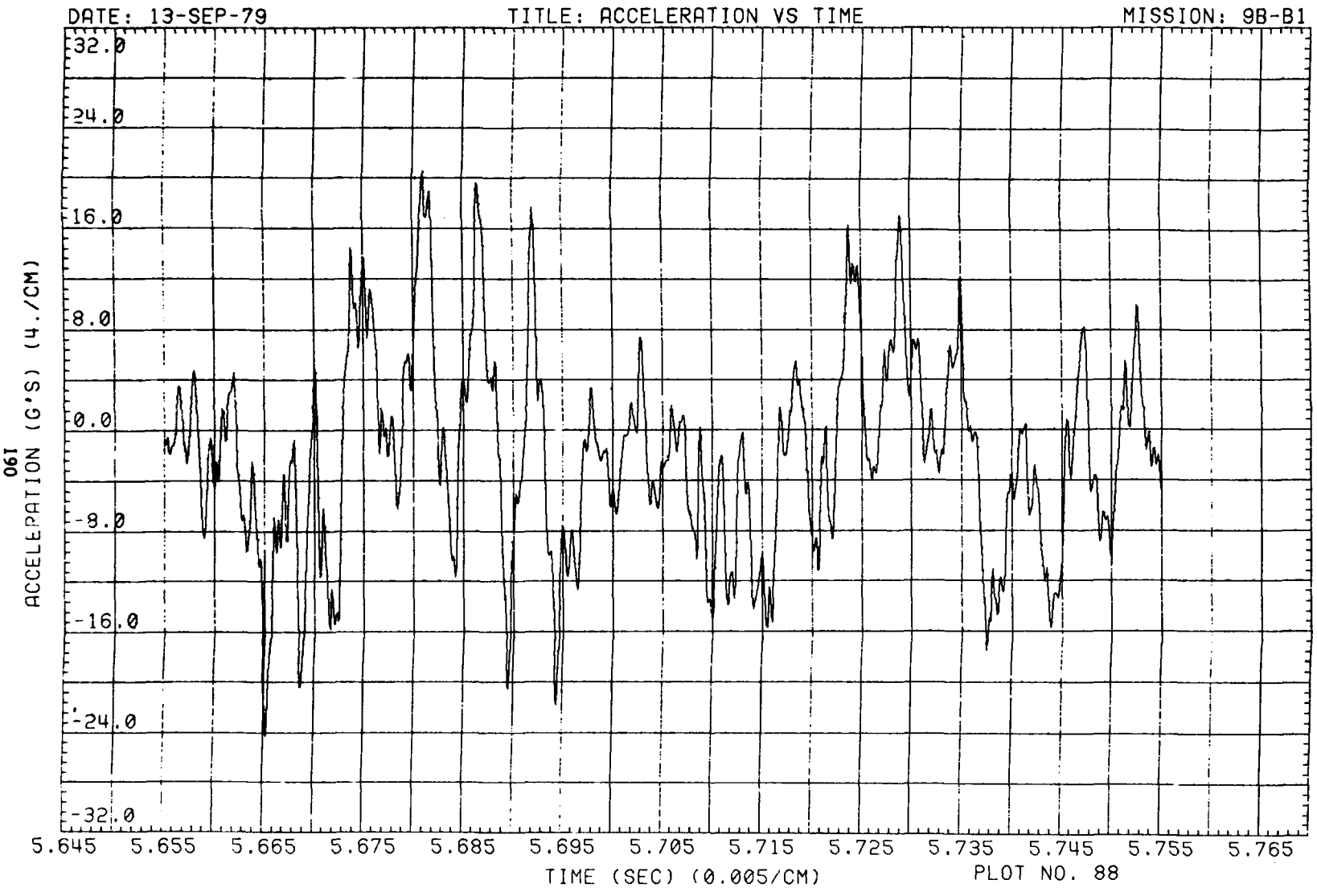

Figure 51. (Concluded)

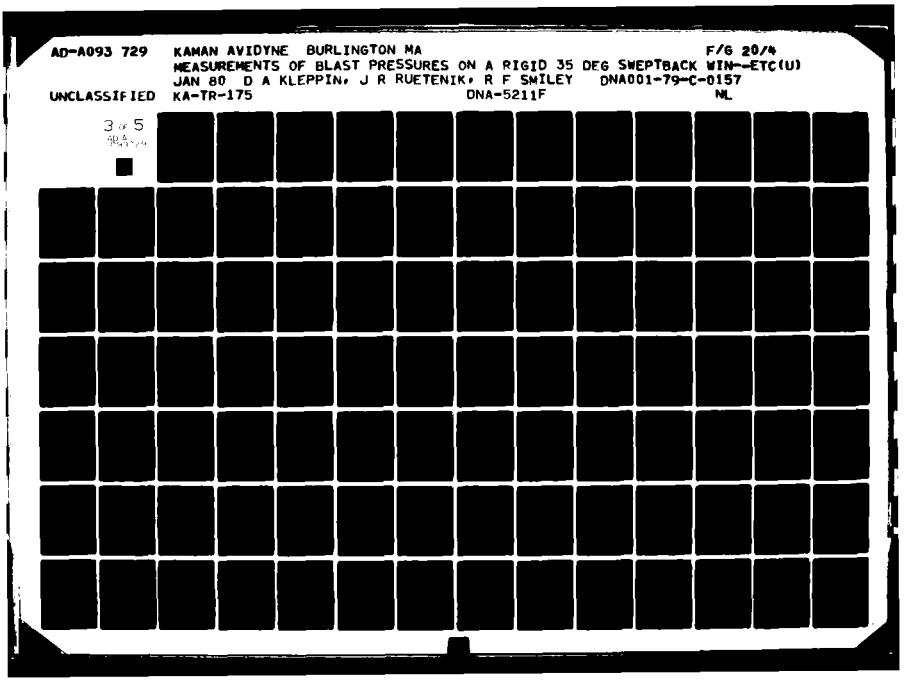
AD-A093 729
KAMAN AVIDYNE BURLINGTON MA
F/G 20/4
MEASUREMENTS OF BLAST PRESSURES ON A RIGID 35 DEG SWEPTBACK WIN--ETC(U)
JAN 80 D A KLEPPIN, J R RUETENIK, R F SMILEY DNA001-79-C-0157
UNCLASSIFIED
KA-TR-175
DNA-5211F
NL
3 of 5

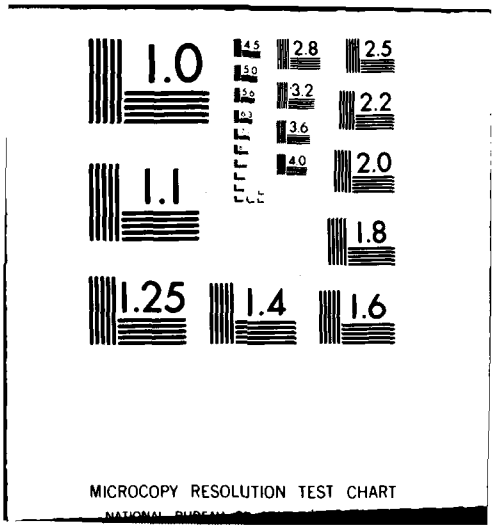
1.0
1.1
1.25
1.4
1.6
1.8
2.0
2.2
2.5
2.8
3.2
3.6
4.0
4.5
5.0
5.6
6.3
MICROCOPY RESOLUTION TEST CHART

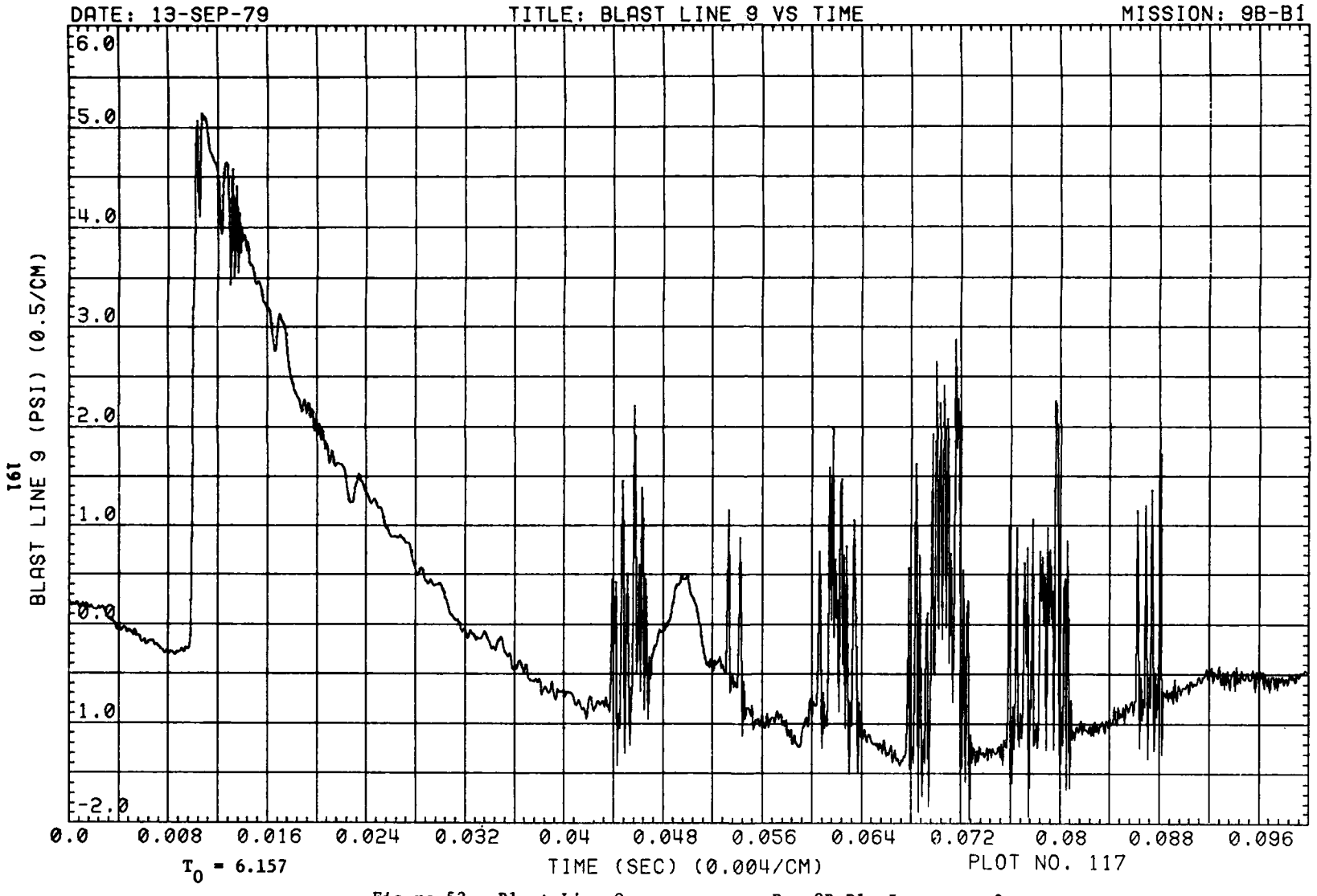

Figure 52. Blast-Line Overpressures, Run 9B-B1, Intercept 3

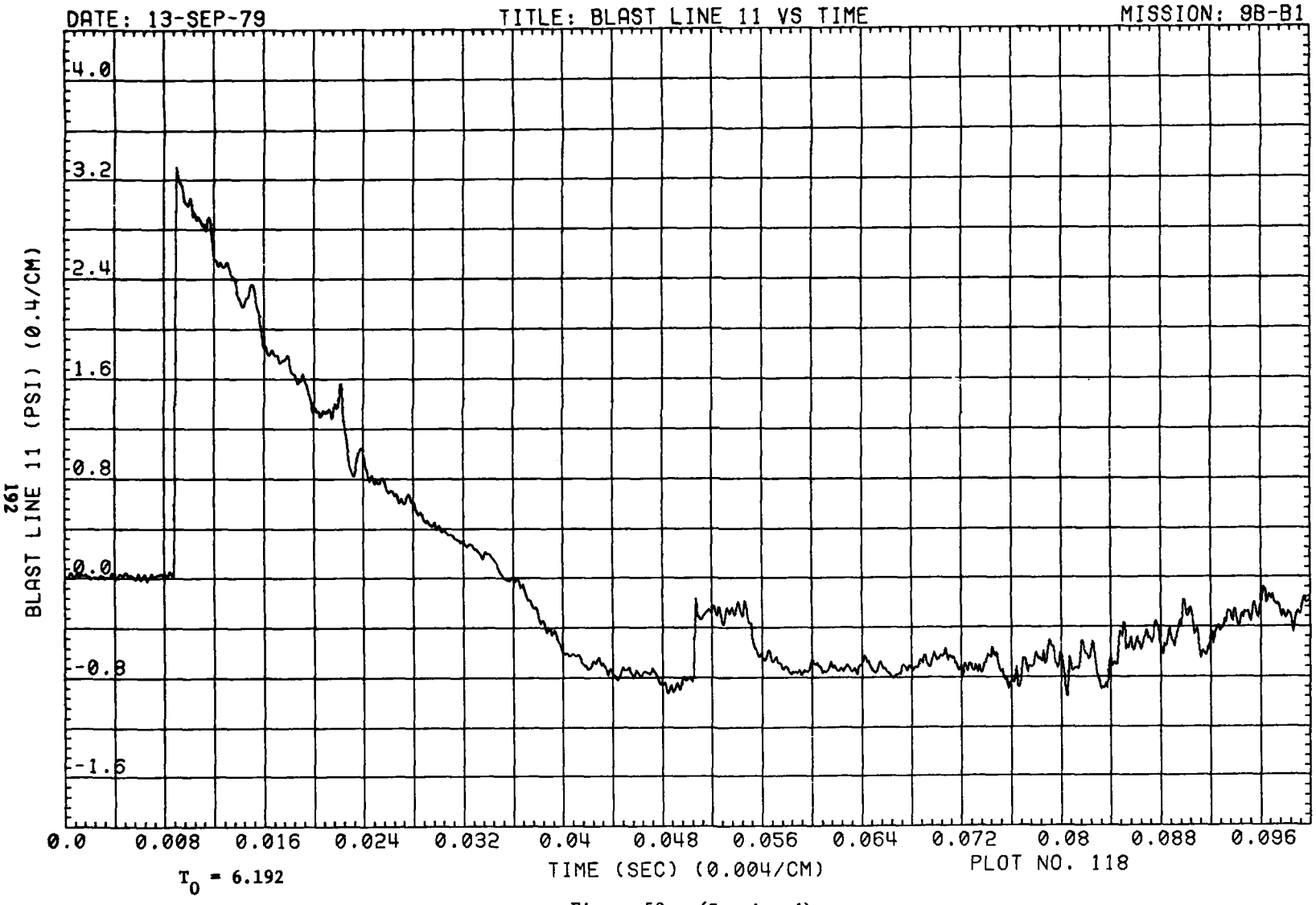

Figure 52. (Continued)

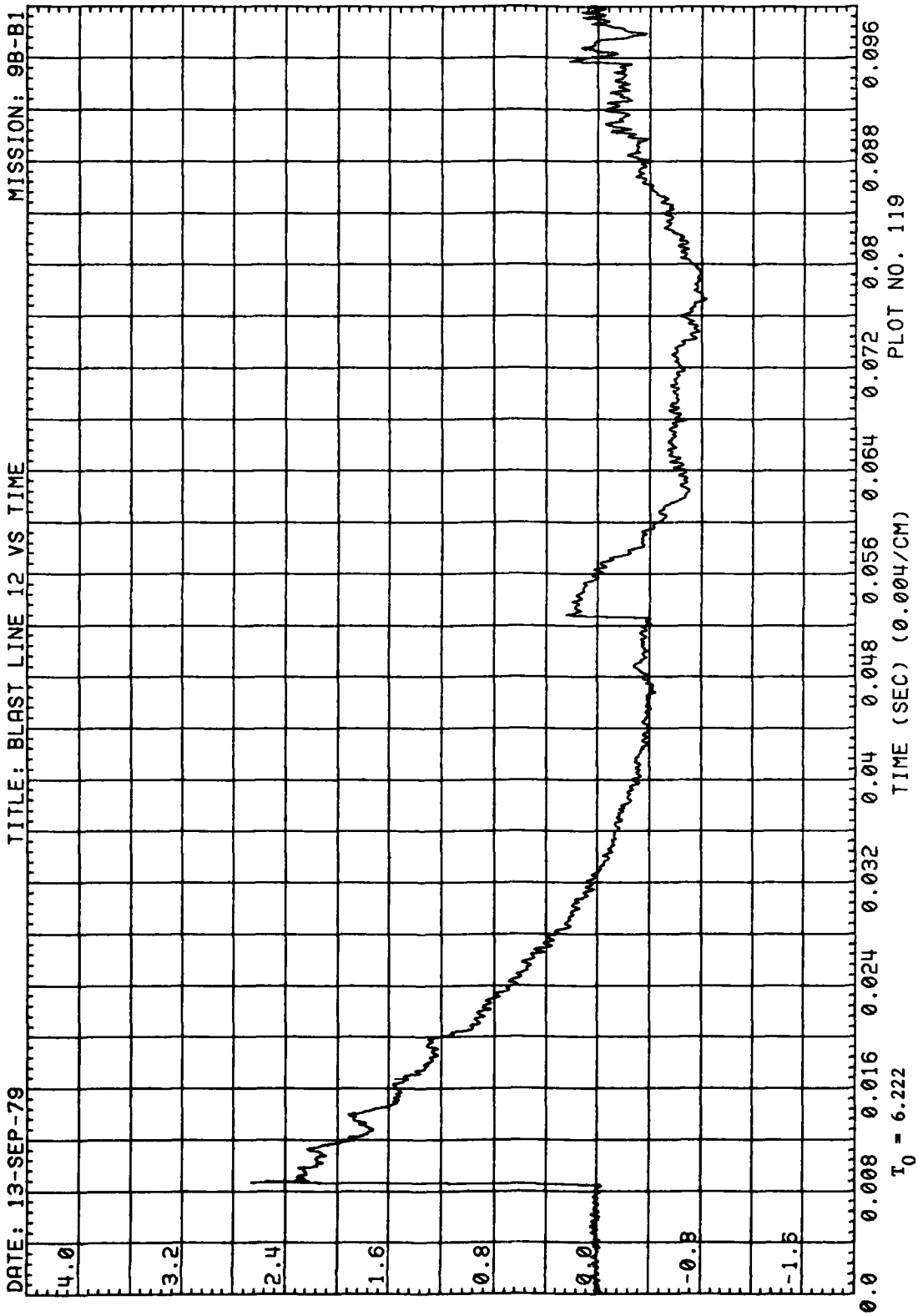

Figure 52. (Concluded)

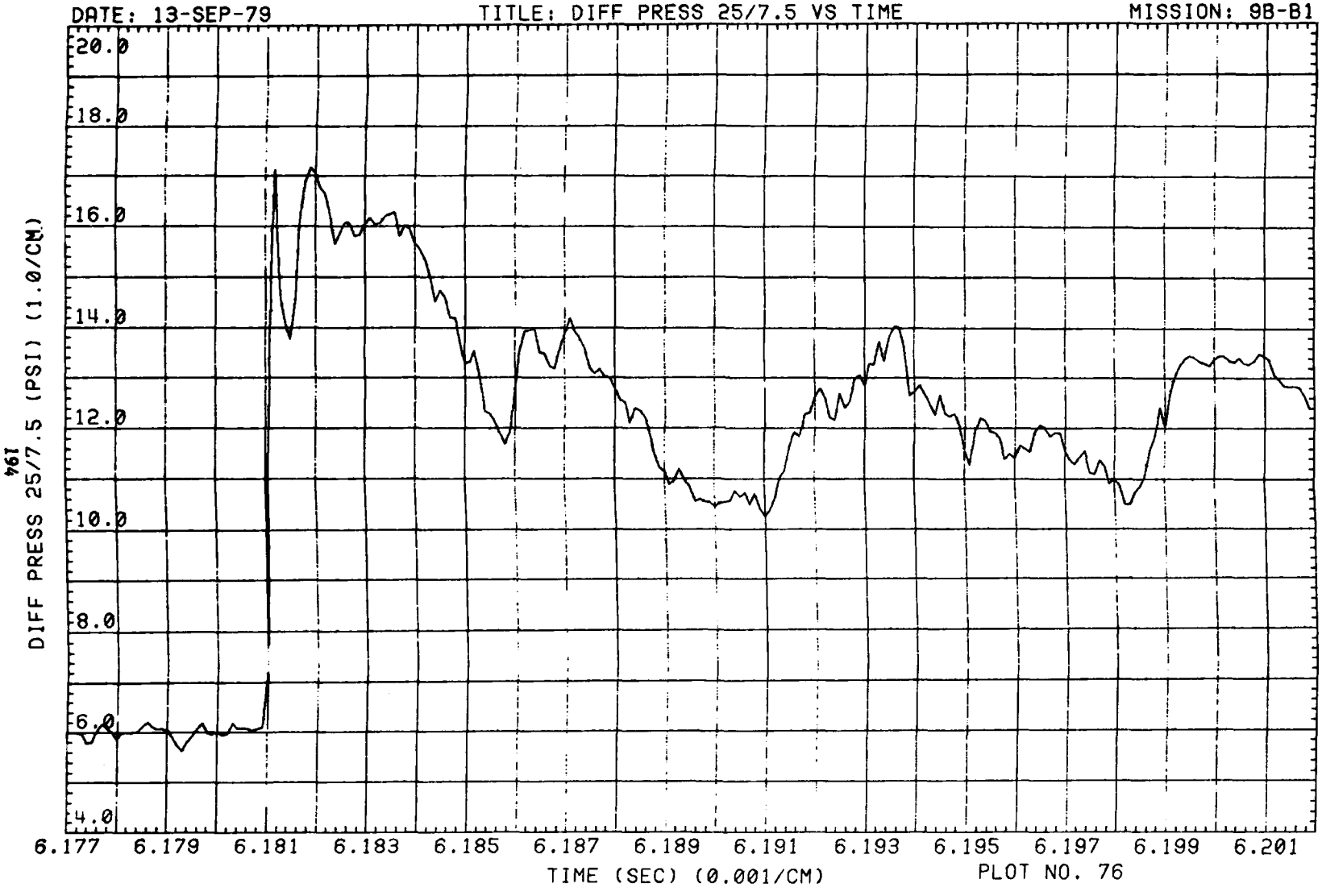

Figure 53. Differential Wing Pressures, Run 9B-B1, Intercept 3

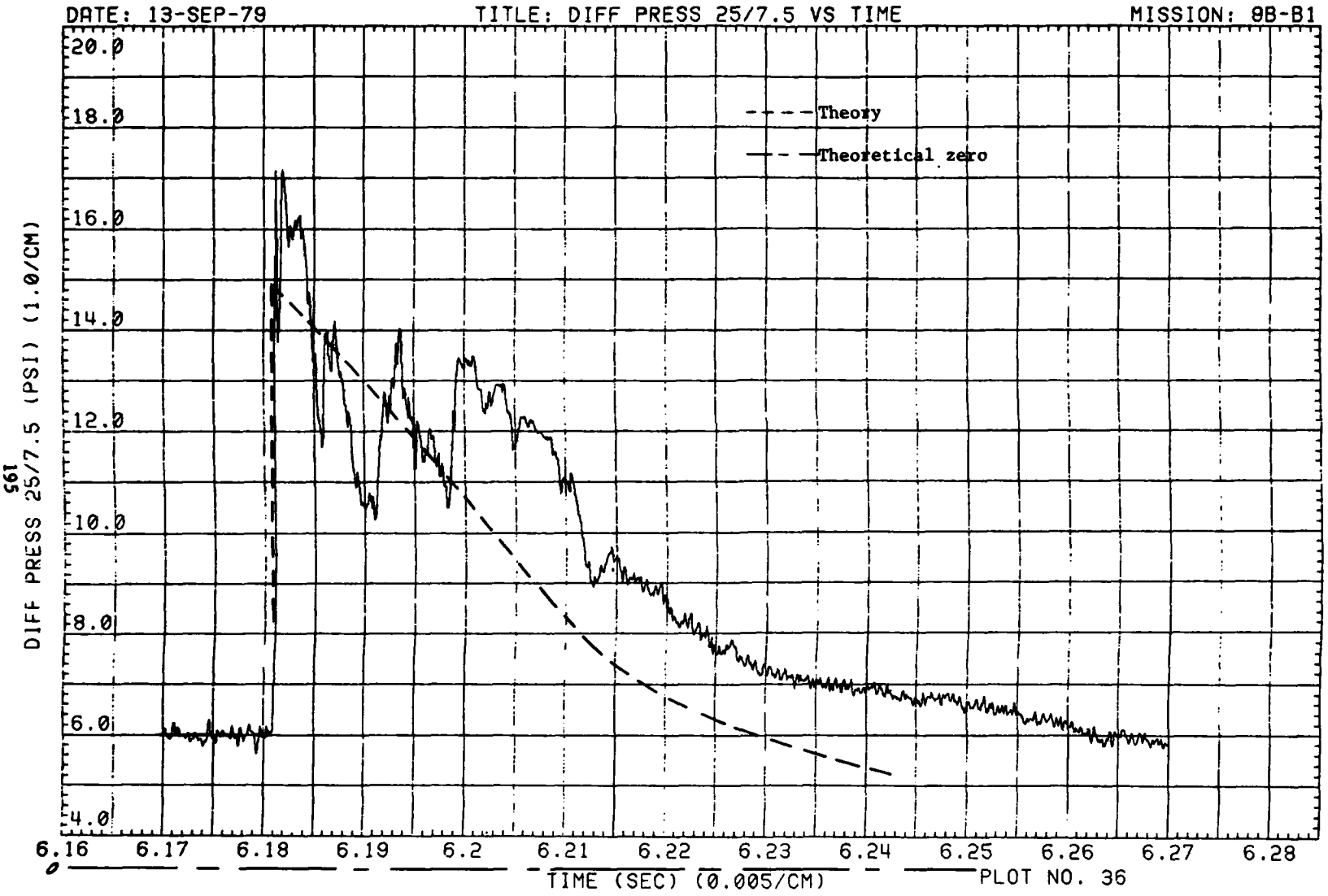

Figure 53. (Continued)

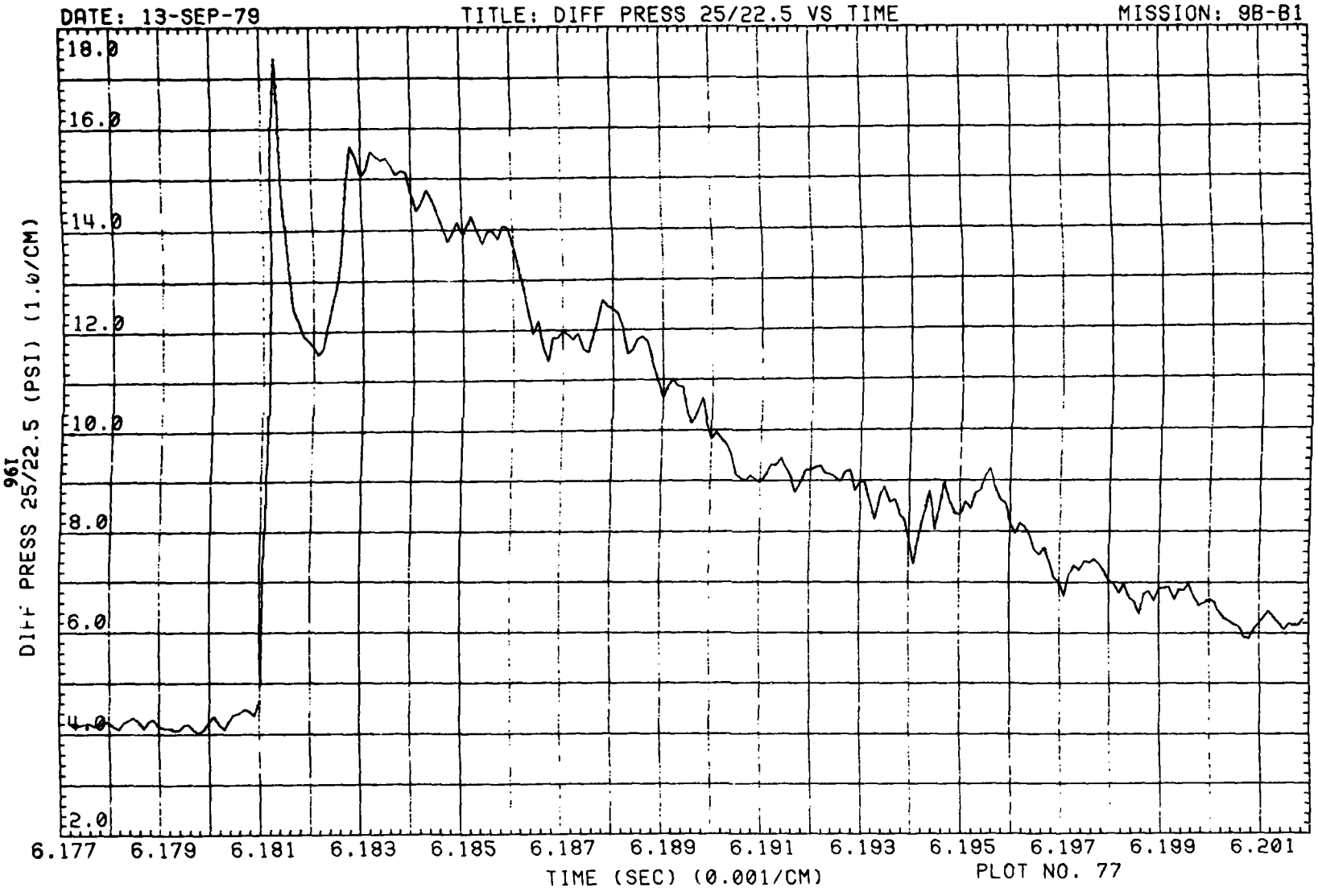

Figure 53. (Continued)

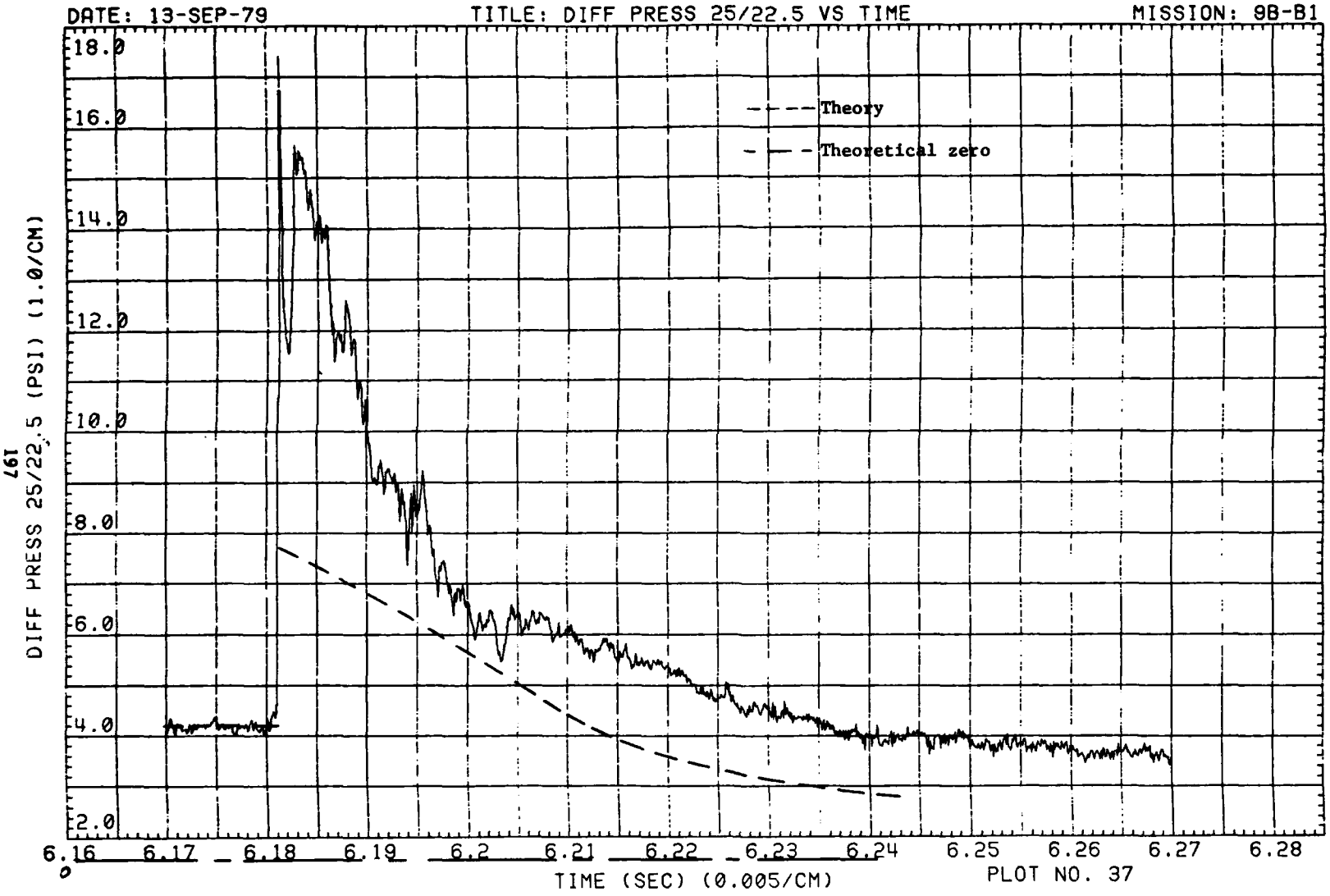

Figure 53. (Continued)

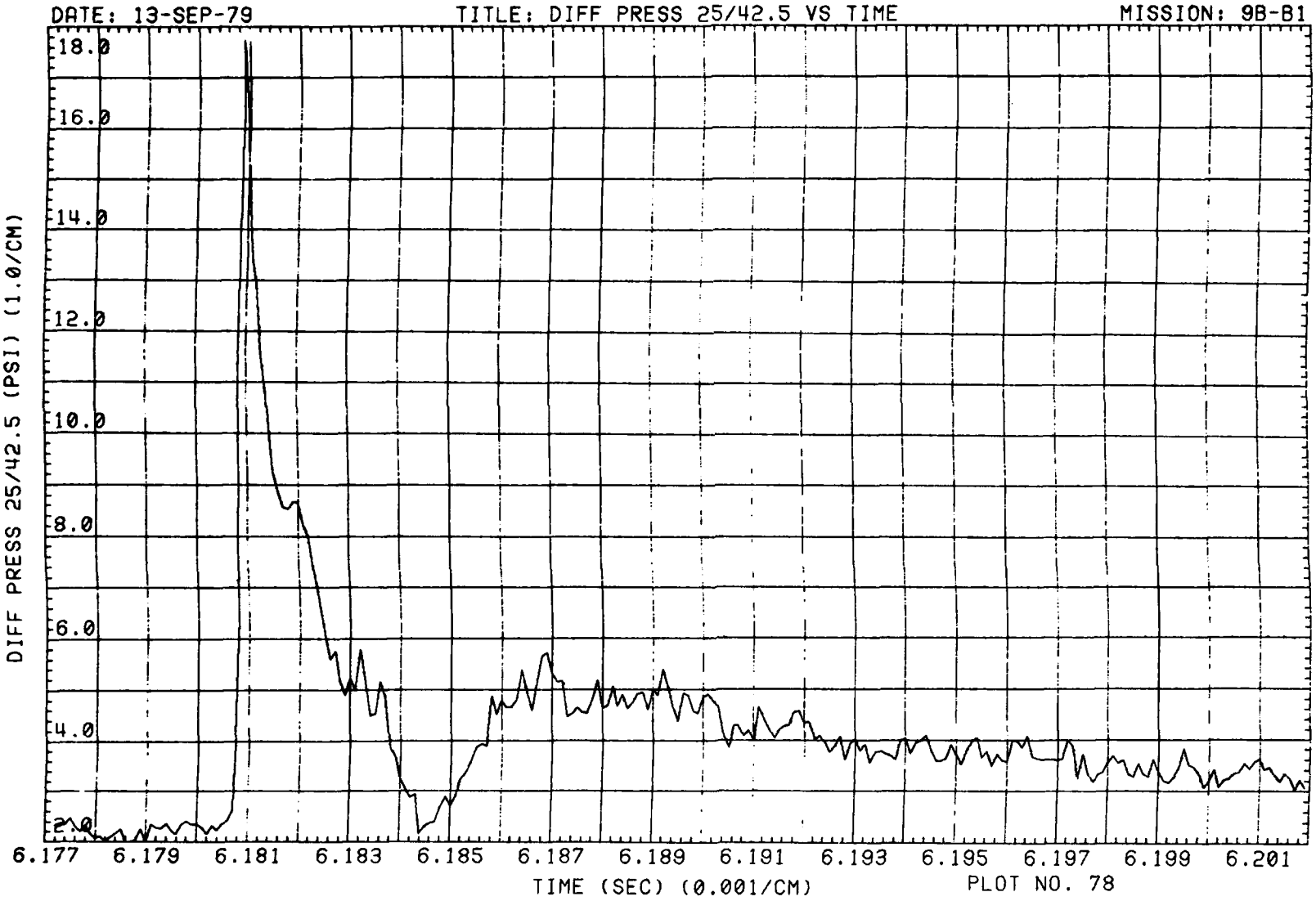

Figure 53. (Continued)

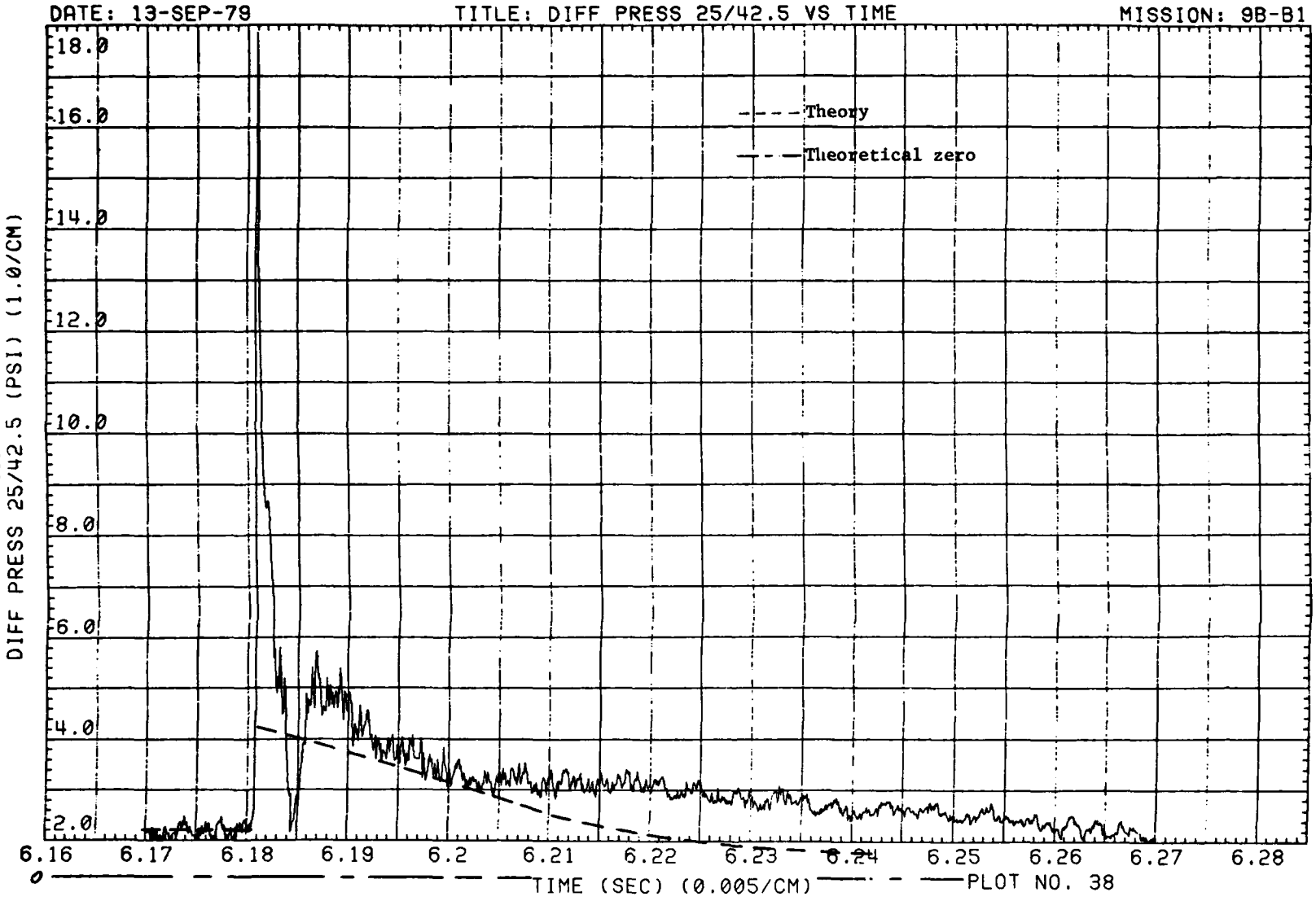

Figure 53. (Continued)

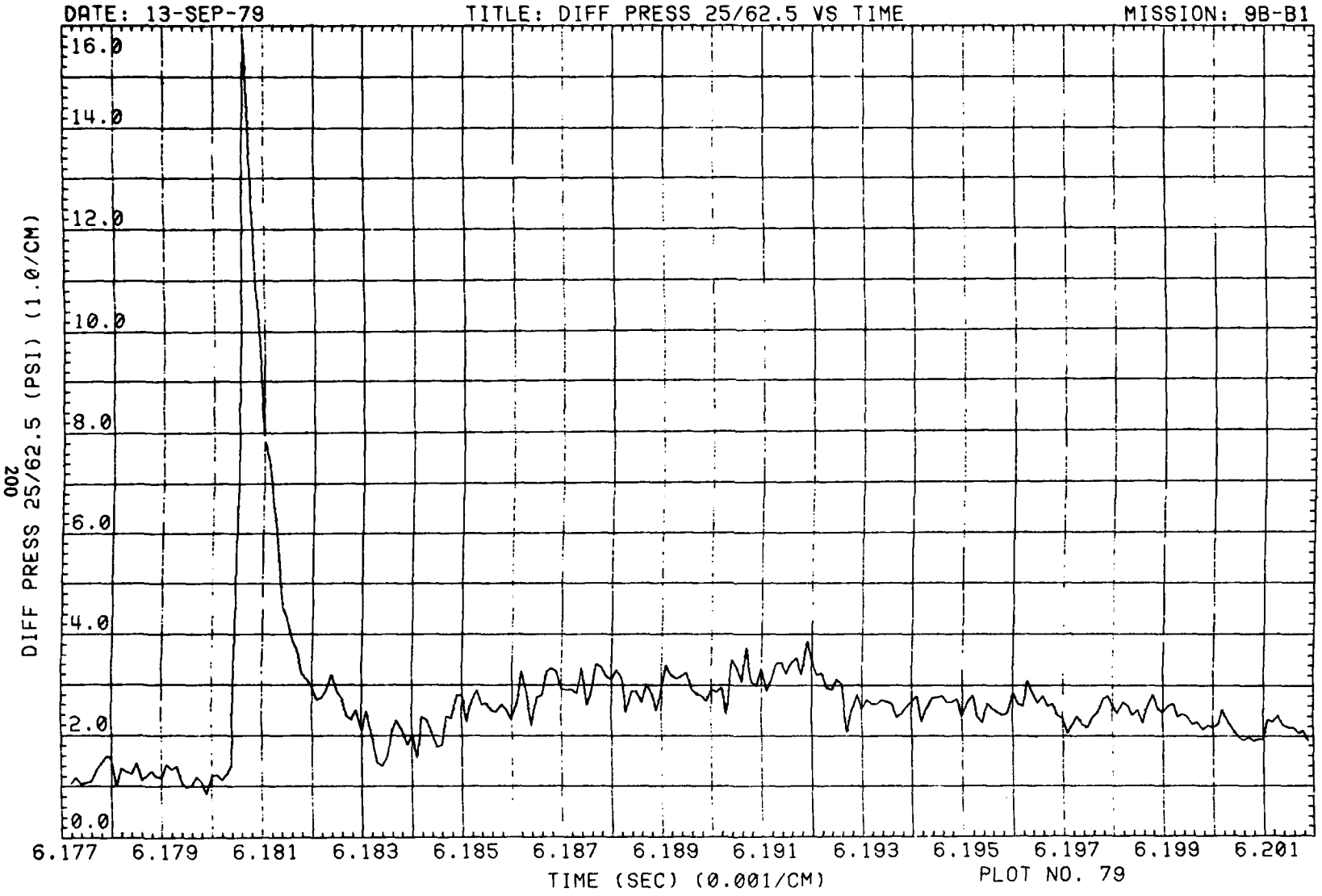

Figure 53. (Continued)

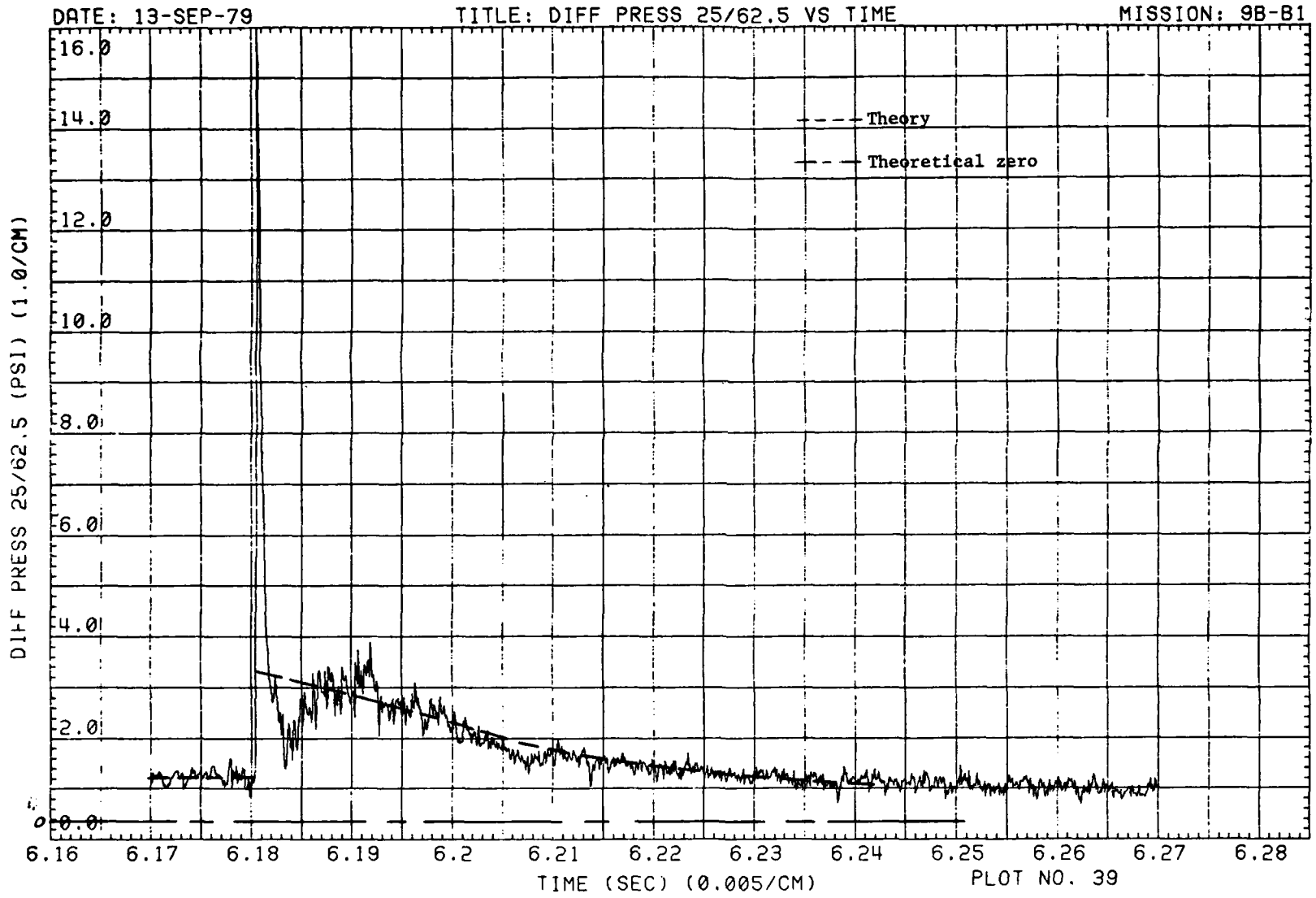

Figure 53. (Continued)

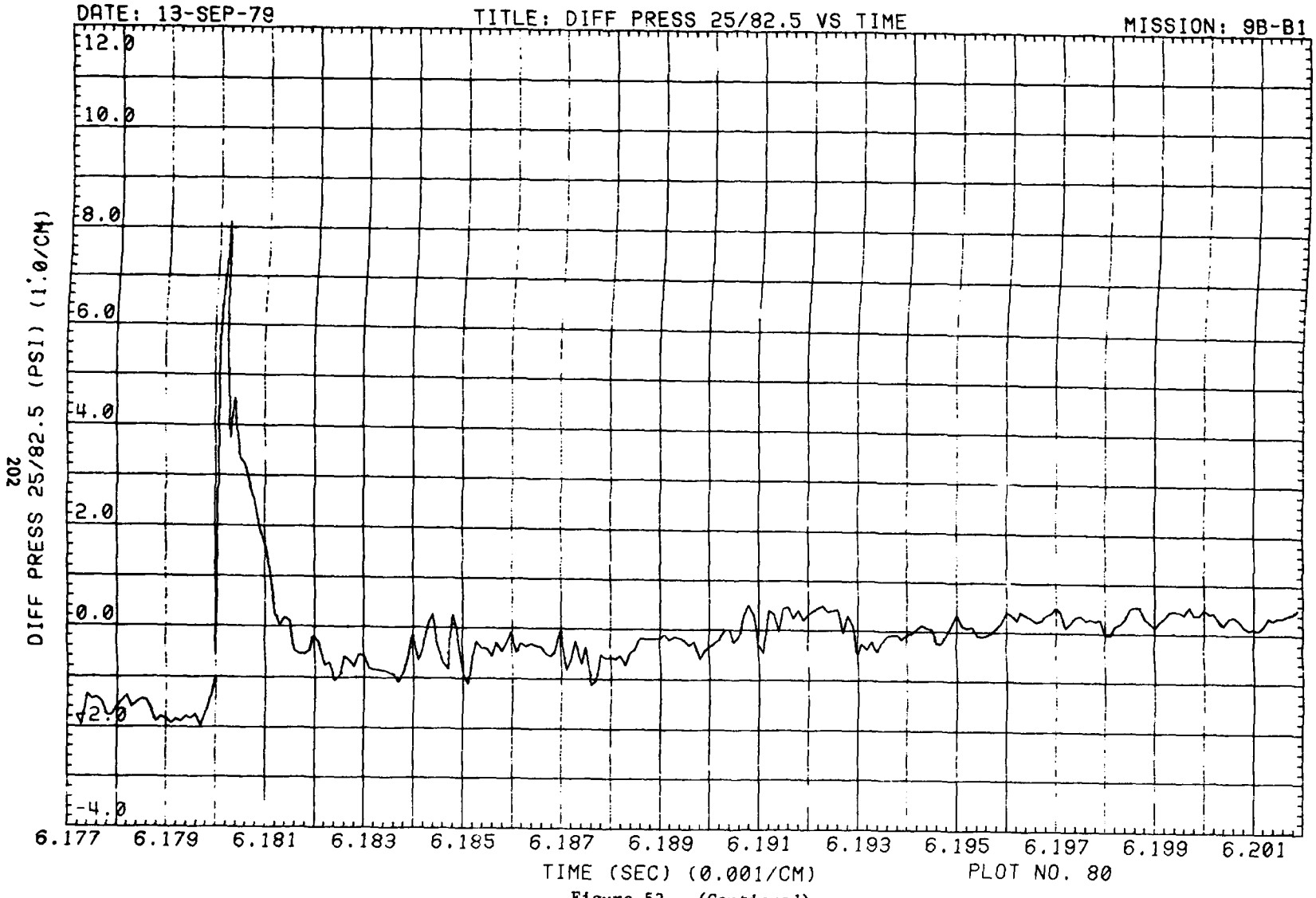

Figure 53. (Continued)

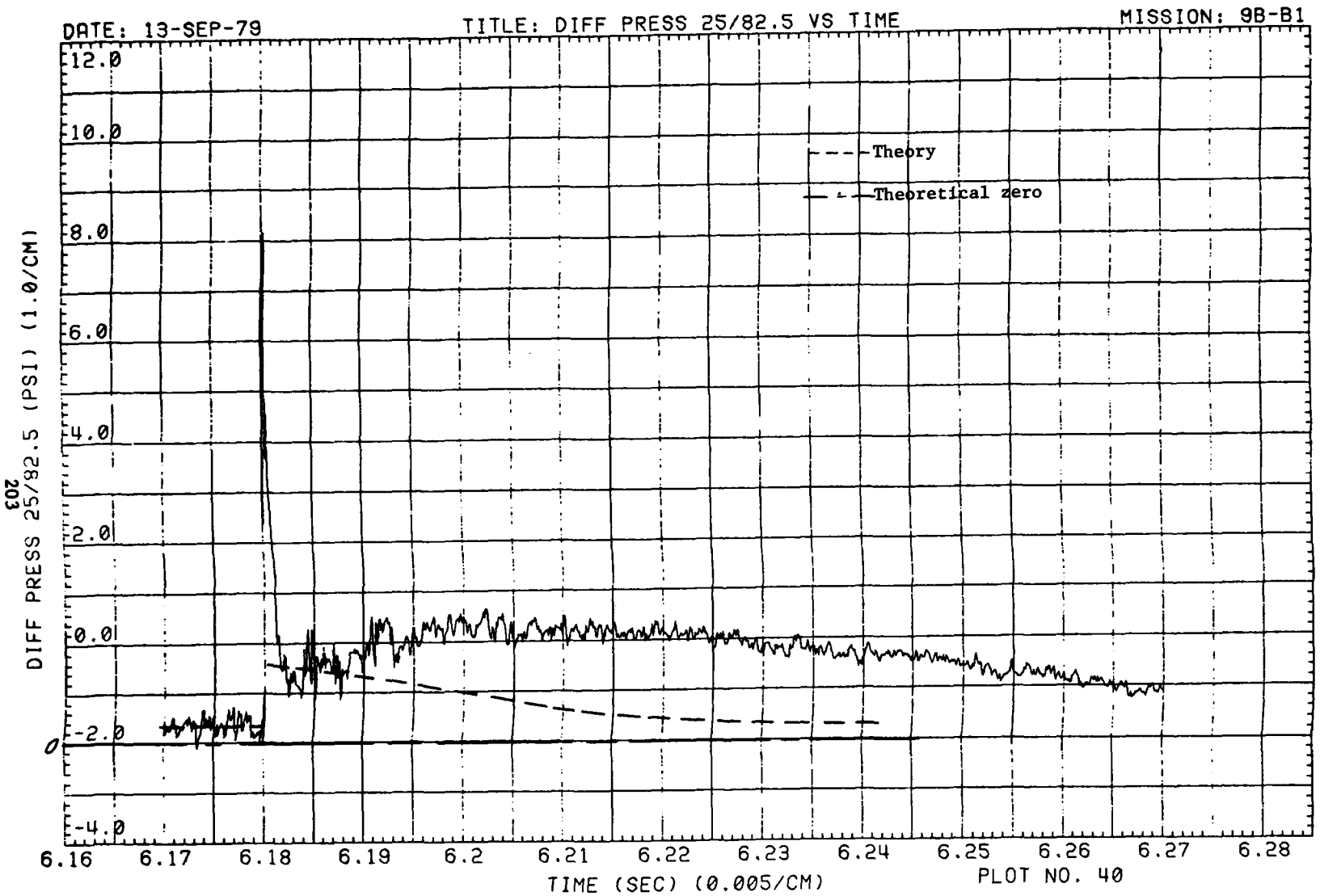

Figure 53. (Continued)

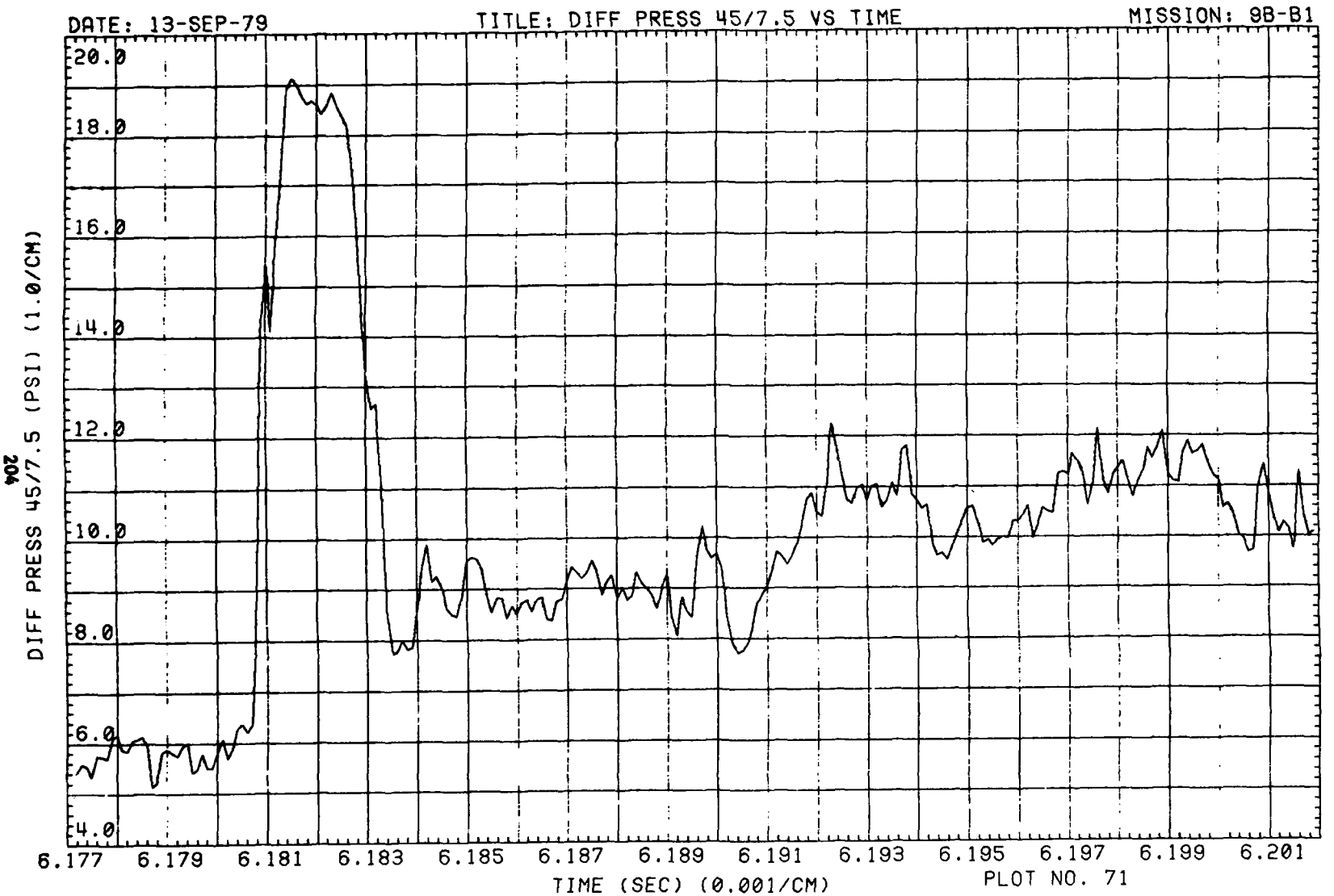

Figure 53. (Continued)

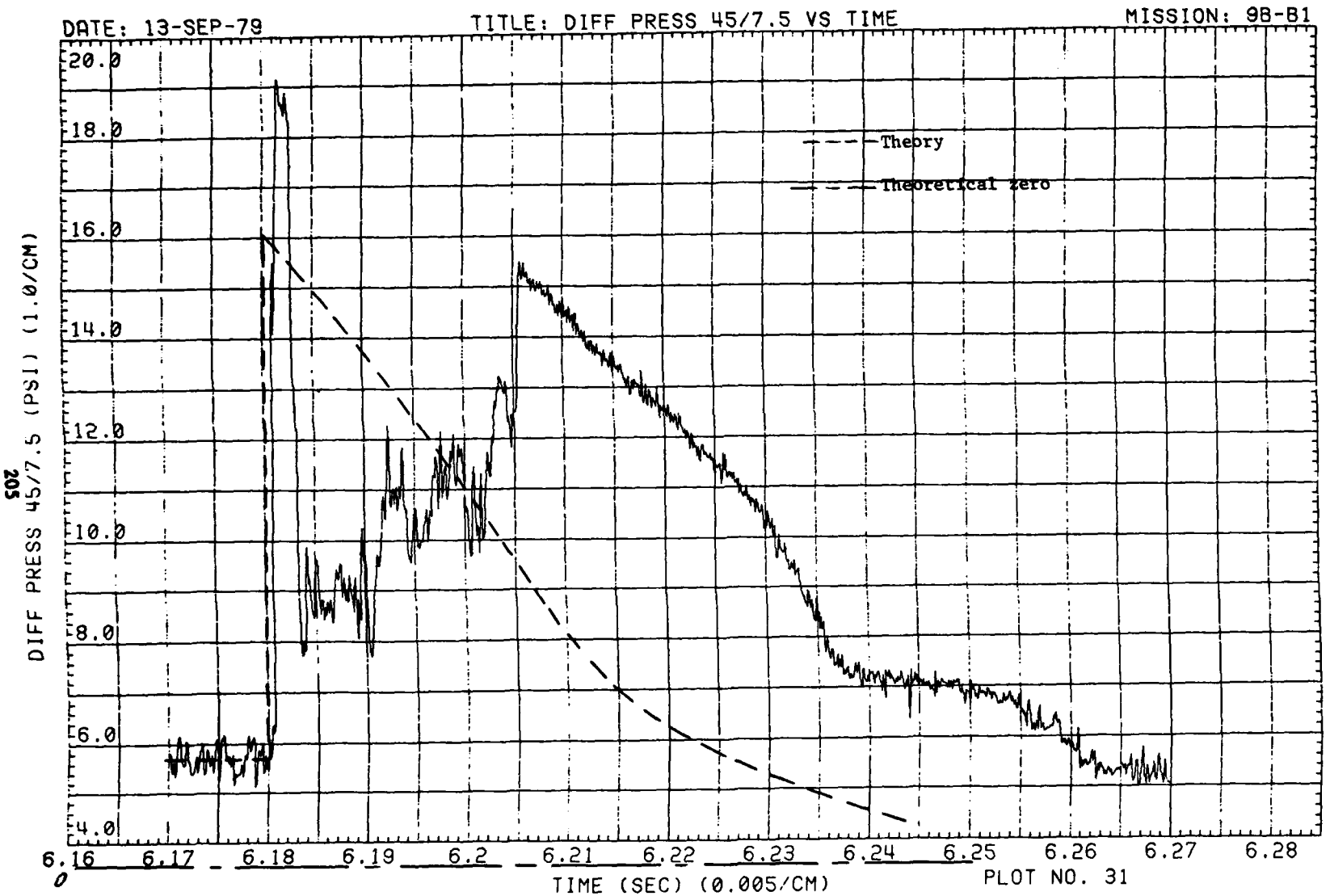

Figure 53. (Continued)

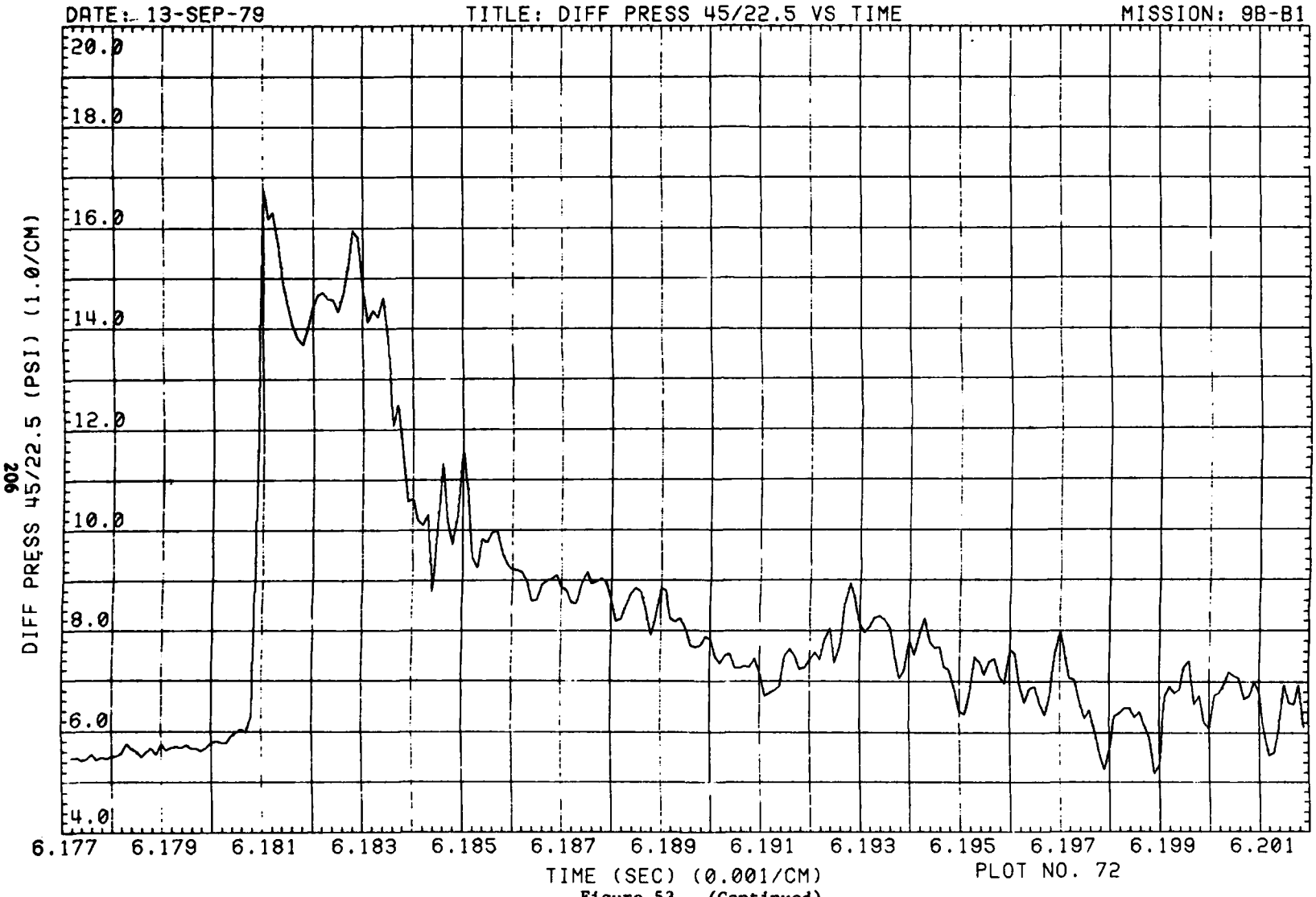

Figure 53. (Continued)

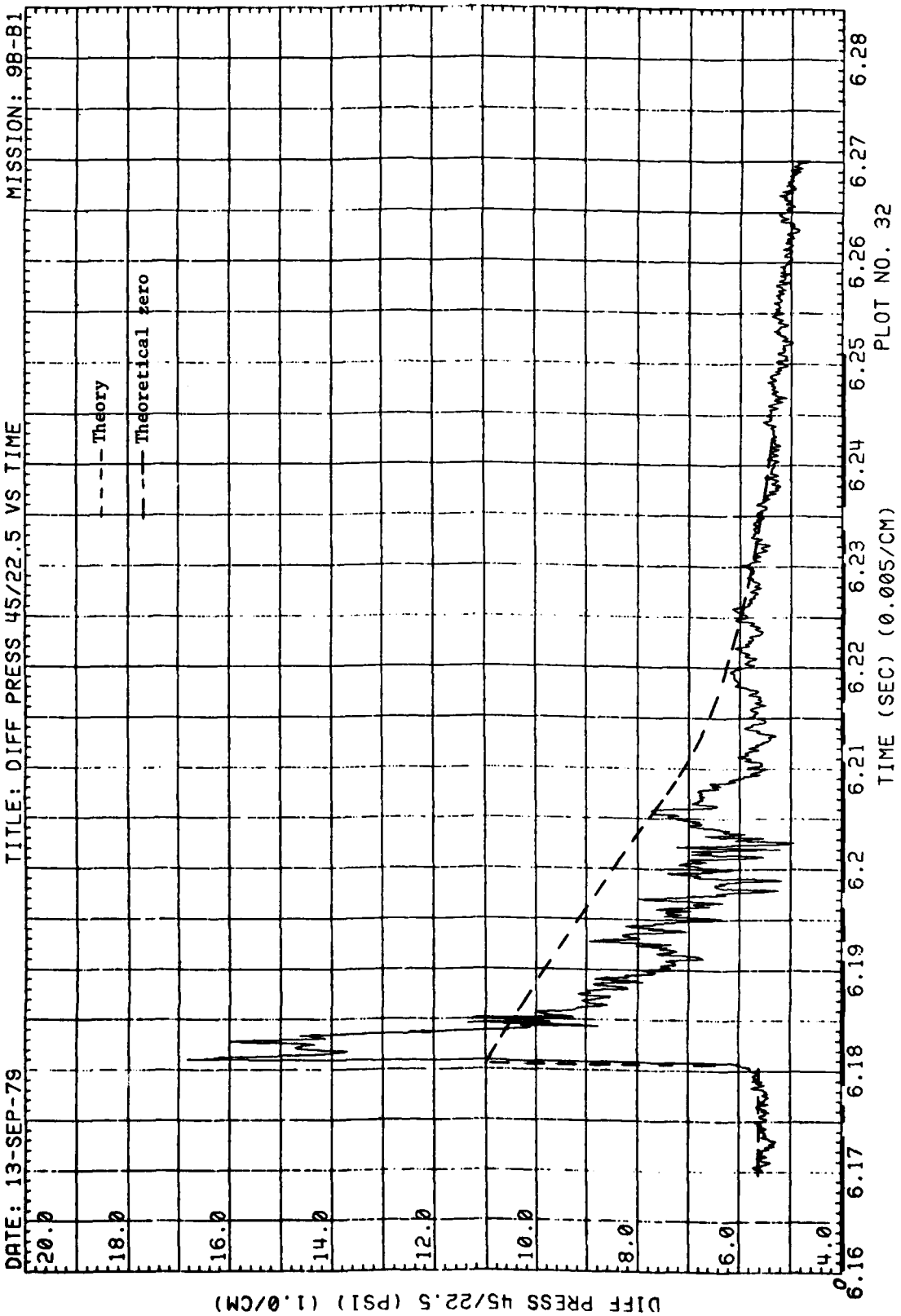

Figure 53. (Continued)

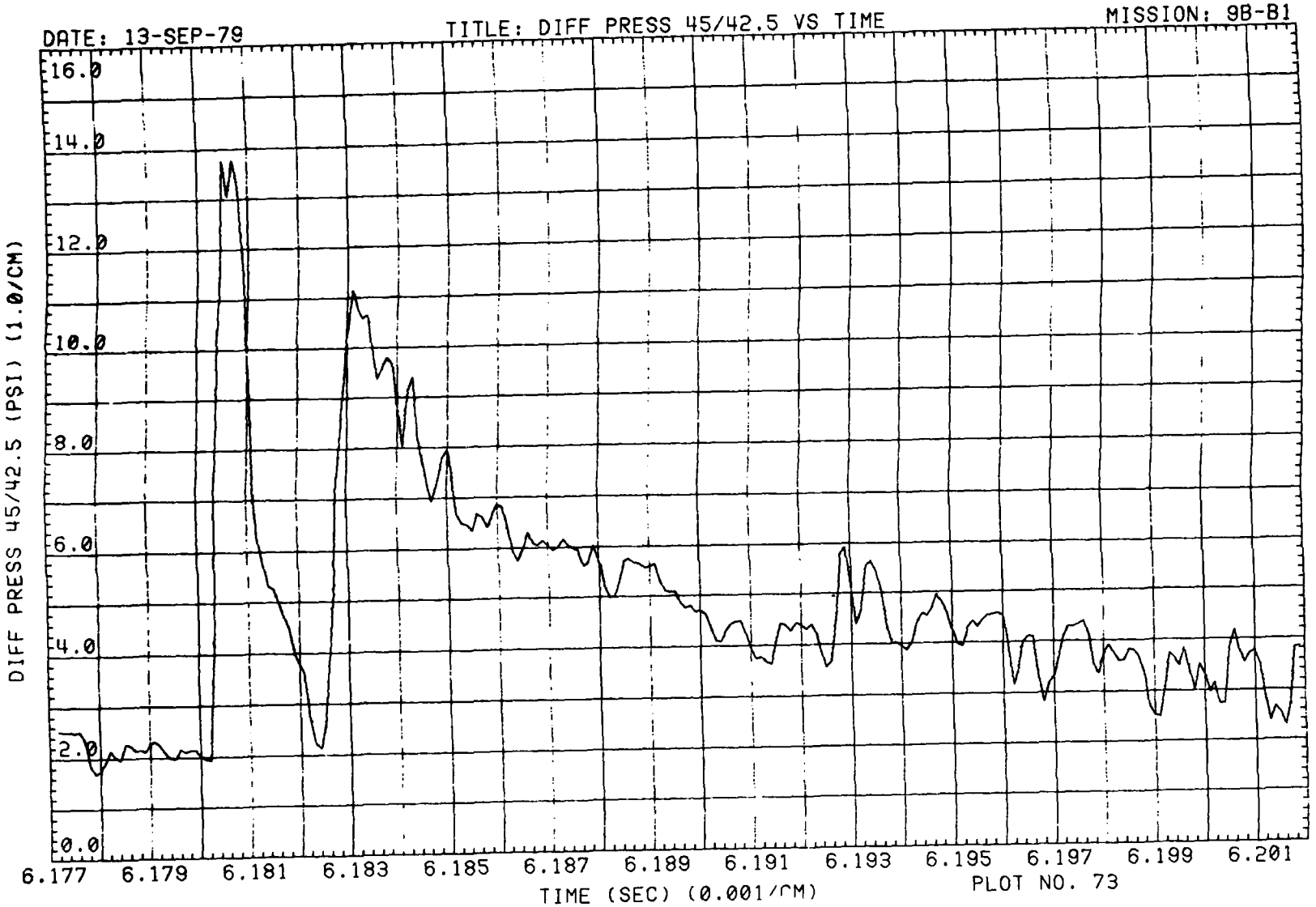

Figure 53. (Continued)

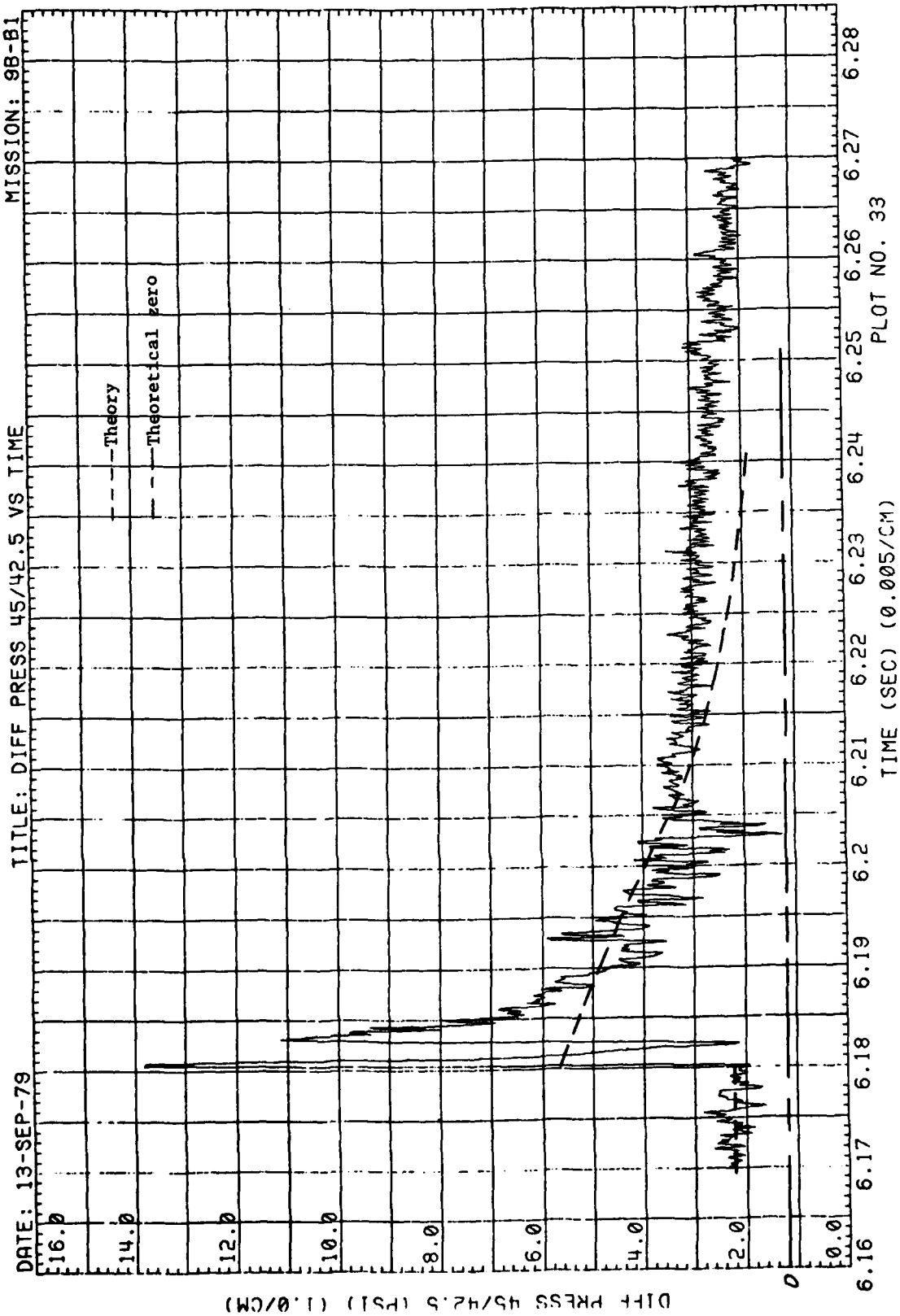

Figure 53. (Continued)

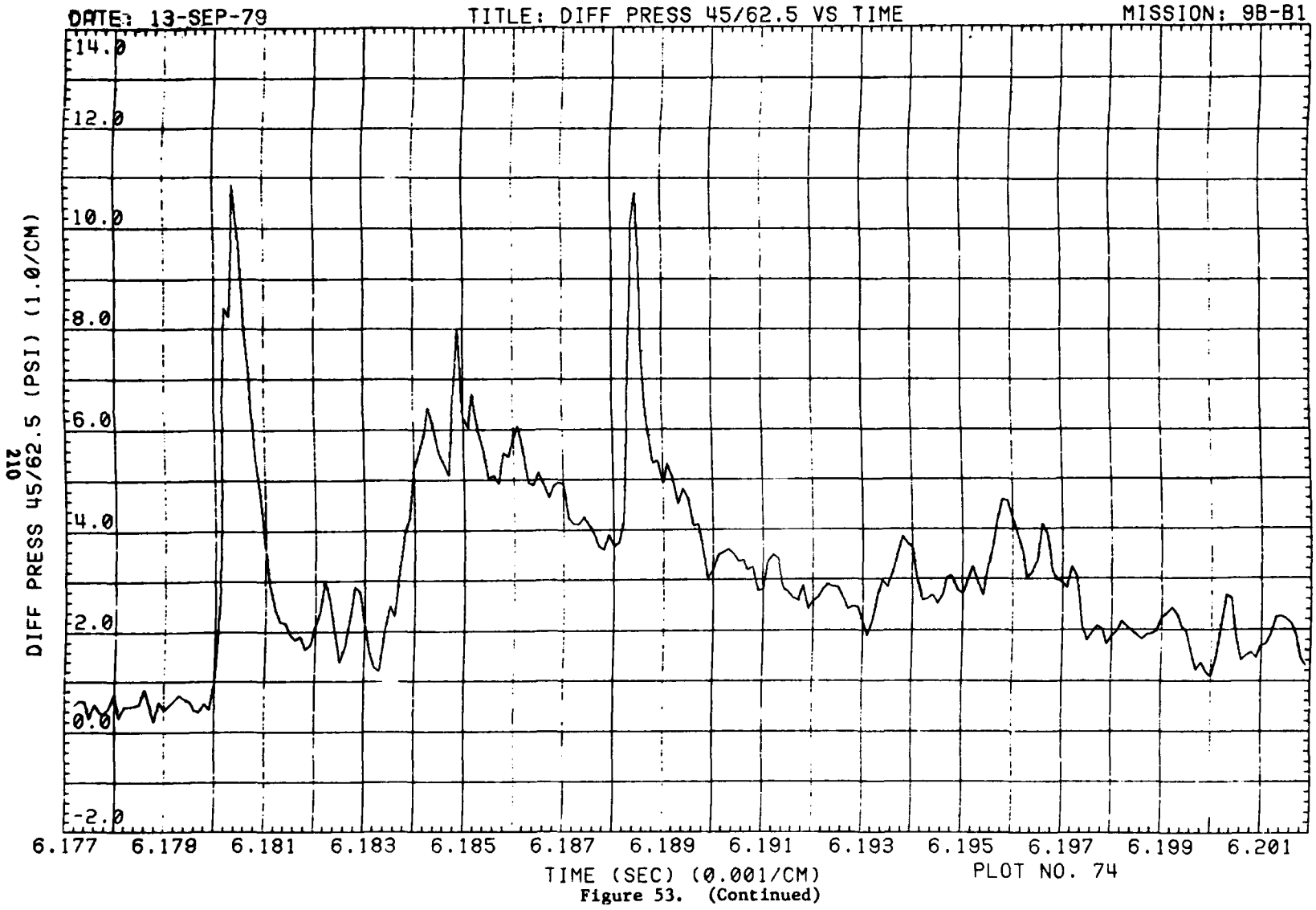

Figure 53. (Continued)

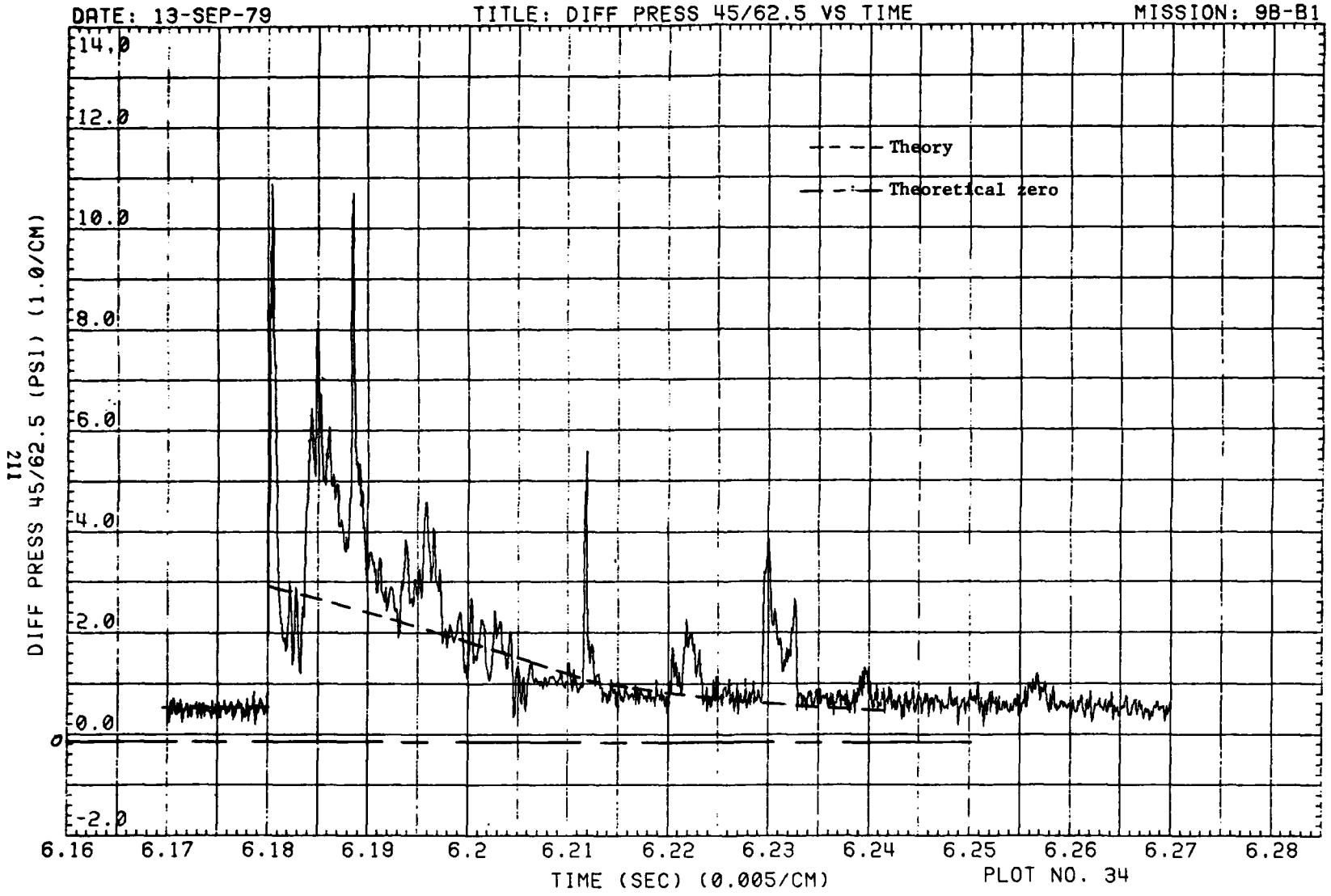

Figure 53. (Continued)

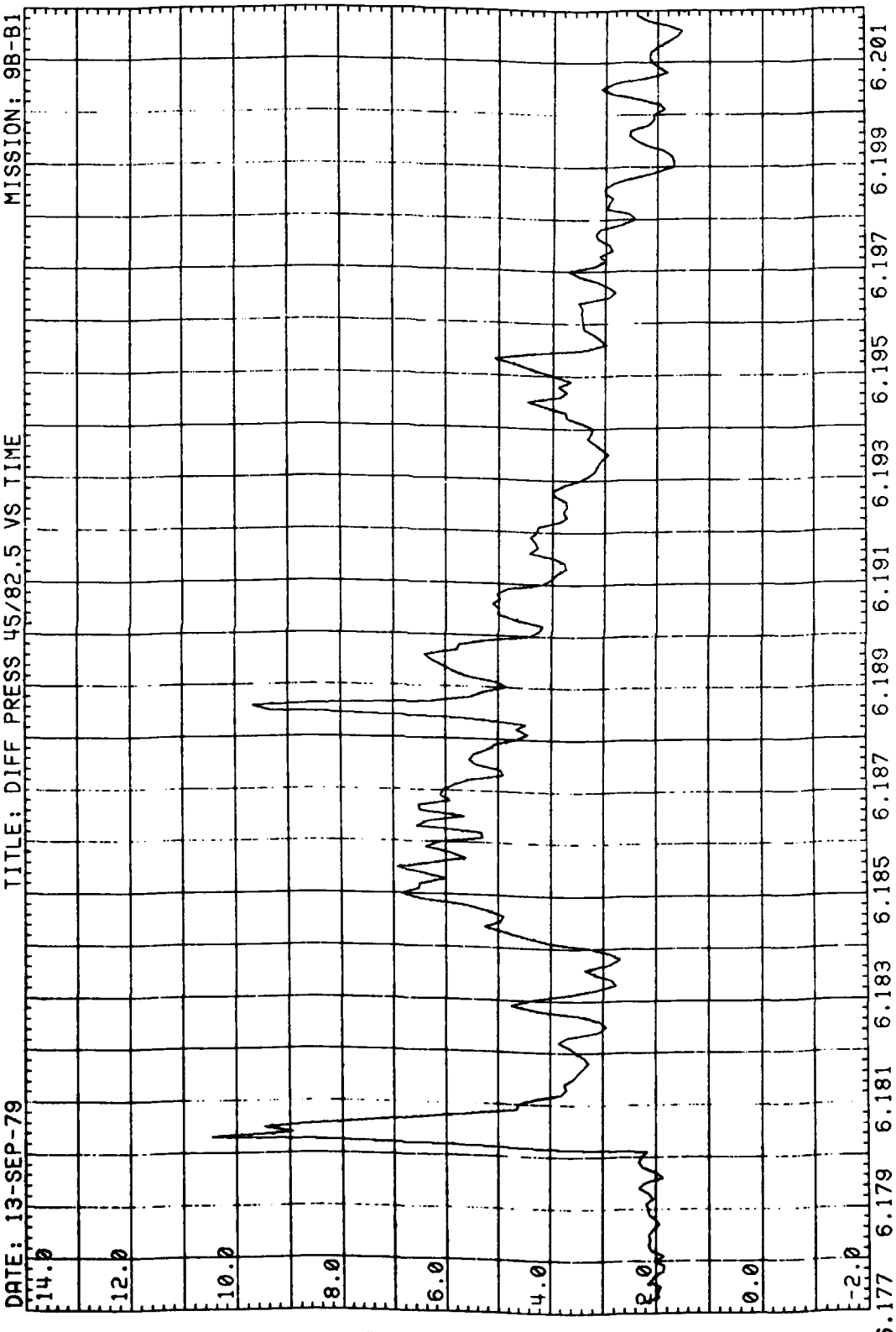

Figure 53. (Continued)

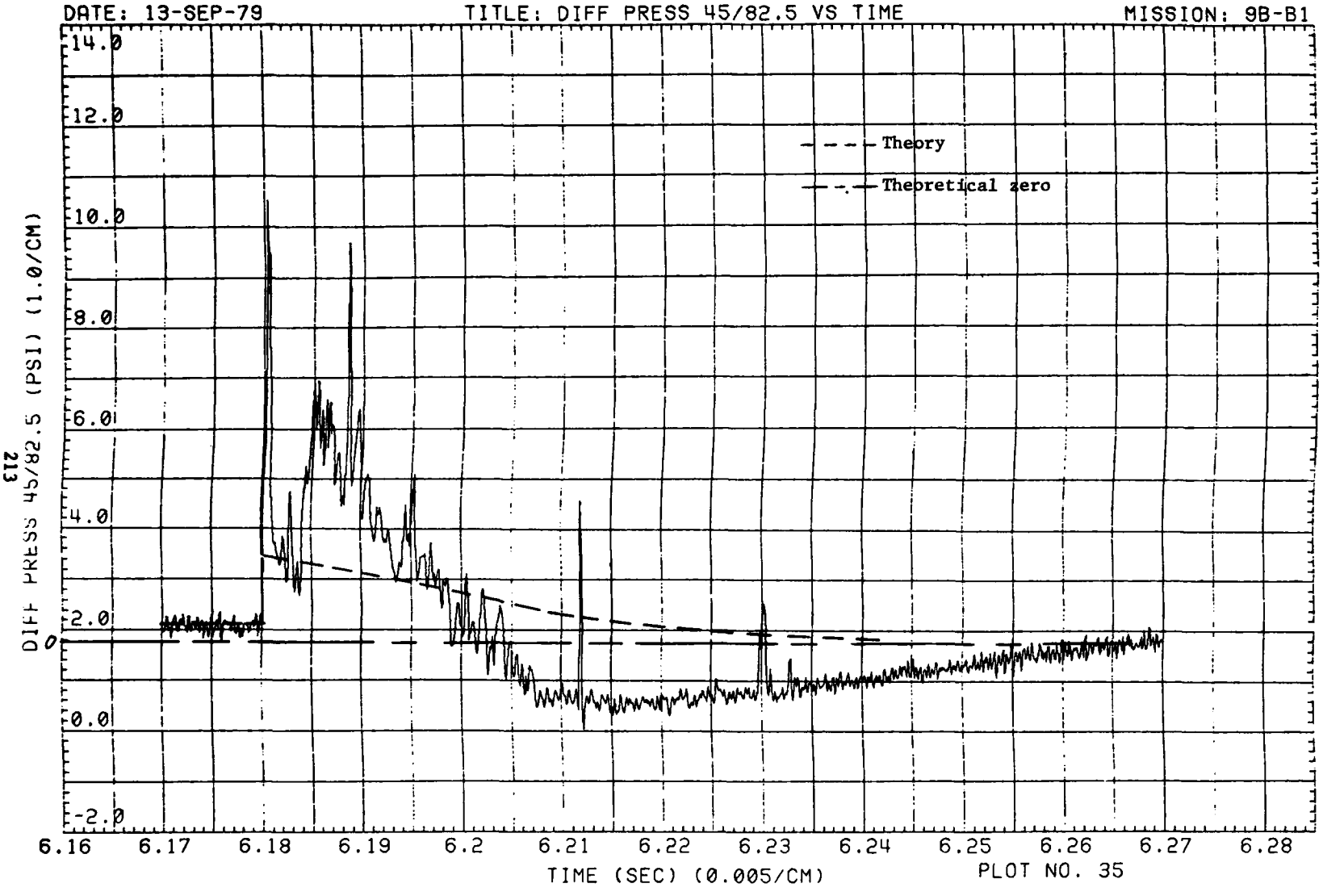

Figure 53. (Continued)

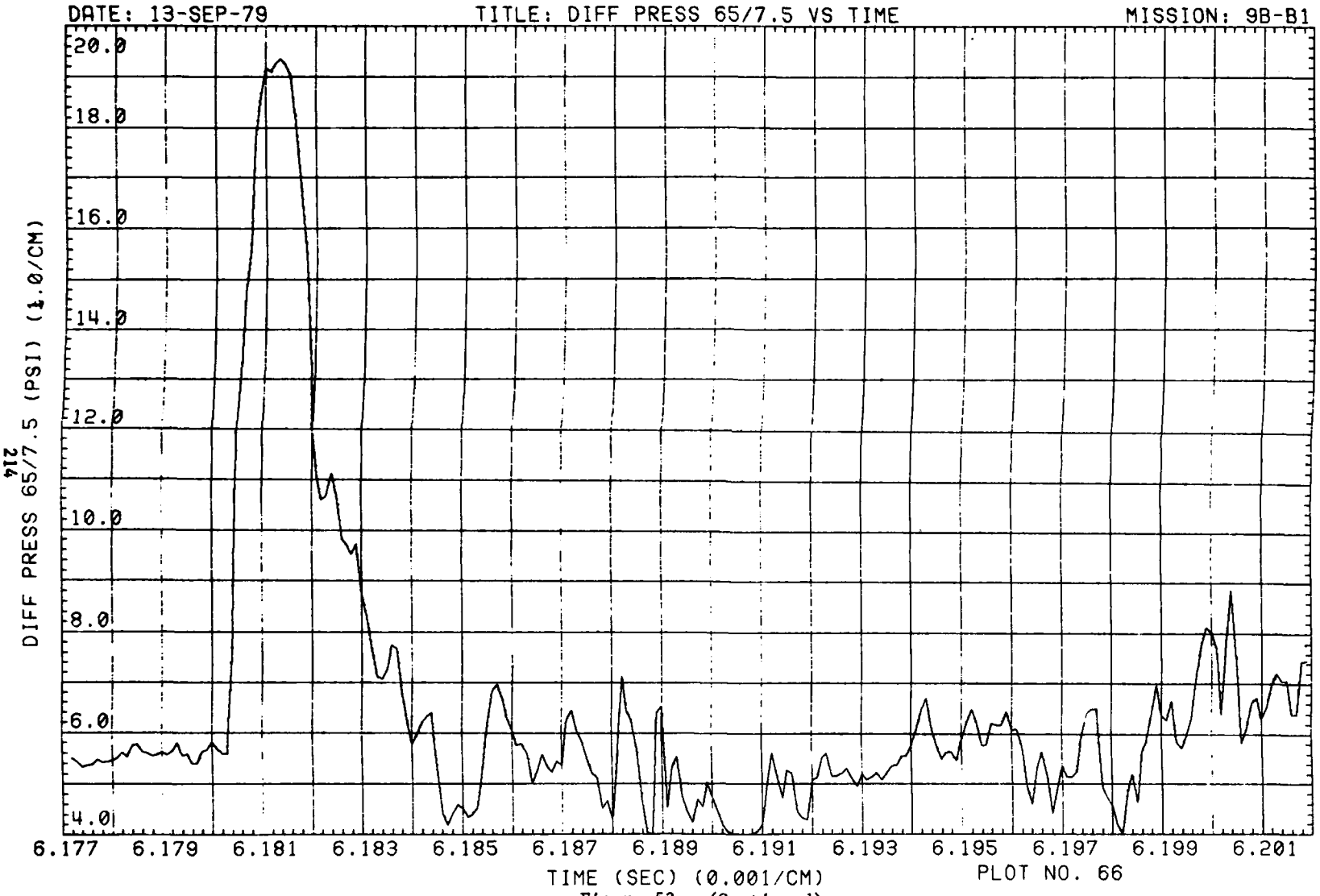

214

Figure 53. (Continued)

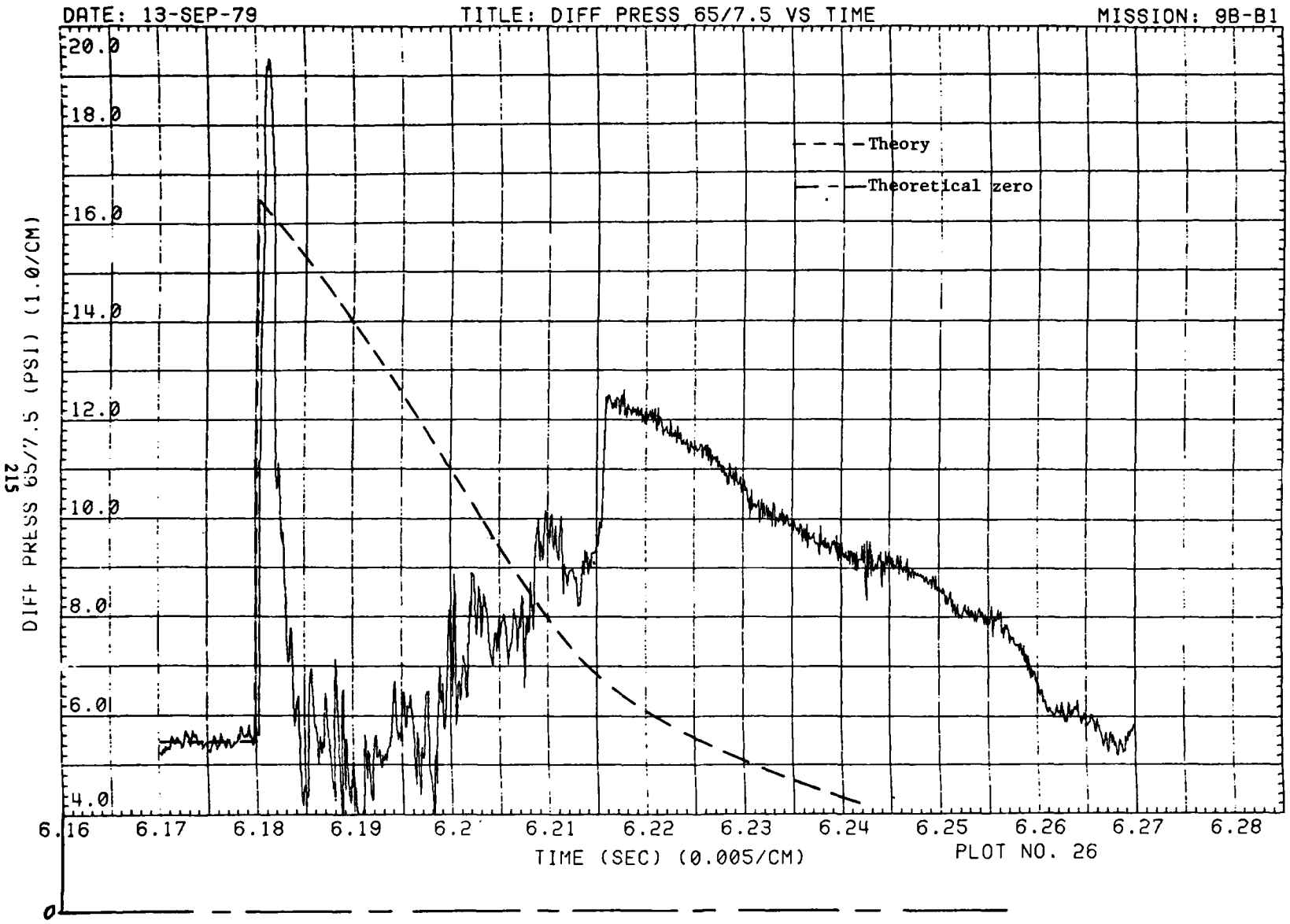

Figure 53. (Continued)

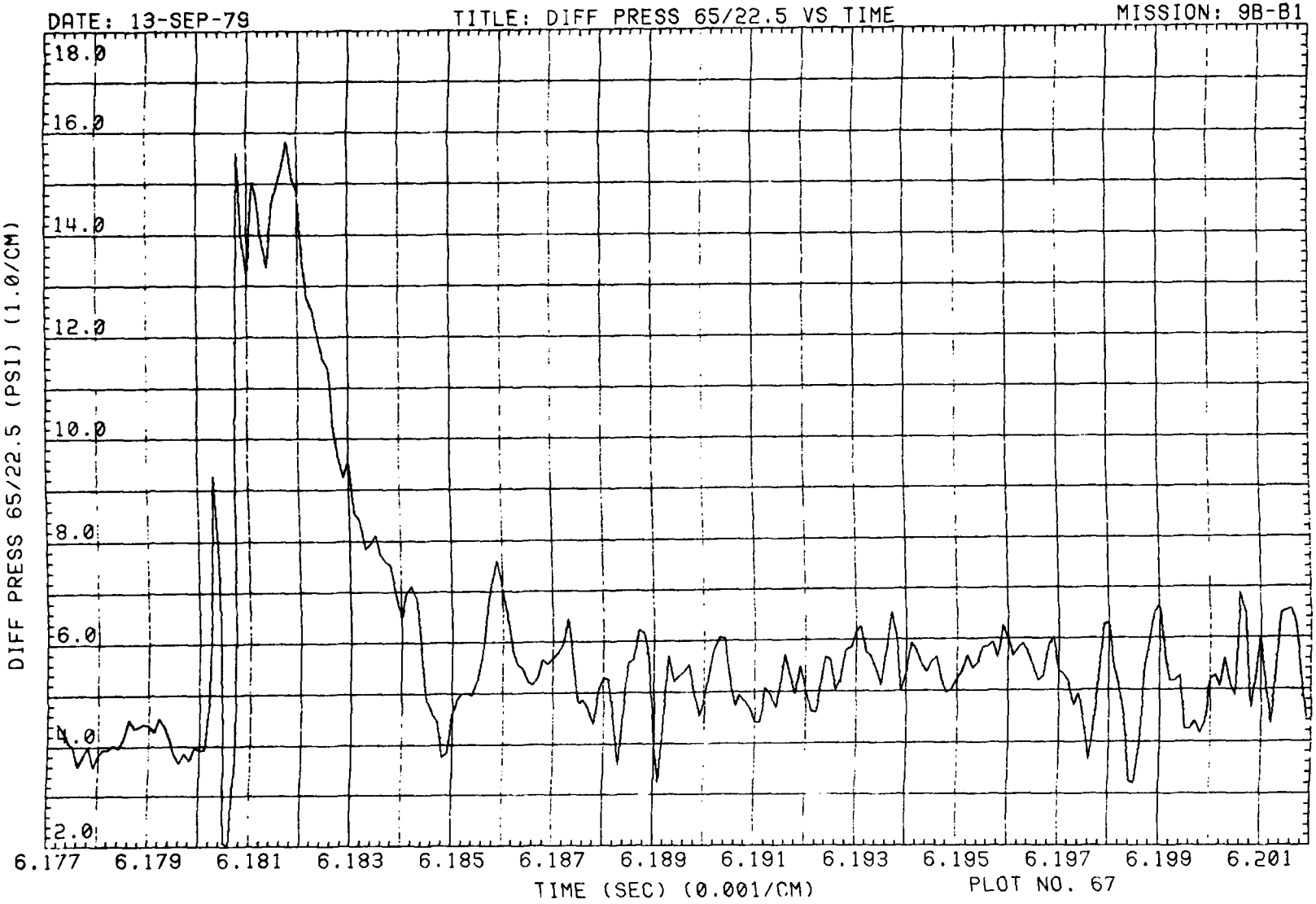

Figure 53. (Continued)

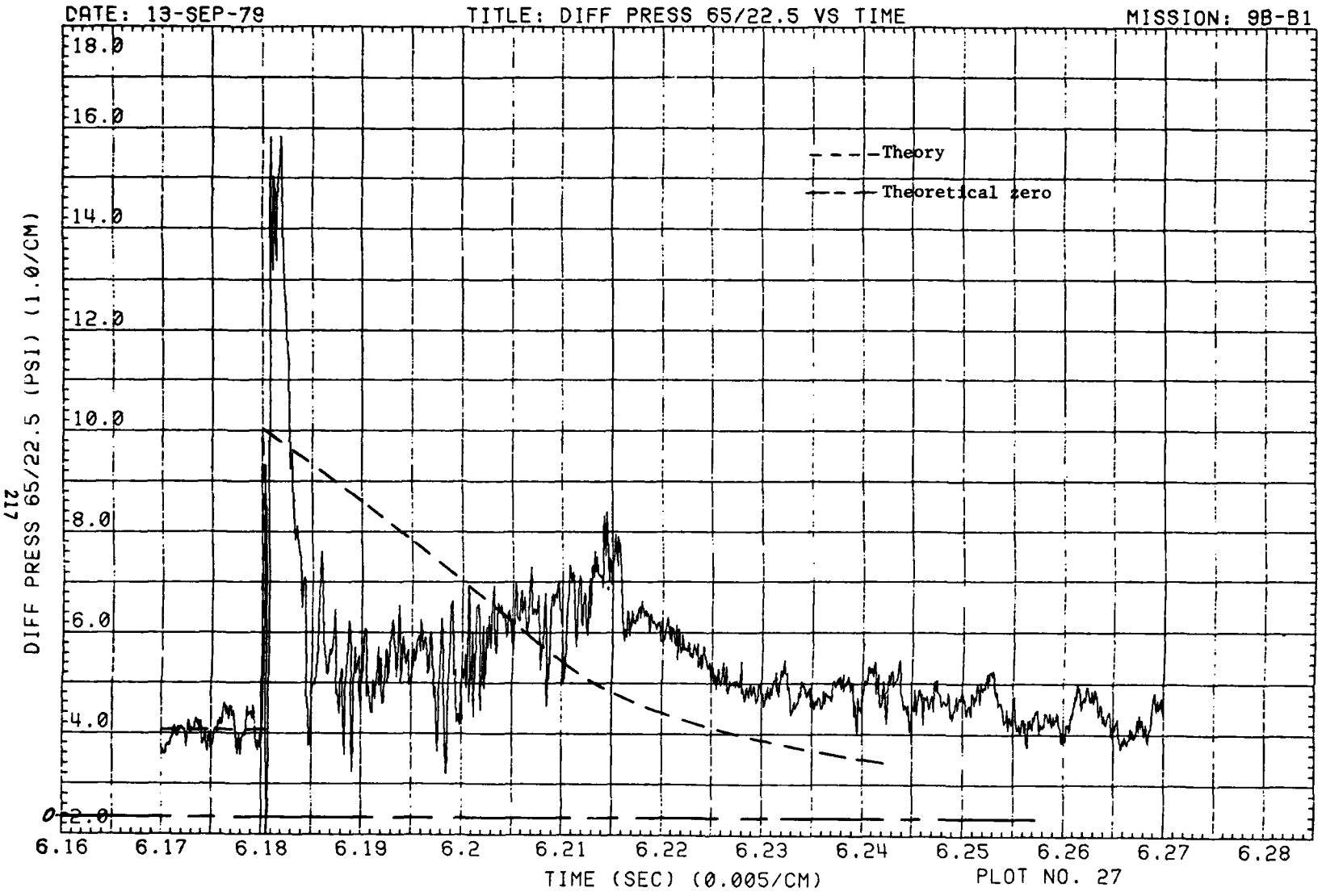

Figure 53. (Continued)

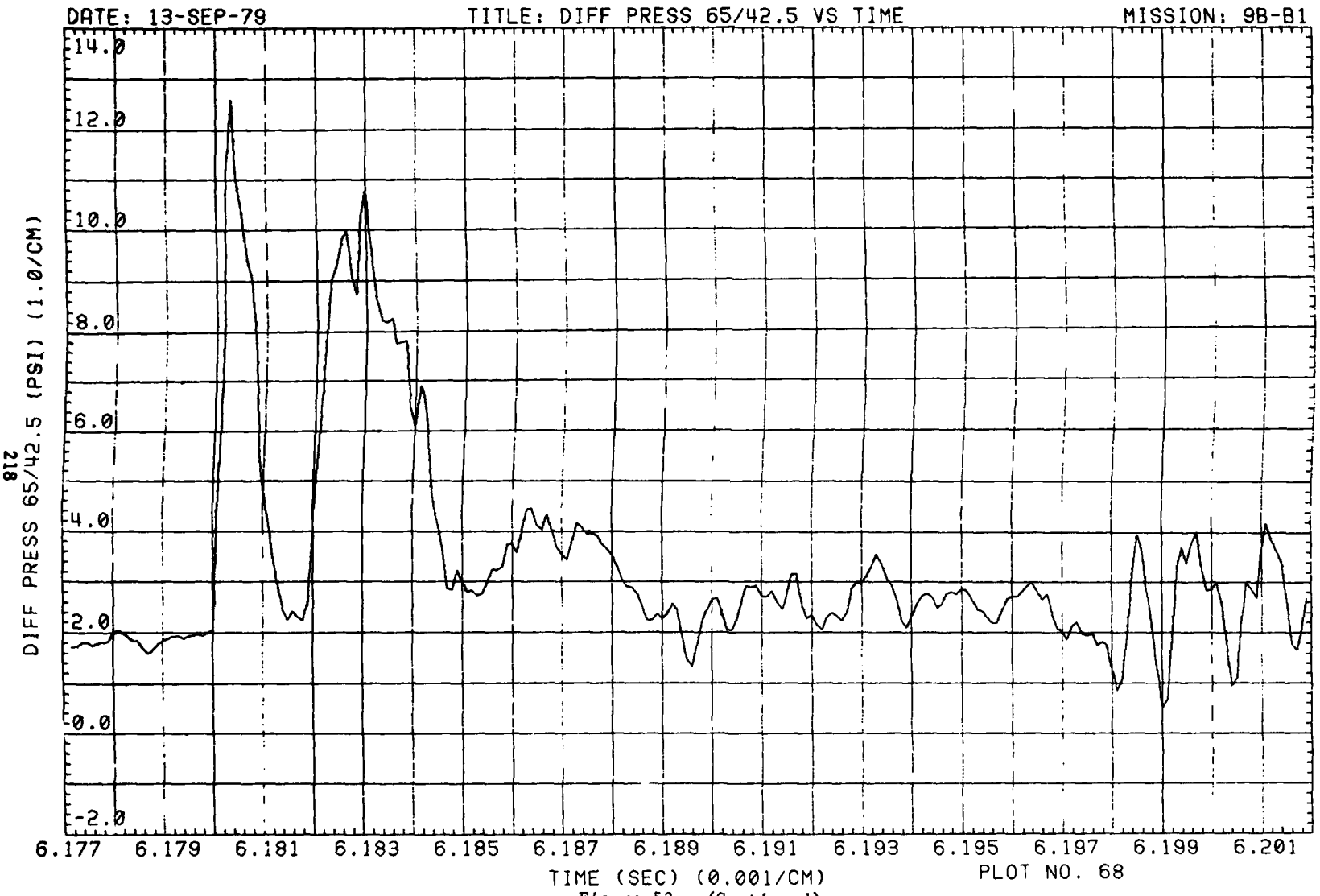

Figure 53. (Continued)

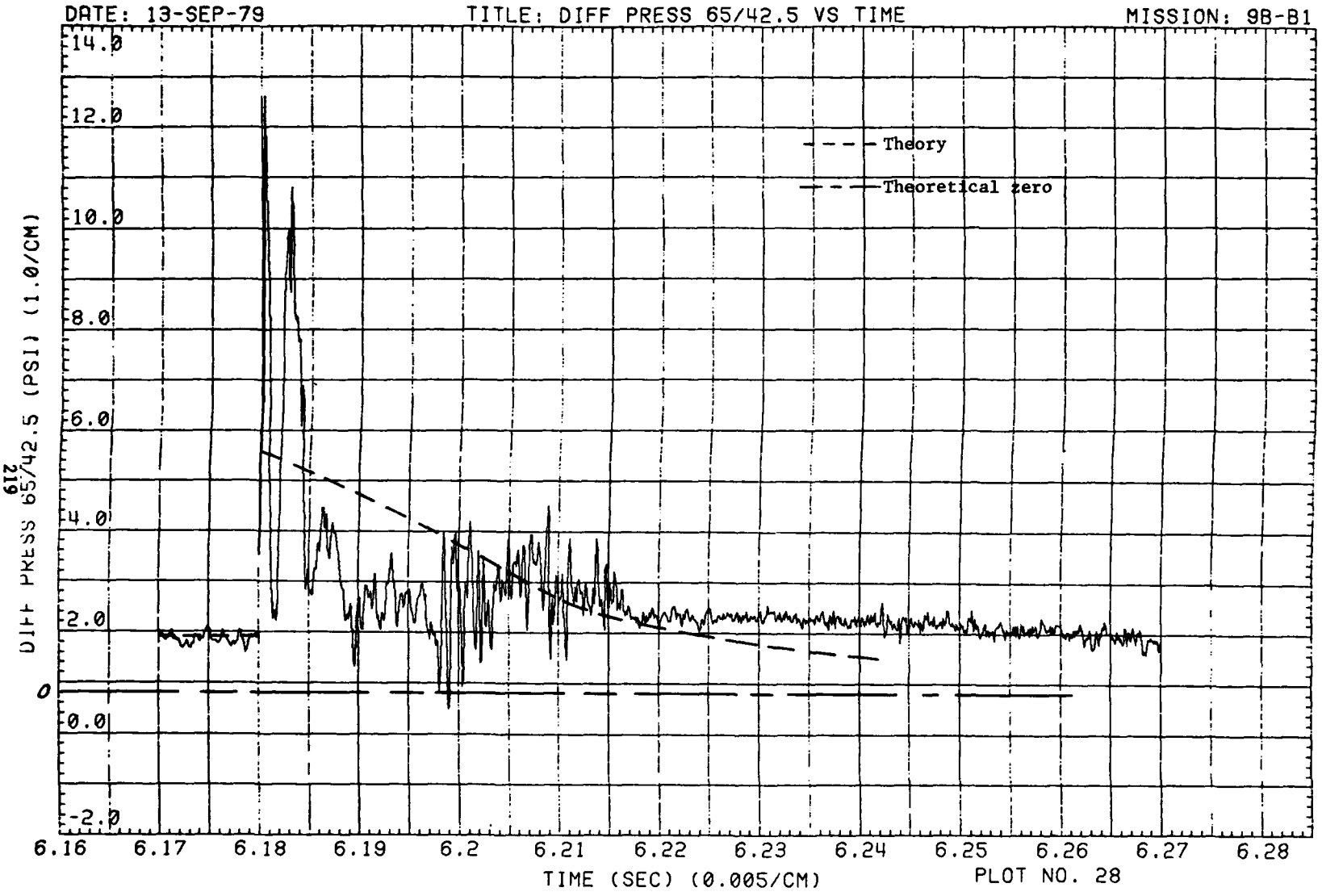

Figure 53. (Continued)

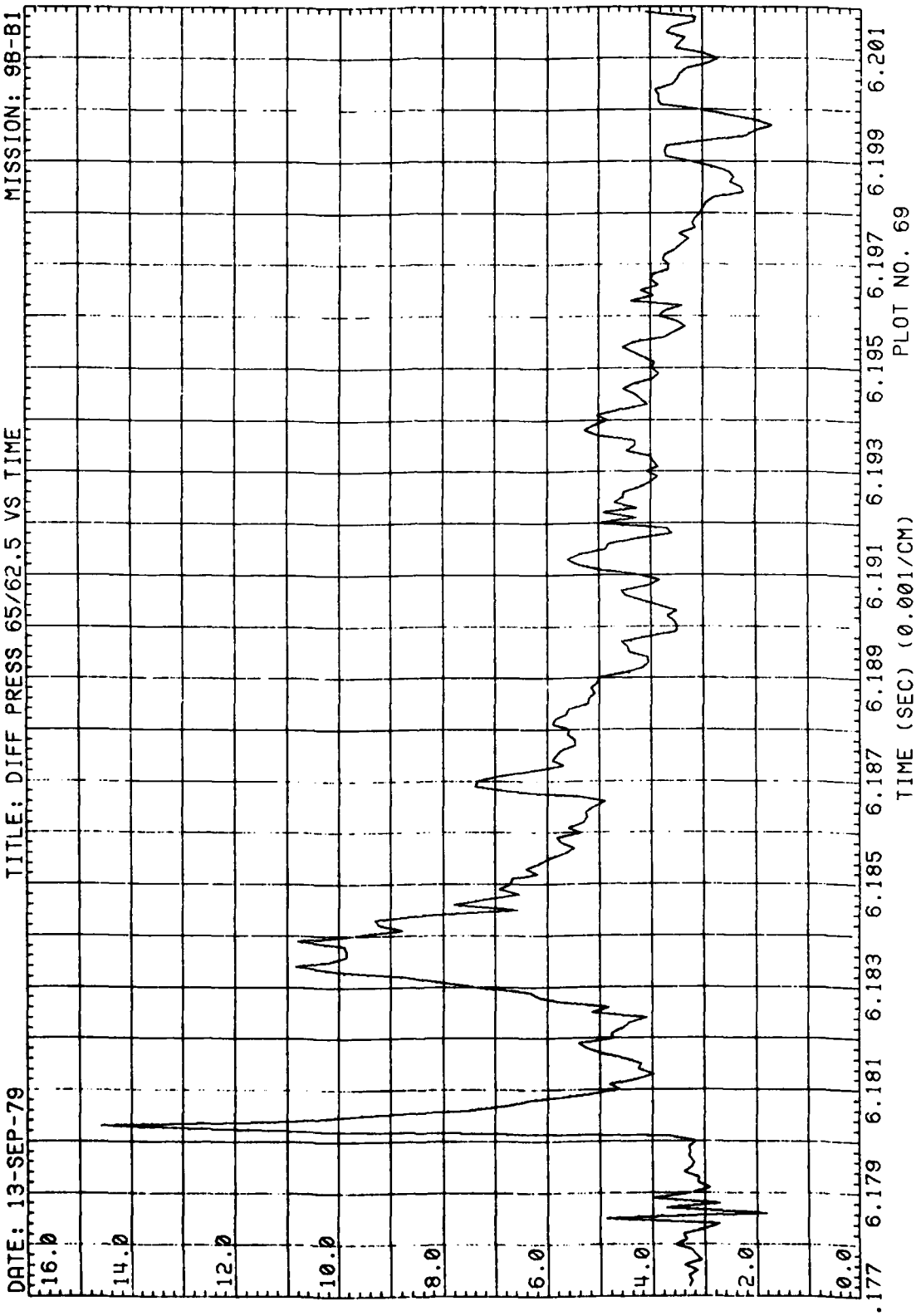

Figure 53. (Continued)

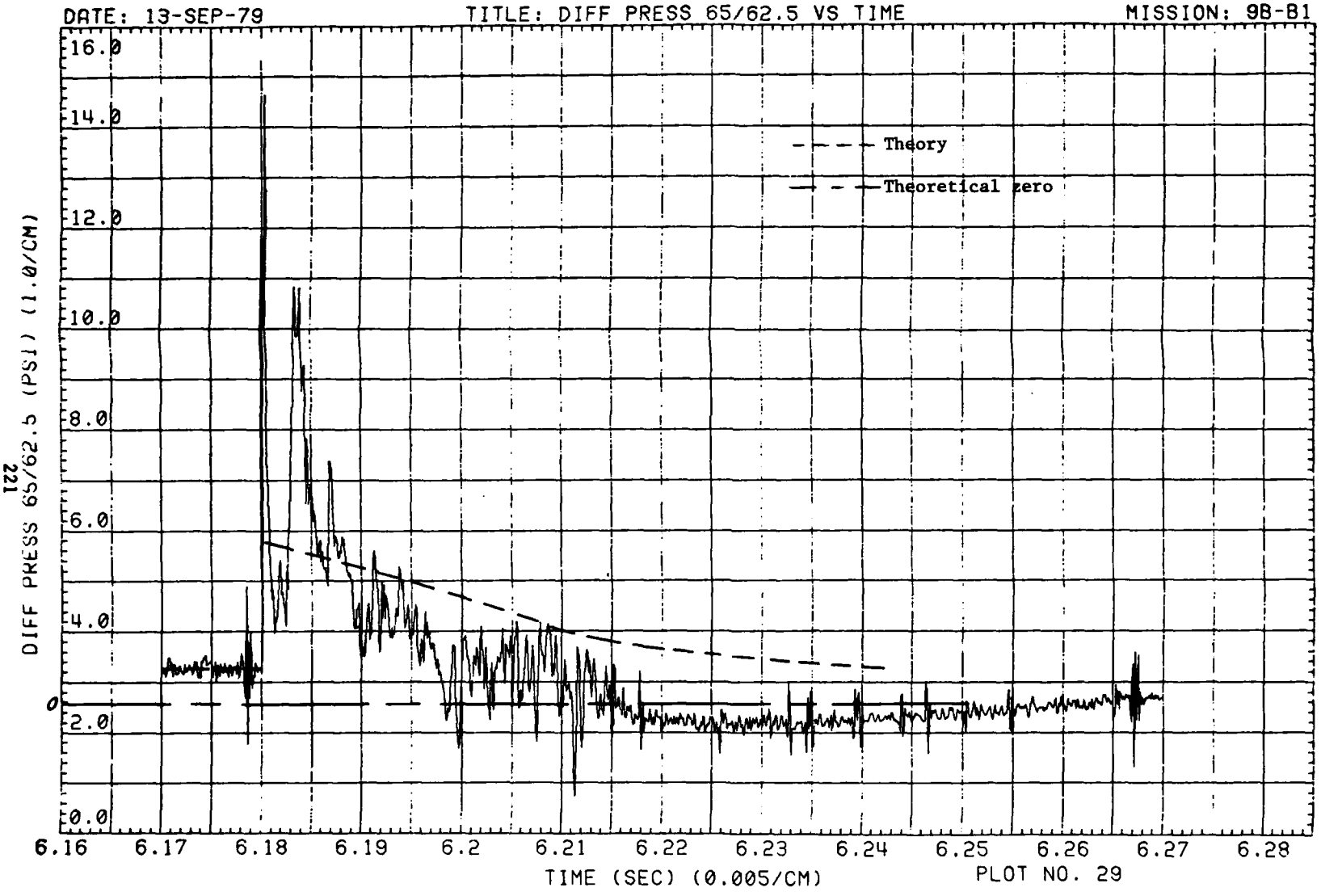

Figure 53. (Continued)

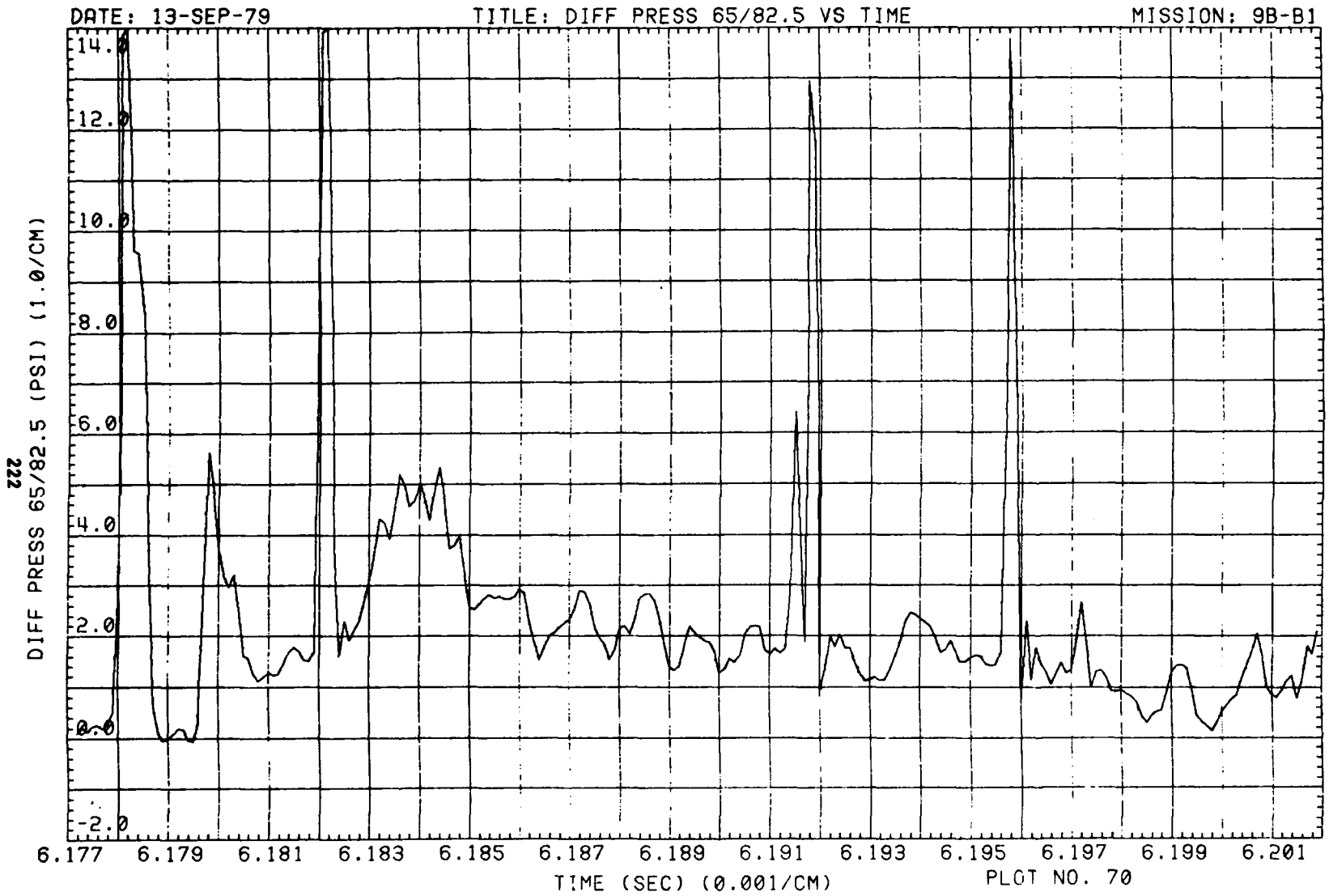

Figure 53. (Continued)

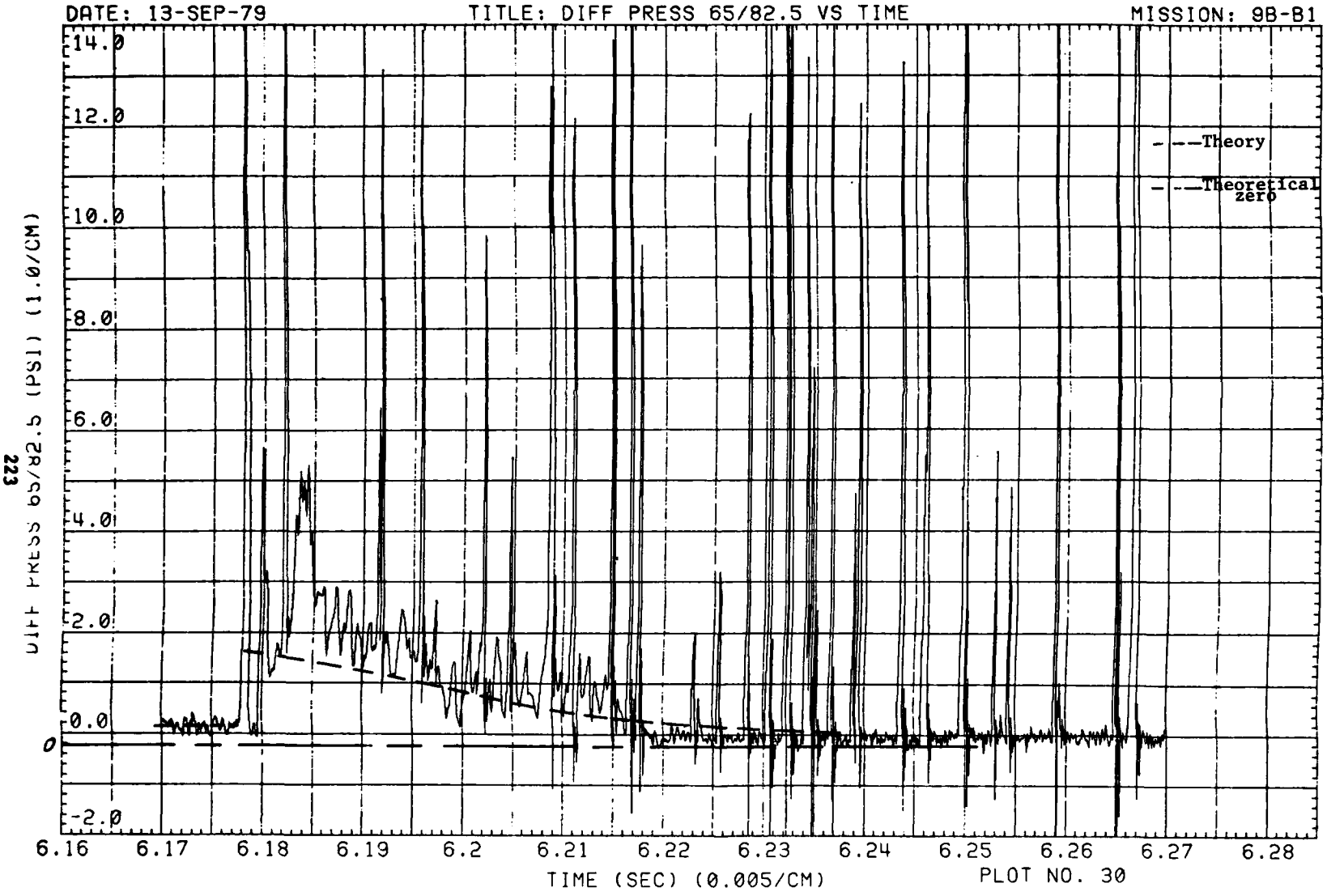

Figure 53. (Continued)

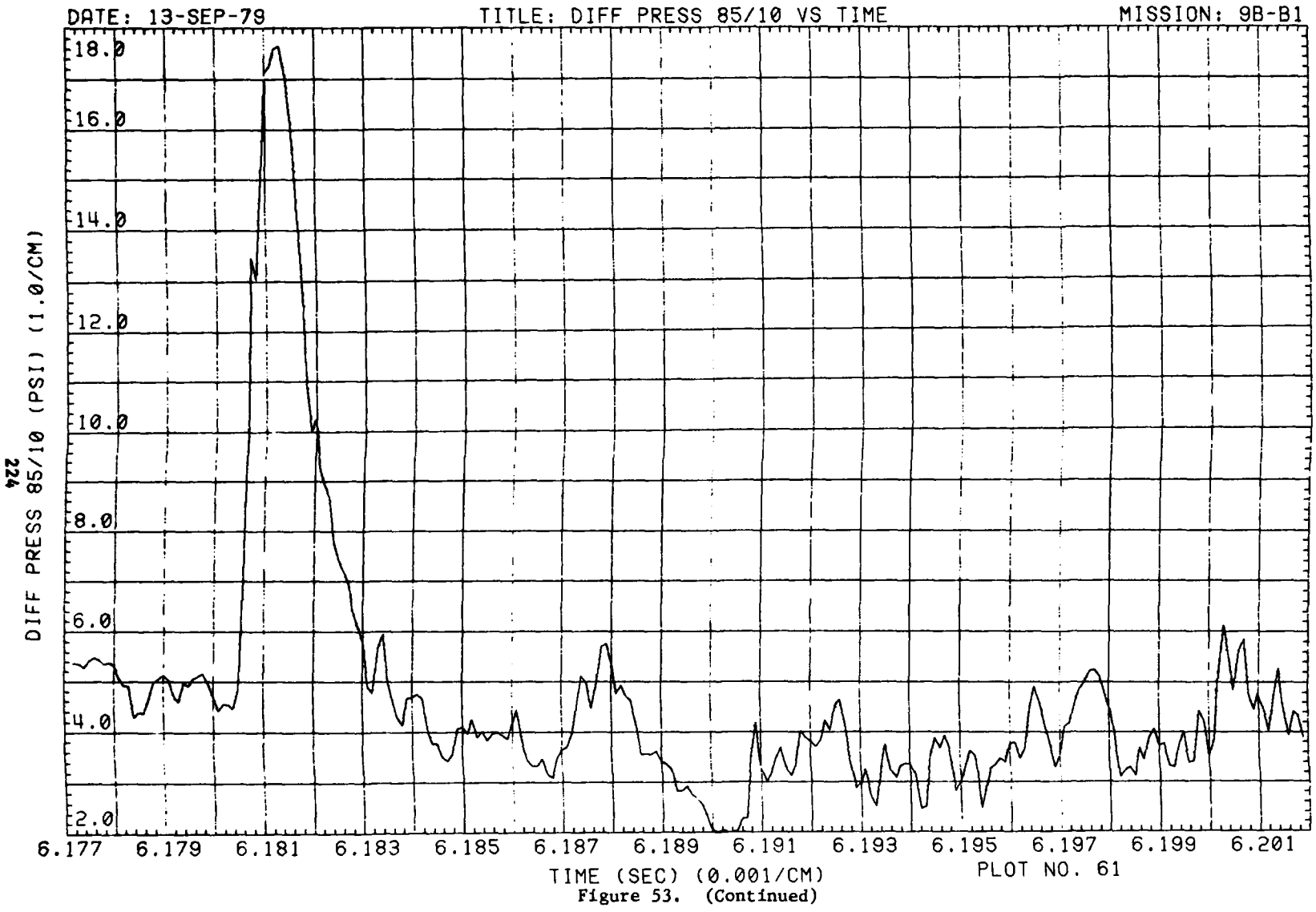

Figure 53. (Continued)

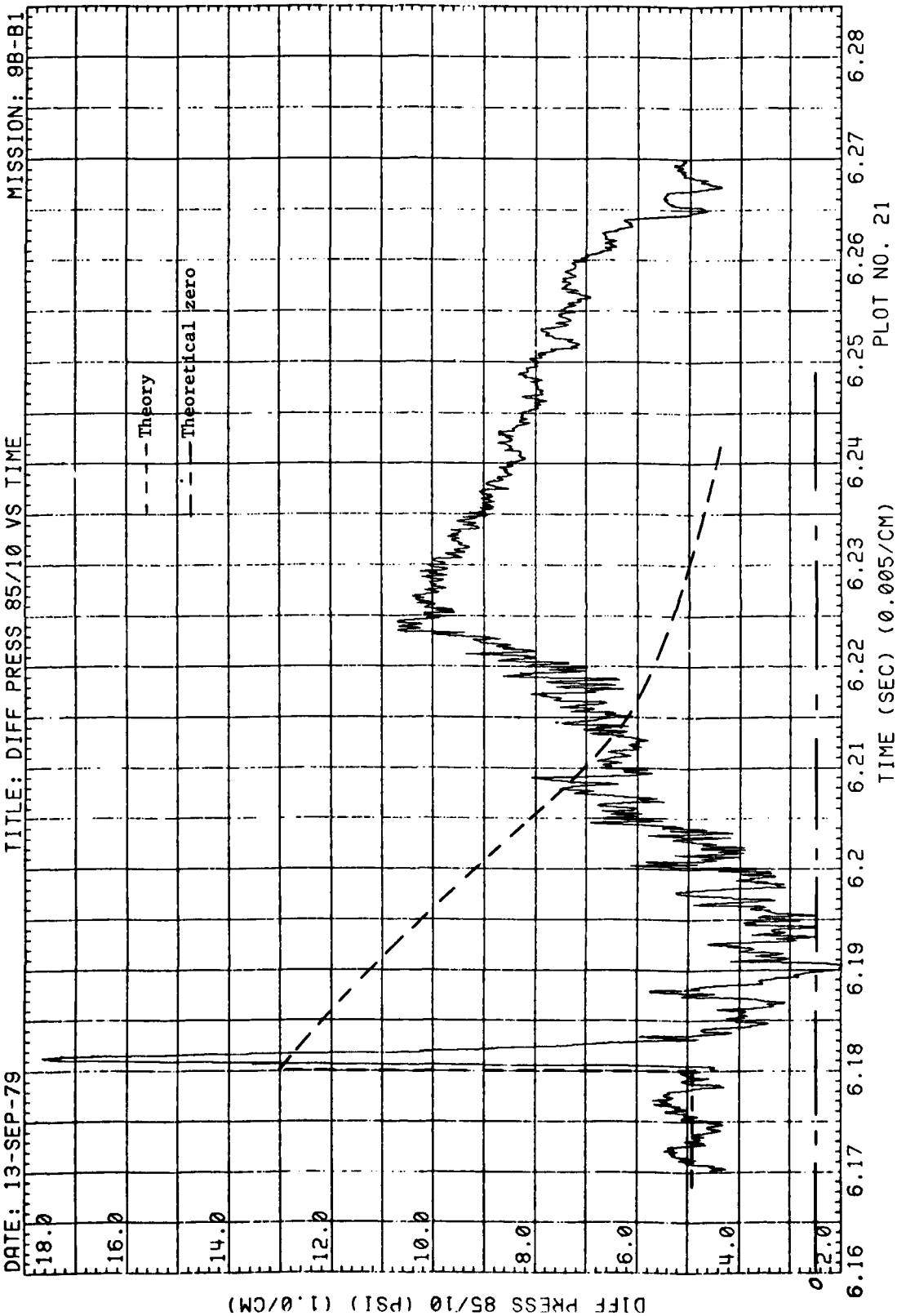

Figure 53. (Continued)

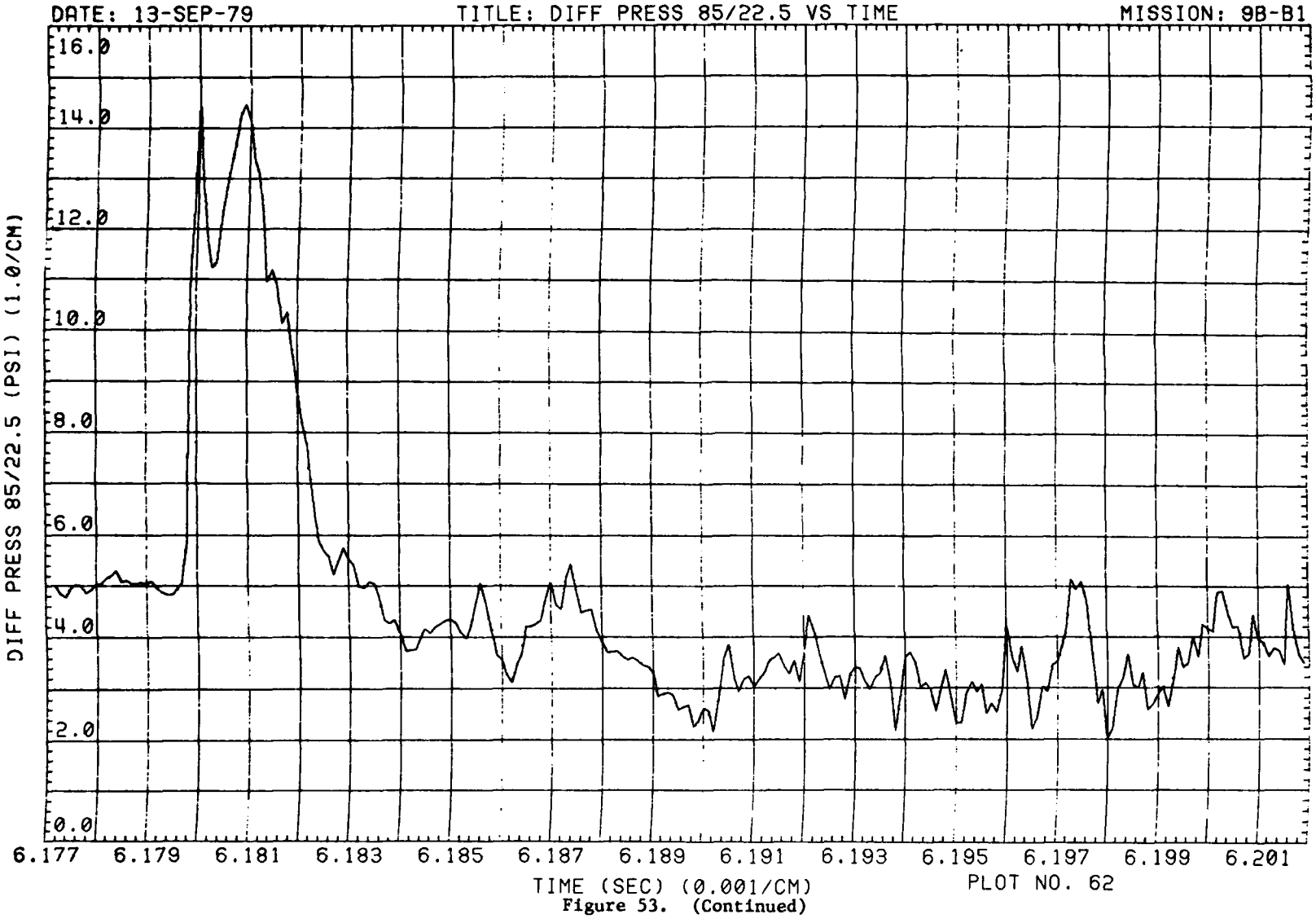

Figure 53. (Continued)

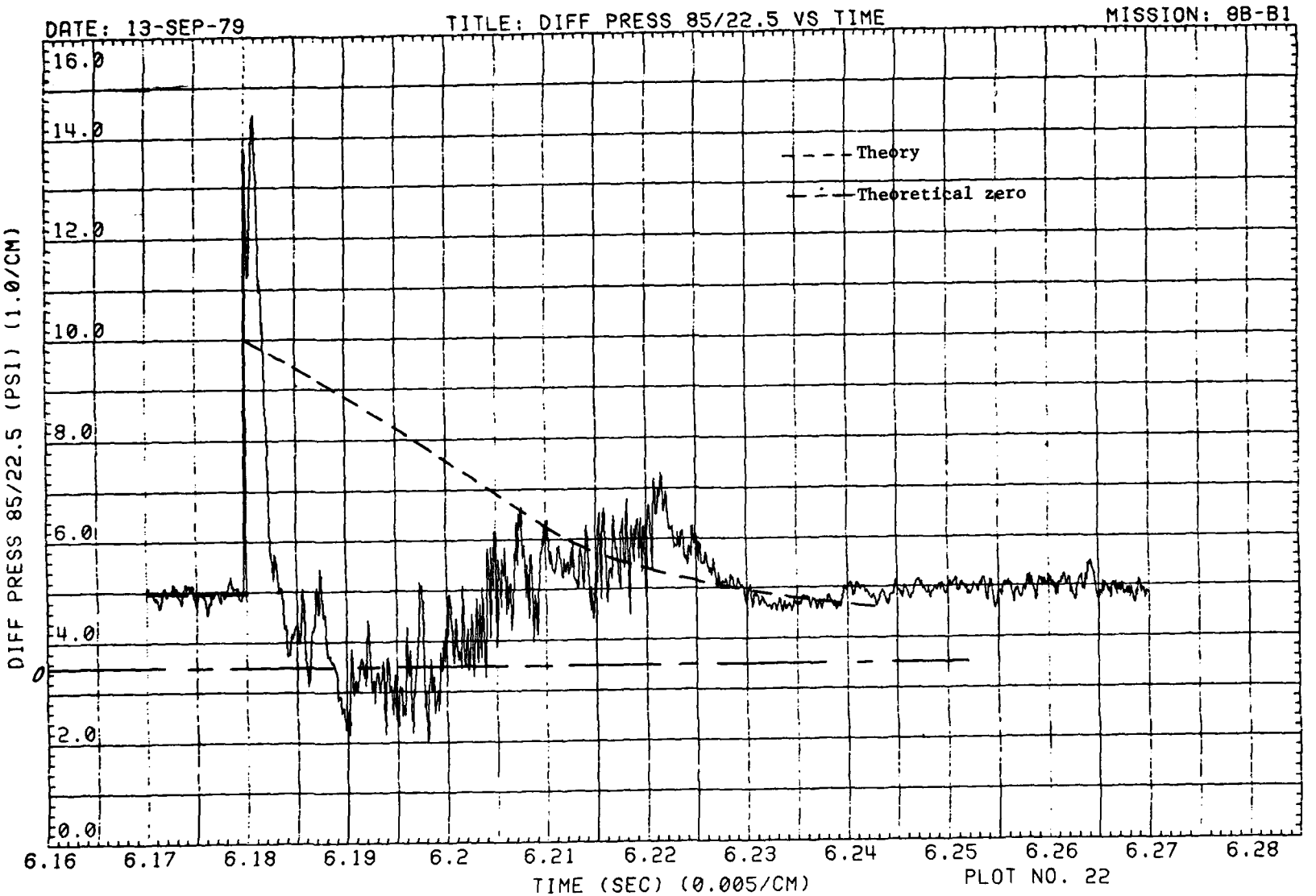

Figure 53. (Continued)

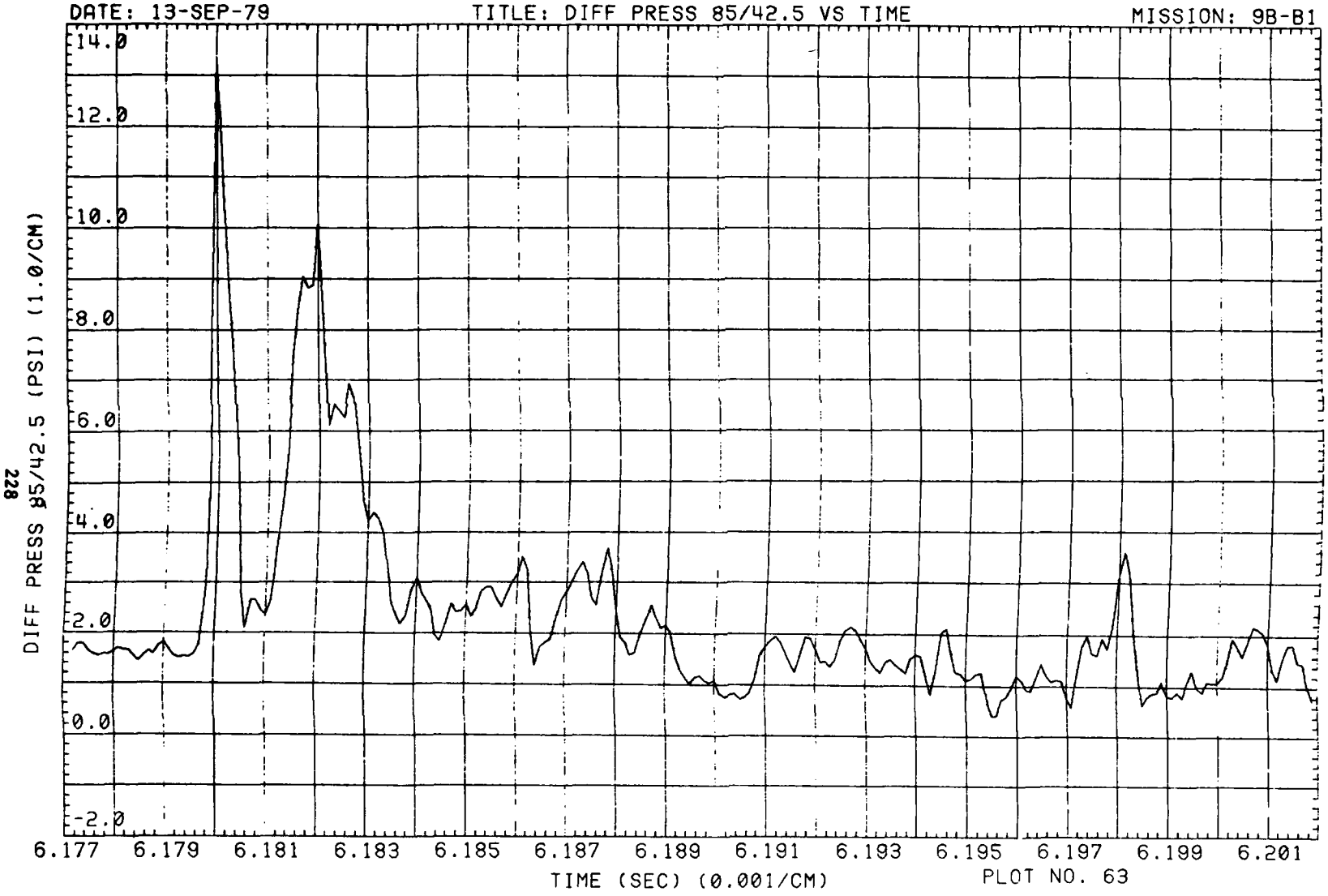

Figure 53. (Continued)

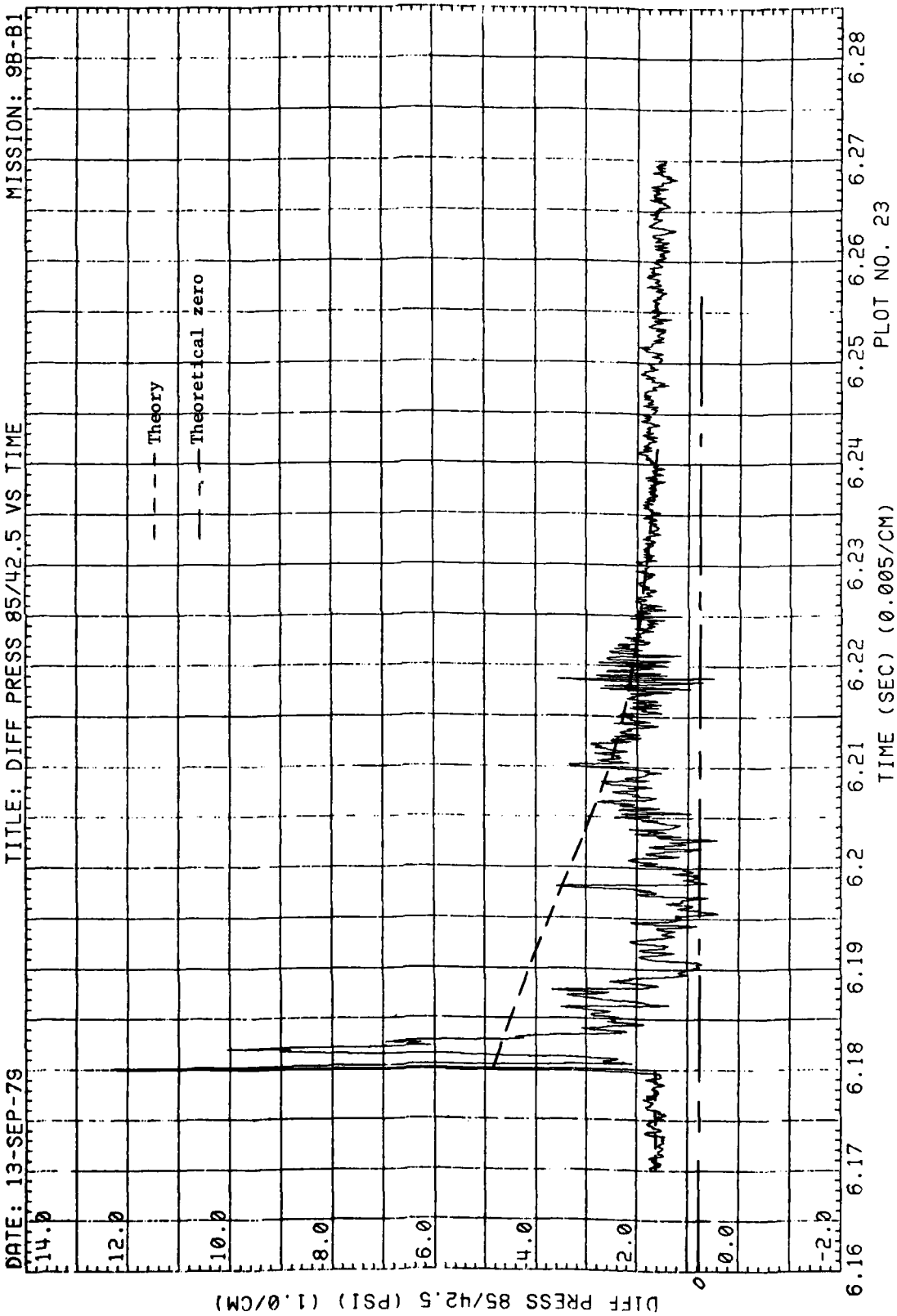

Figure 53. (Continued)

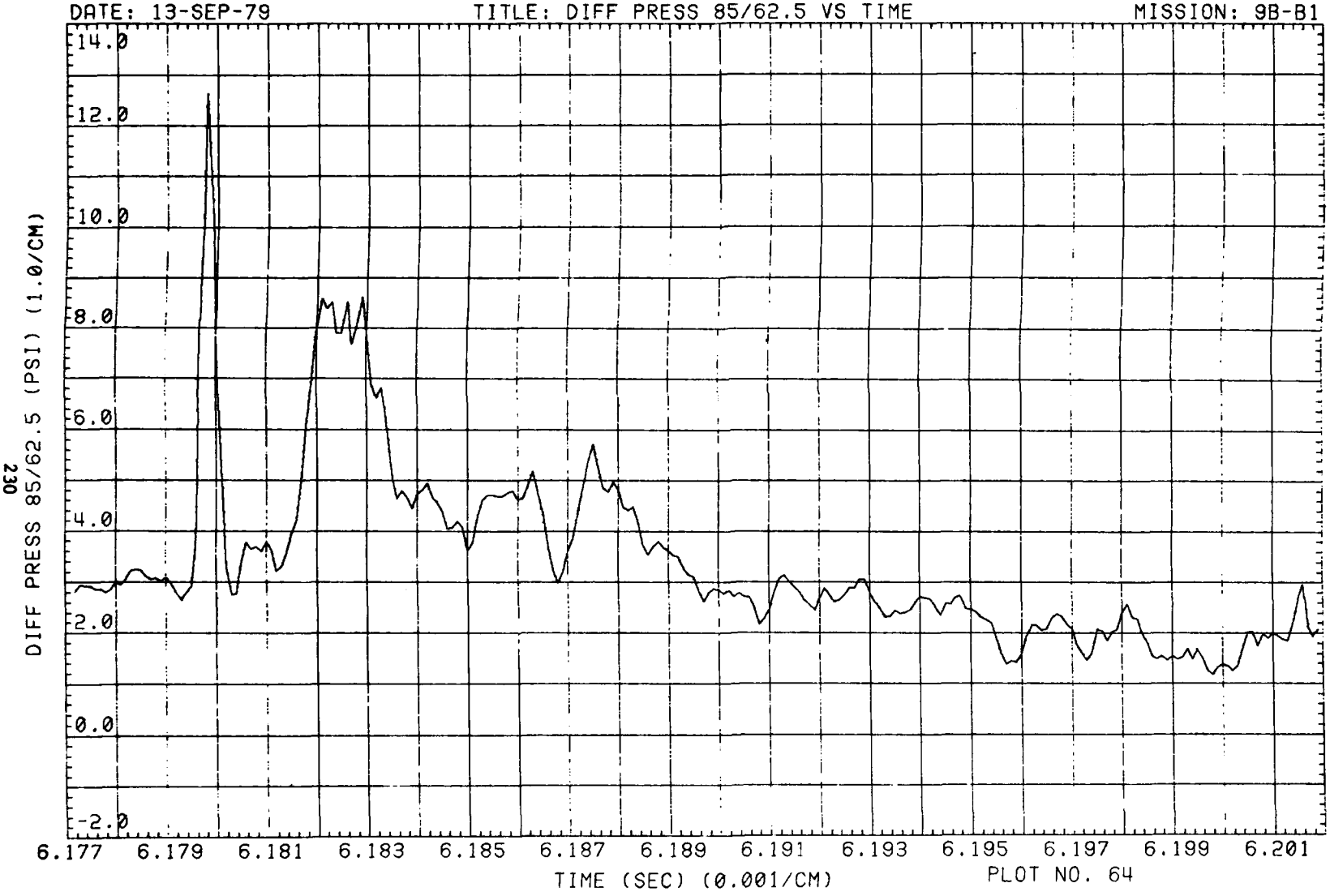

Figure 53. (Continued)

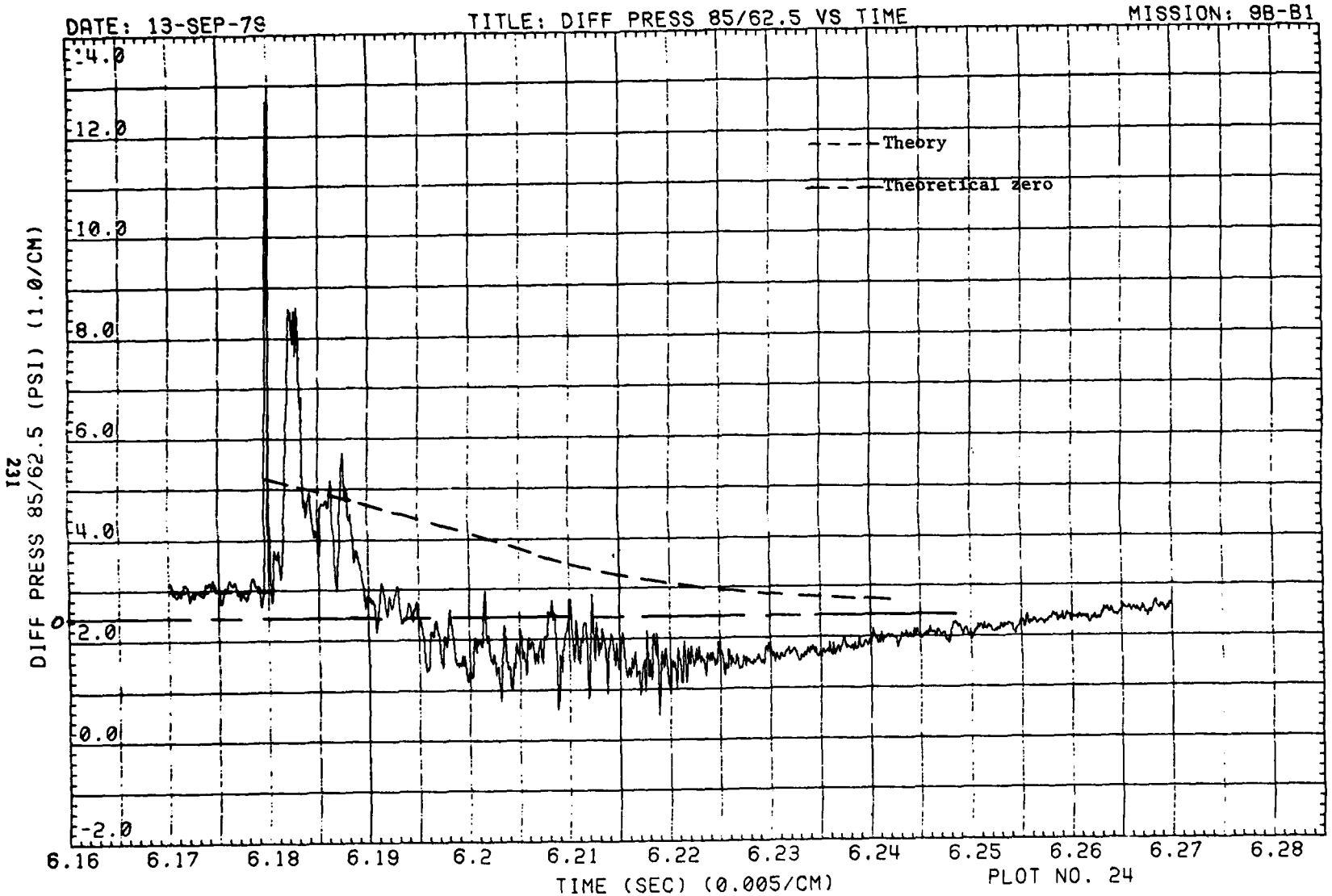

Figure 53. (Continued)

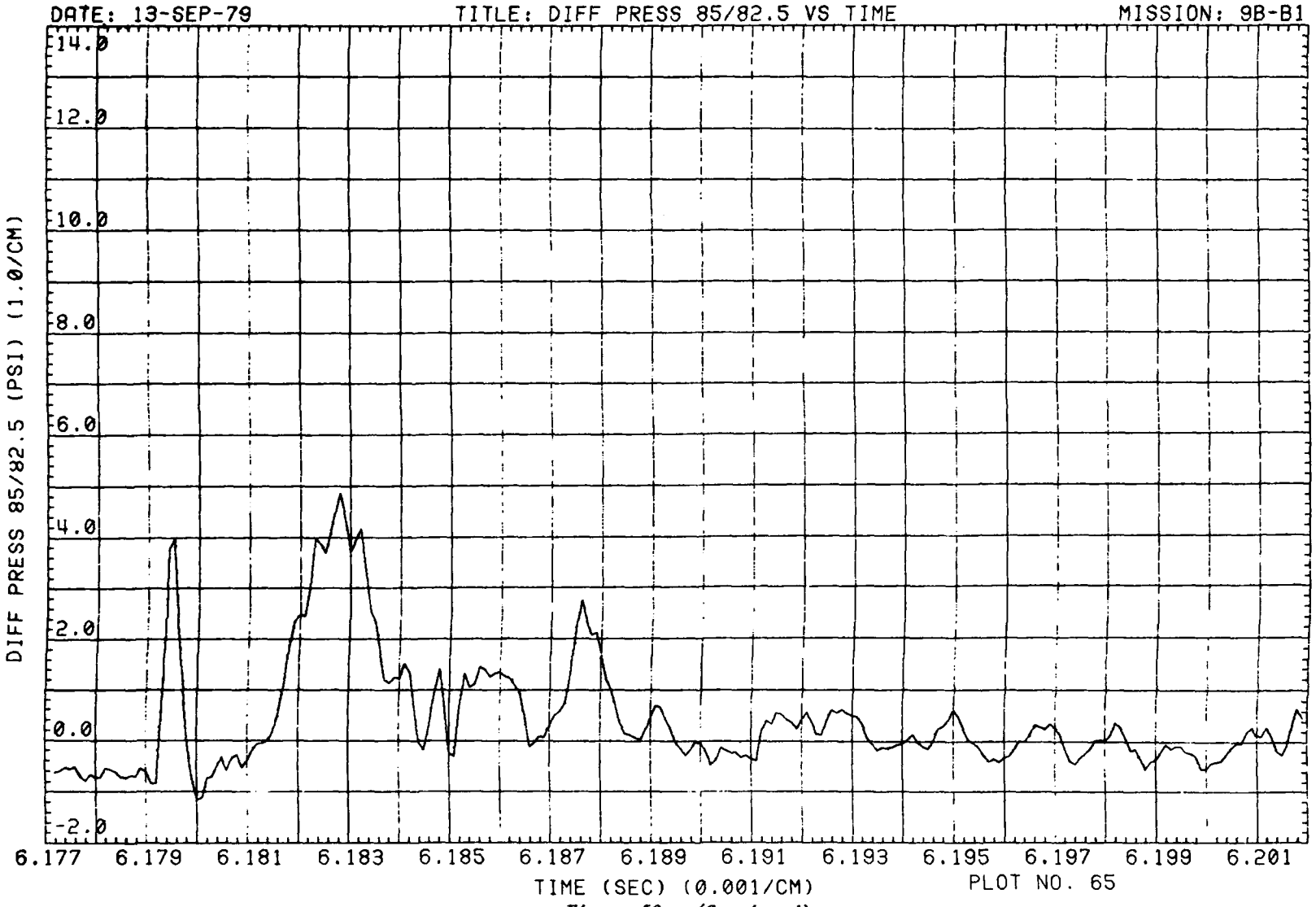

Figure 53. (Continued)

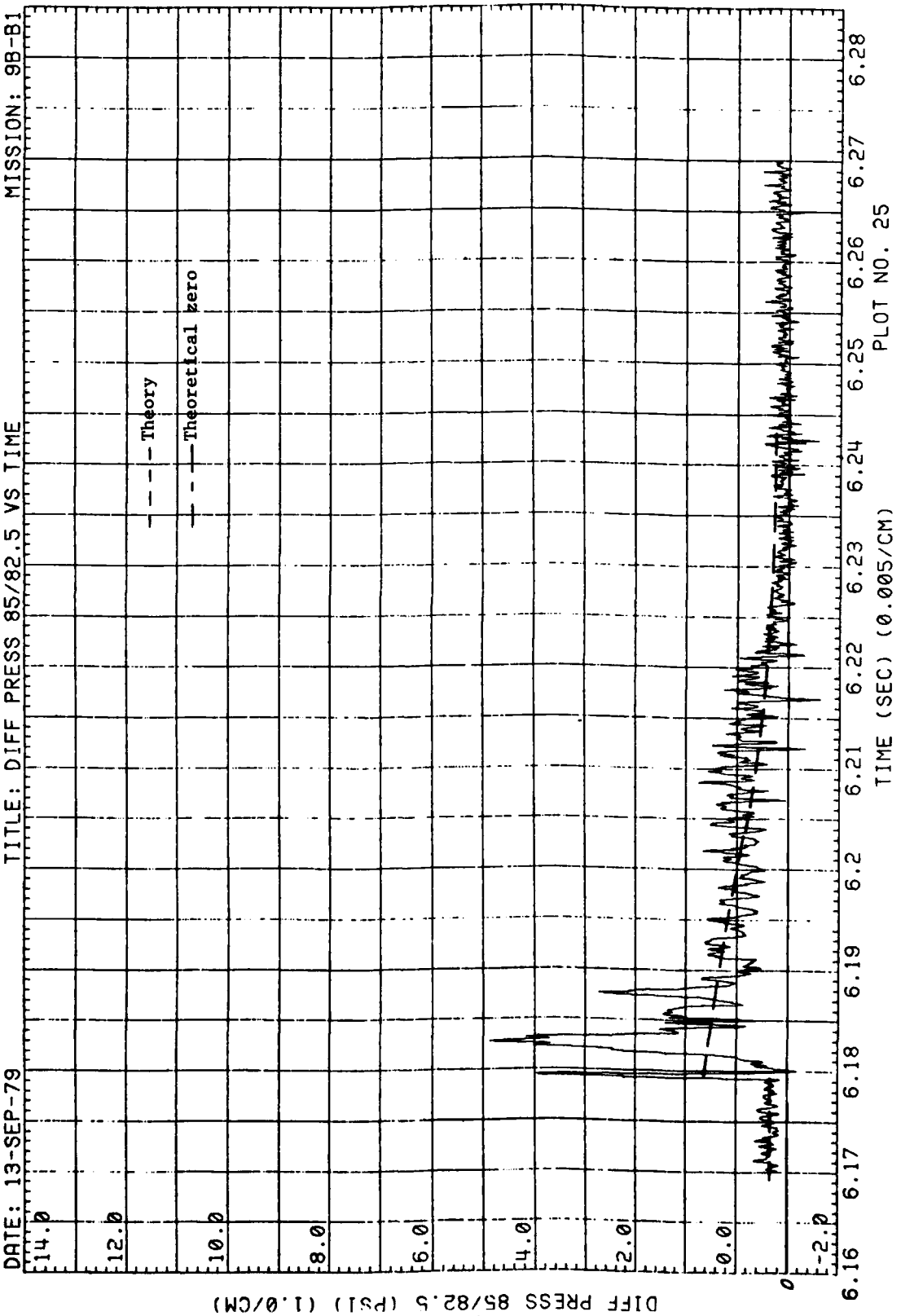

Figure 53. (Concluded)

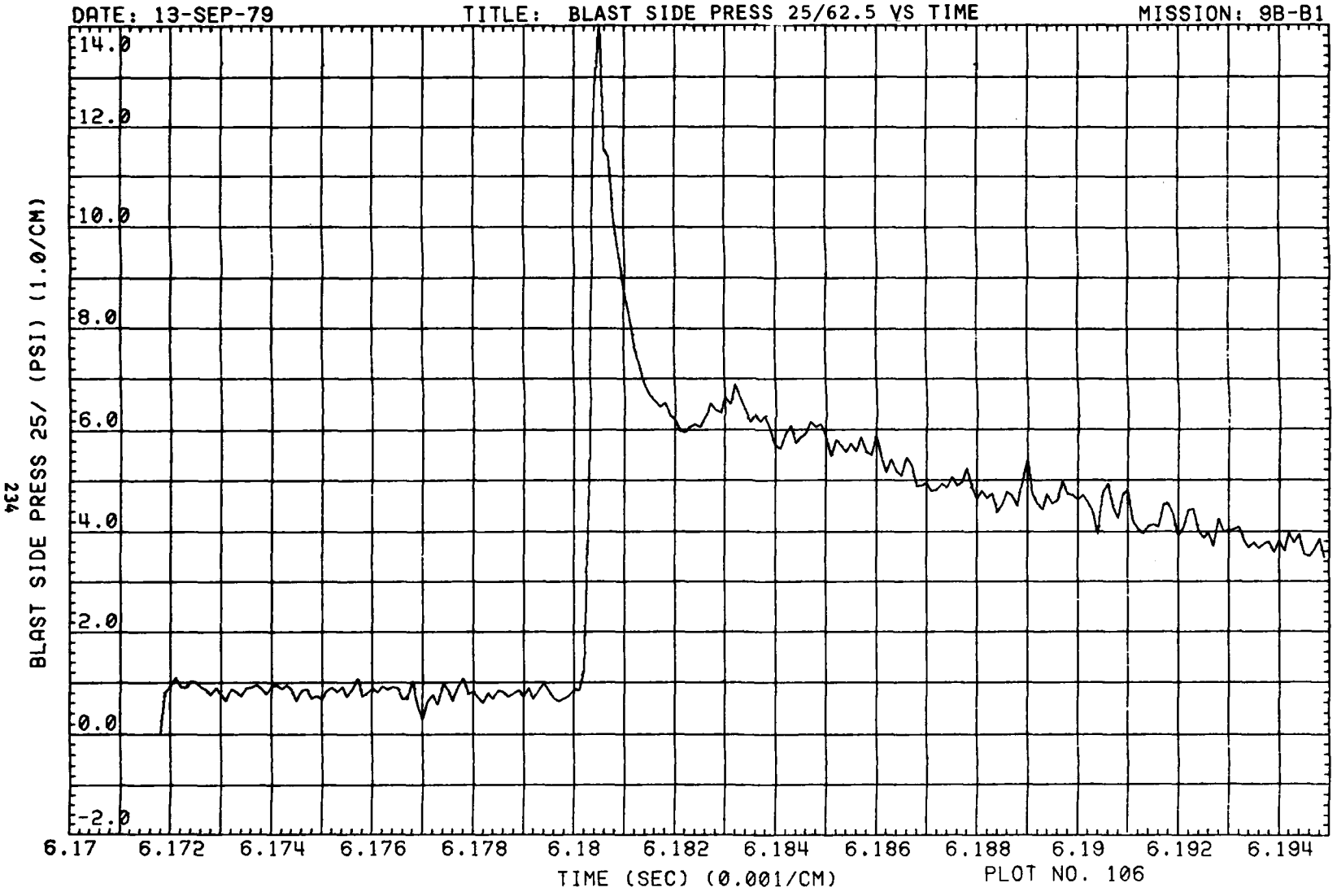

Figure 54. Blastward and Leeward Wing Pressures, Run 9B-B1, Intercept 3

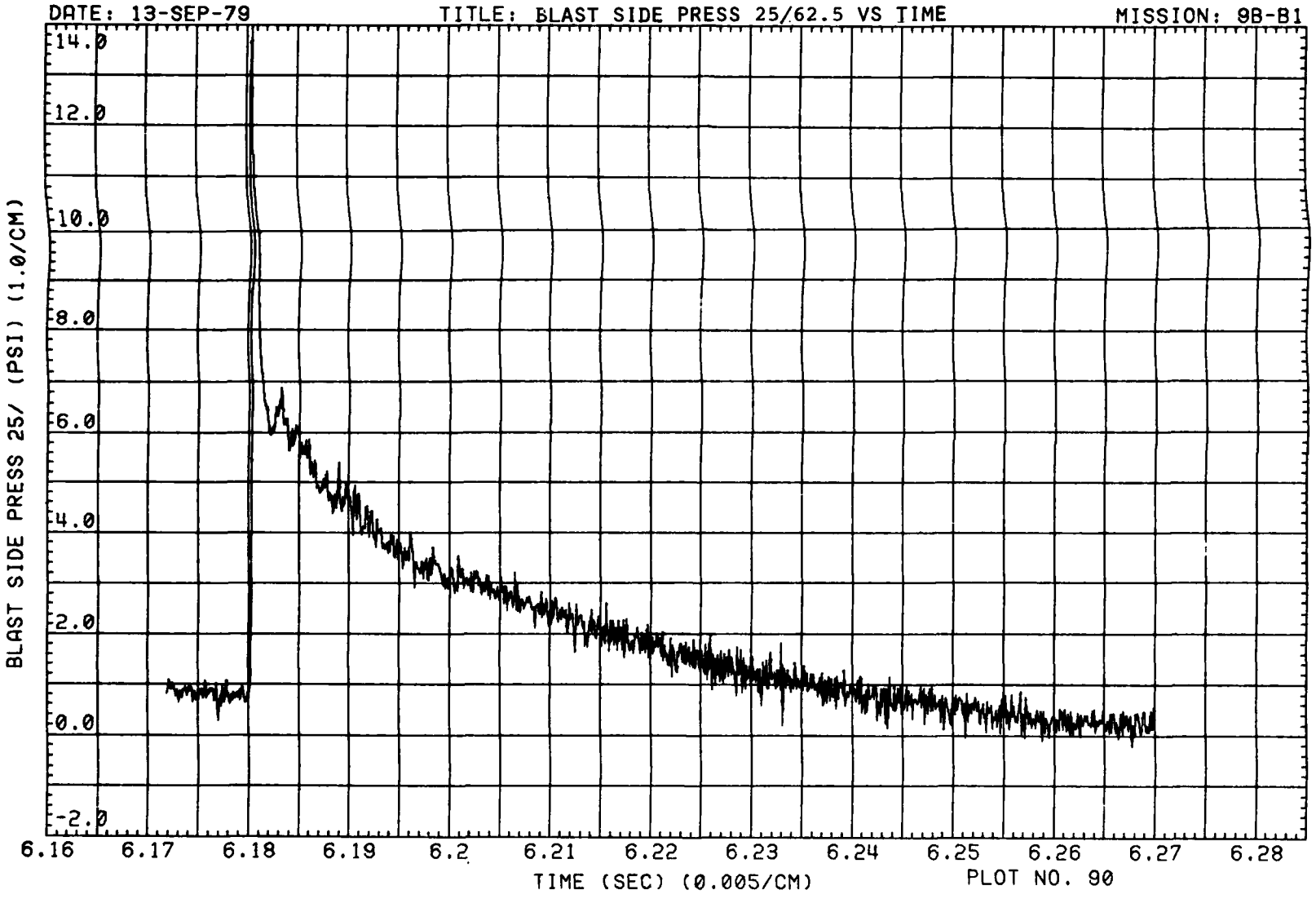

Figure 54. (Continued)

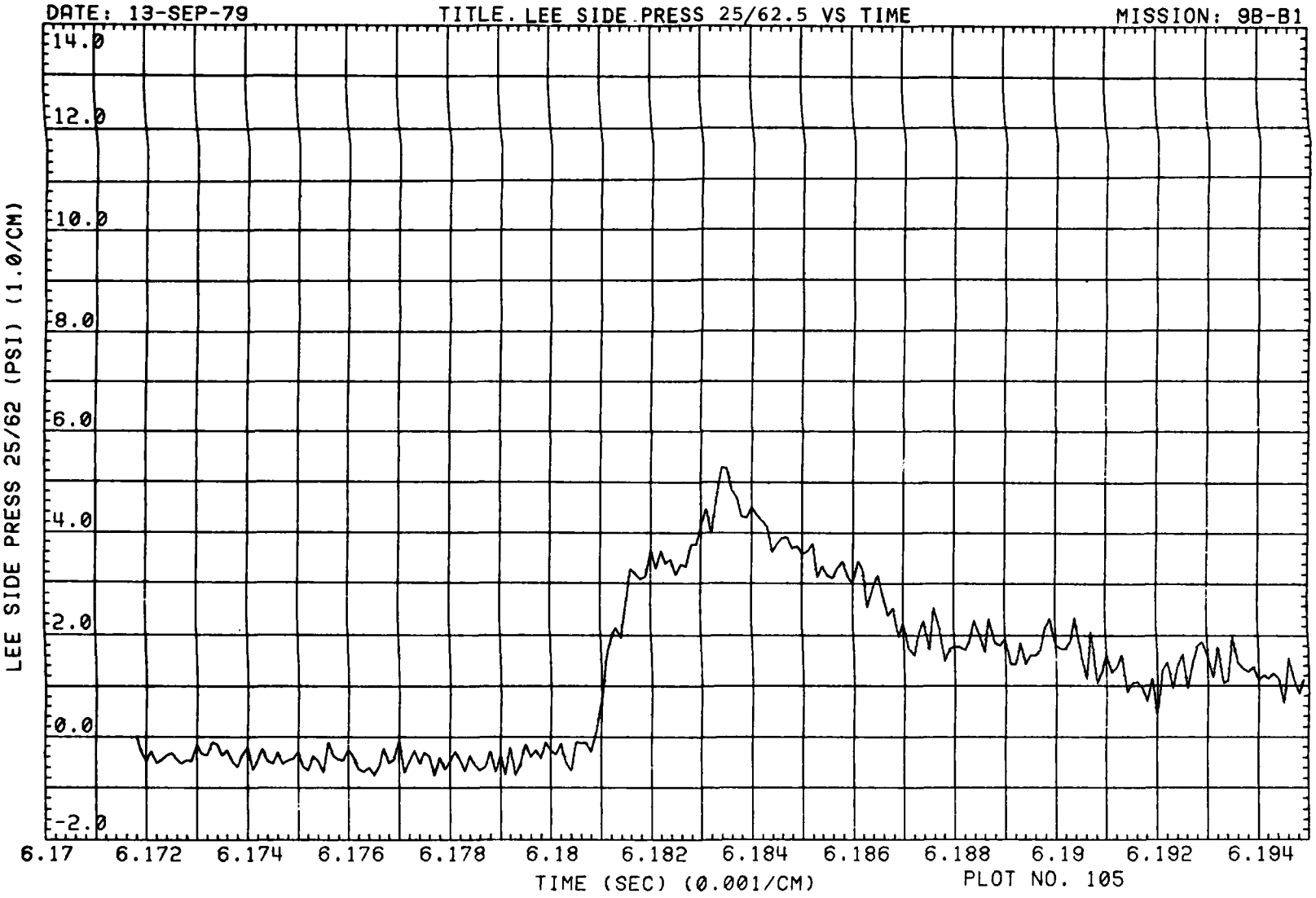

Figure 54. (Continued)

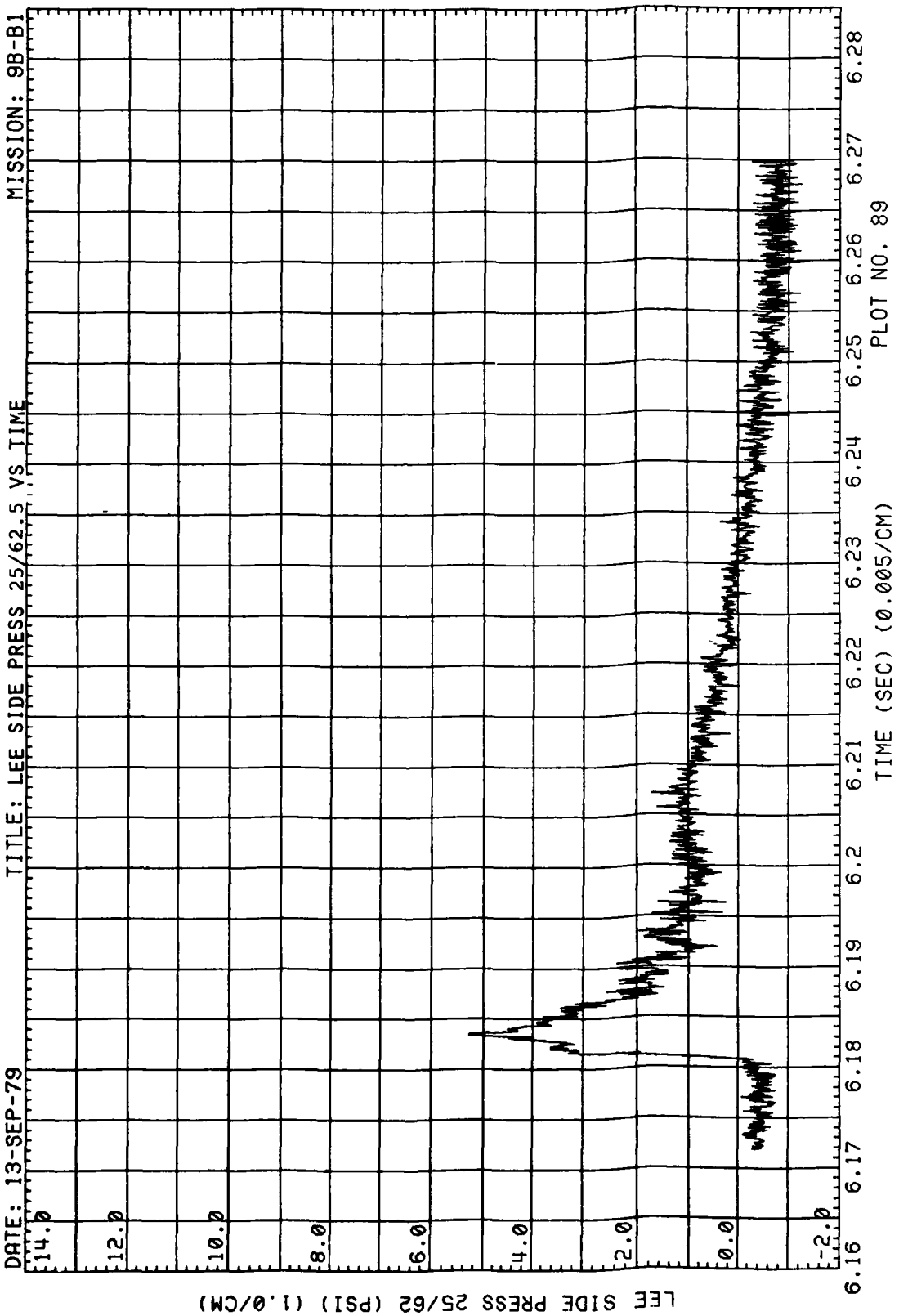

Figure 54. (Concluded)

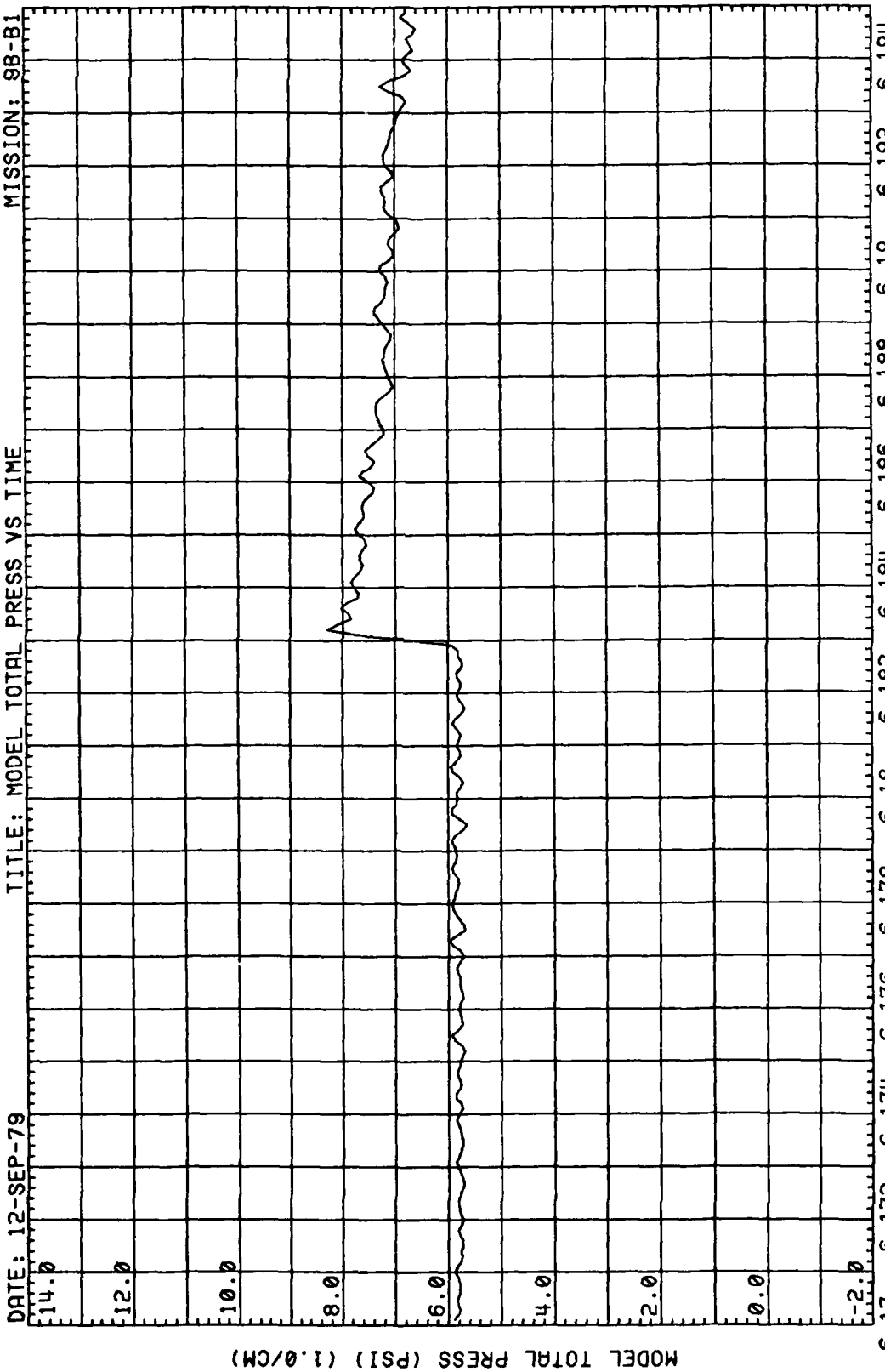

Figure 55. Total Pressure at Model, Run 9B-B1, Intercept 3

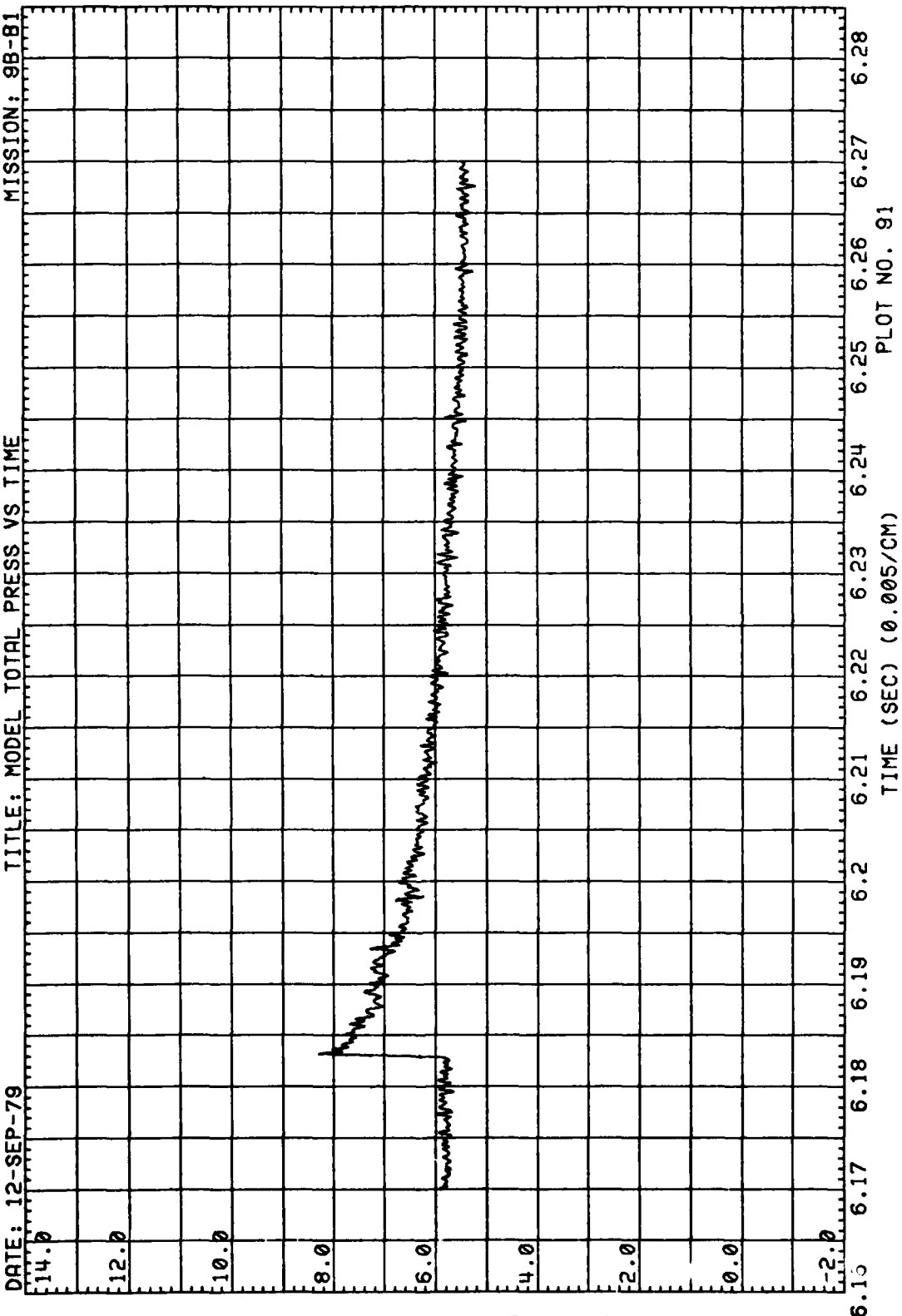

Figure 55. (Concluded)

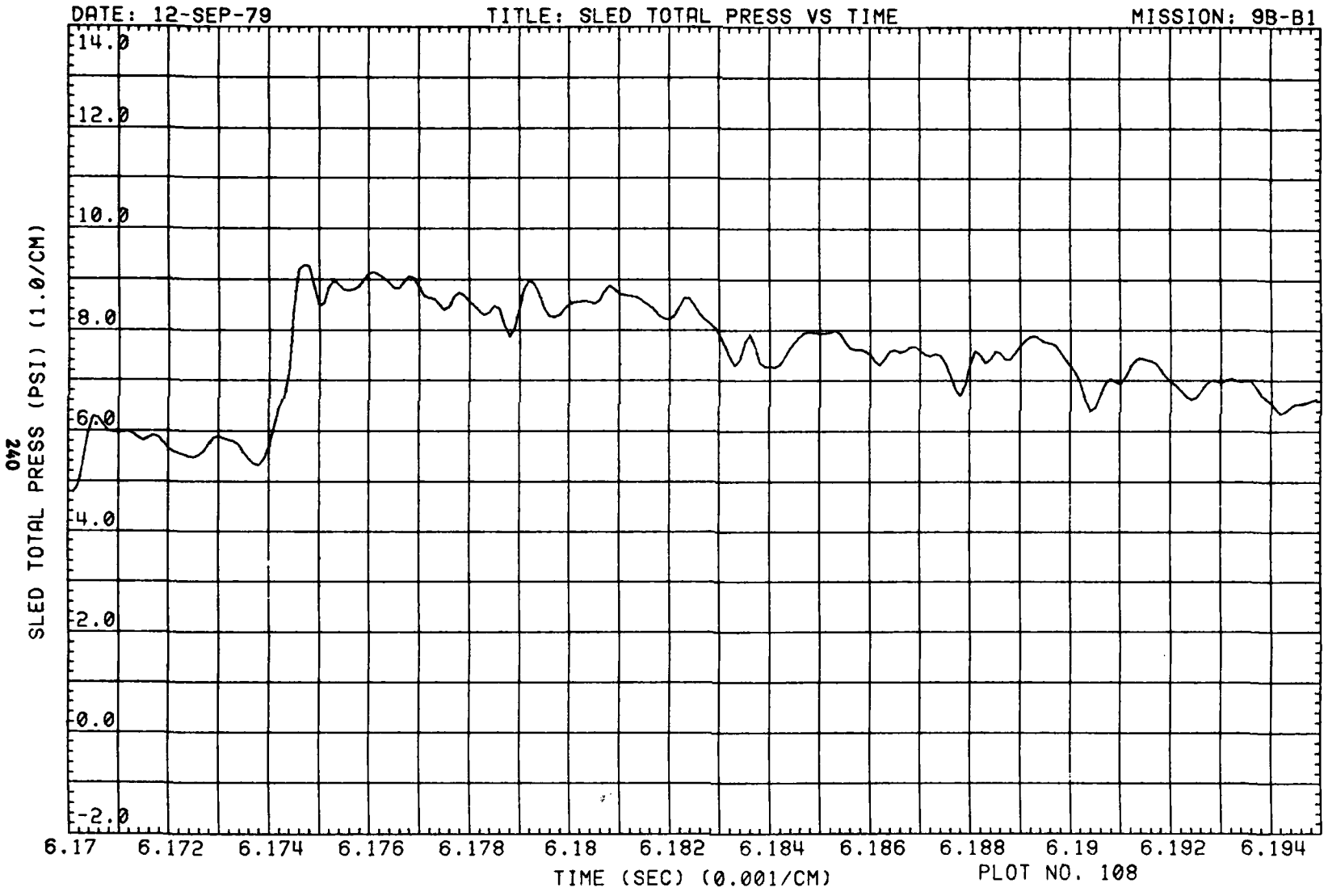

Figure 56. Total Pressure at Sled, Run 9B-B1, Intercept 3

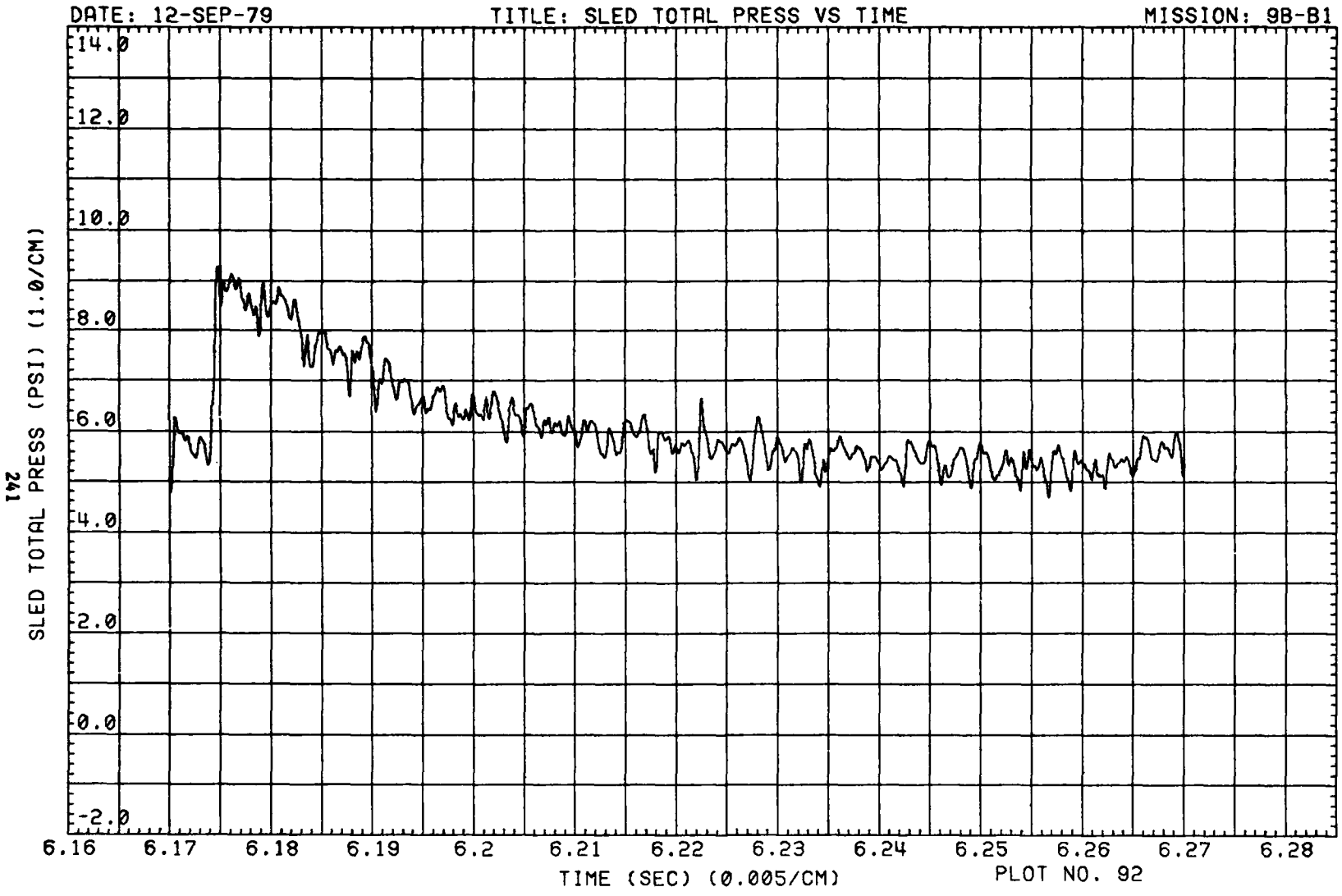

Figure 56. (Concluded)

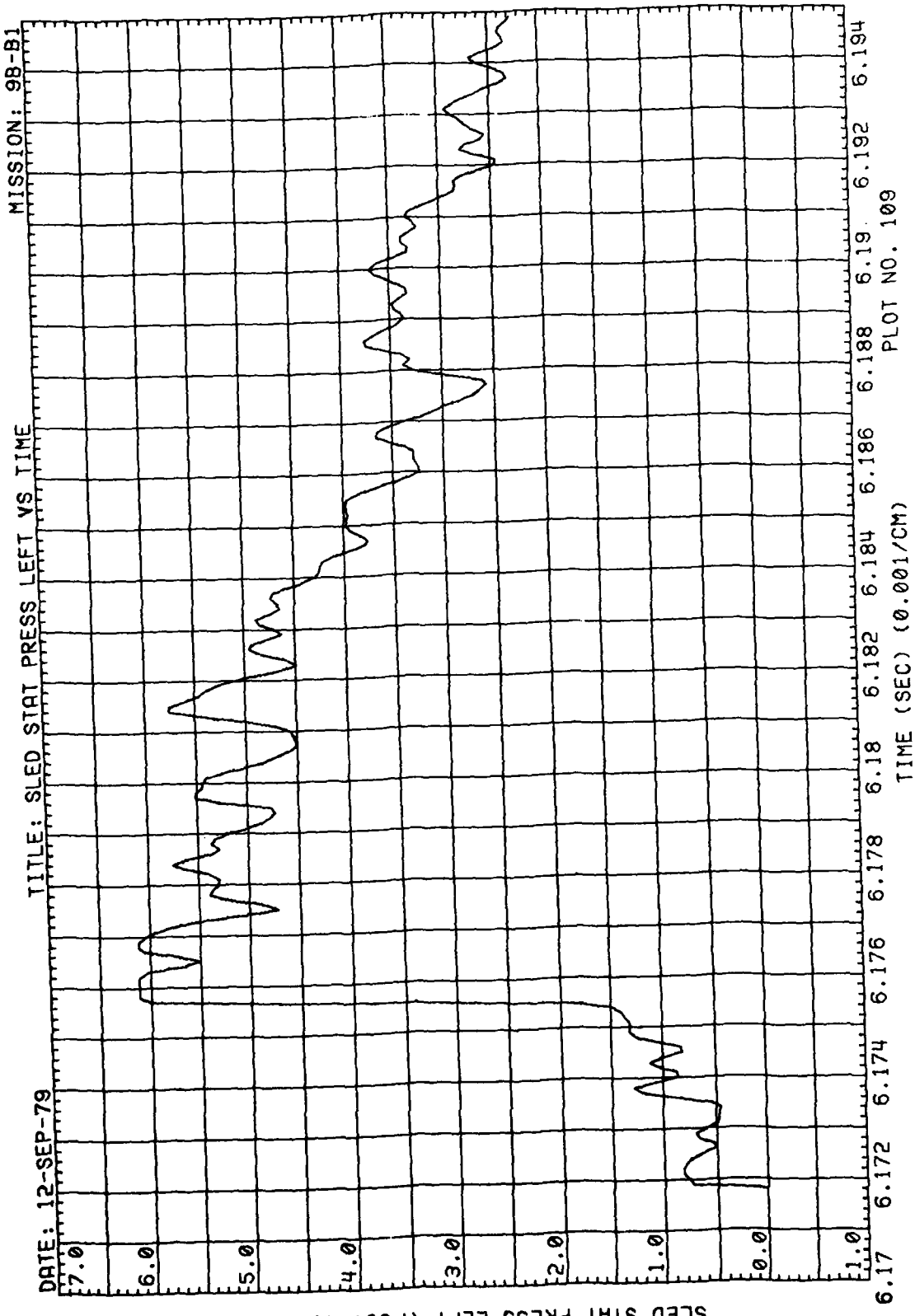

Figure 57. Left Side Static Pressure at Sled, Run 9B-B1, Intercept 3

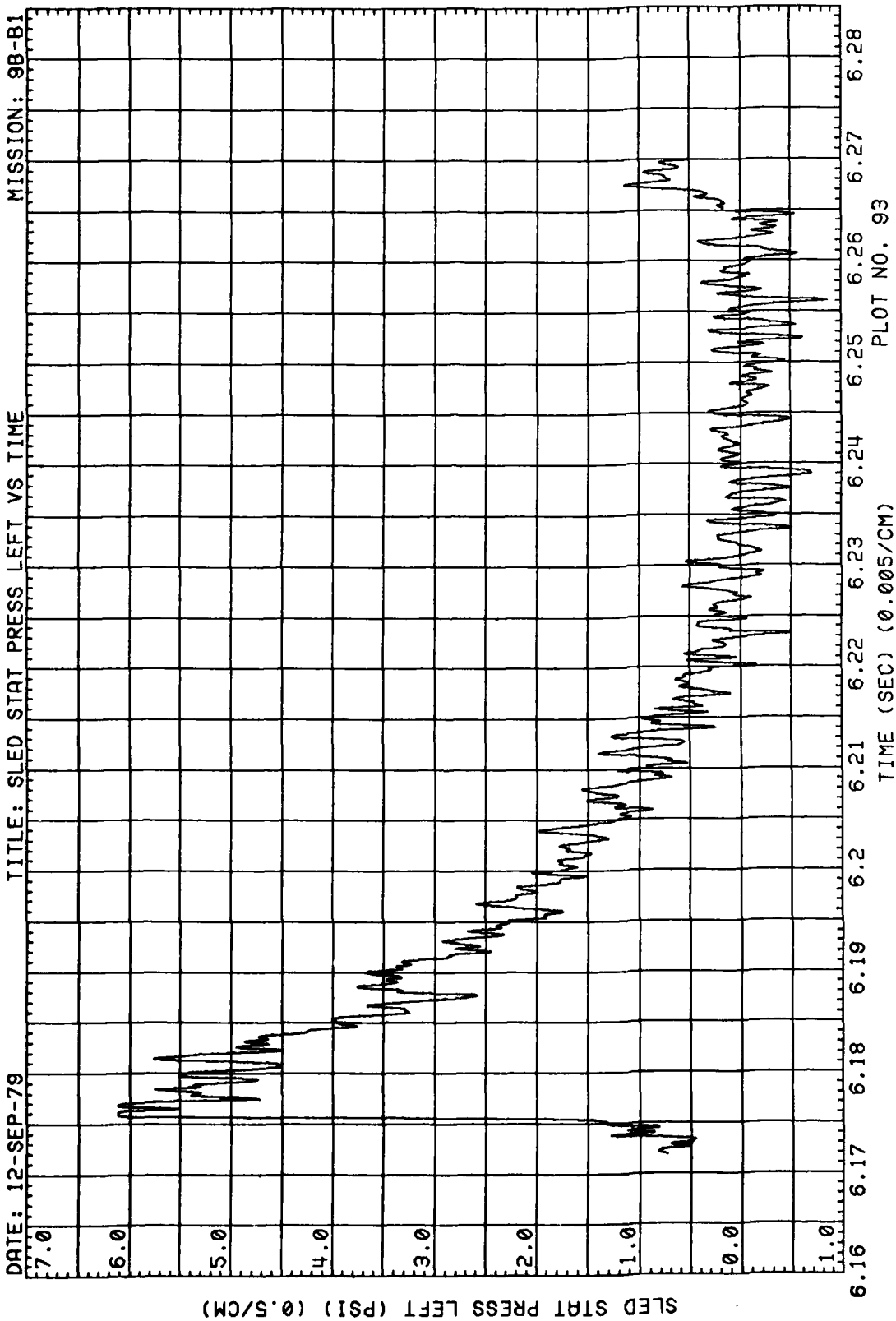

Figure 57. (Concluded)

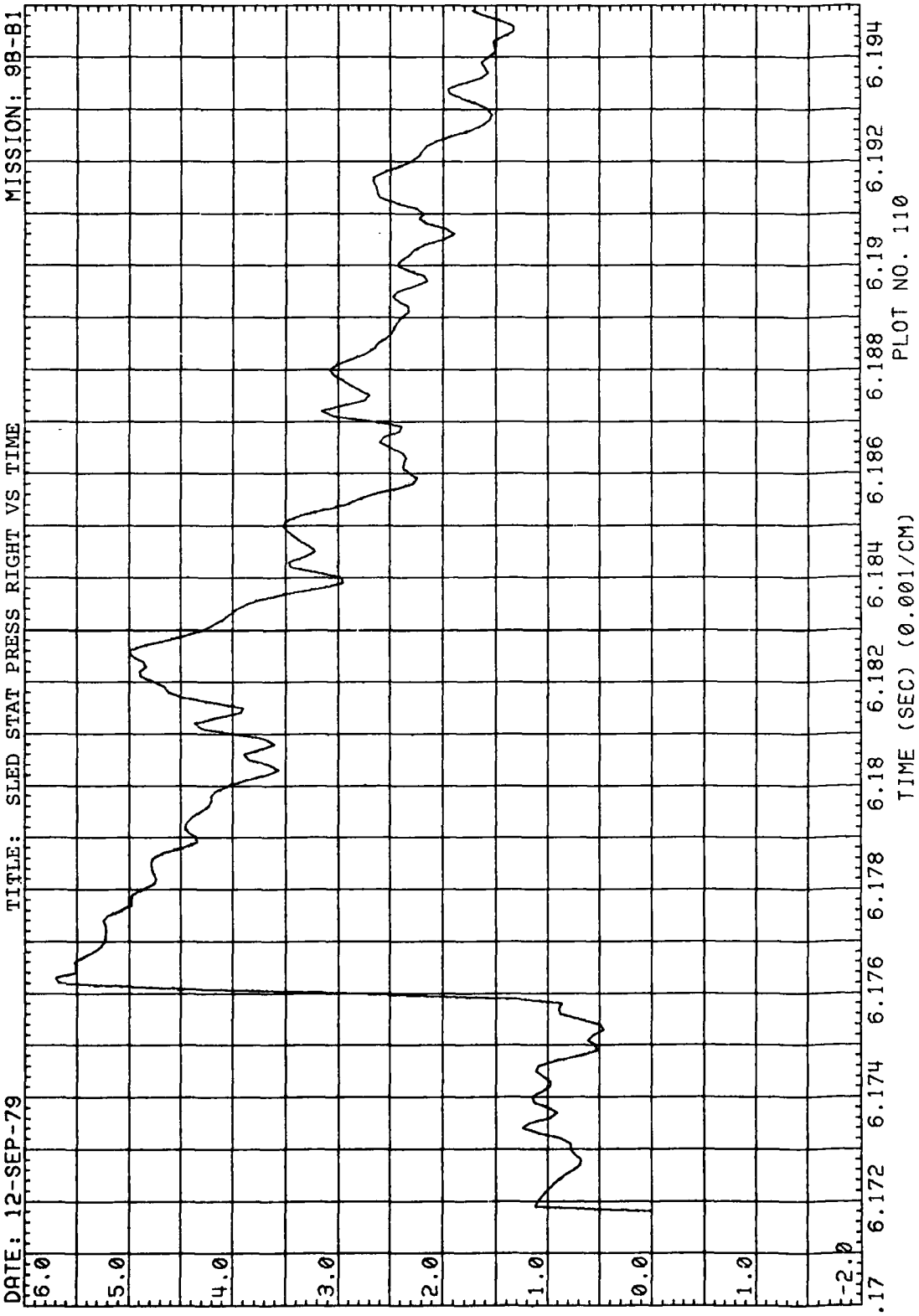

Figure 58. Right Side Static Pressure at Sled, Run 9B-B1, Intercept 3

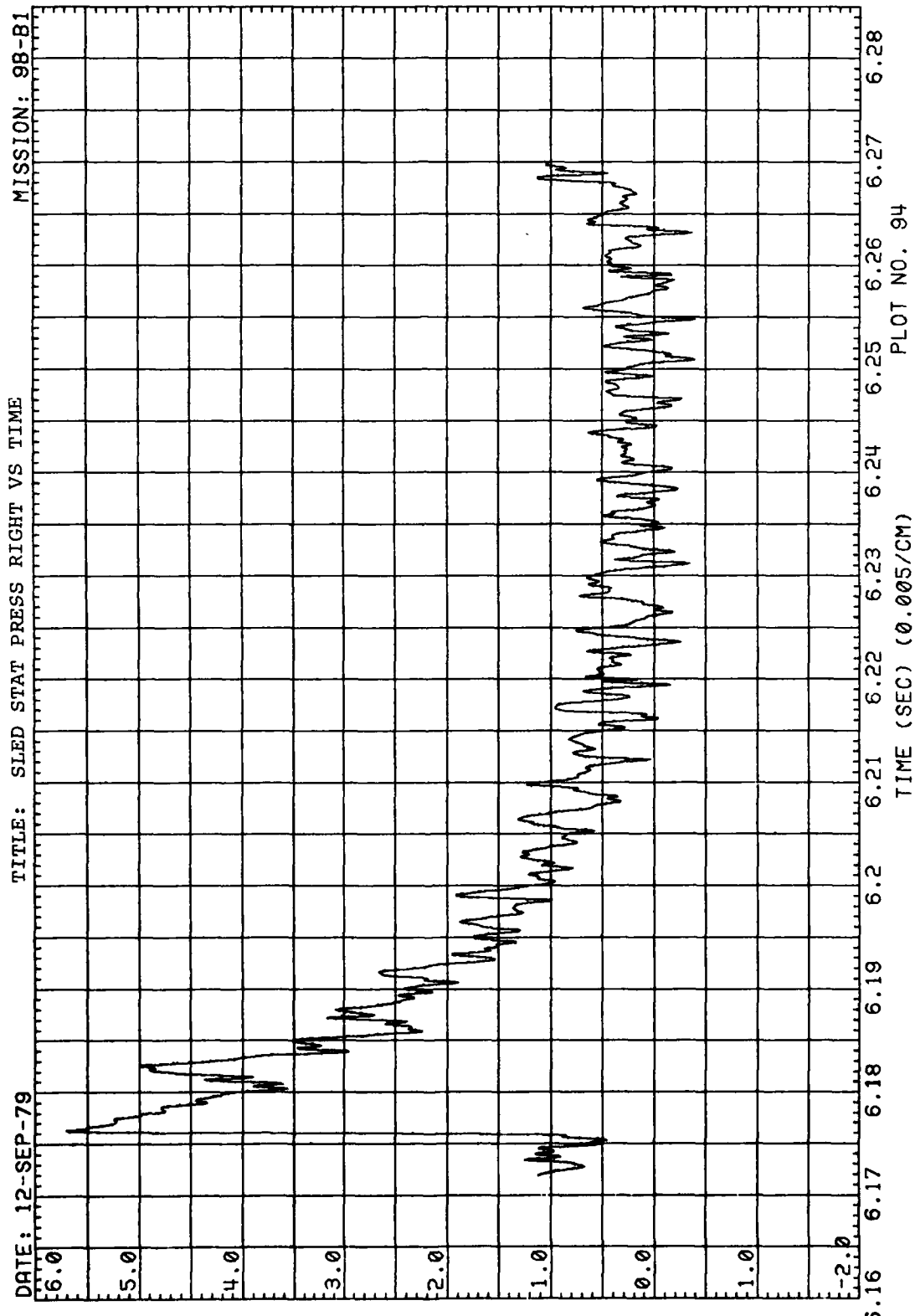

Figure 58. (Concluded)

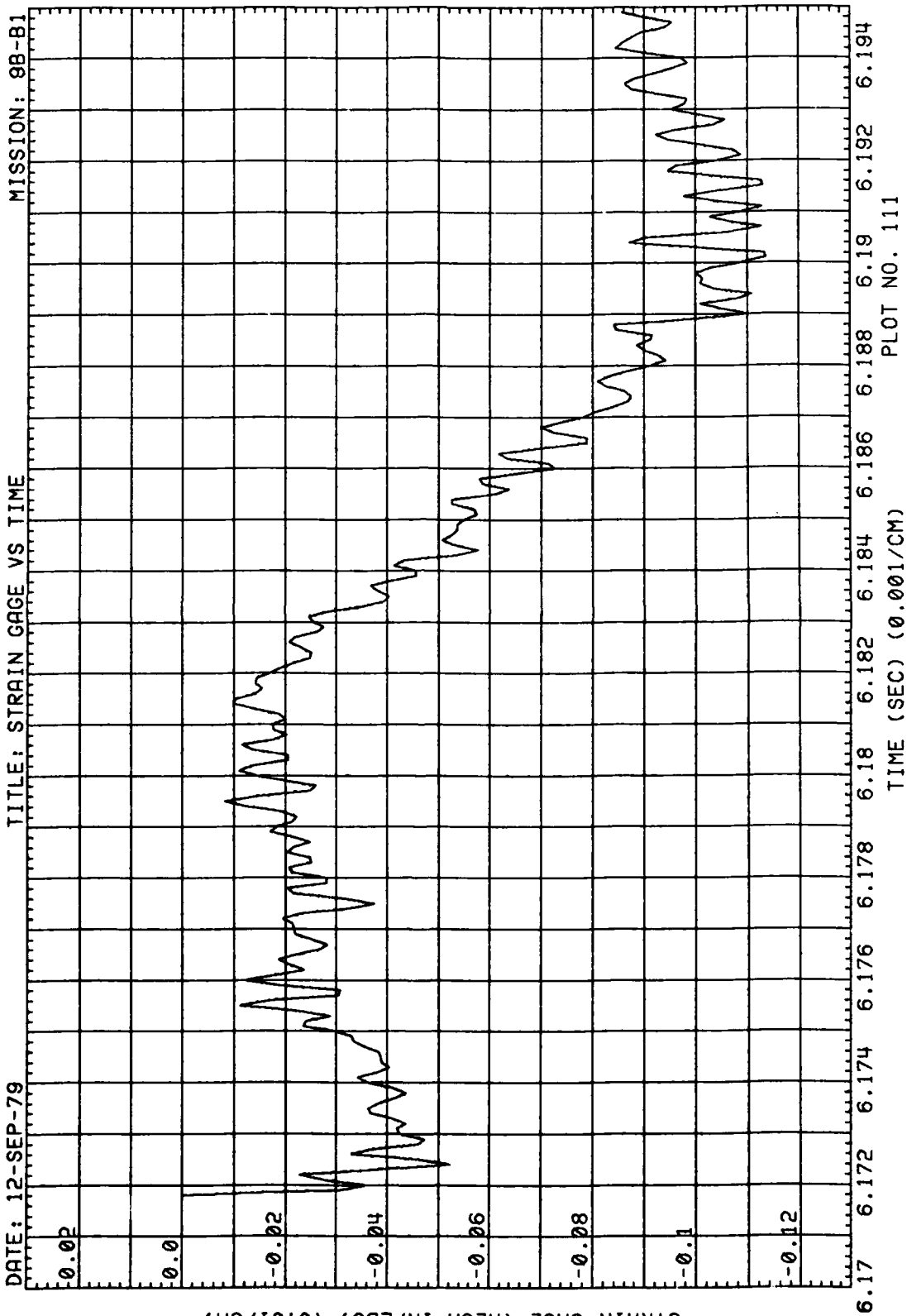

Figure 59. Strain at Model Support, Run 9B-B1, Intercept 3

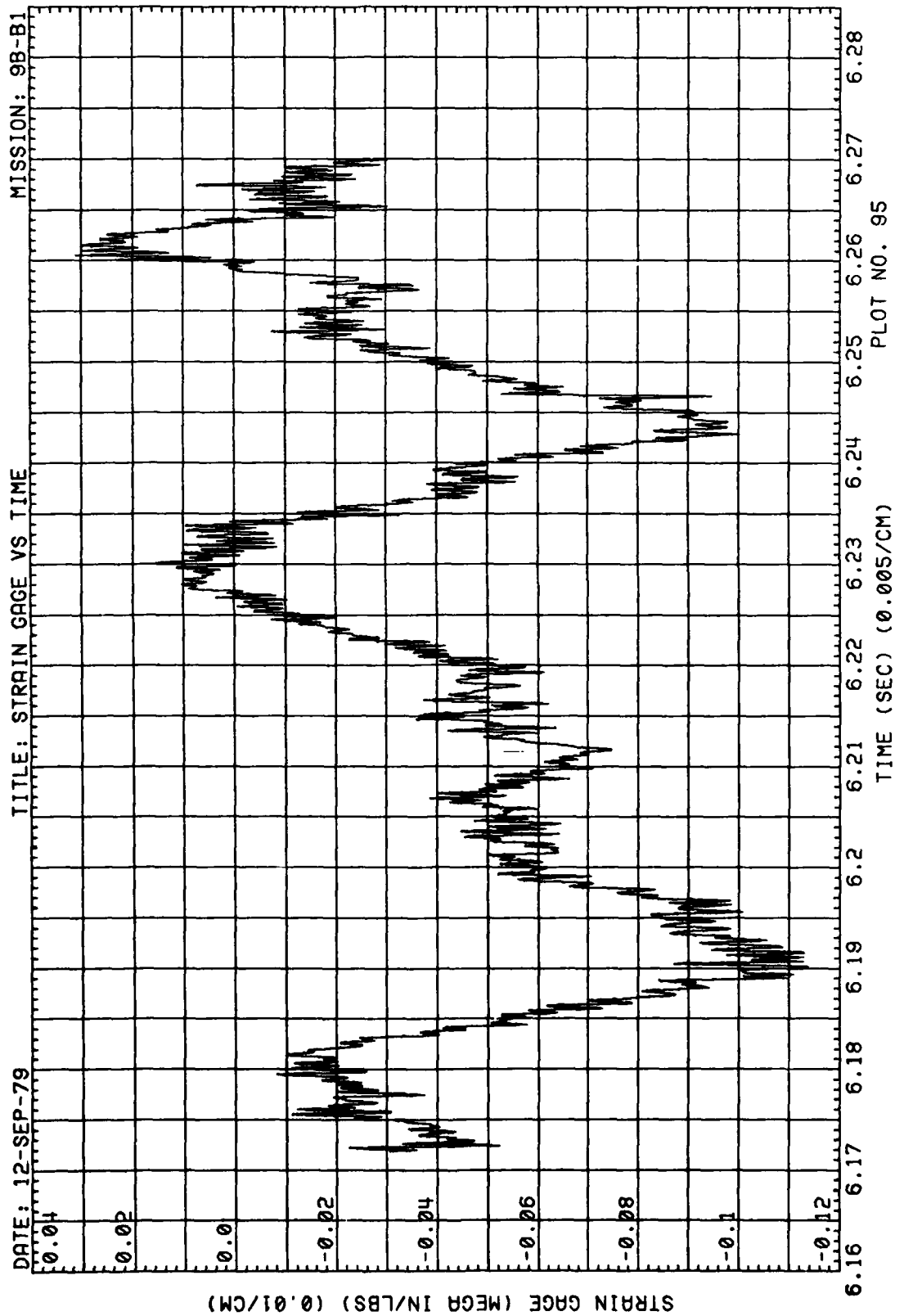

Figure 59. (Concluded)

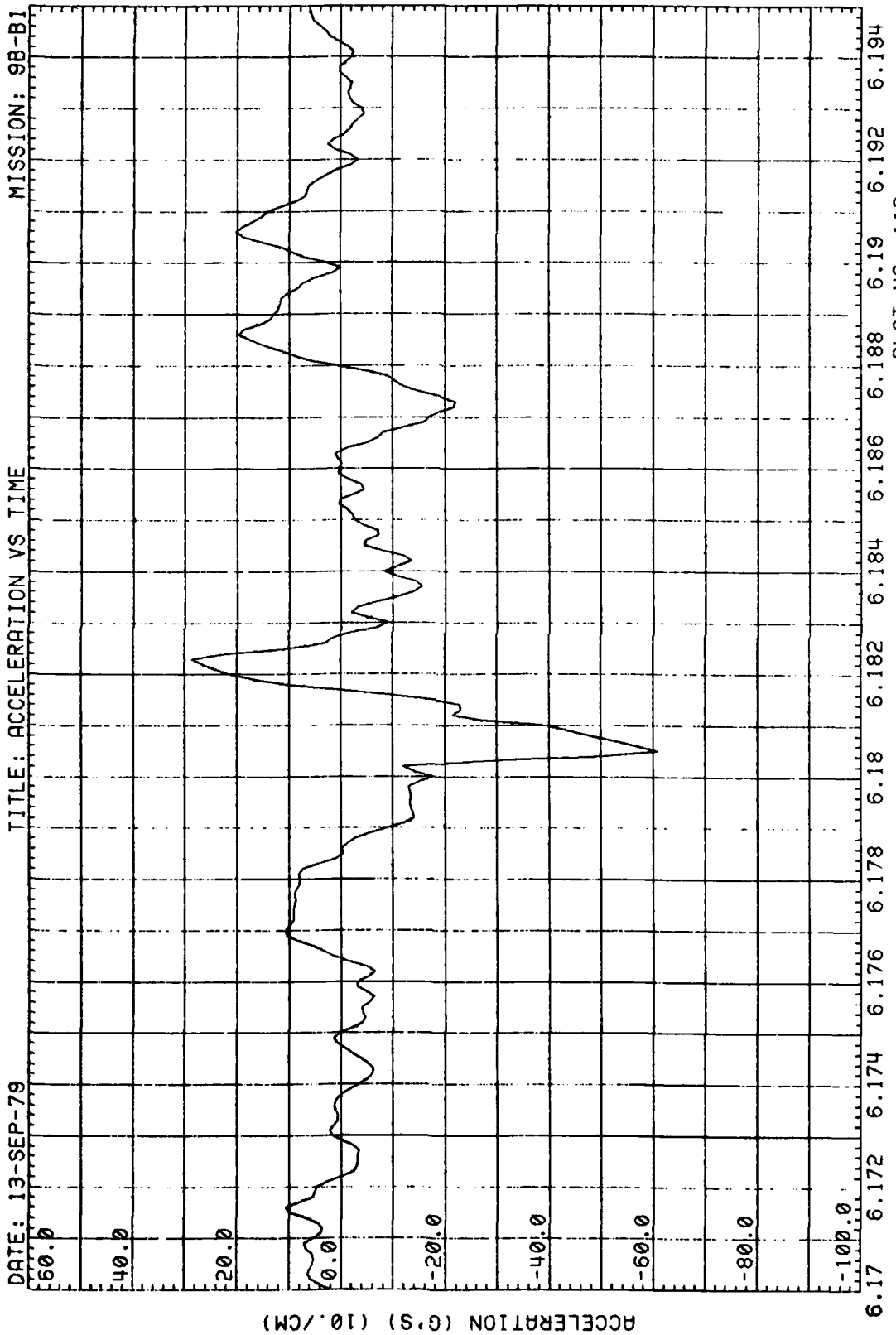

Figure 60. Wing Acceleration, Run 9B-B1, Intercept 3

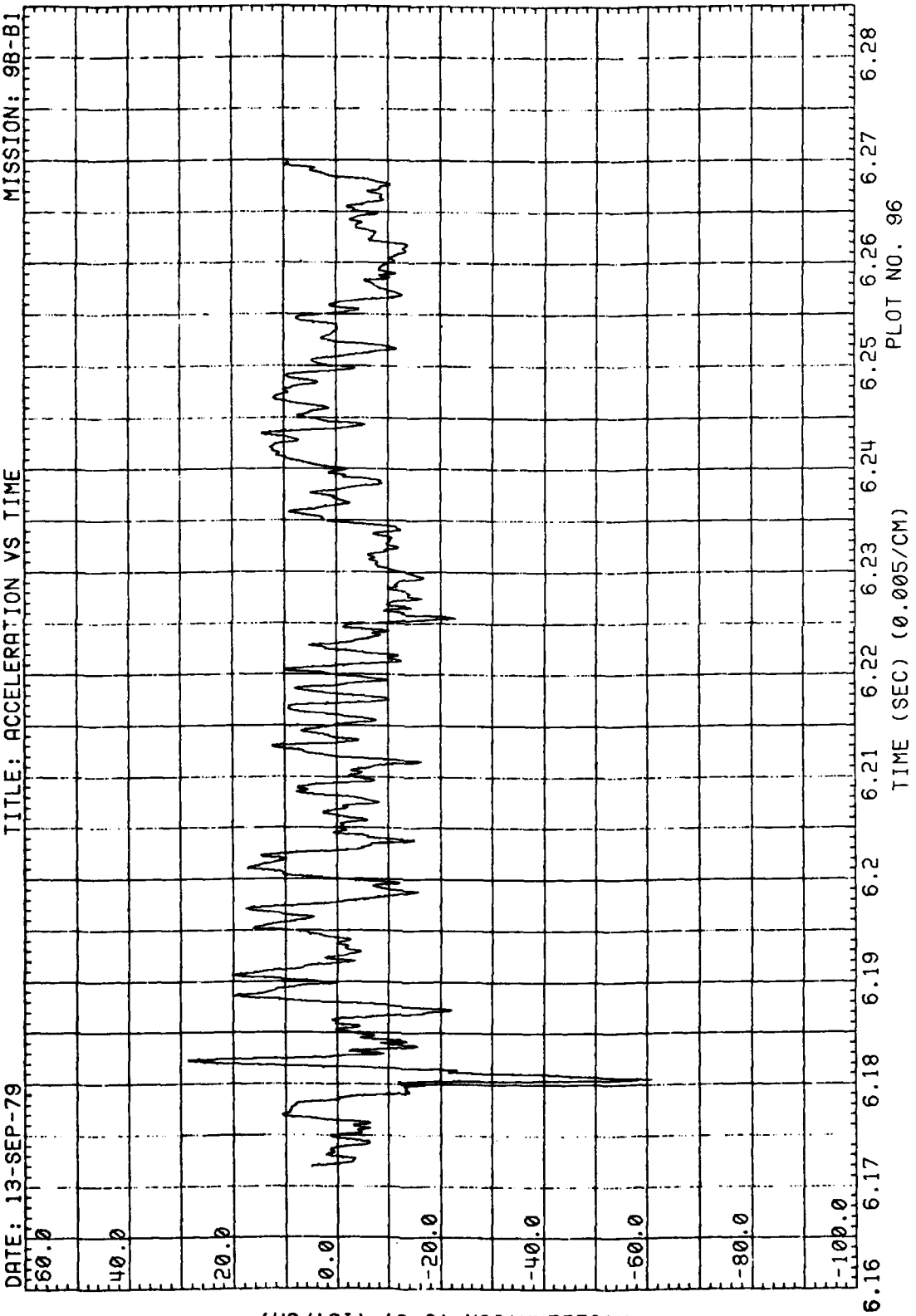

Figure 60. (Concluded)

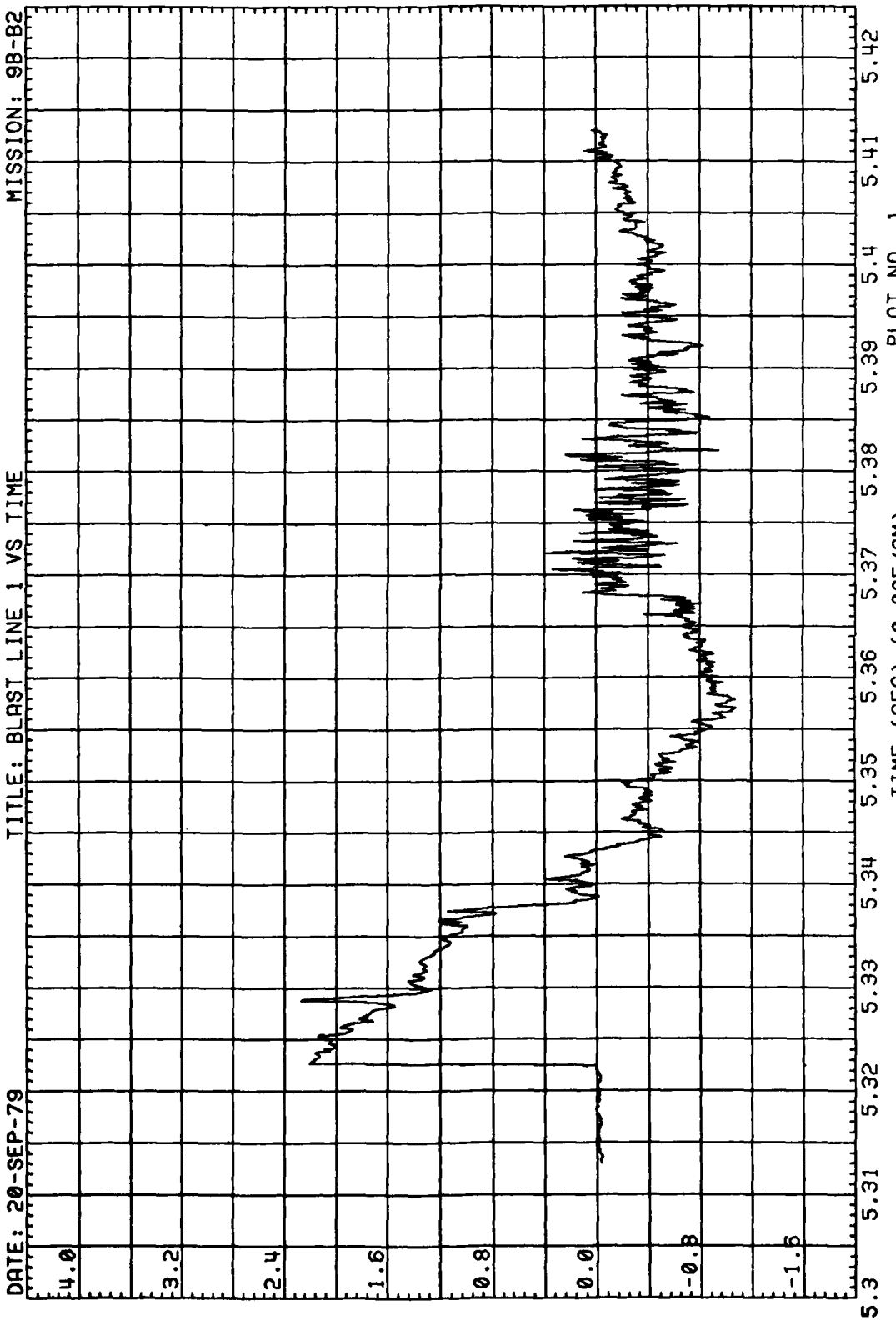

Figure 61. Blast-Line Overpressures, Run 9B-B2, Intercept 1

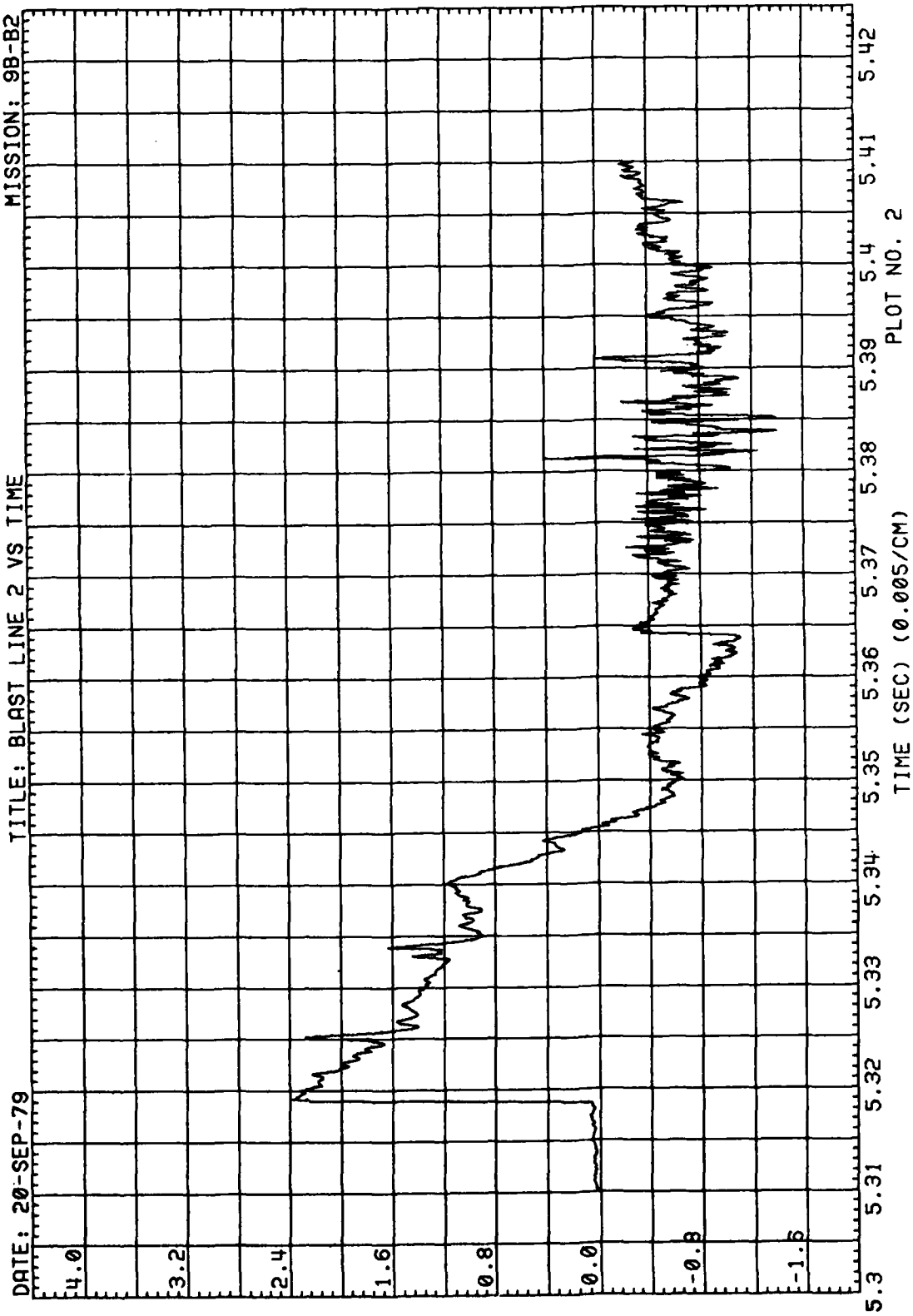

Figure 61. (Continued)

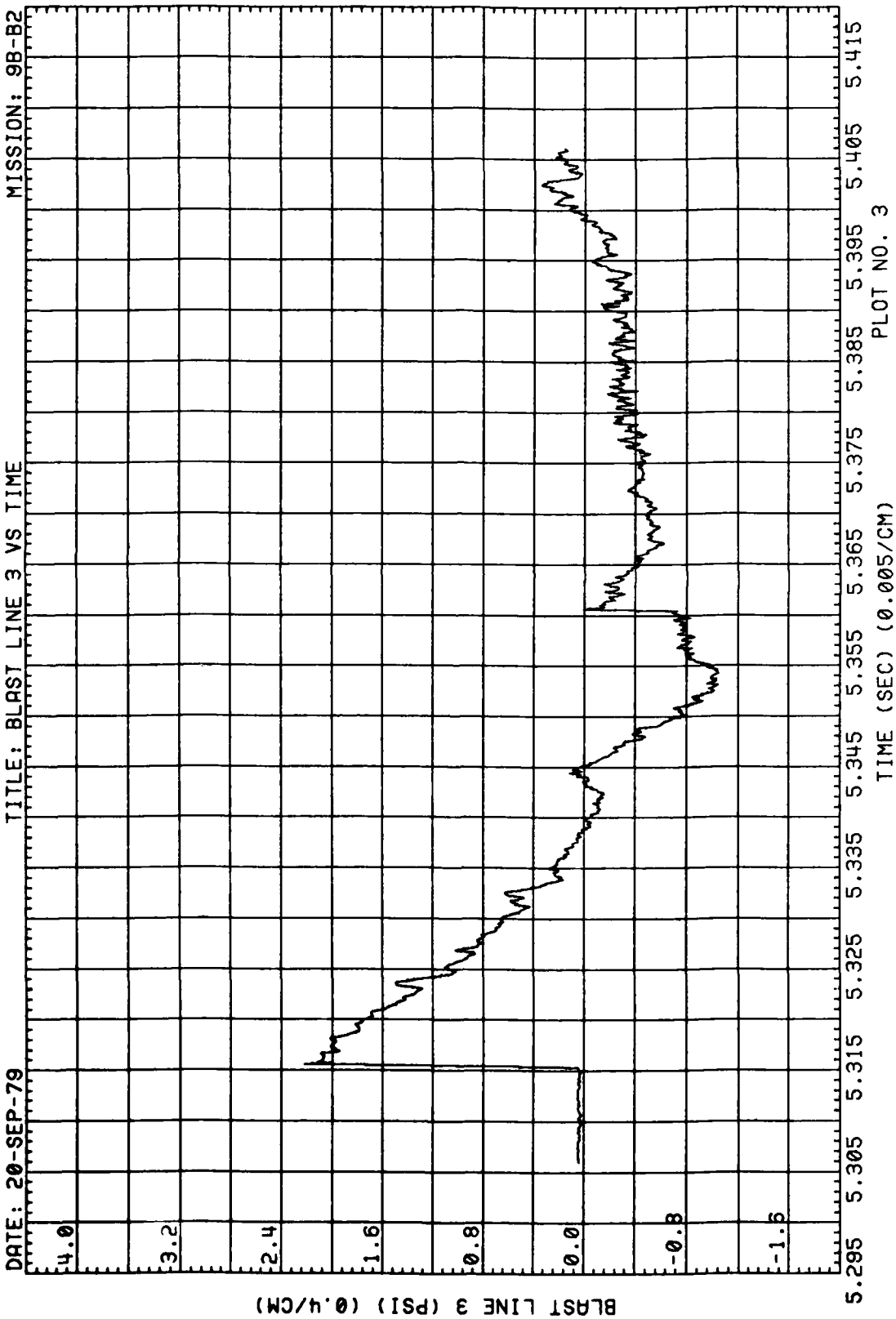

Figure 61. (Continued)

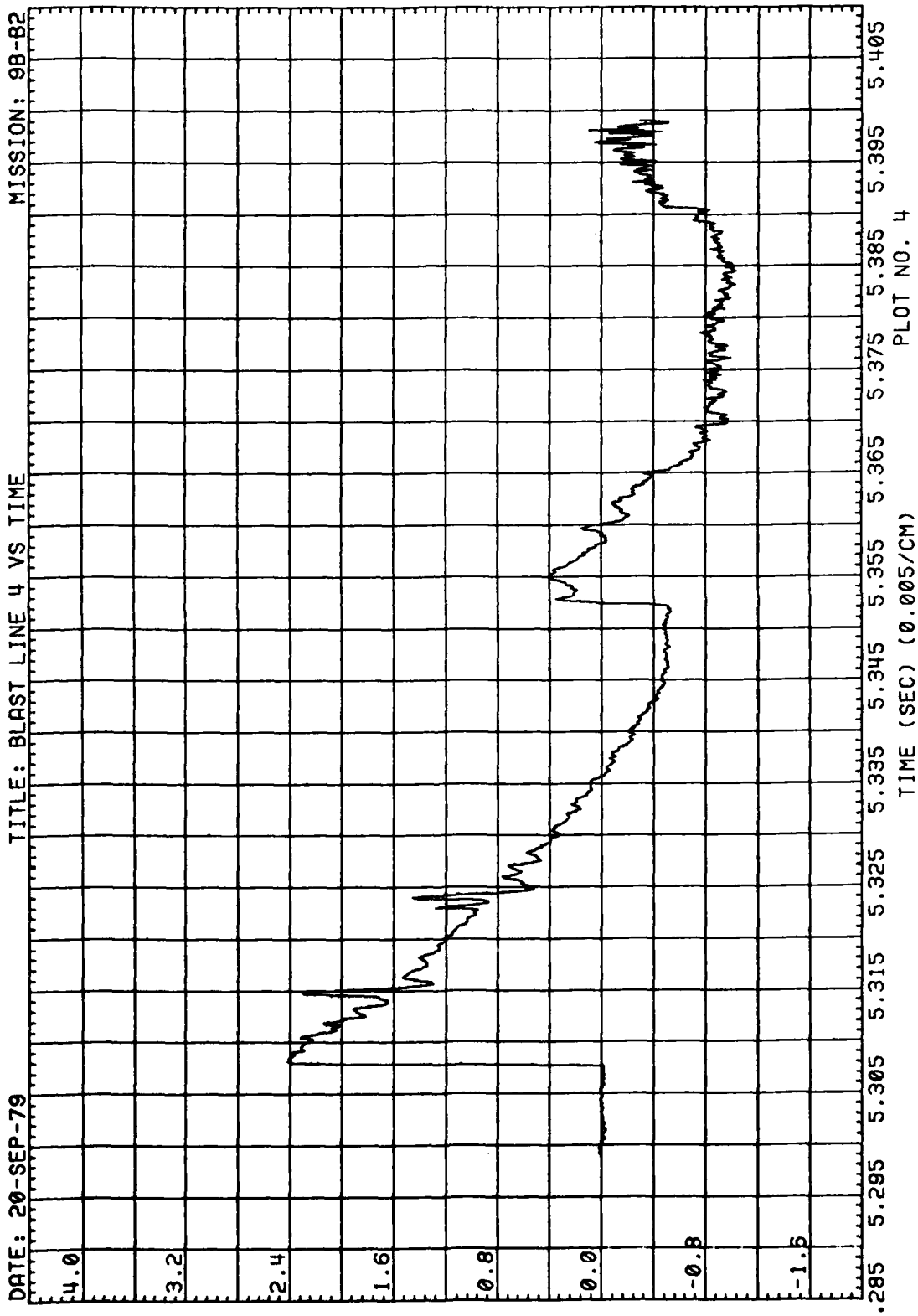

Figure 61. (Concluded)

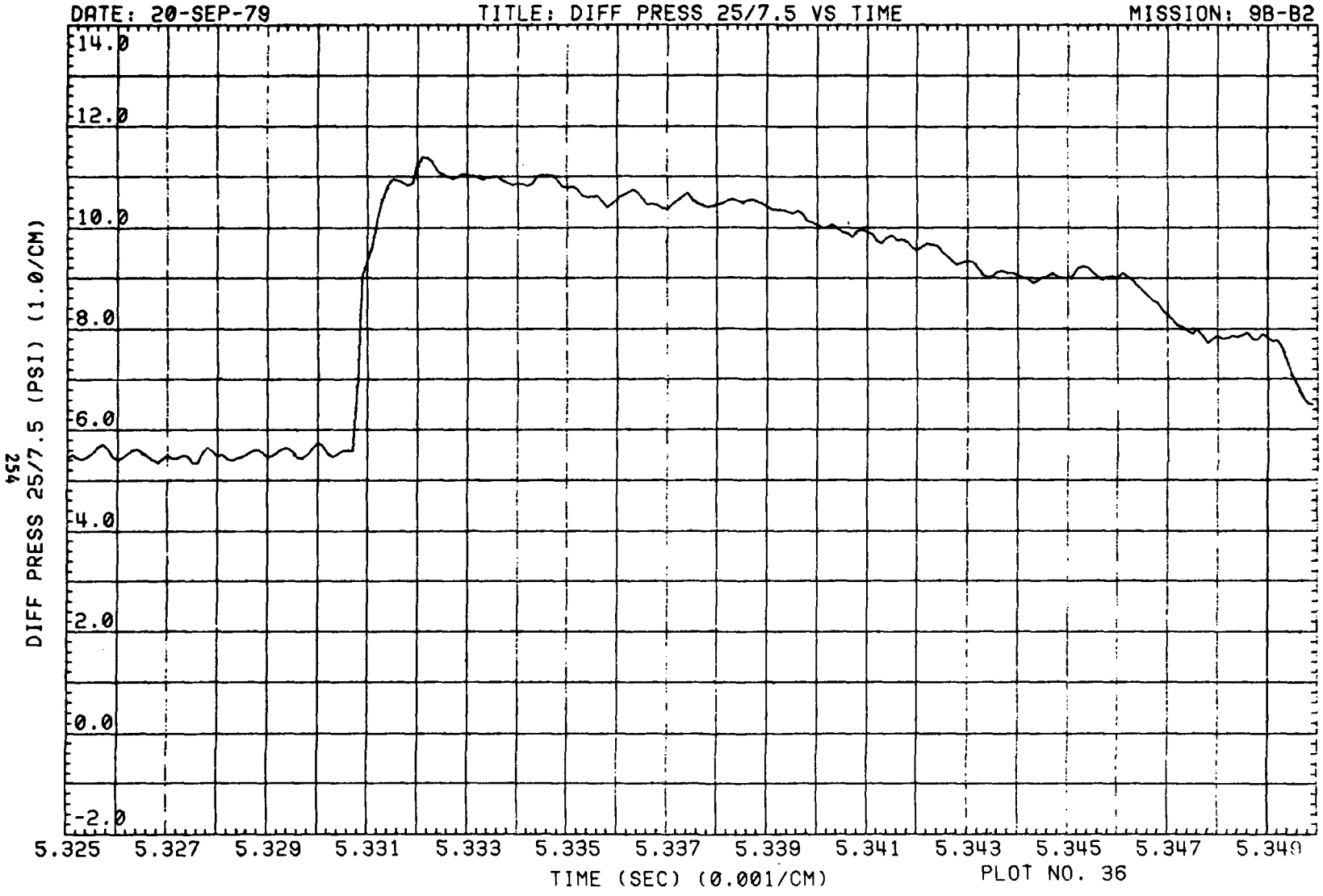

Figure 62. Differential Wing Pressures, Run 9B-B2, Intercept 1

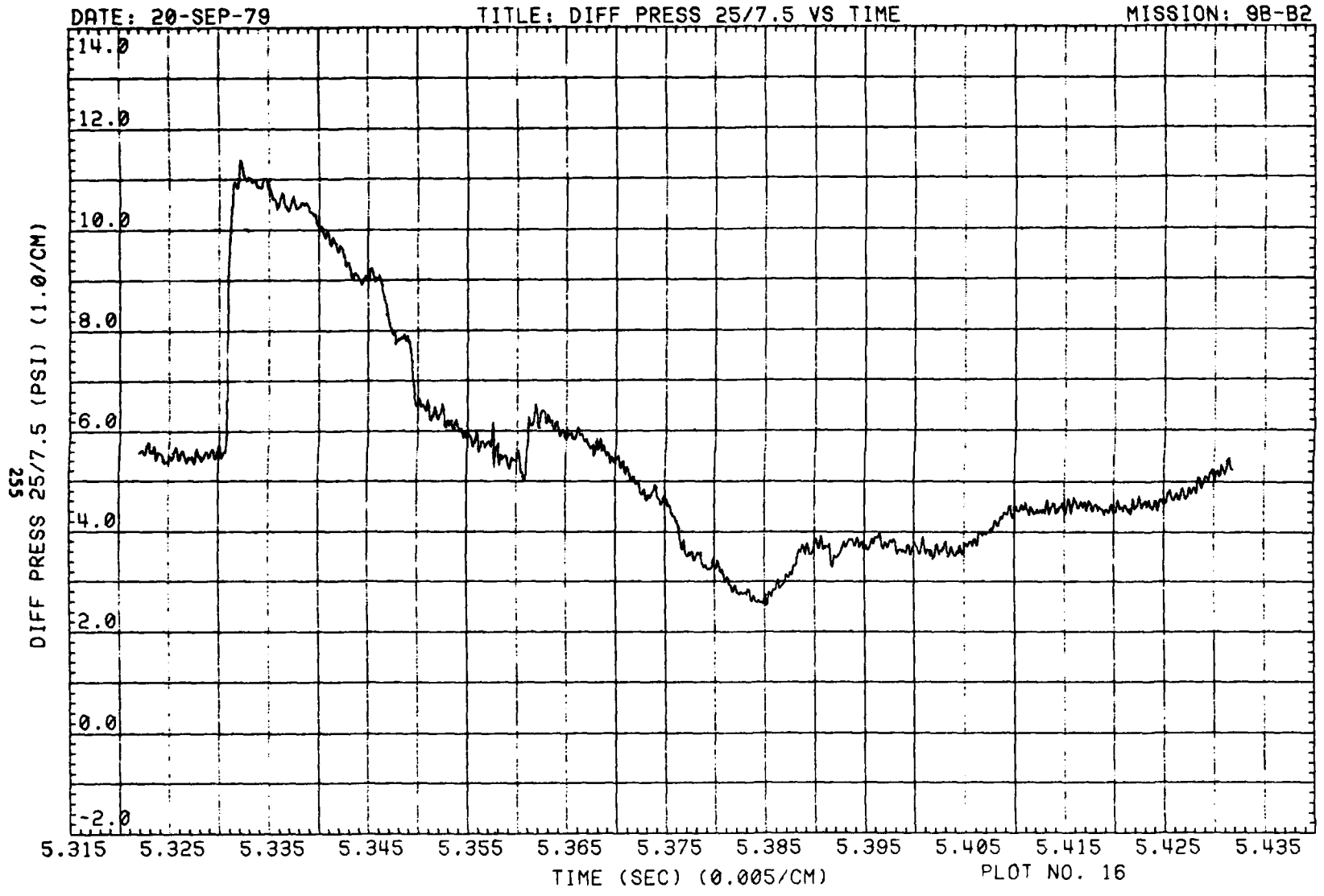

Figure 62. (Continued)

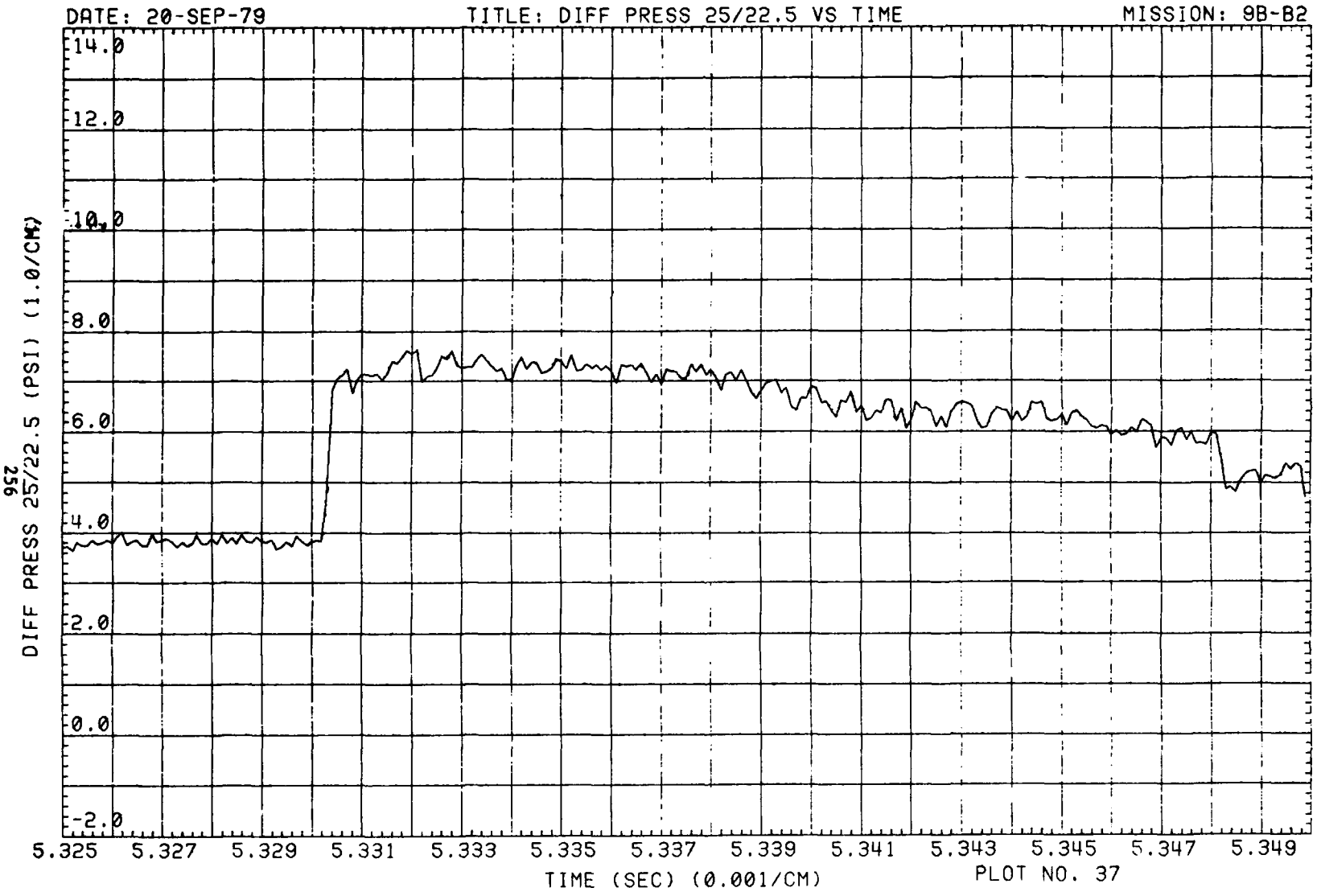

Figure 62. (Continued)

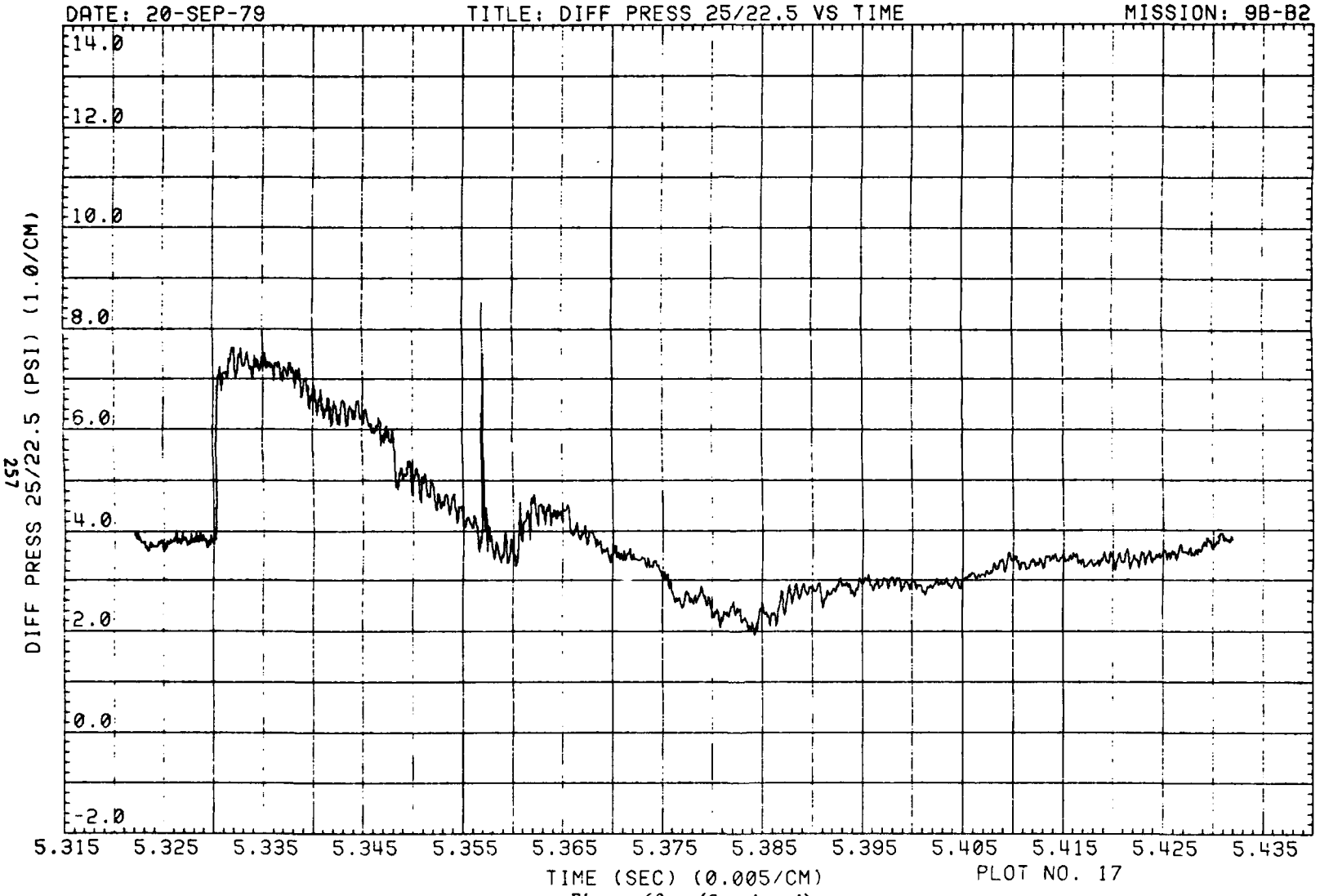

Figure 62. (Continued)

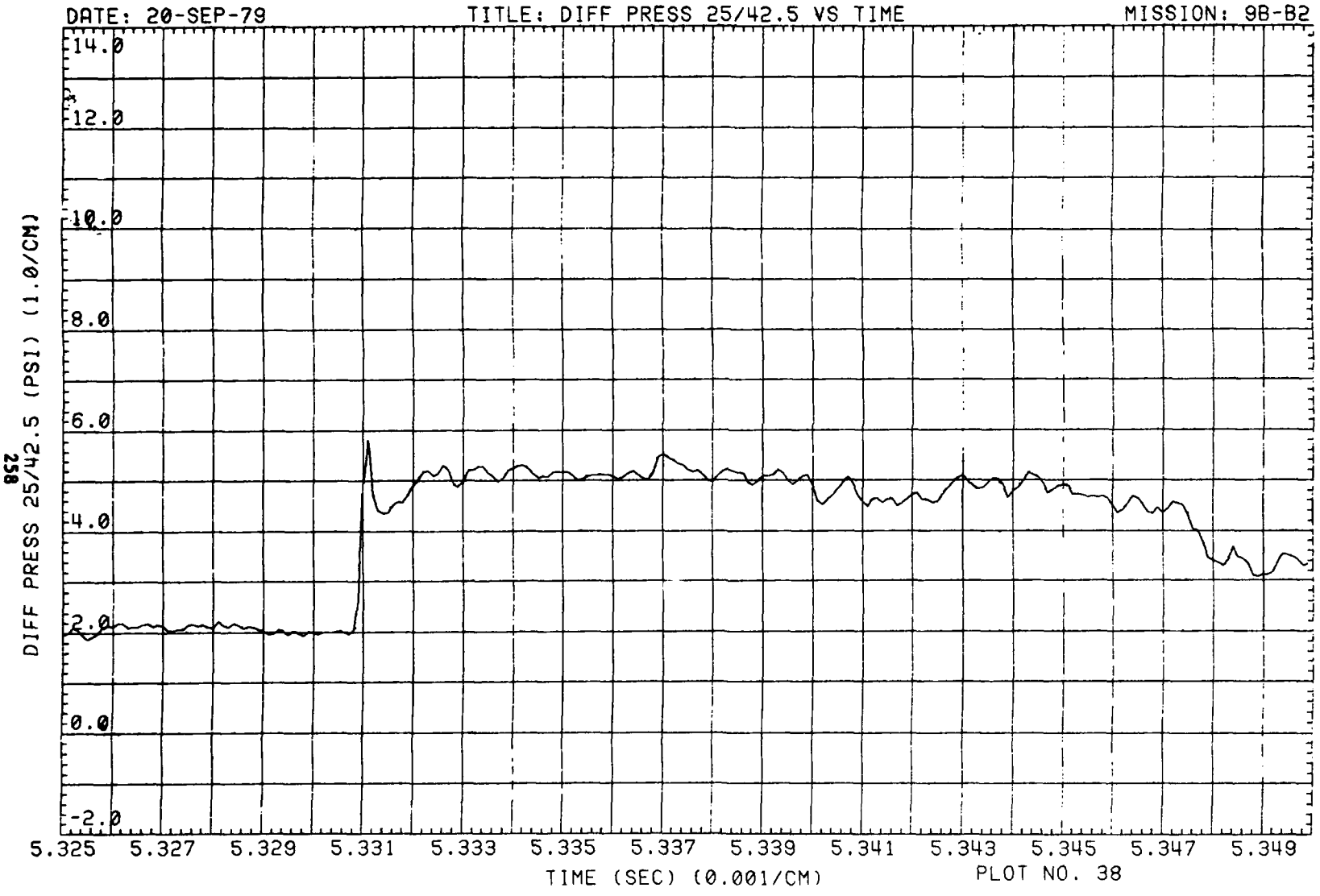

Figure 62. (Continued)

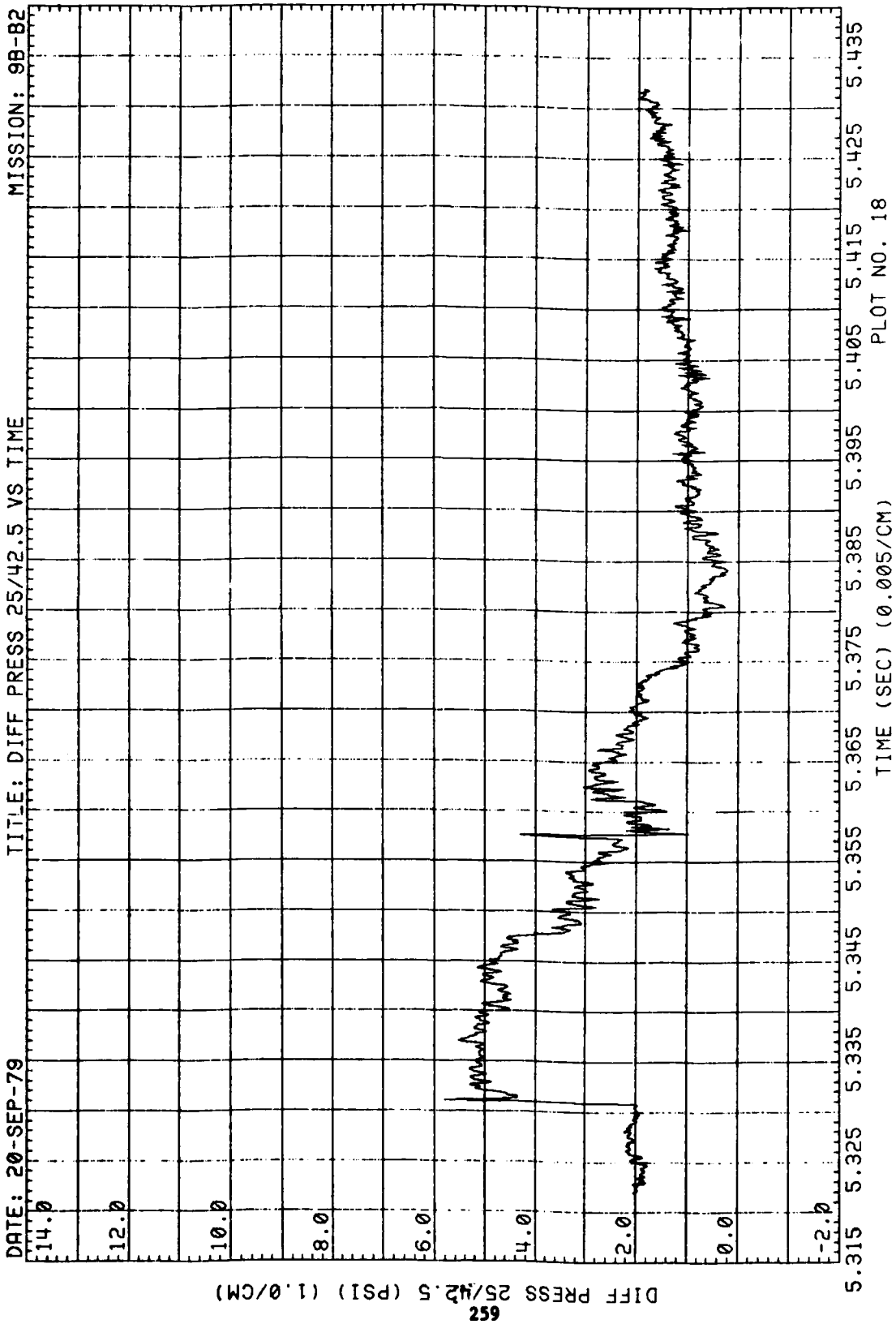

Figure 62. (Continued)

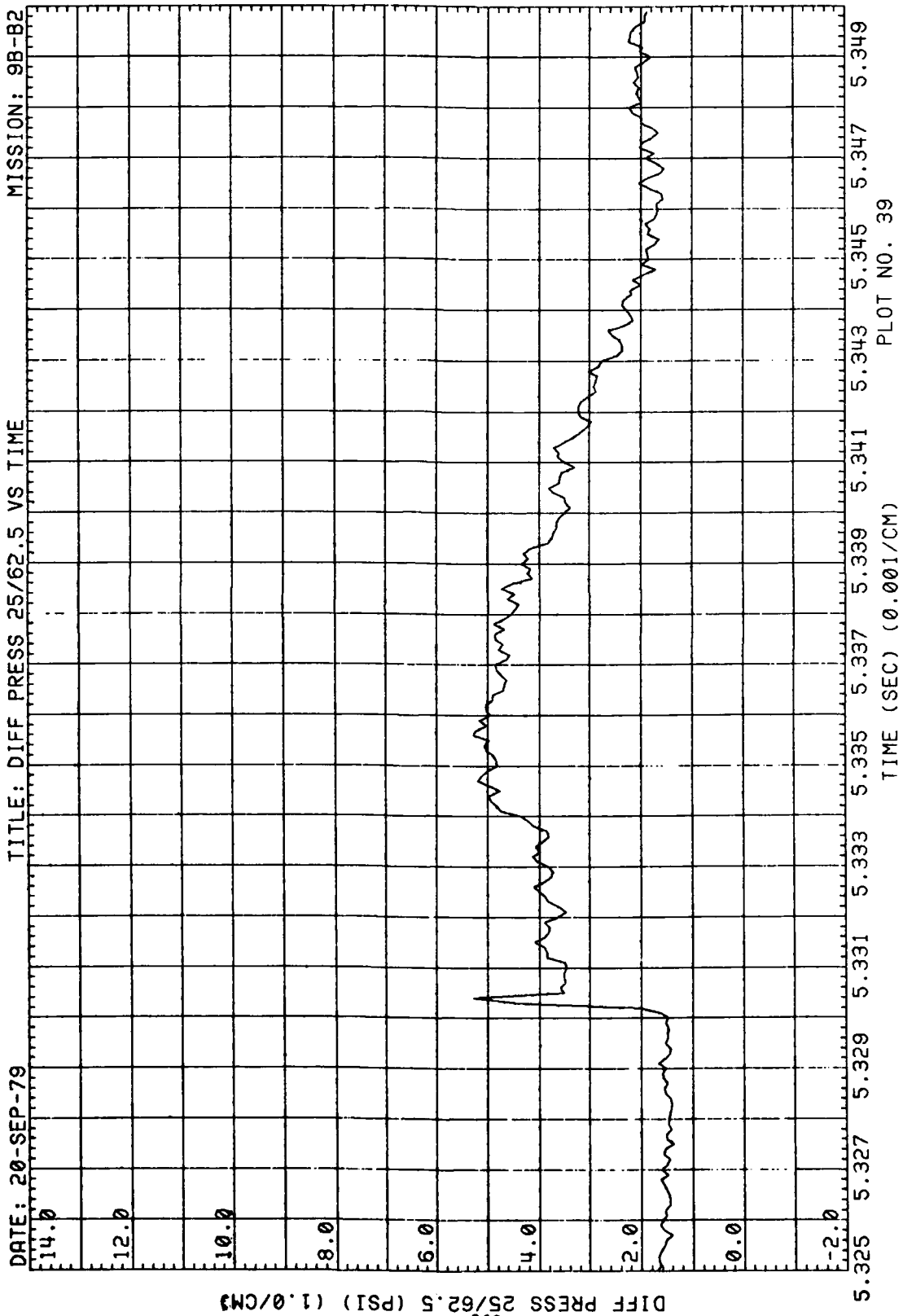

Figure 62. (Continued)

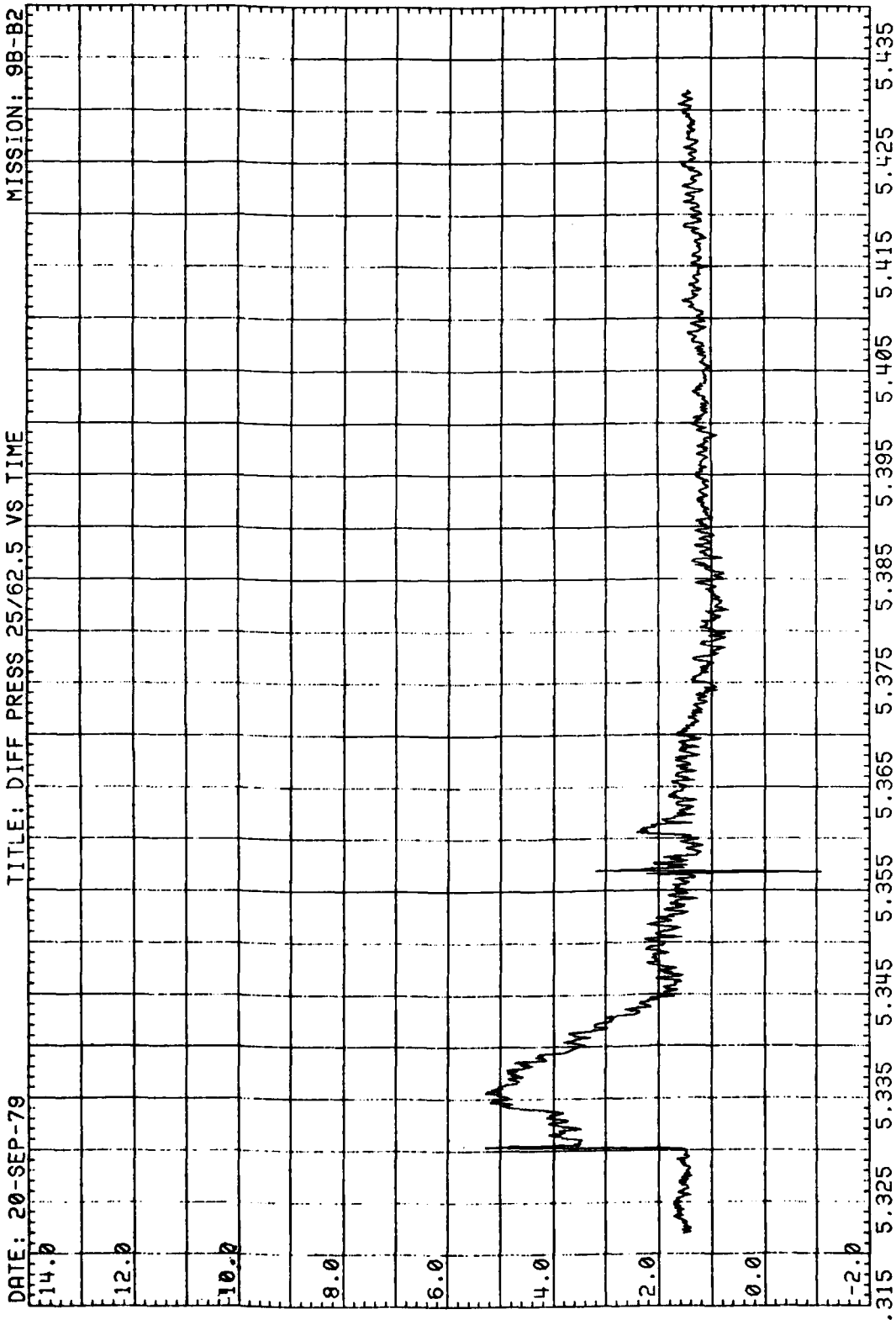

Figure 62. (Continued)

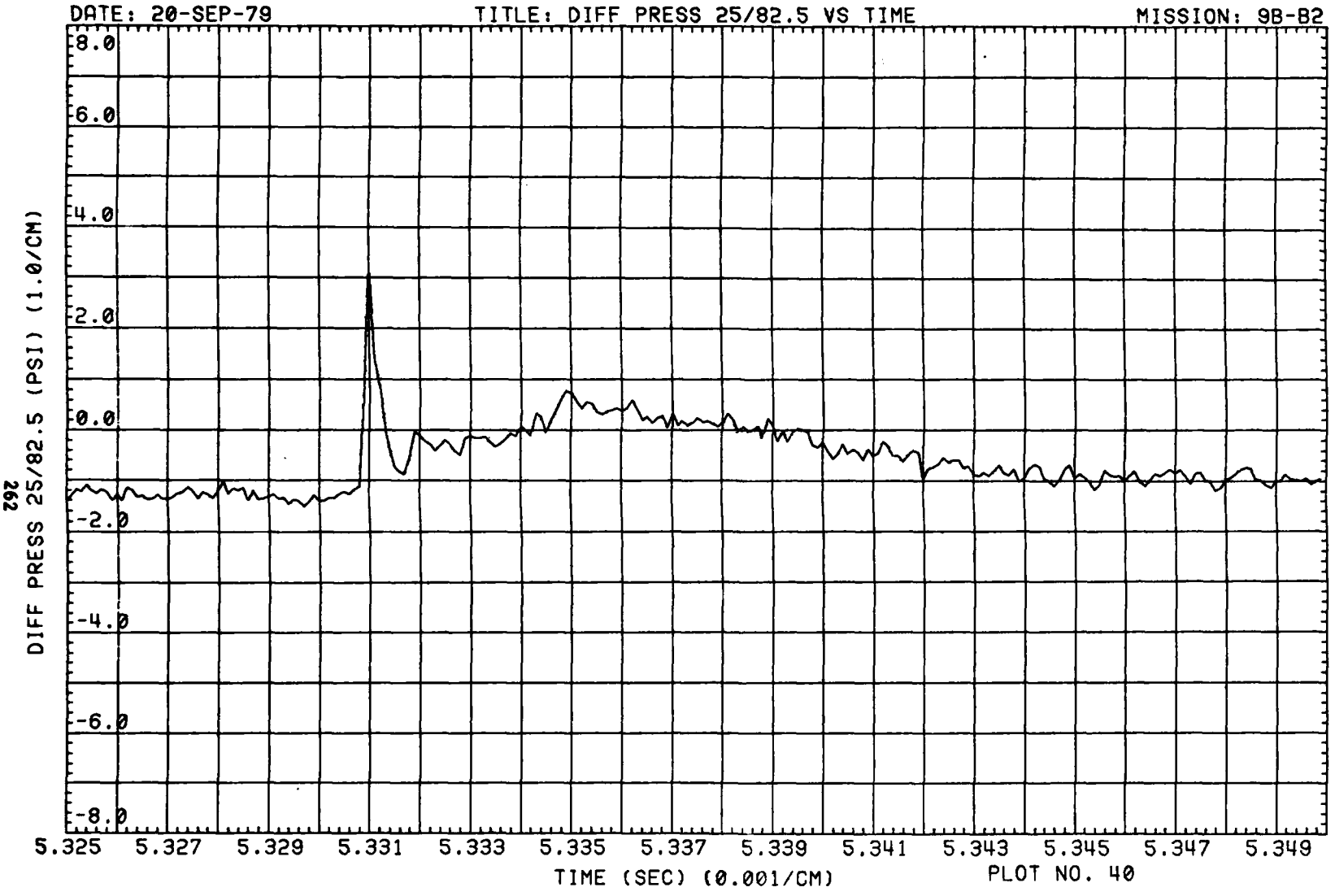

Figure 62. (Continued)

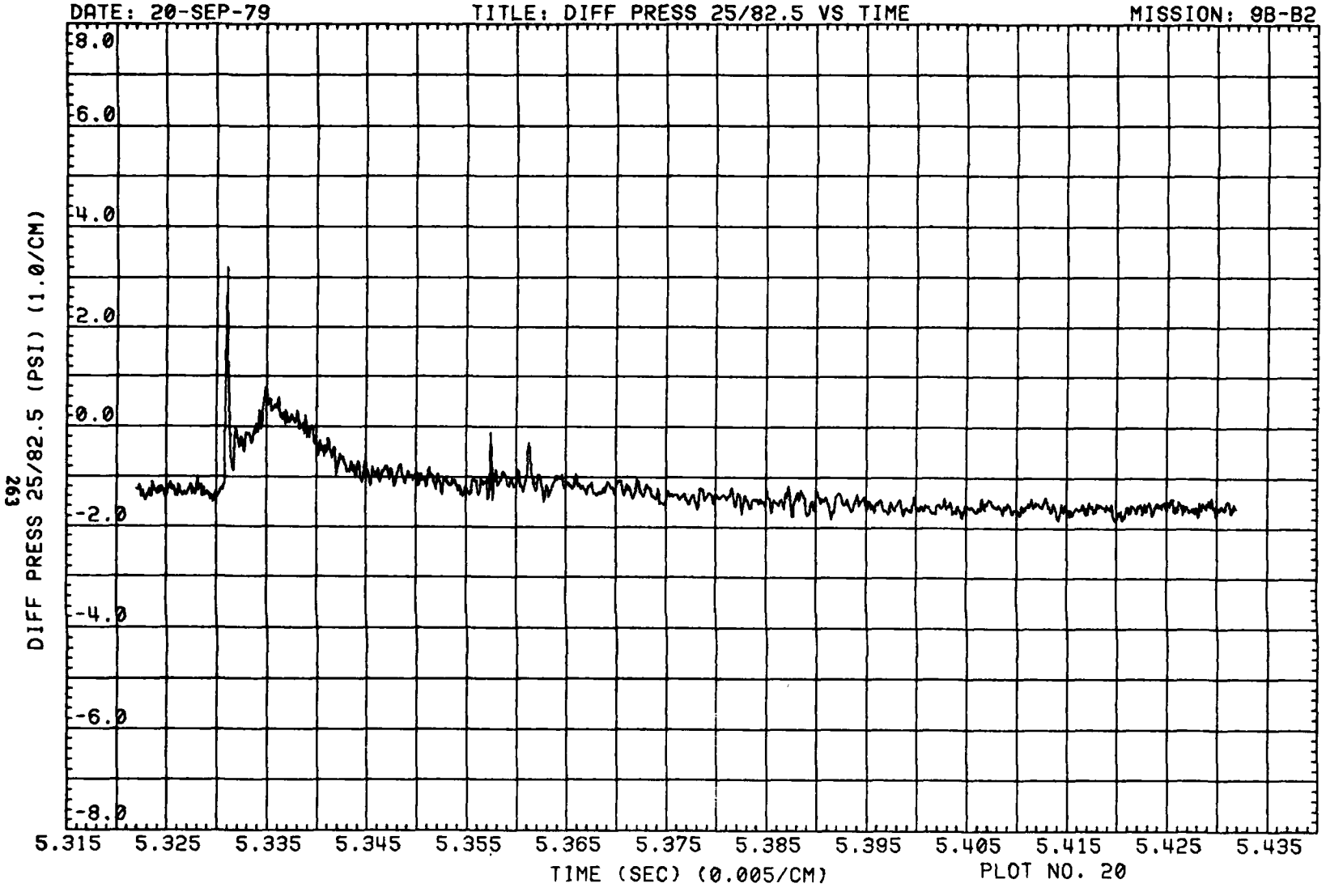

Figure 62. (Continued)

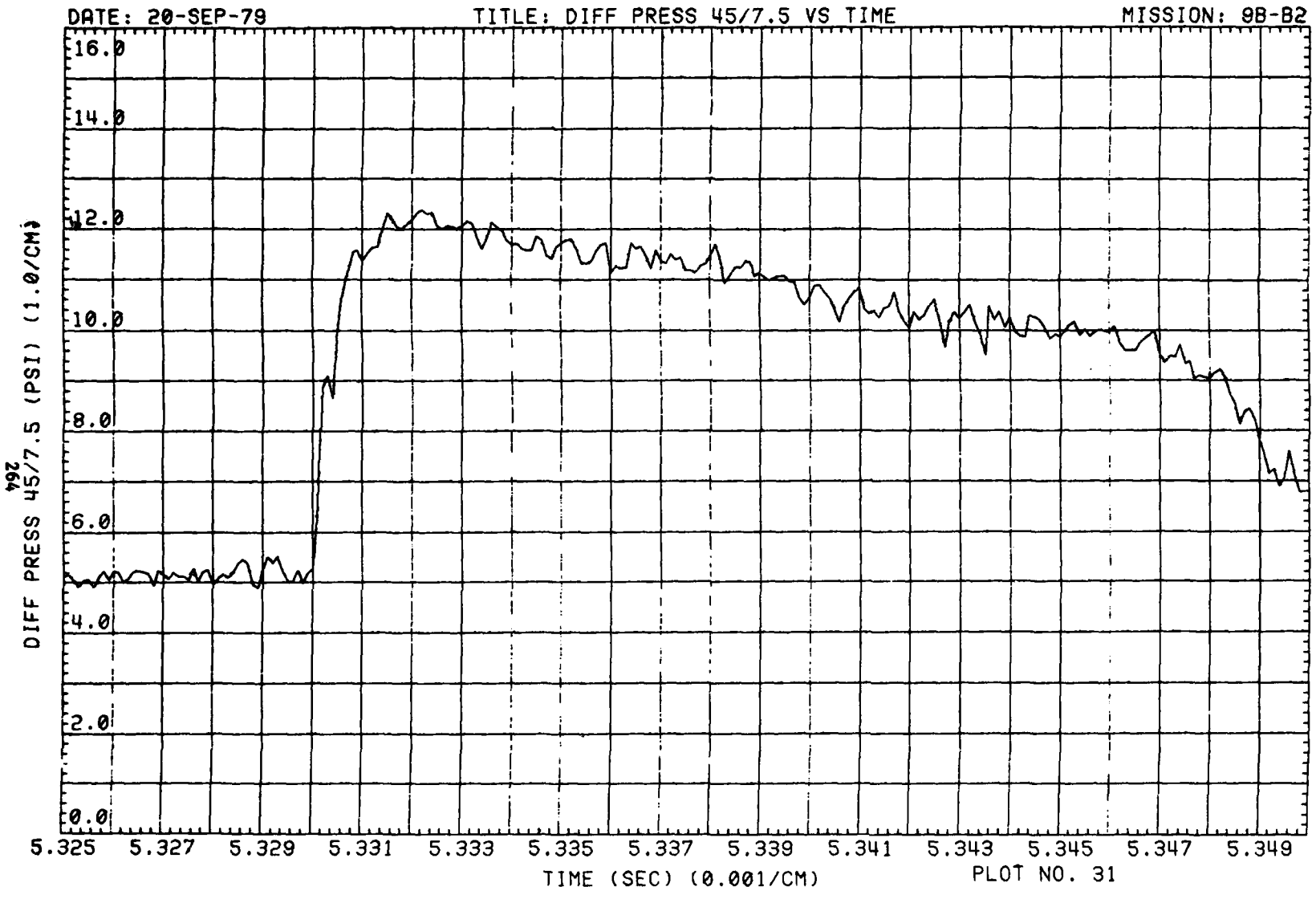

Figure 62. (Continued)

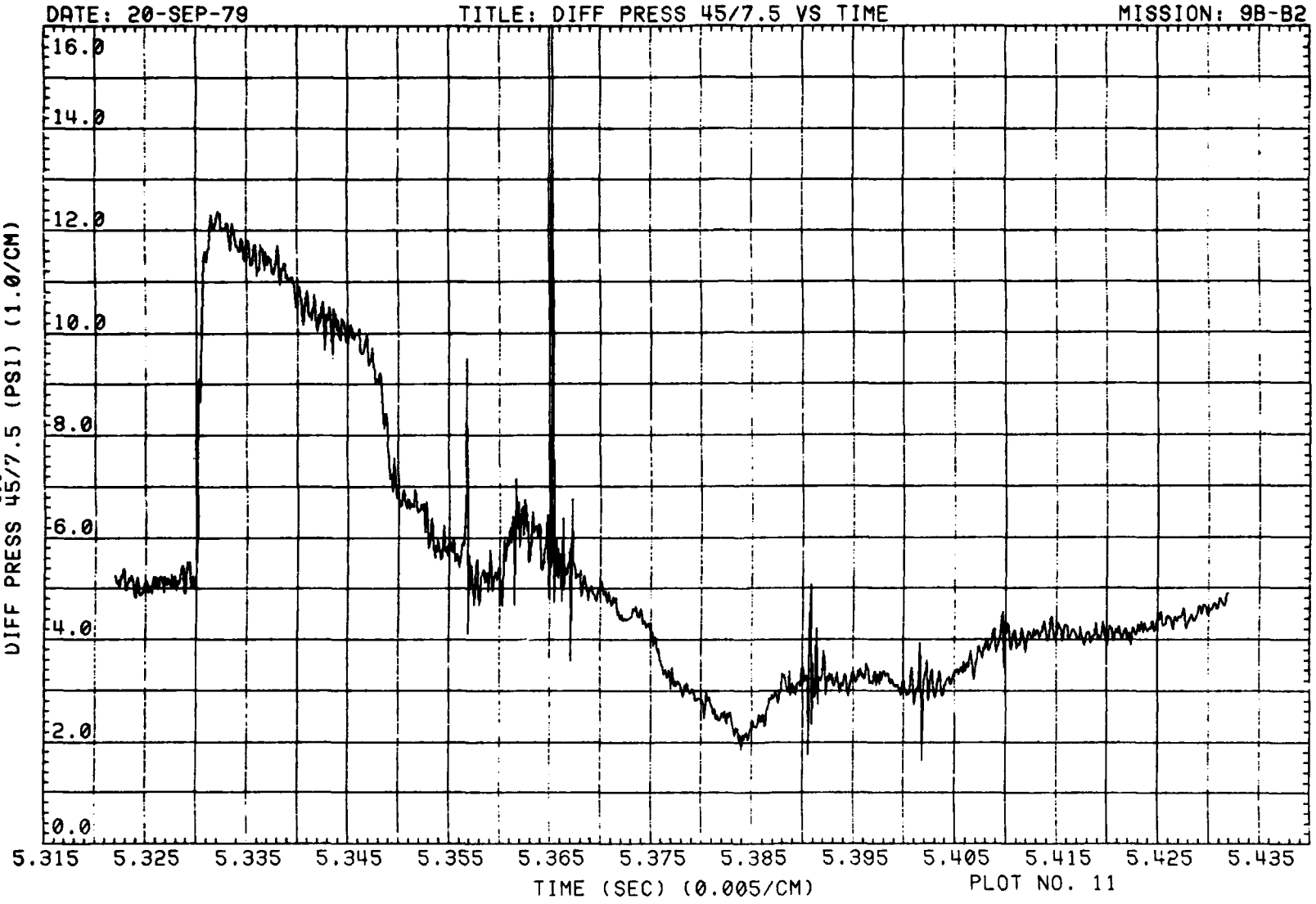

Figure 62. (Continued)

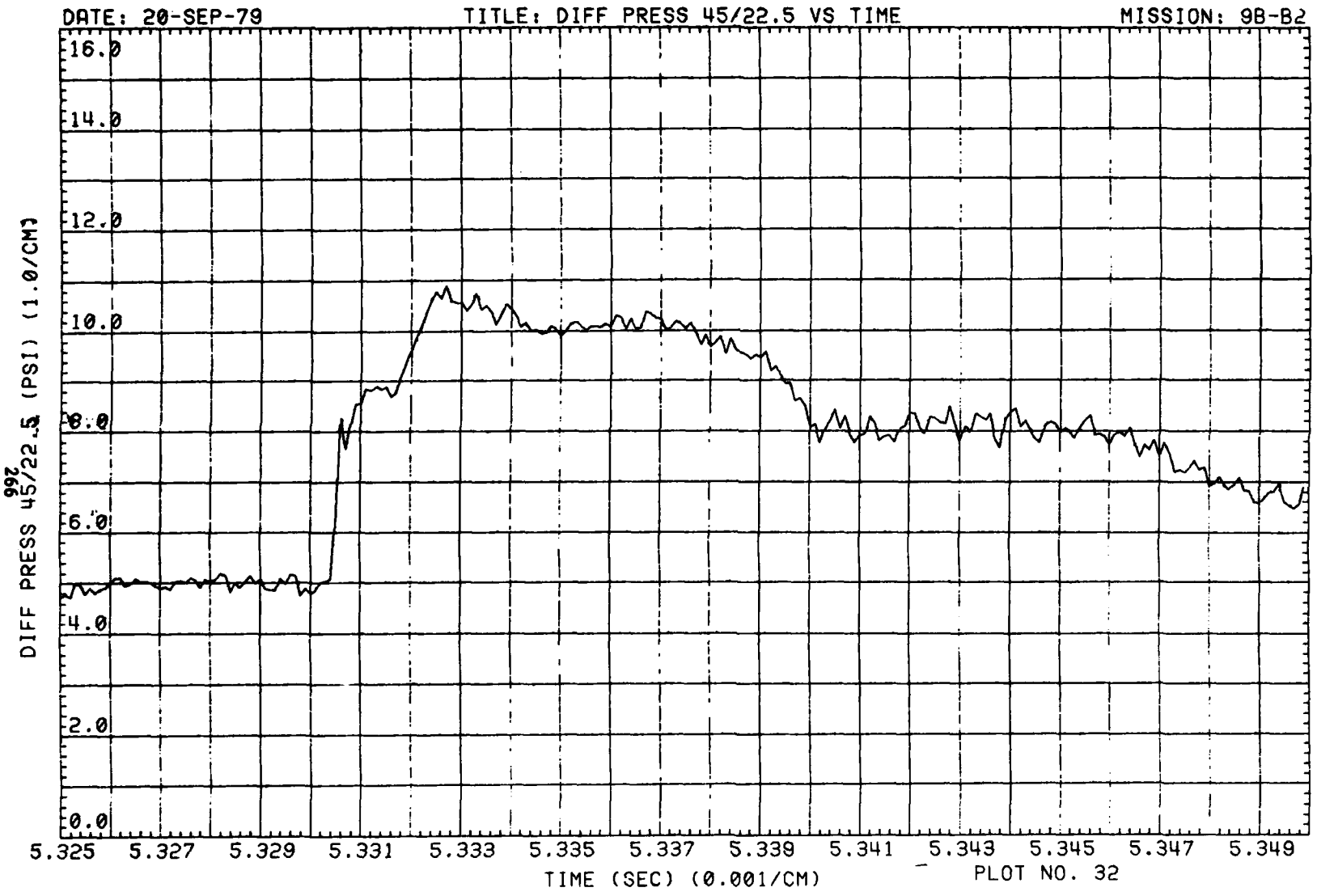

Figure 62. (Continued)

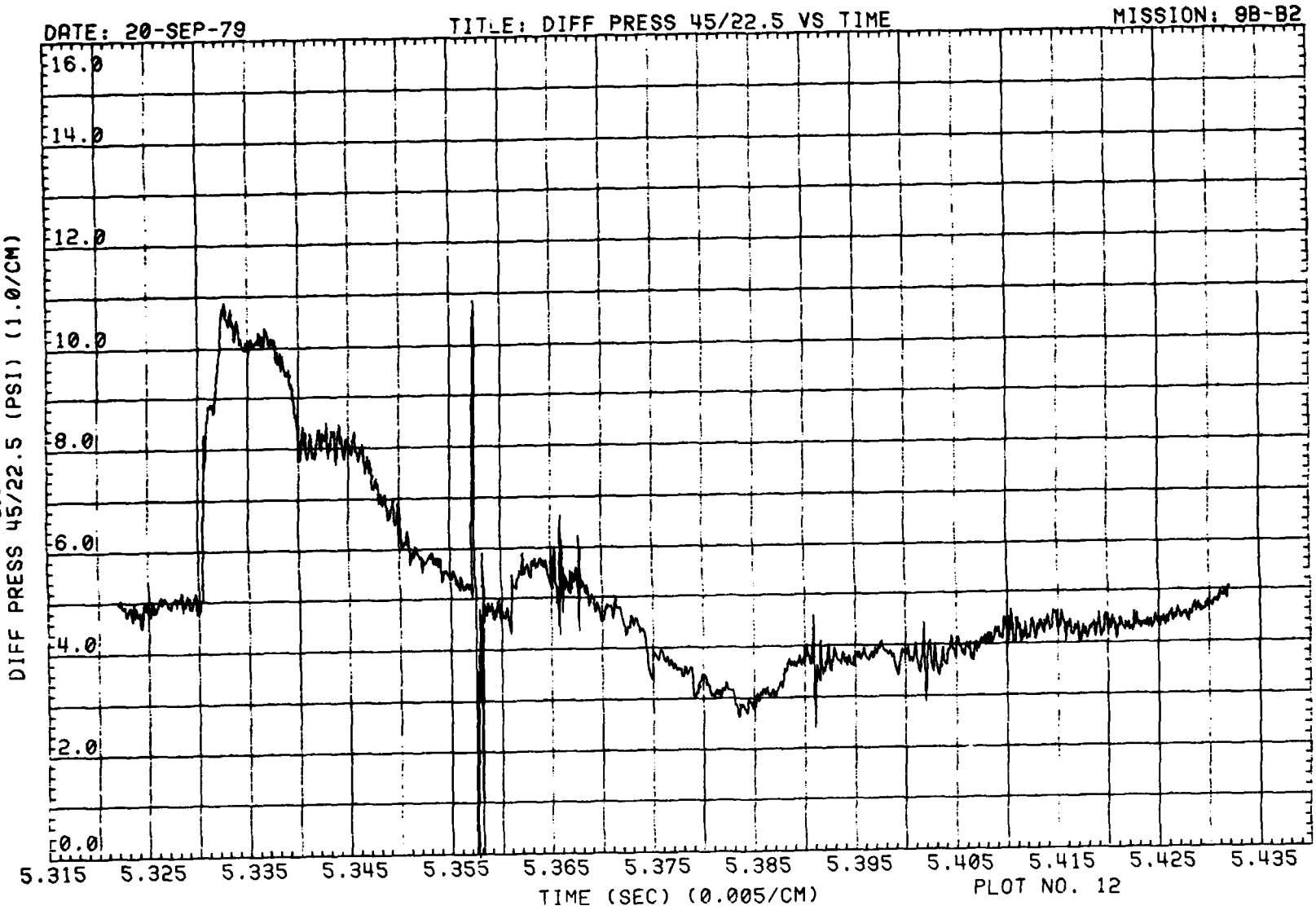

Figure 62. (Continued)

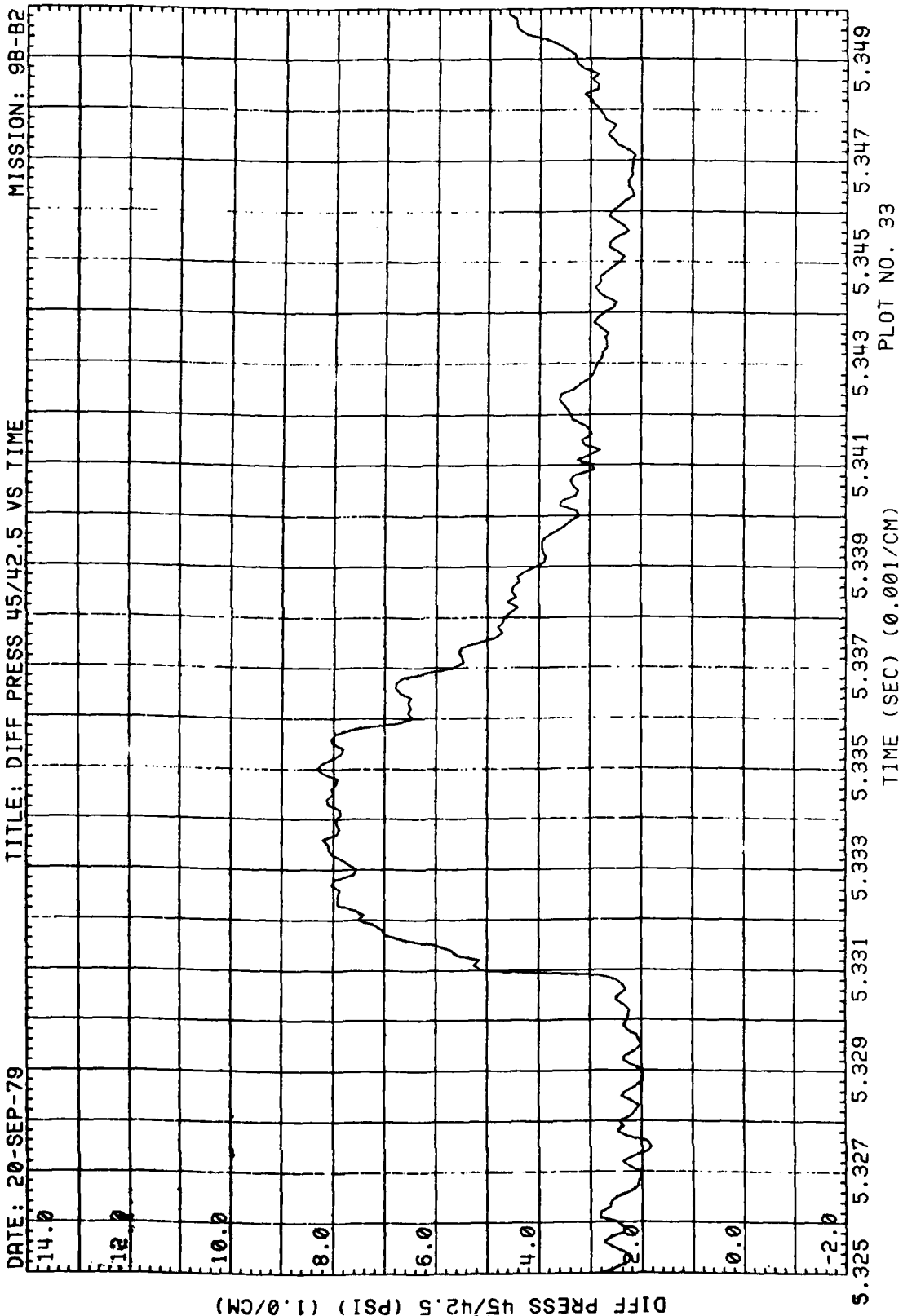

Figure 62. (Continued)

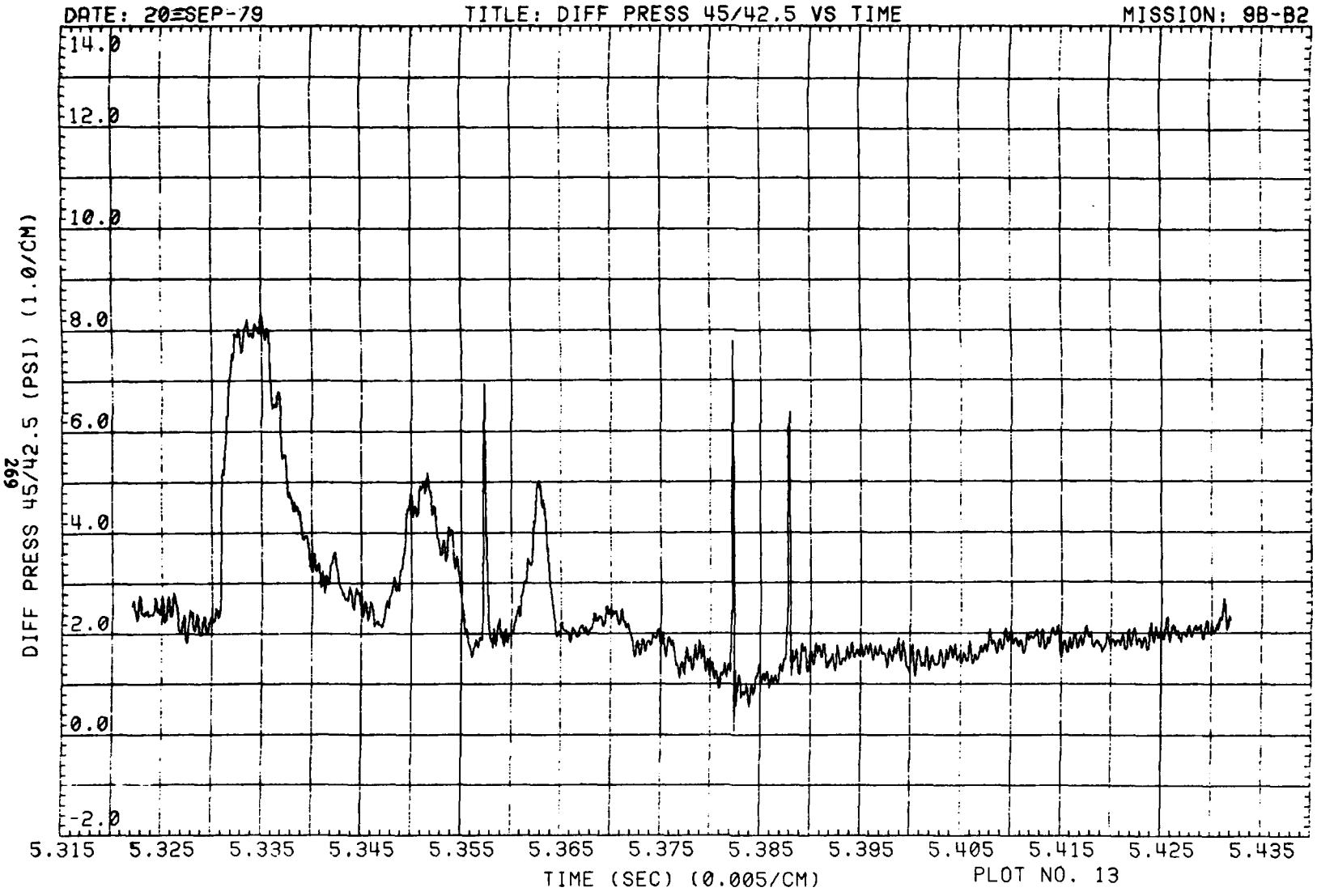

Figure 62. (Continued)

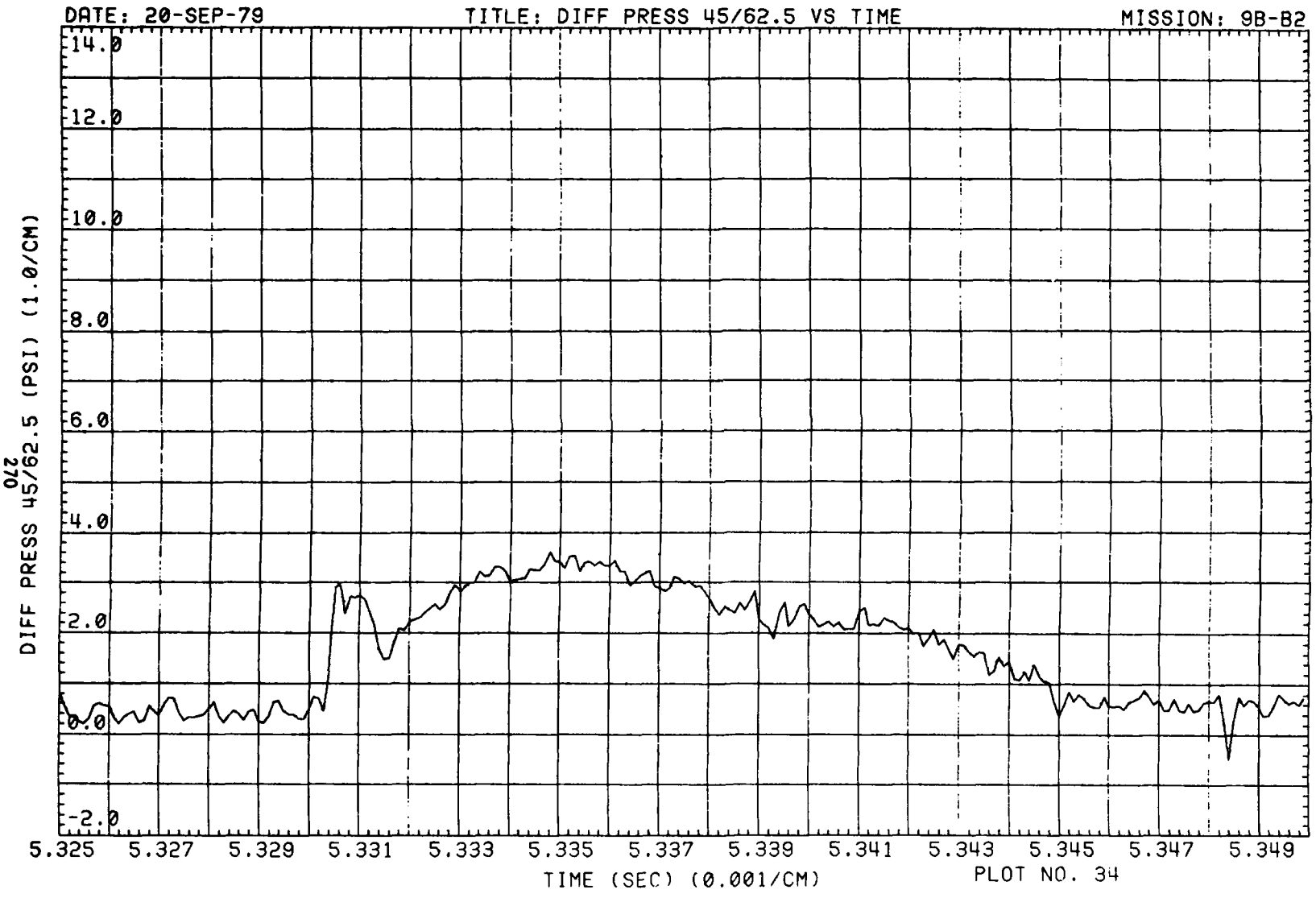

Figure 62. (Continued)

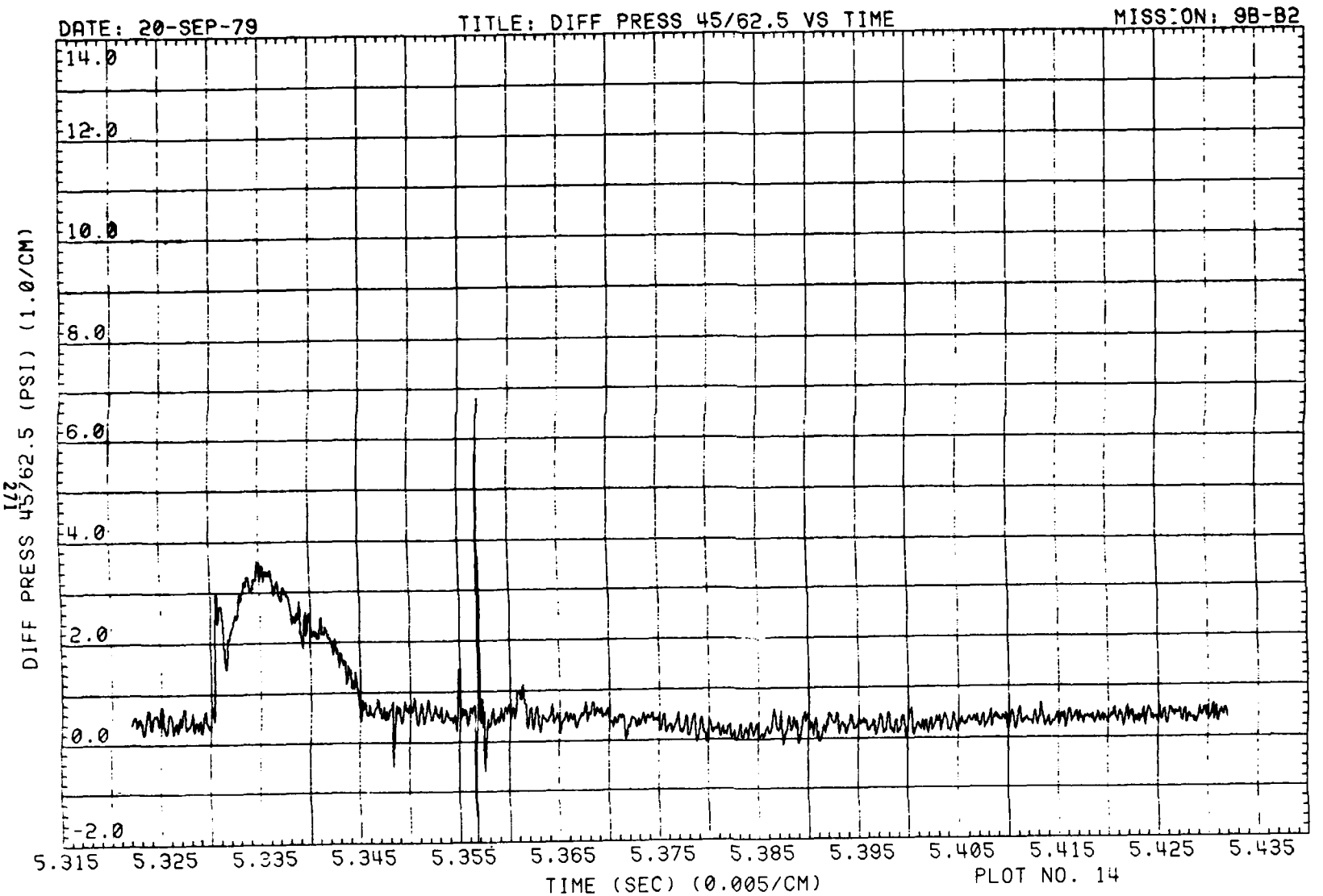

Figure 62. (Continued)

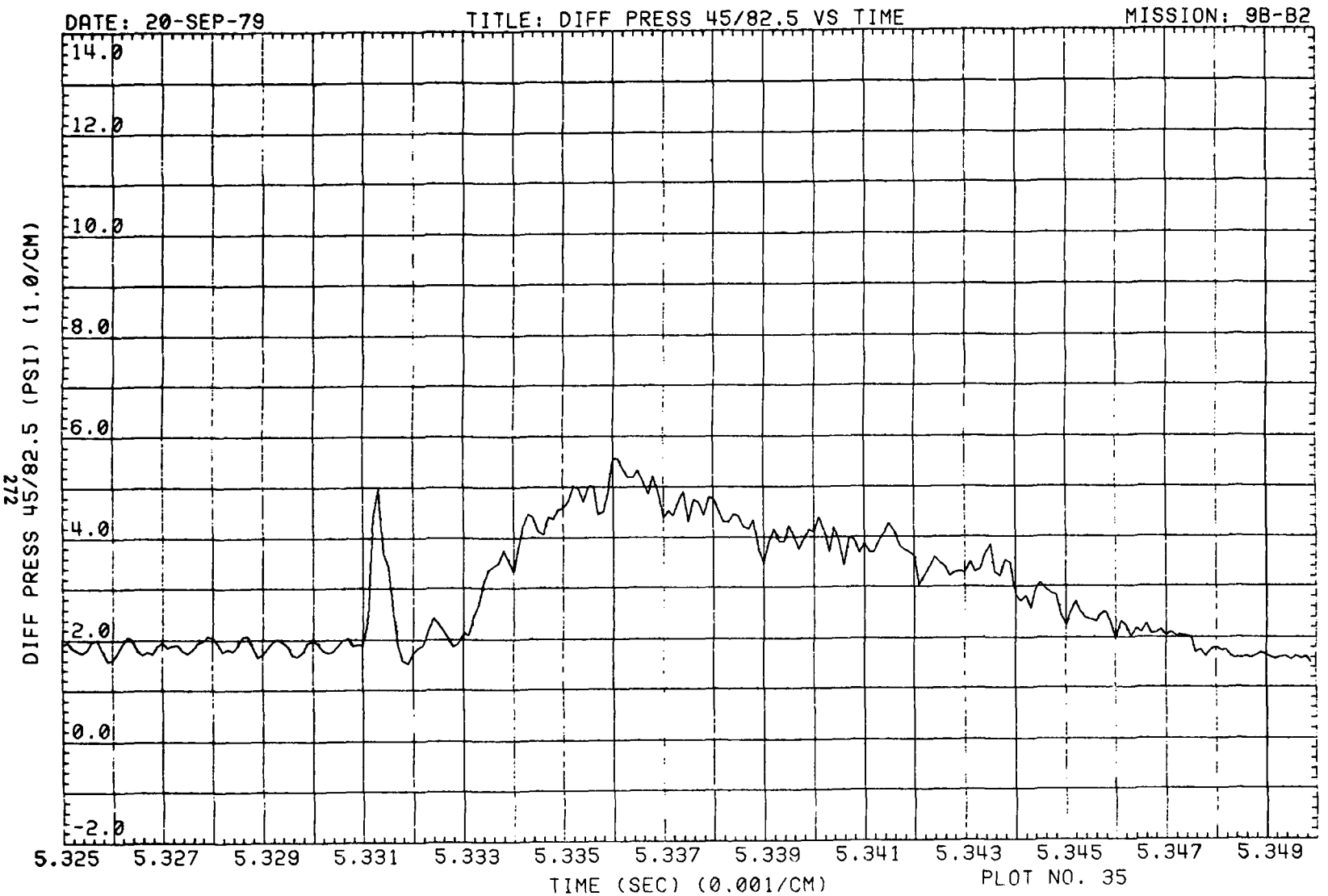

Figure 62. (Continued)

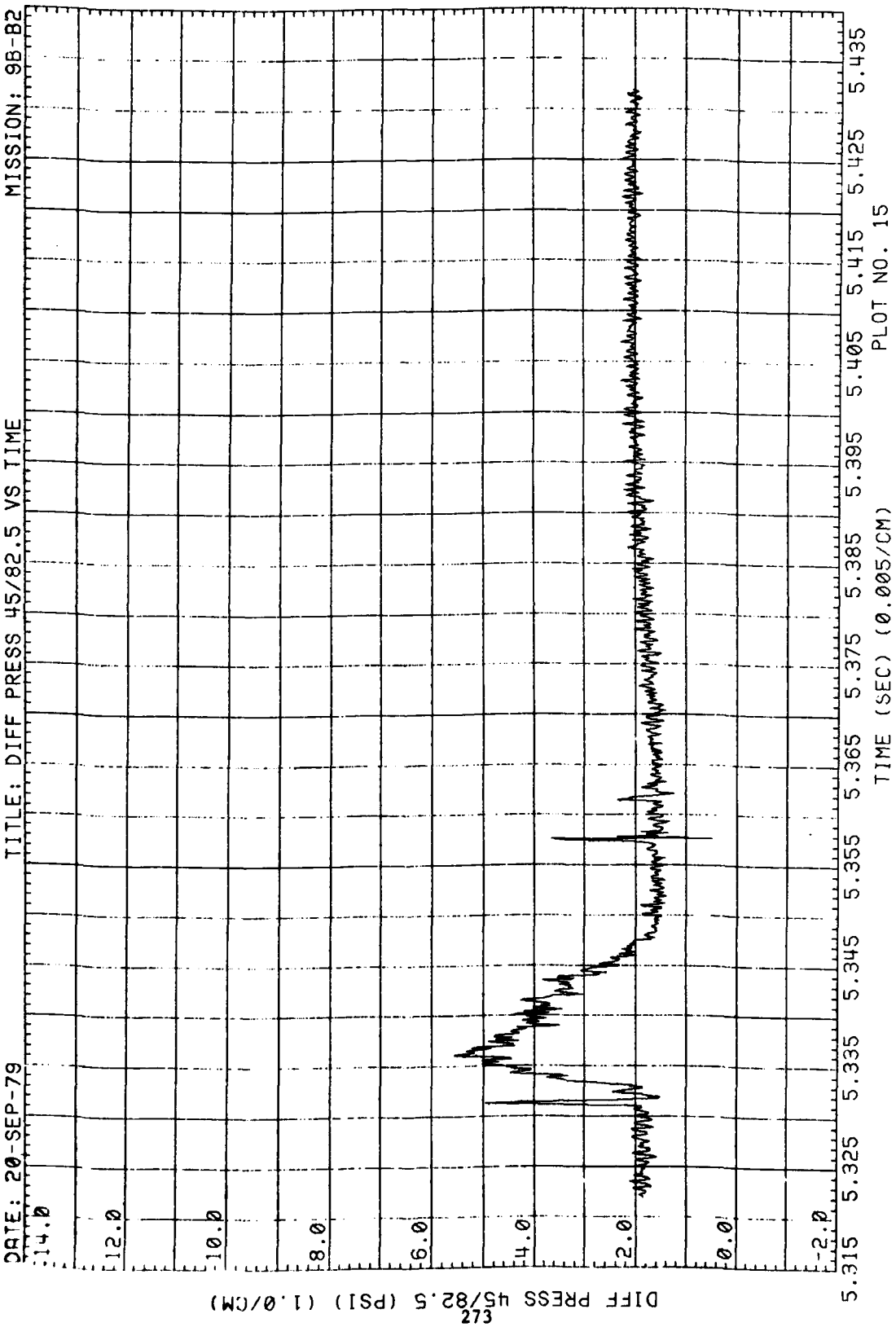

Figure 62. (Continued)

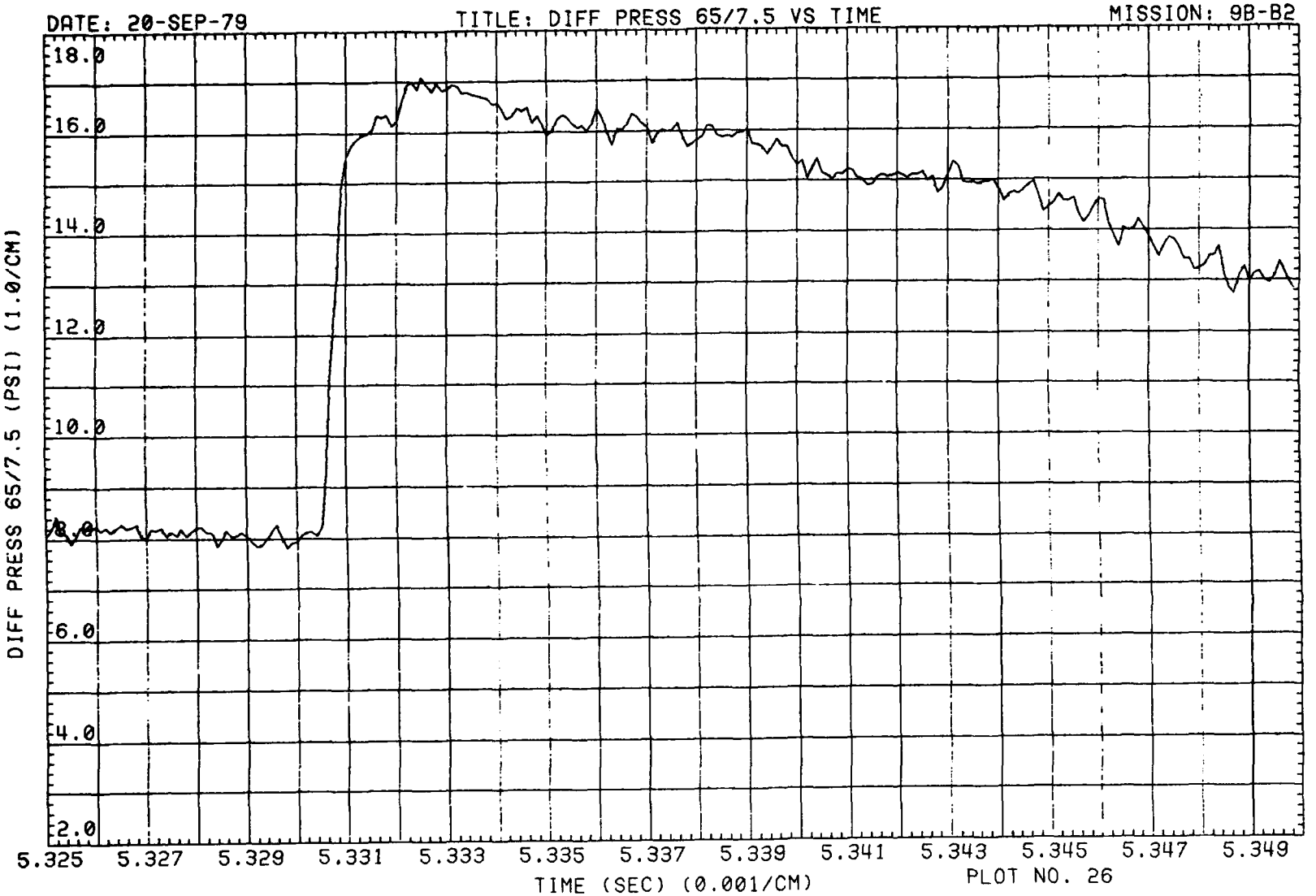

Figure 62. (Continued)

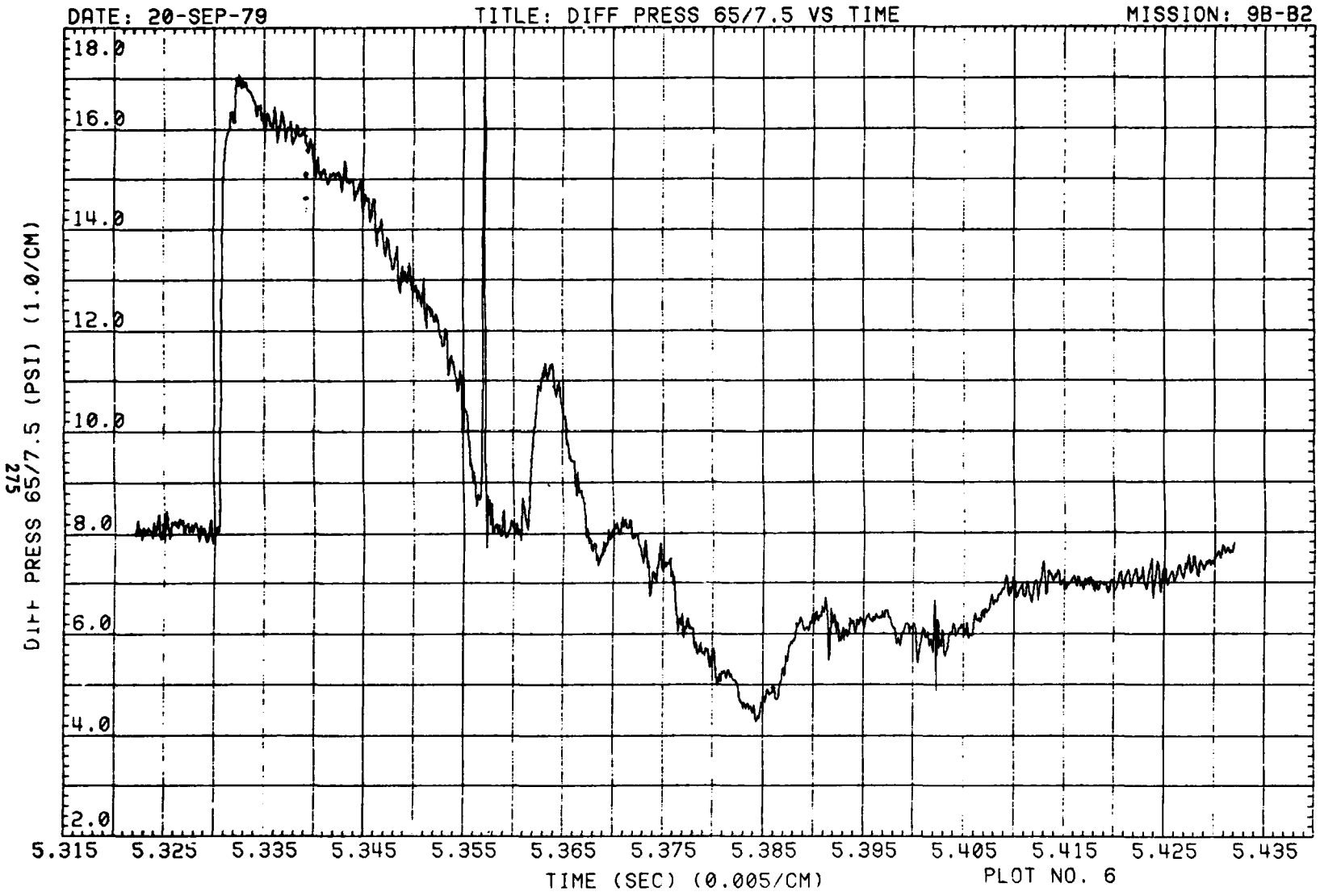

Figure 62. (Continued)

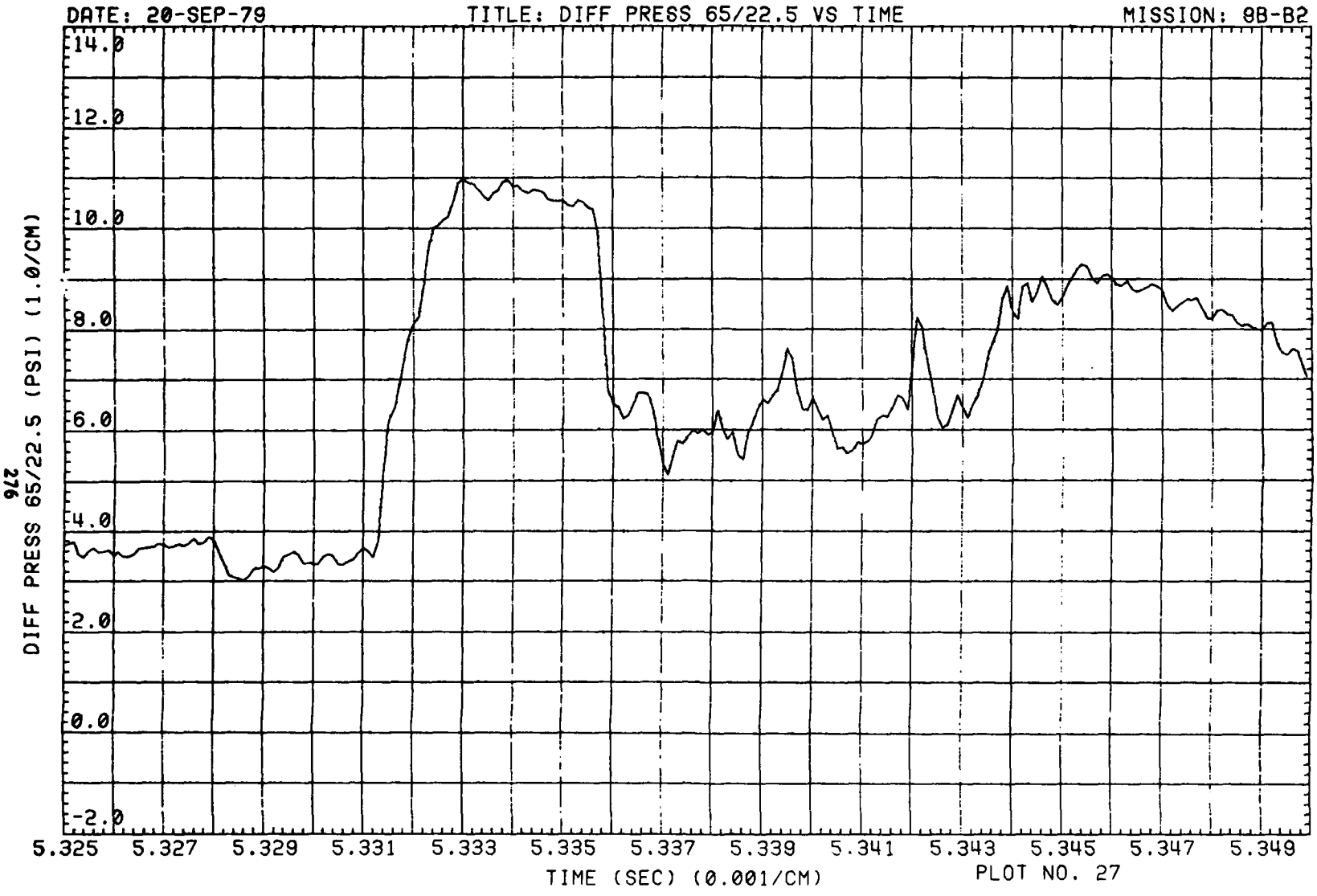

Figure 62. (Continued)

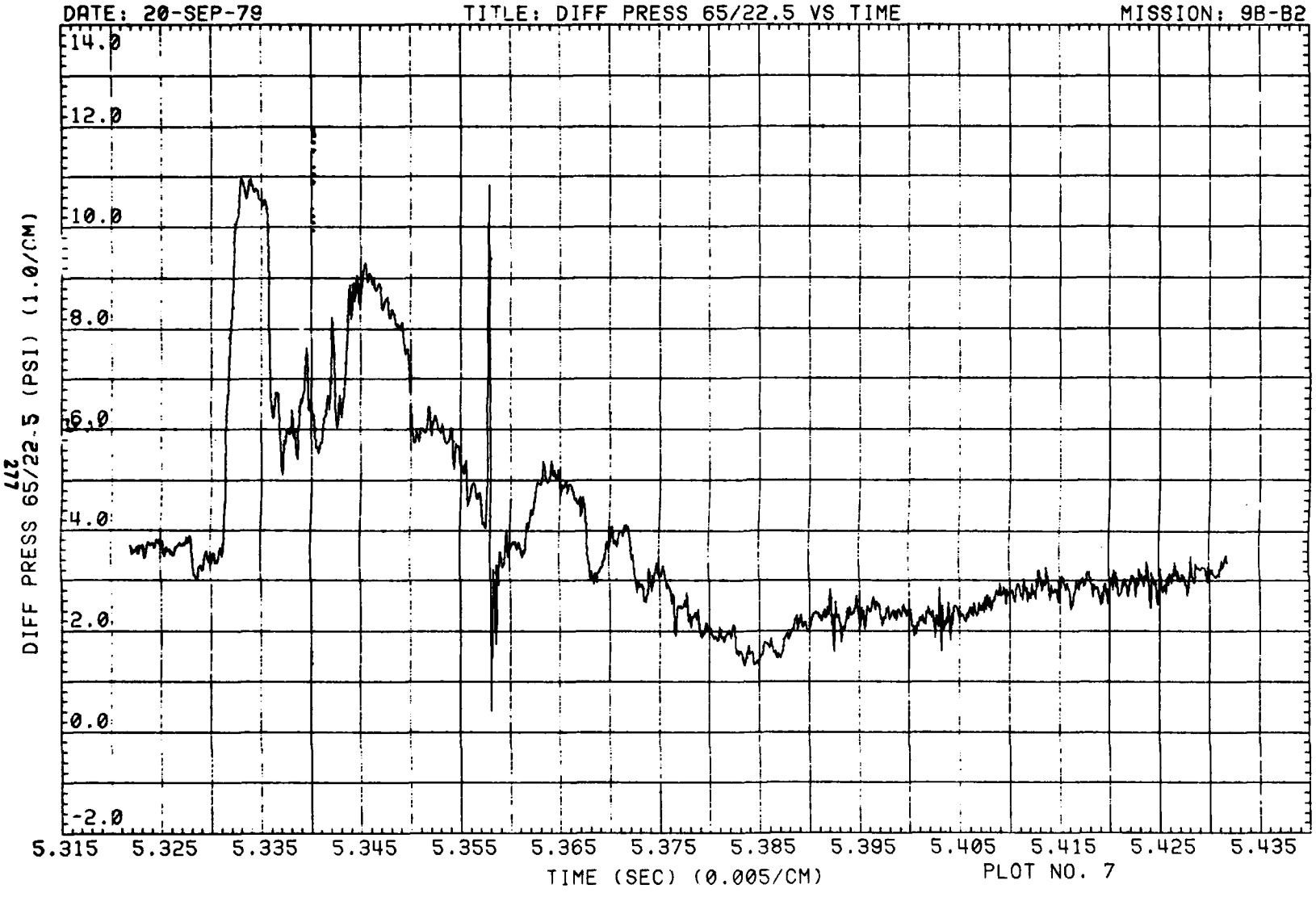

Figure 62. (Continued)

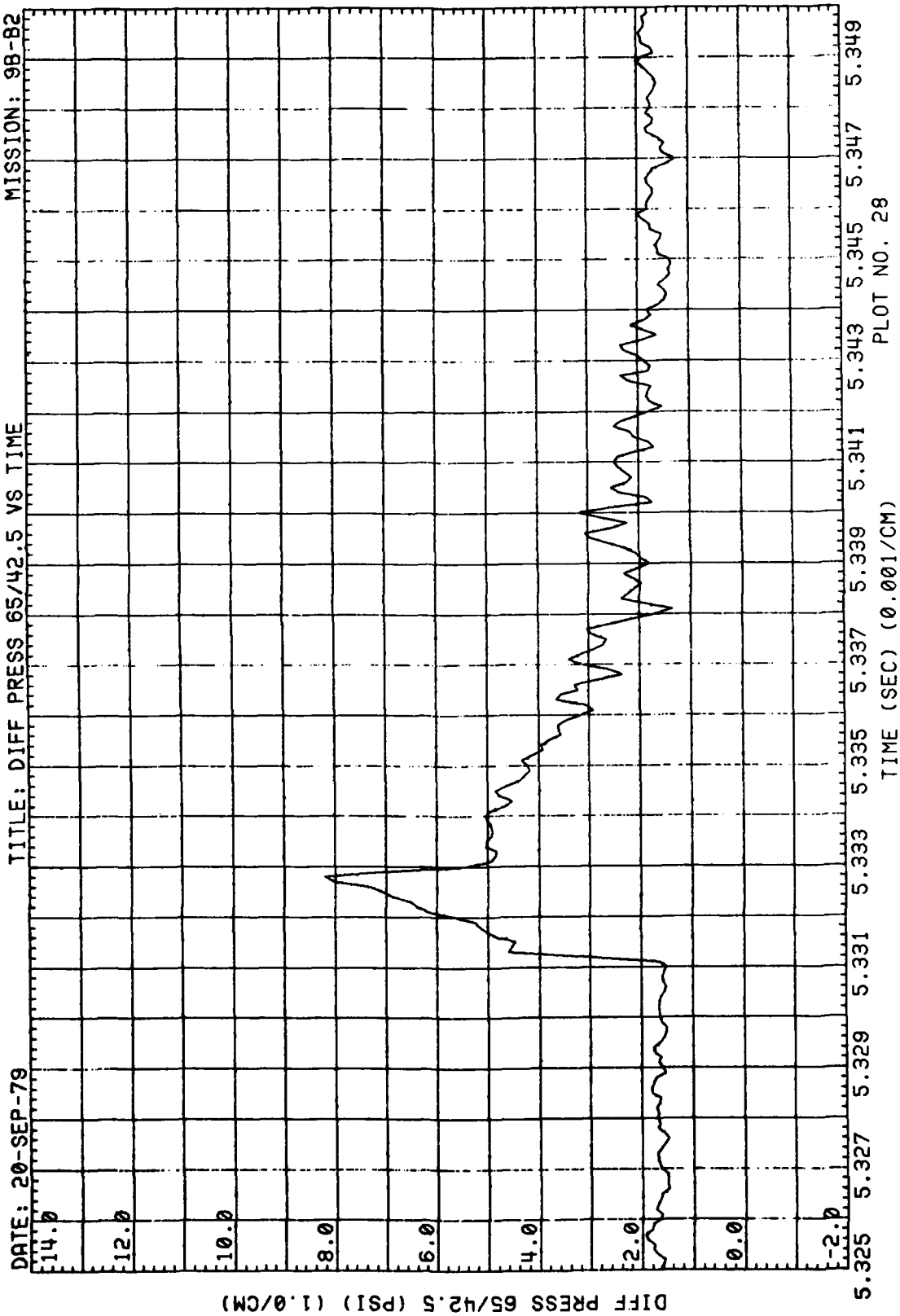

Figure 62. (Continued)

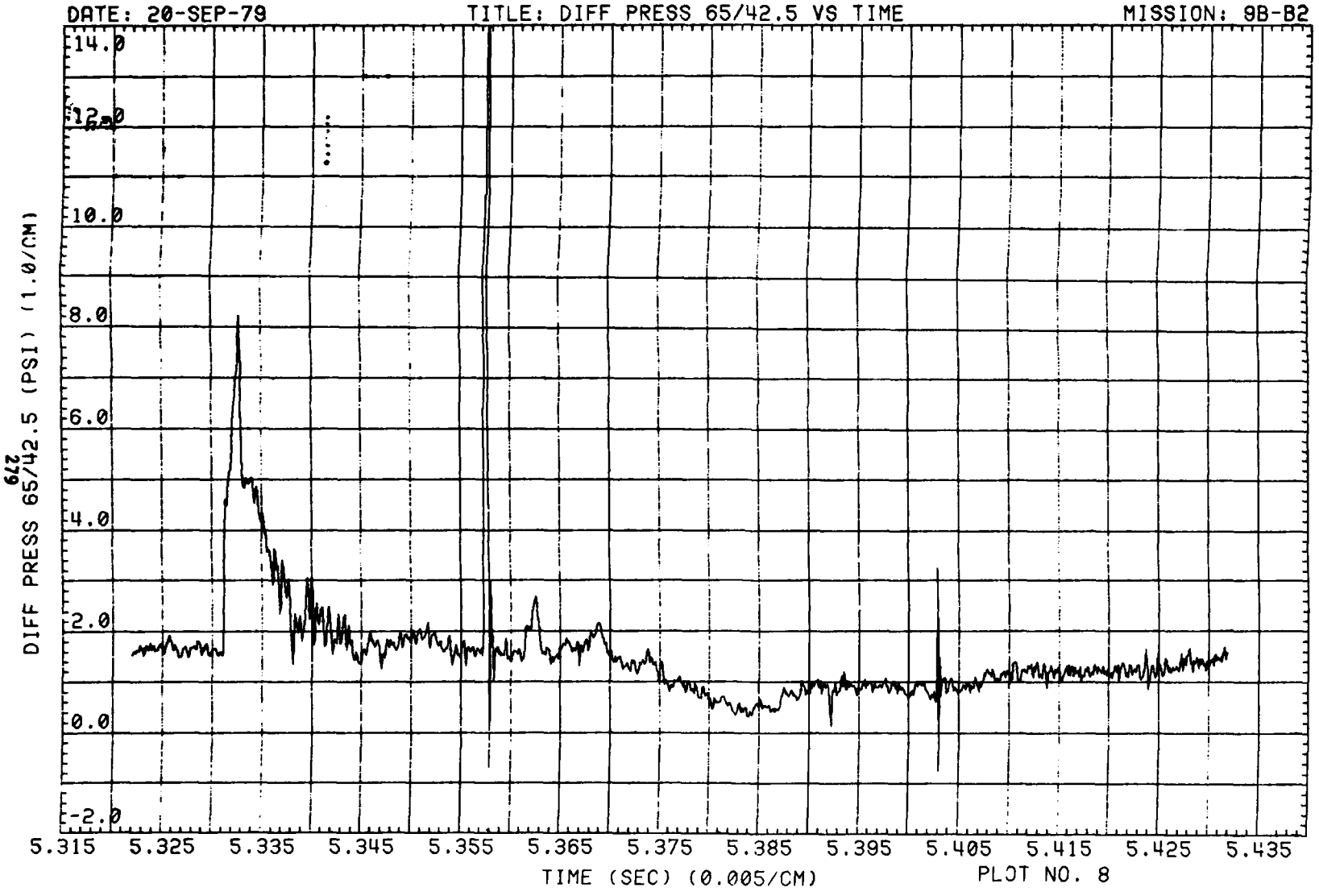

Figure 62. (Continued)

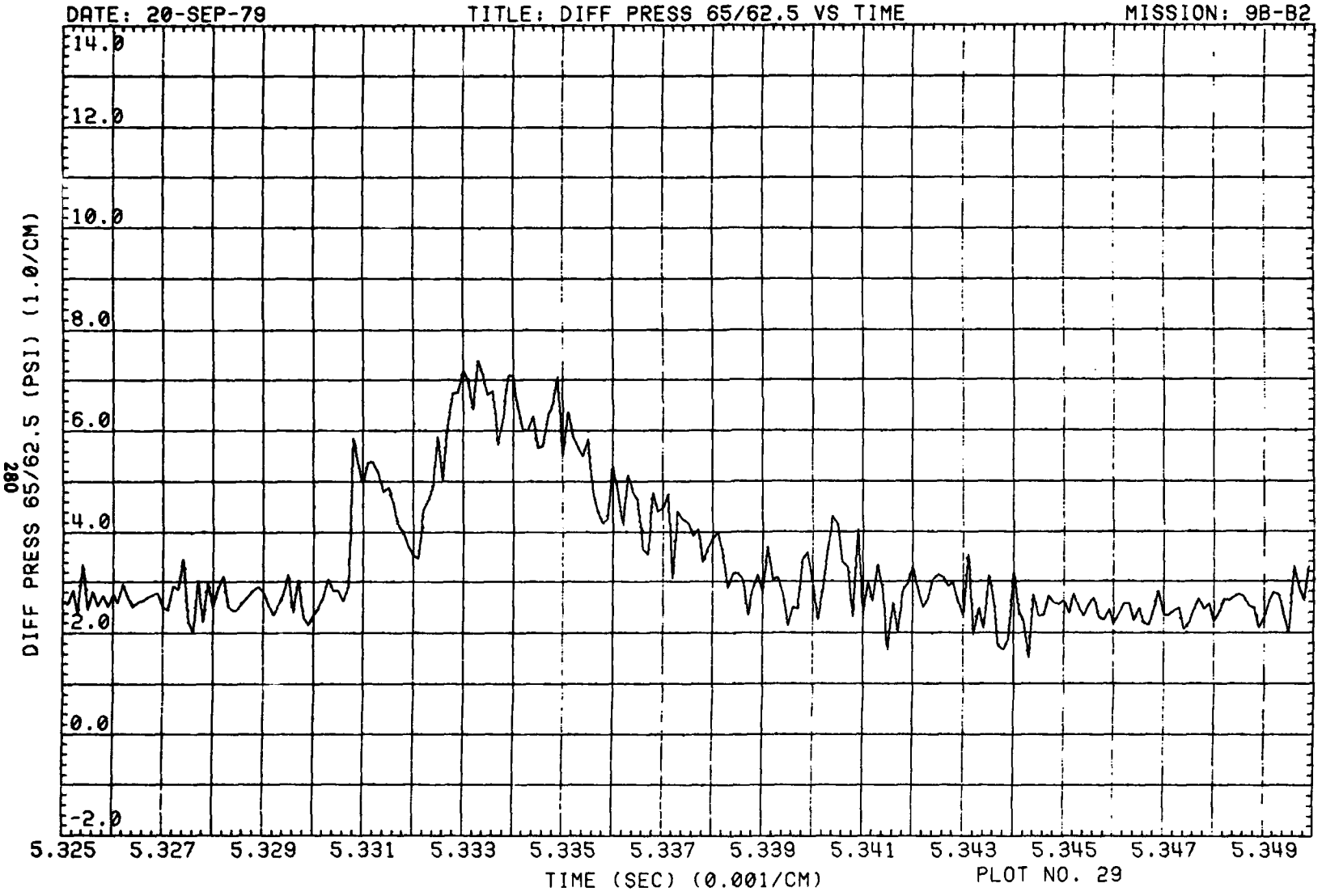

Figure 62. (Continued)

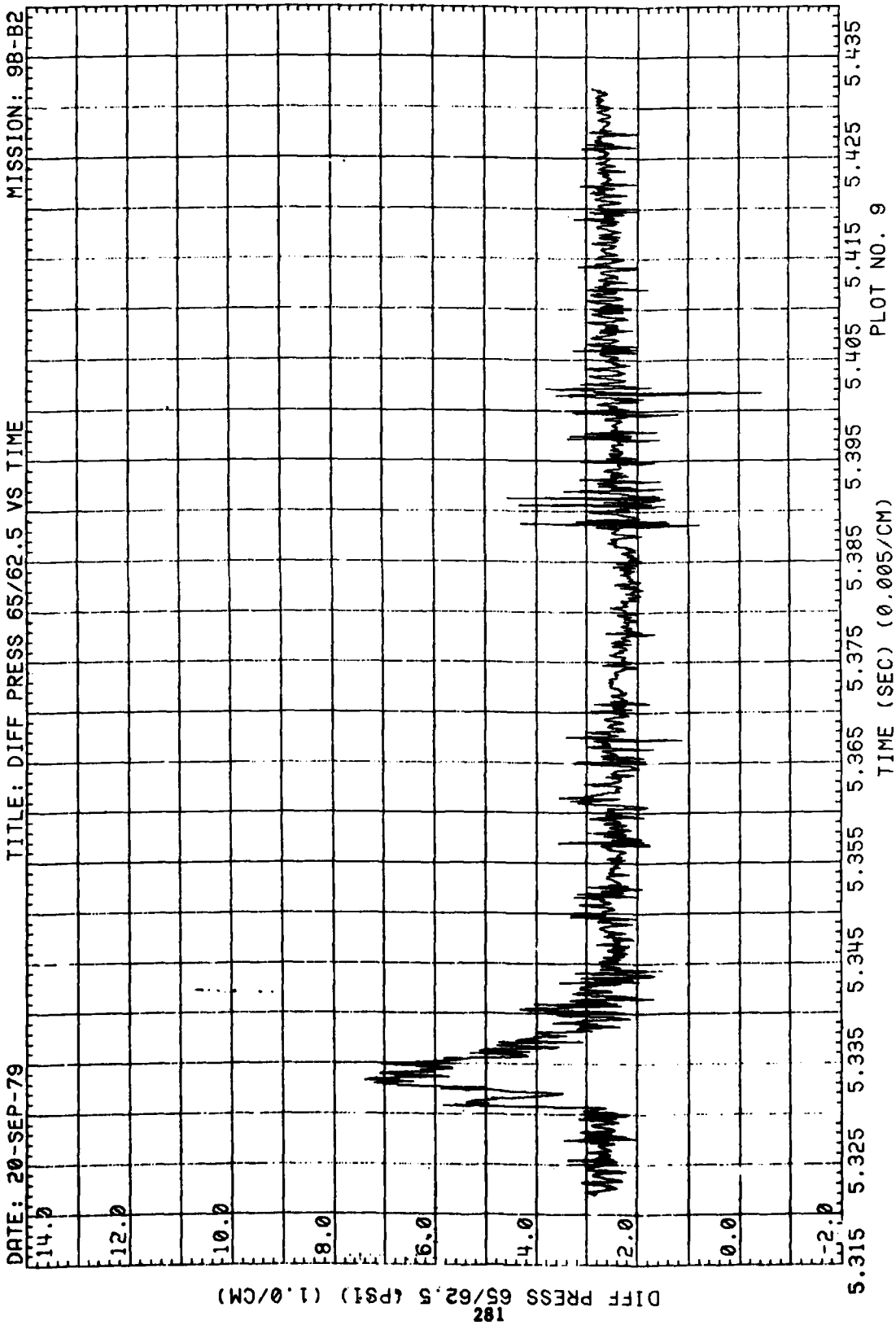

Figure 62. (Continued)

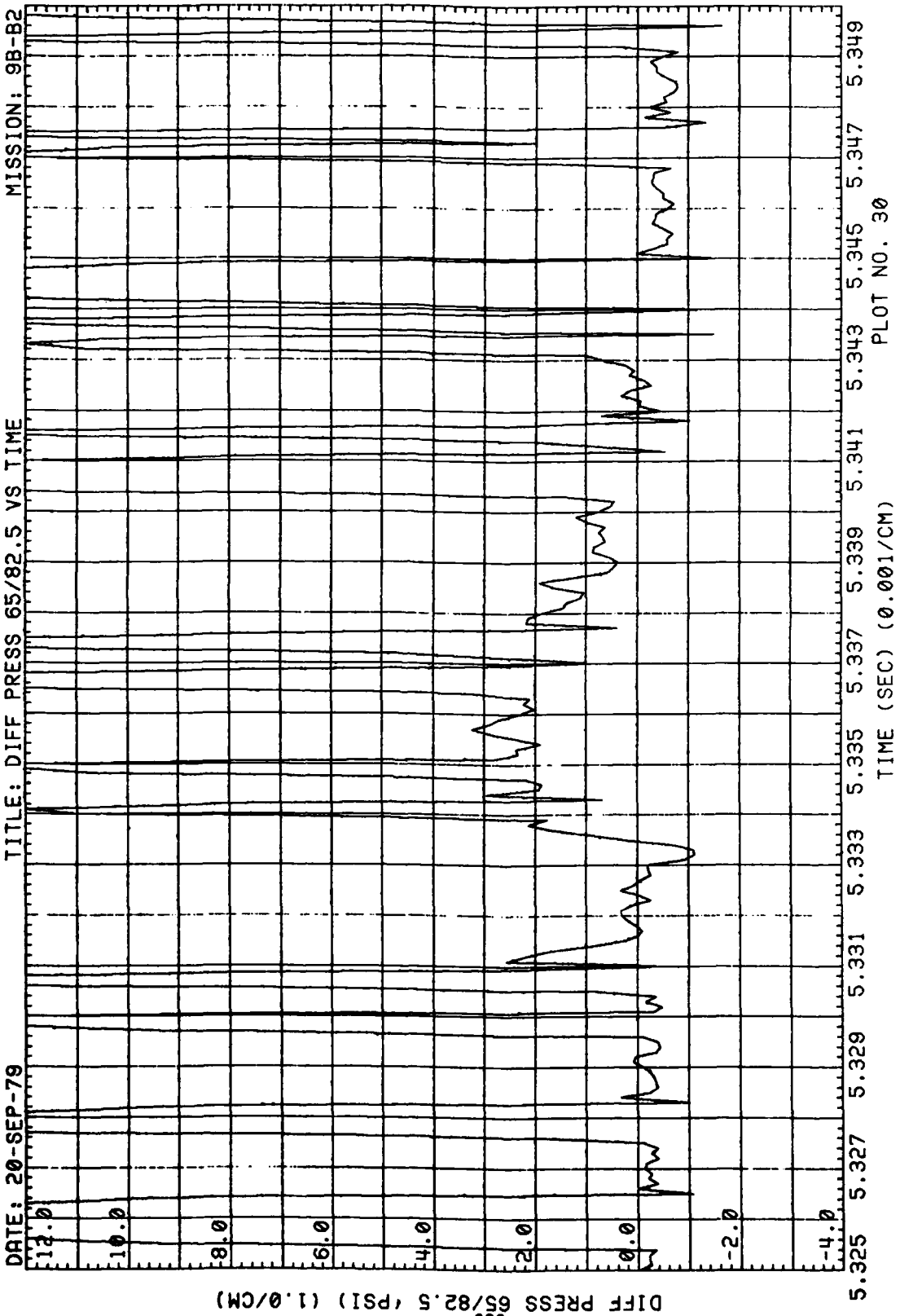

Figure 62. (Continued)

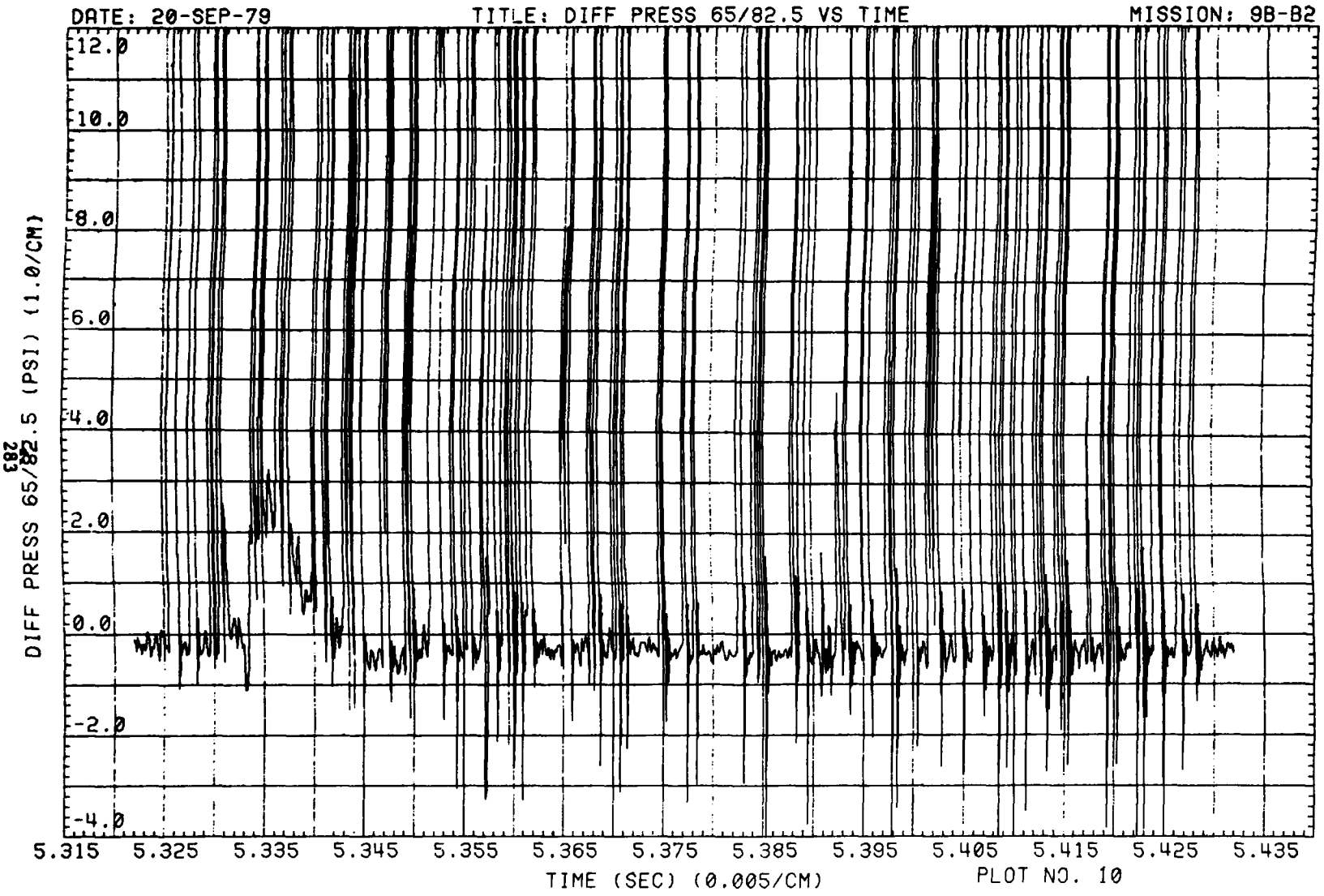

Figure 62. (Continued)

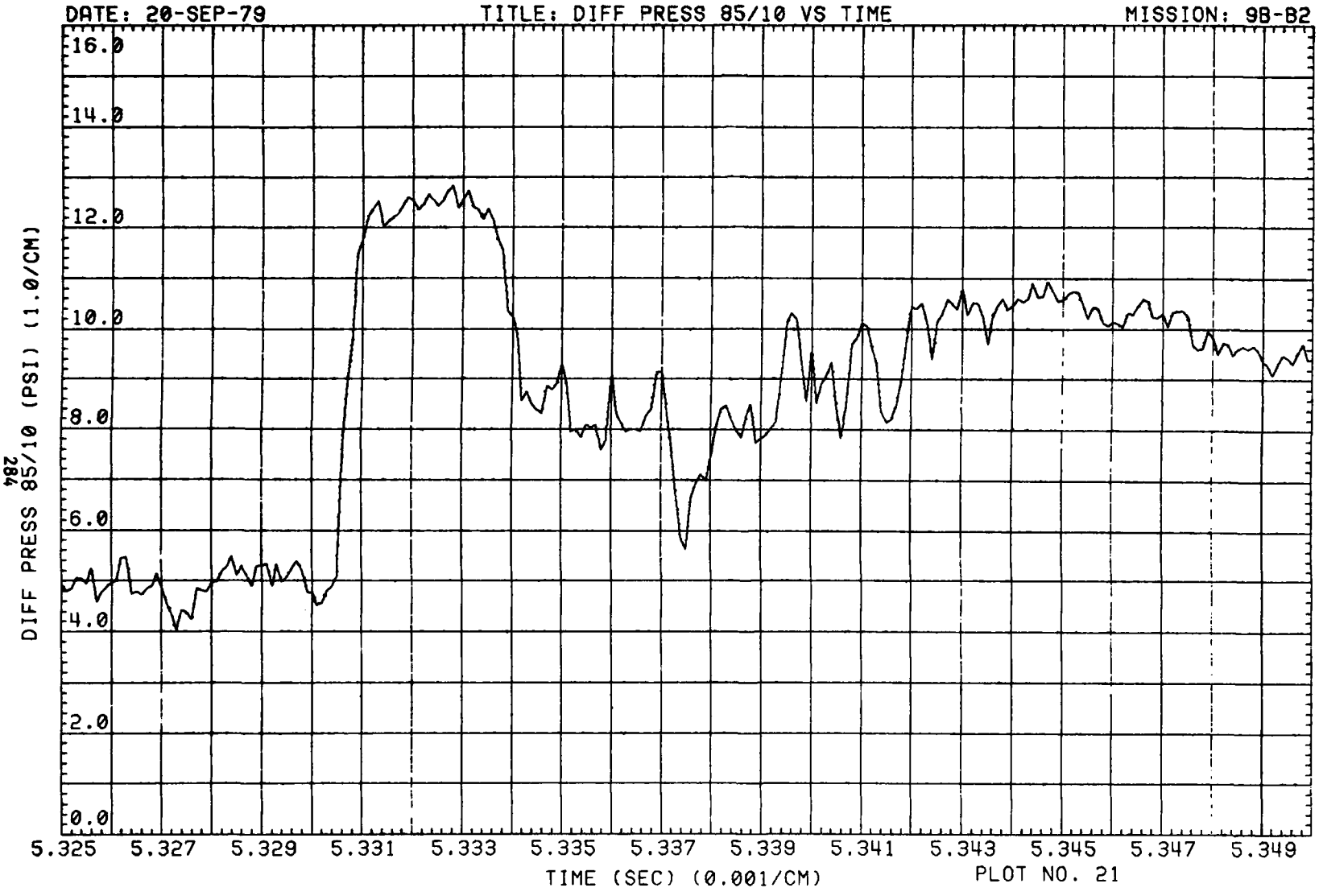

Figure 62. (Continued)

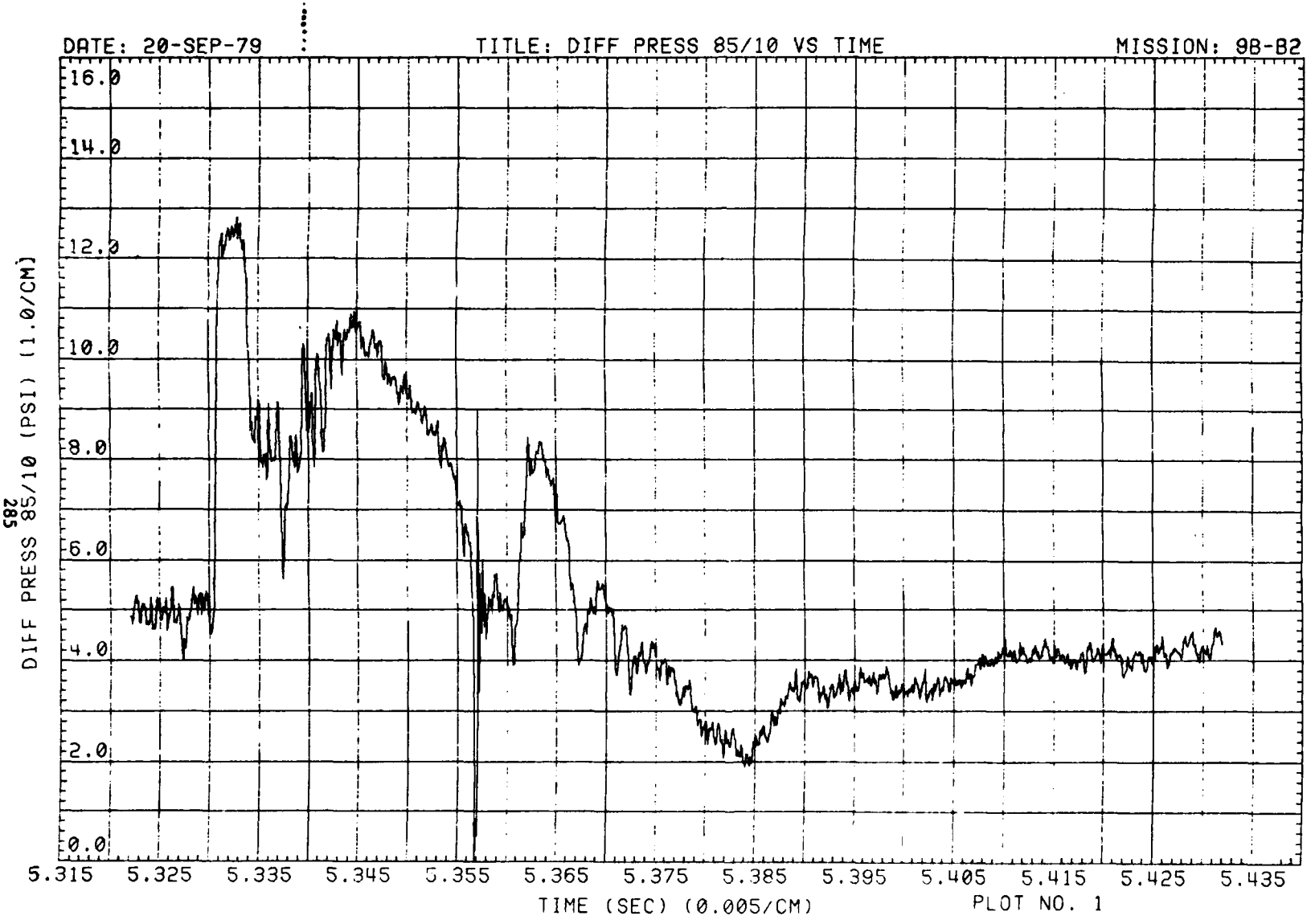

Figure 62. (Continued)

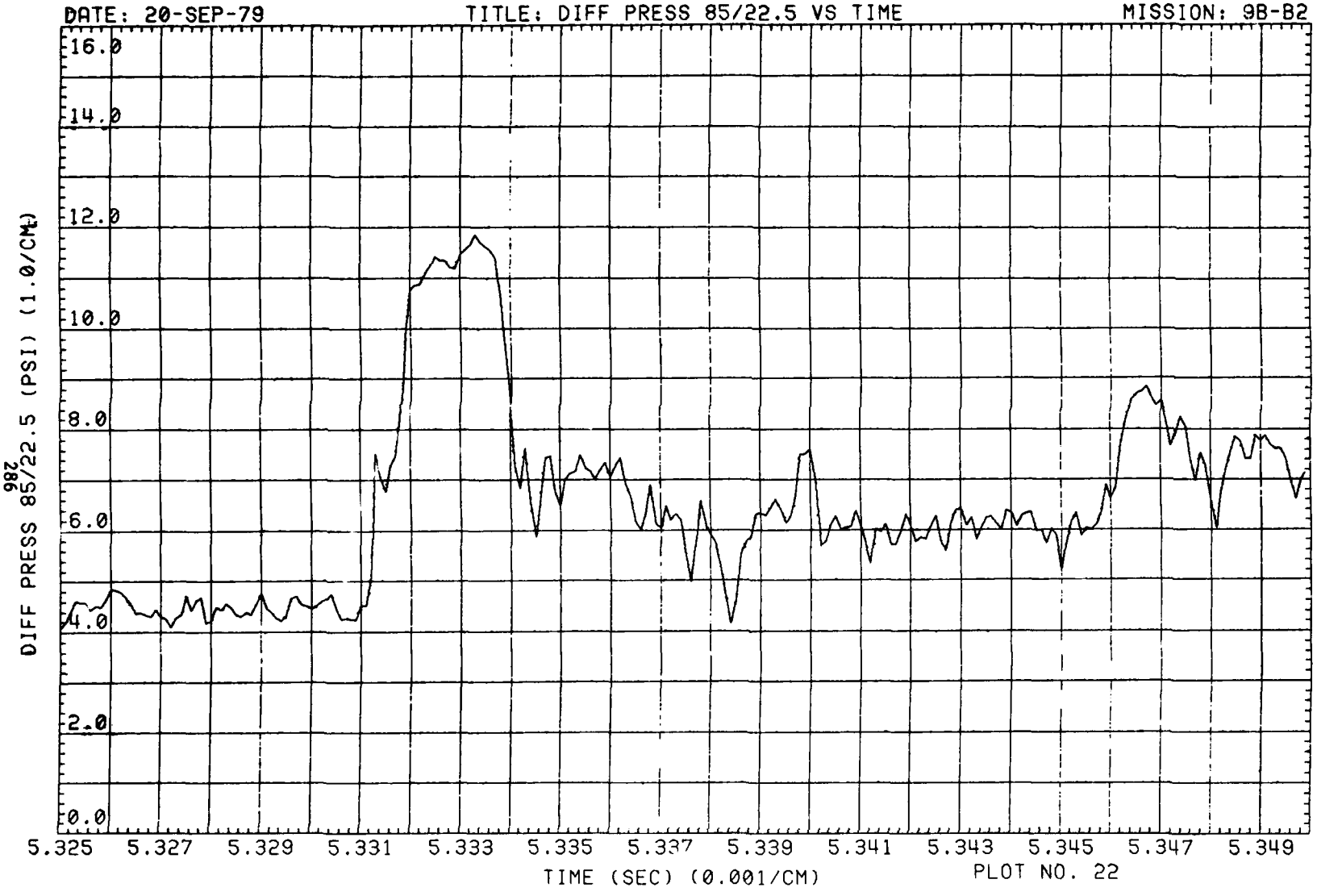

Figure 62. (Continued)

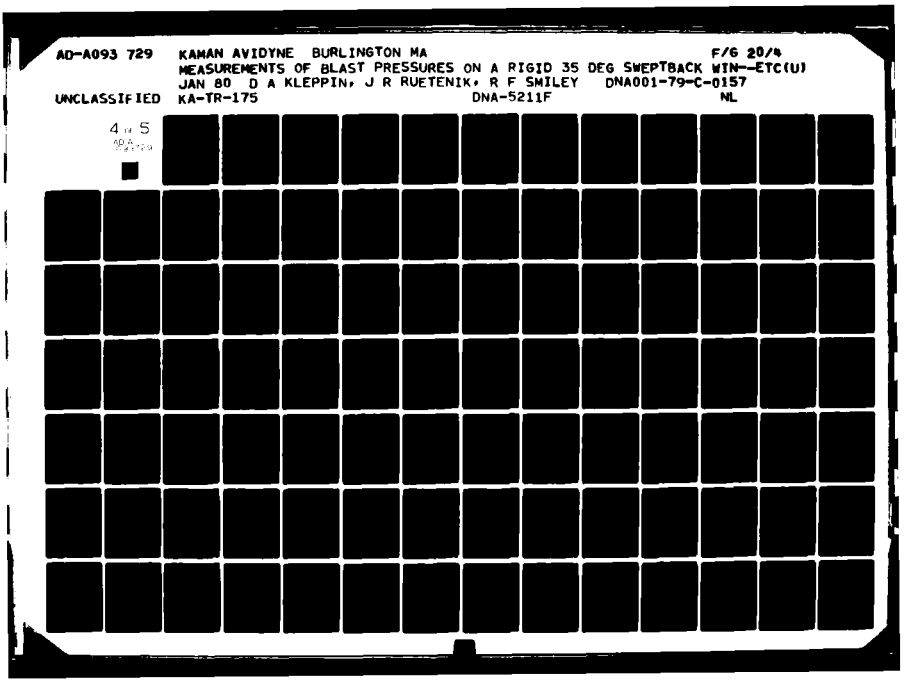
AD-A093 729
KAMAN AVIDYNE BURLINGTON MA
F/G 20/4
MEASUREMENTS OF BLAST PRESSURES ON A RIGID 35 DEG SWEPTBACK WIN--ETC(U)
JAN 80 D A KLEPPIN, J R RUETENIK, R F SMILEY
DNA001-79-C-0157
UNCLASSIFIED
KA-TR-175
DNA-5211F
NL
4 OF 5
AD A

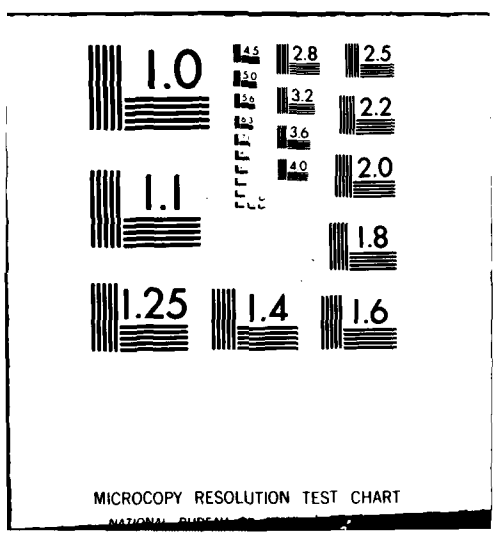
1.0
1.1
1.25
1.4
1.6
1.8
2.0
2.2
2.5
2.8
3.2
3.6
4.0
MICROCOPY RESOLUTION TEST CHART

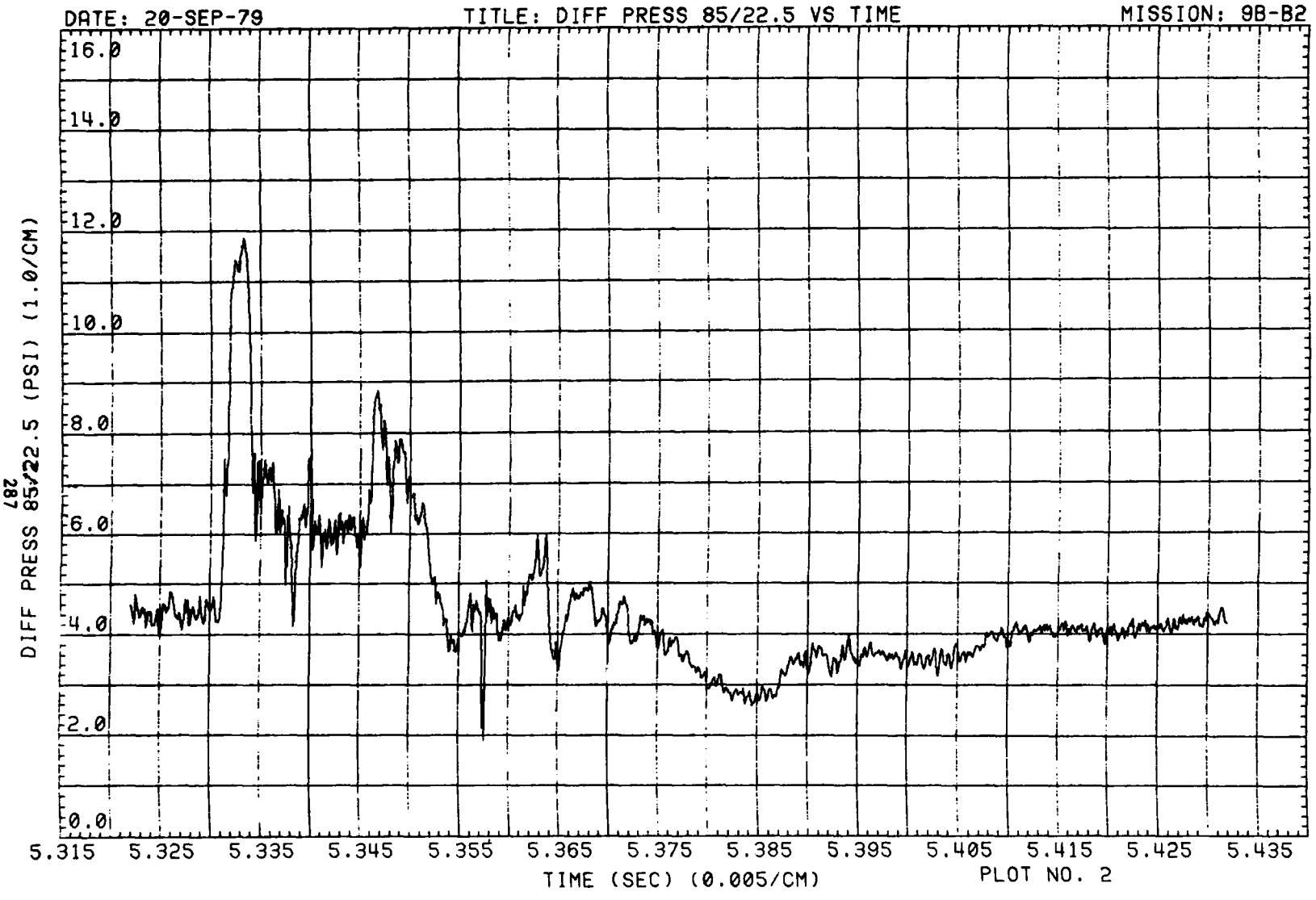

Figure 62. (Continued)

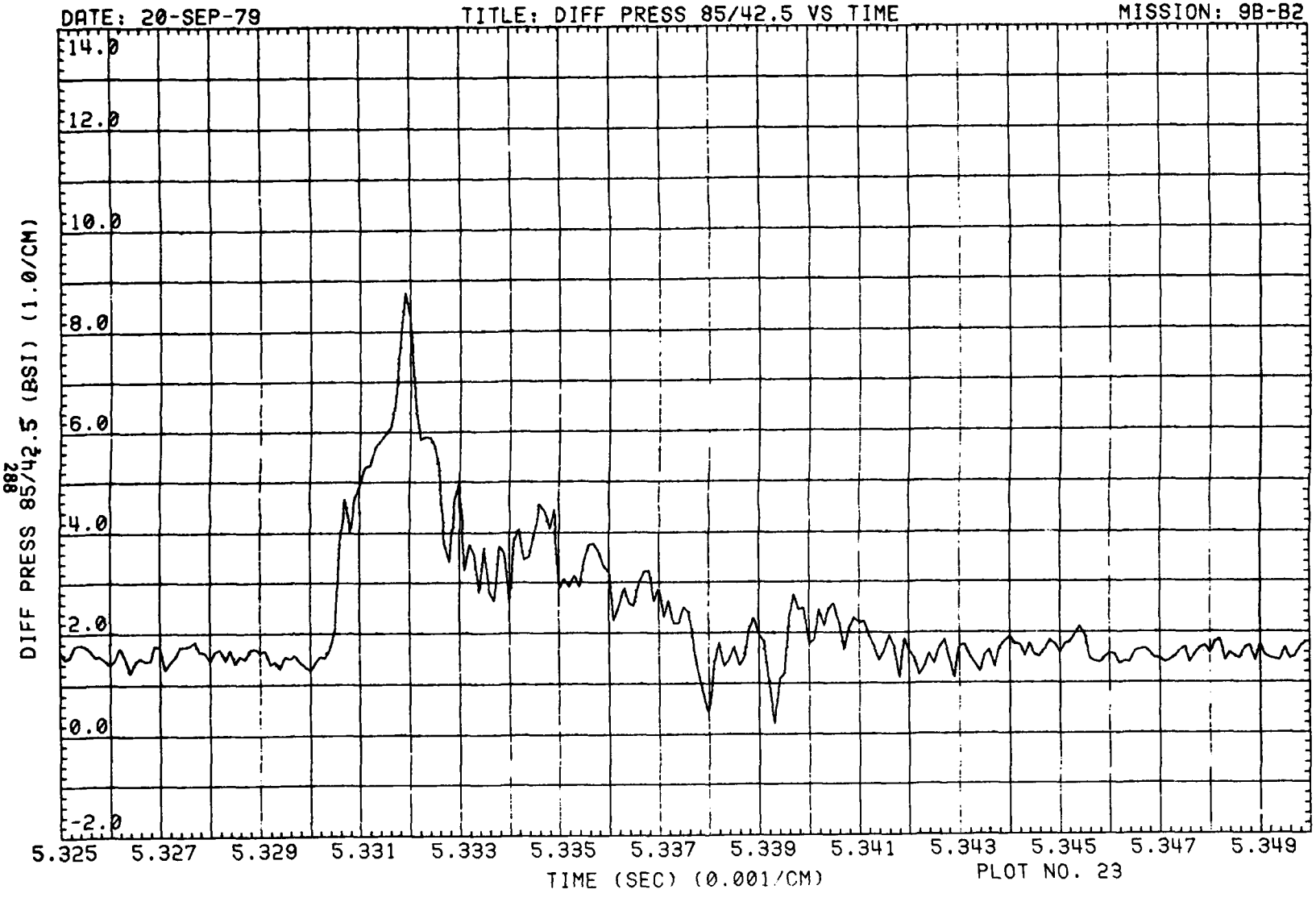

Figure 62. (Continued)

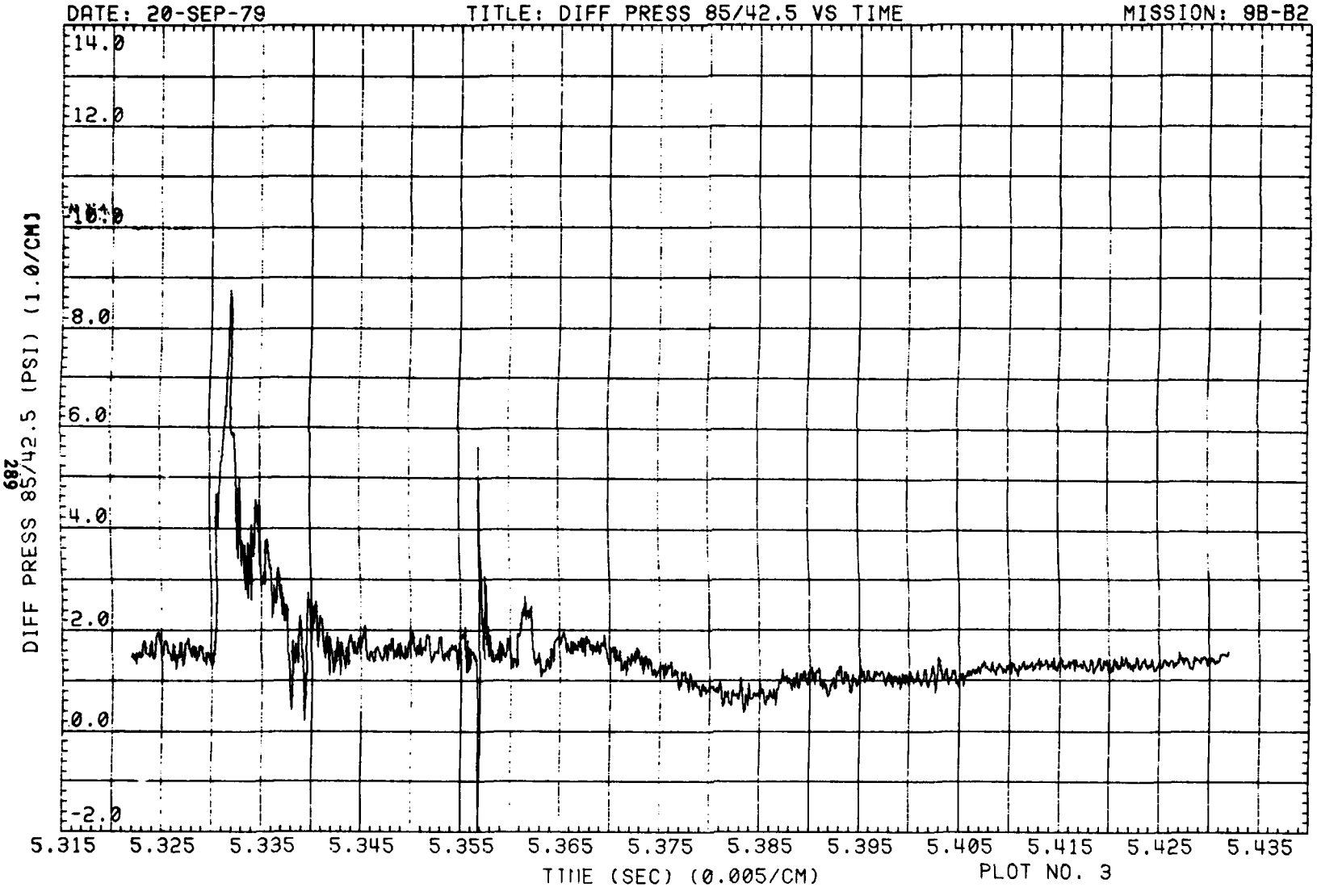

Figure 62. (Continued)

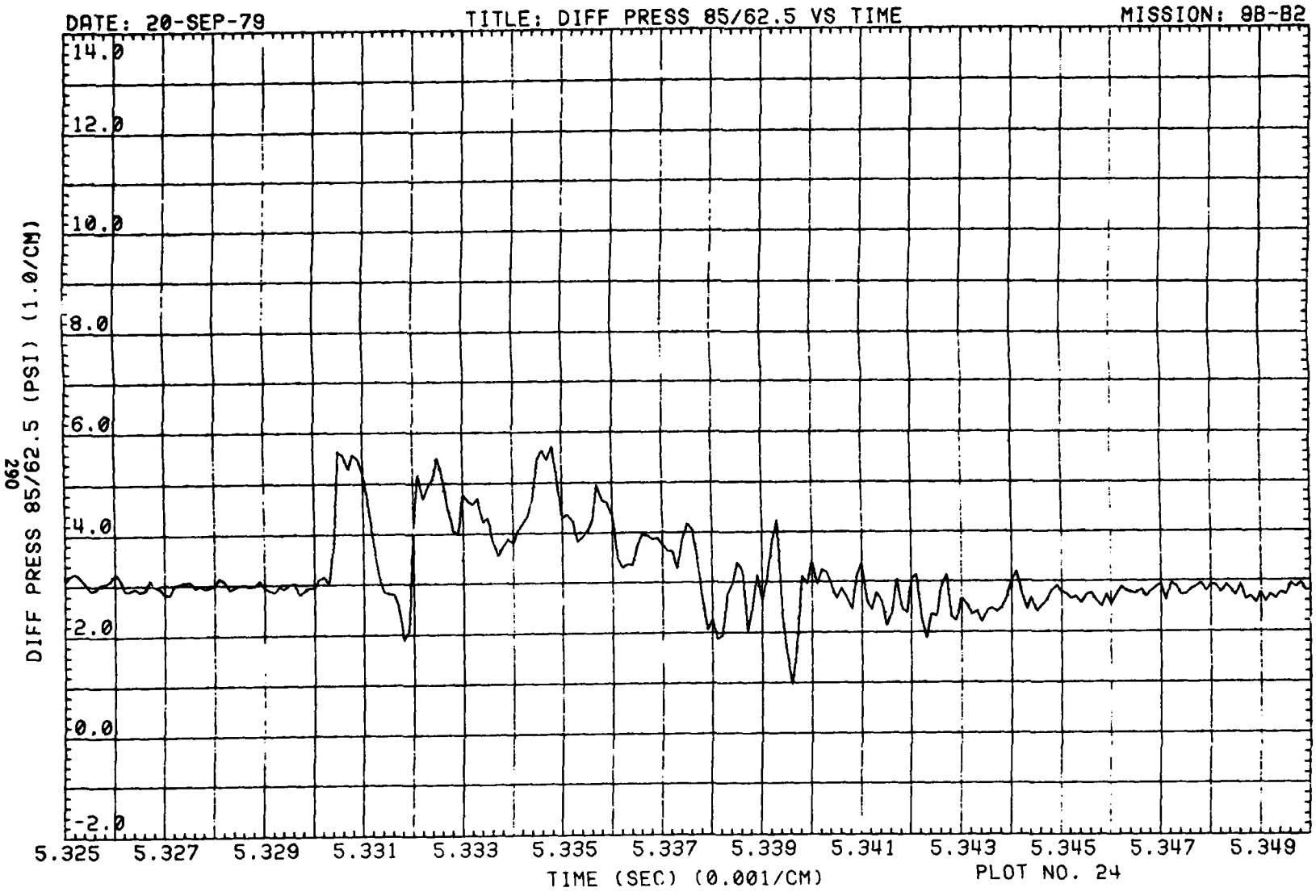

Figure 62. (Continued)

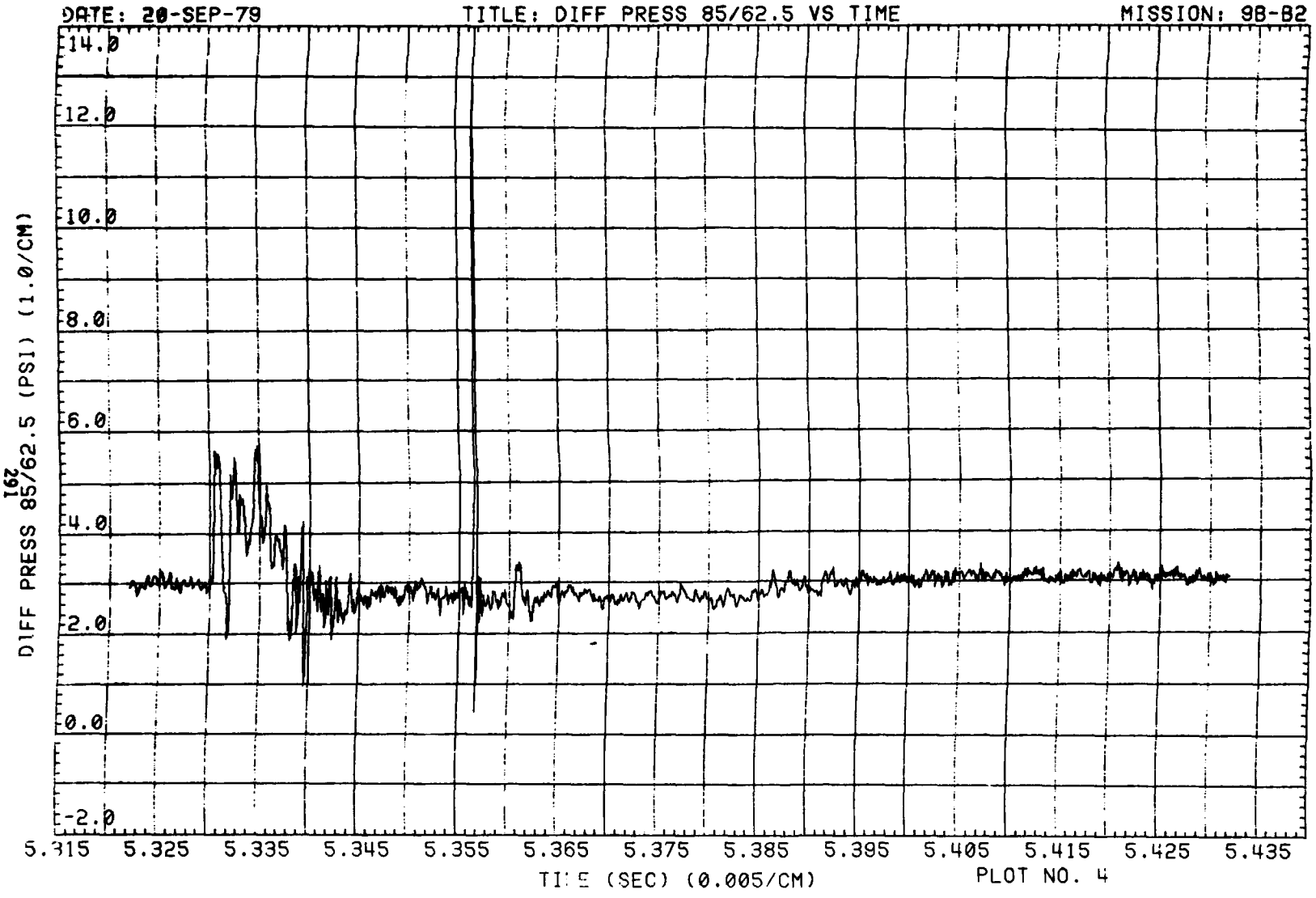

Figure 62. (Continued)

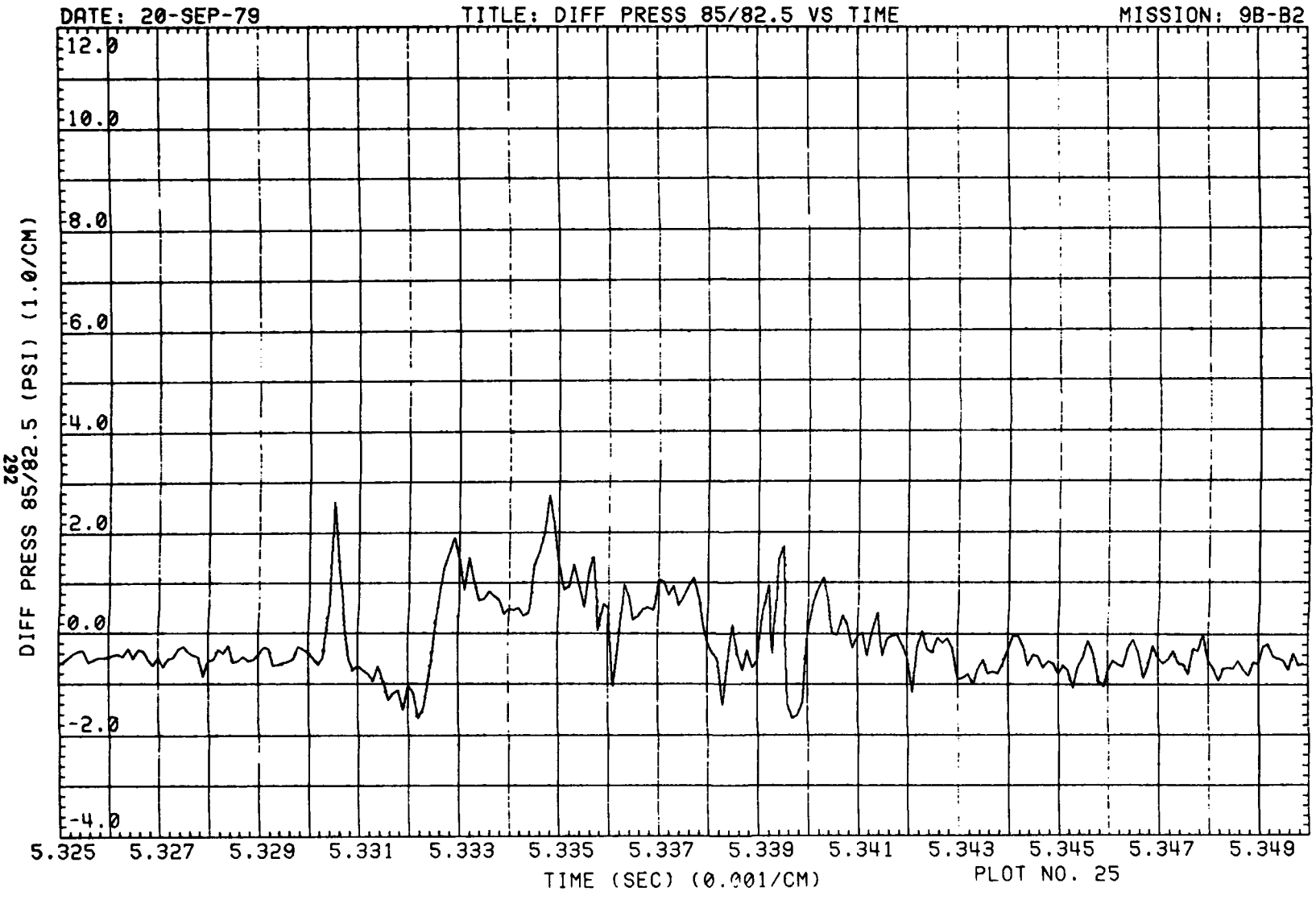

Figure 62. (Continued)

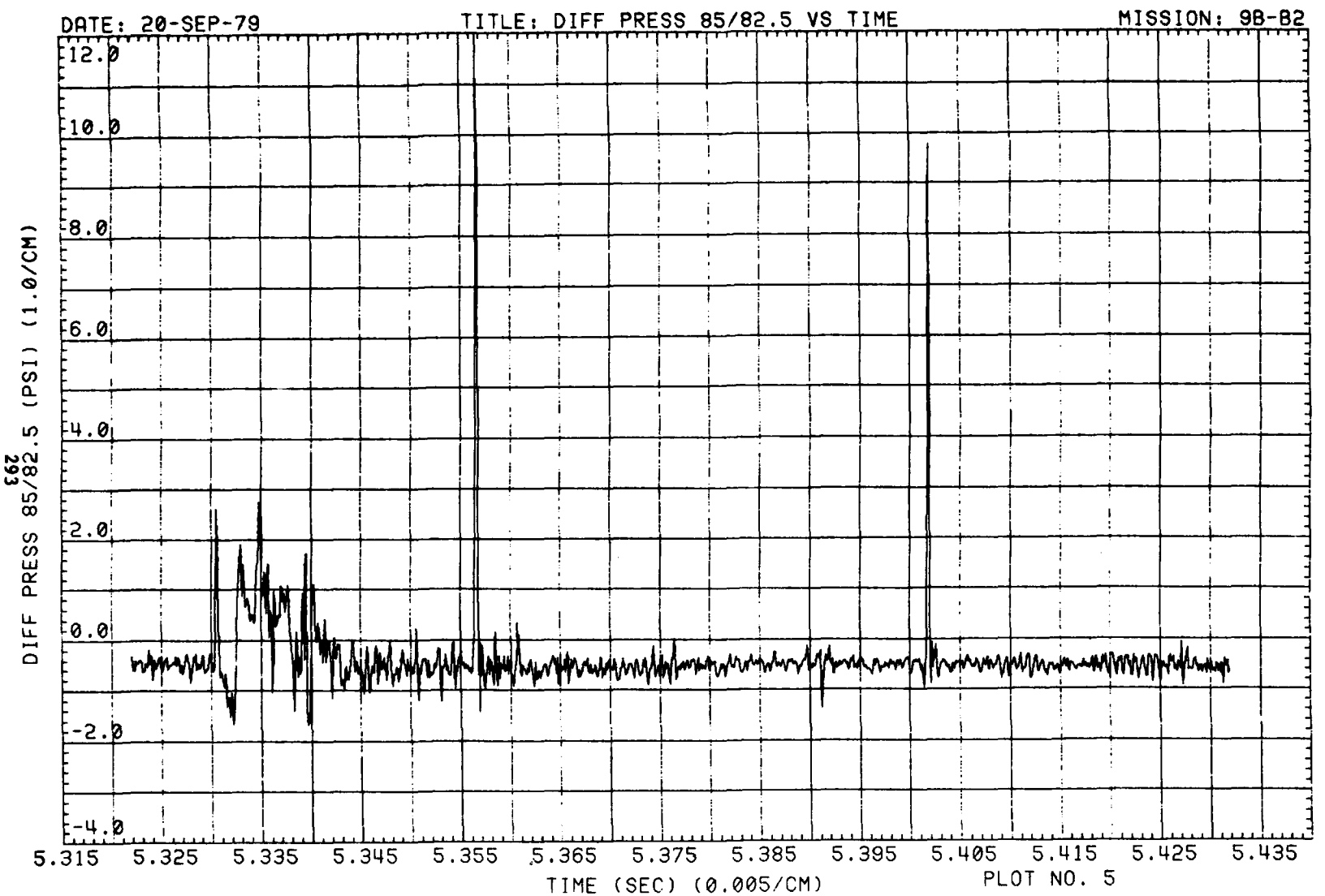

Figure 62. (Concluded)

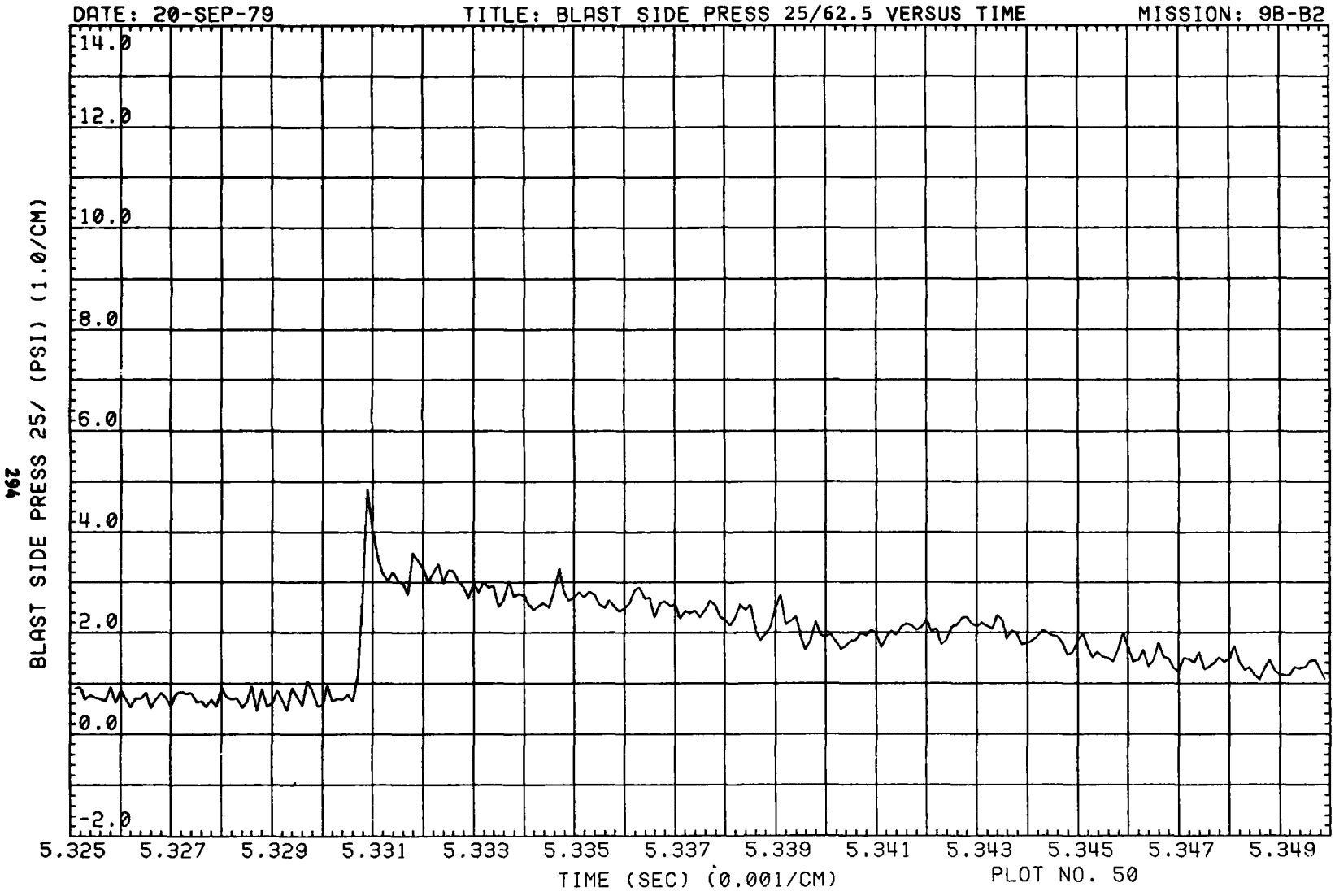

Figure 63. Blastward and Leeward Wing Pressure, Run 9B-B2, Intercept 1

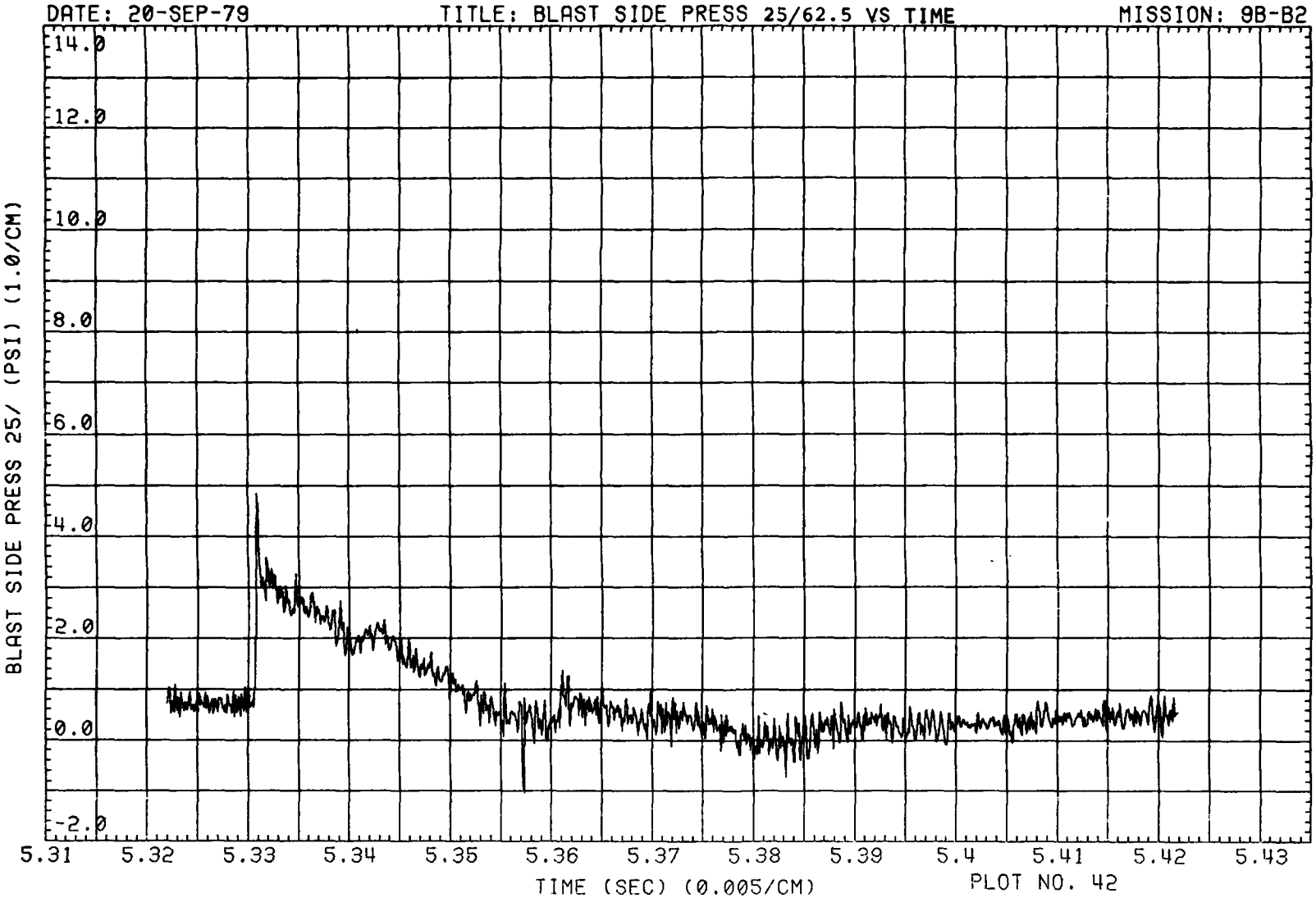

Figure 63. (Continued)

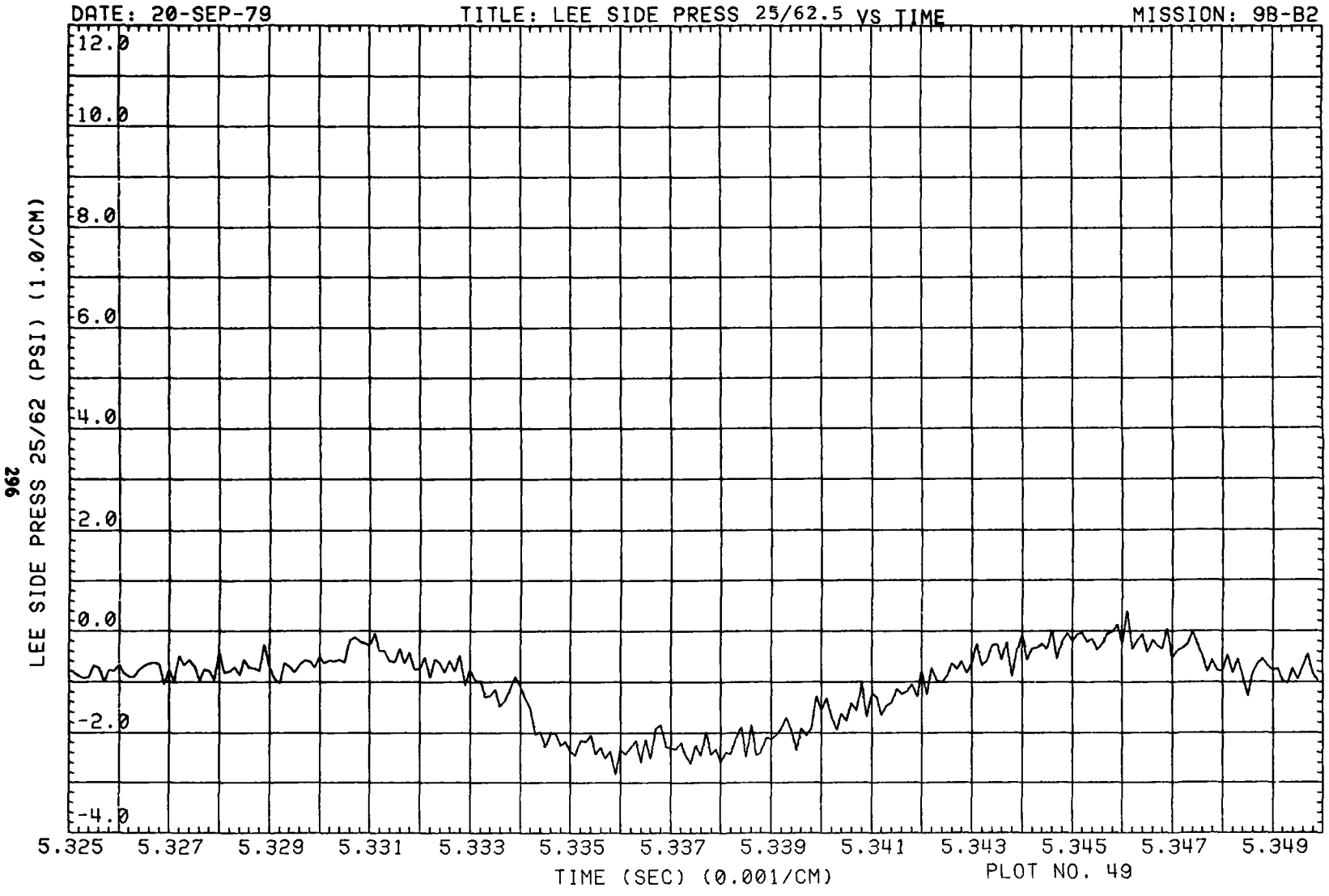

Figure 63. (Continued)

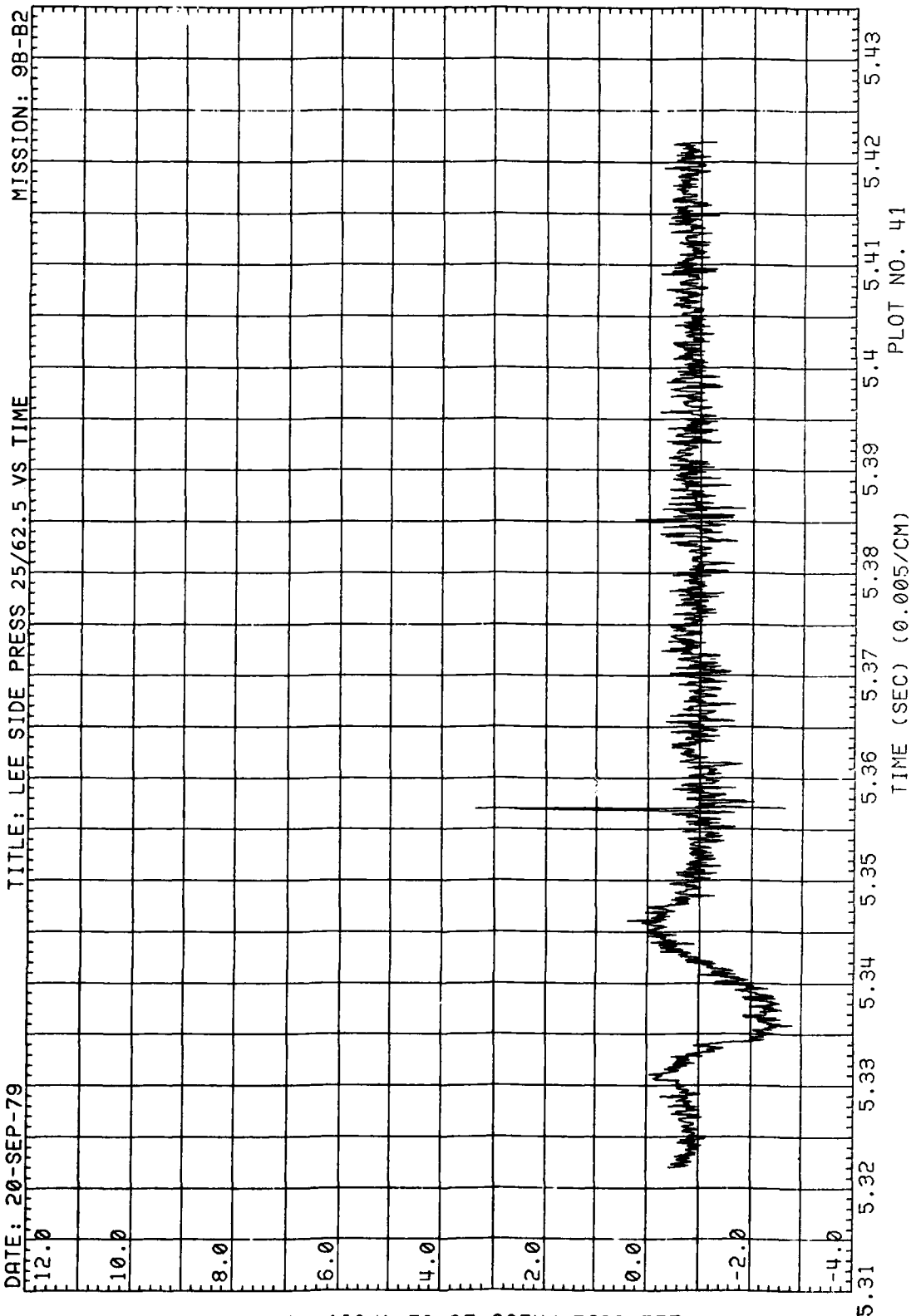

Figure 63. (Concluded)

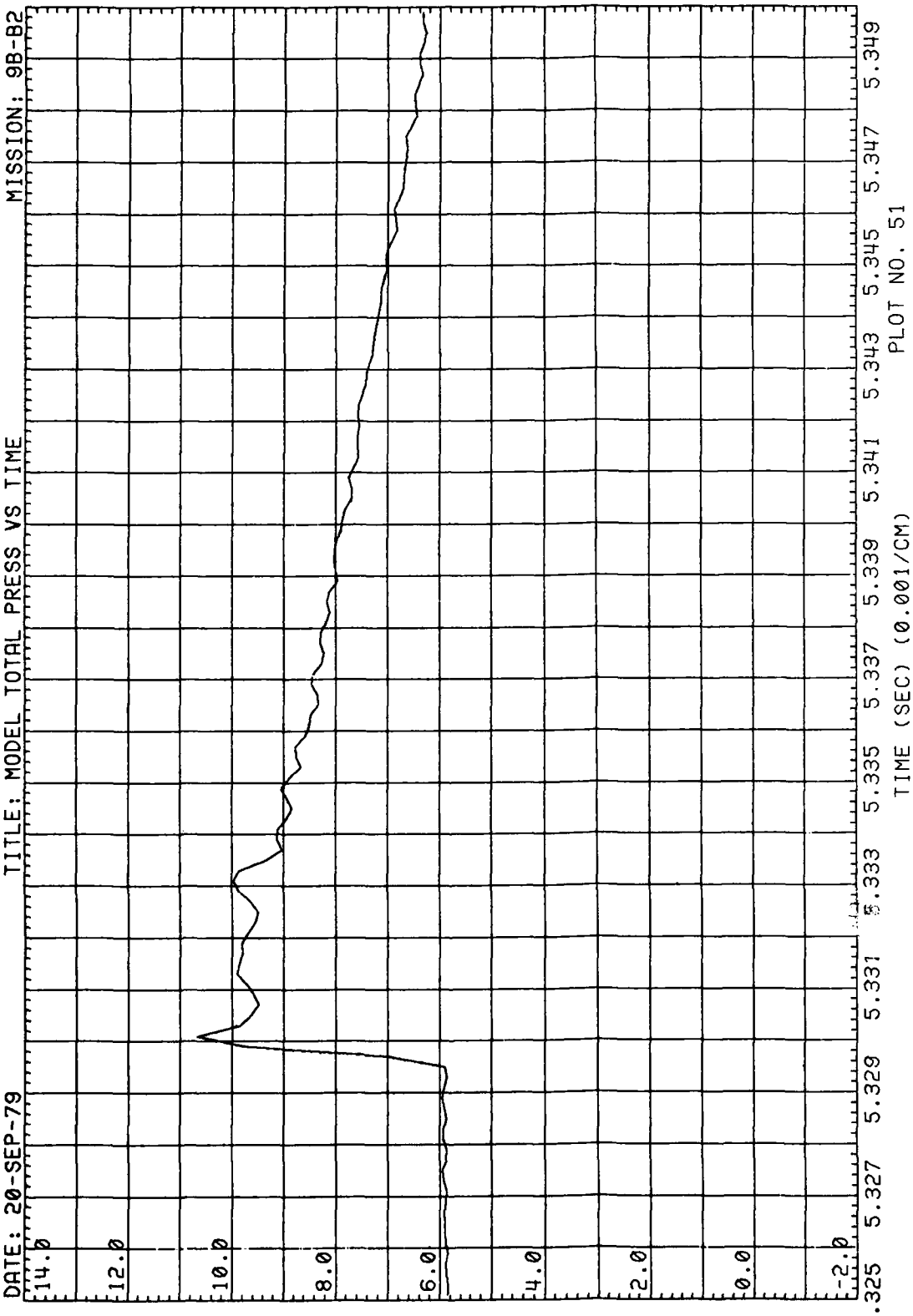

Figure 64. Total Pressure at Model, Run 9B-B2, Intercept 1

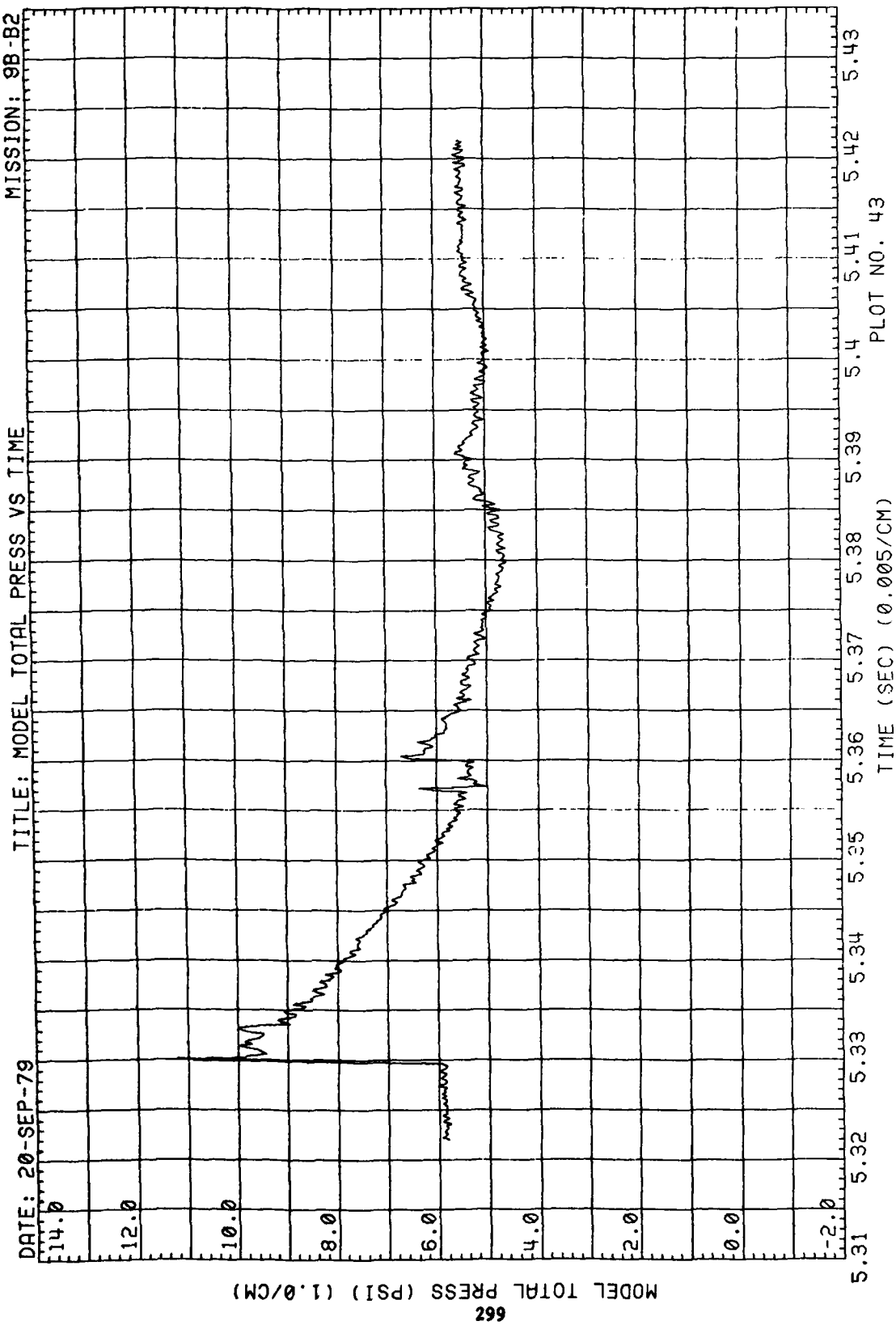

Figure 64. (Concluded)

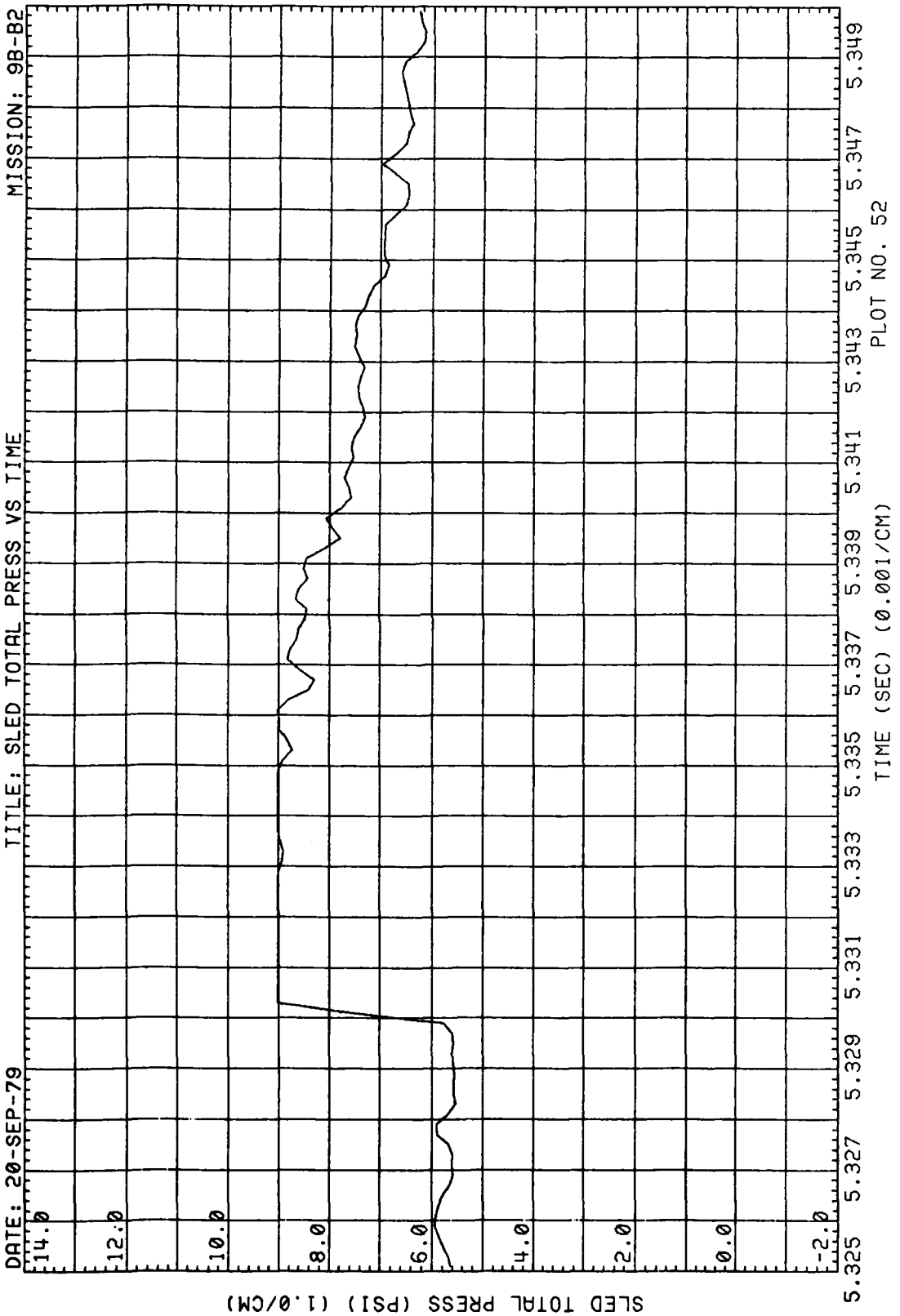

Figure 65. Total Pressure at Sled, Run 9B-B2, Intercept 1

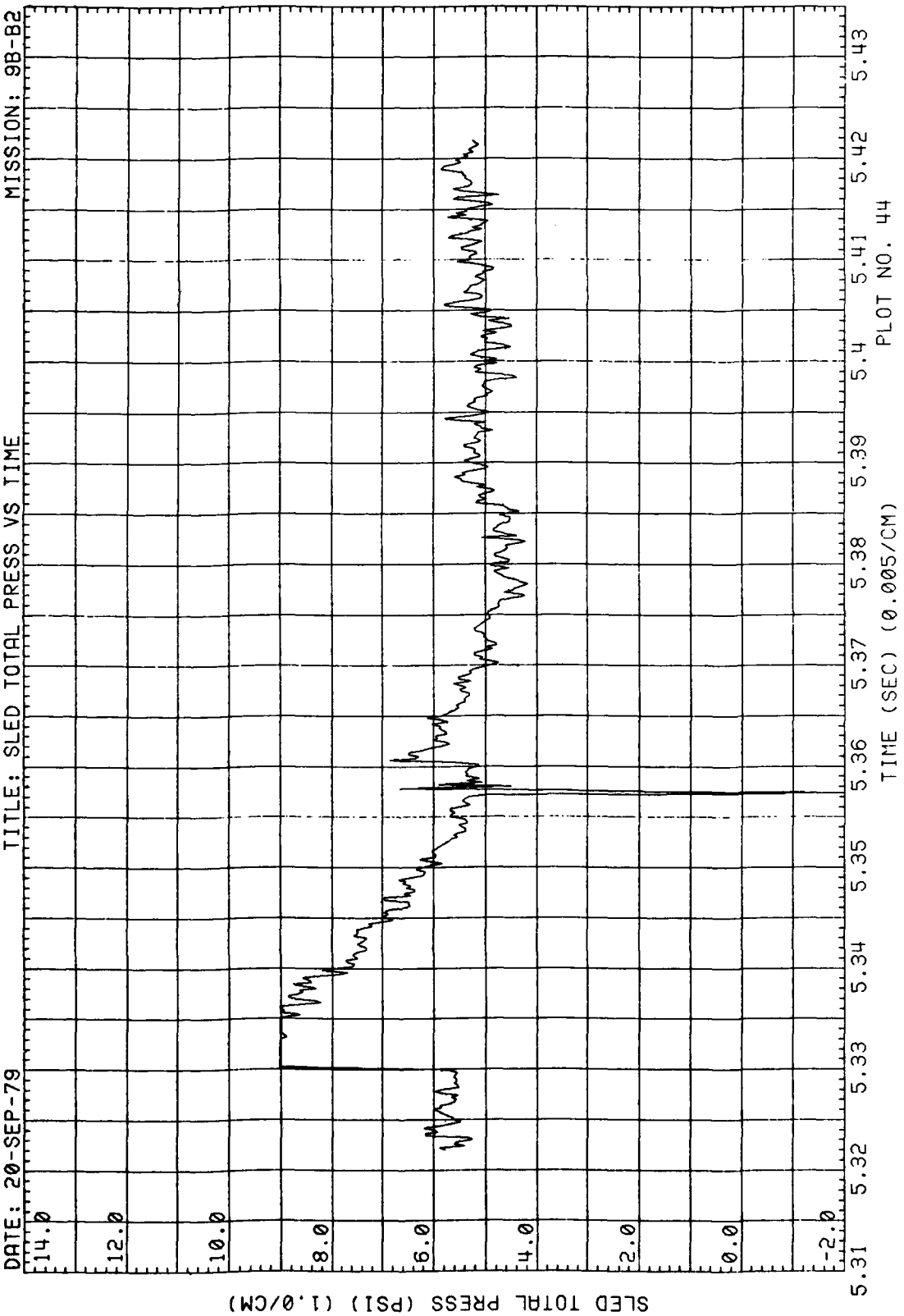

Figure 65. (Concluded)

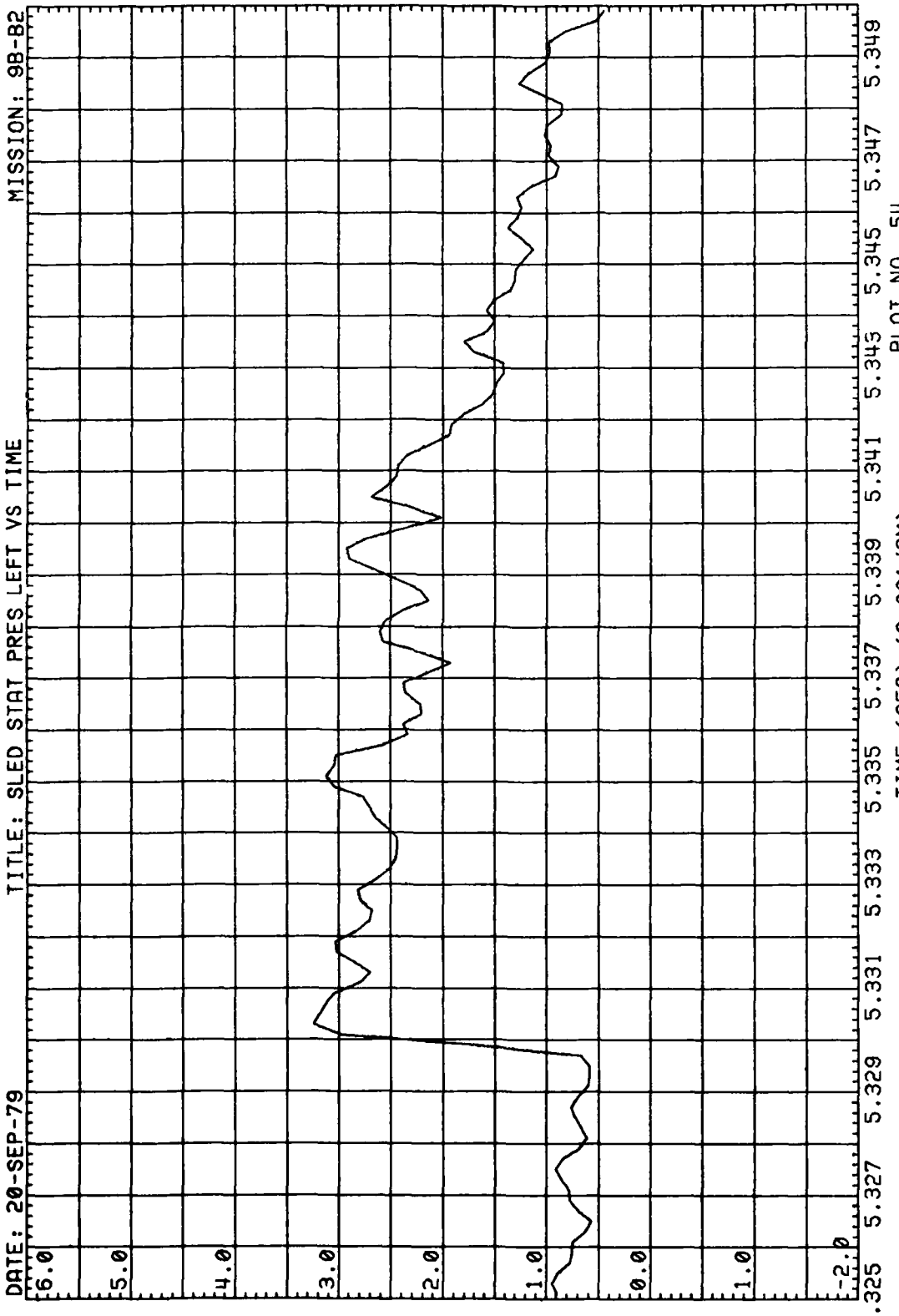

Figure 66. Left Side Static Pressure at Sled, Run 9B-B2, Intercept 1

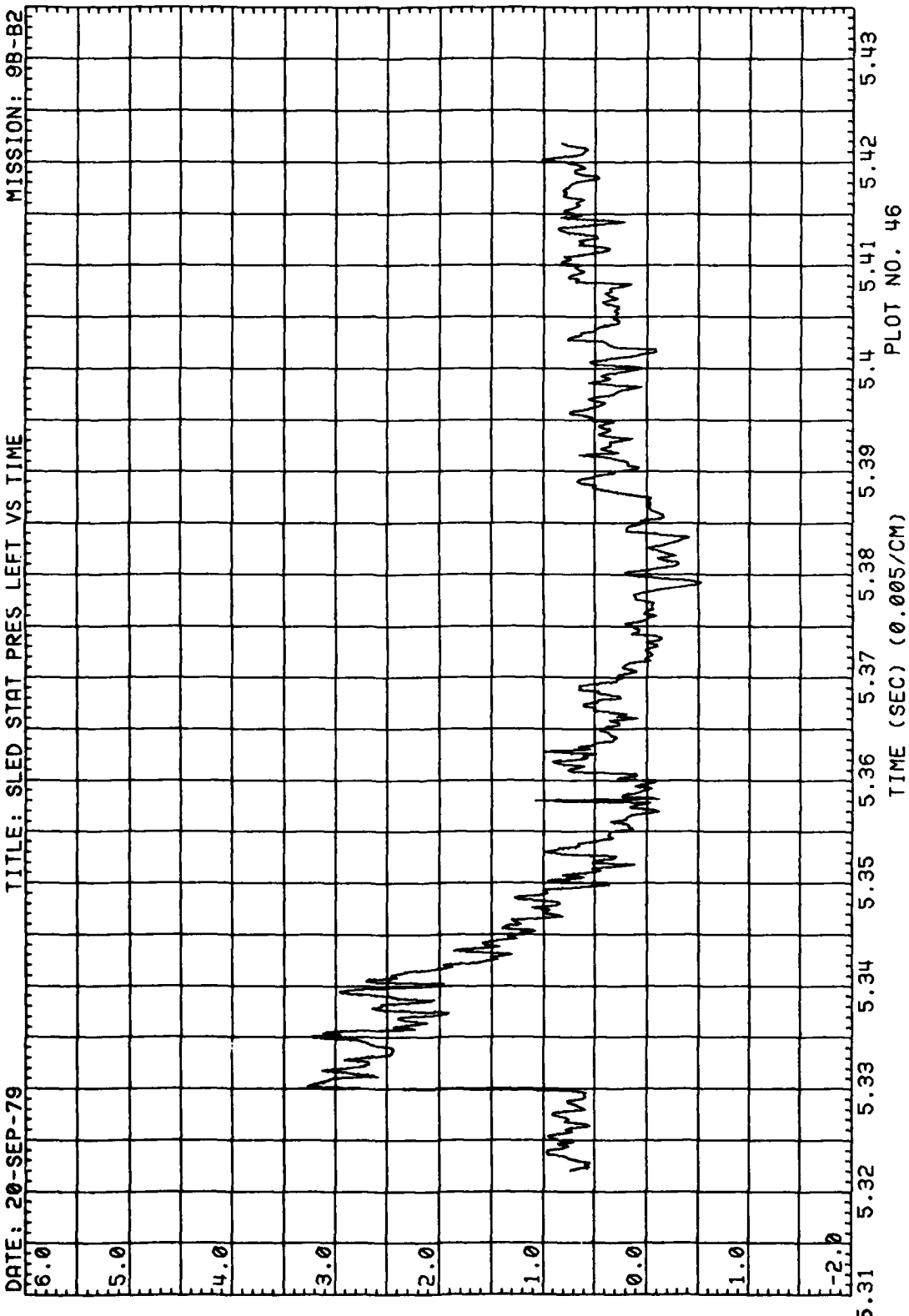

Figure 66. (Concluded)

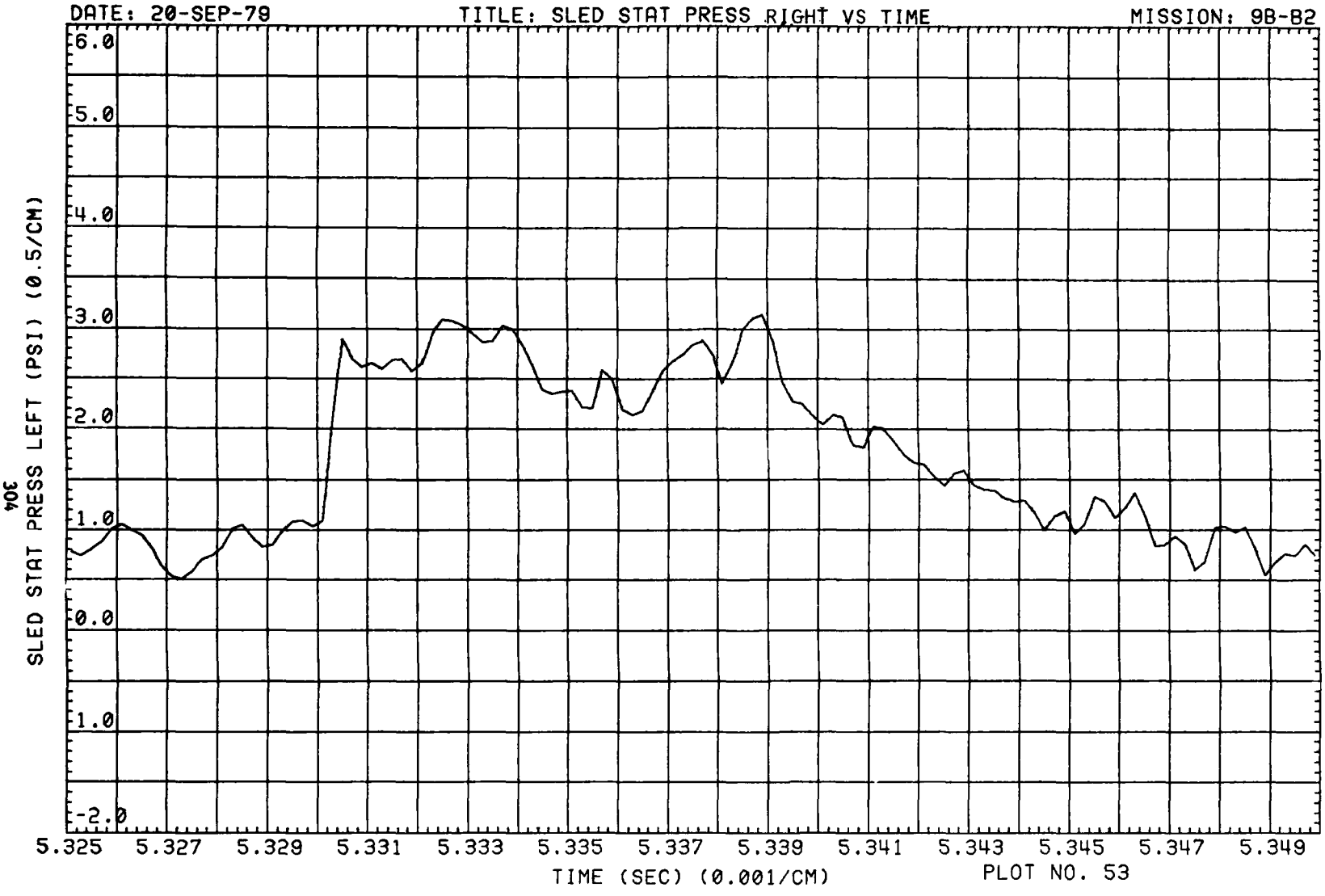

Figure 67. Right Side Static Pressure at Sled, Run 9B-B2, Intercept 1

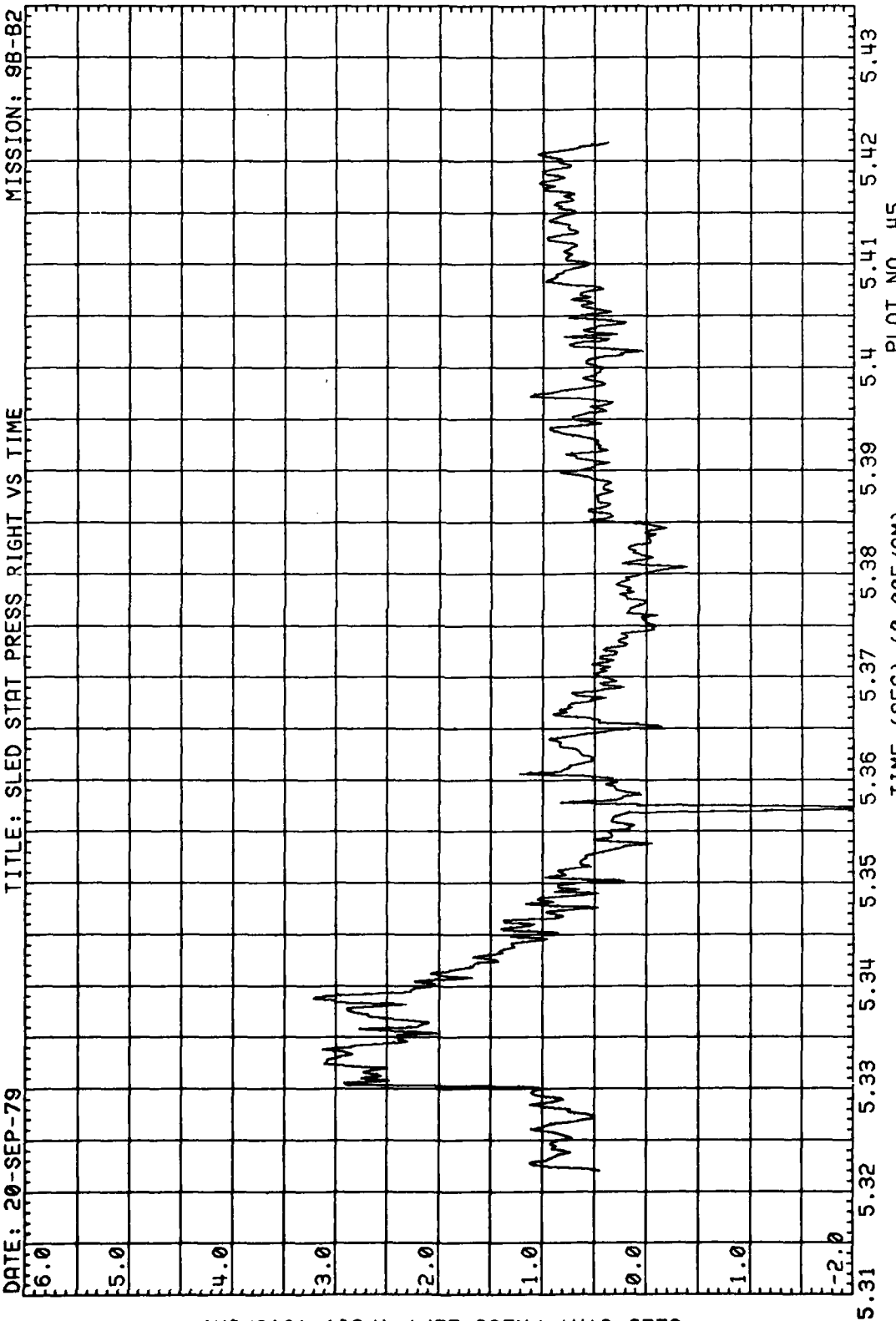

Figure 67. (Concluded)

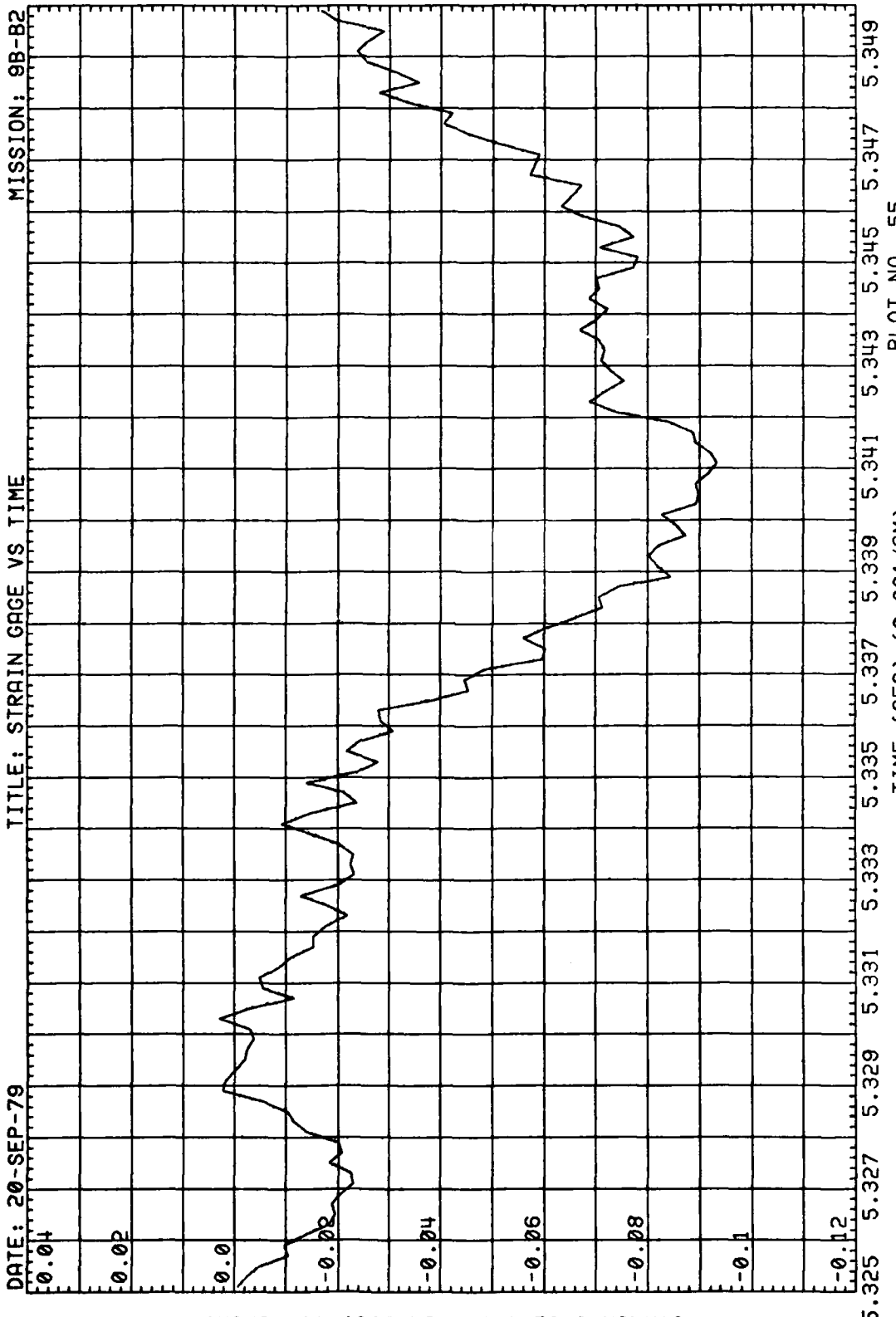

Figure 68. Strain at Model Support, Run 9B-B2, Intercept 1

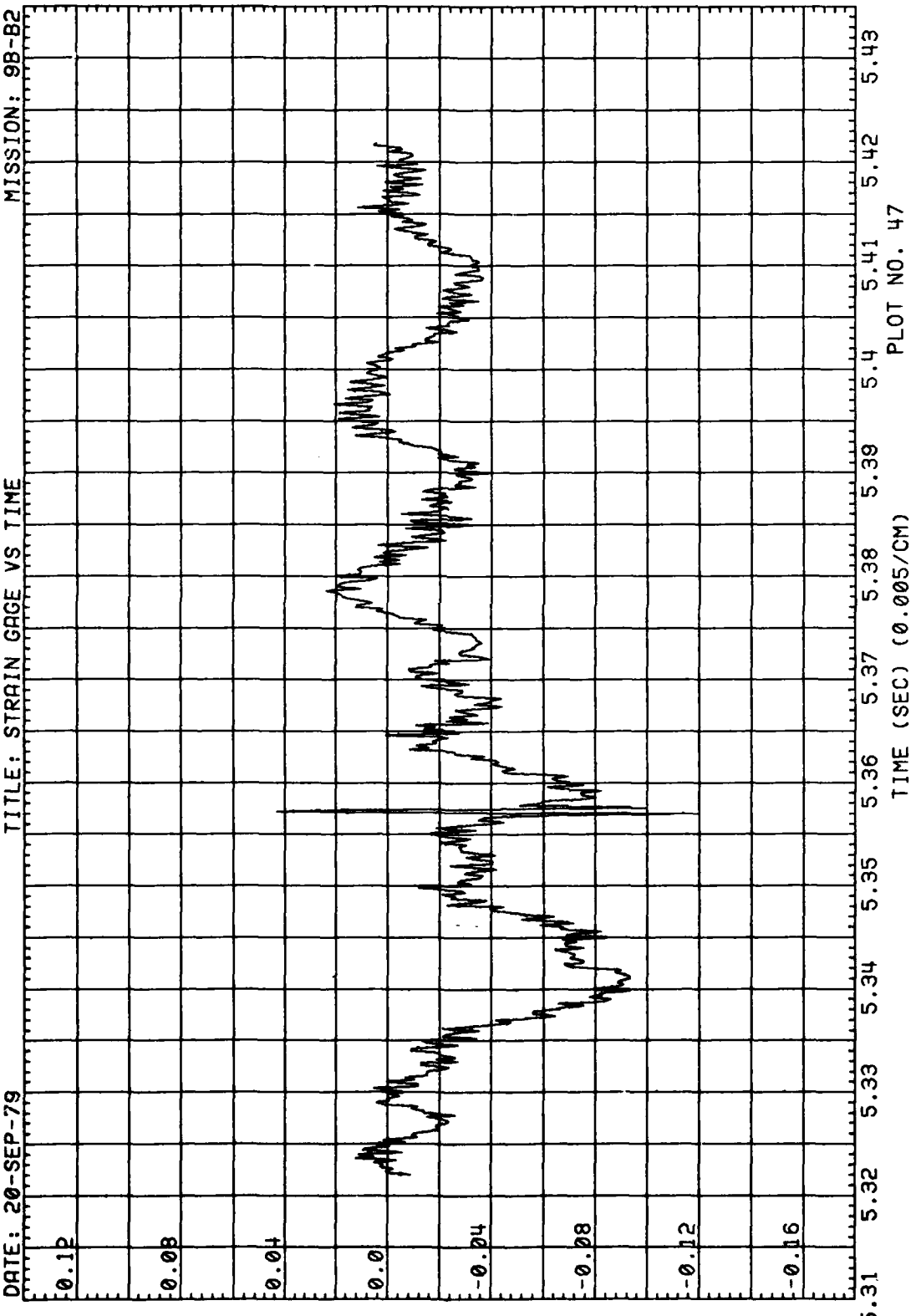

Figure 68. (Concluded)

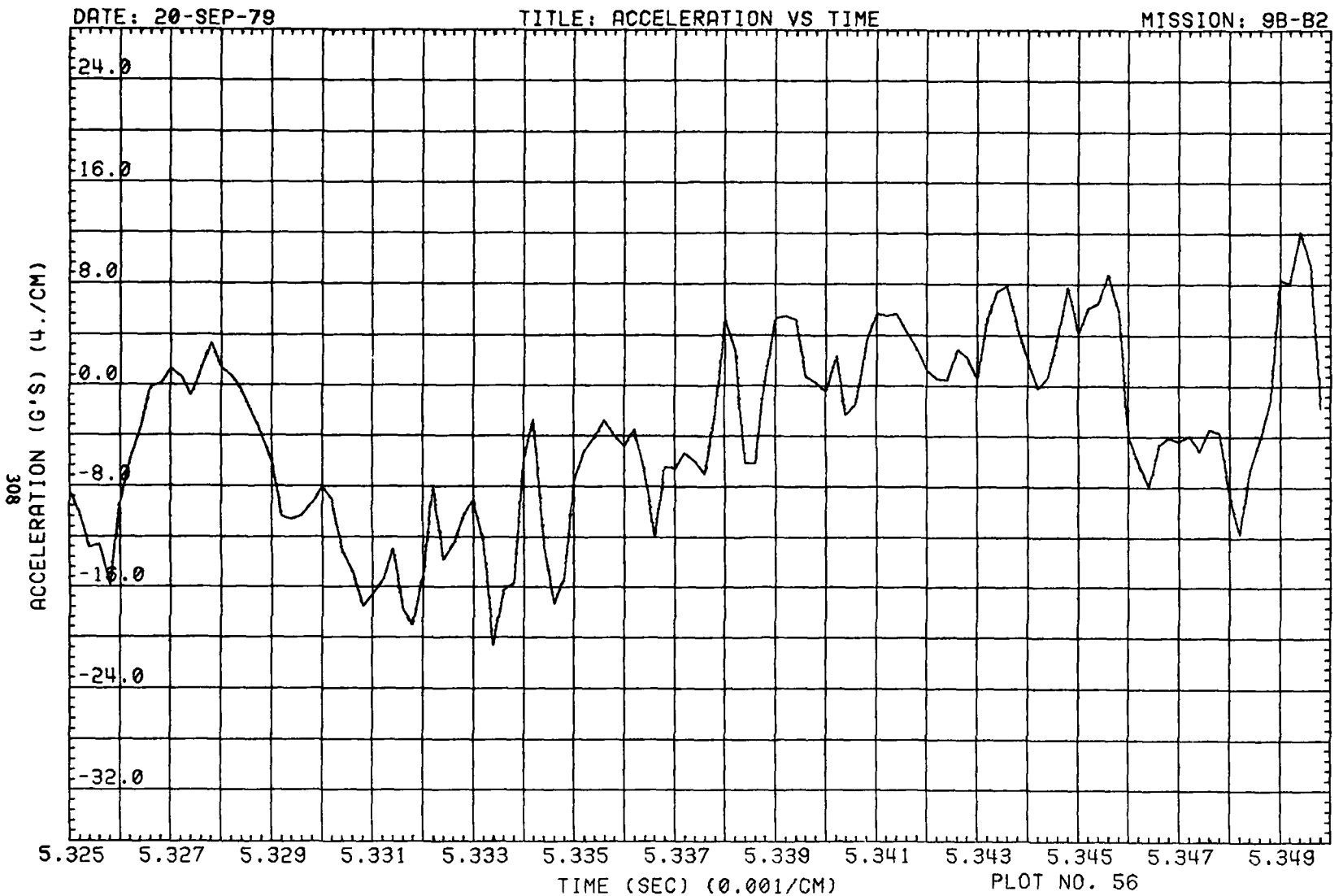

Figure 69. Wing Acceleration, Run 9B-B2, Intercept 1

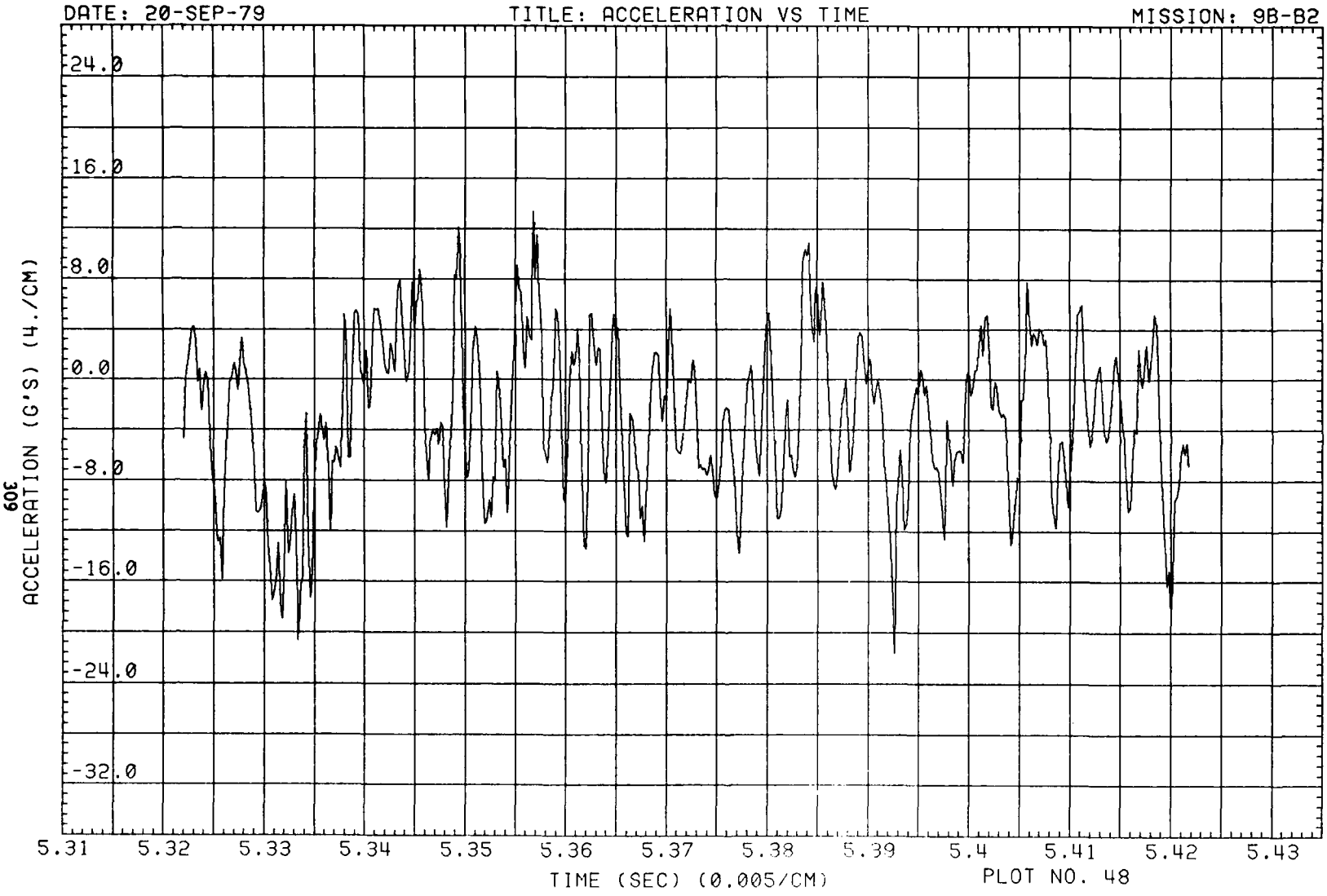

Figure 69. (Concluded)

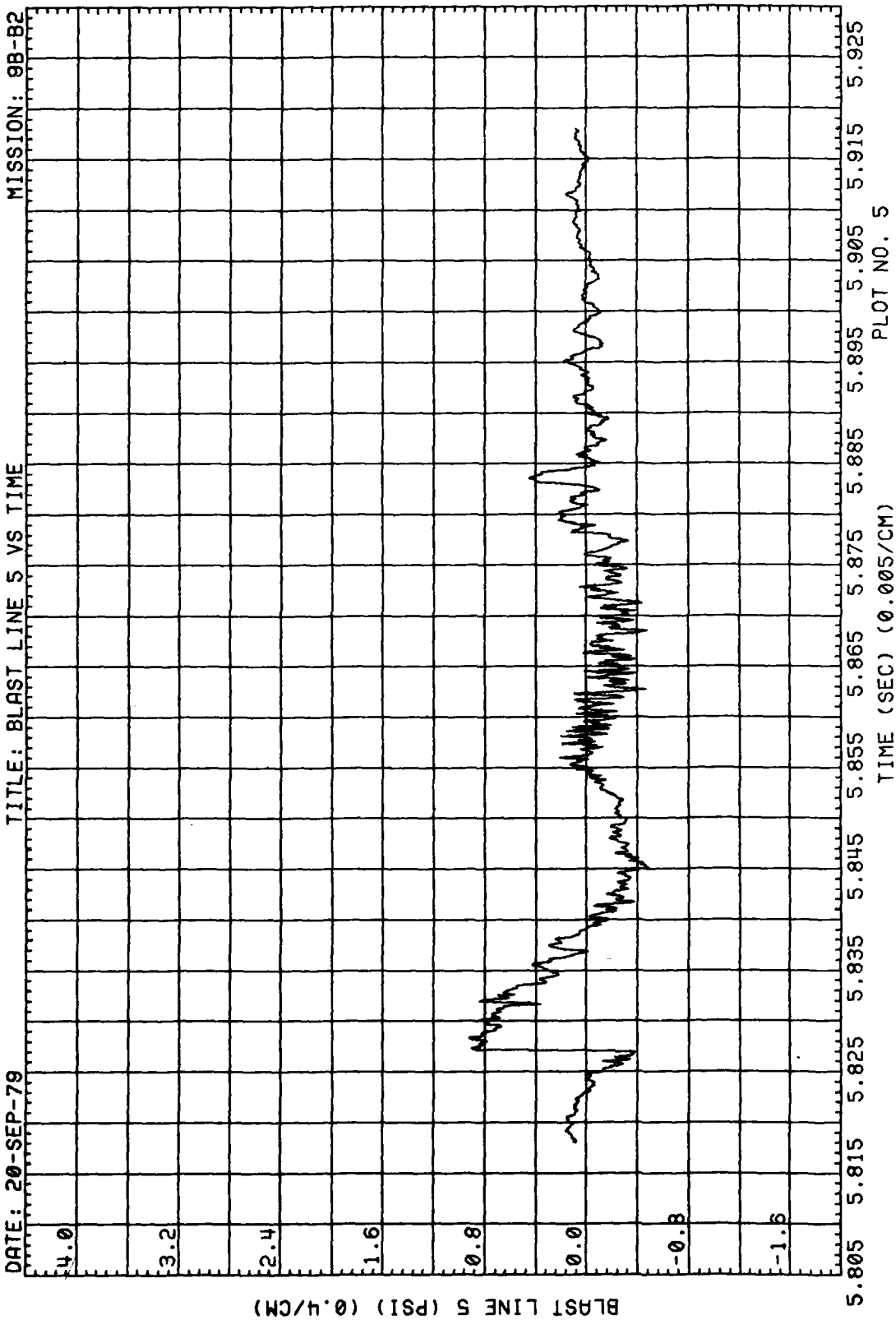

Figure 70. Blast-Line Pressure, Run 9B-B2, Intercept 2

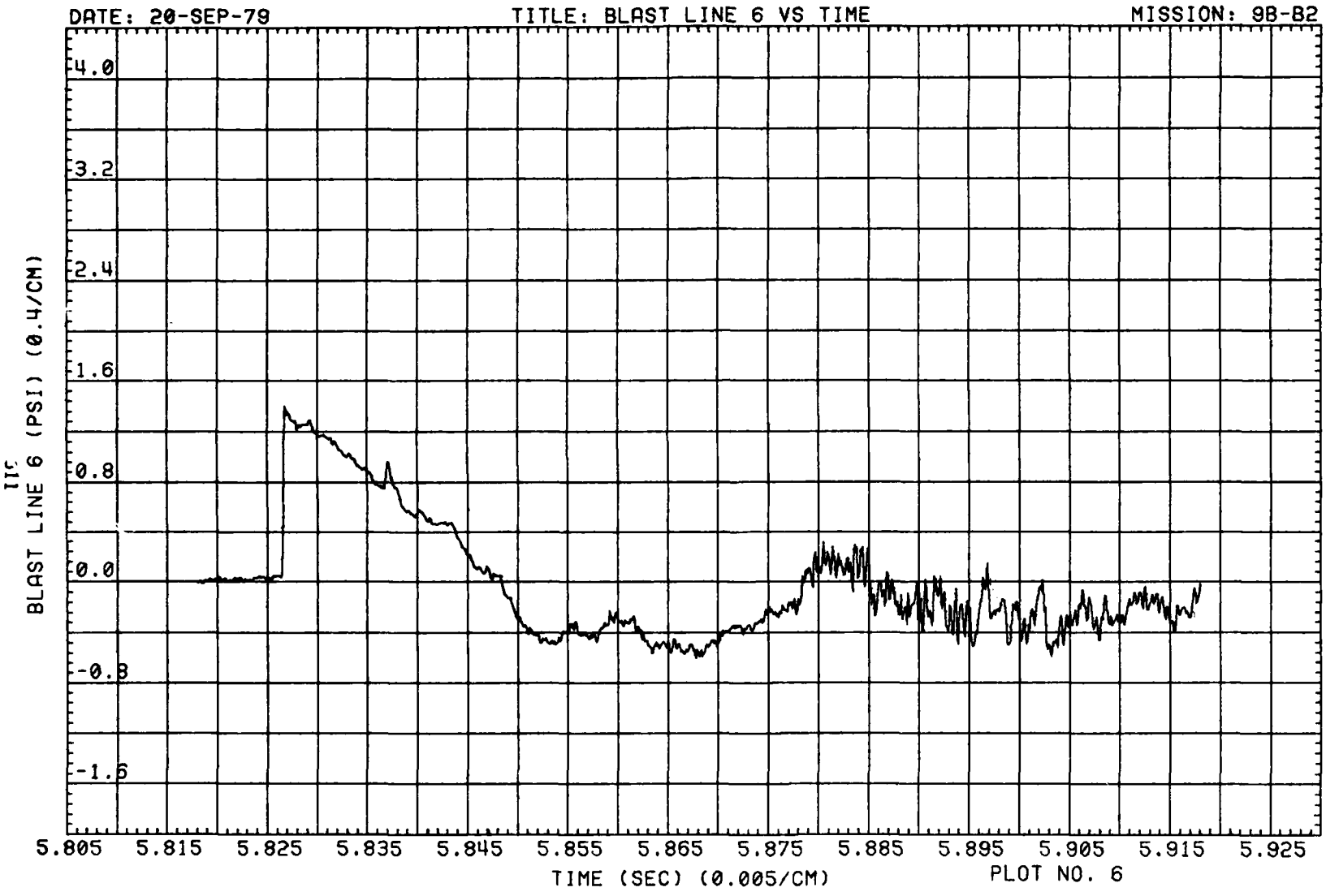

Figure 70. (Continued)

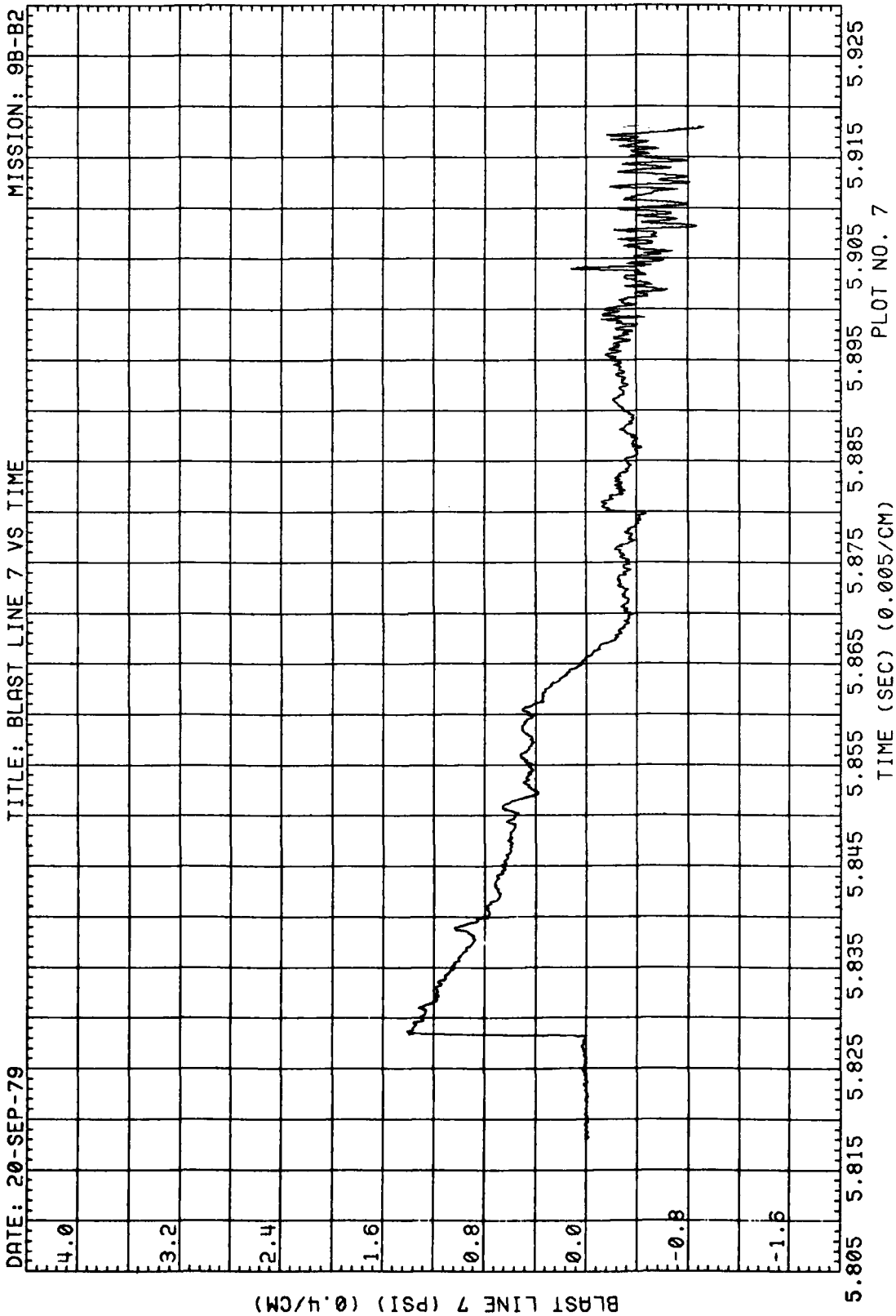

Figure 70. (Continued)

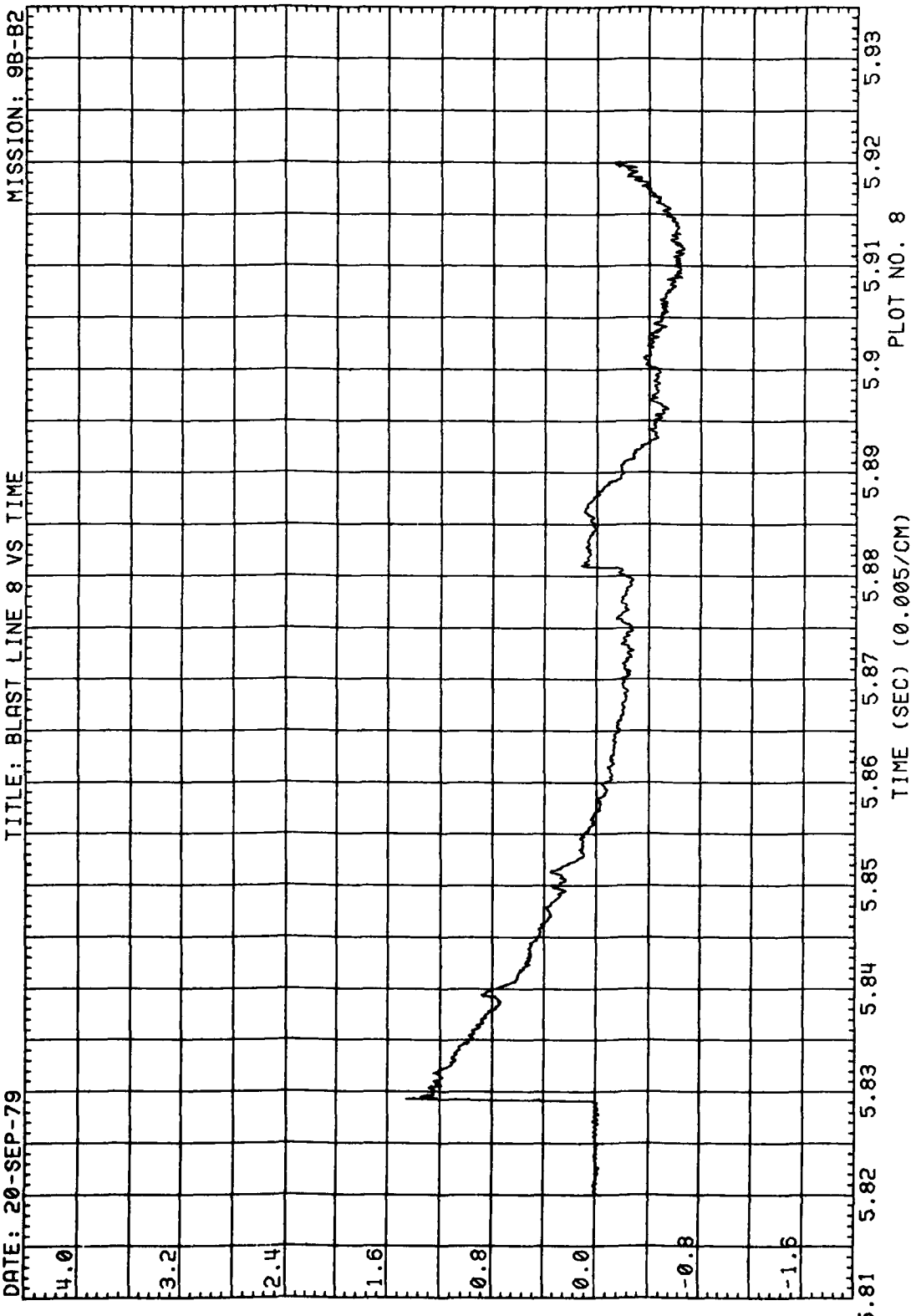

Figure 70. (Concluded)

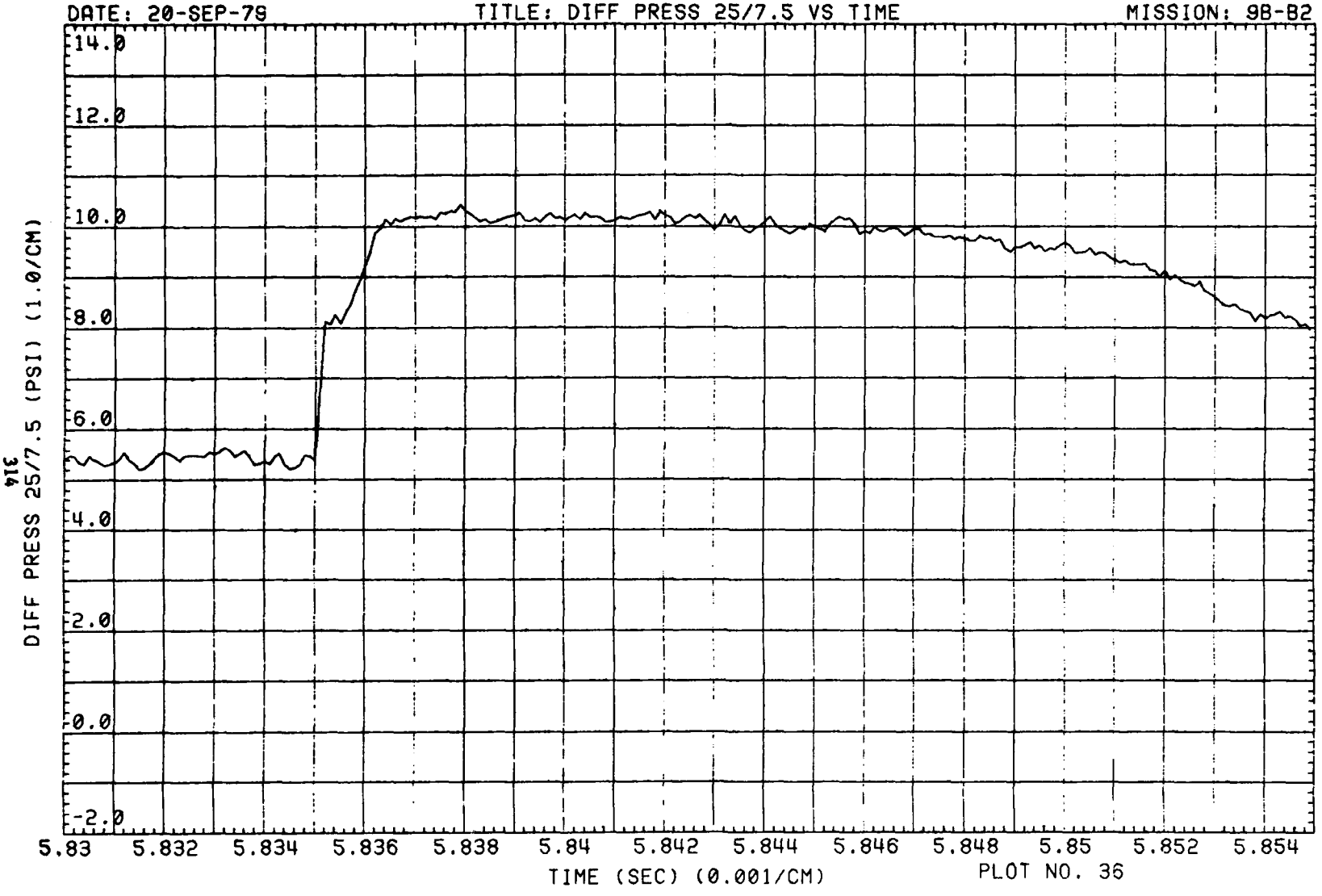

Figure 71. Differential Wing Pressures, Run 9B-B2, Intercept 2

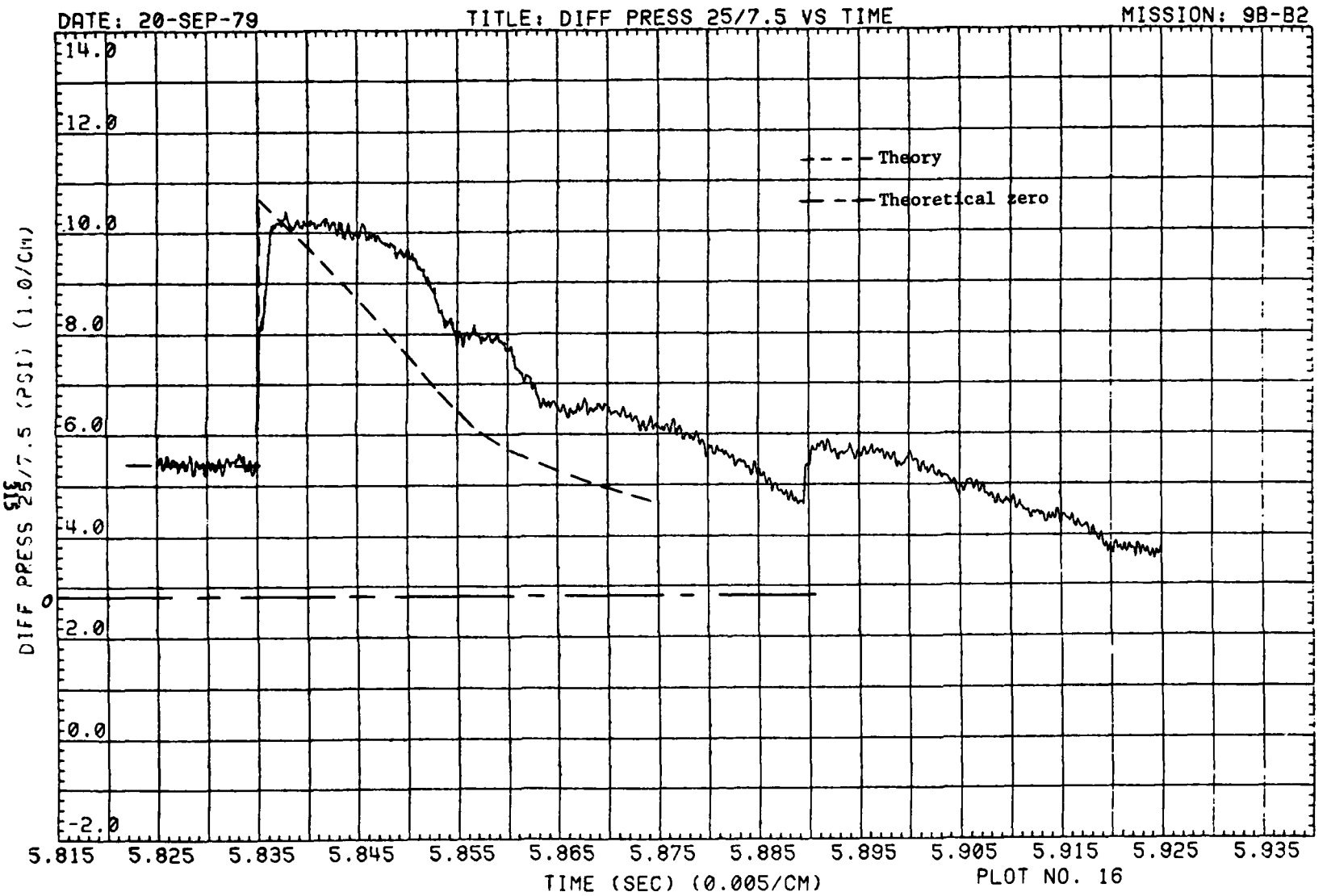

Figure 71. (Continued)

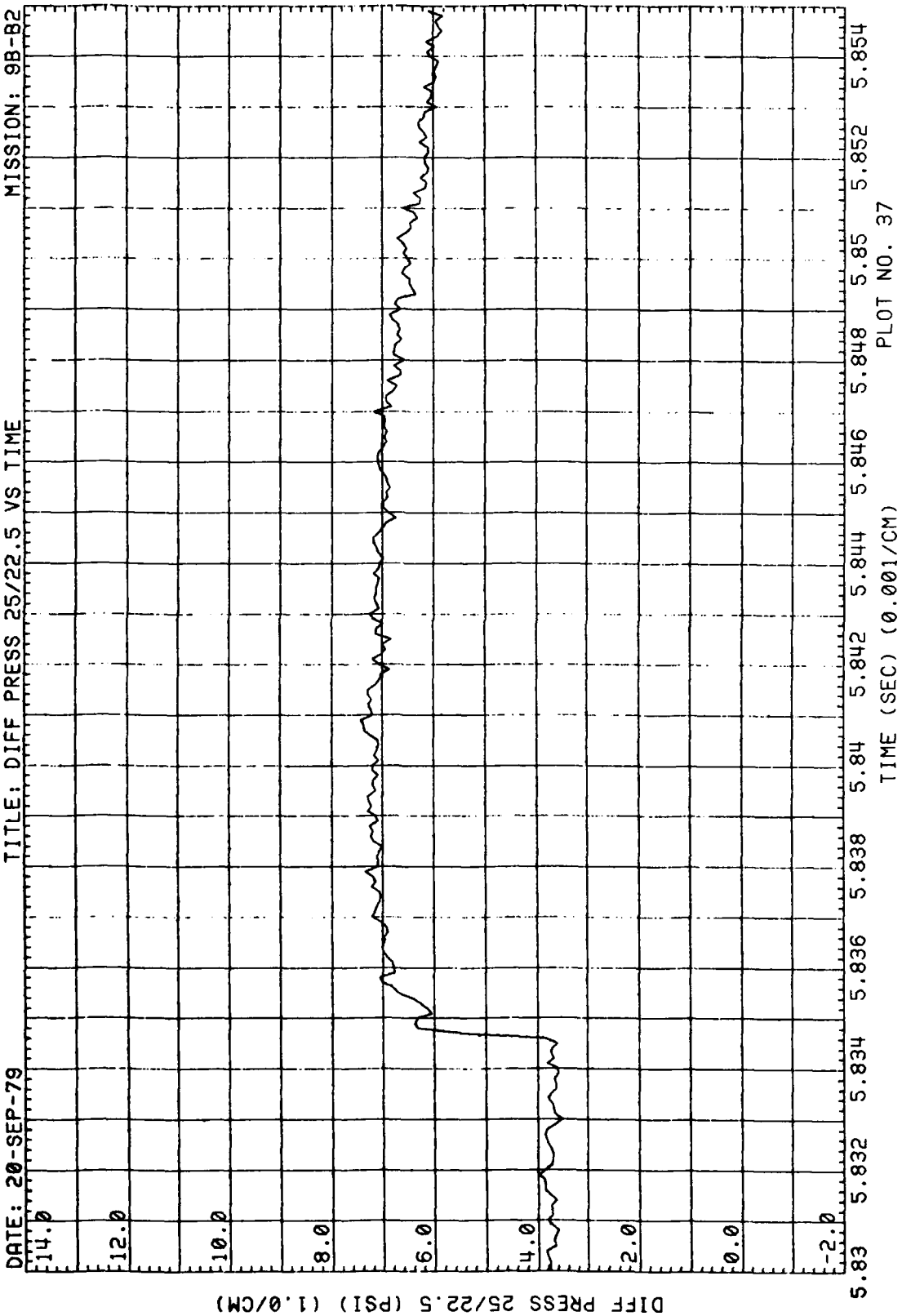

Figure 71. (Continued)

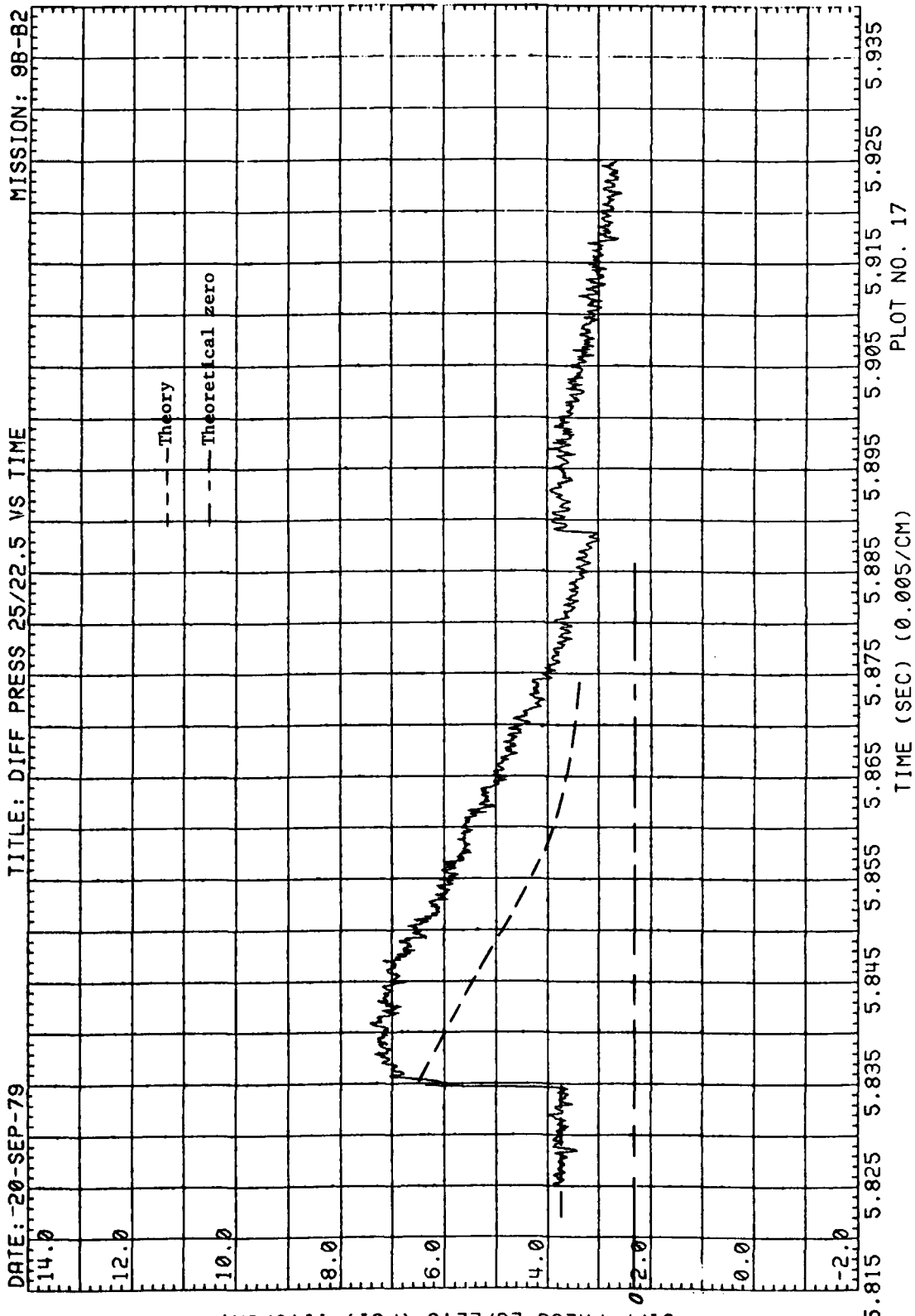

Figure 71. (Continued)

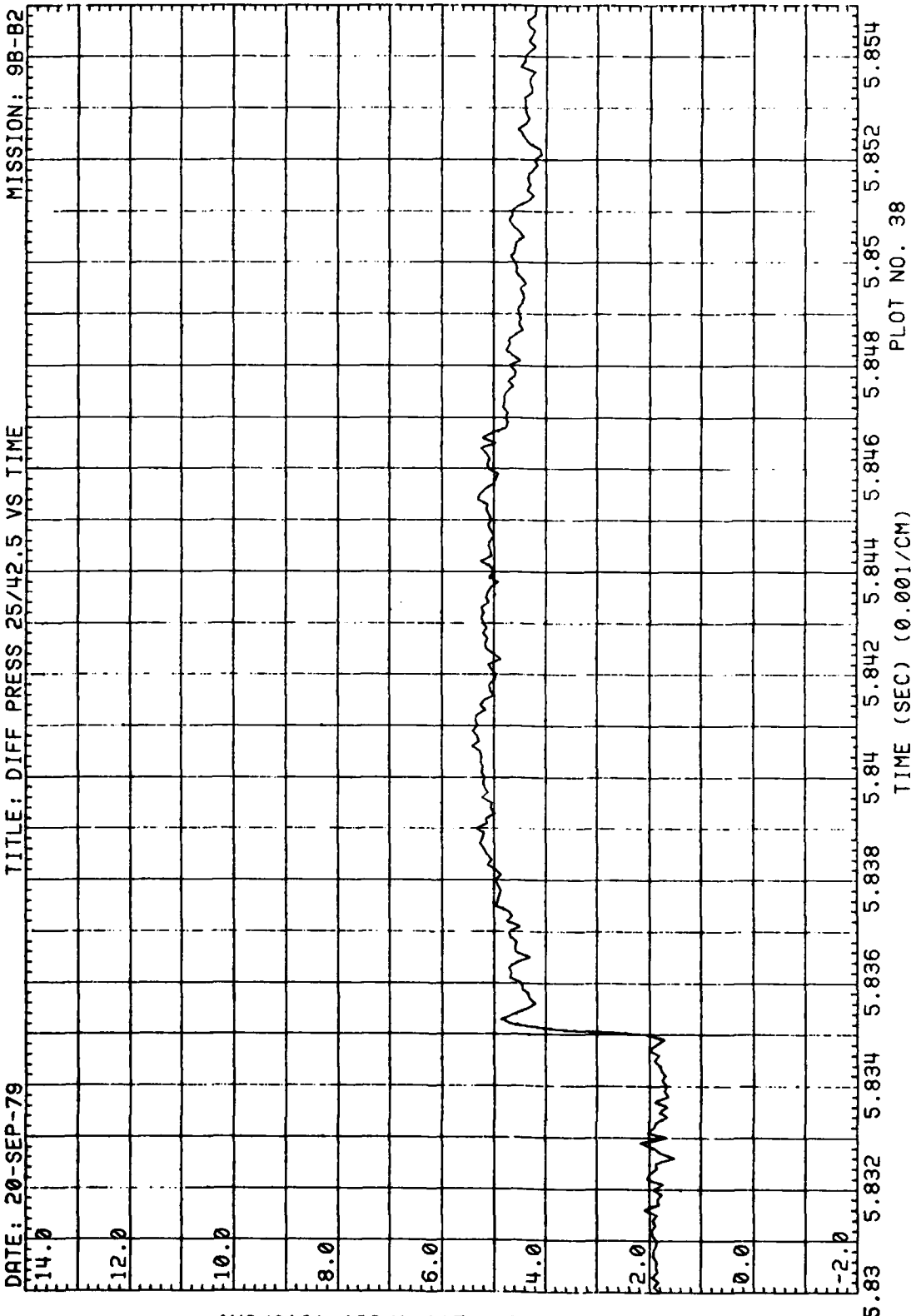

Figure 71. (Continued)

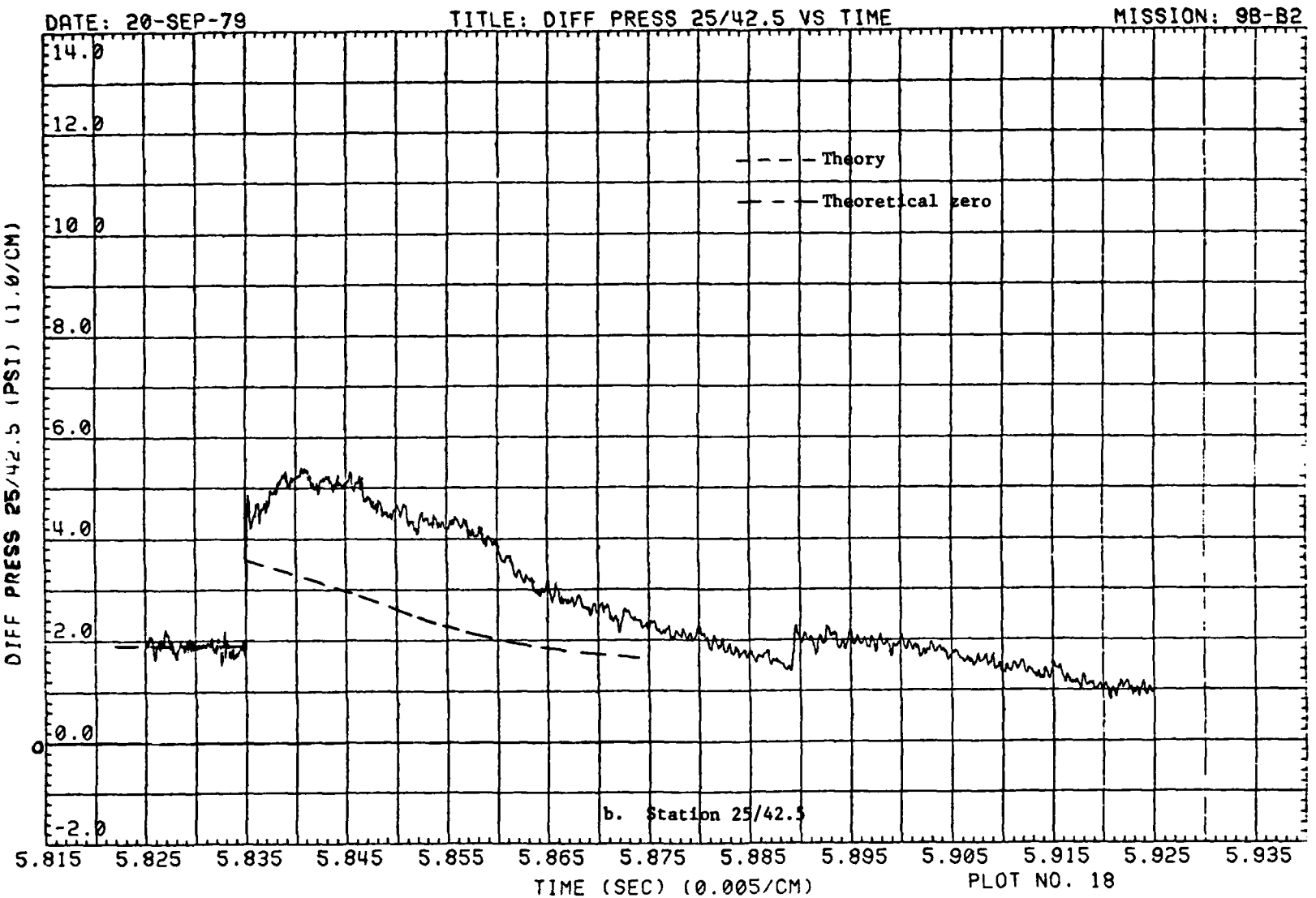

Figure 71. (Continued)

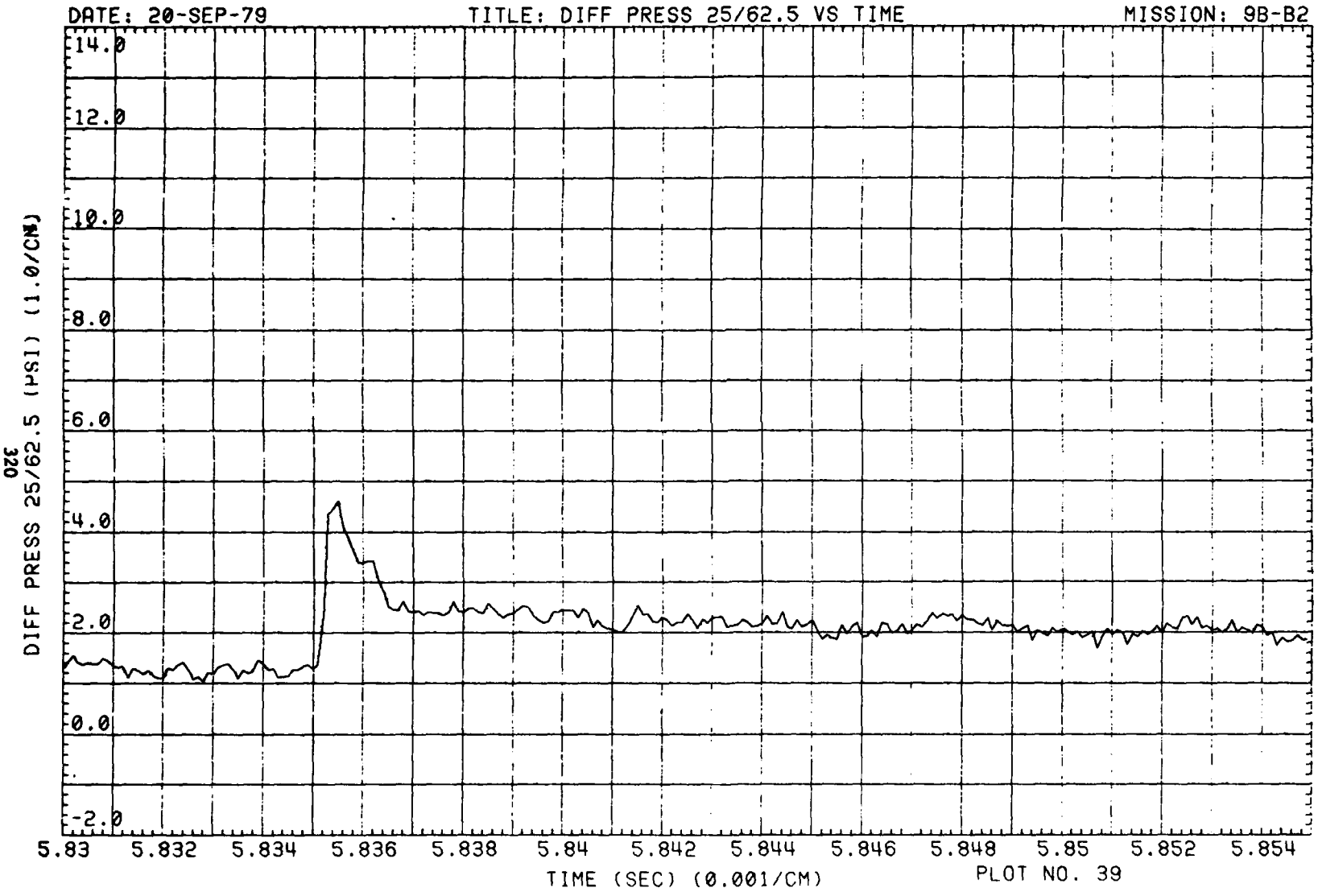

Figure 71. (Continued)

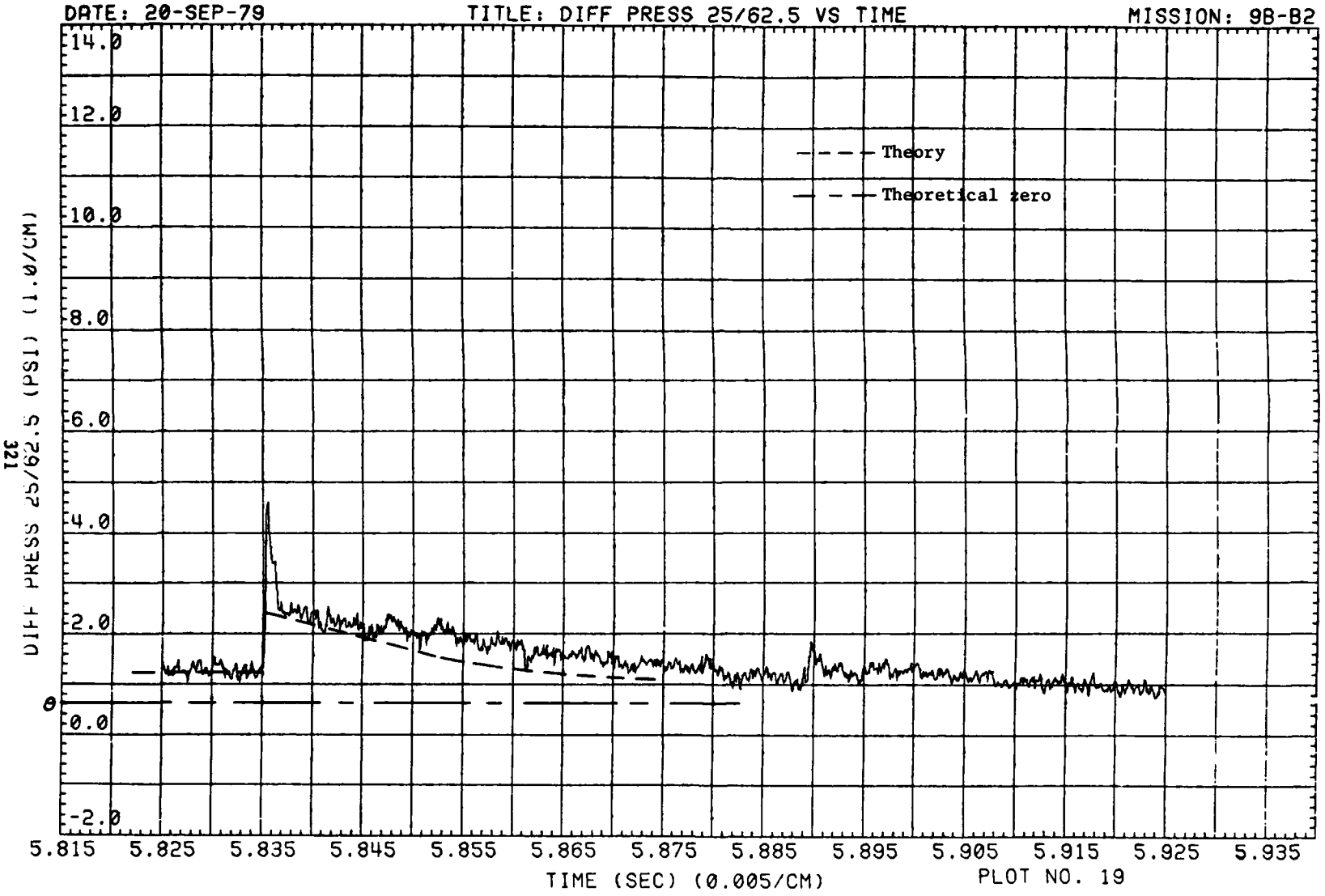

Figure 71. (Continued)

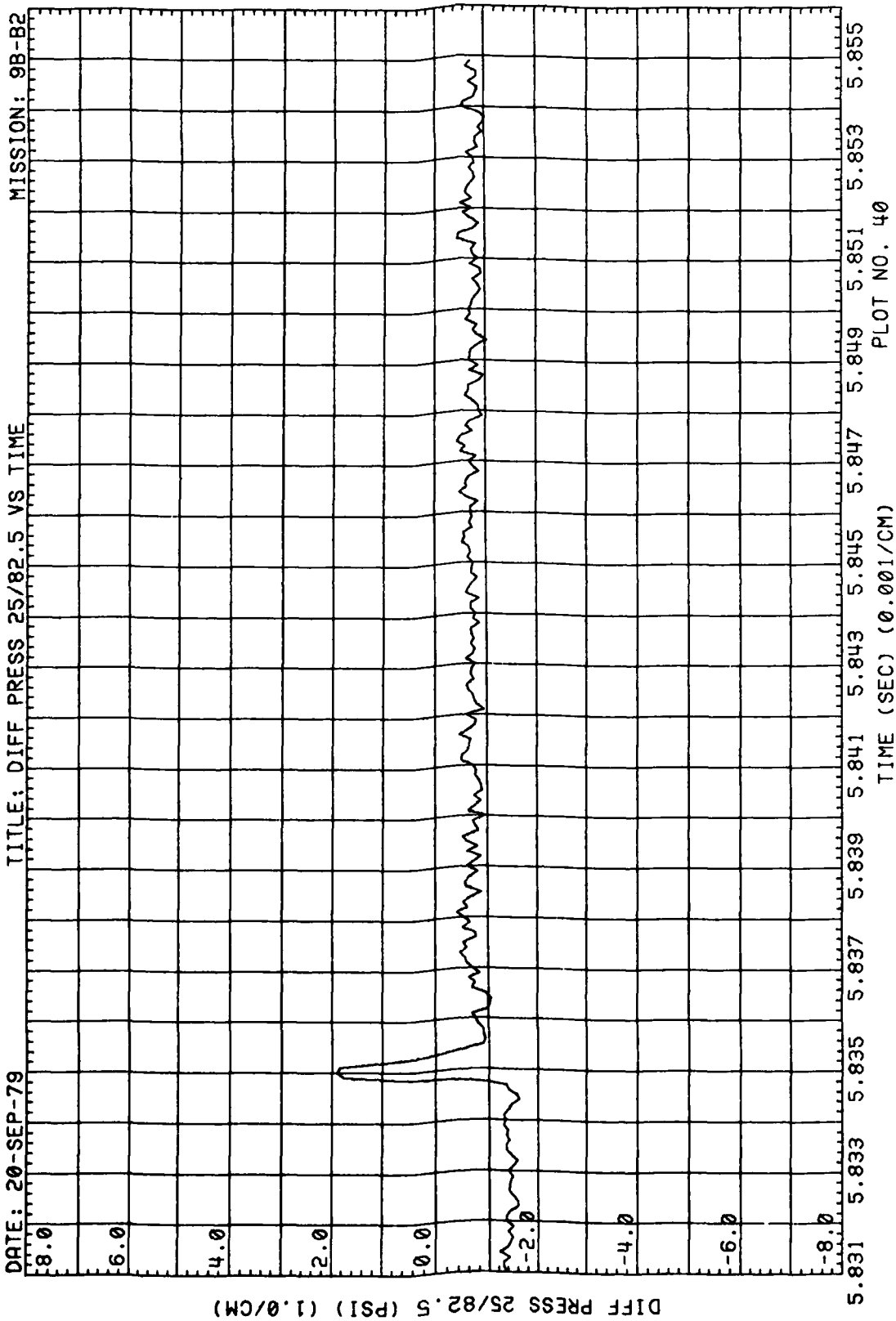

Figure 71. (Continued)

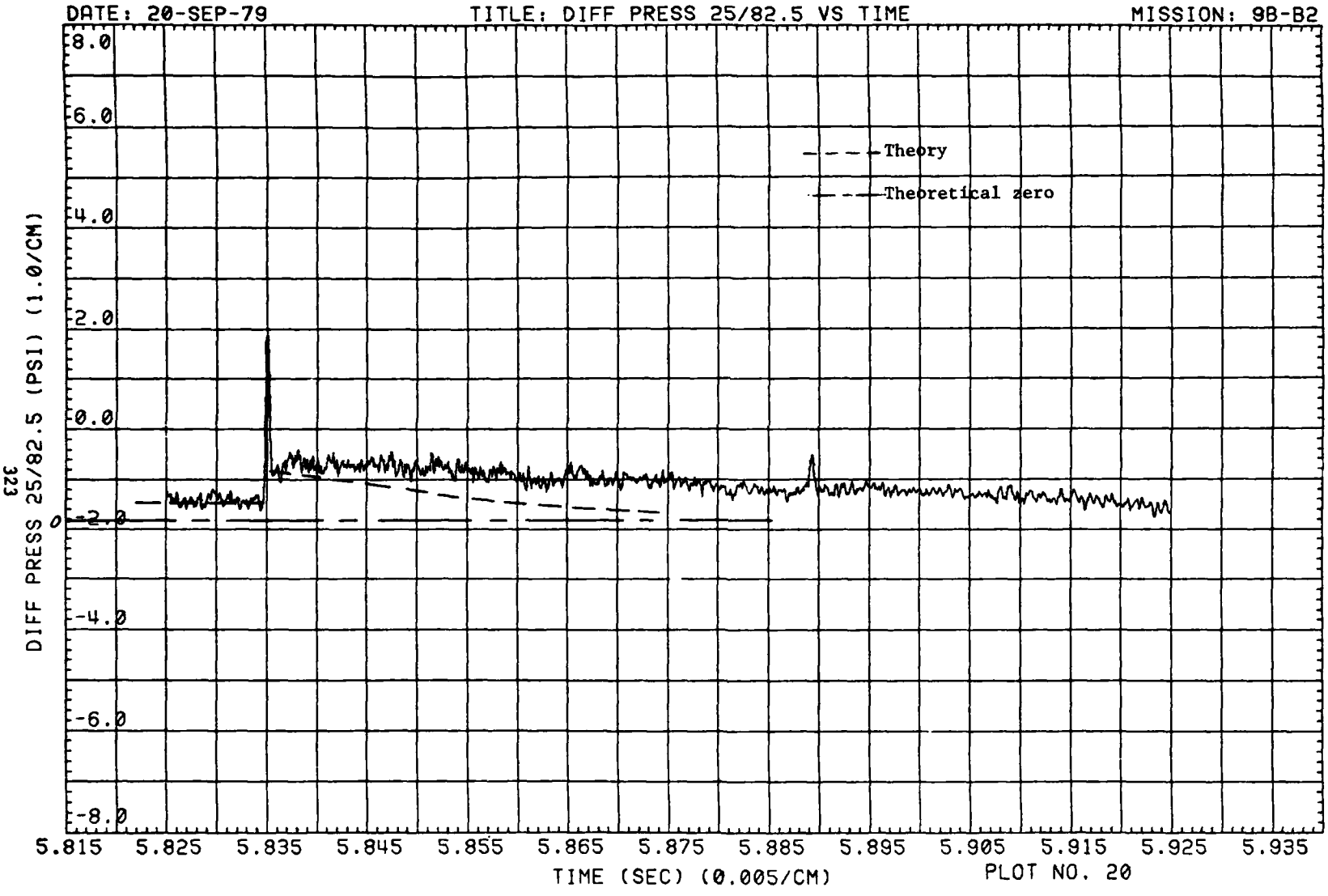

Figure 71. (Continued)

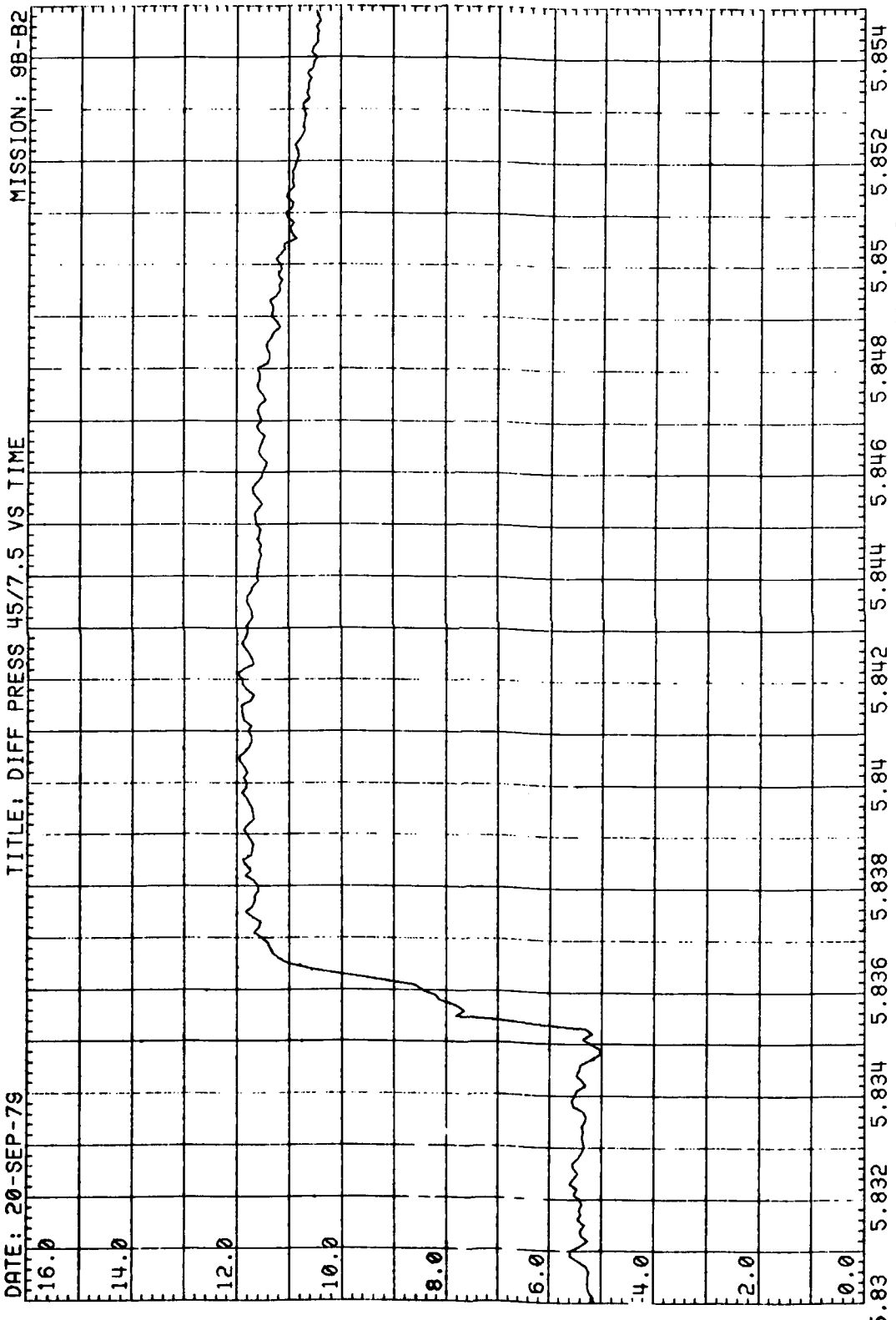

Figure 71. (Continued)

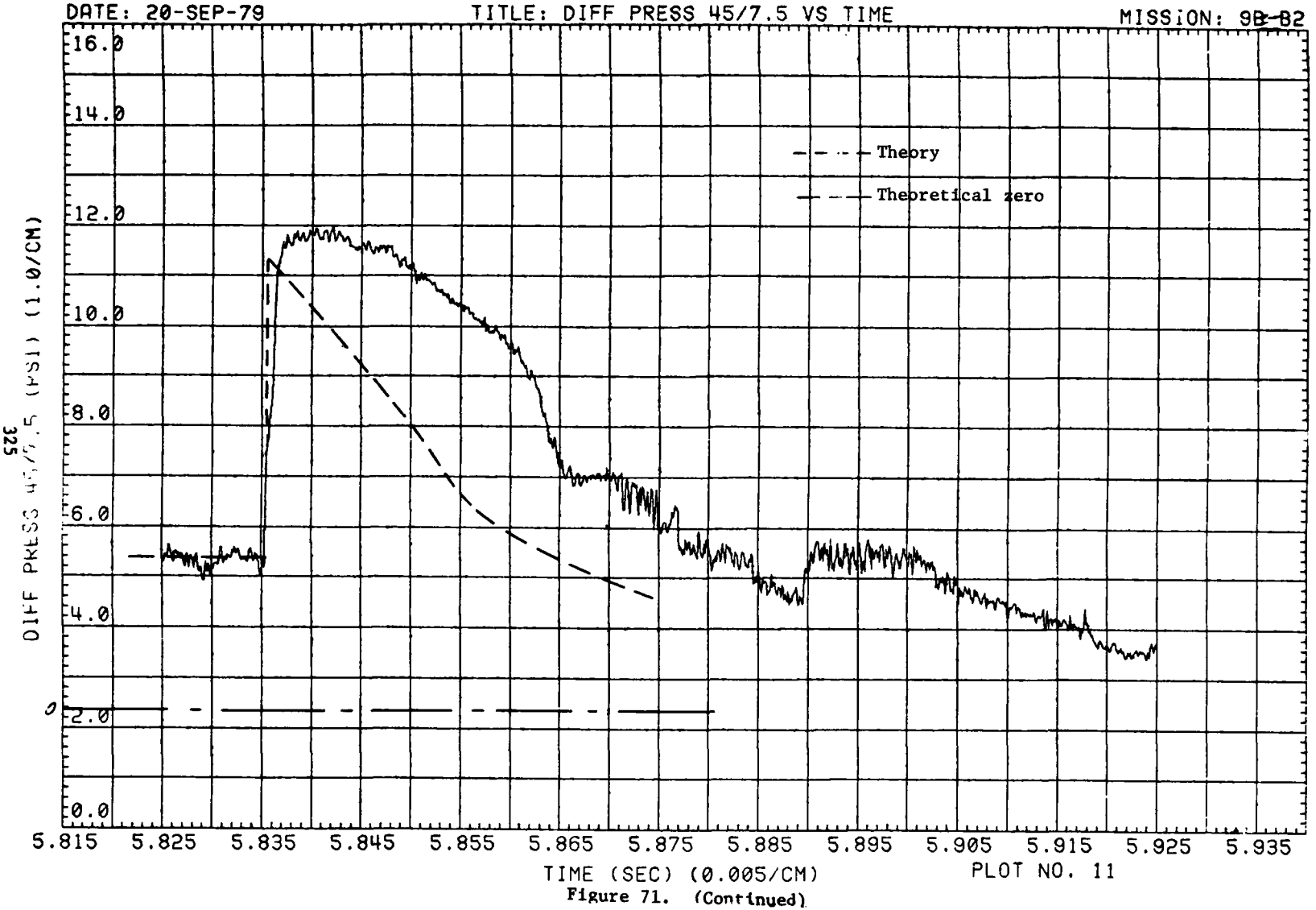

Figure 71. (Continued)

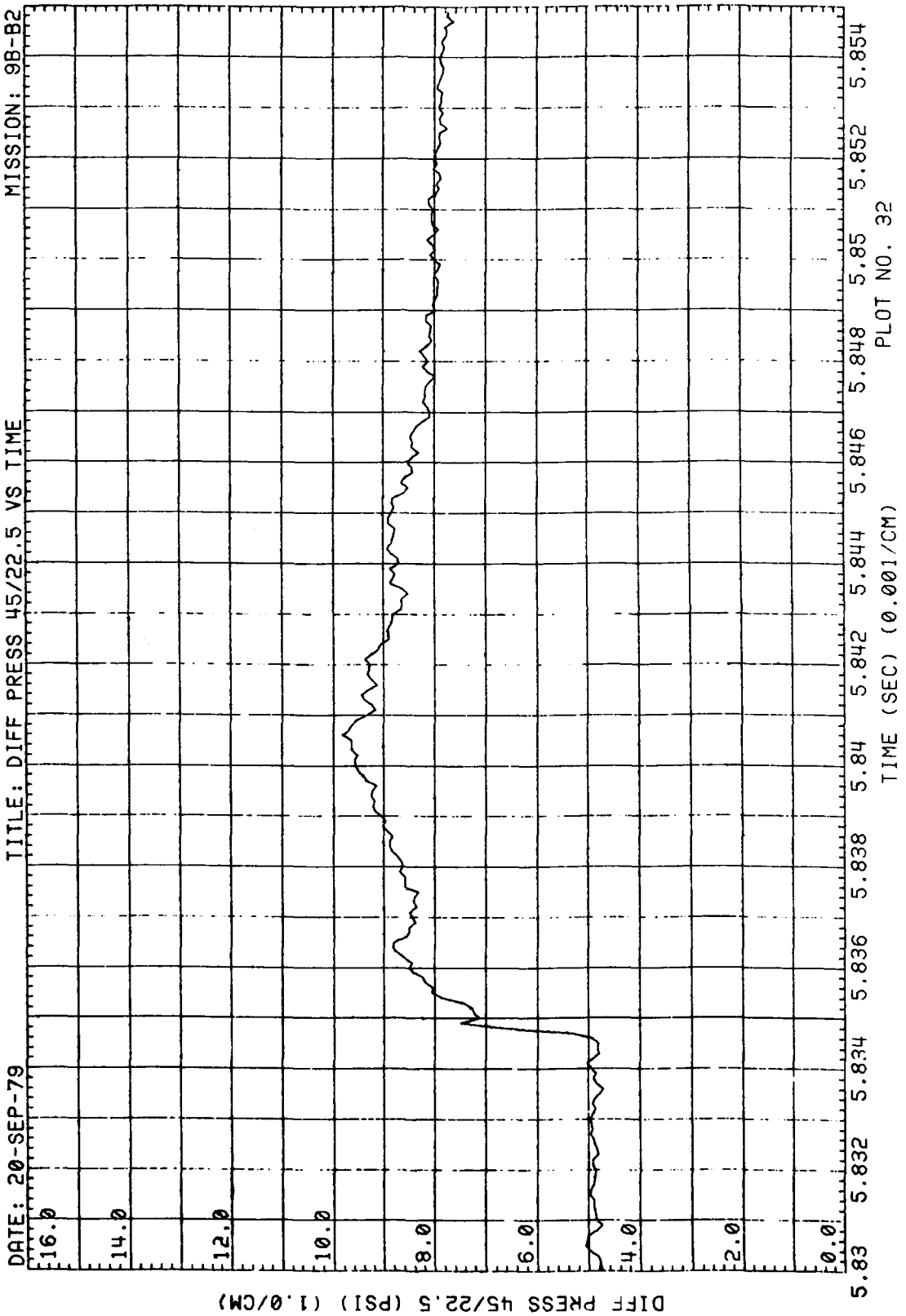

Figure 71. (Continued)

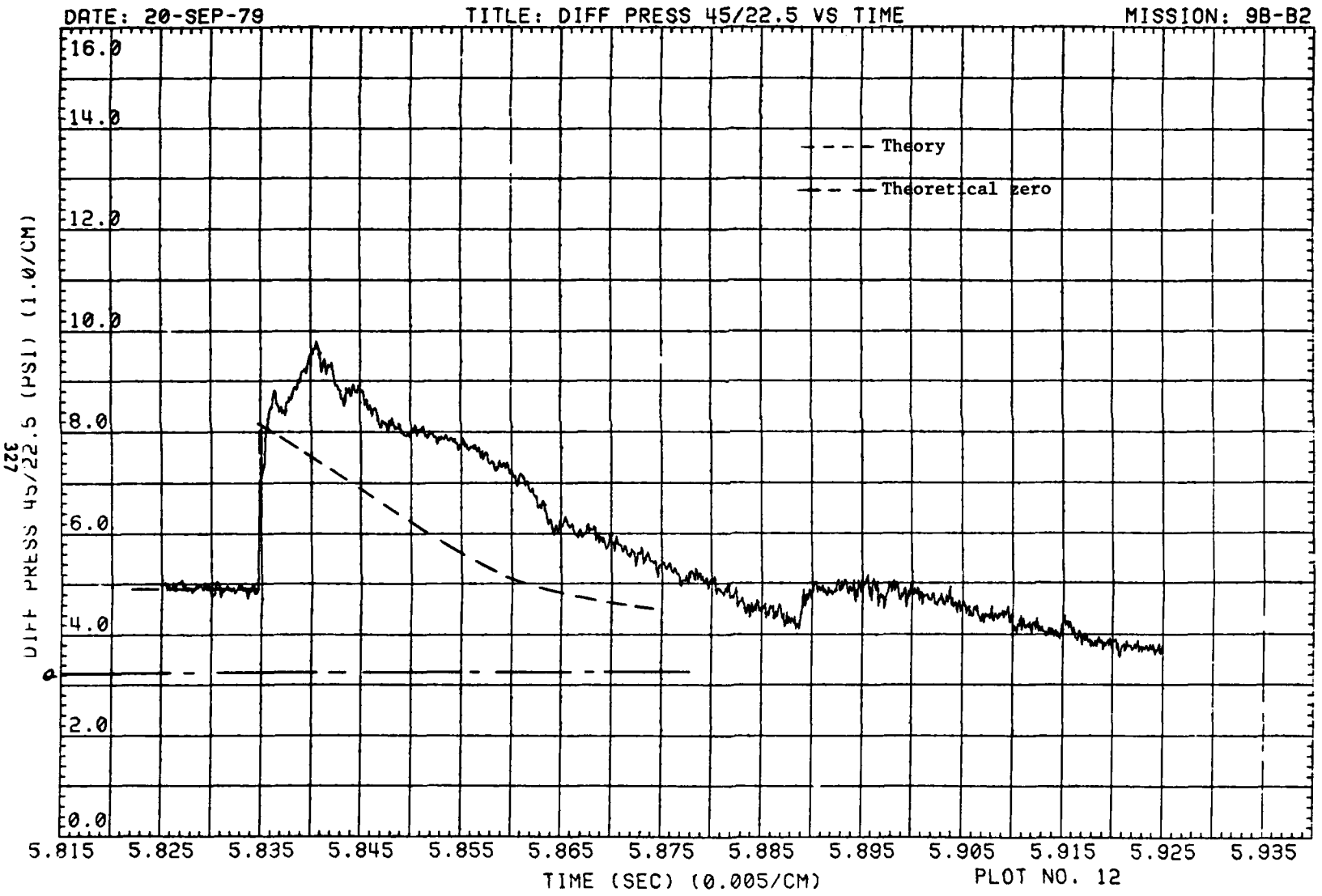

Figure 77. (Continued)

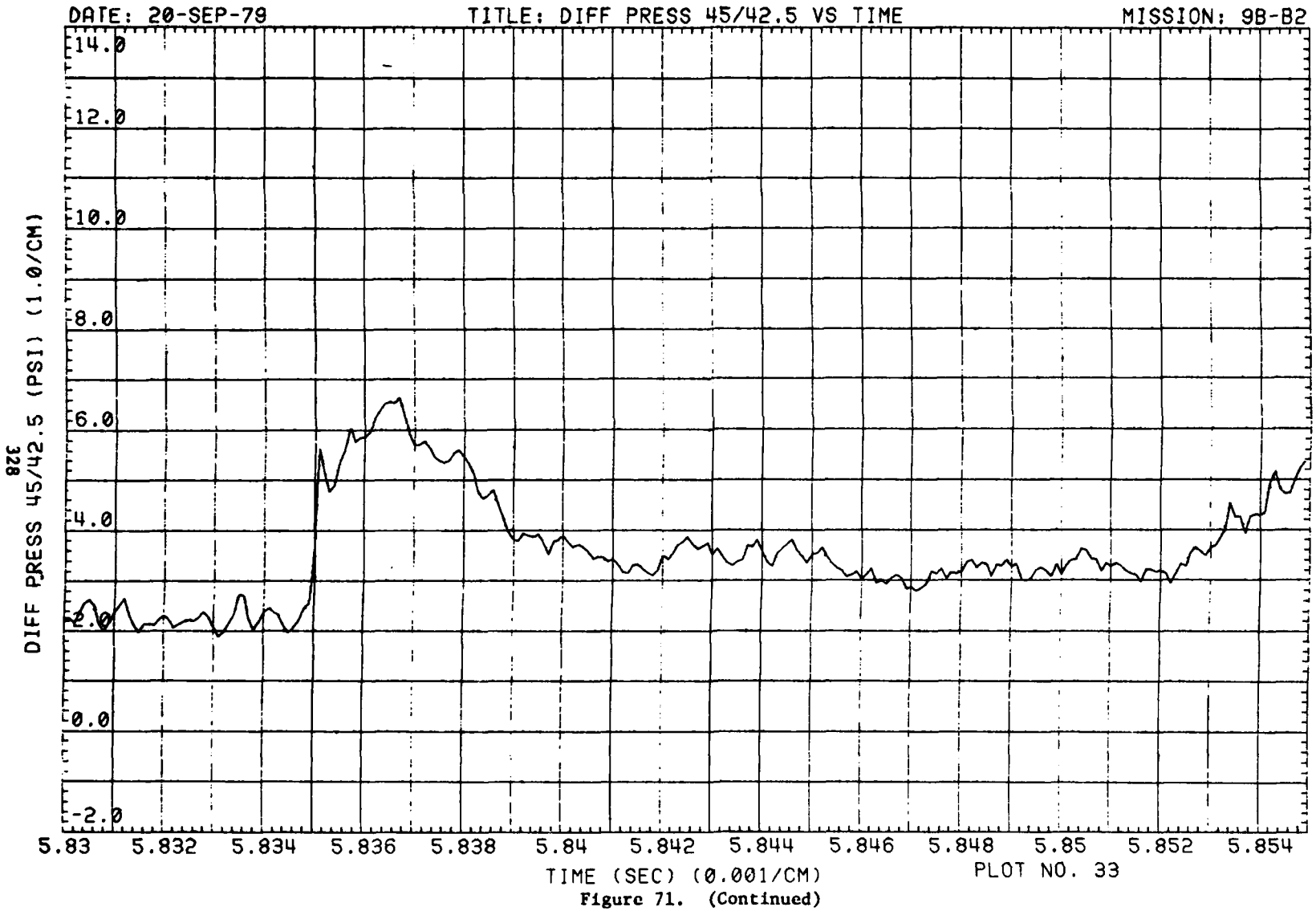

Figure 71. (Continued)

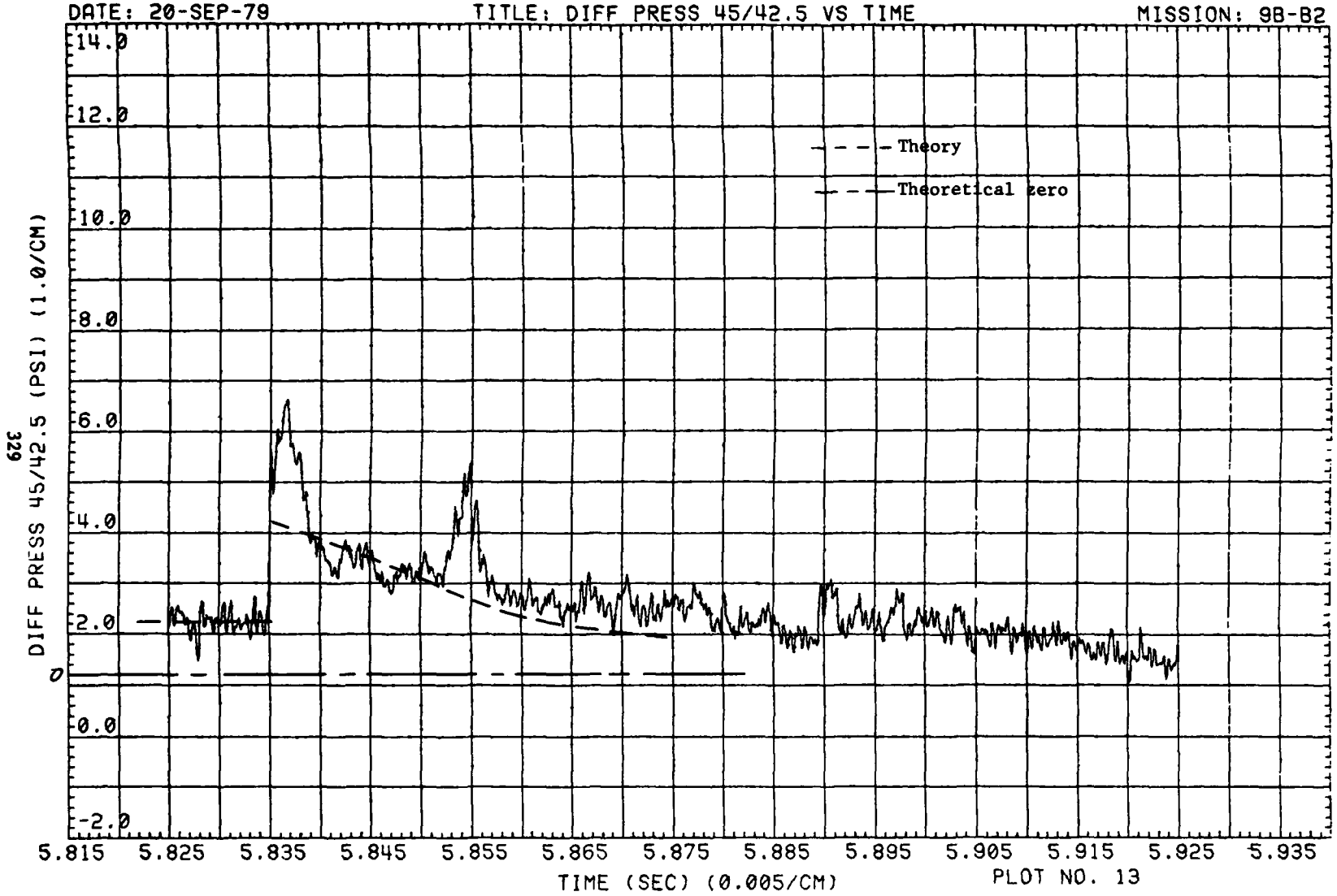

Figure 71. (Continued)

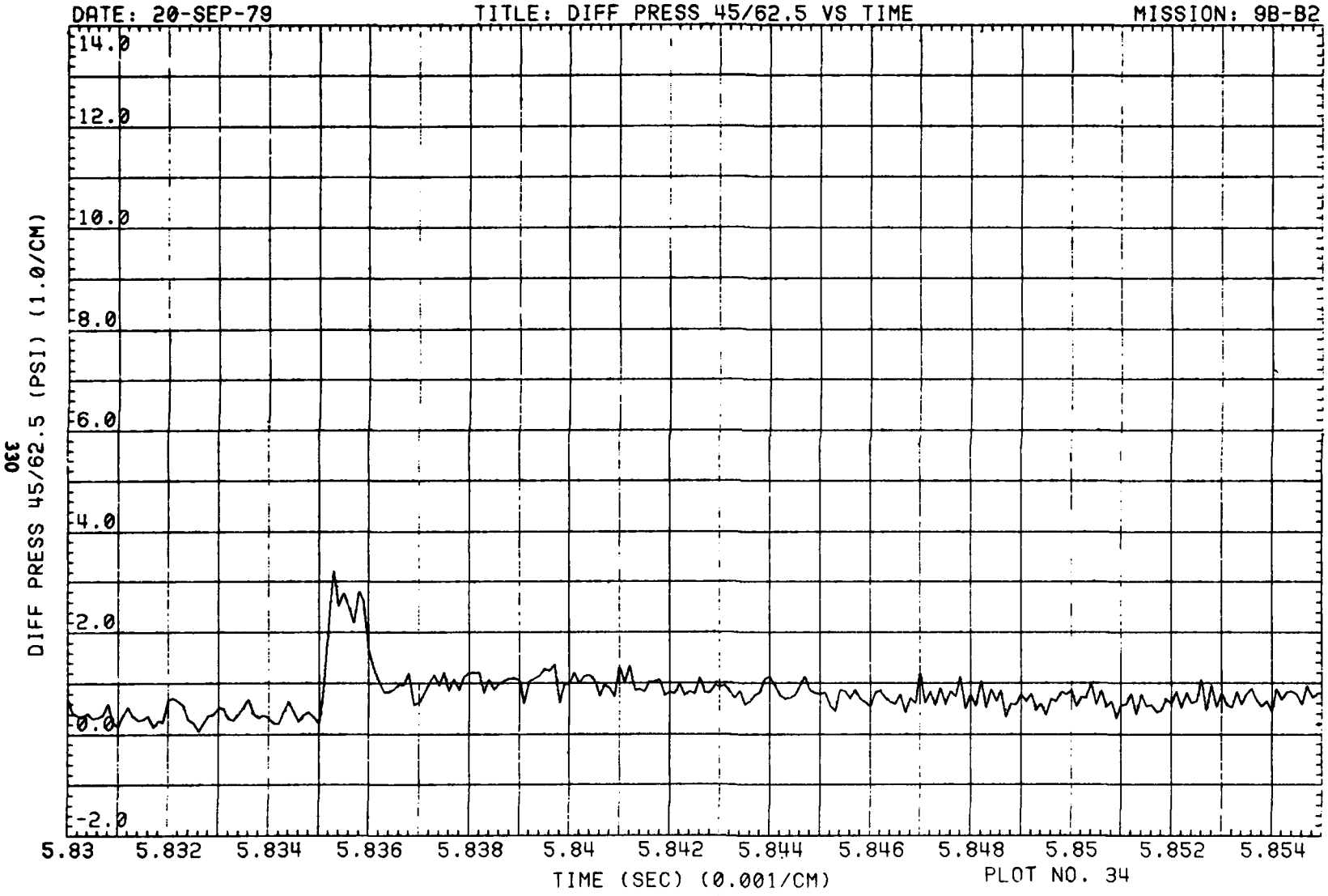

Figure 71. (Continued)

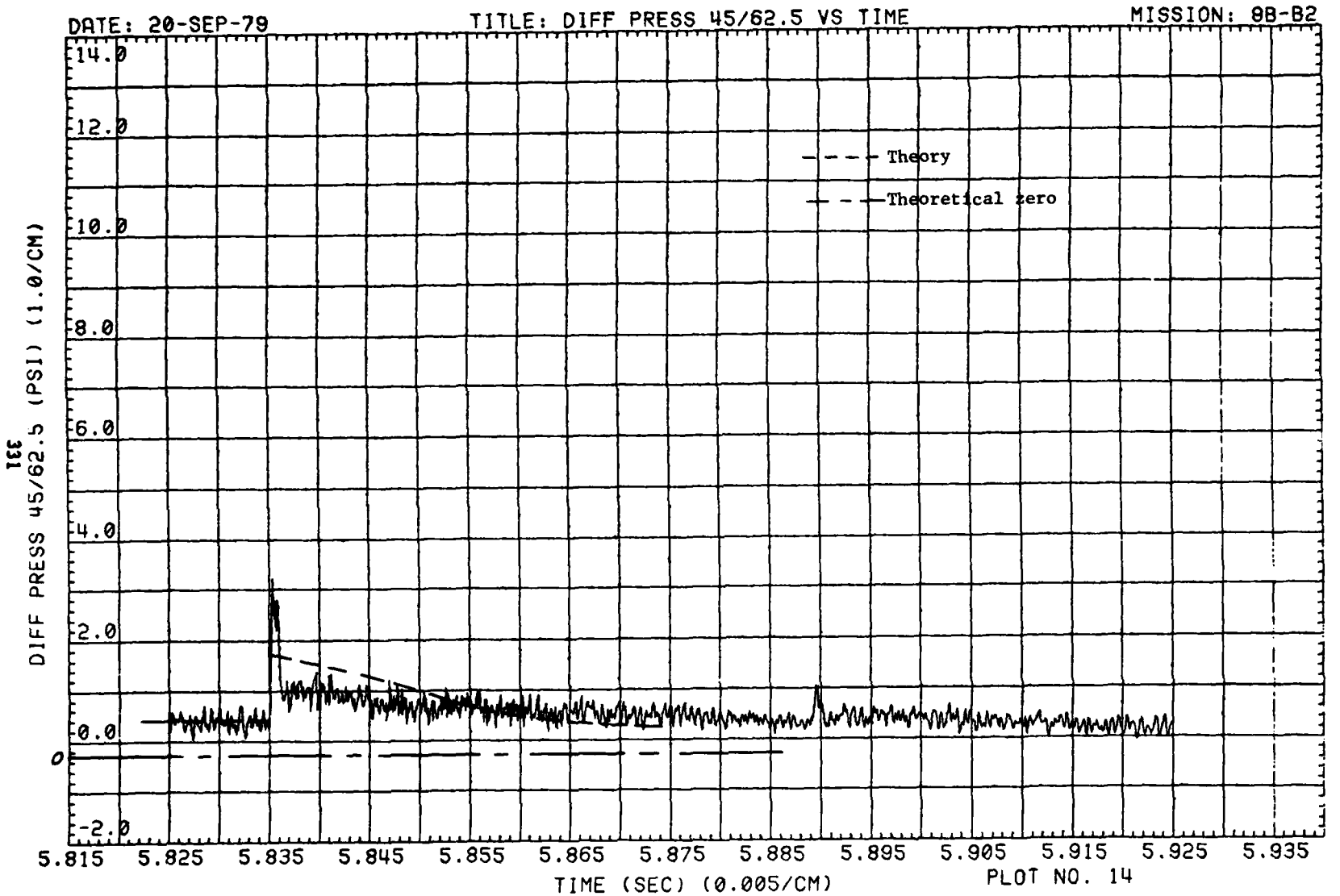

Figure 71. (Continued)

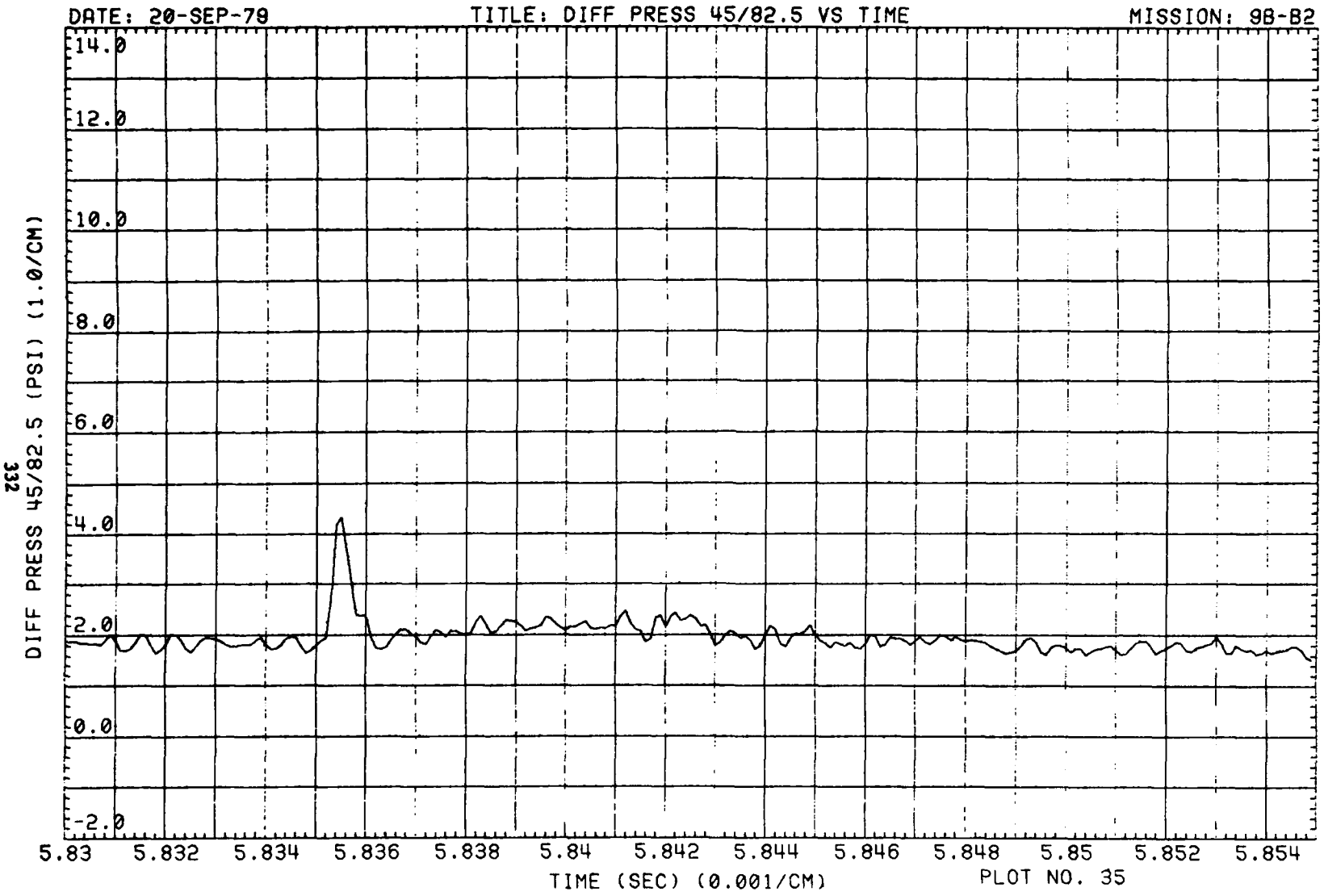

Figure 71. (Continued)

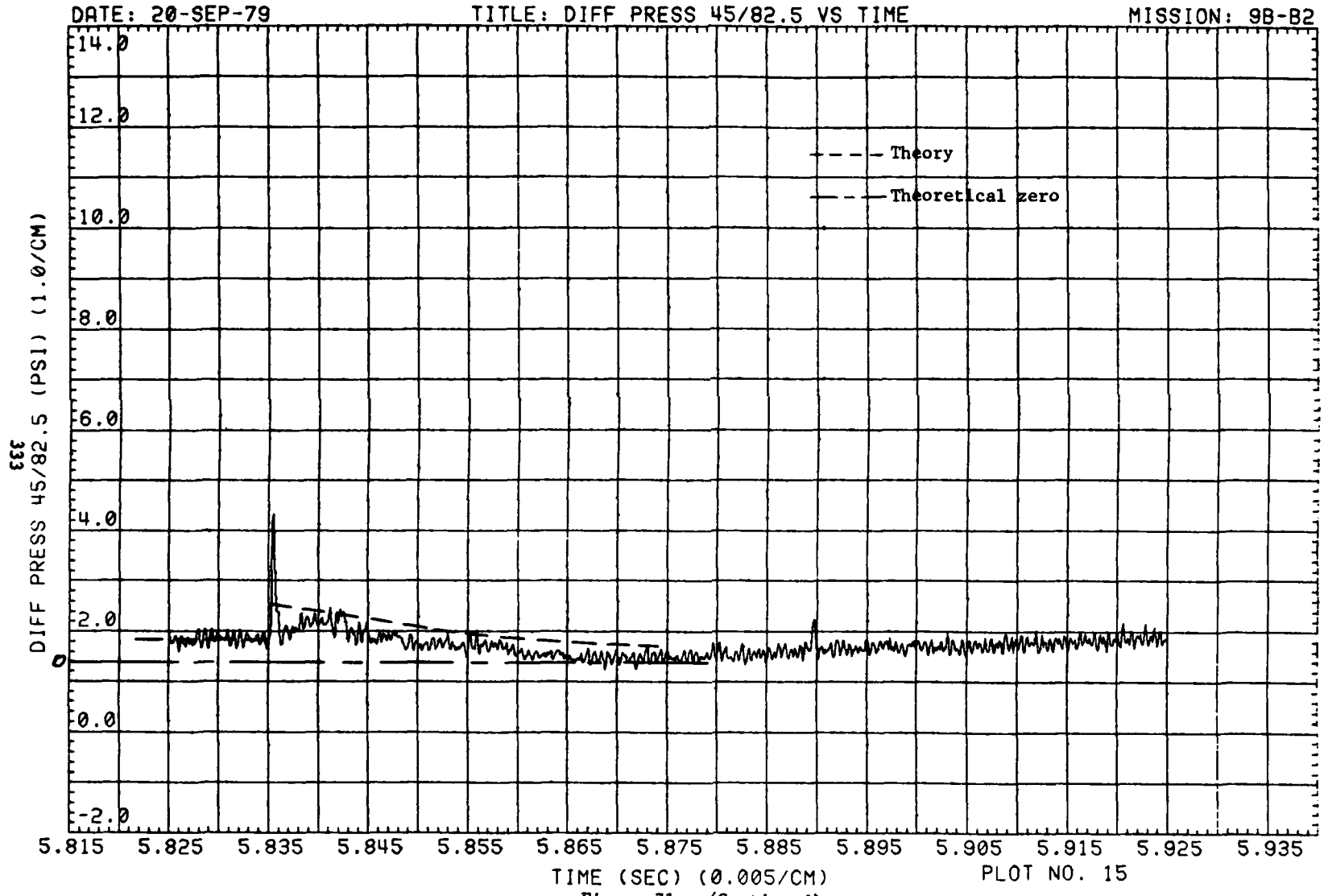

Figure 71. (Continued)

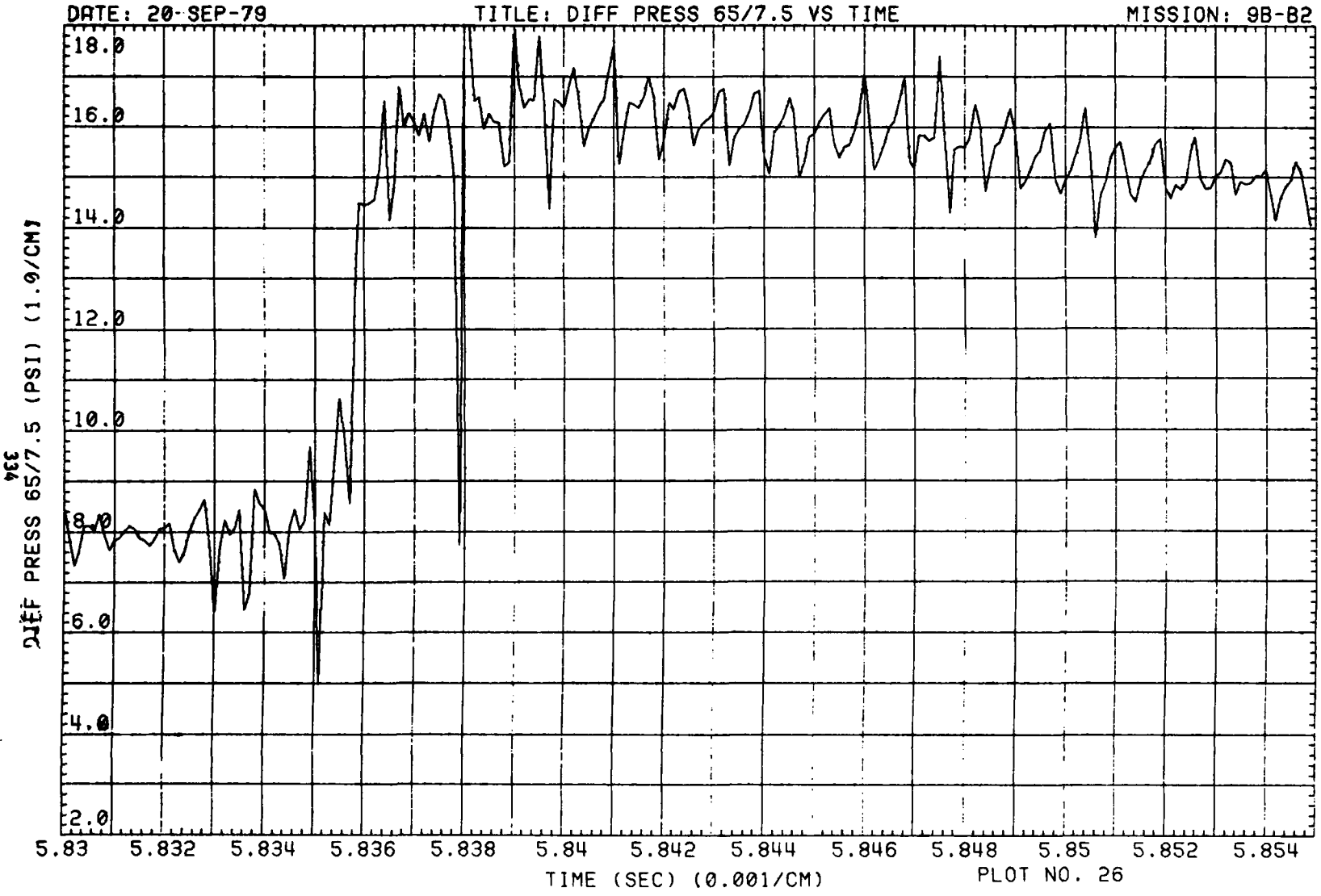

Figure 71. (Continued)

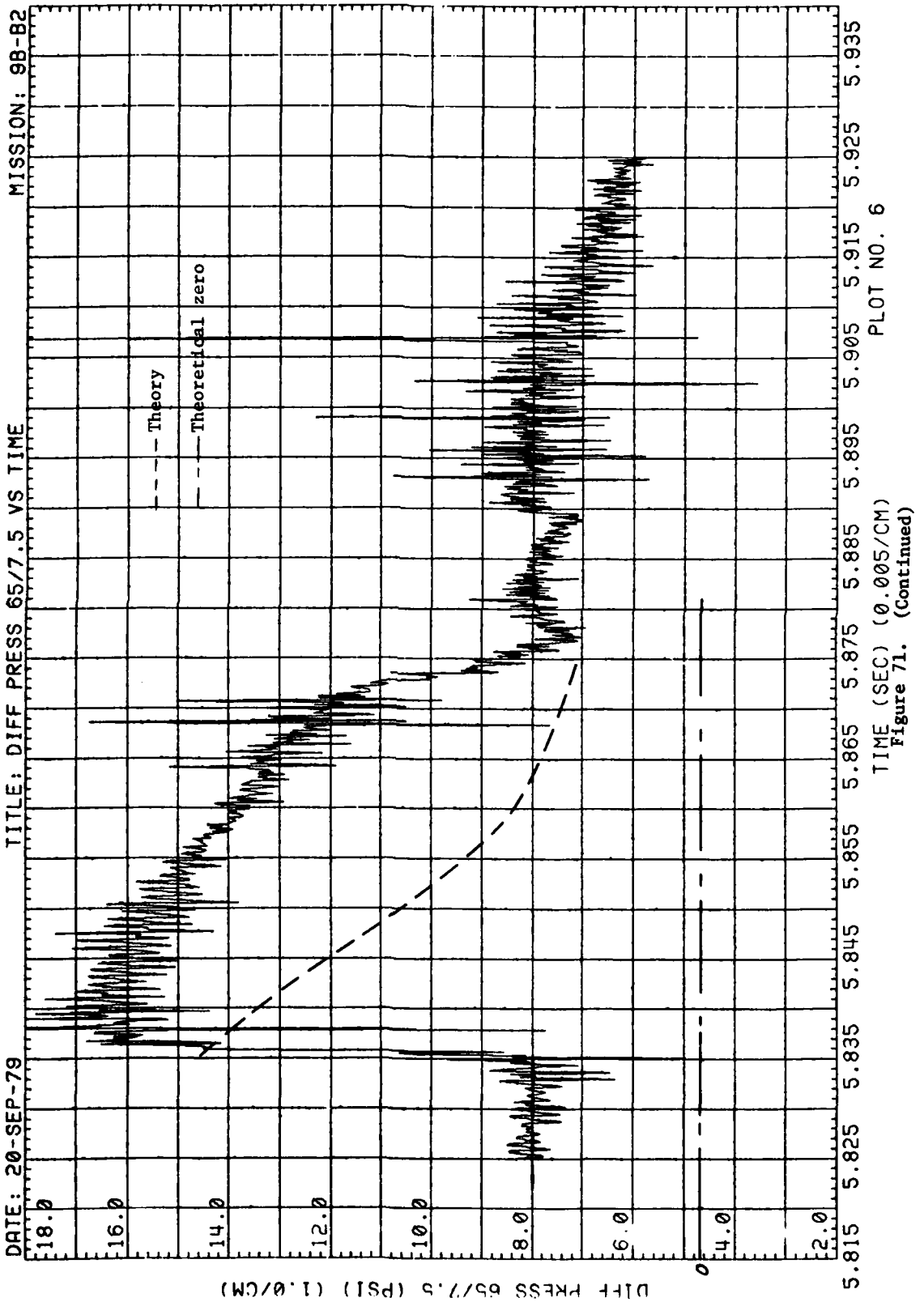

Figure 71. (Continued)

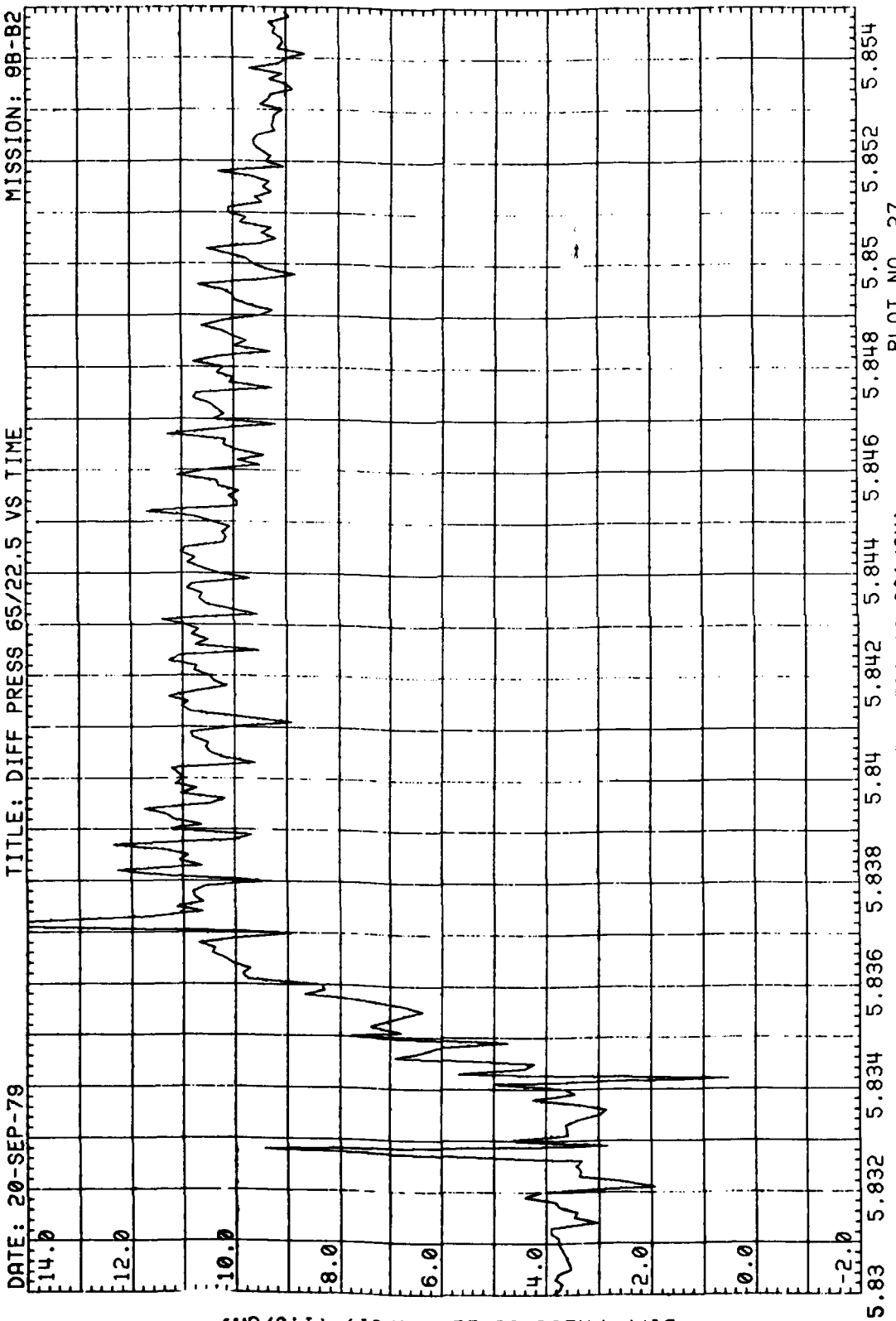

Figure 71. (Continued)

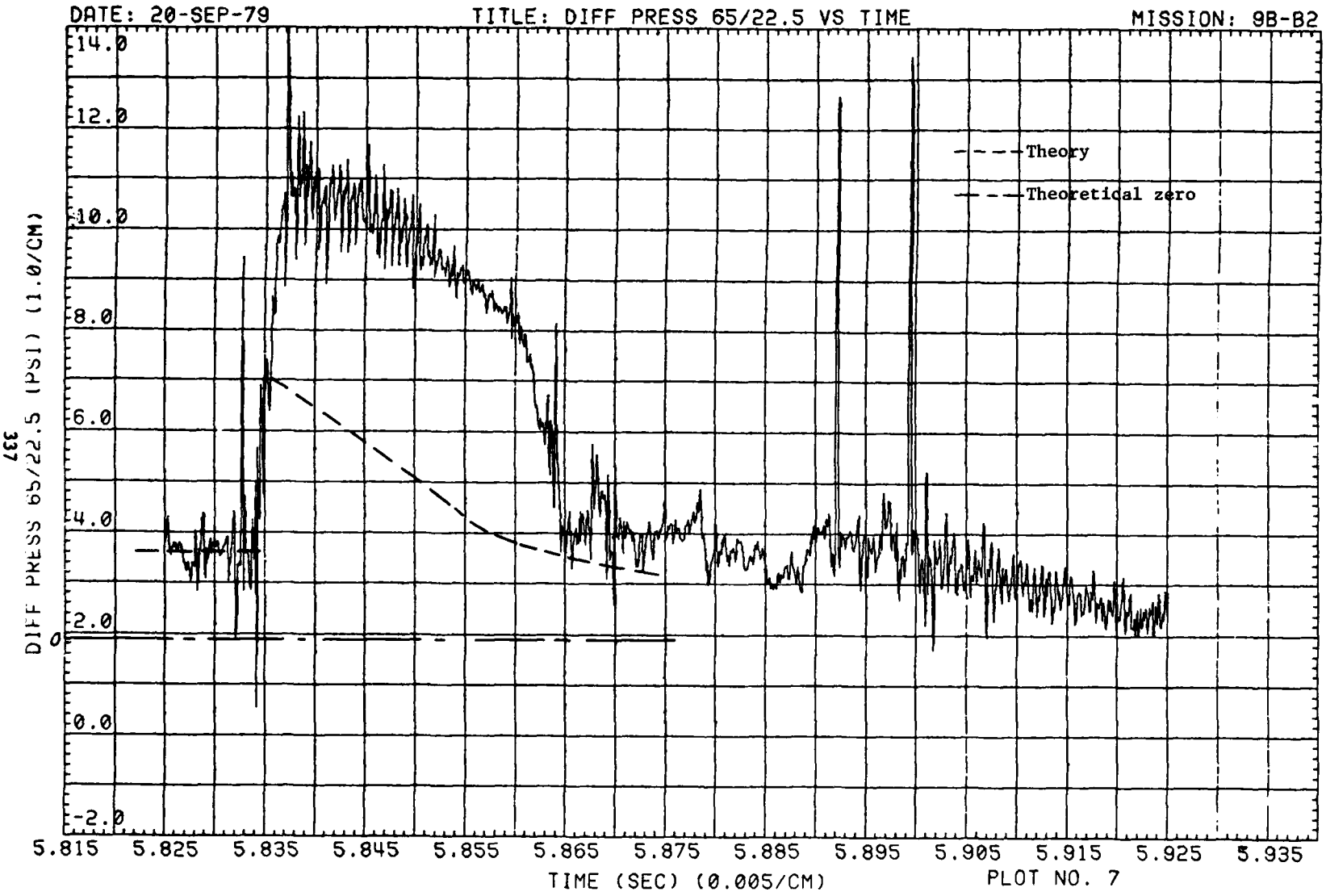

Figure 71. (Continued)

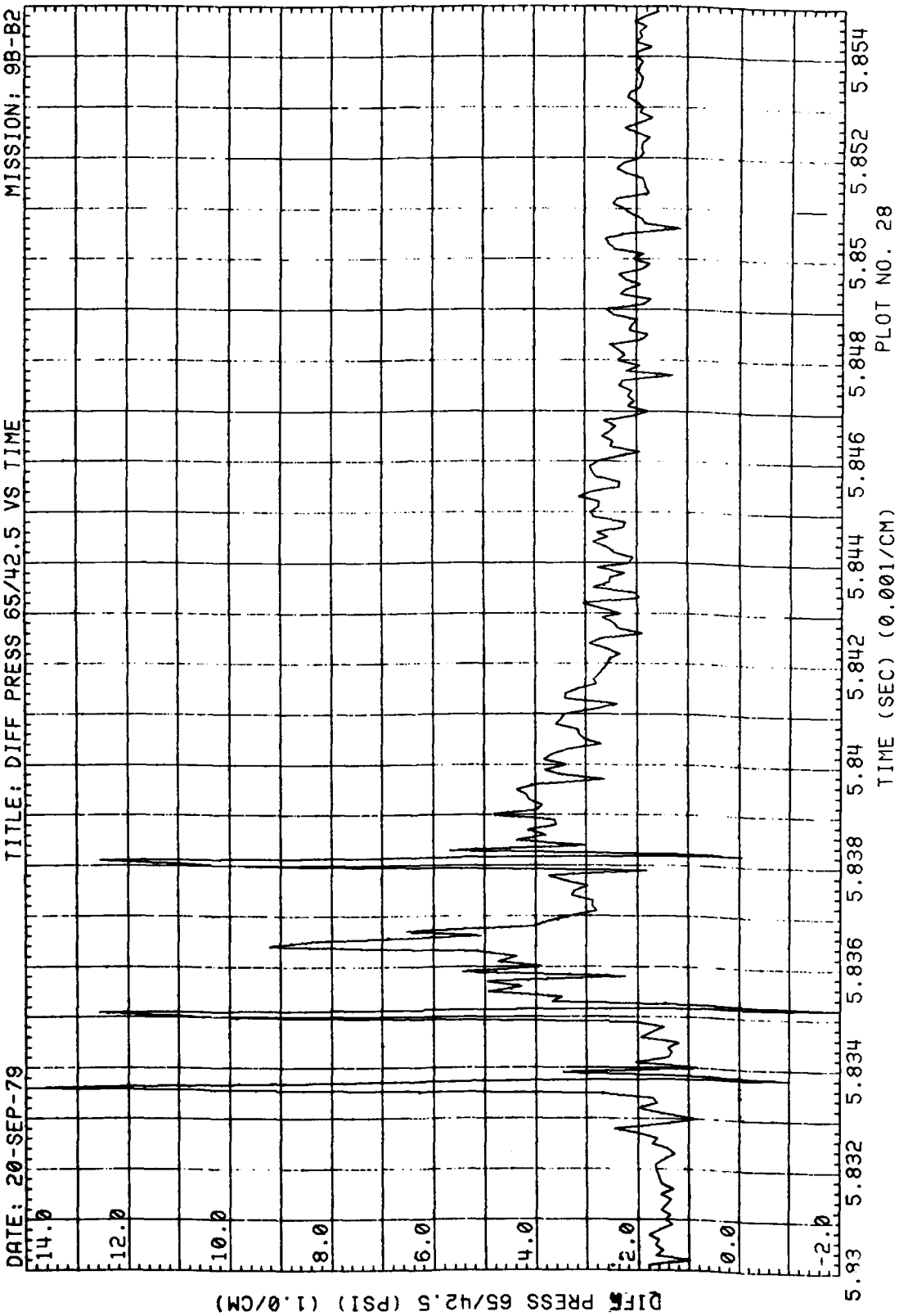

Figure 71. (Continued)

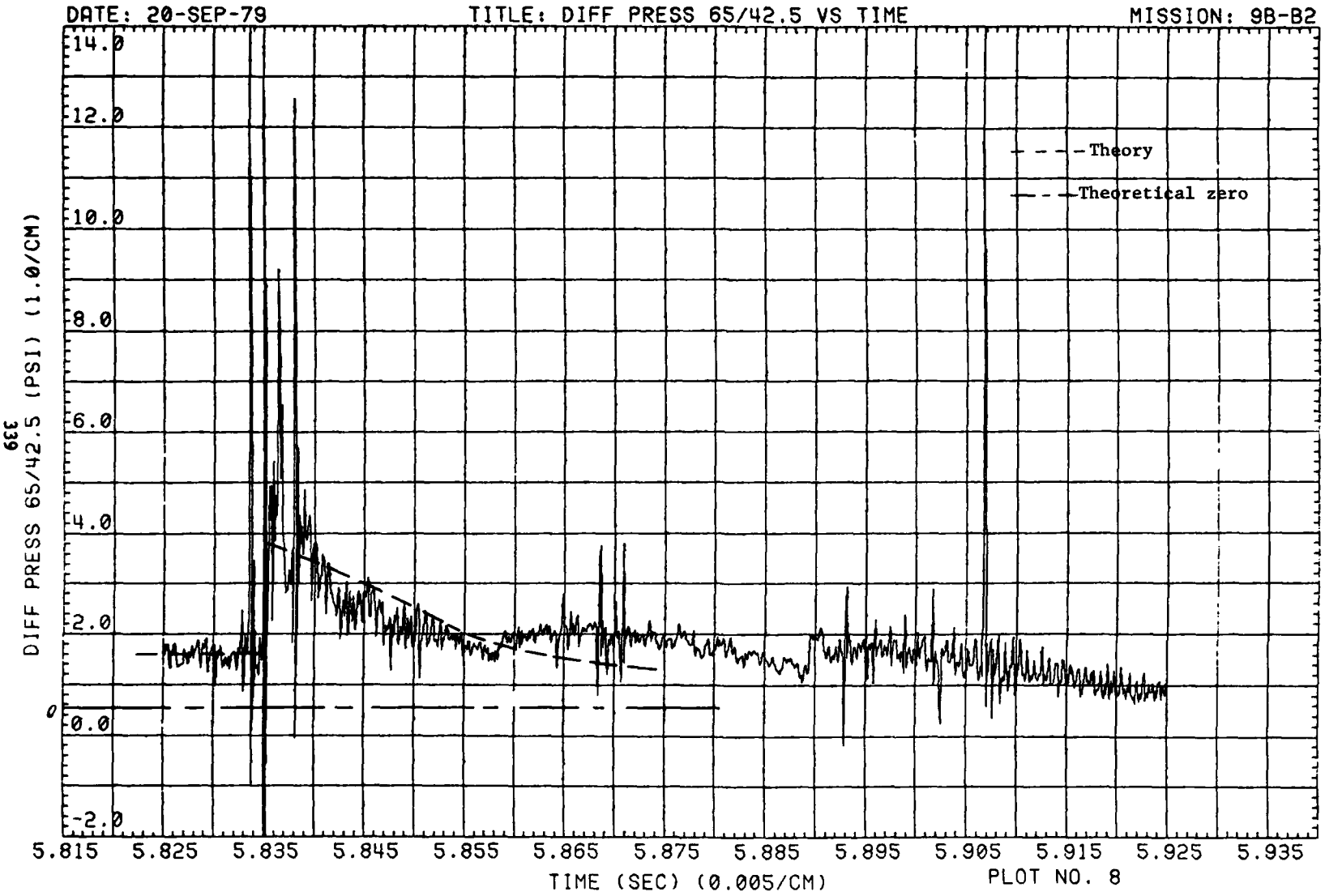

Figure 71. (Continued)

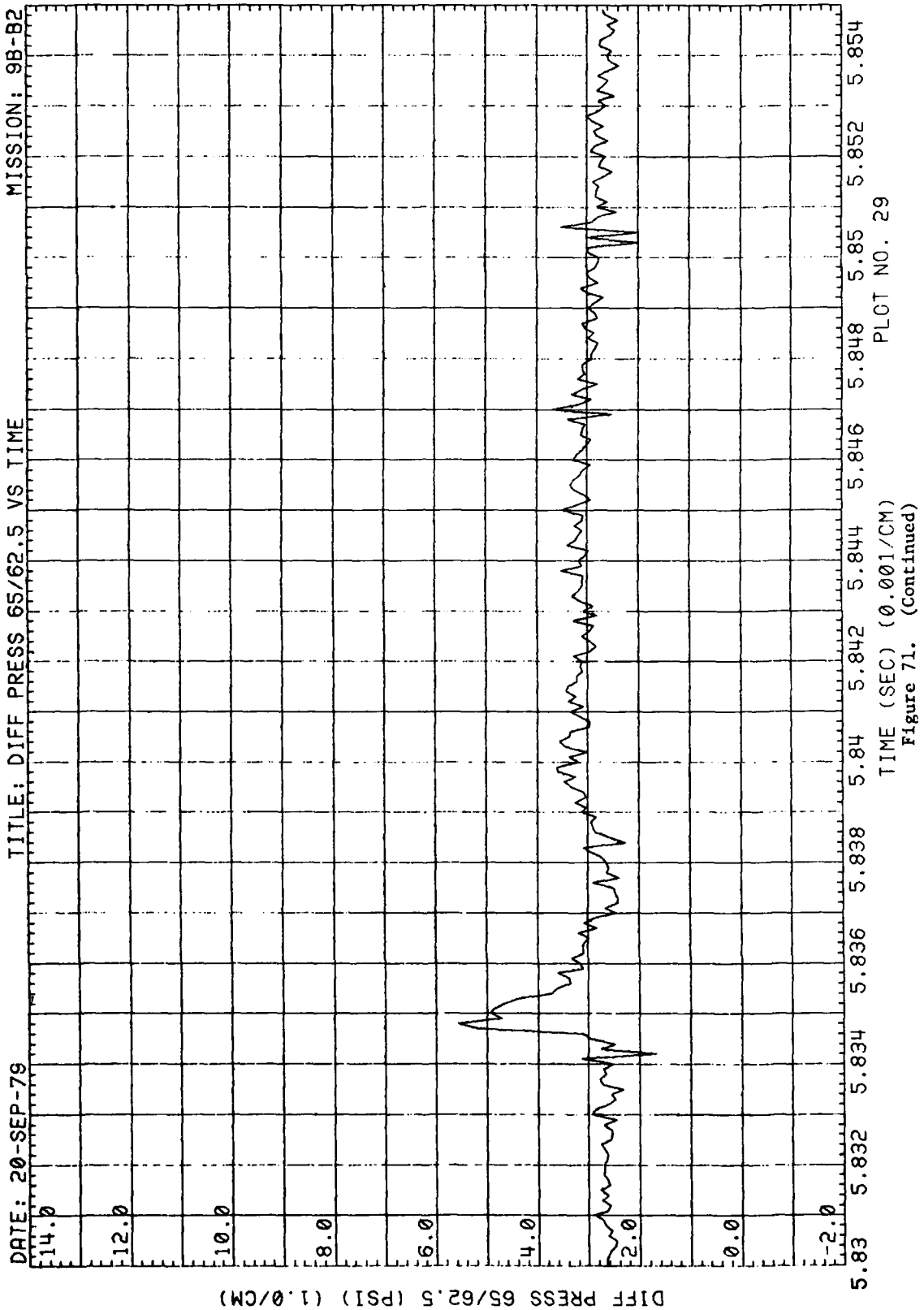

Figure 71. (Continued)

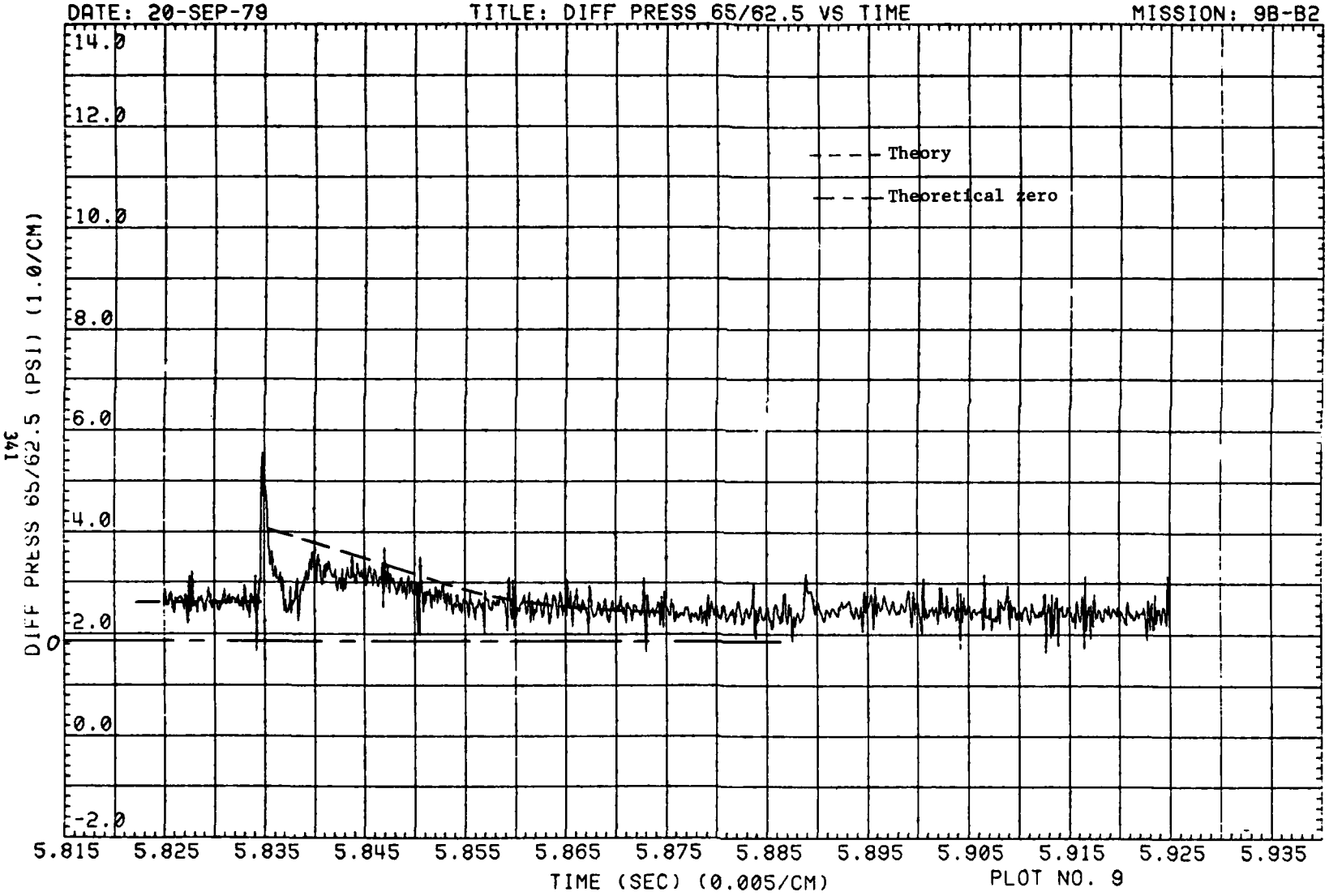

Figure 71. (Continued)

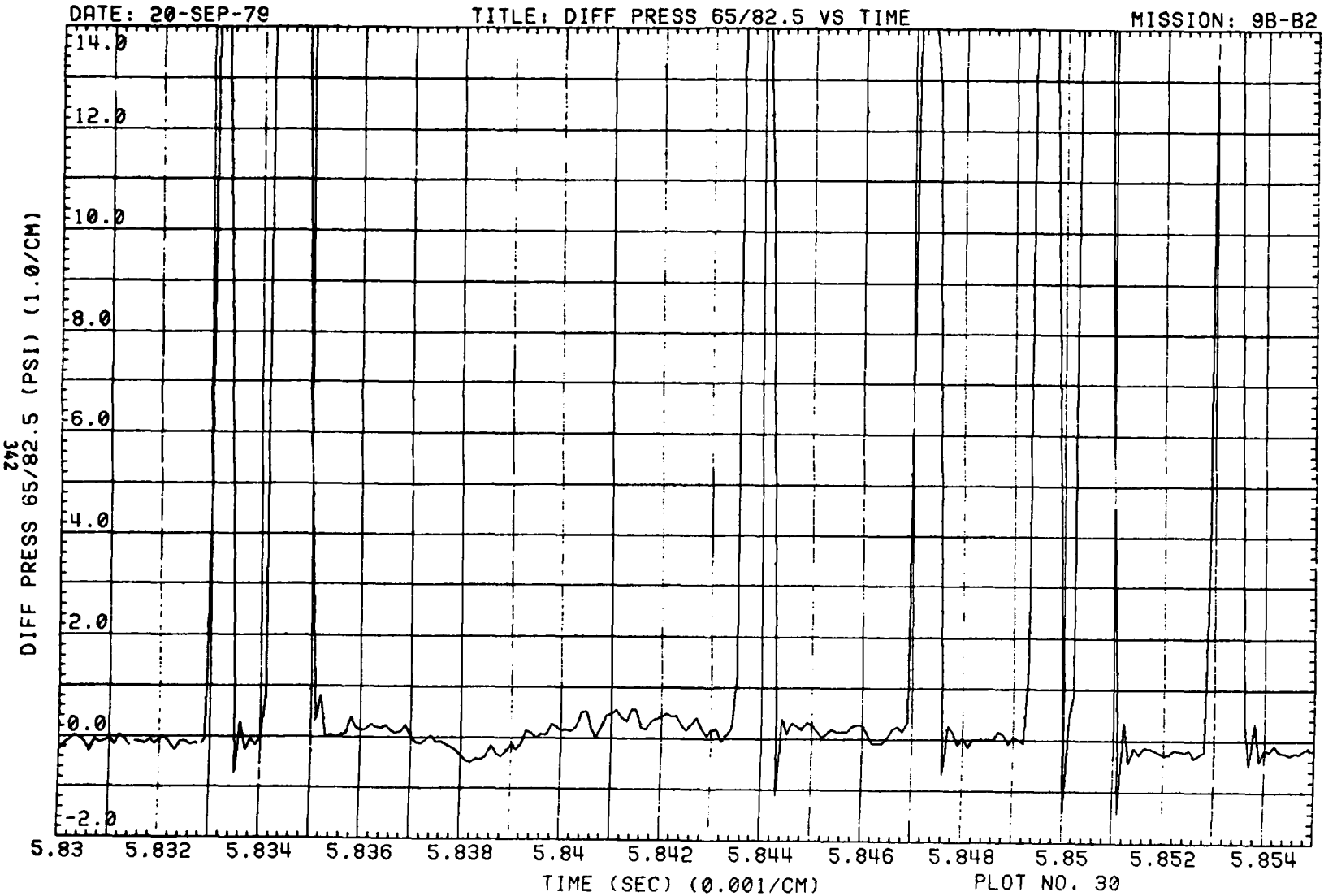

Figure 71. (Continued)

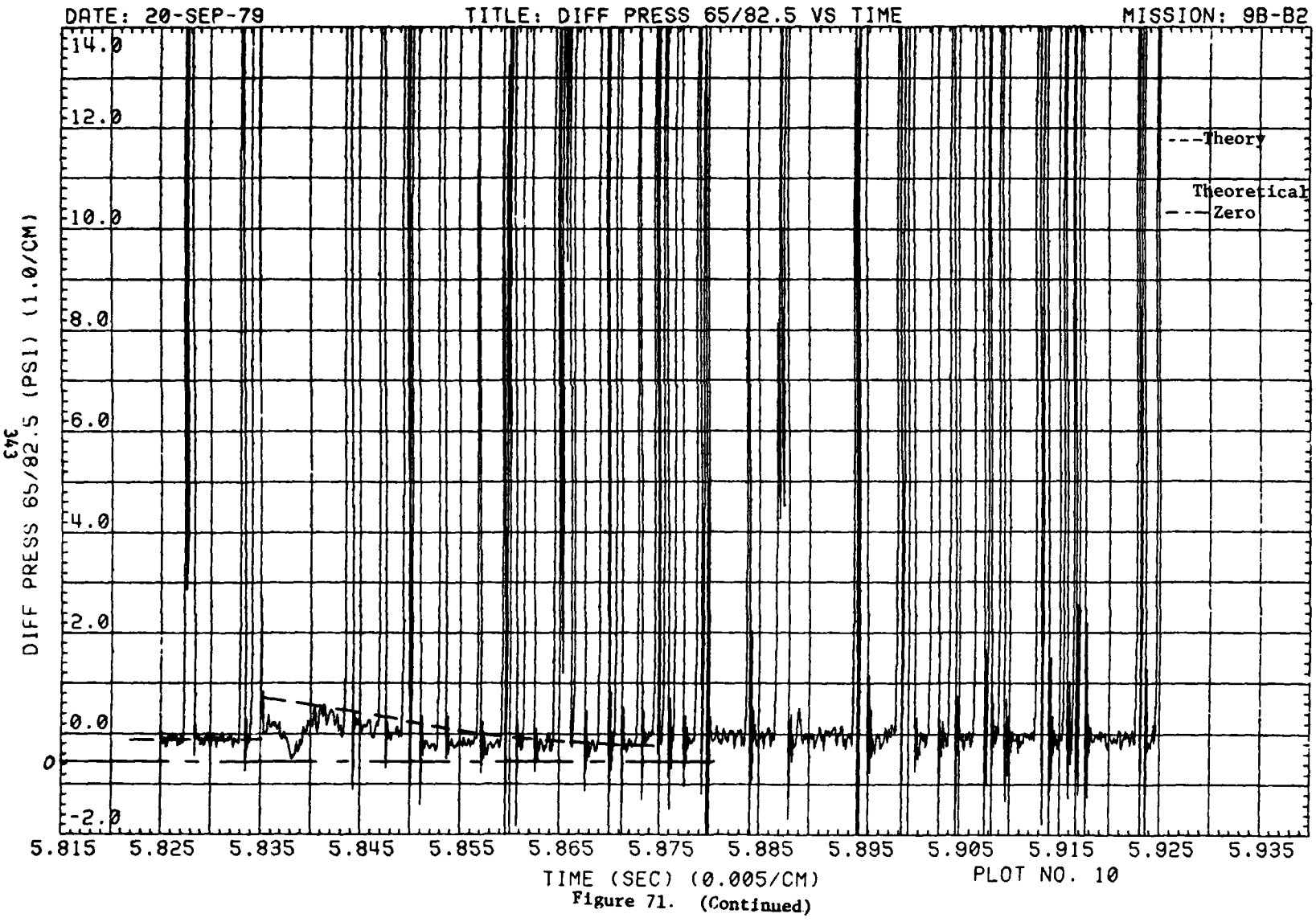

Figure 71. (Continued)

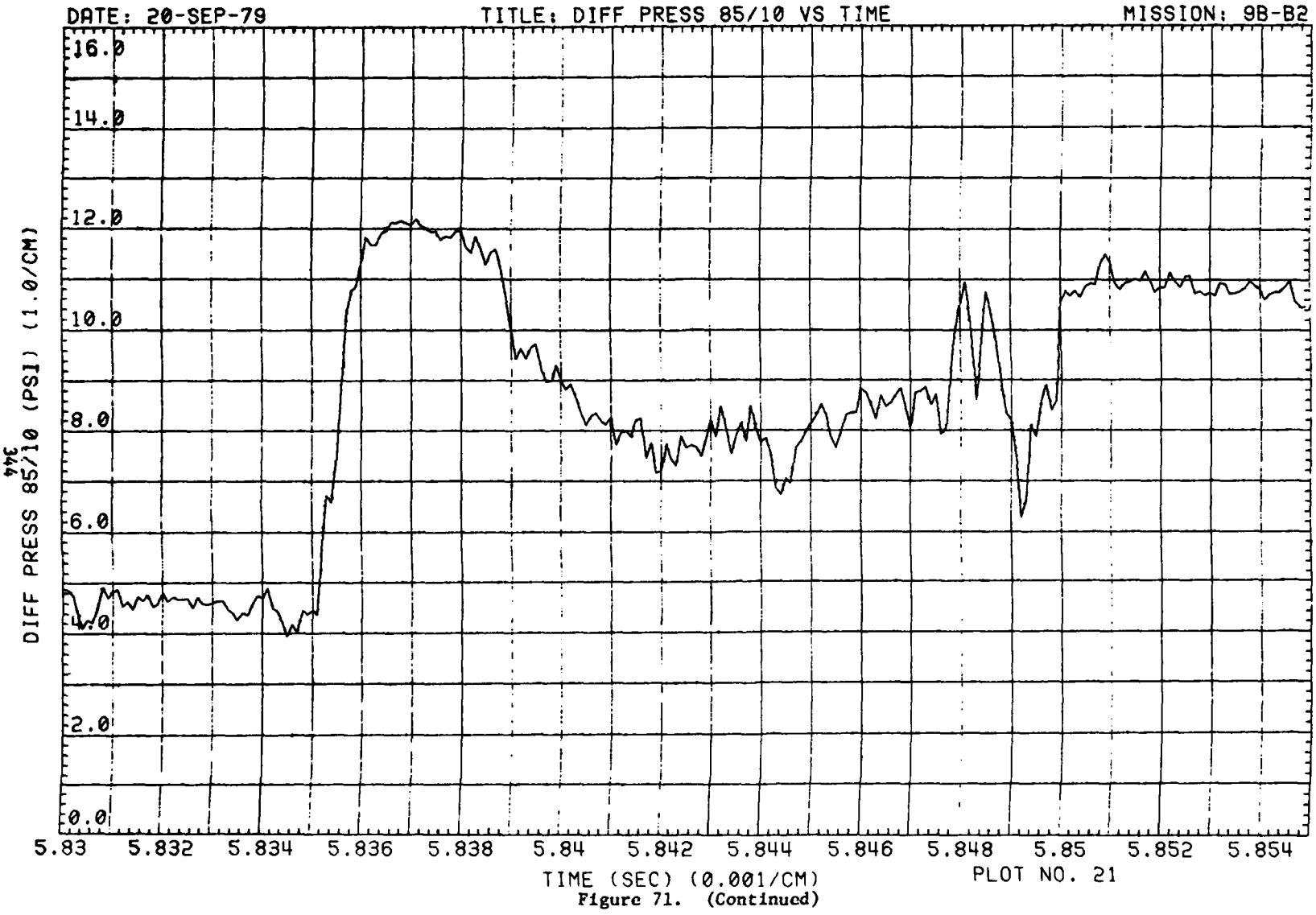

Figure 71. (Continued)

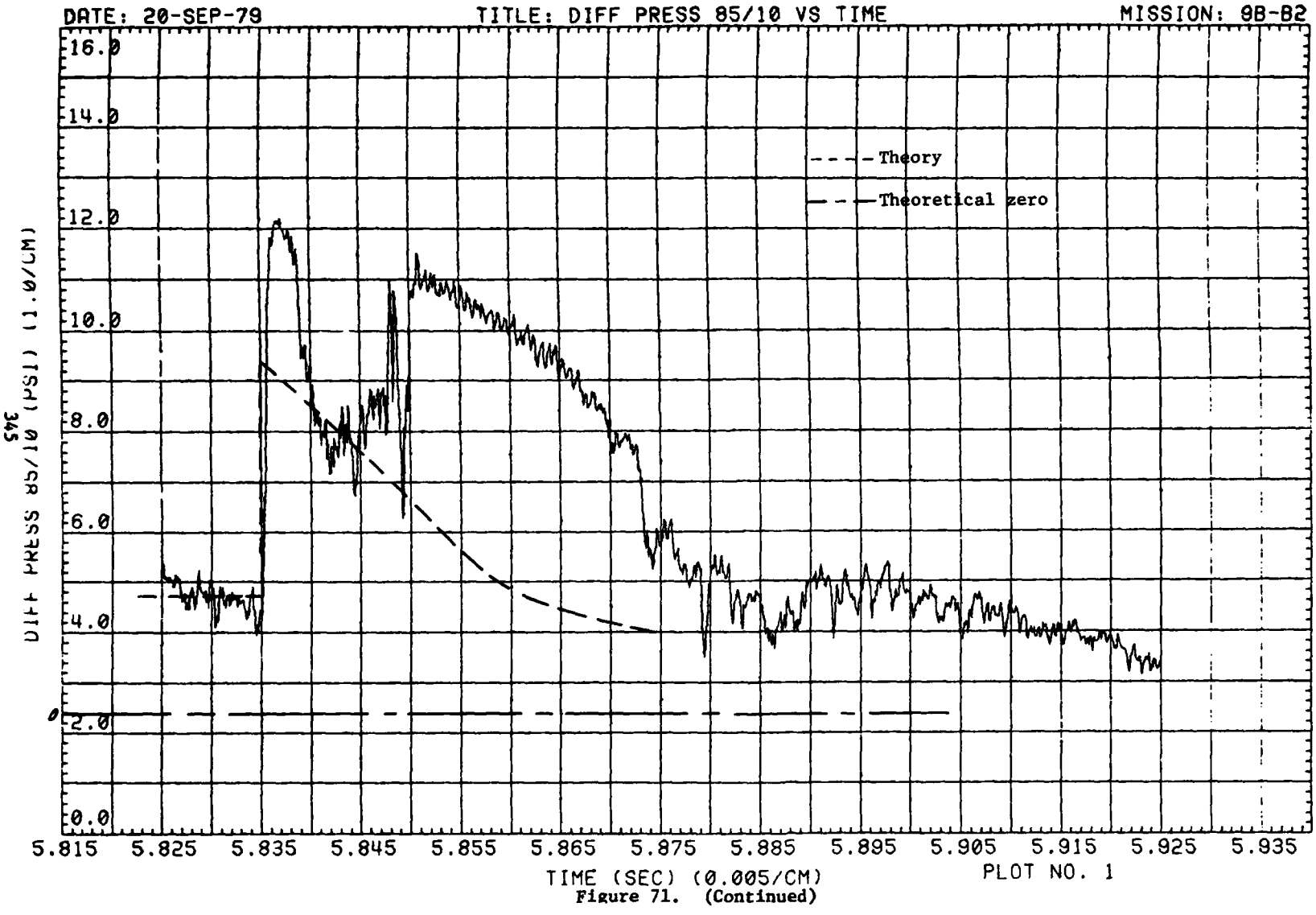

Figure 71. (Continued)

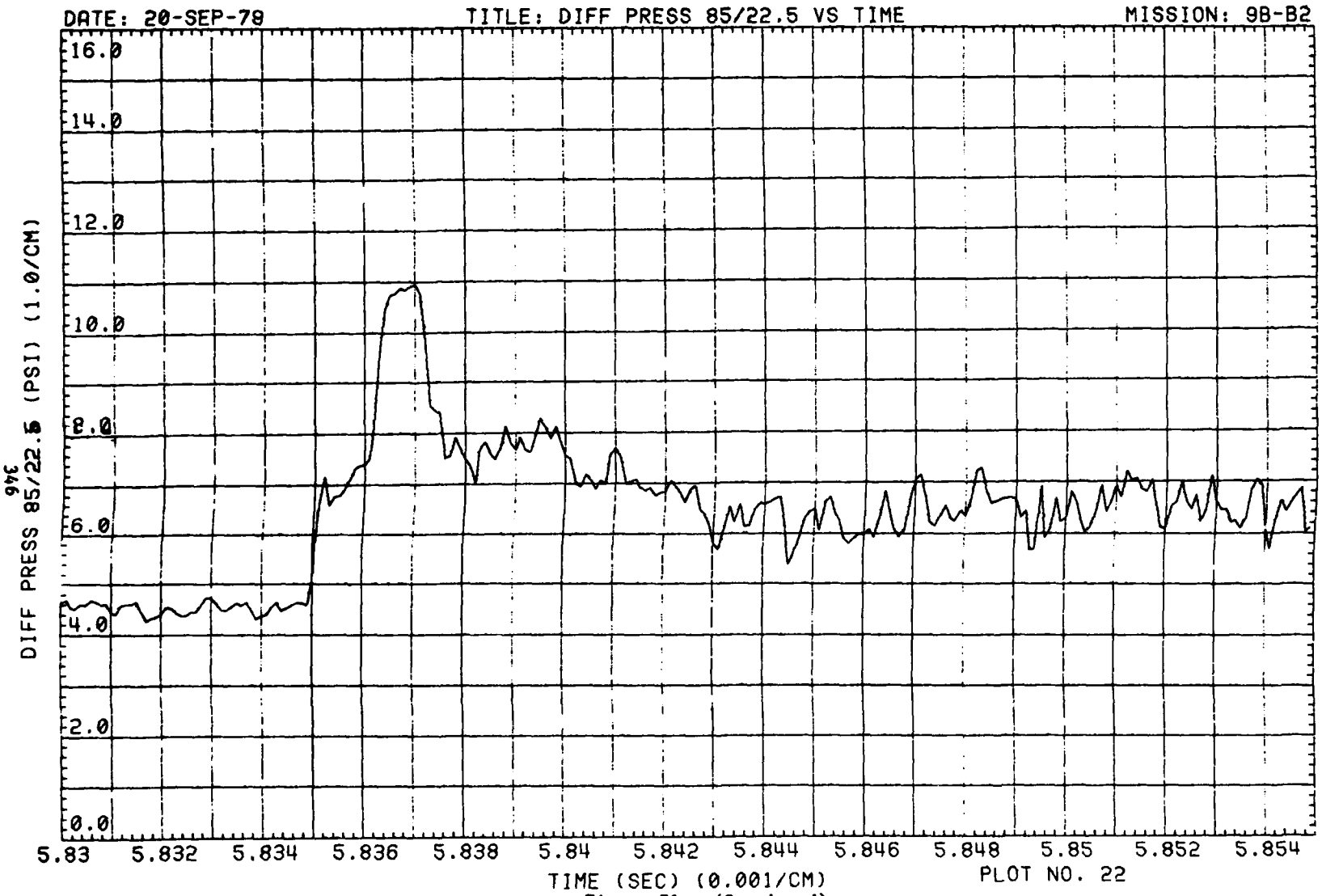

Figure 71. (Continued)

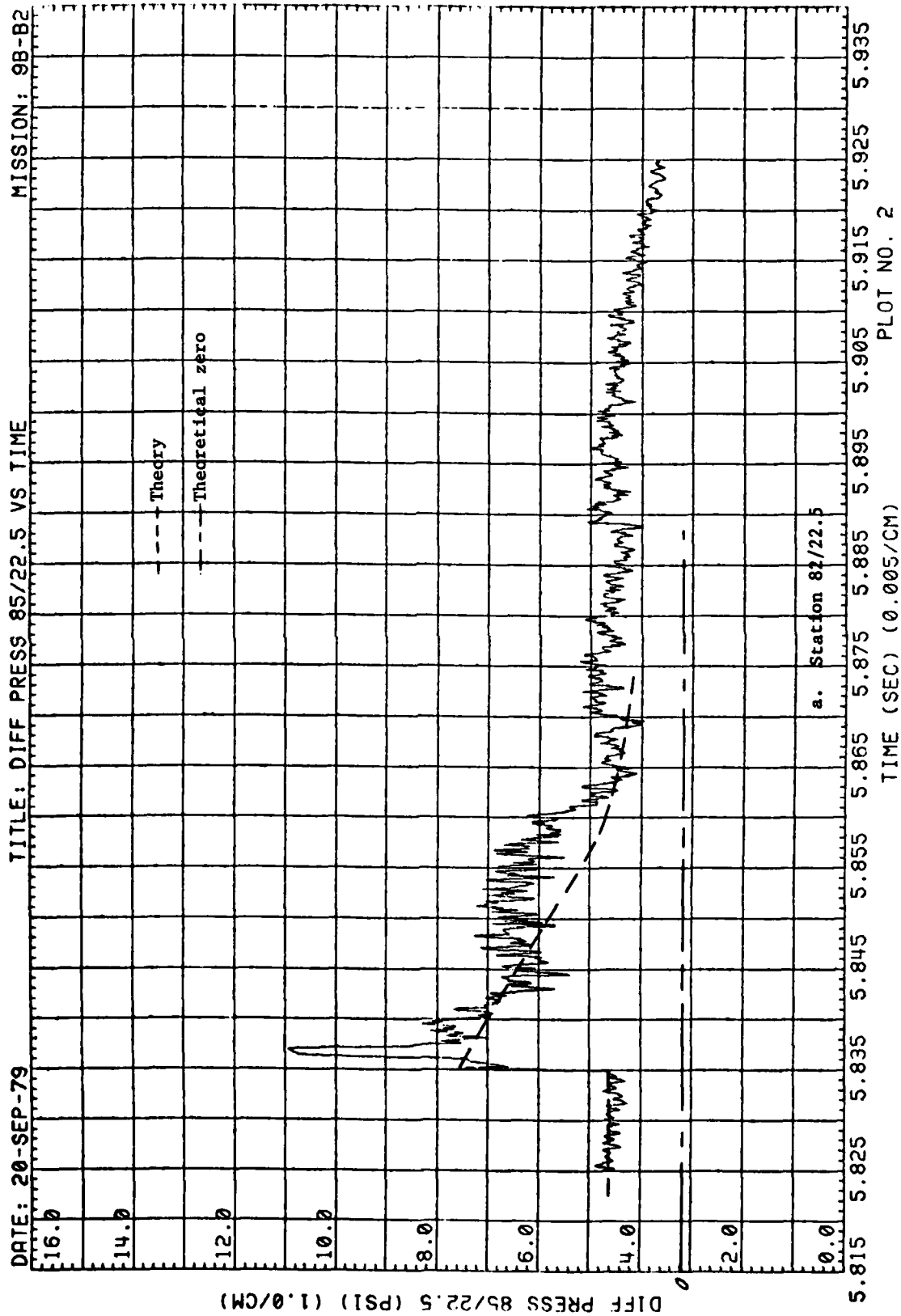

Figure 71. (Continued)

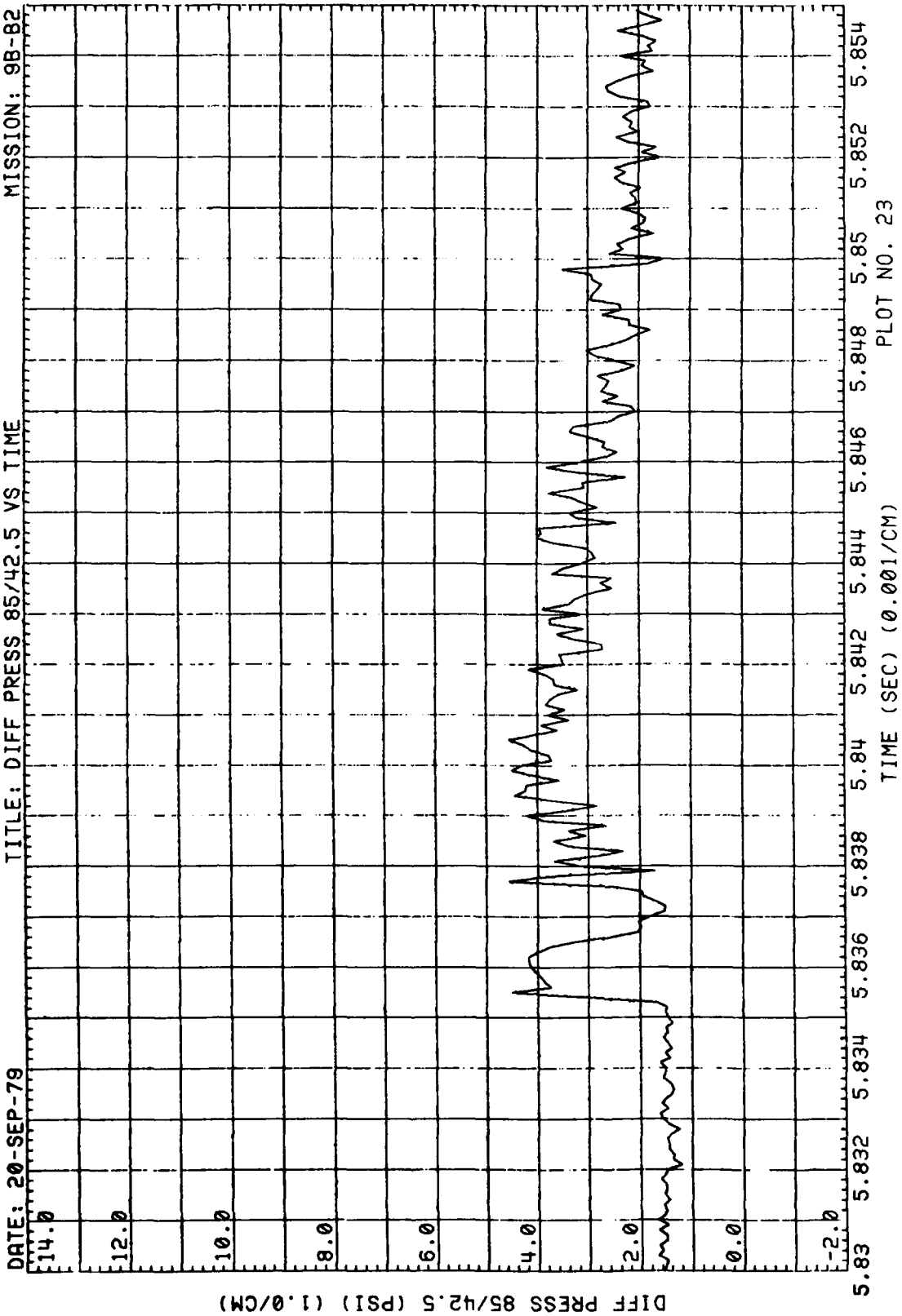

Figure 71. (Continued)

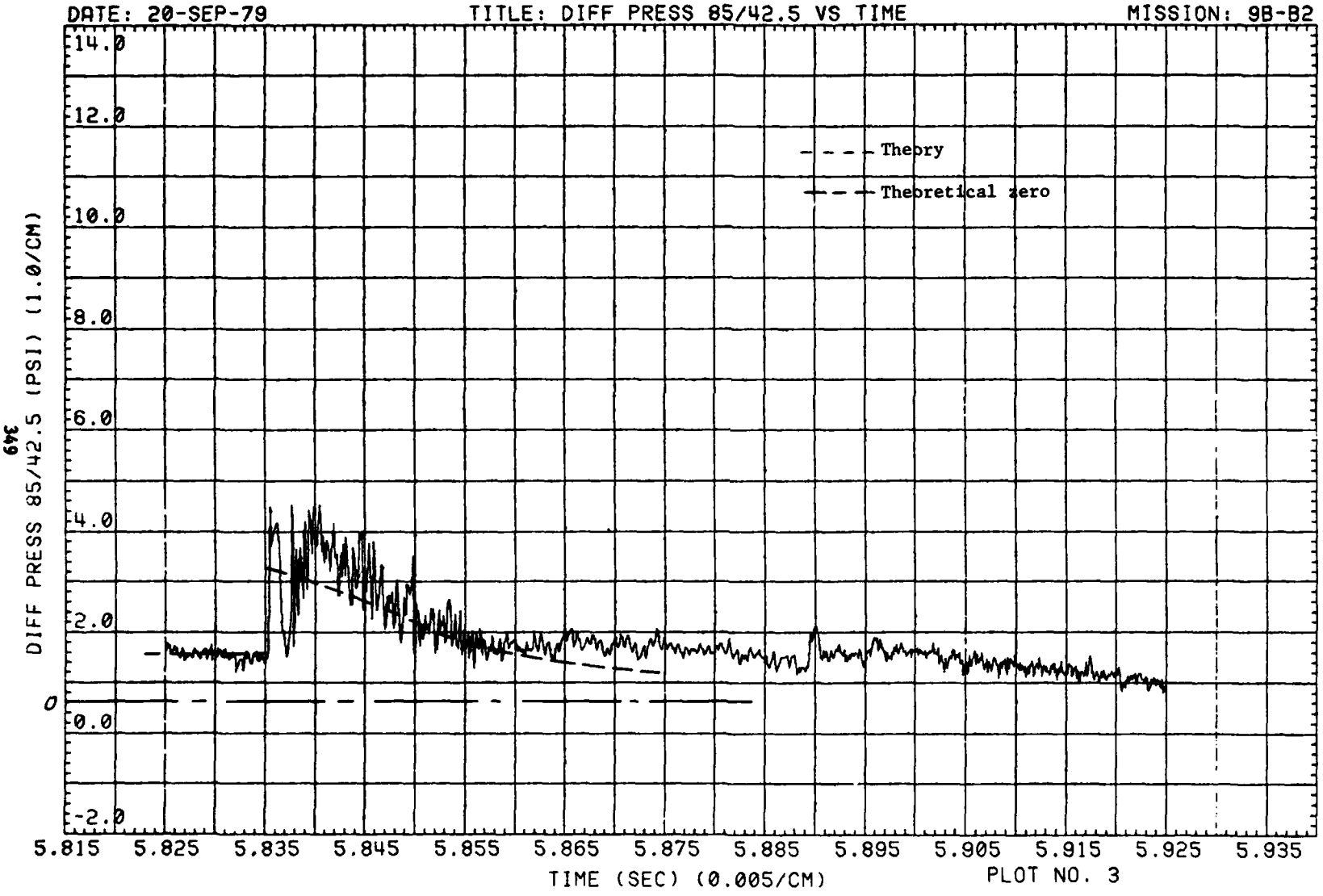

Figure 71. (Continued)

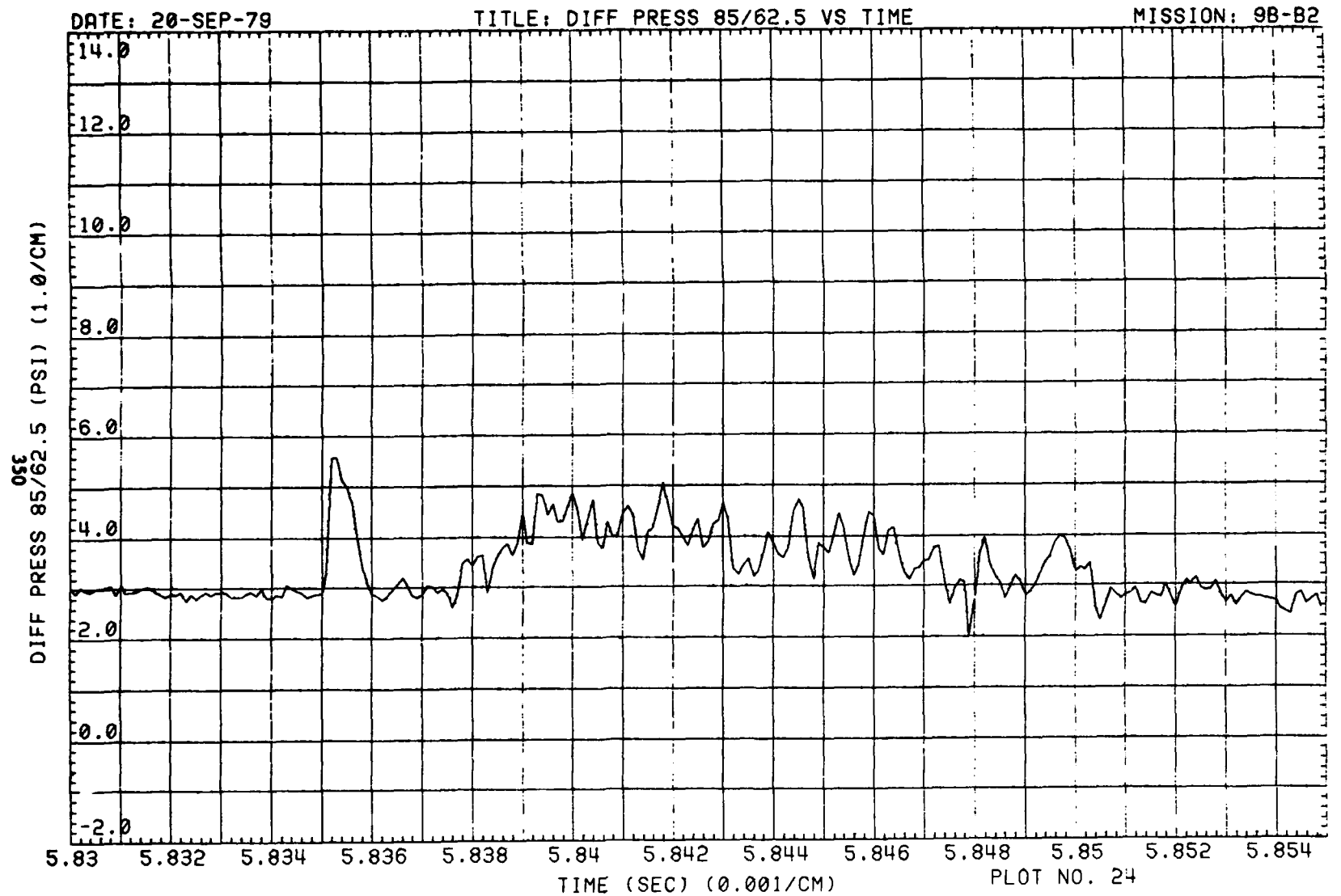

Figure 71. (Continued)

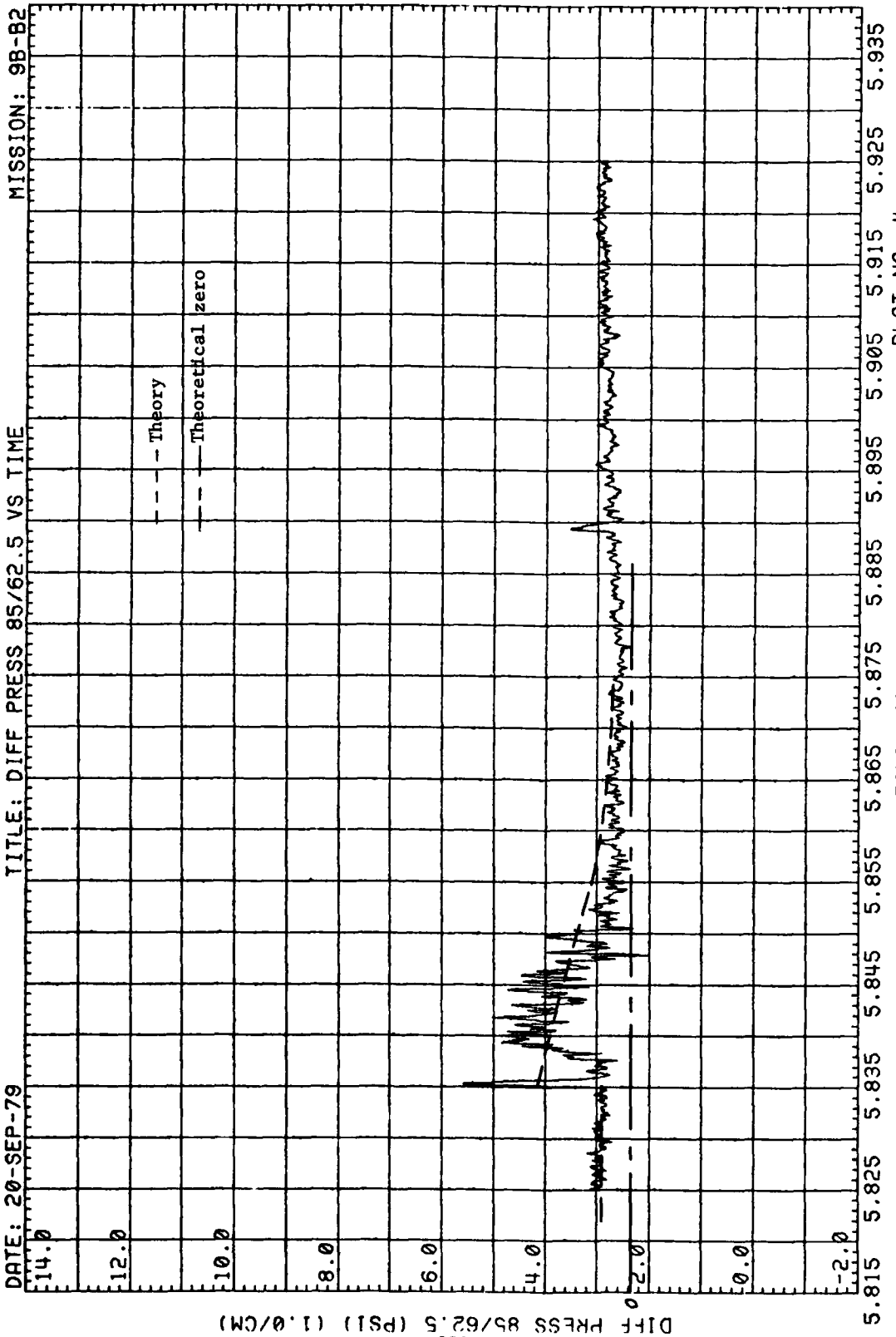

Figure 71. (Continued)

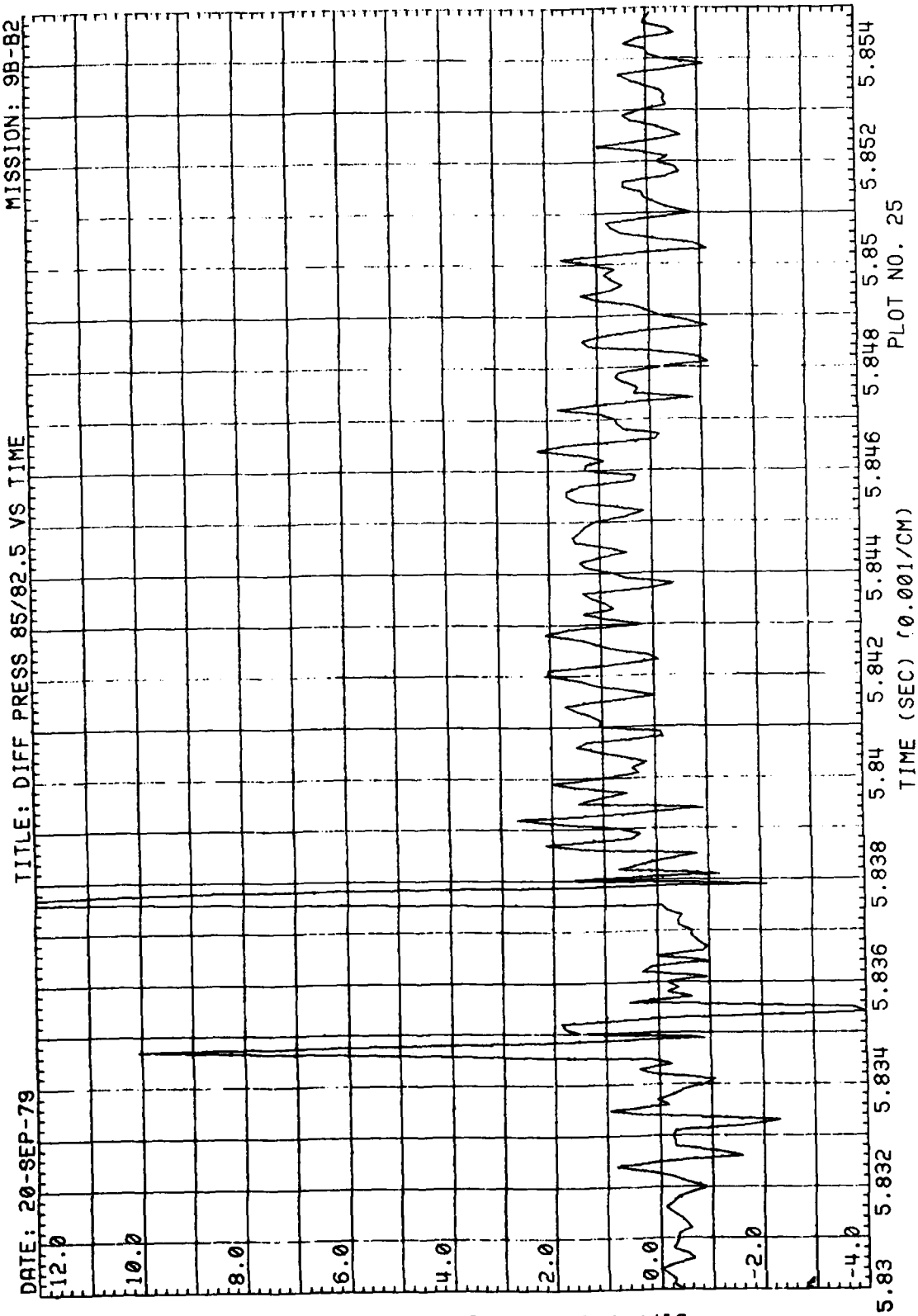

Figure 71. (Continued)

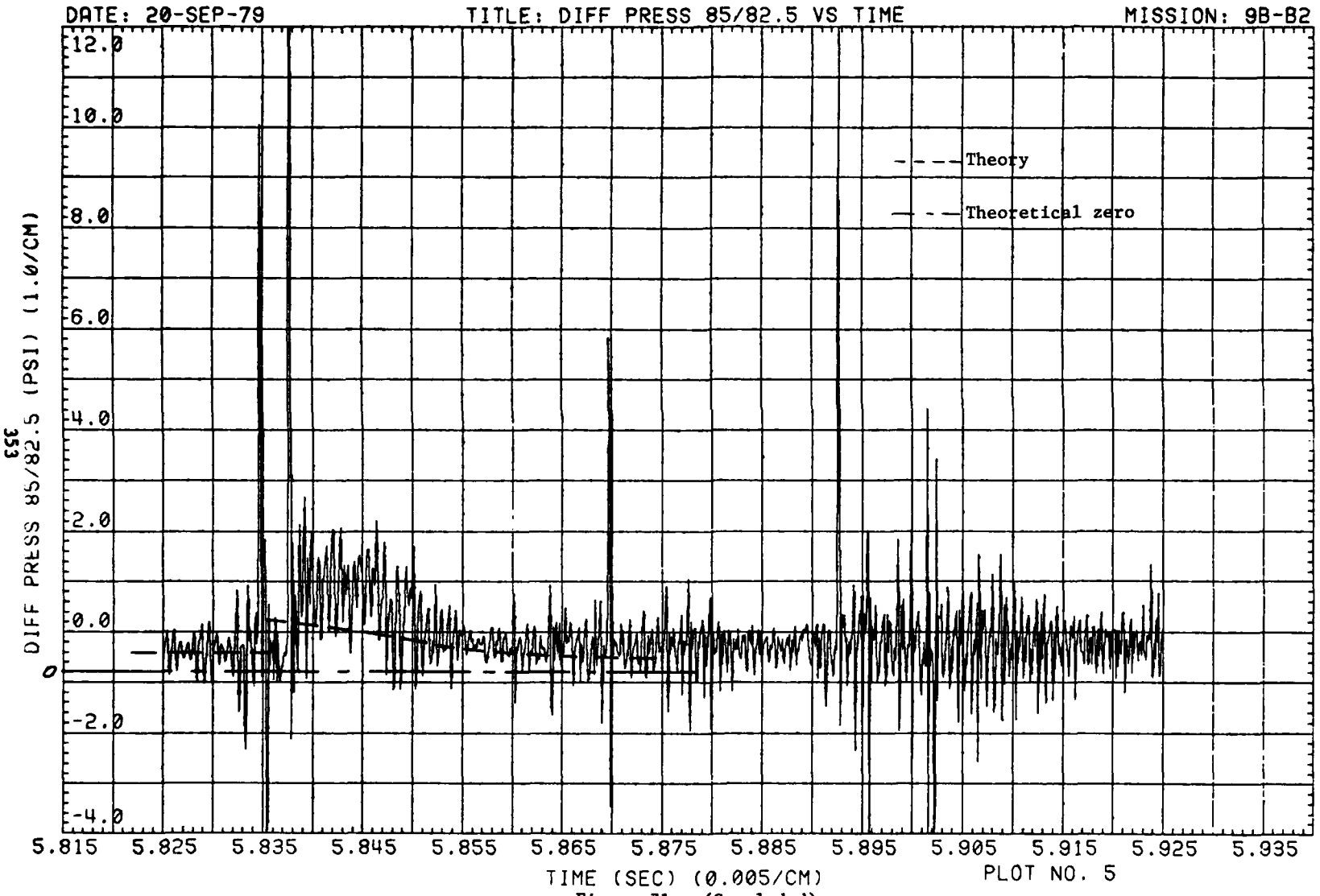

Figure 71. (Concluded)

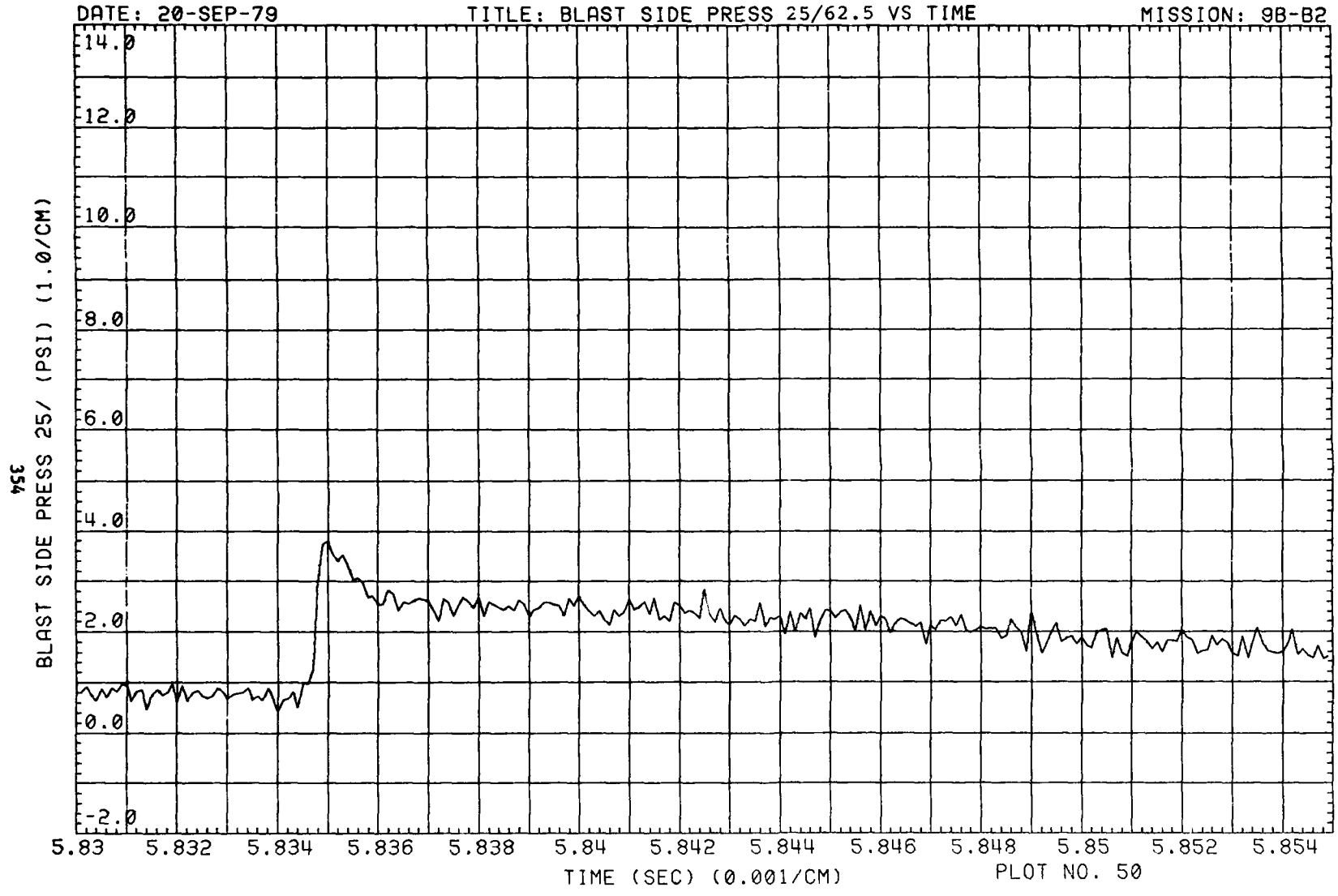

Figure 72. Blastward and Leeward Wing Pressures, Run 9B-B2, Intercept 2

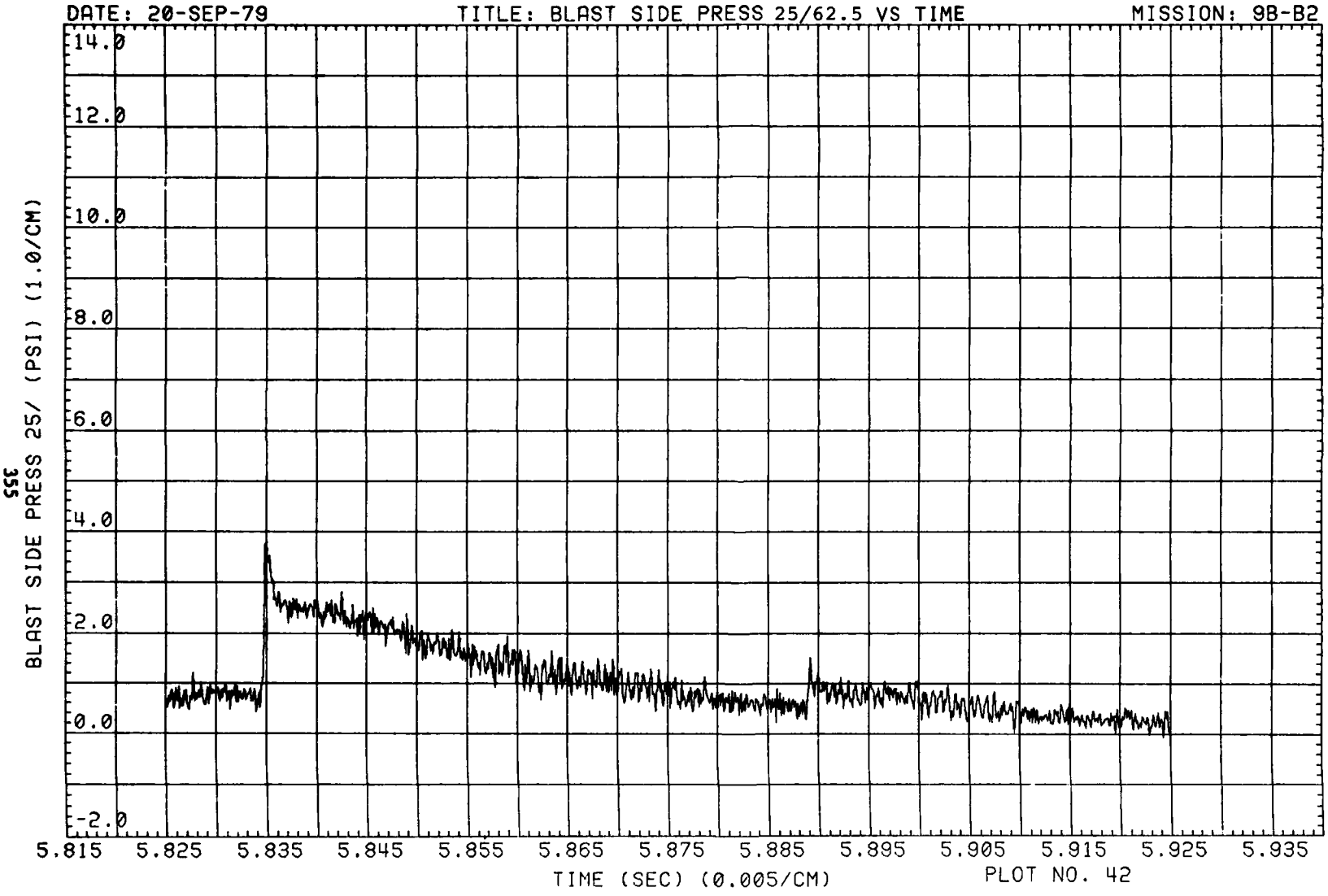

Figure 72. (Continued)

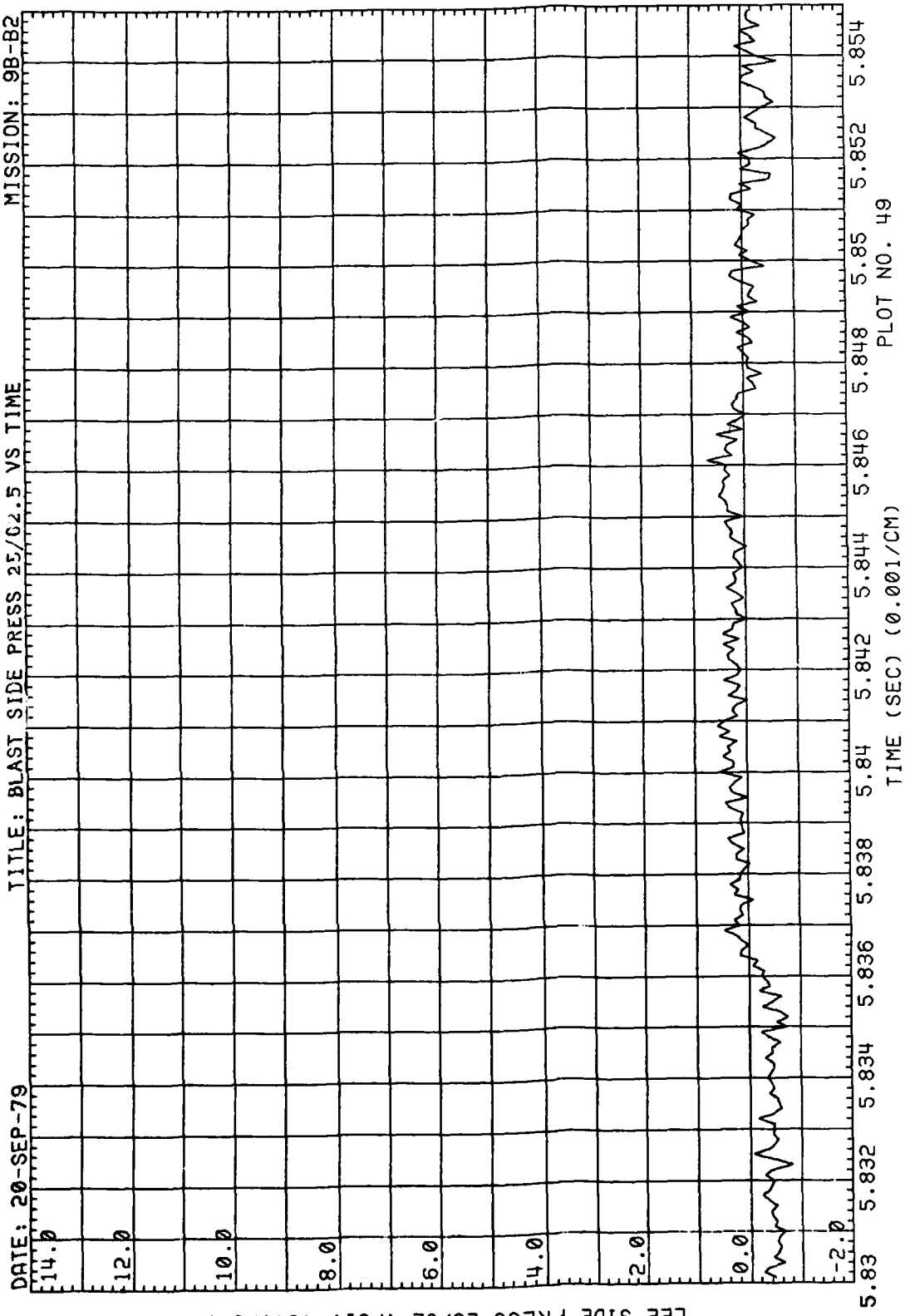

Figure 72. (Continued)

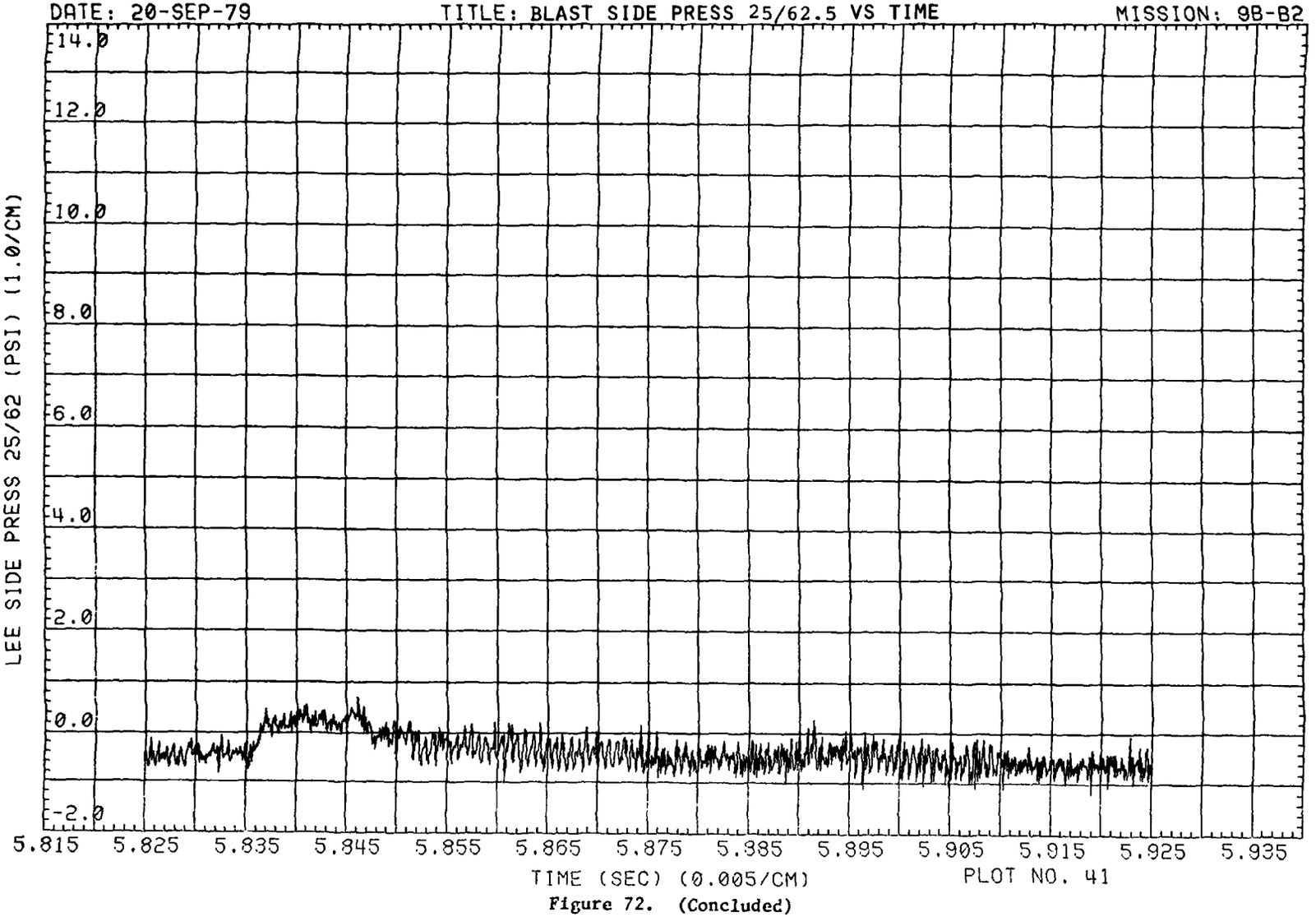

Figure 72. (Concluded)

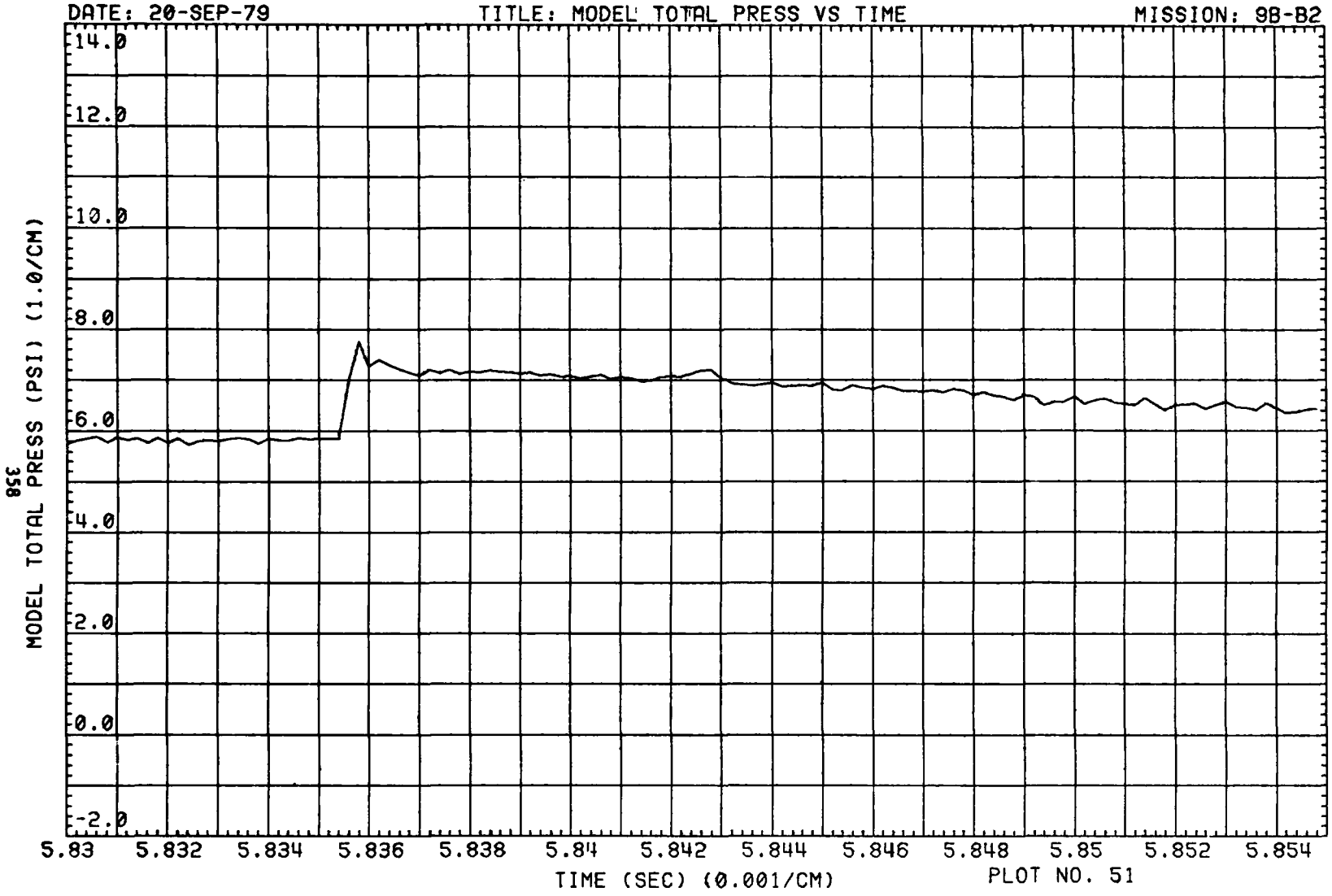

Figure 73. Total Pressure at Model, Run 9B-B2, Intercept 2

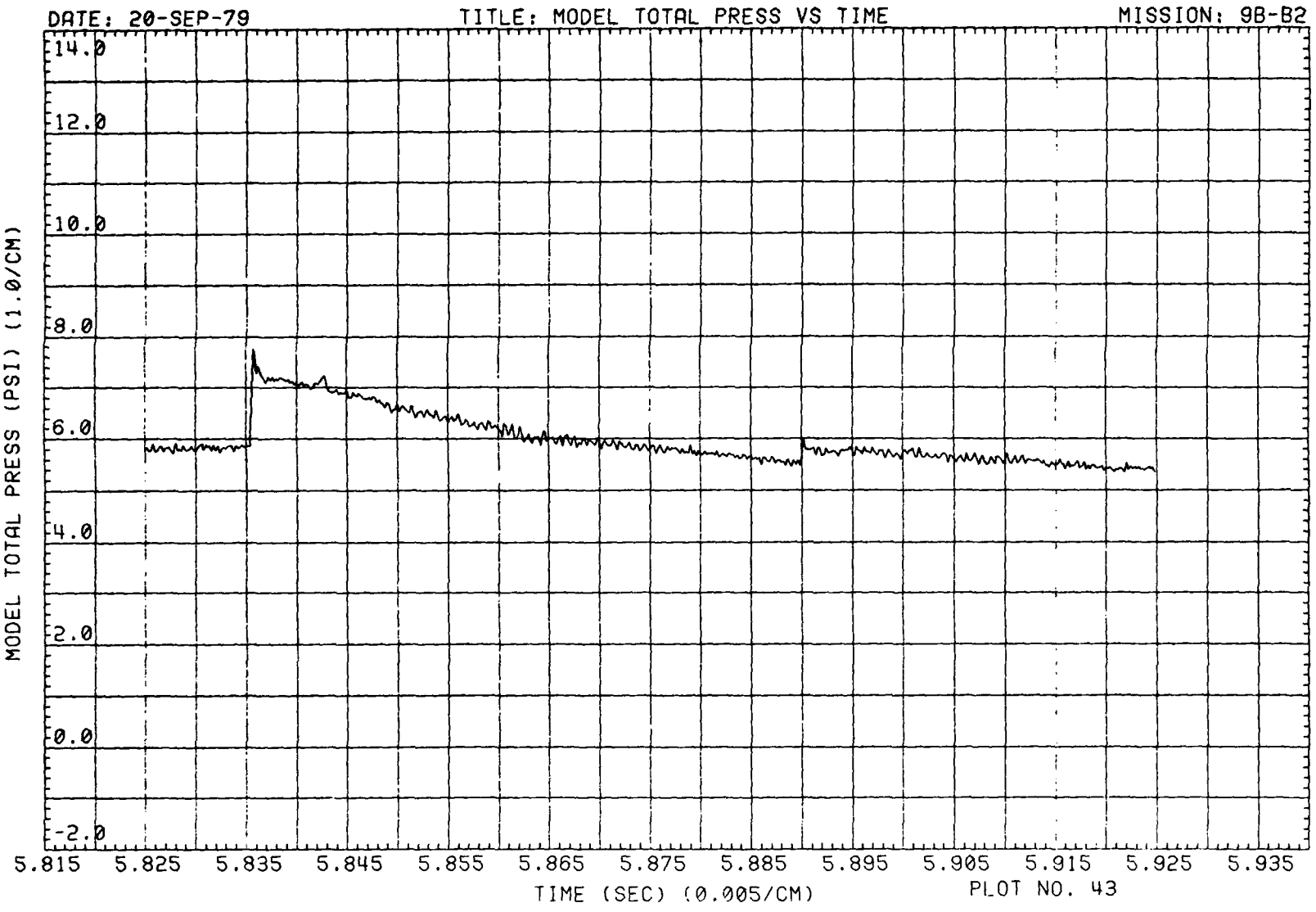

Figure 73. (Concluded)

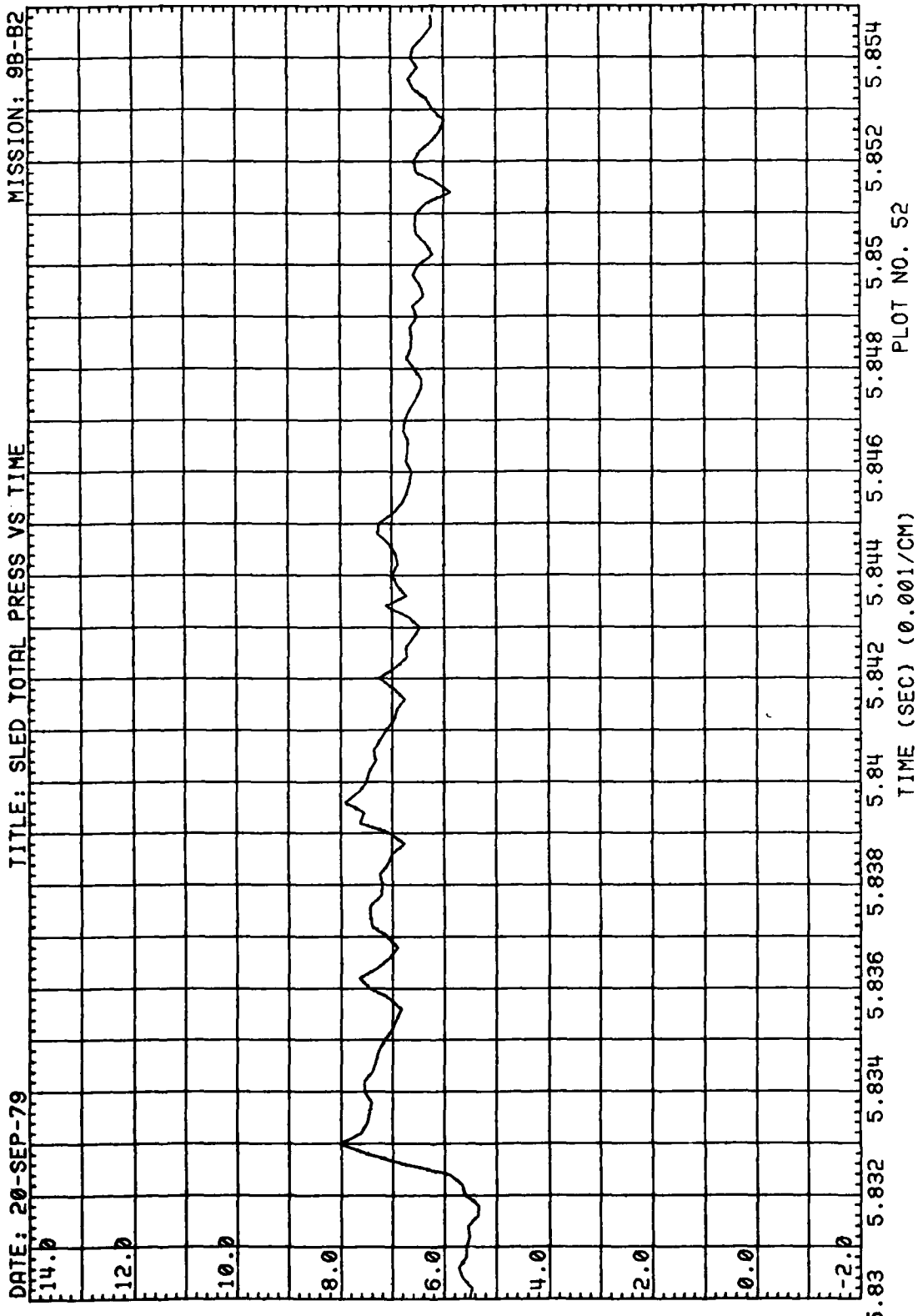

Figure 74. Total Pressure at Sled, Run 9B-B2, Intercept 2

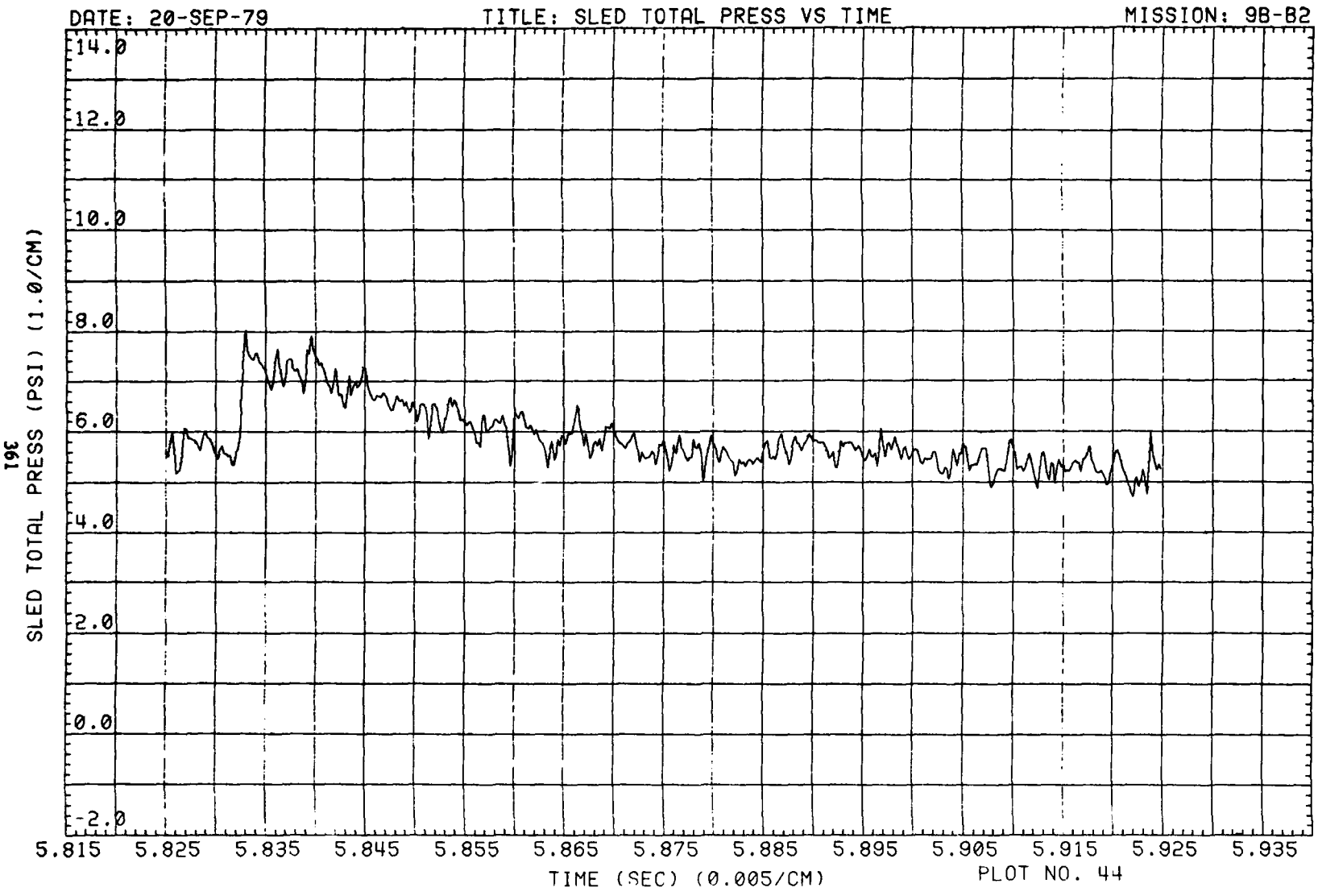

Figure 74. (Concluded)

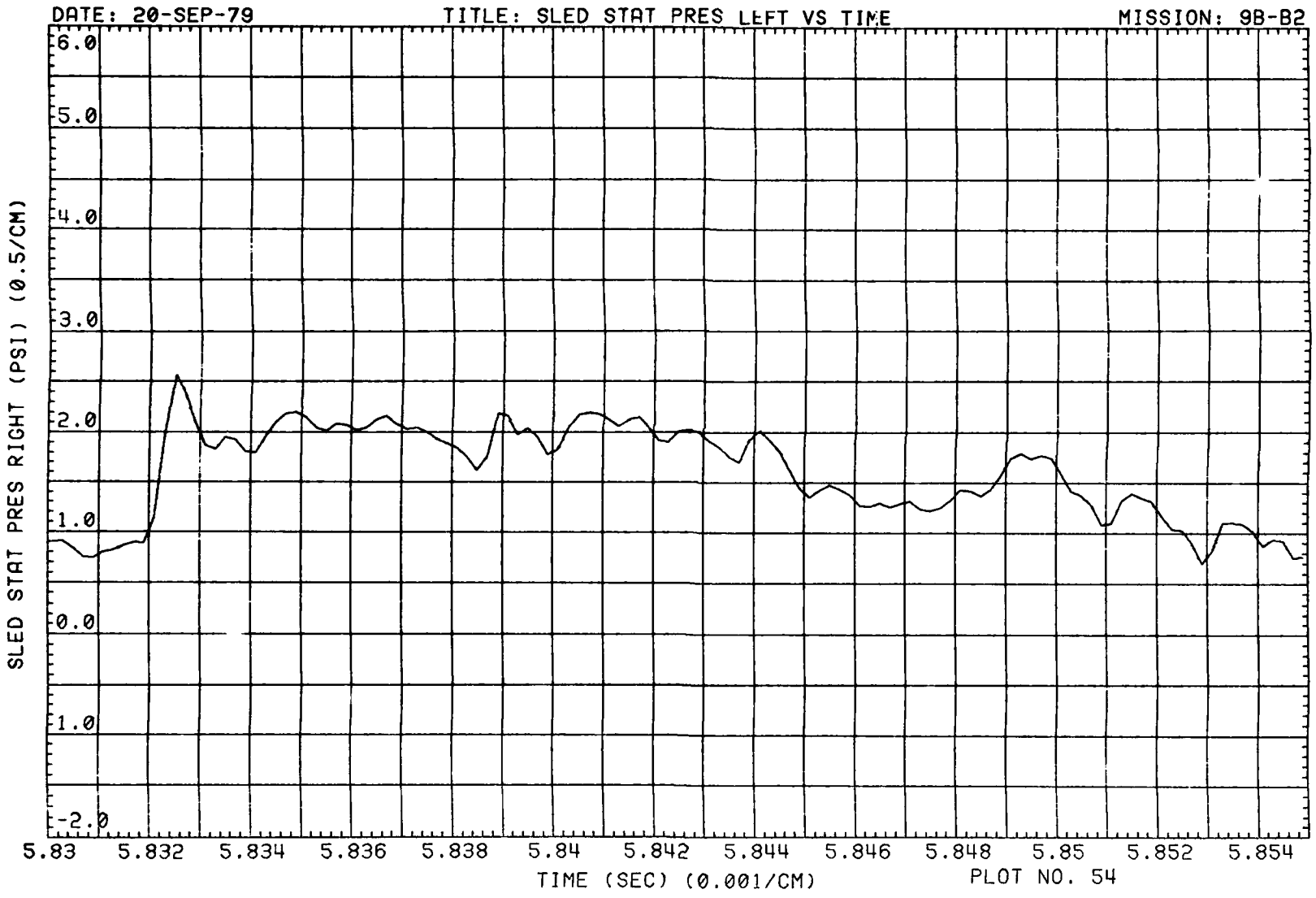

Figure 75. Left Side Static Pressure at Sled, Run 9B-B2, Intercept 2

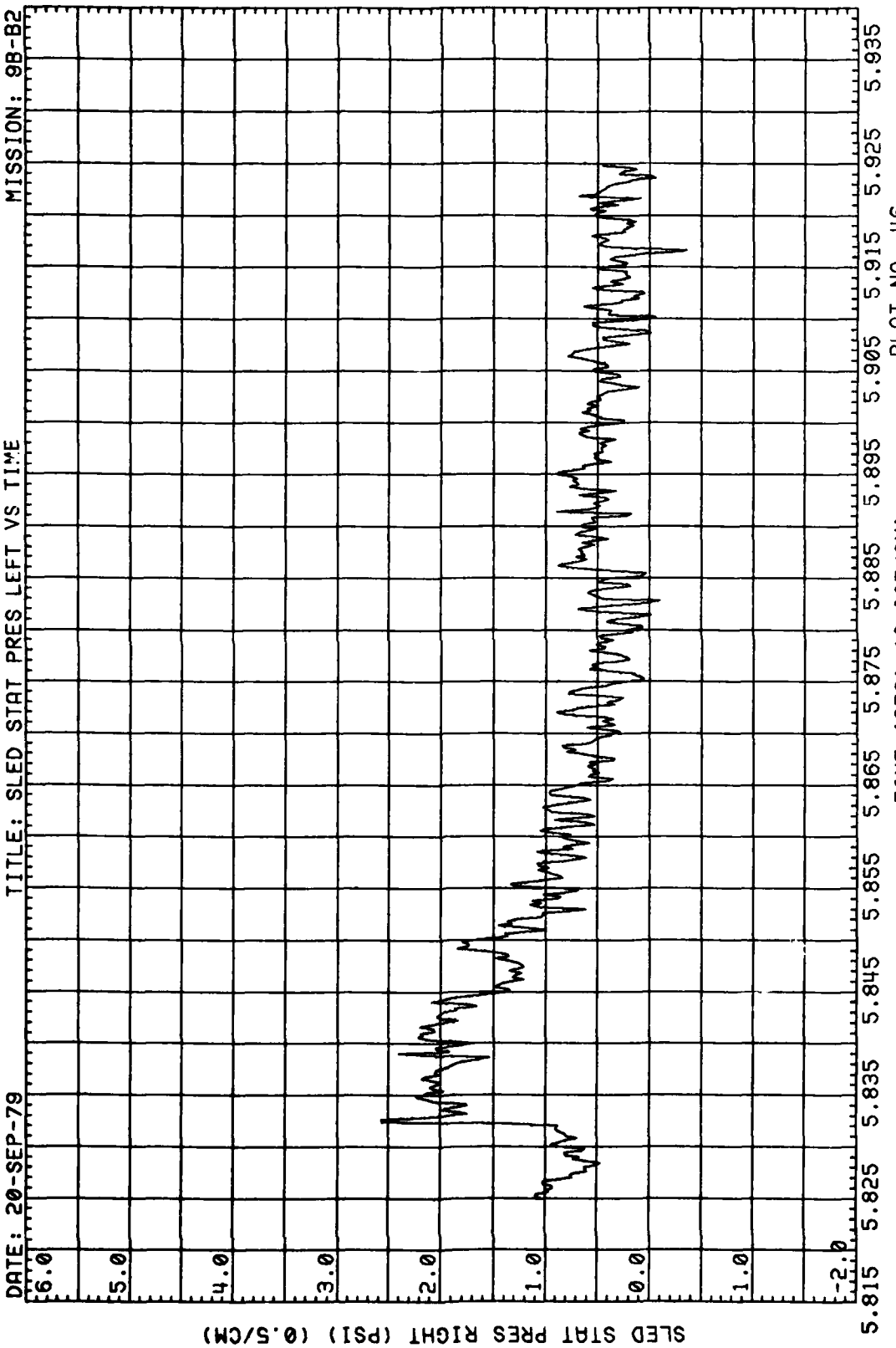

Figure 75. (Concluded)

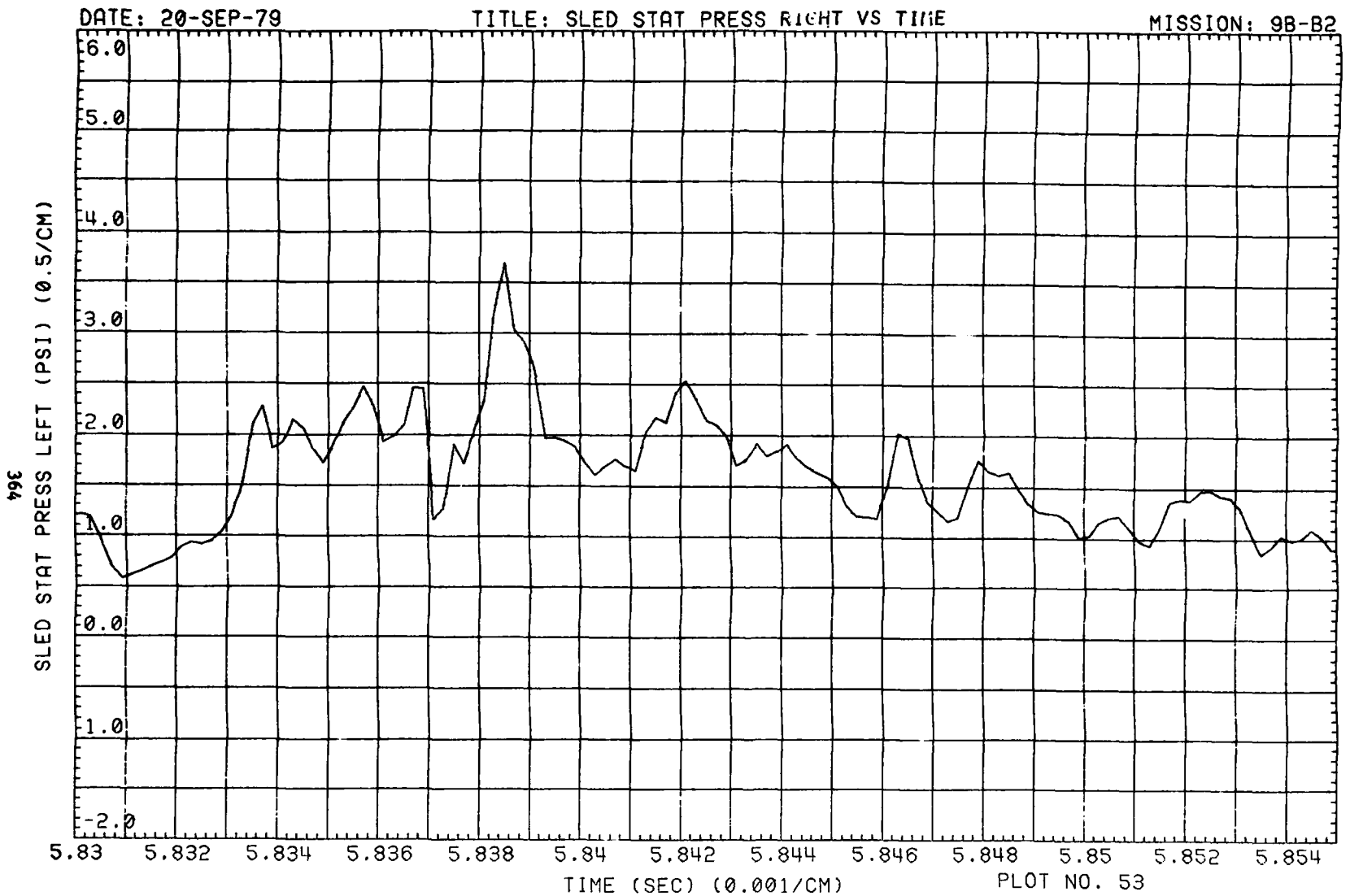

Figure 76. Right Side Static Pressure at Sled, Run 9B-B2, Intercept 2

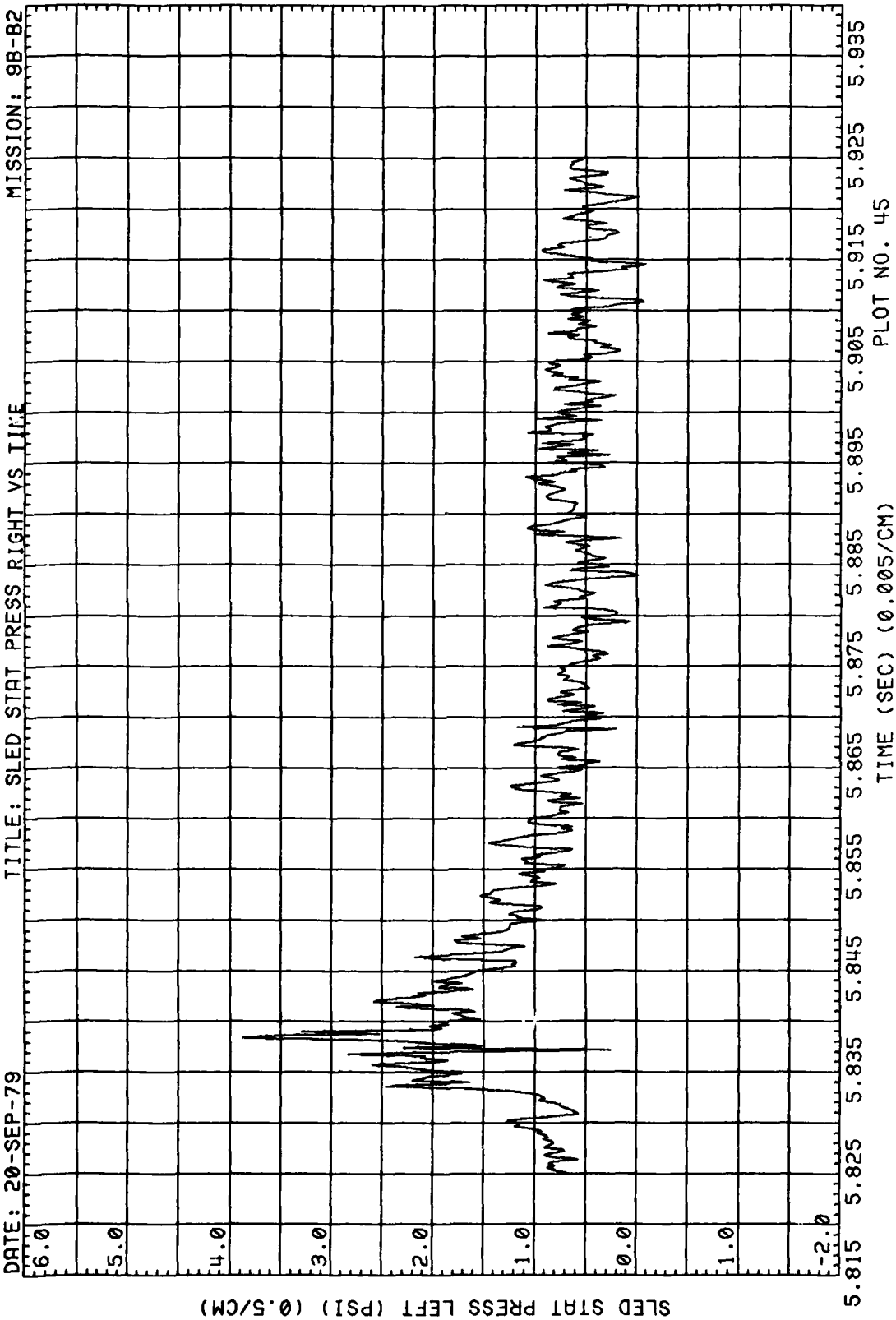

Figure 76. (Concluded)

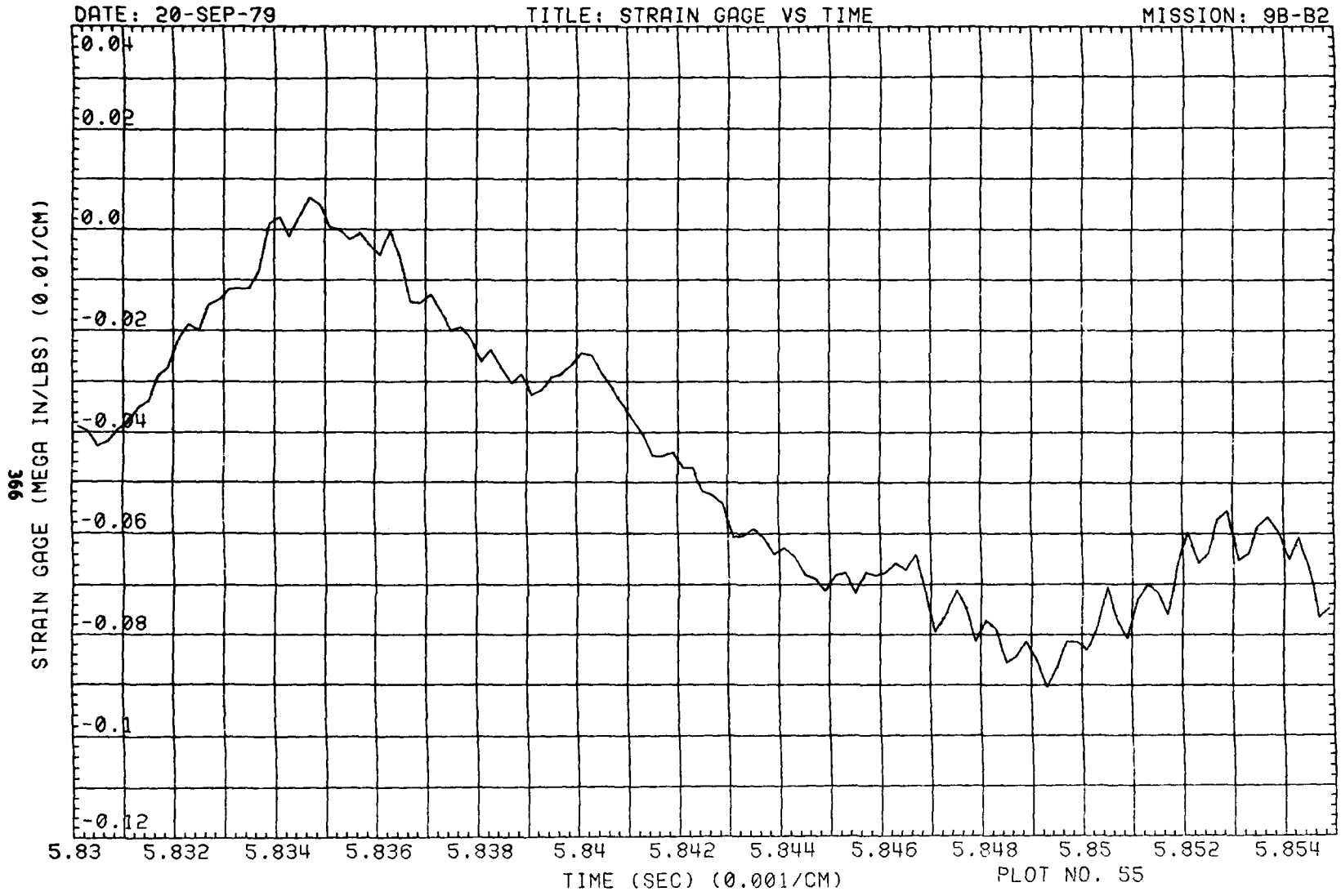

Figure 77. Strain at Model Support, Run 9B-B2, Intercept 2

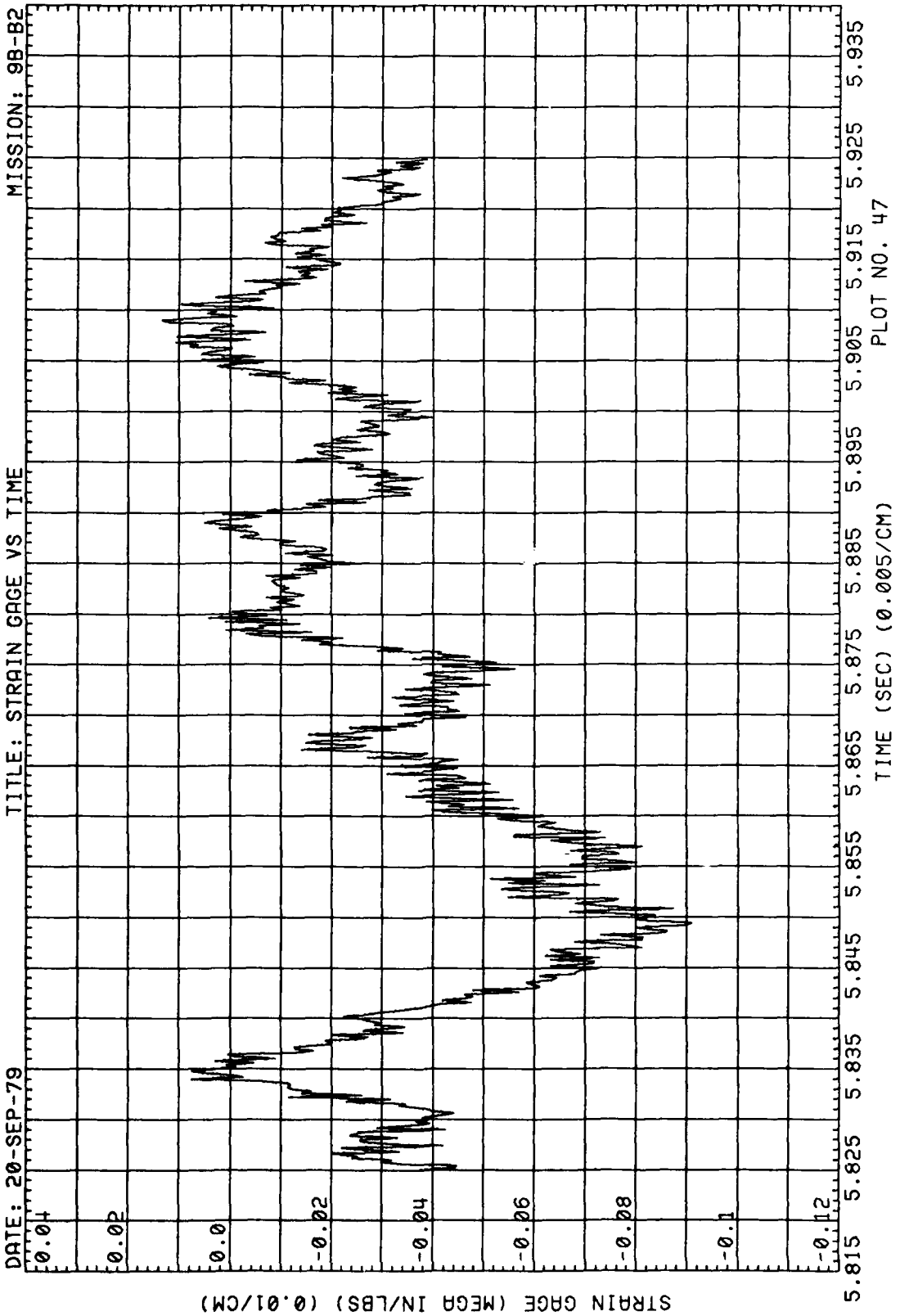

Figure 77. (Concluded)

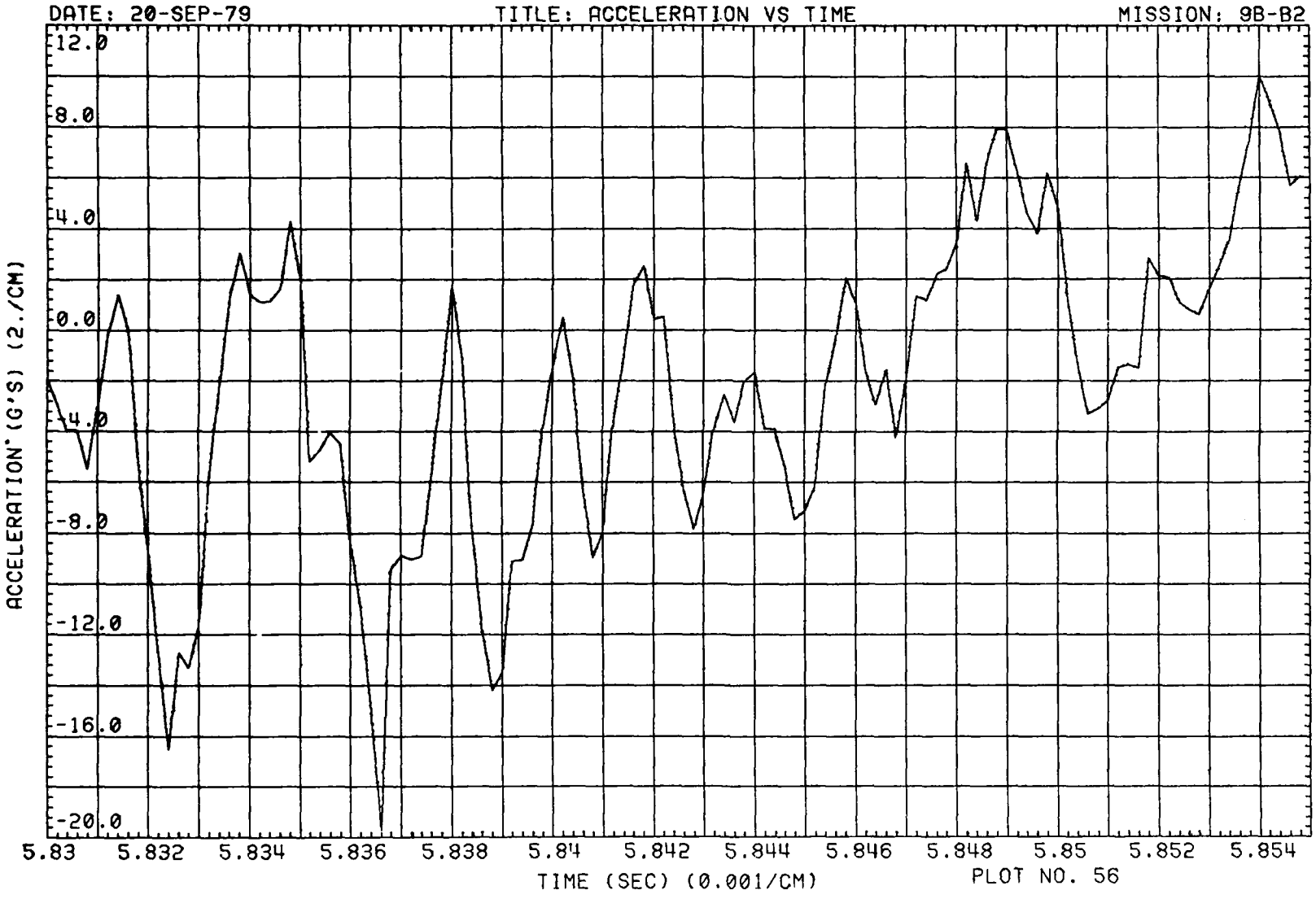

Figure 78. Wing Acceleration, Run 9B-B2, Intercept 2

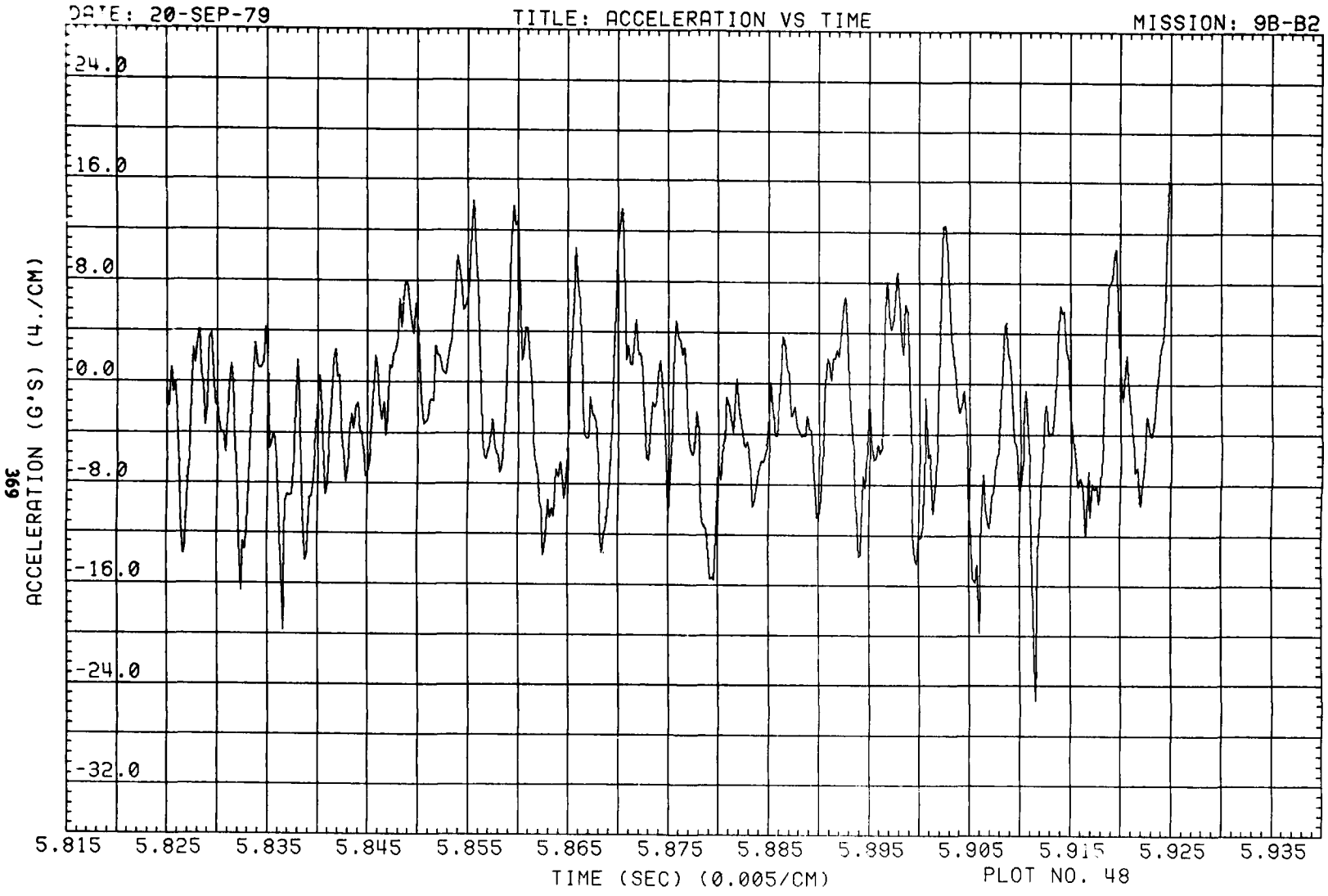

Figure 78. (Concluded)

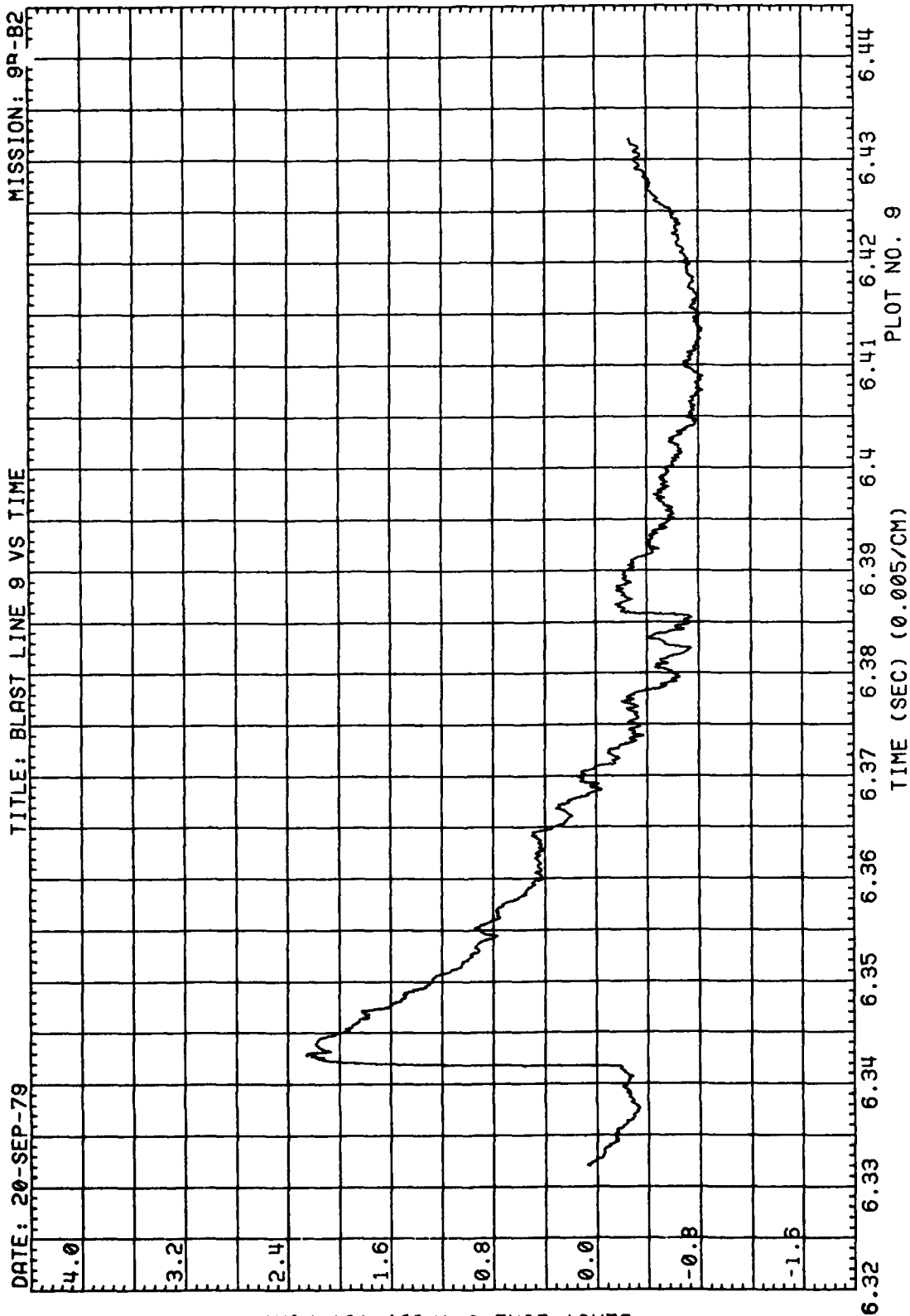

Figure 79. Blast-Line Overpressures, Run 9B-B2, Intercept 3

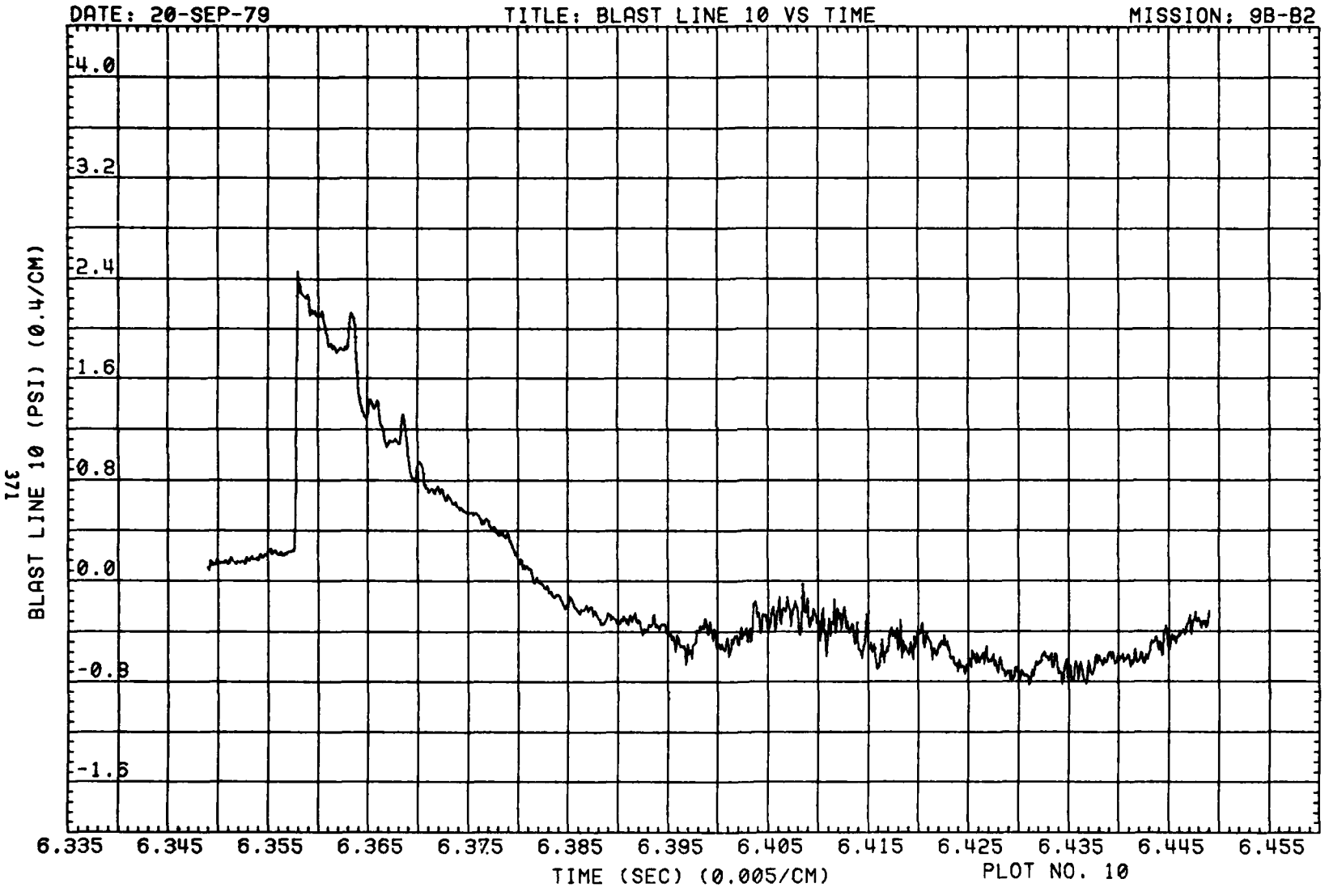

Figure 79. (Continued)

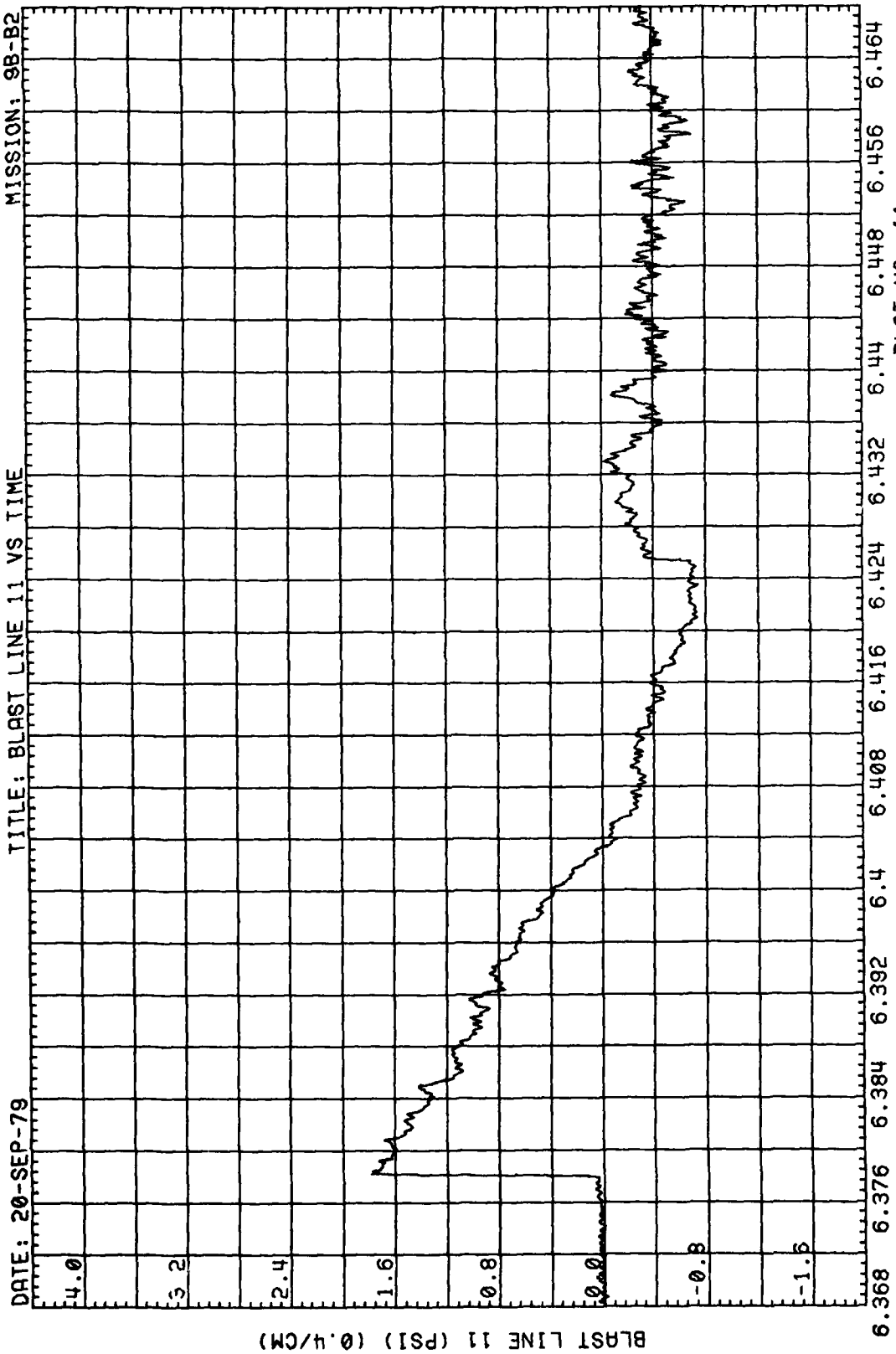

Figure 79. (Continued)

Figure 79. (Concluded)

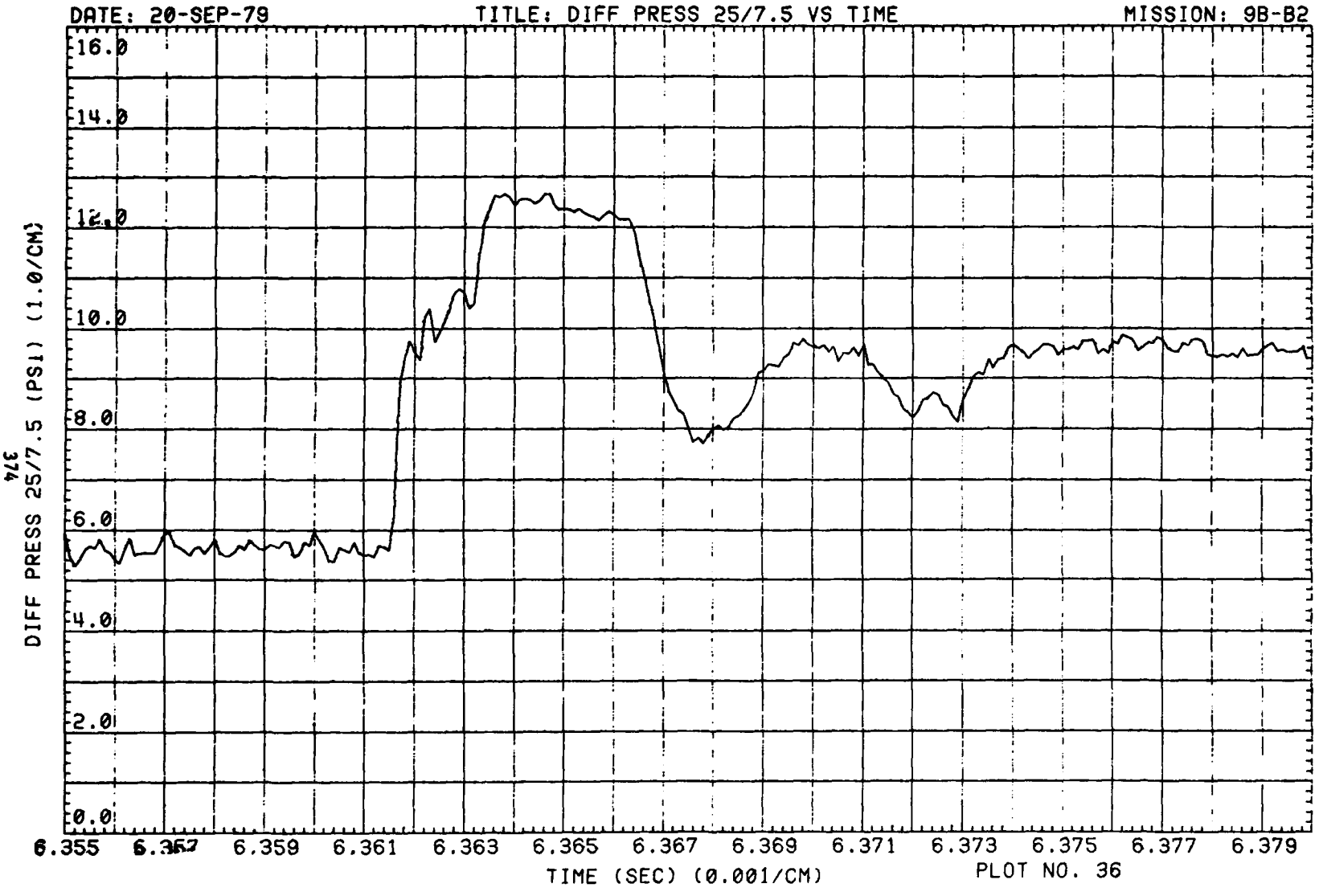

Figure 80. Differential Wing Pressures, Run 9B-B2, Intercept 3

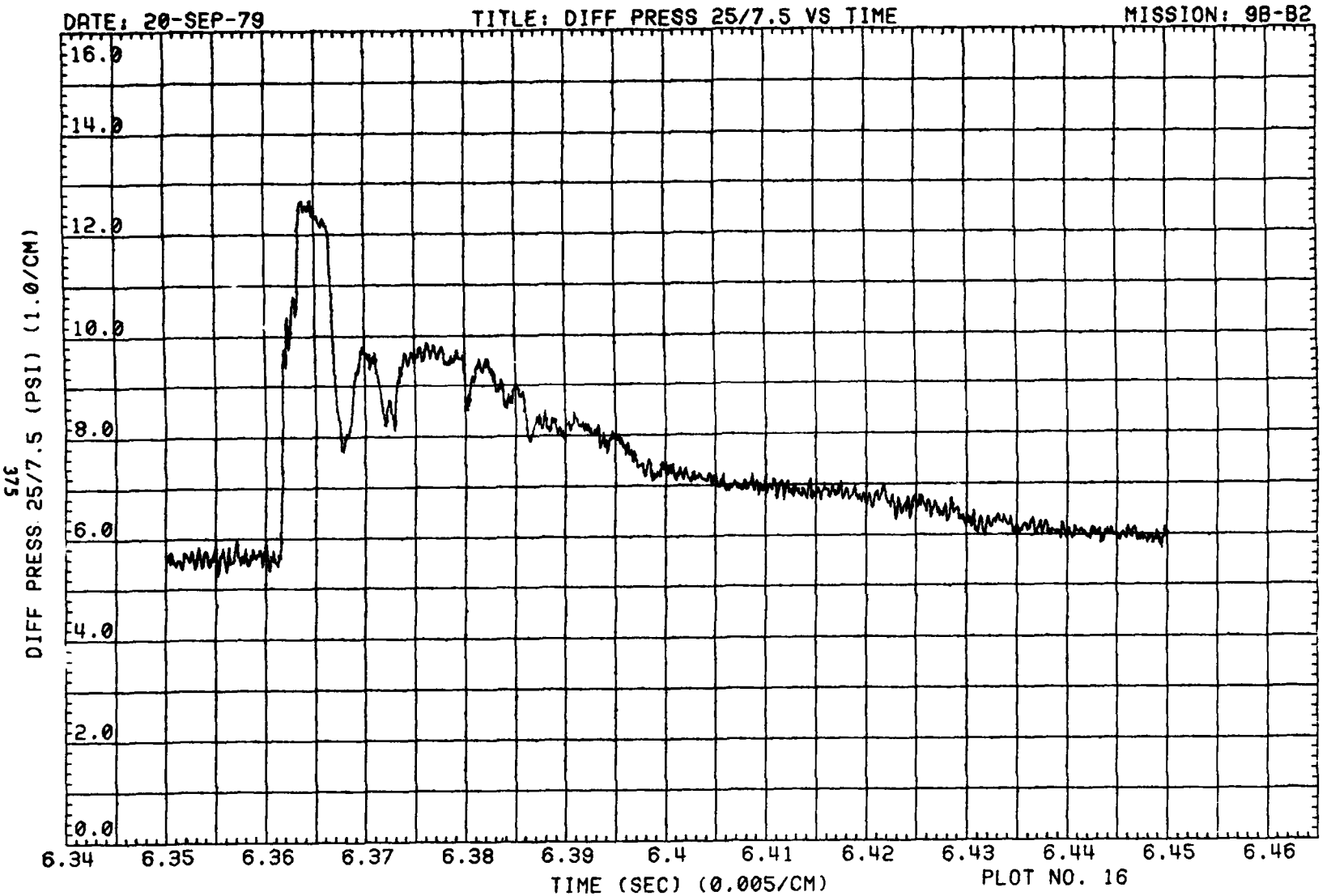

Figure 80. (Continued)

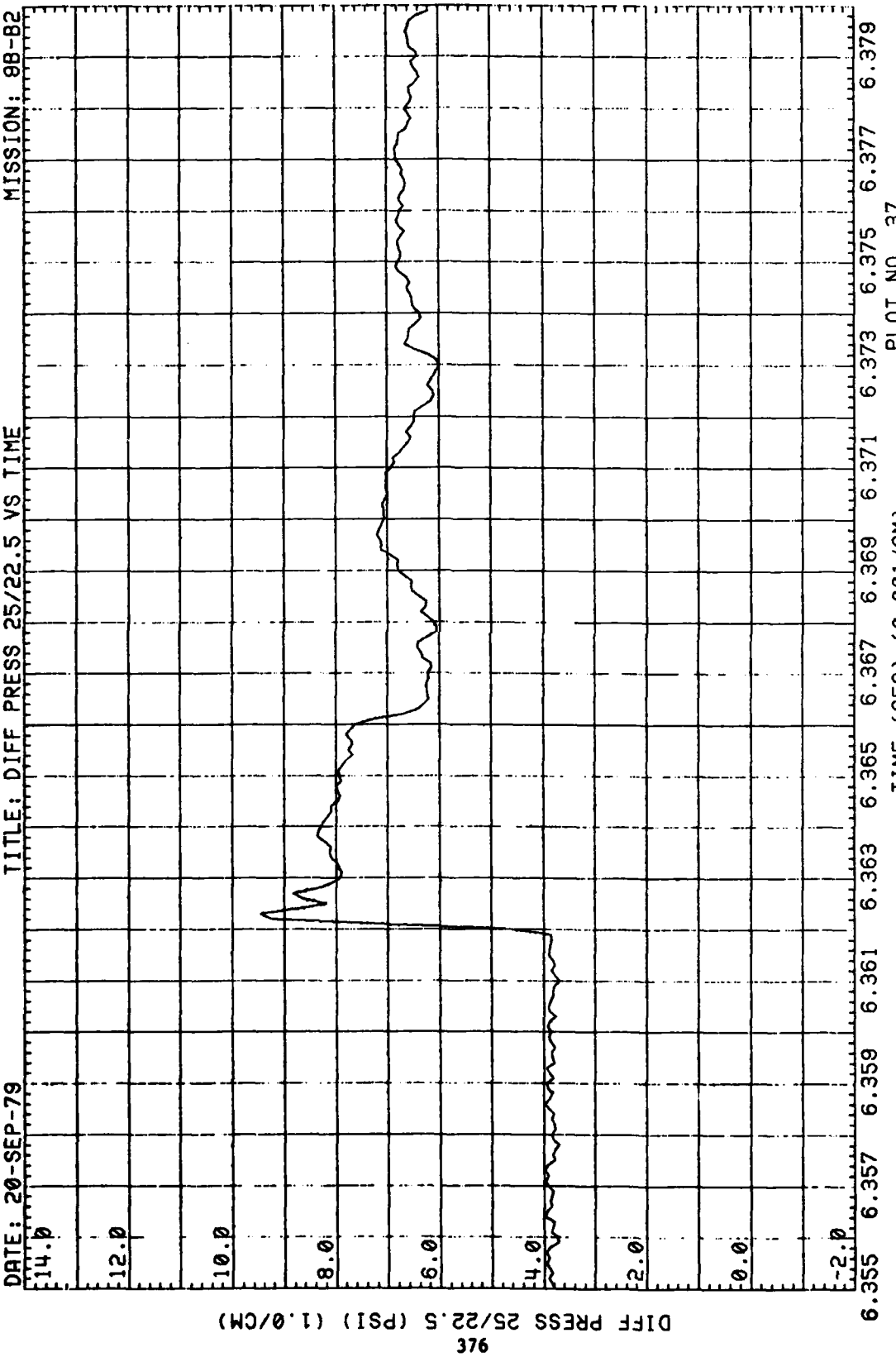

Figure 80. (Continued)

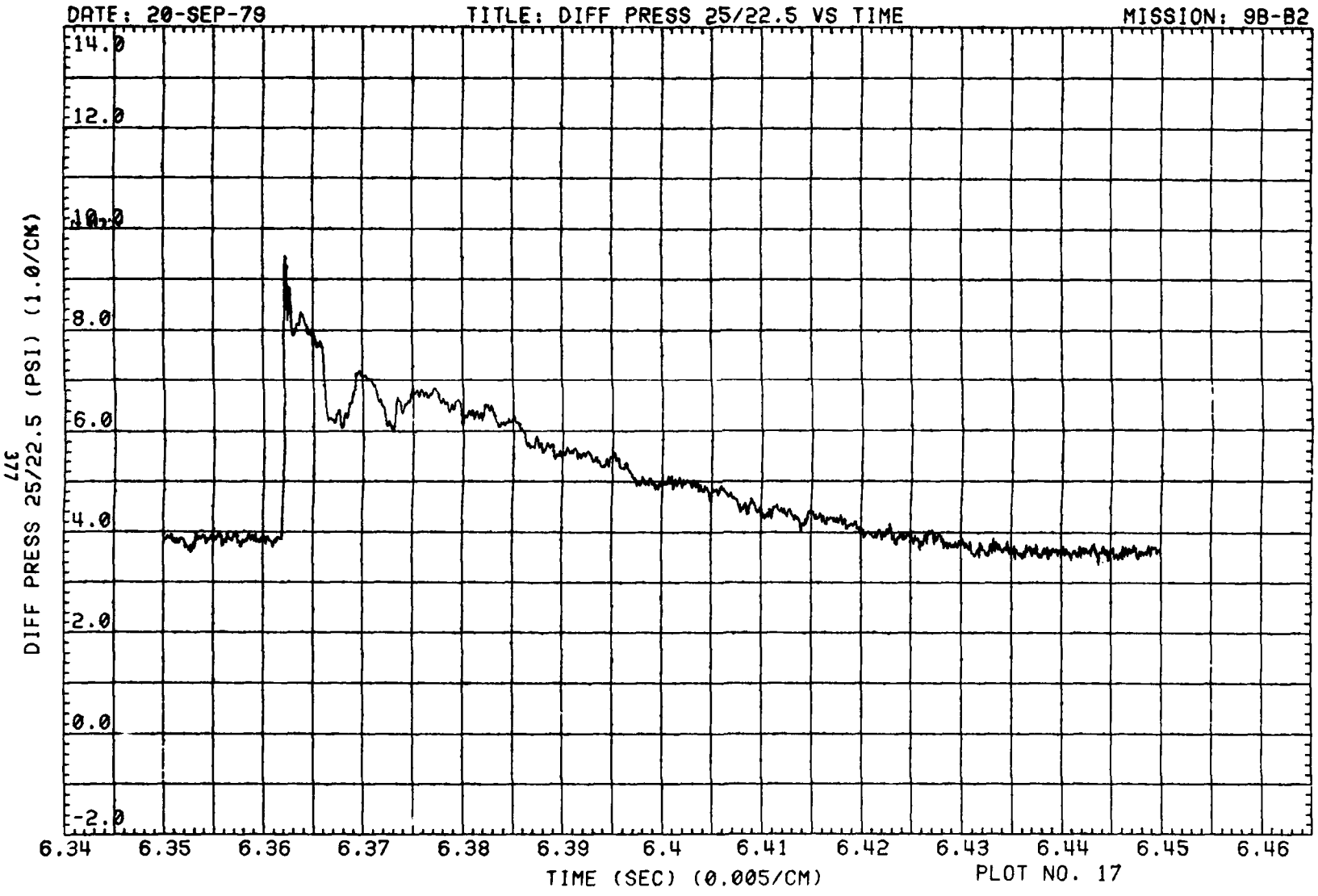

Figure 80. (Continued)

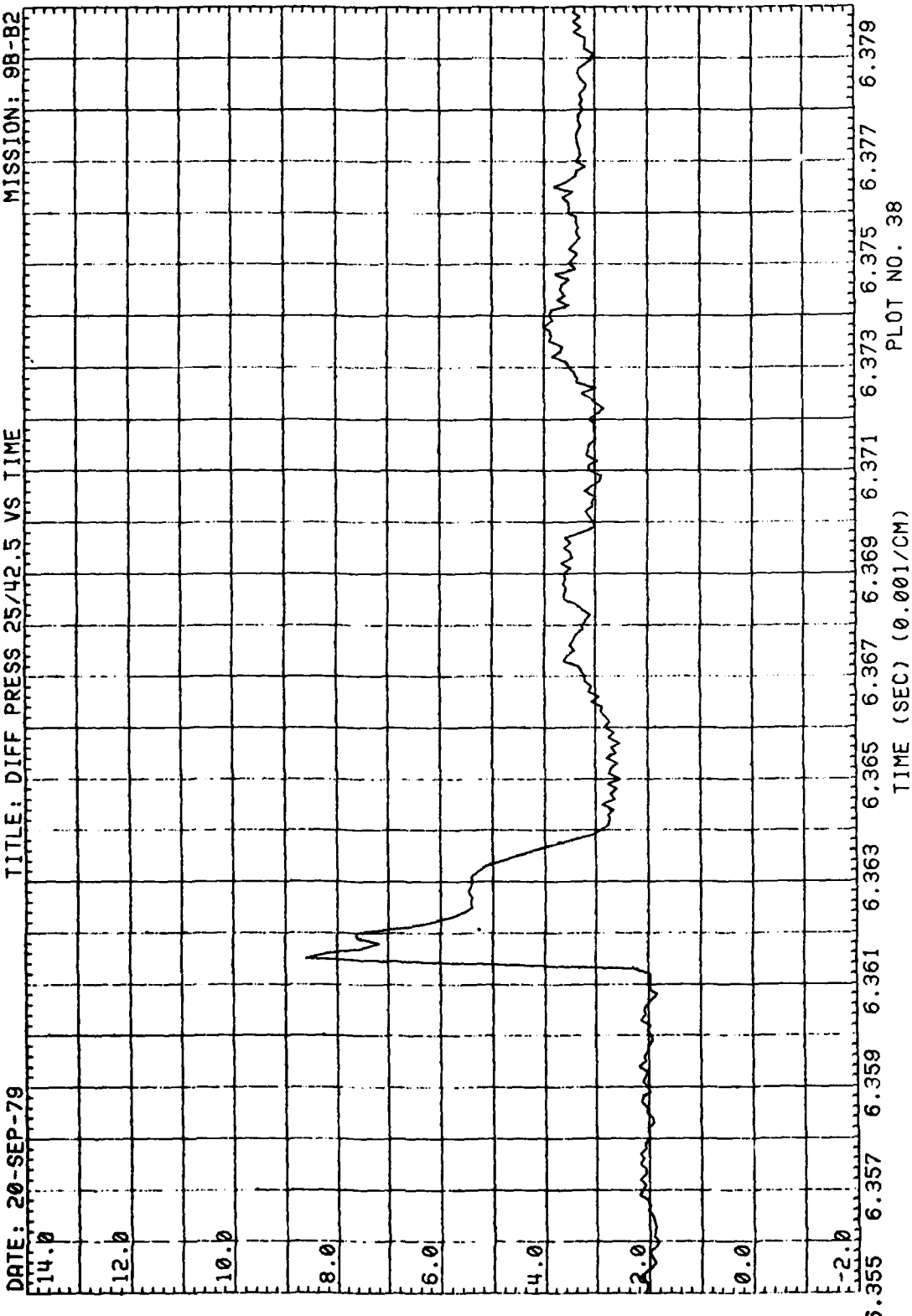

Figure 80. (Continued)

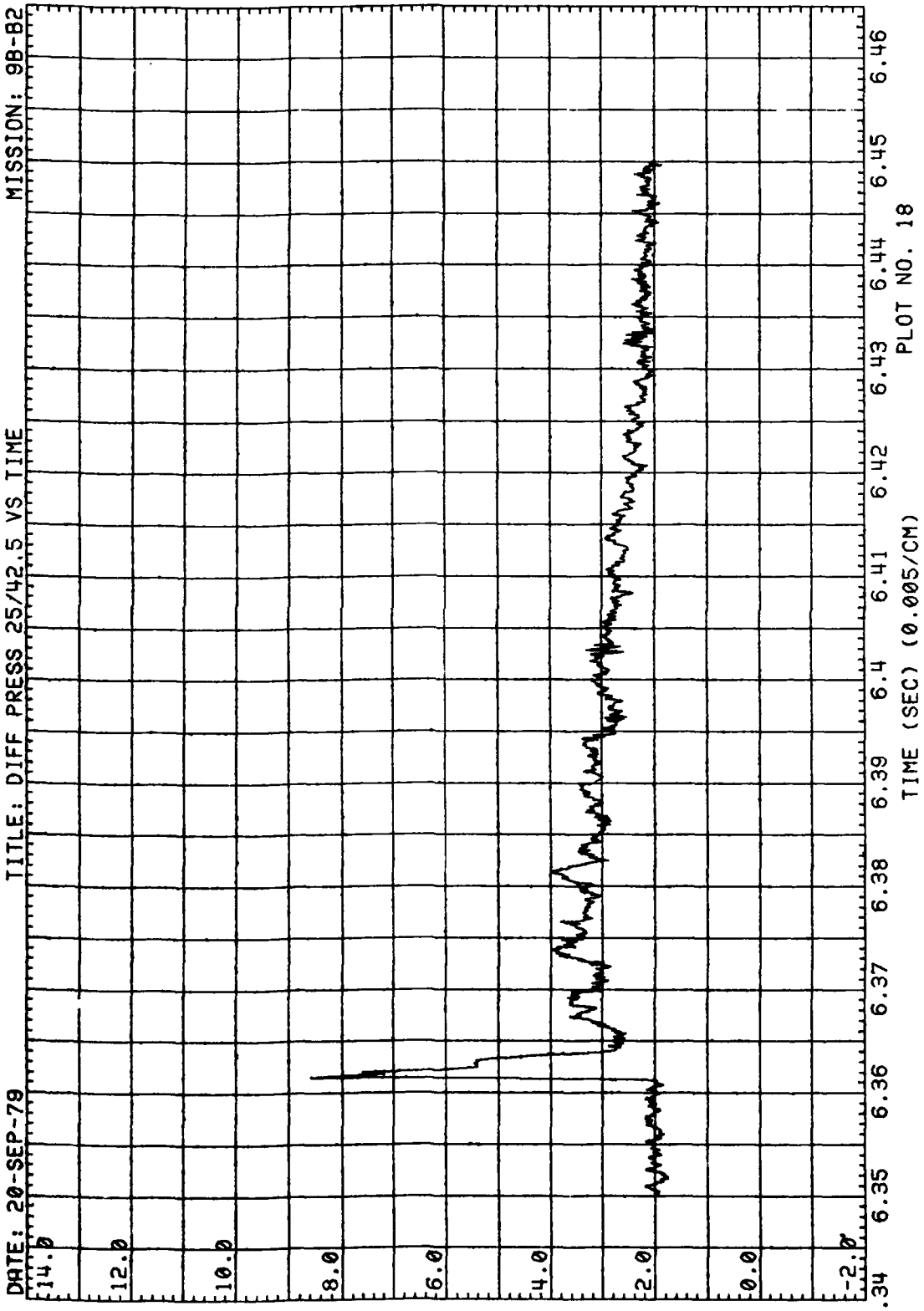

Figure 80. (Continued)

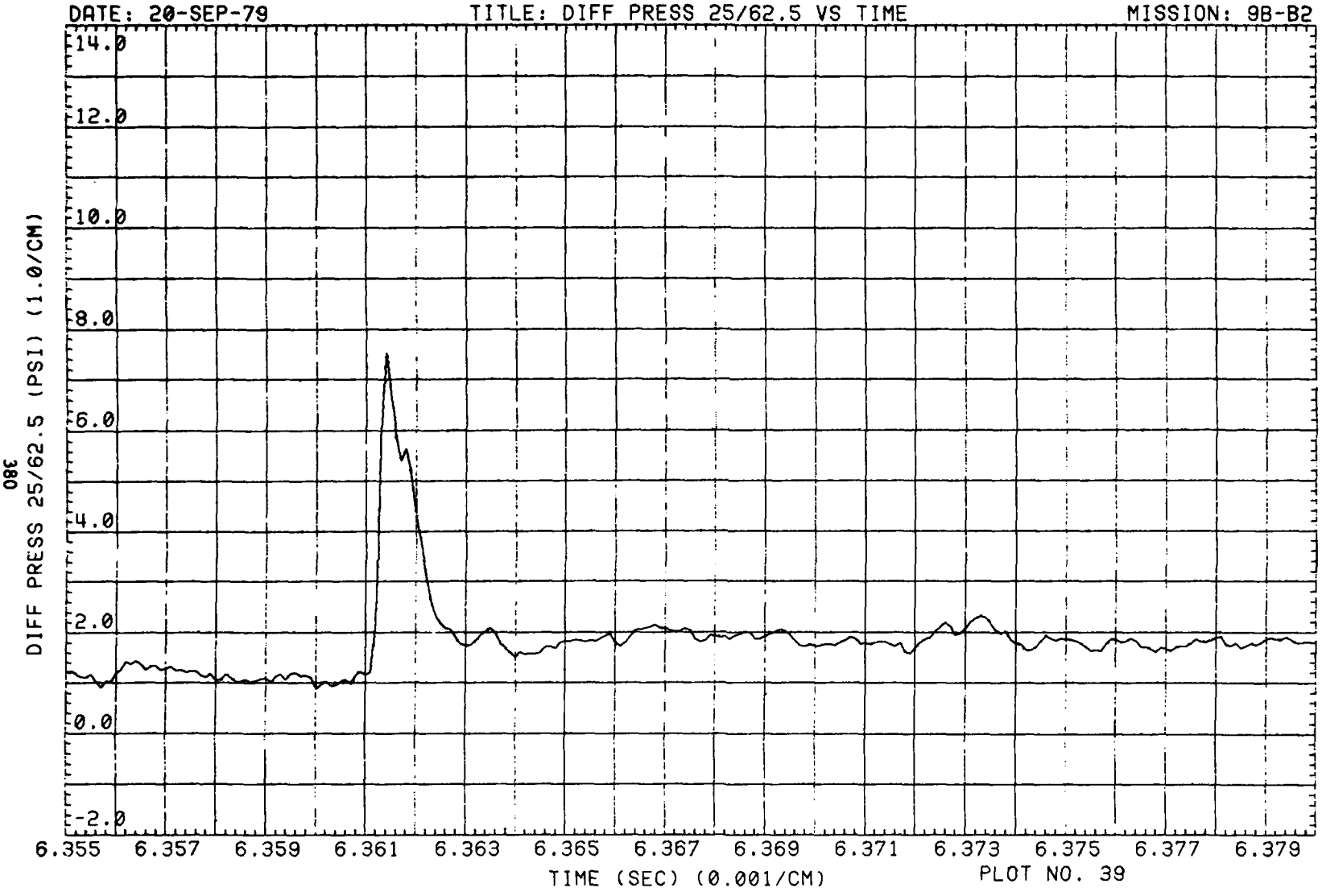

Figure 80. (Continued)

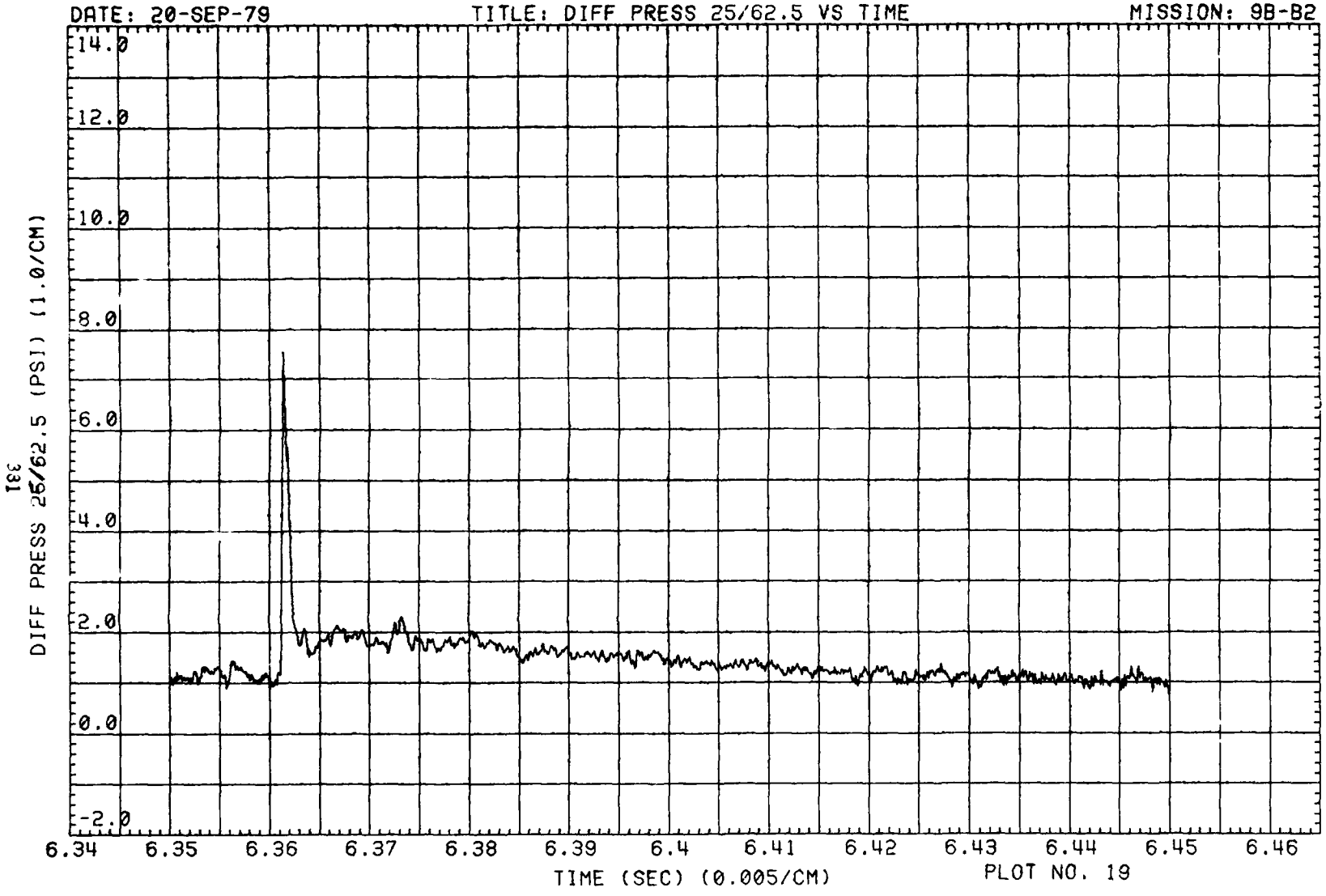

Figure 80. (Continued)

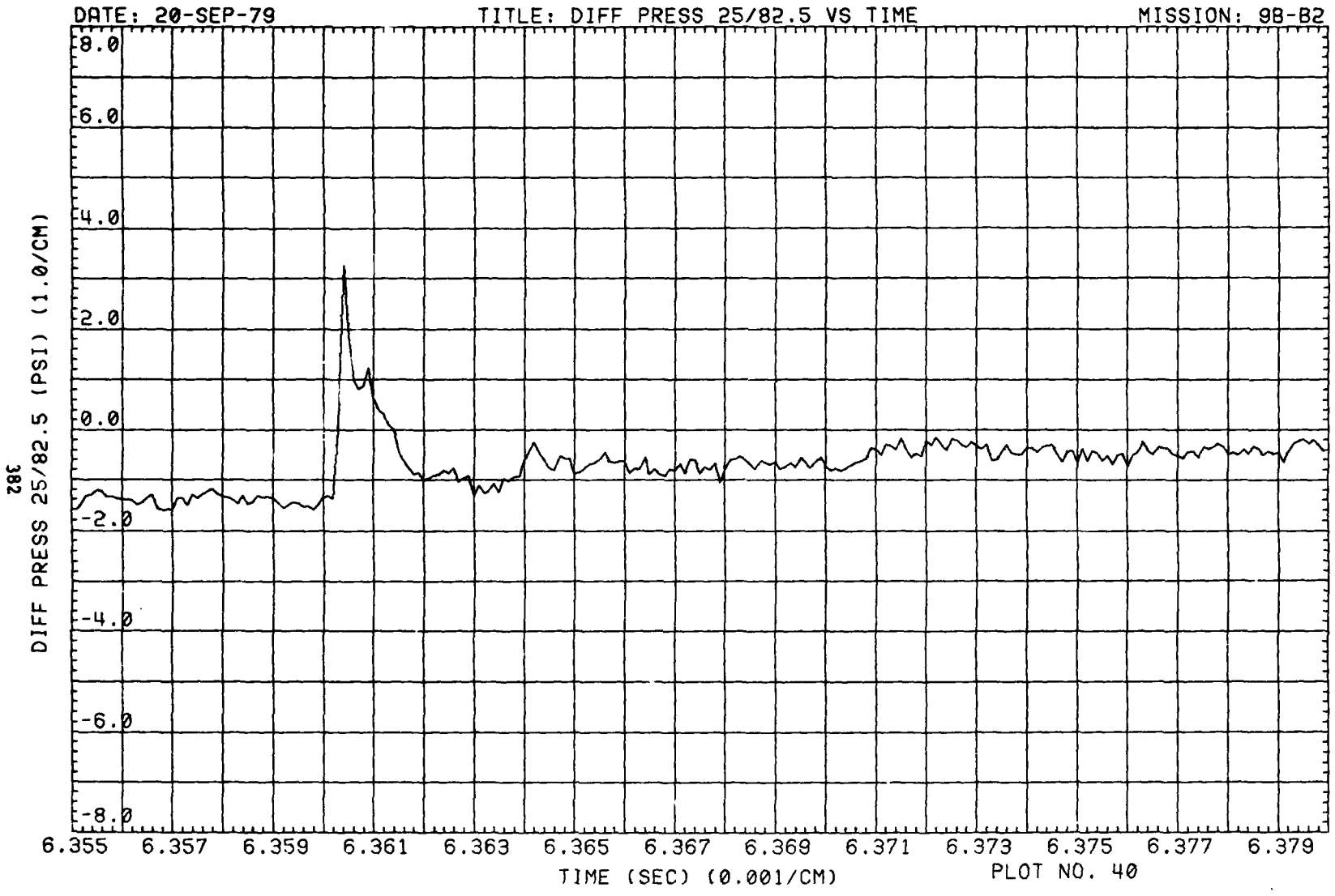

Figure 80. (Continued)

AD-A093 729 KAMAN AVIDYNE BURLINGTON MA F/G 20/4
MEASUREMENTS OF BLAST PRESSURES ON A RIGID 35 DEG SWEPTBACK WIN--ETC(U)
JAN 80 D A KLEPPIN, J R RUETENIK, R F SMILEY DNA001-79-C-0157
UNCLASSIFIED KA-TR-175 DNA-5211F NL

5 of 5
AD A093729

END
DATE FILMED
2-81
DTIC

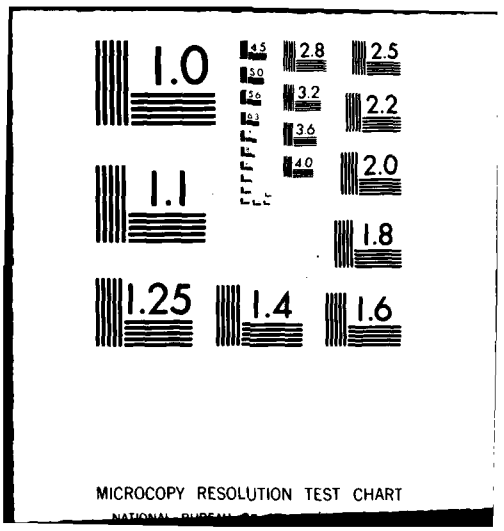
1.0
1.1
1.25
1.4
1.6
1.8
2.0
2.2
2.5
2.8
3.2
3.6
4.0
4.5
5.0
5.6
6.3
MICROCOPY RESOLUTION TEST CHART

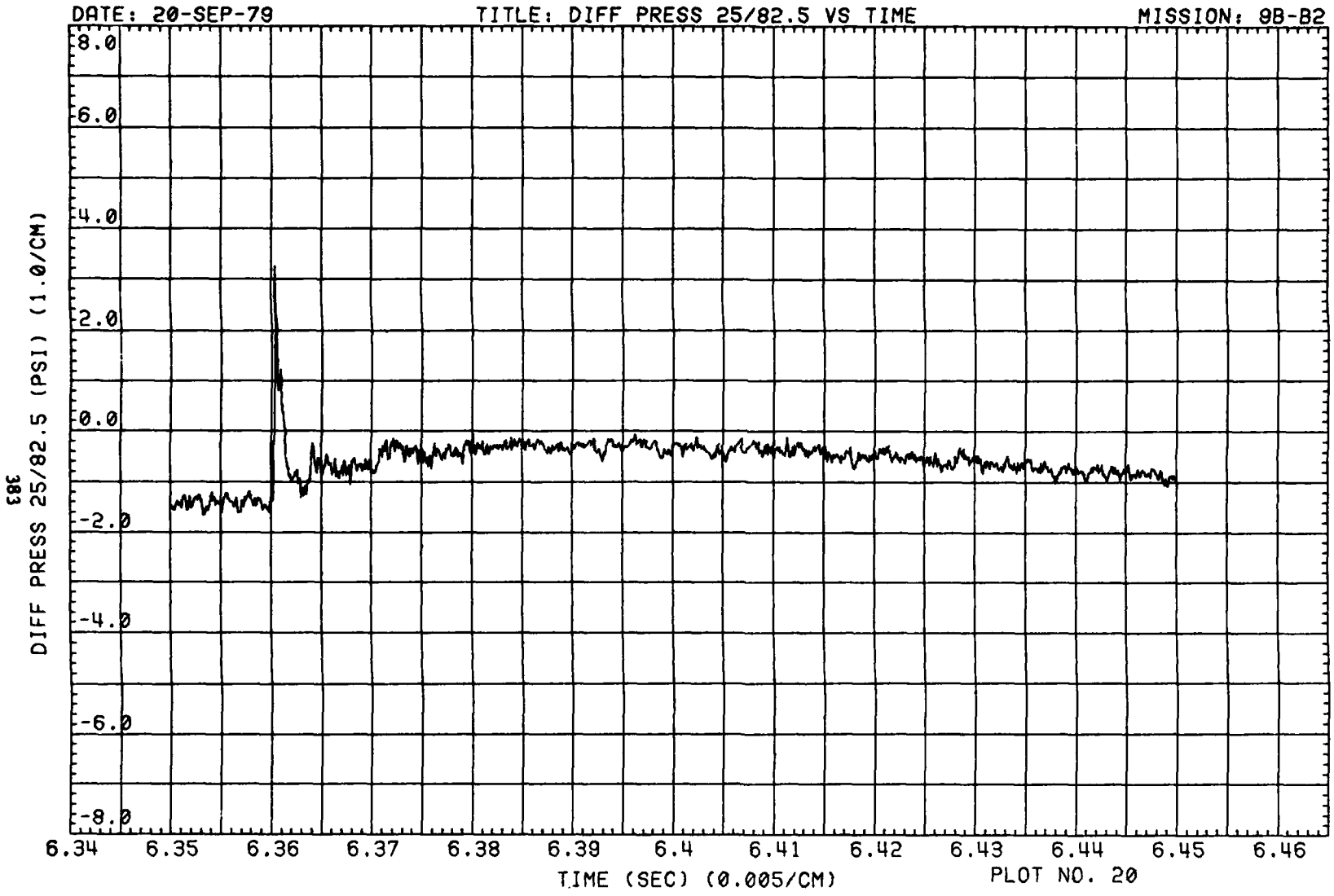

Figure 80. (Continued)

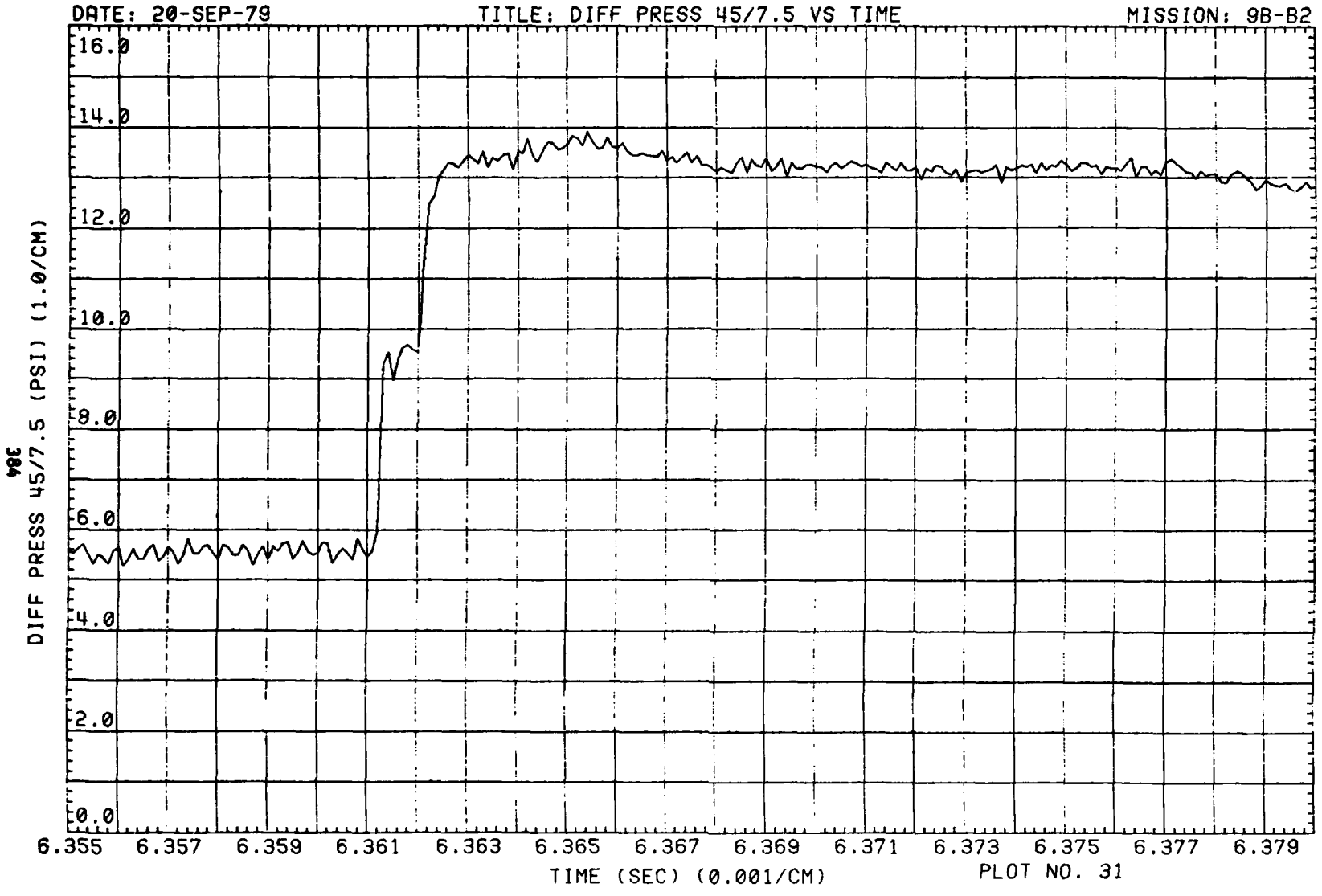

Figure 80. (Continued)

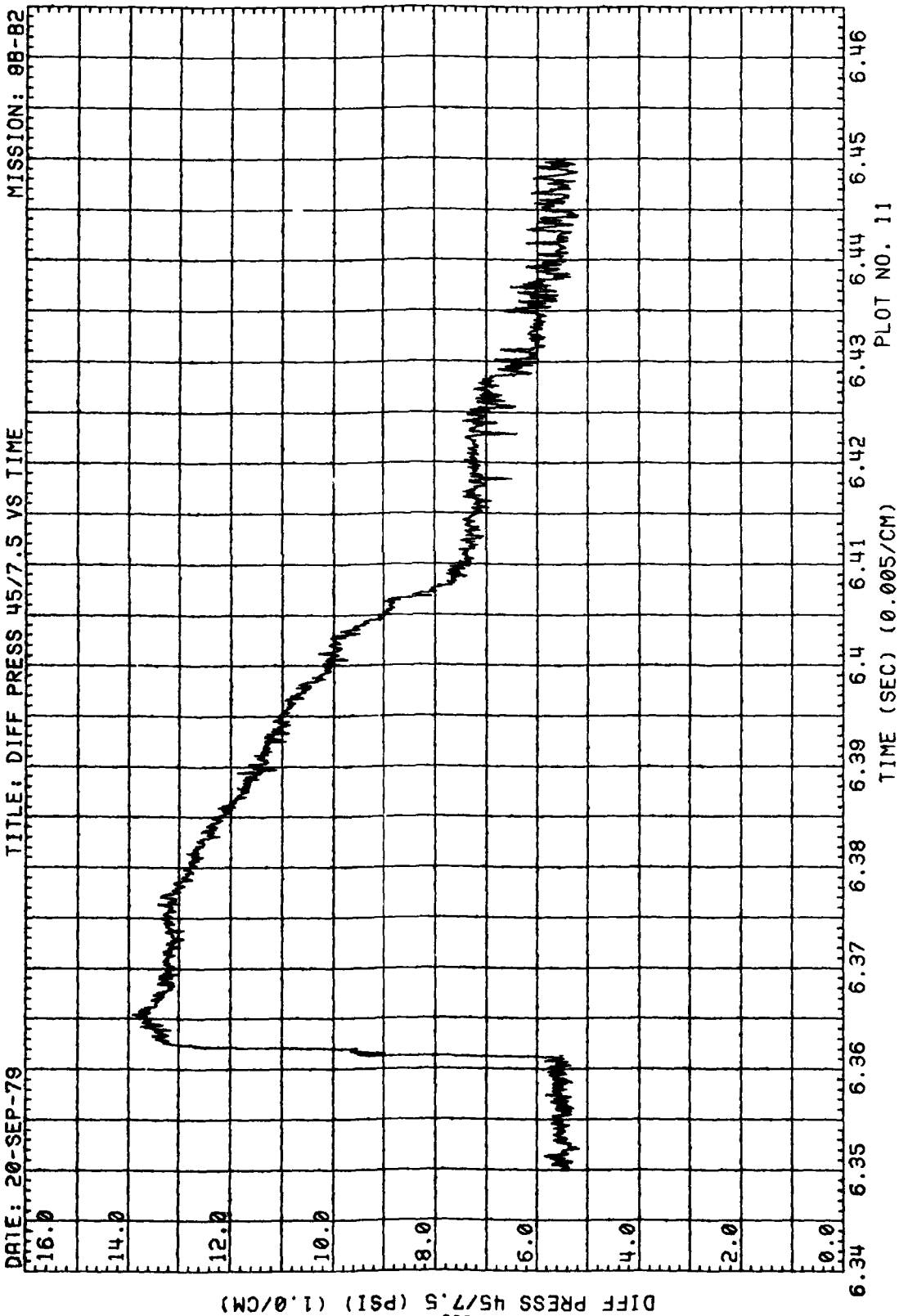

Figure 80. (Continued)

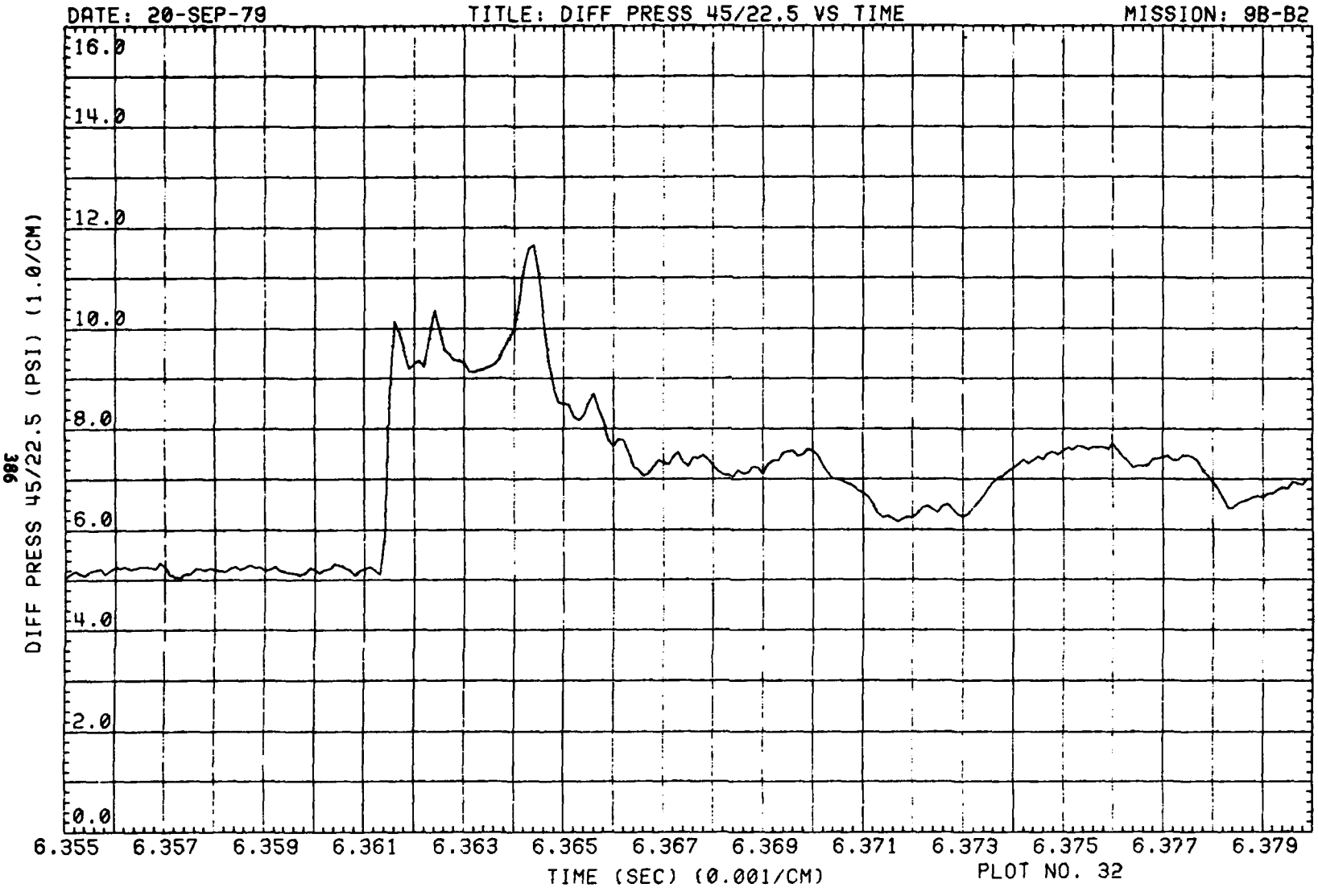

Figure 80. (Continued)

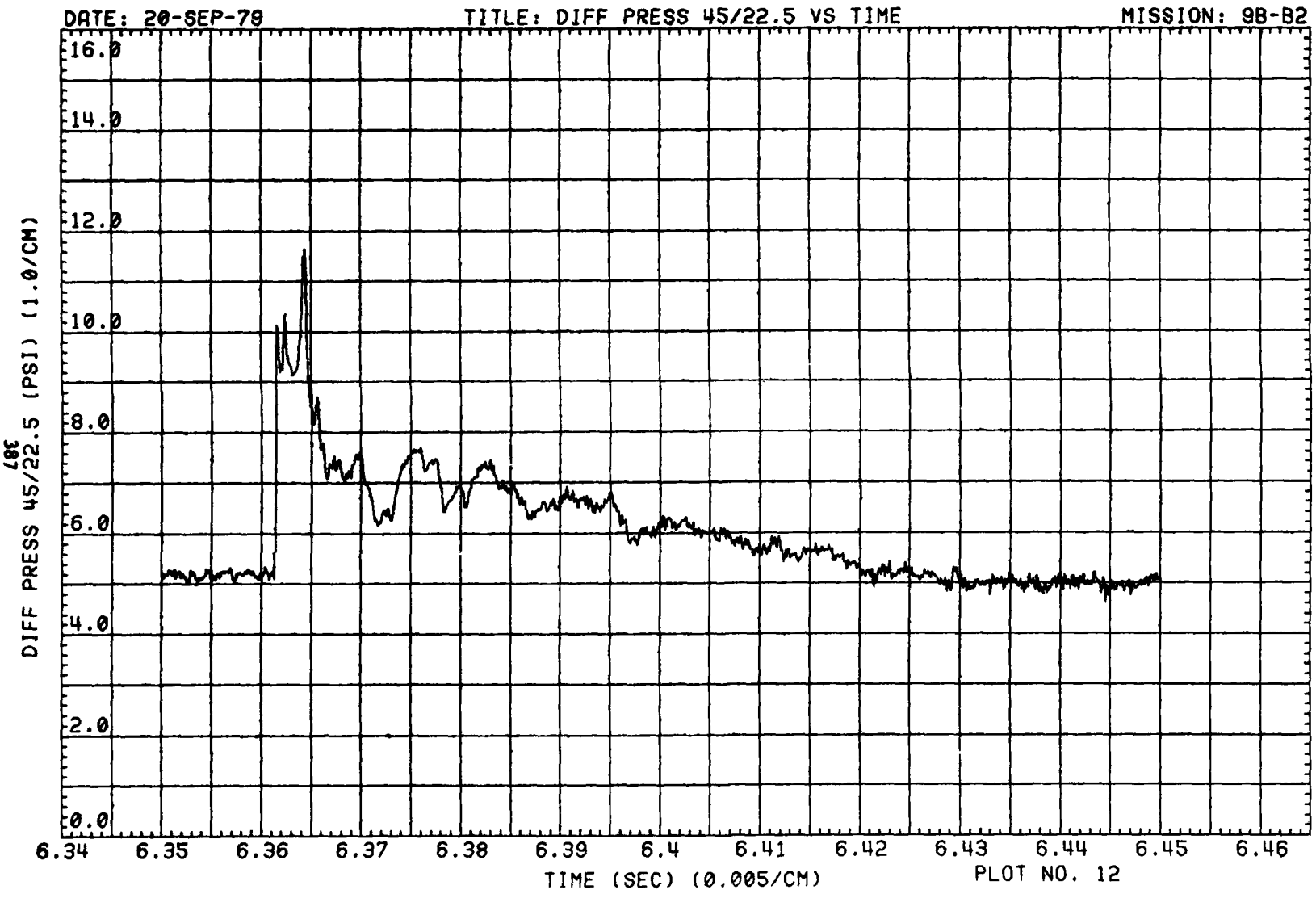

Figure 80. (Continued)

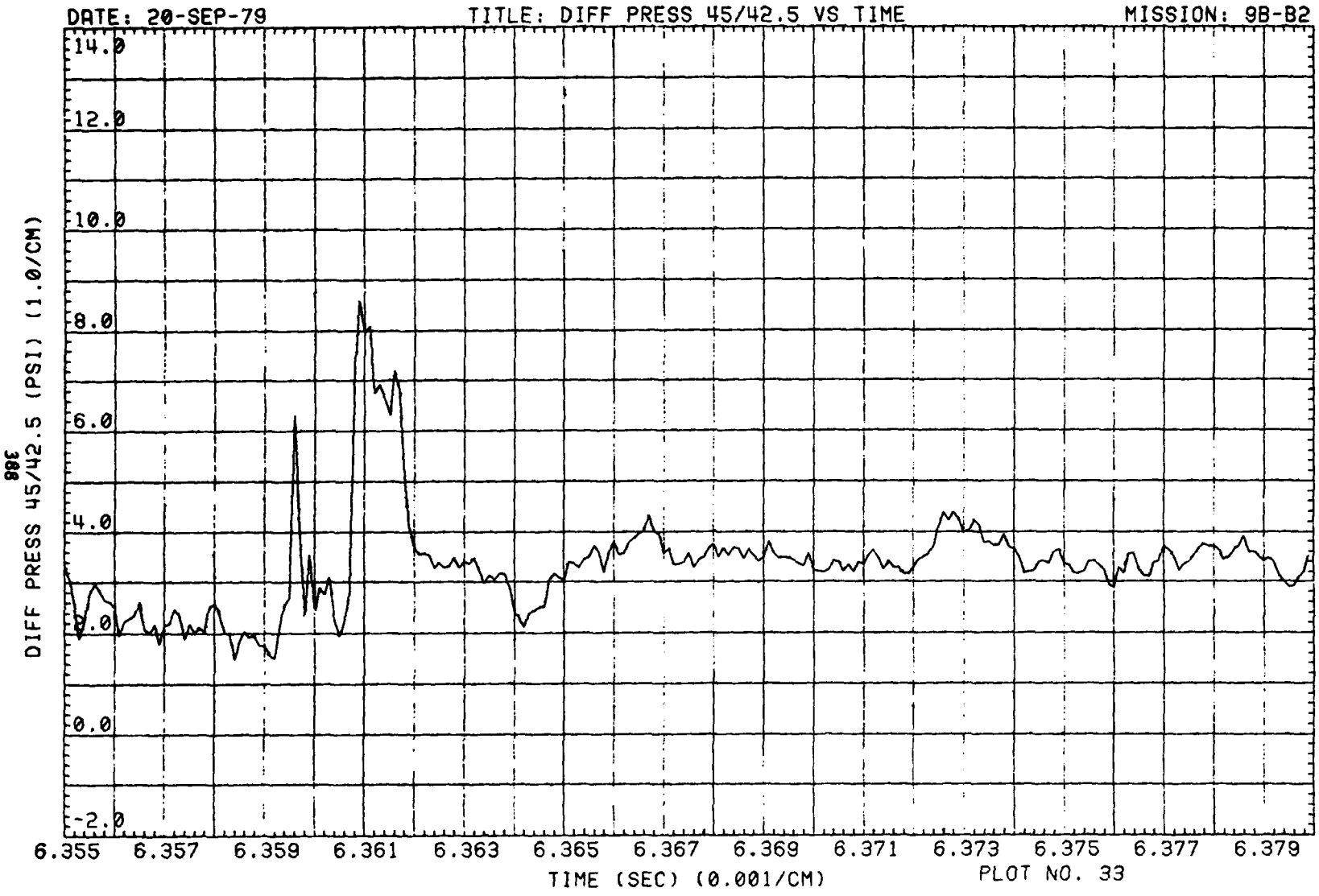

Figure 80. (Continued)

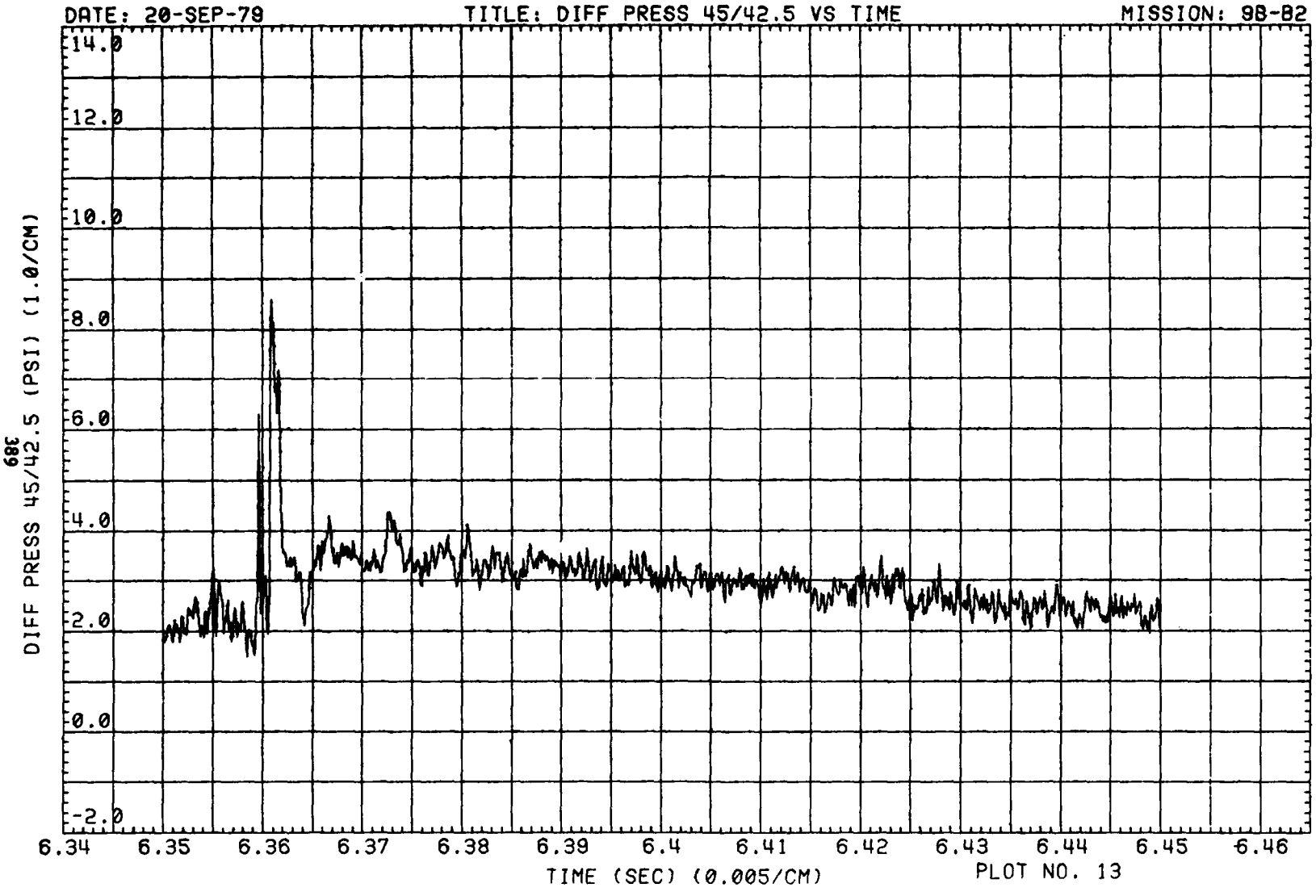

Figure 80. (Continued)

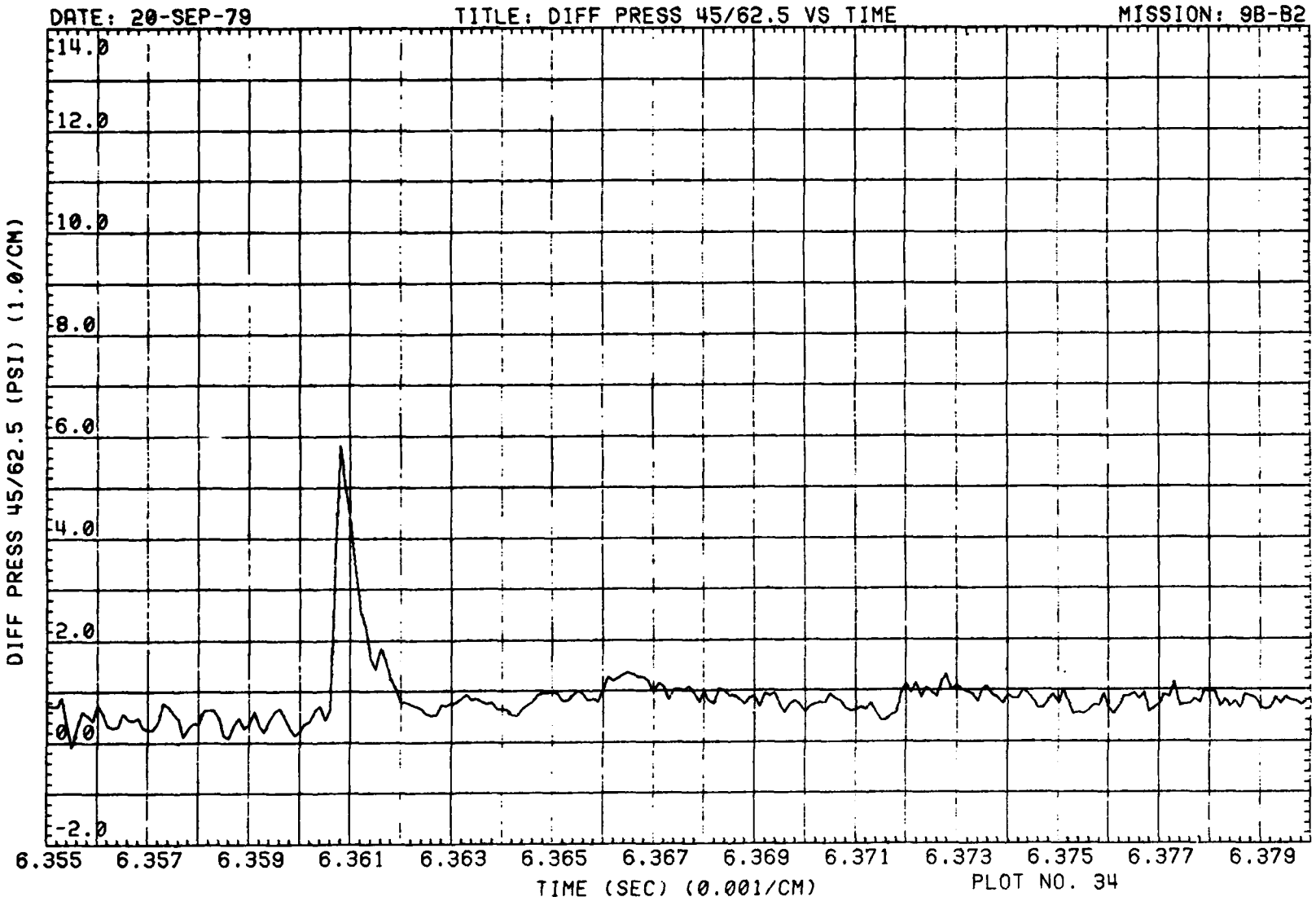

Figure 80. (Continued)

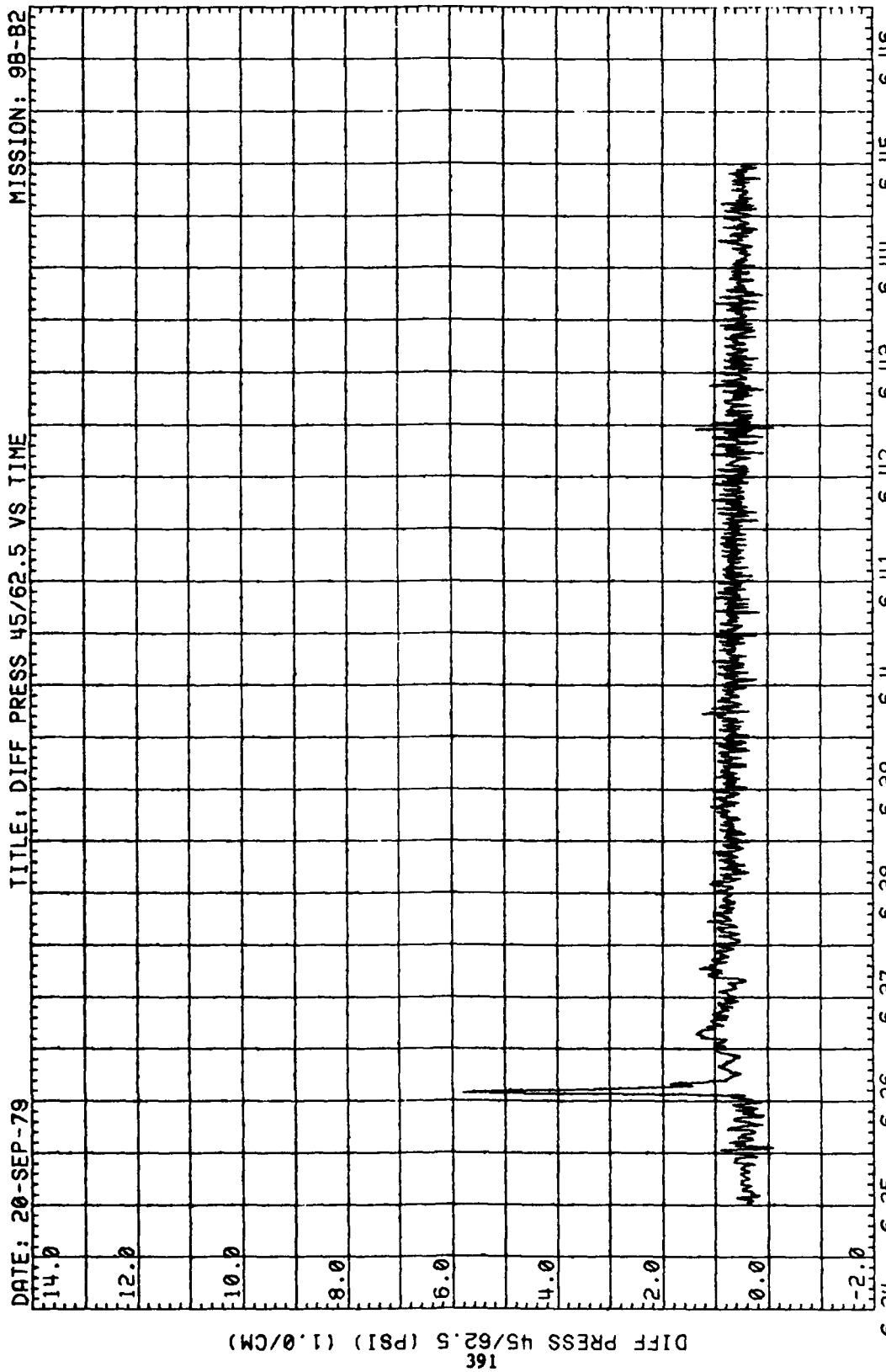

Figure 80. (Continued)

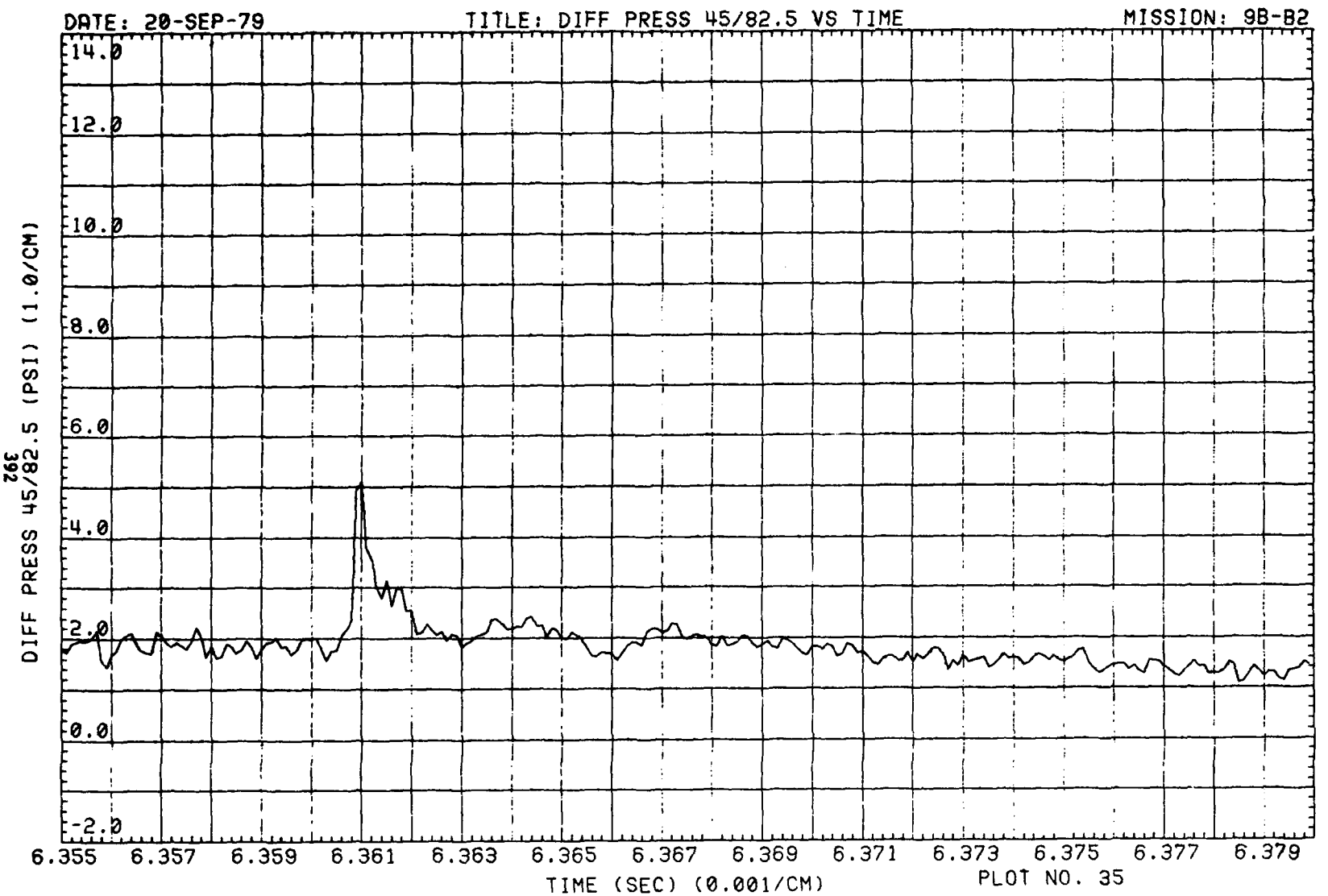

Figure 80. (Continued)

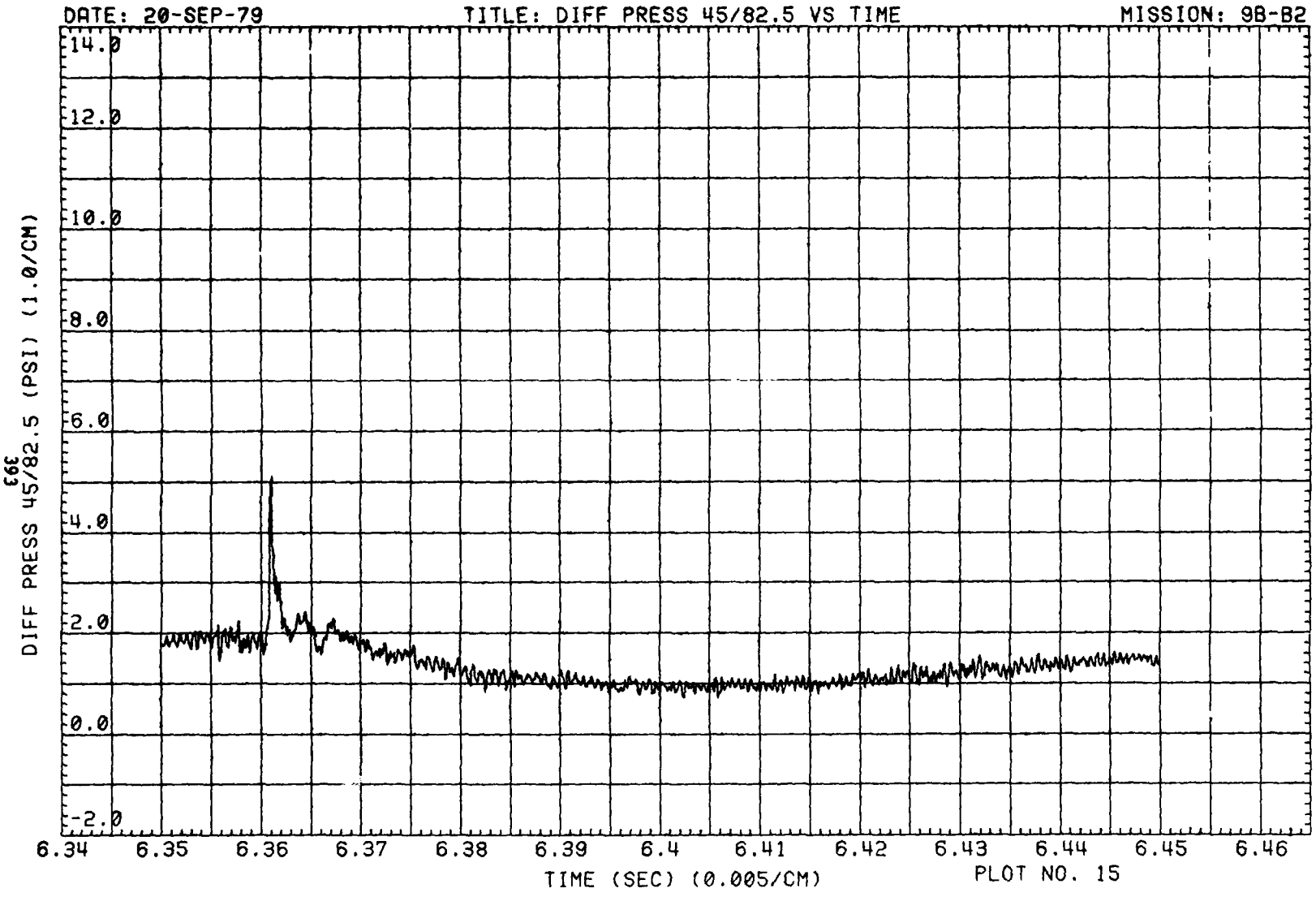

Figure 80. (Continued)

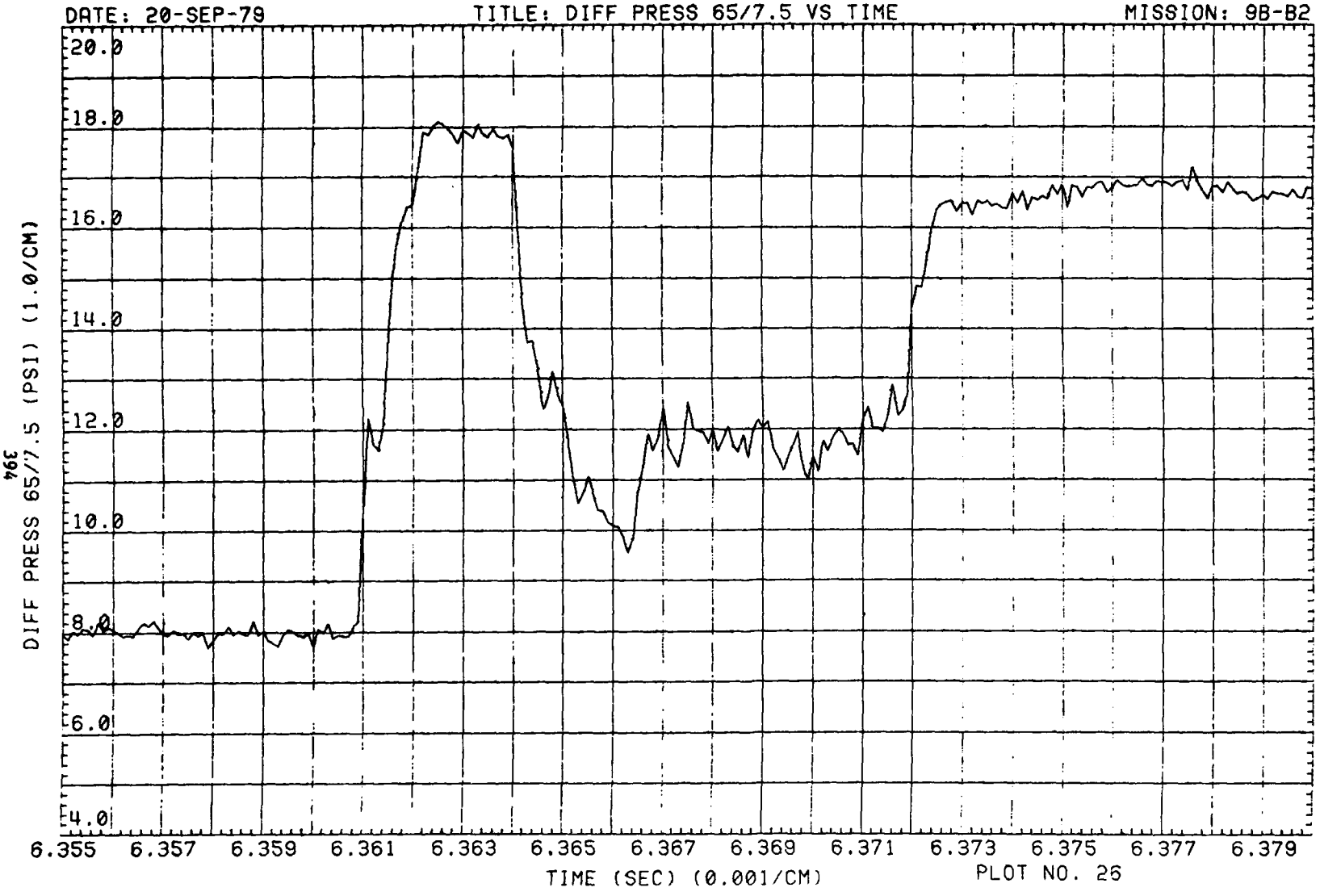

Figure 80. (Continued)

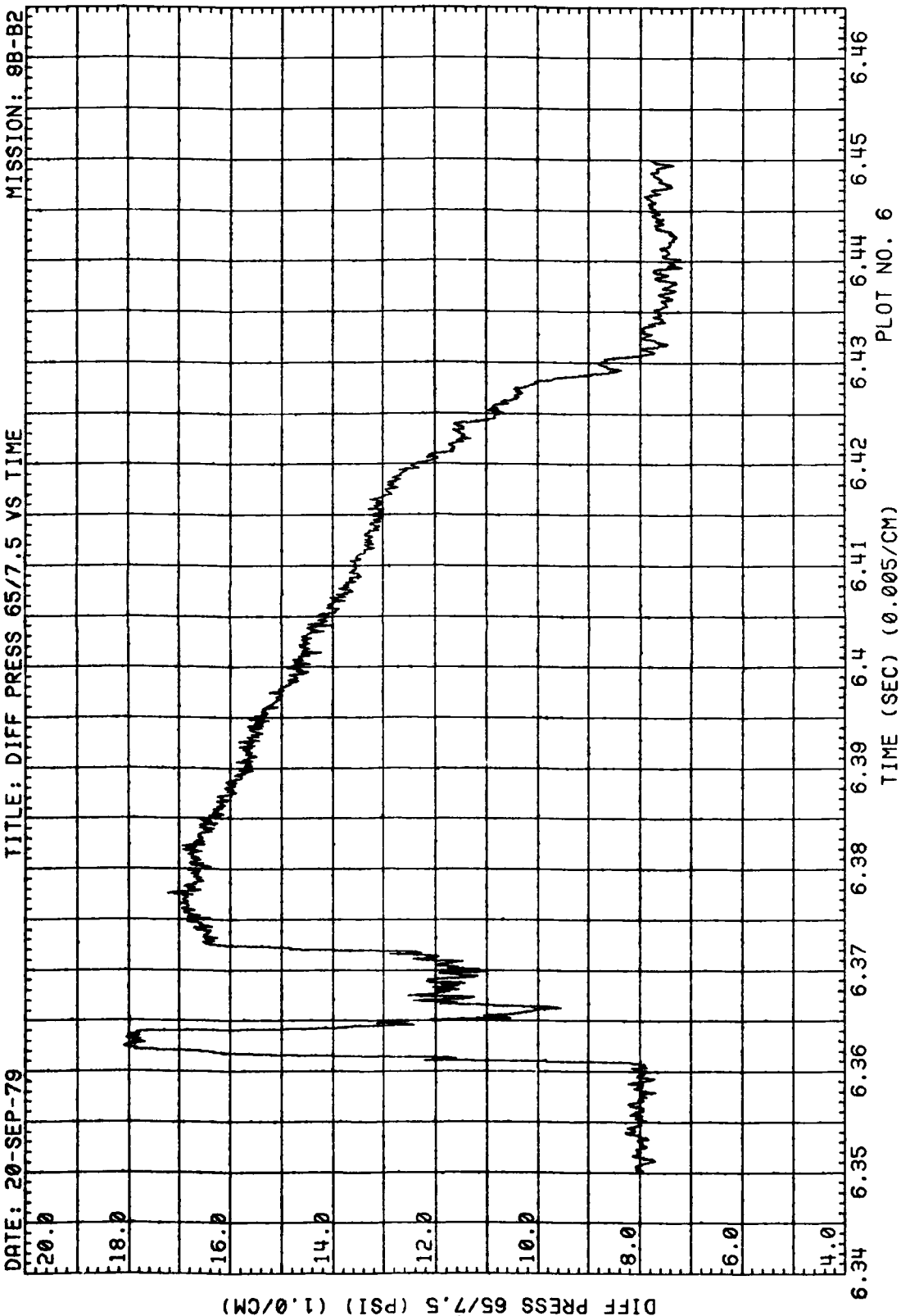

Figure 80. (Continued)

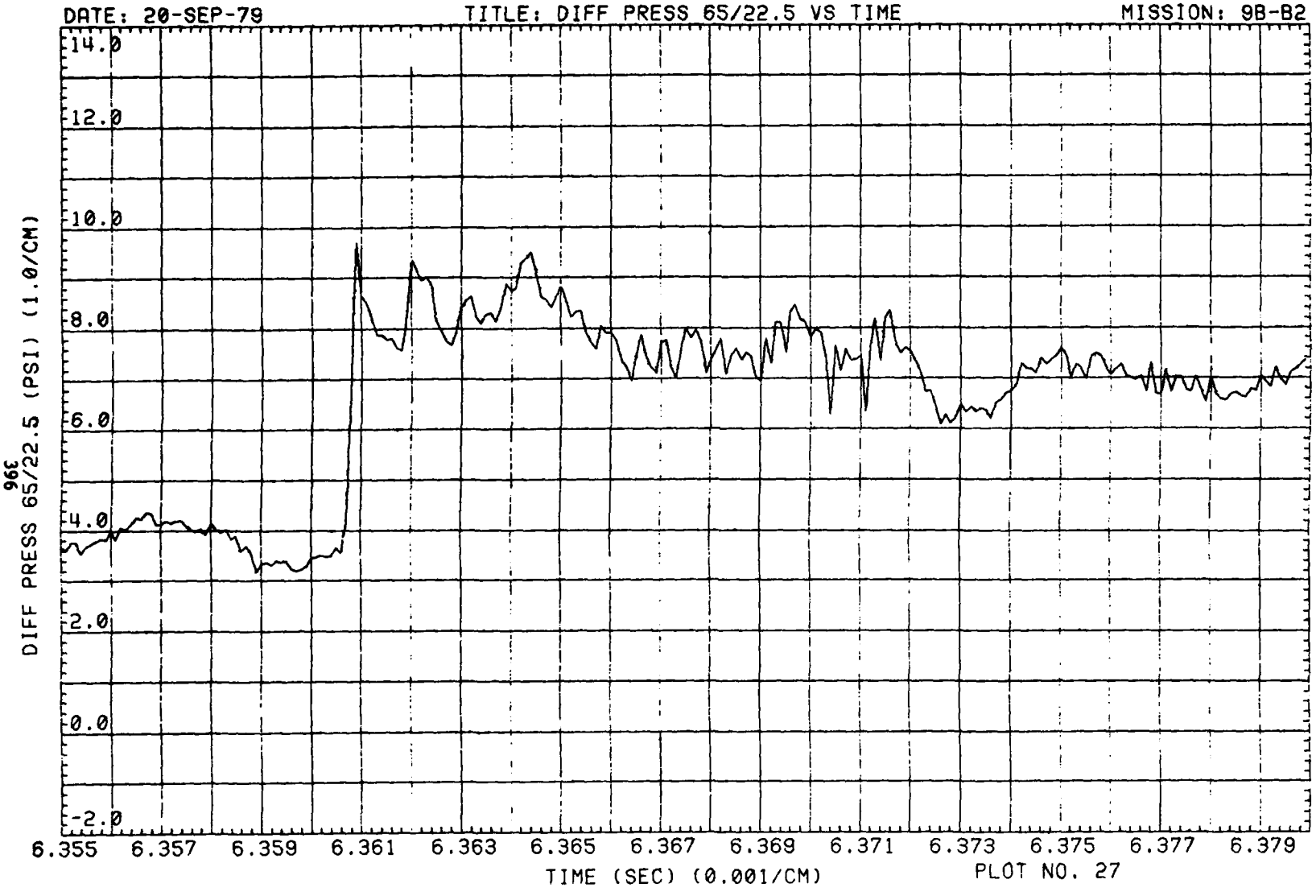

Figure 80. (Continued)

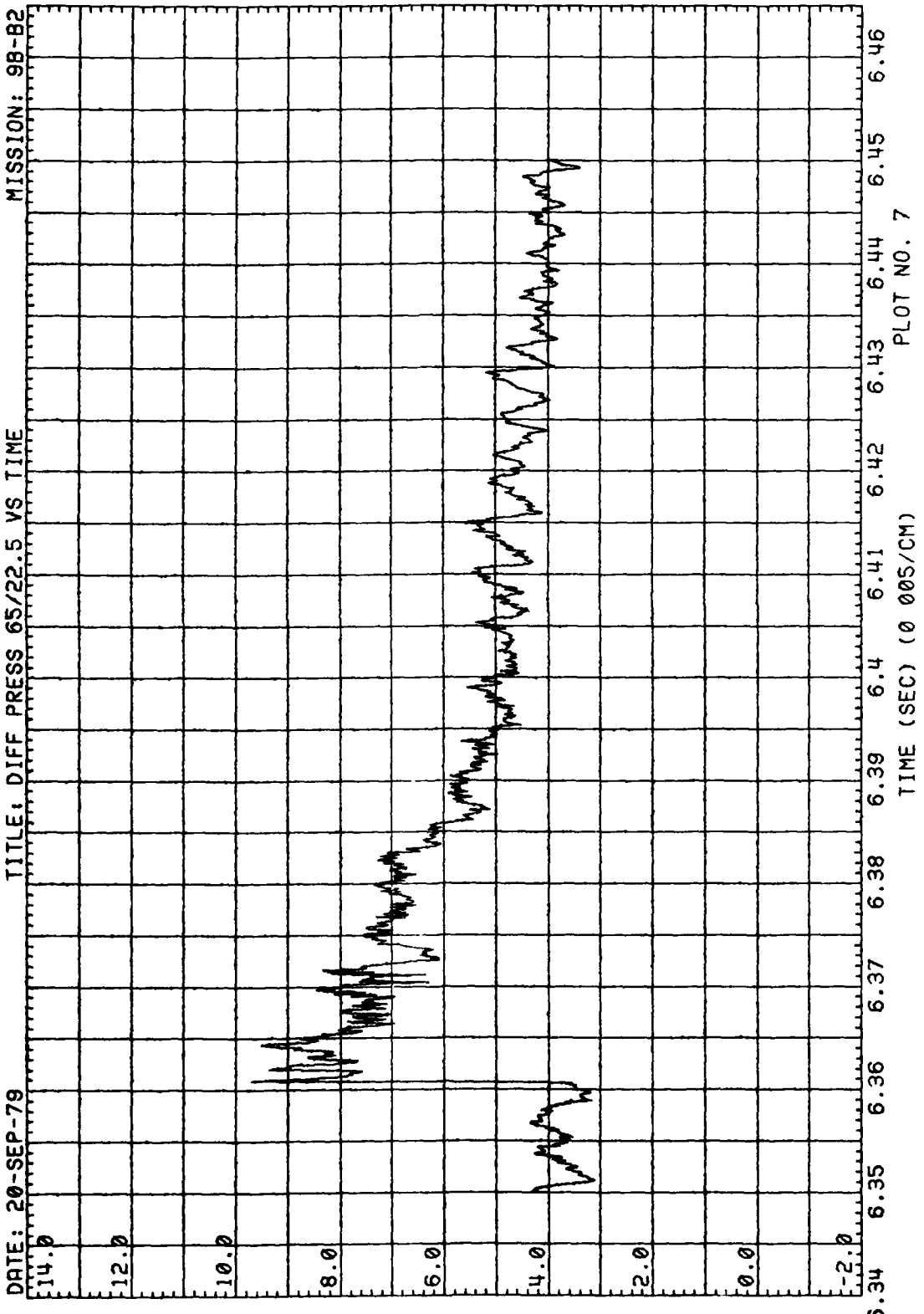

Figure 80. (Continued)

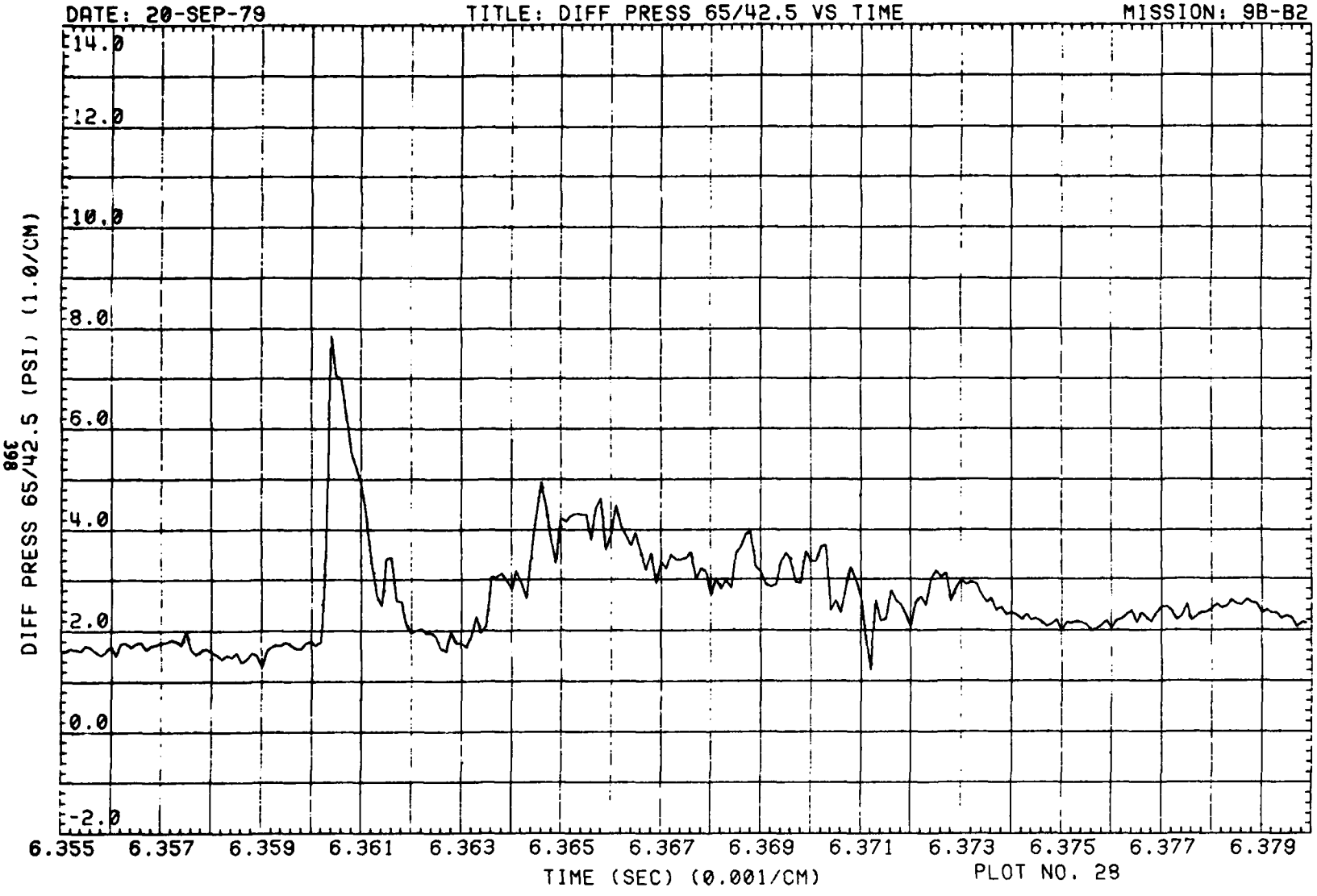

Figure 80. (Continued)

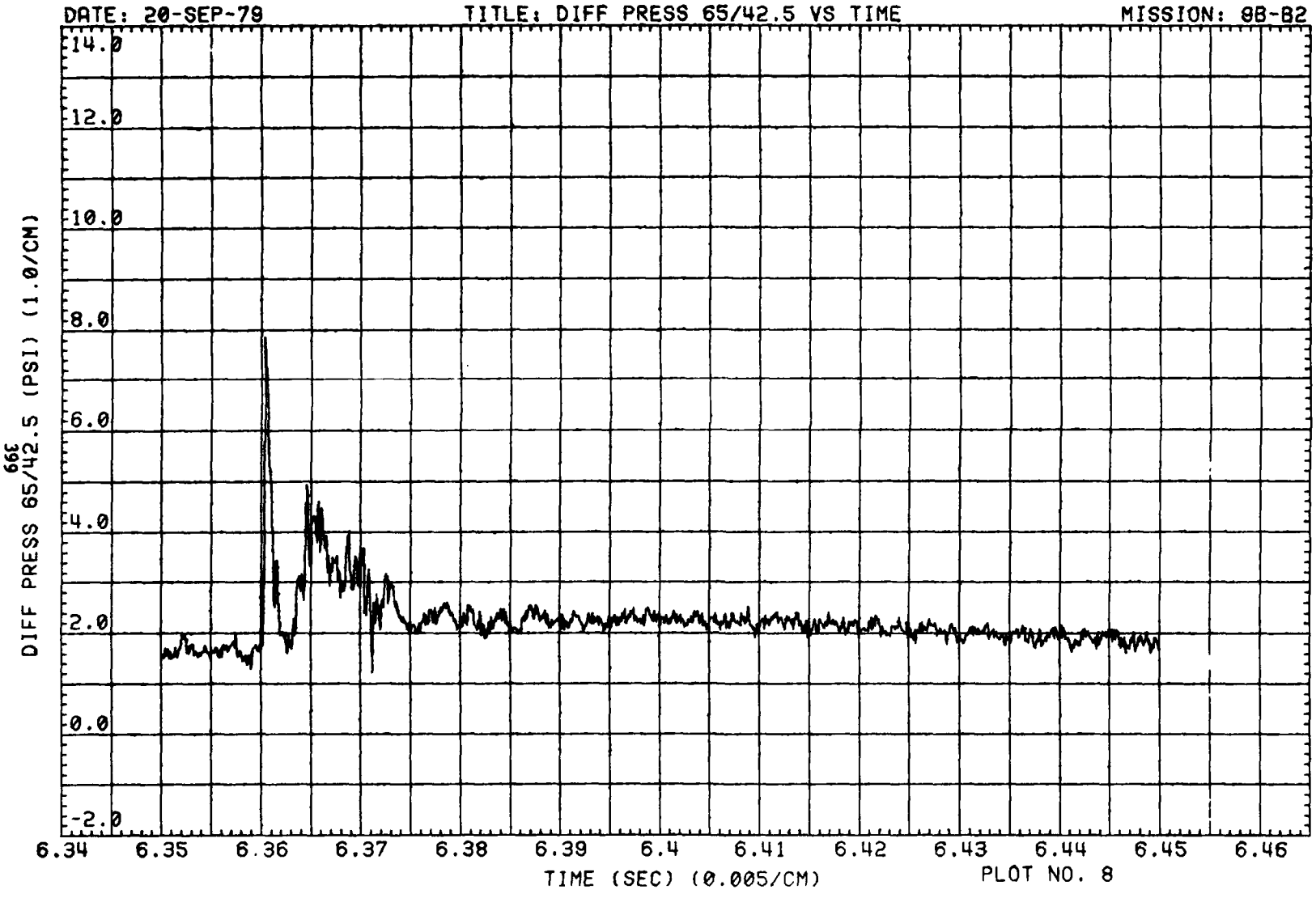

Figure 80. (Continued)

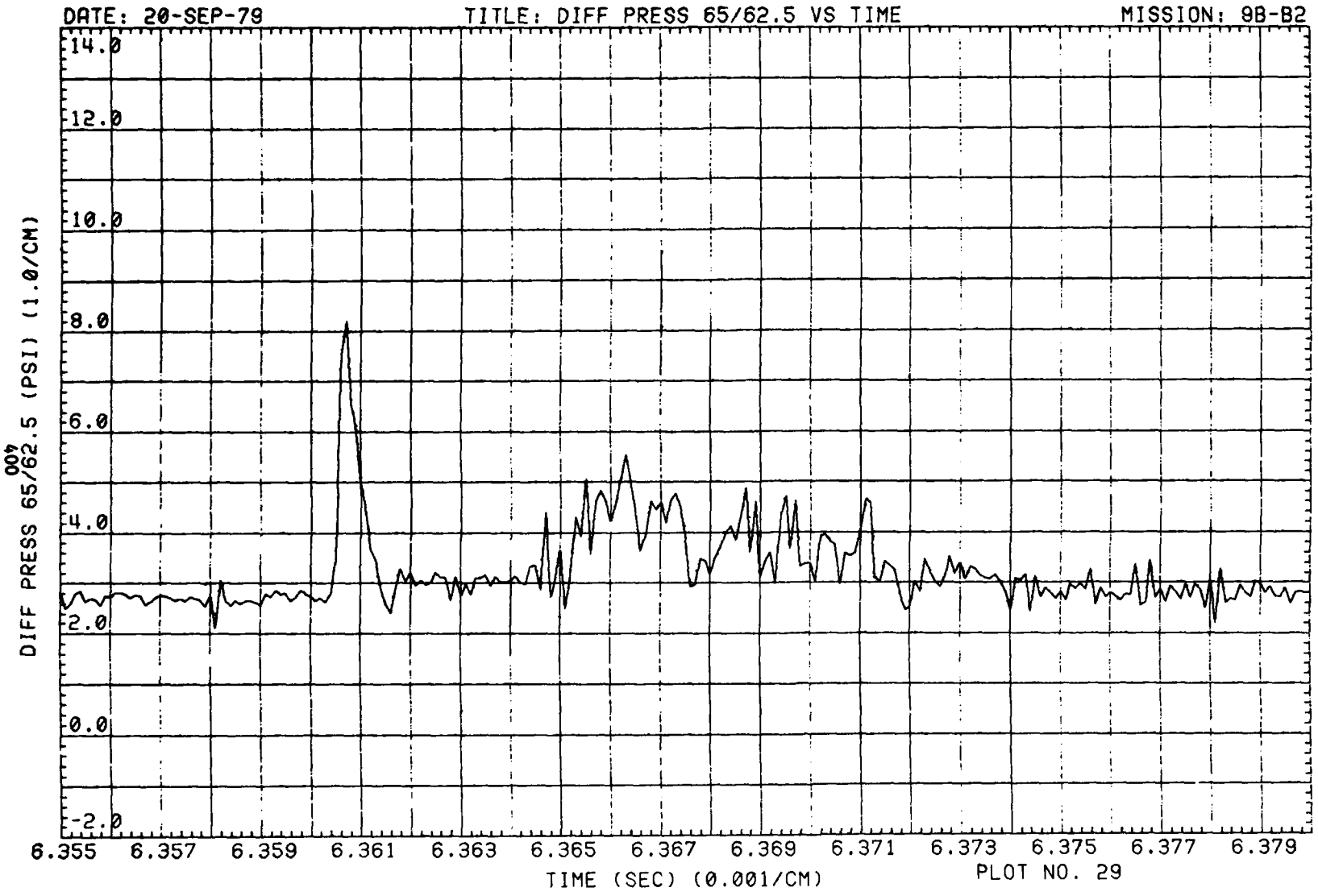

Figure 80. (Continued)

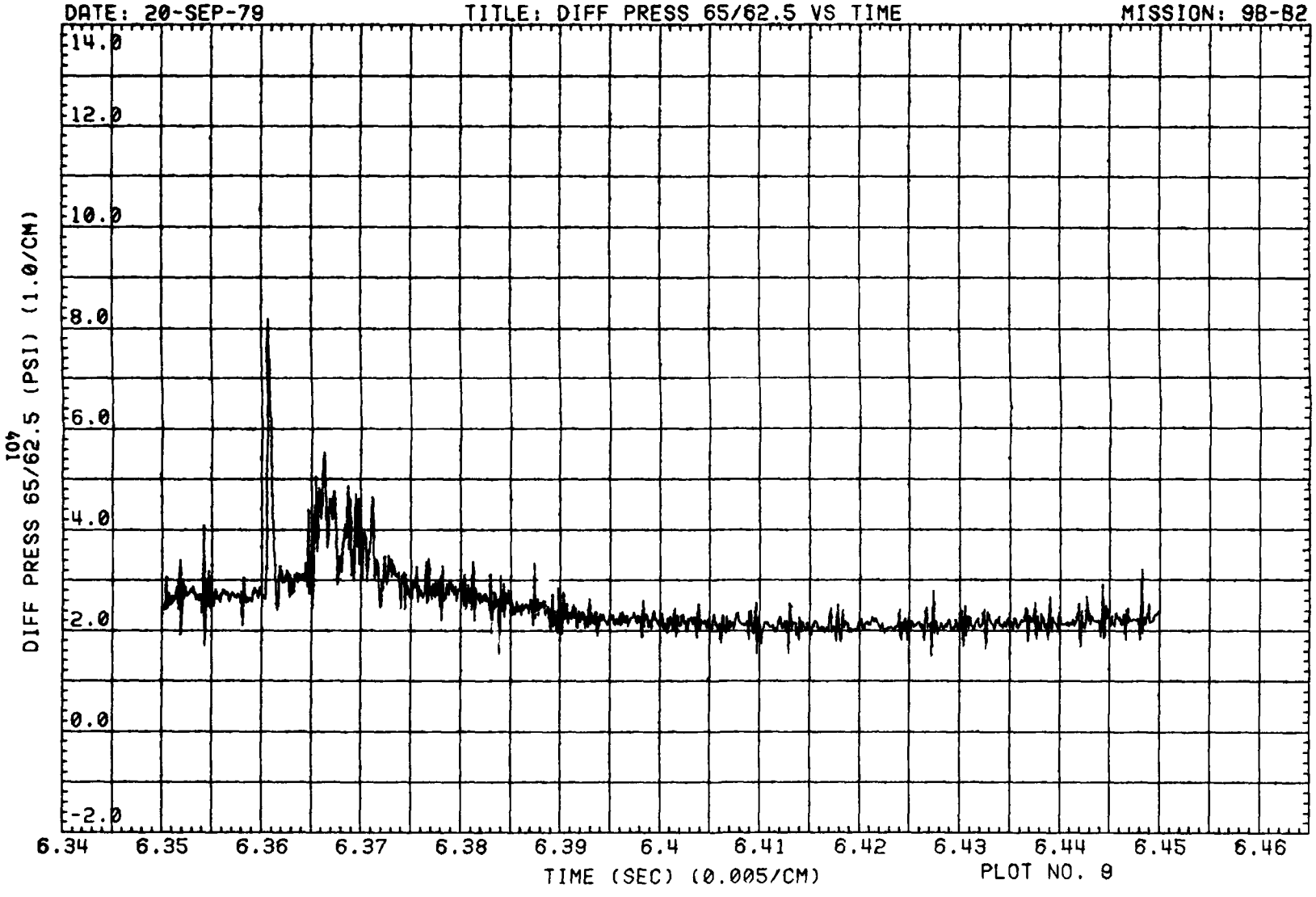

Figure 80. (Continued)

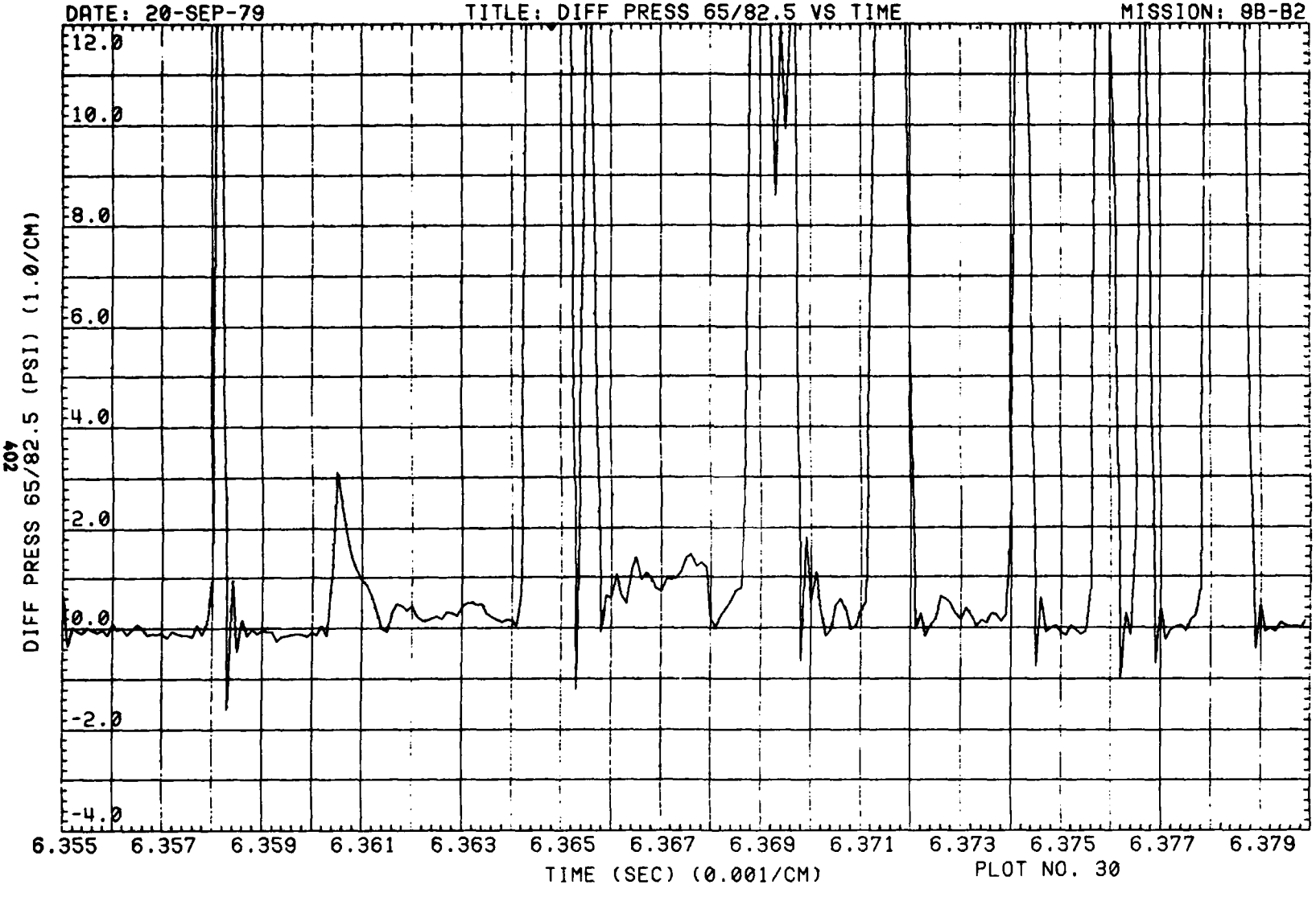

Figure 80. (Continued)

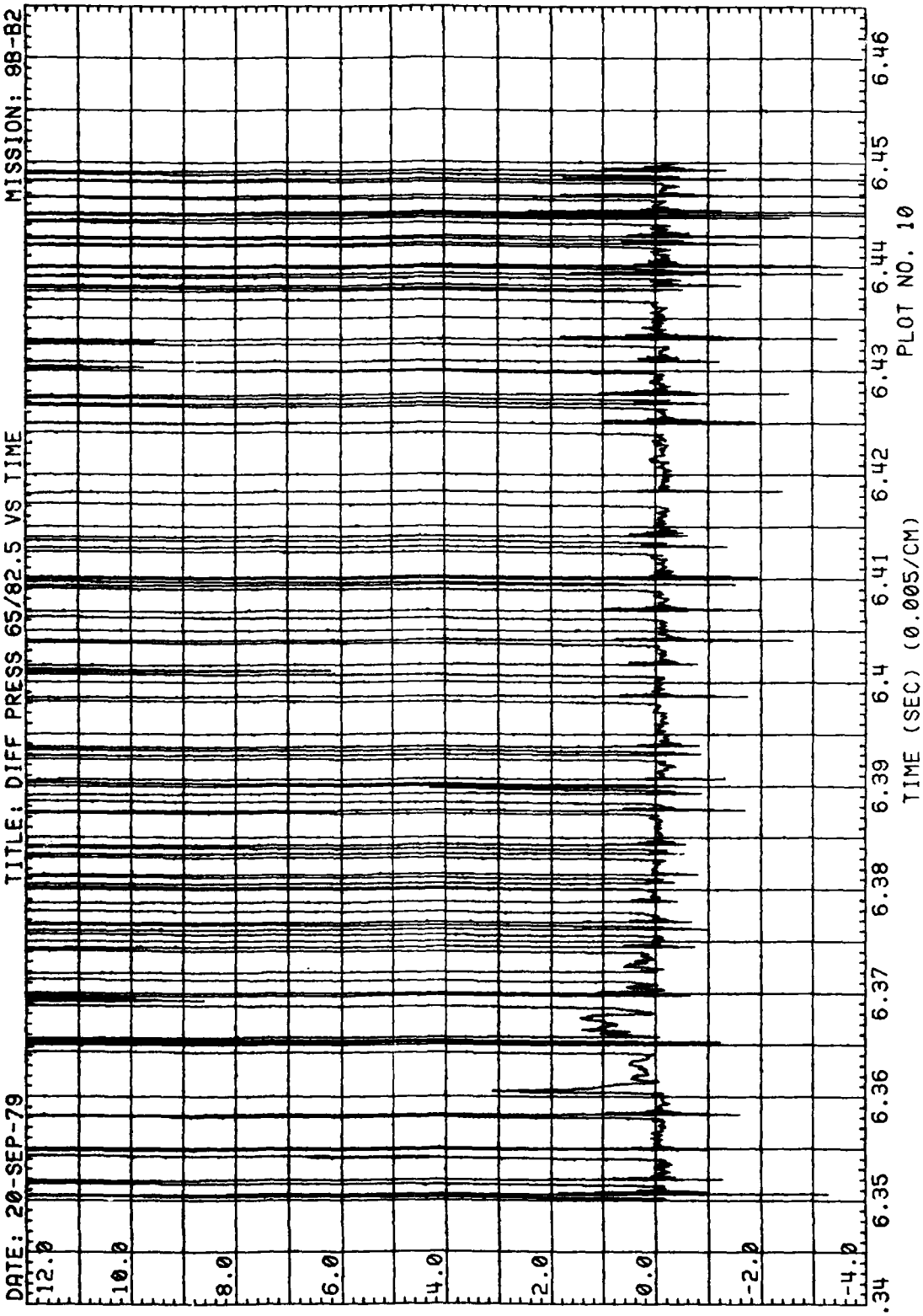

Figure 80. (Continued)

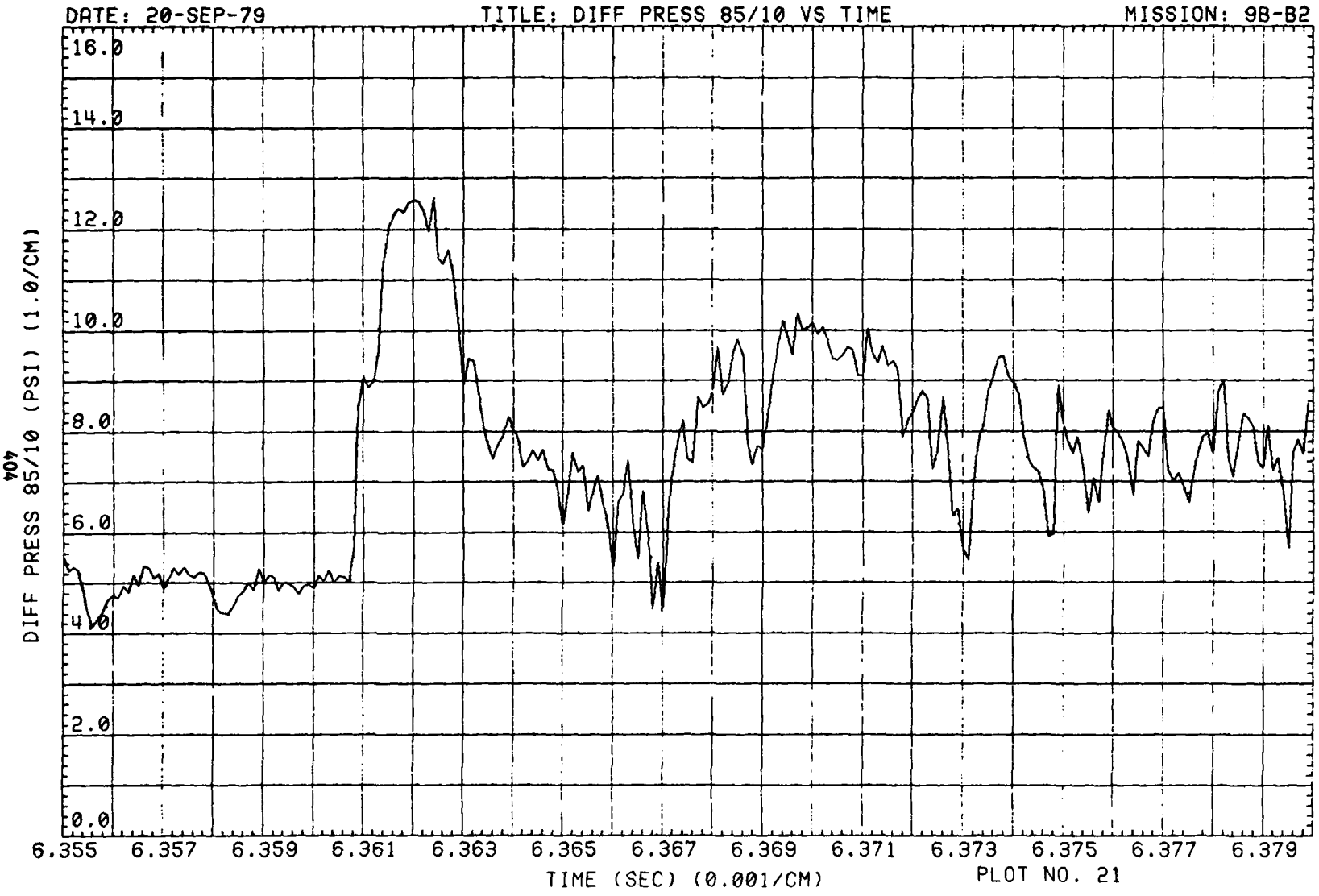

Figure 80. (Continued)

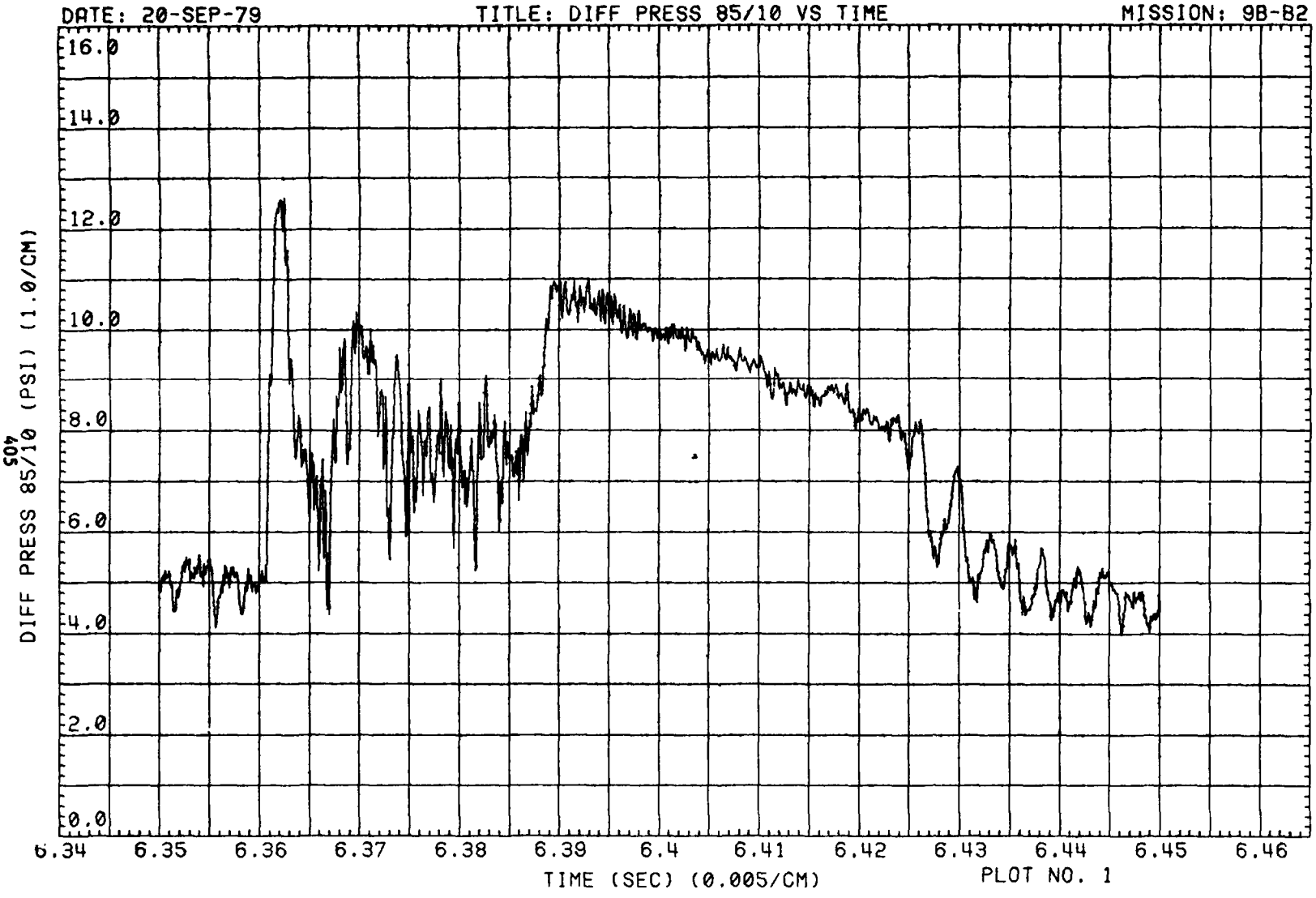

Figure 80. (Continued)

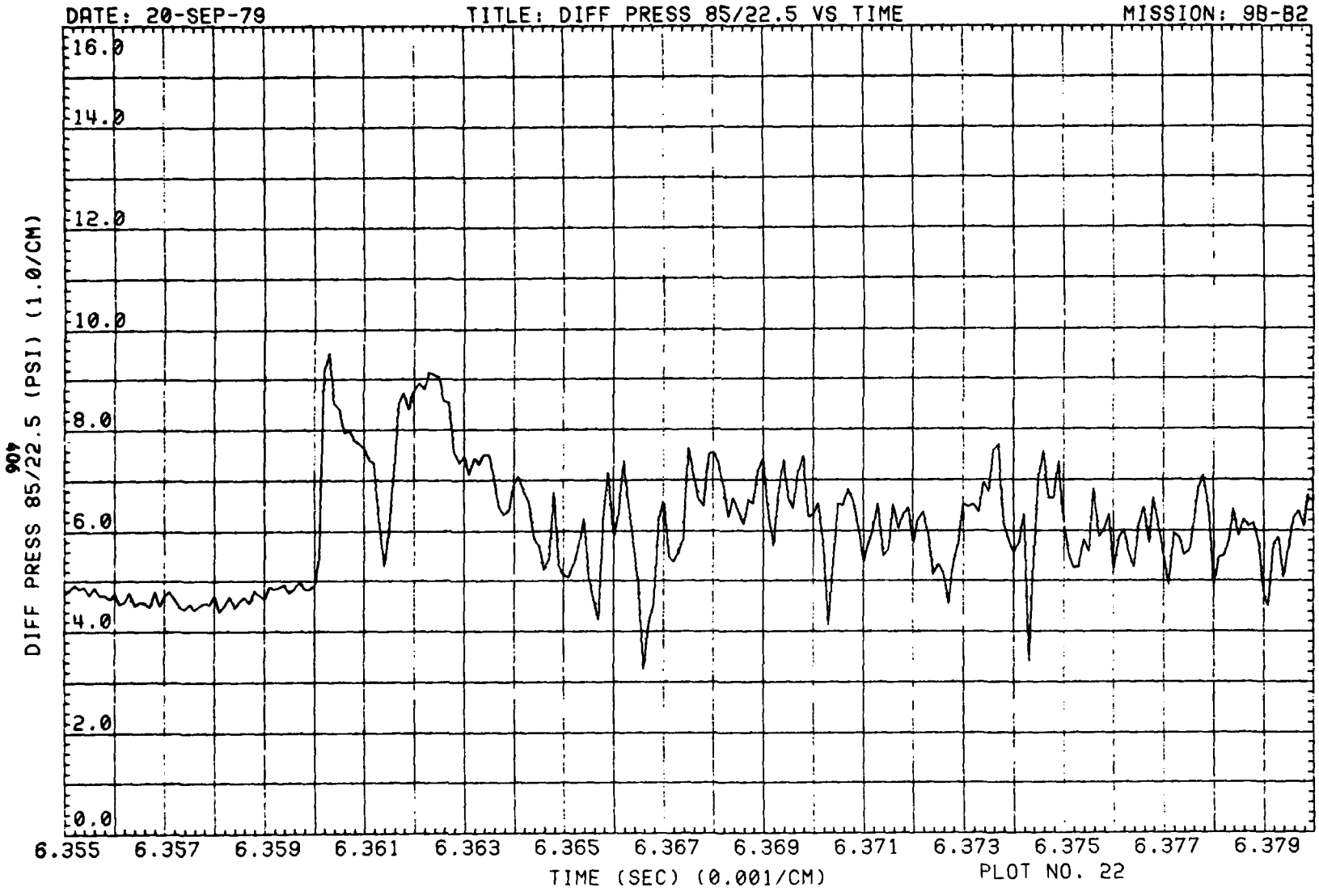

Figure 80. (Continued)

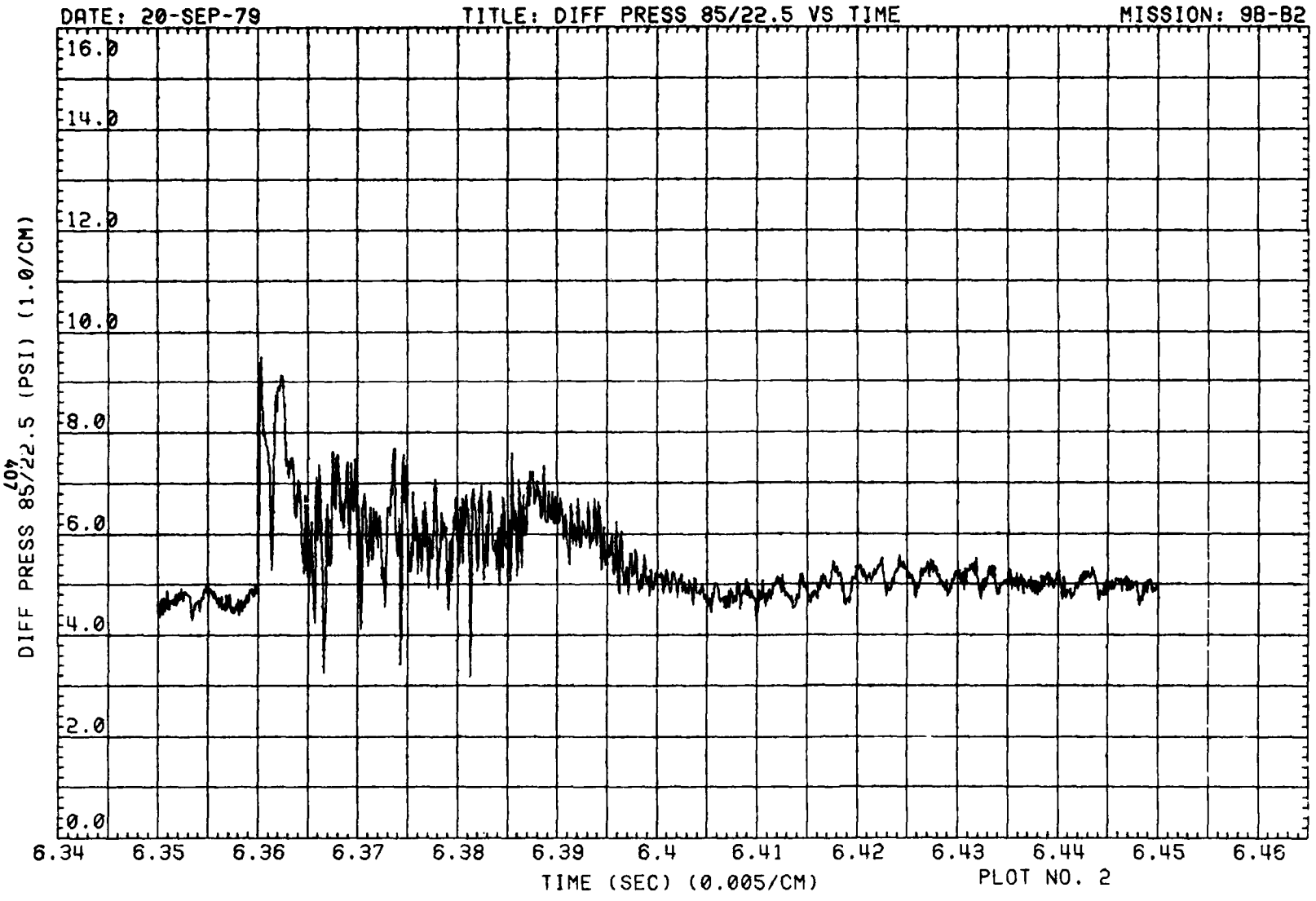

Figure 80. (Continued)

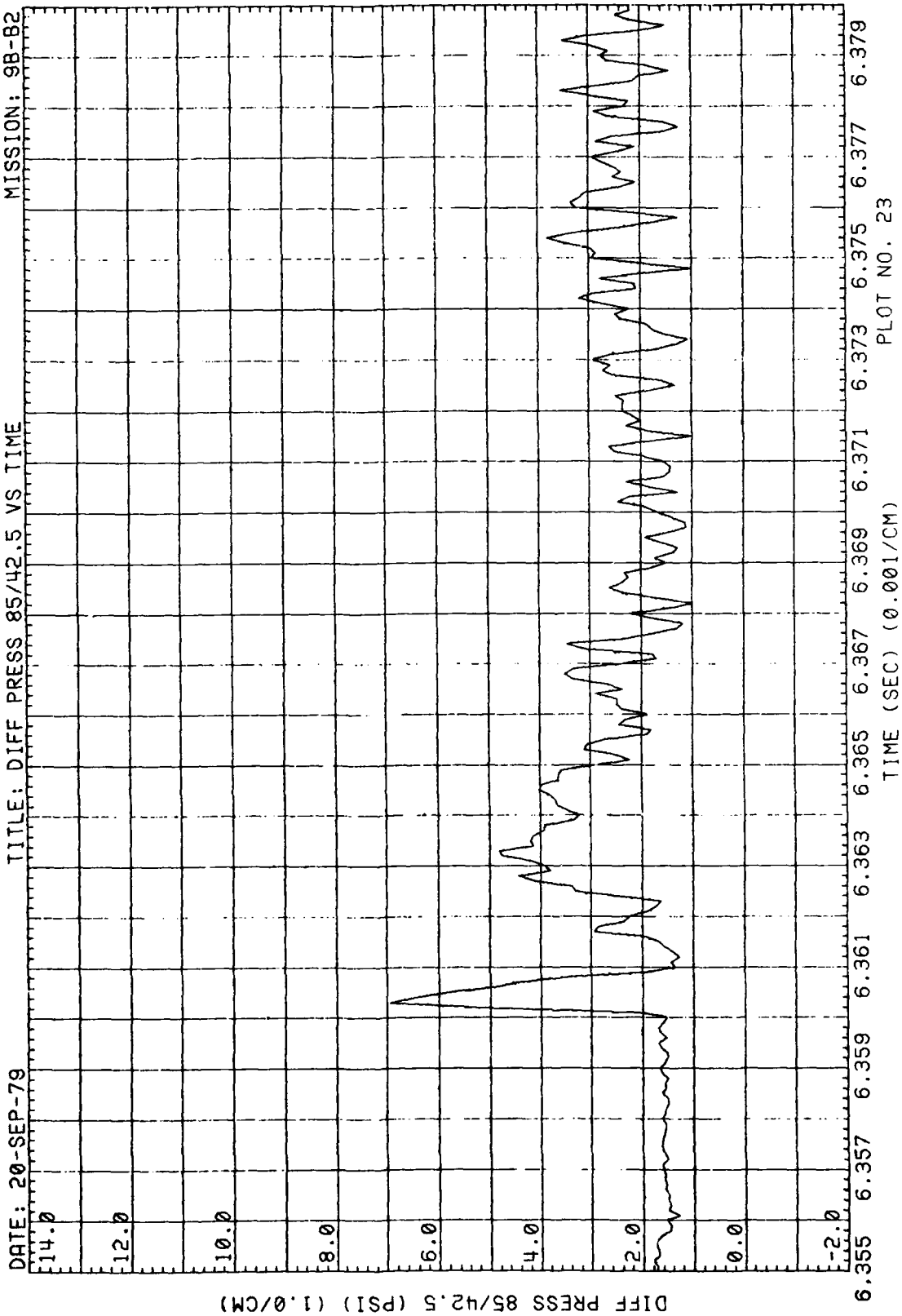

Figure 80. (Continued)

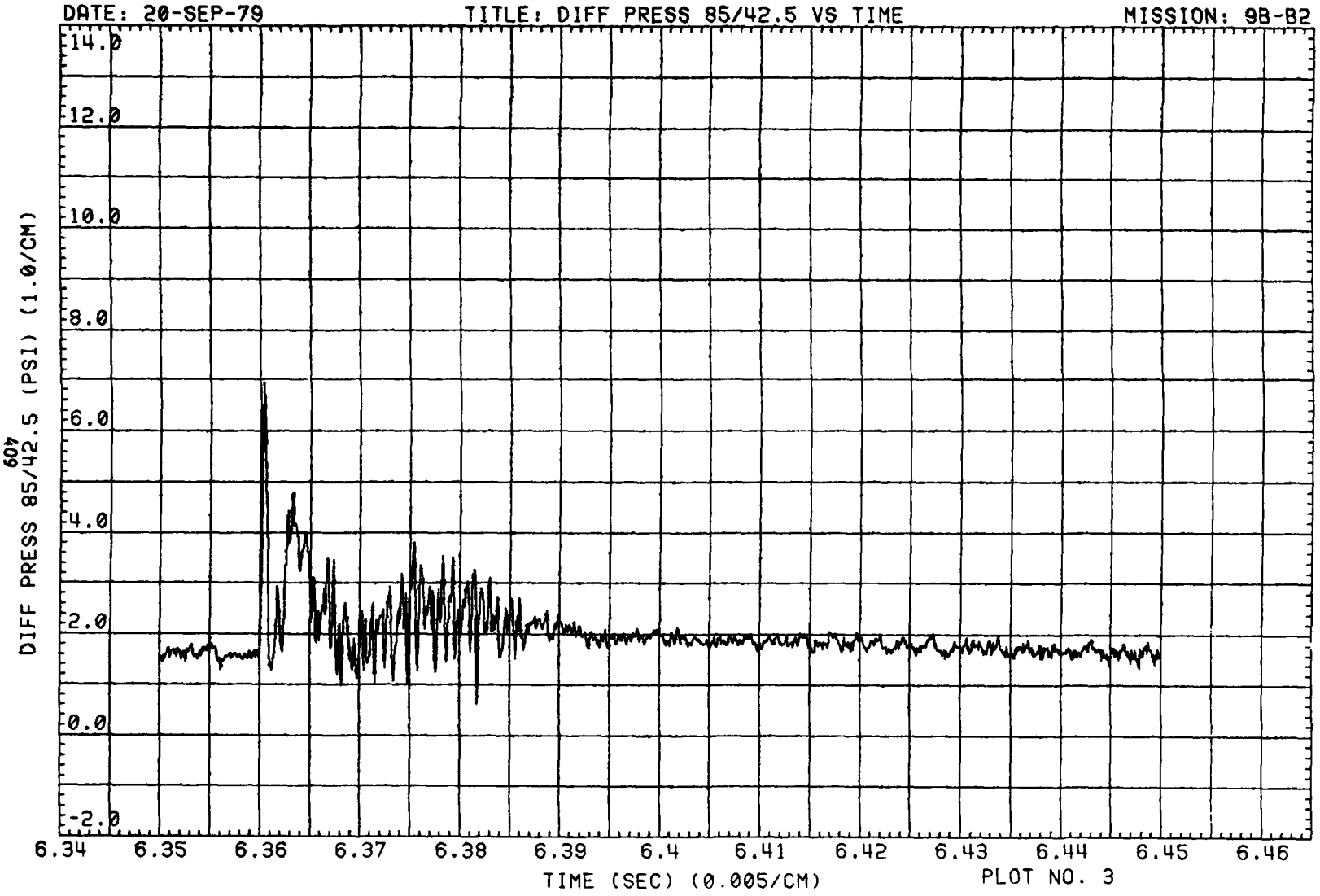

Figure 80. (Continued)

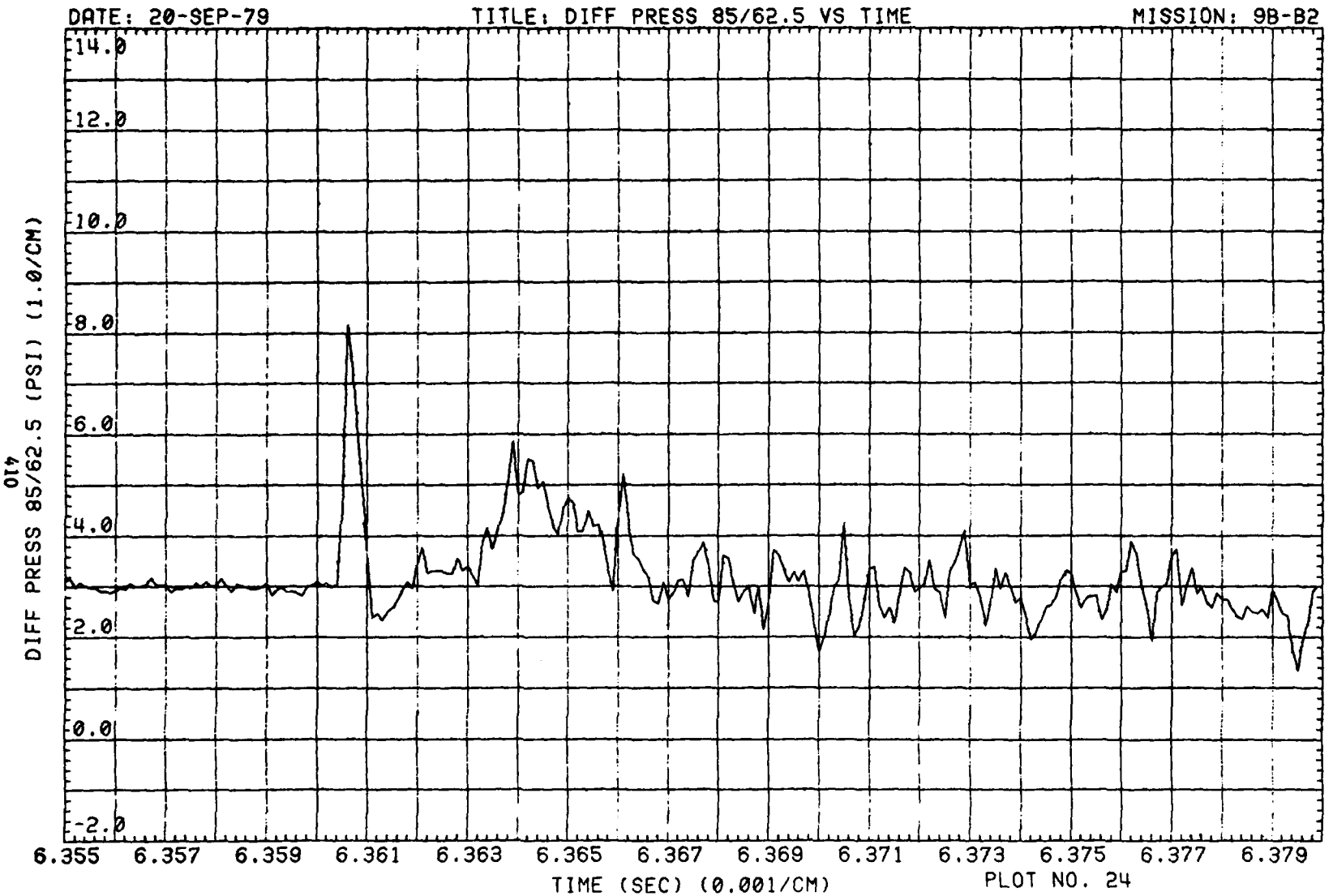

Figure 80. (Continued)

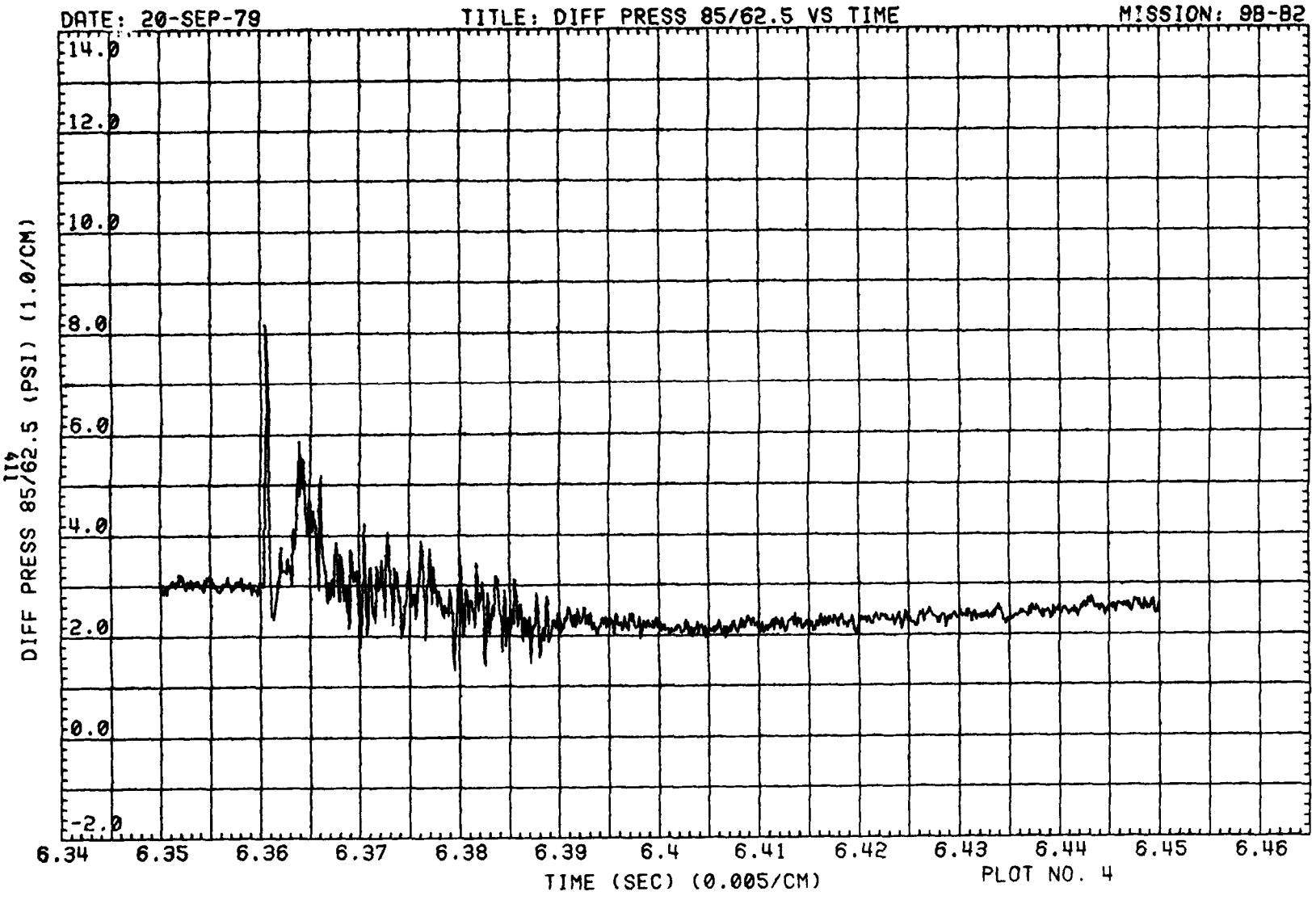

Figure 80. (Continued)

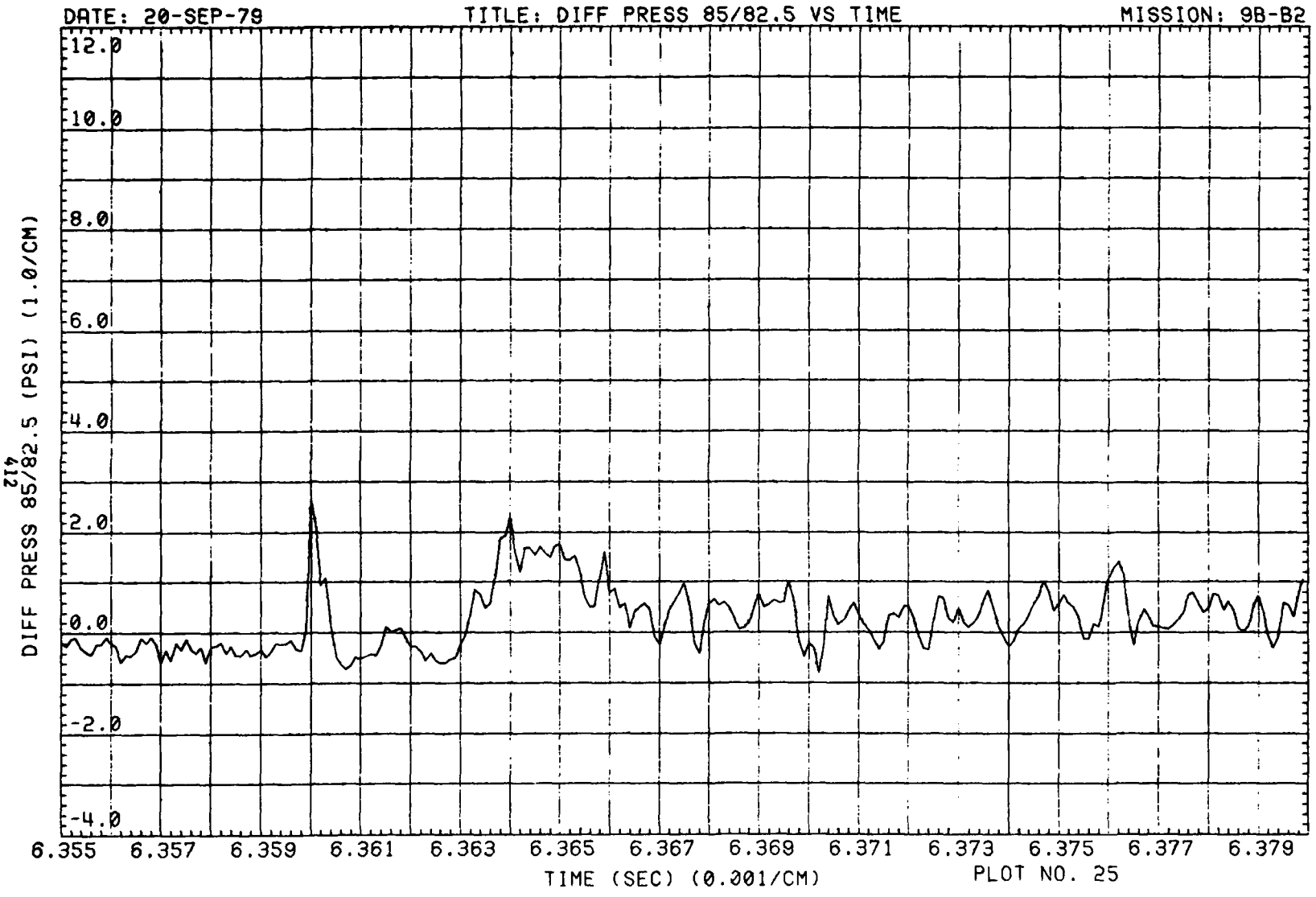

Figure 80. (Continued)

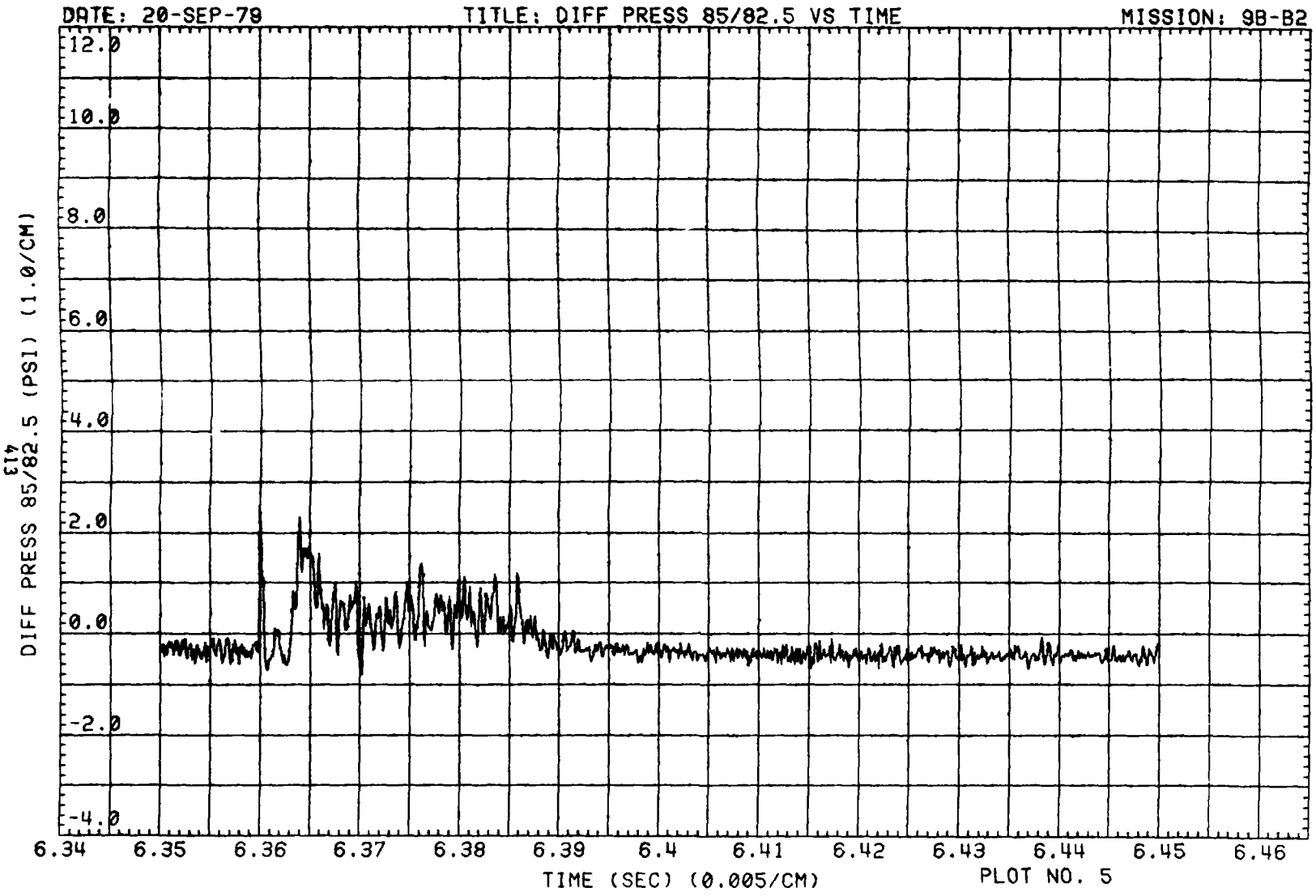

Figure 80. (Concluded)

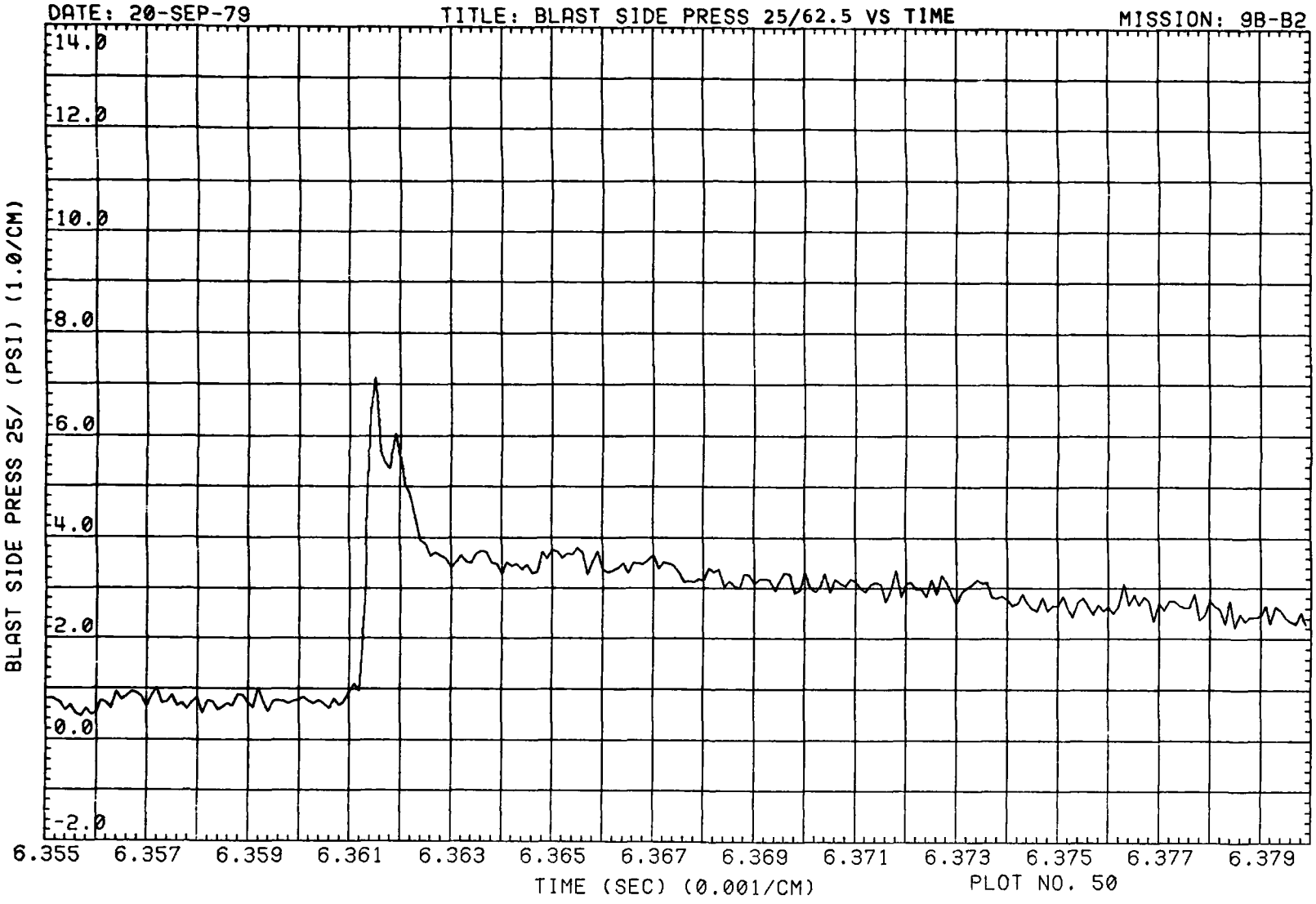

Figure 81. Blastward and Leeward Wing Pressures, Run 9B-B2, Intercept 3

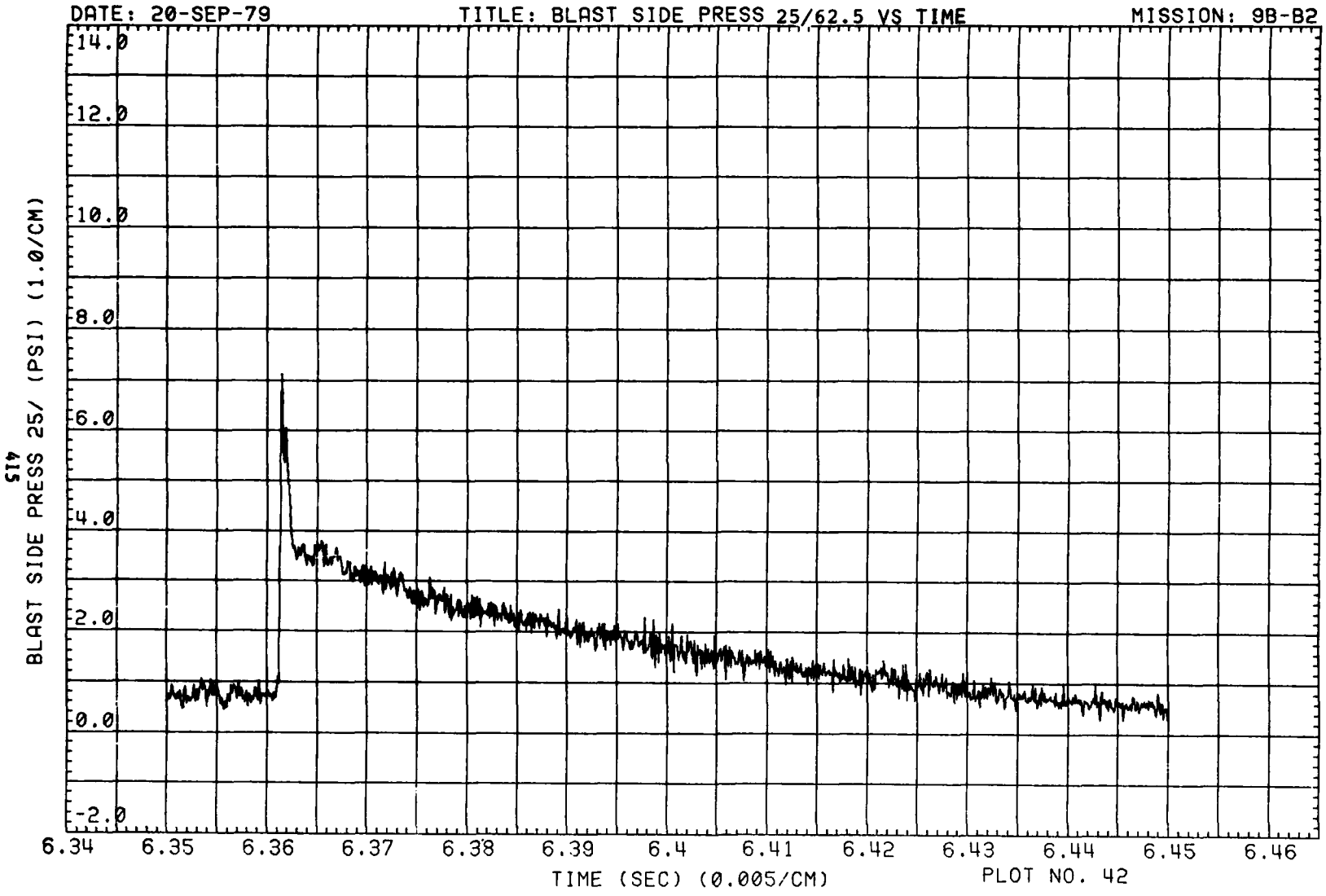

Figure 81. (Continued)

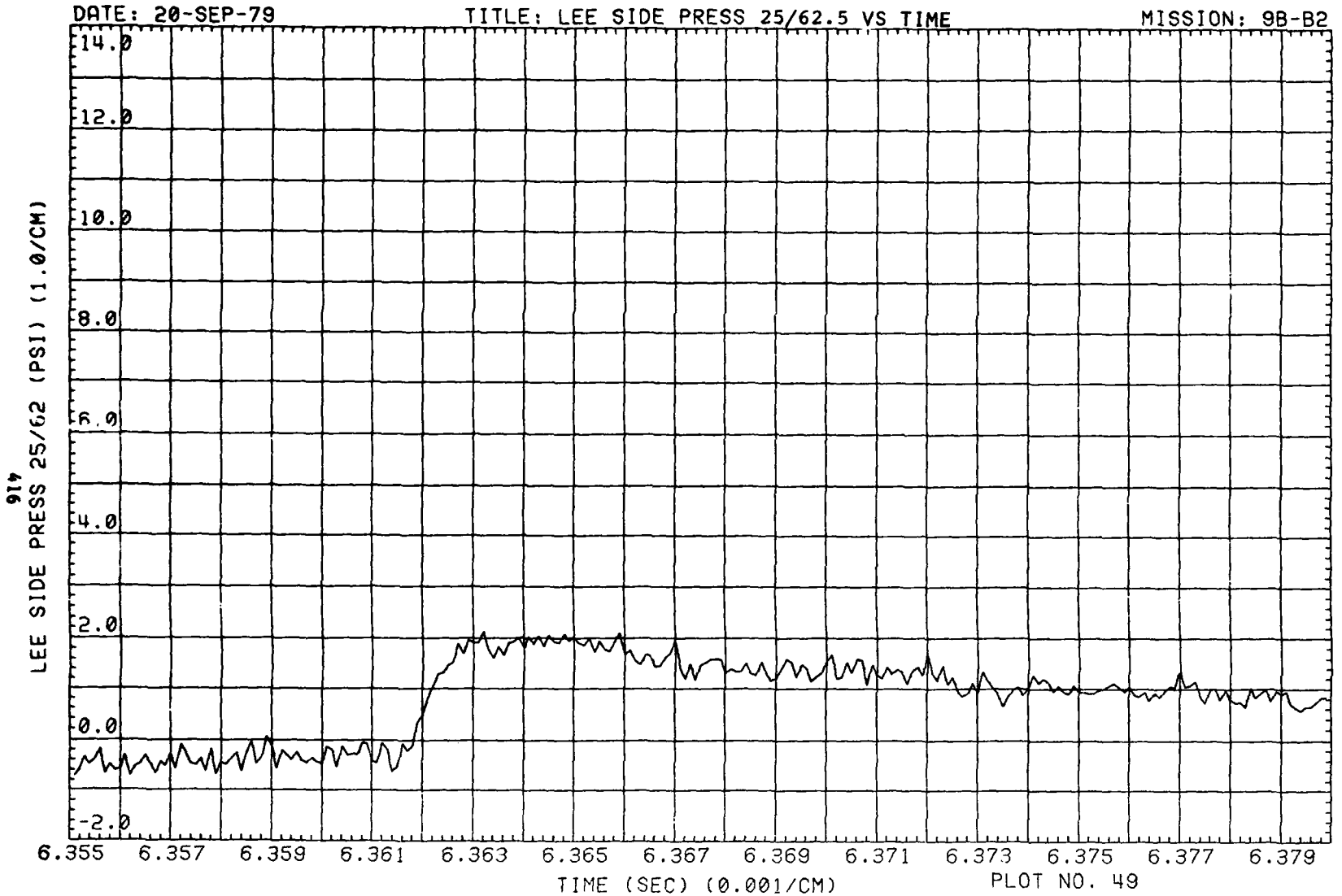

Figure 81. (Continued)

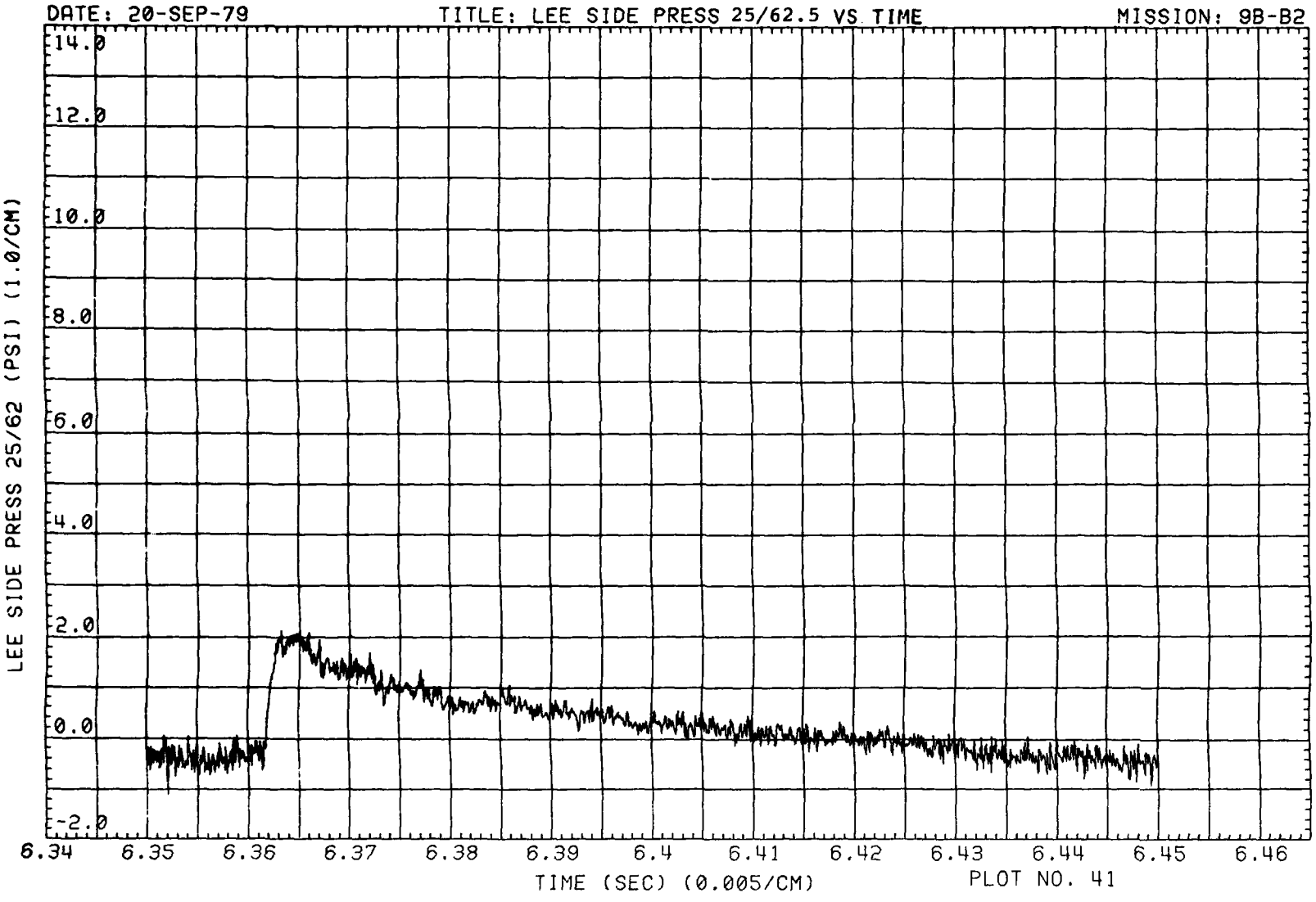

Figure 81. (Concluded)

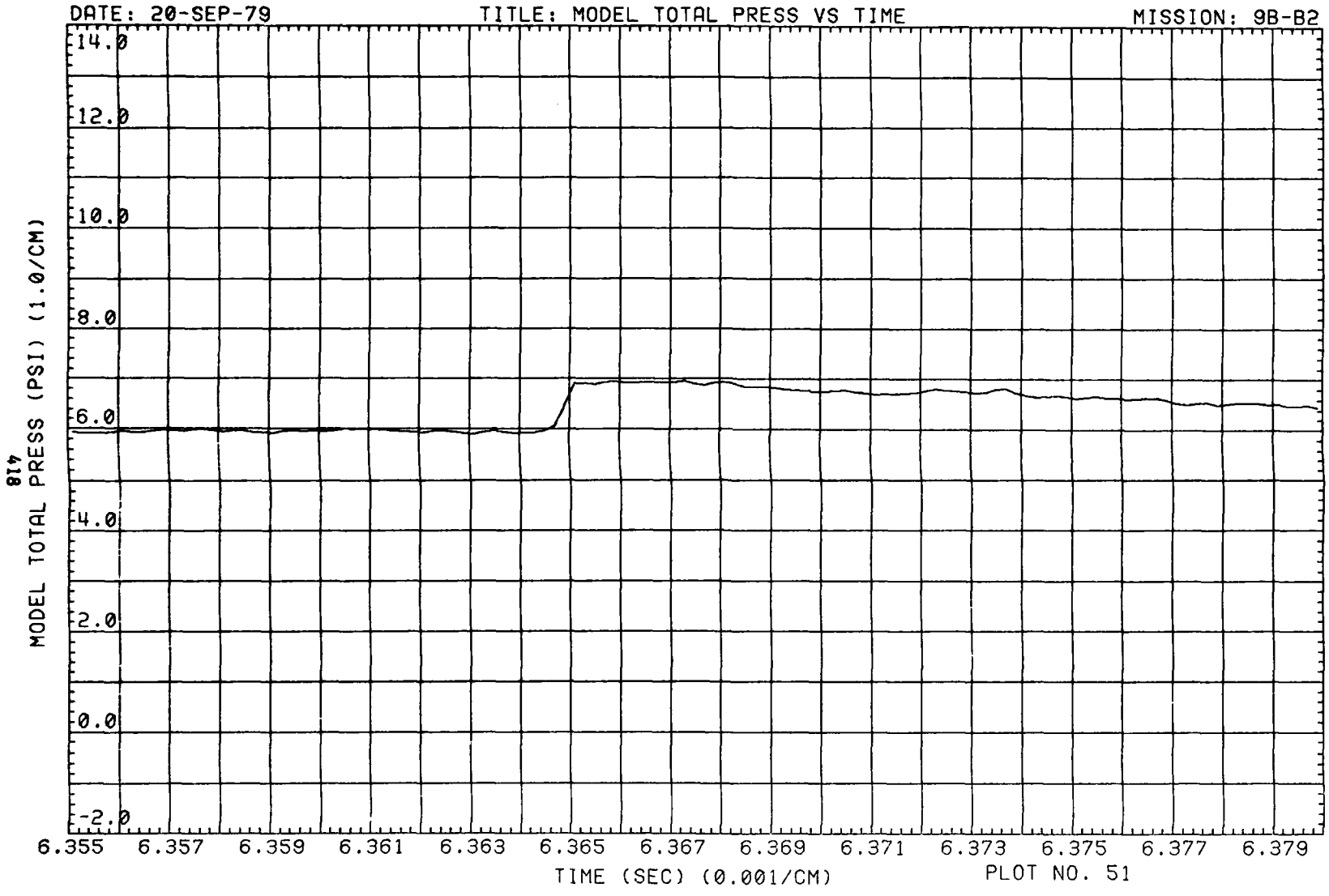

Figure 82. Total Pressure at Model, Run 9B-B2, Intercept 3

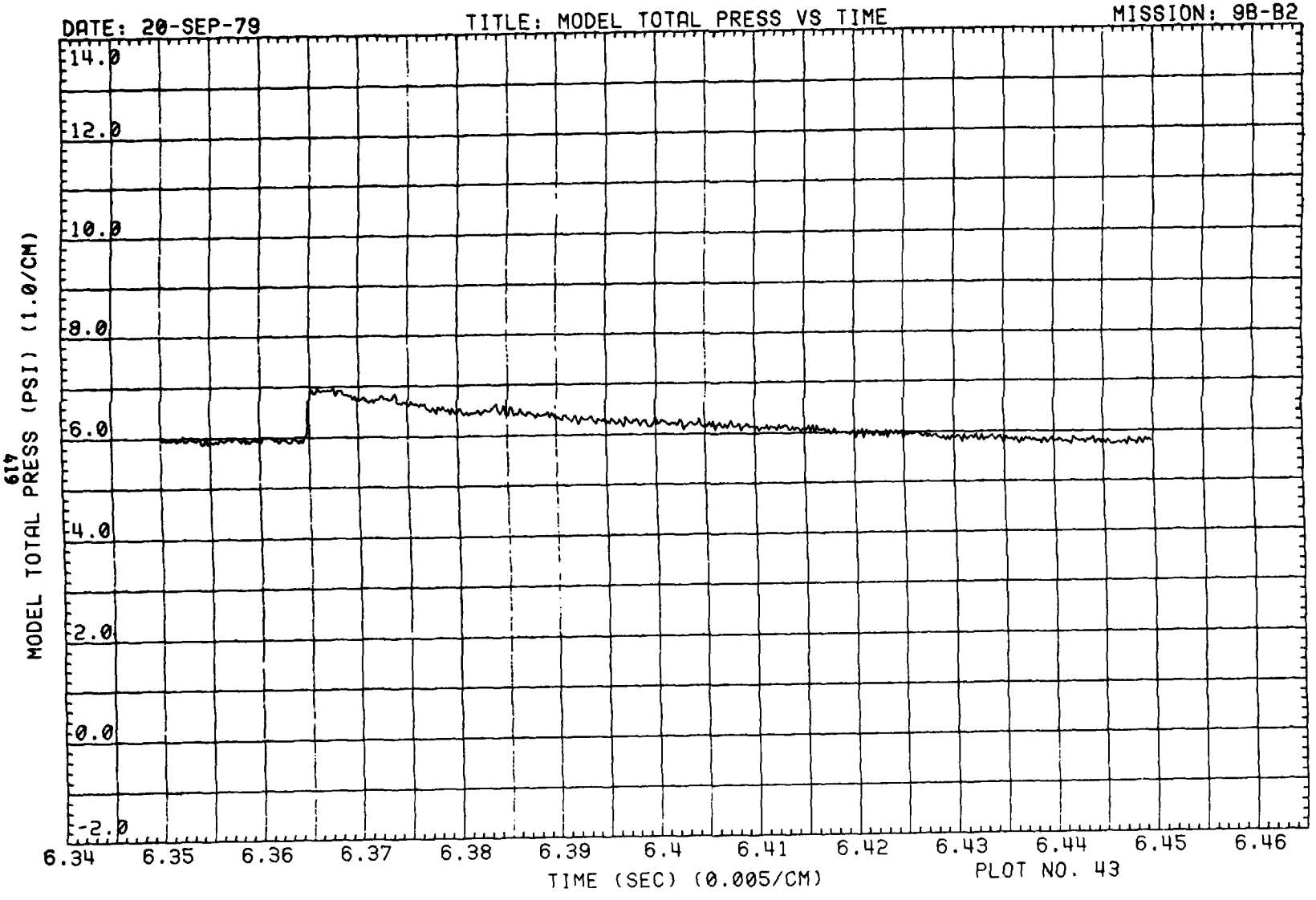

Figure 82. (Concluded)

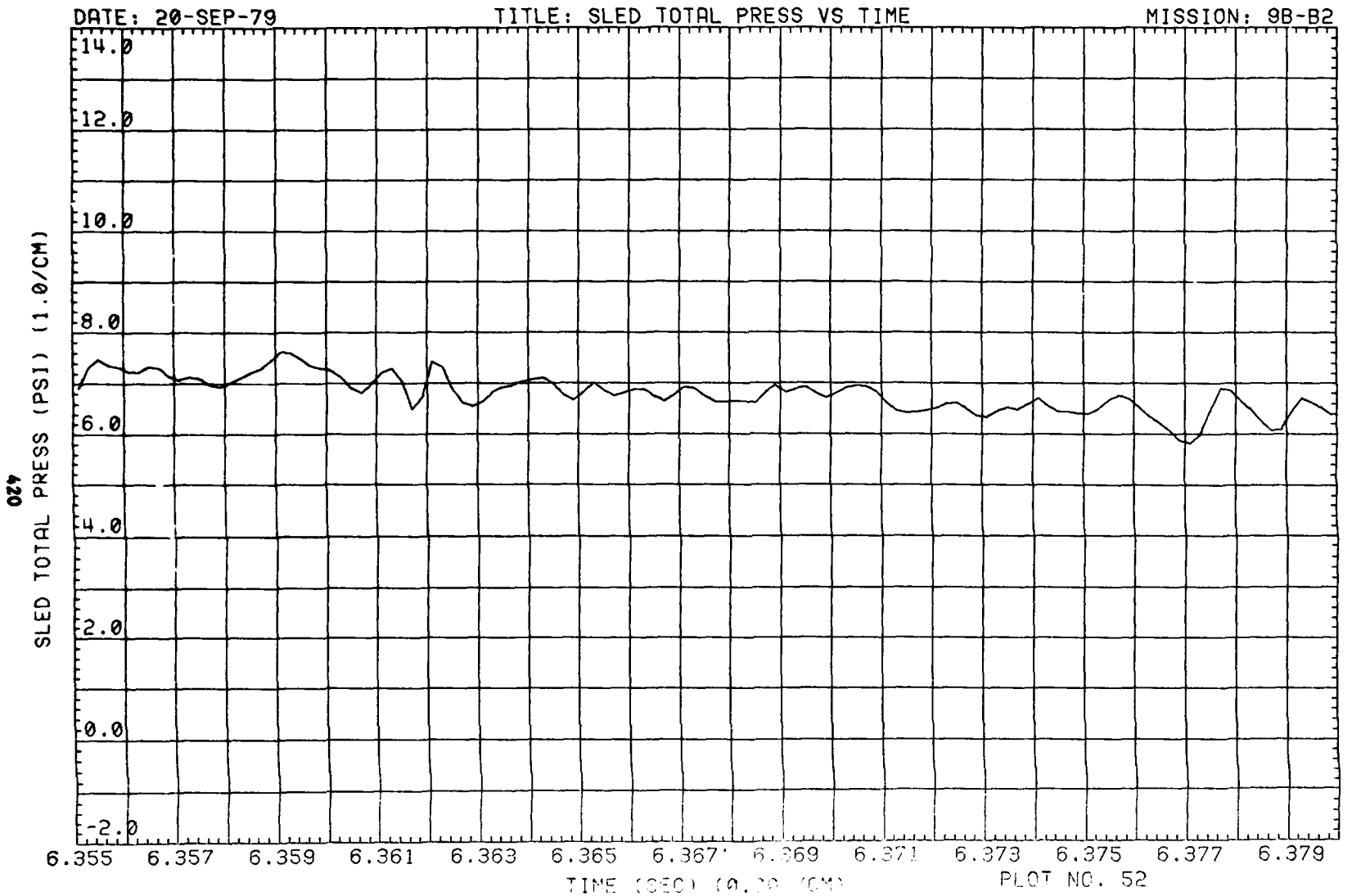

Figure 83. Total Pressure at Sled, Run 9B-B2, Intercept 3

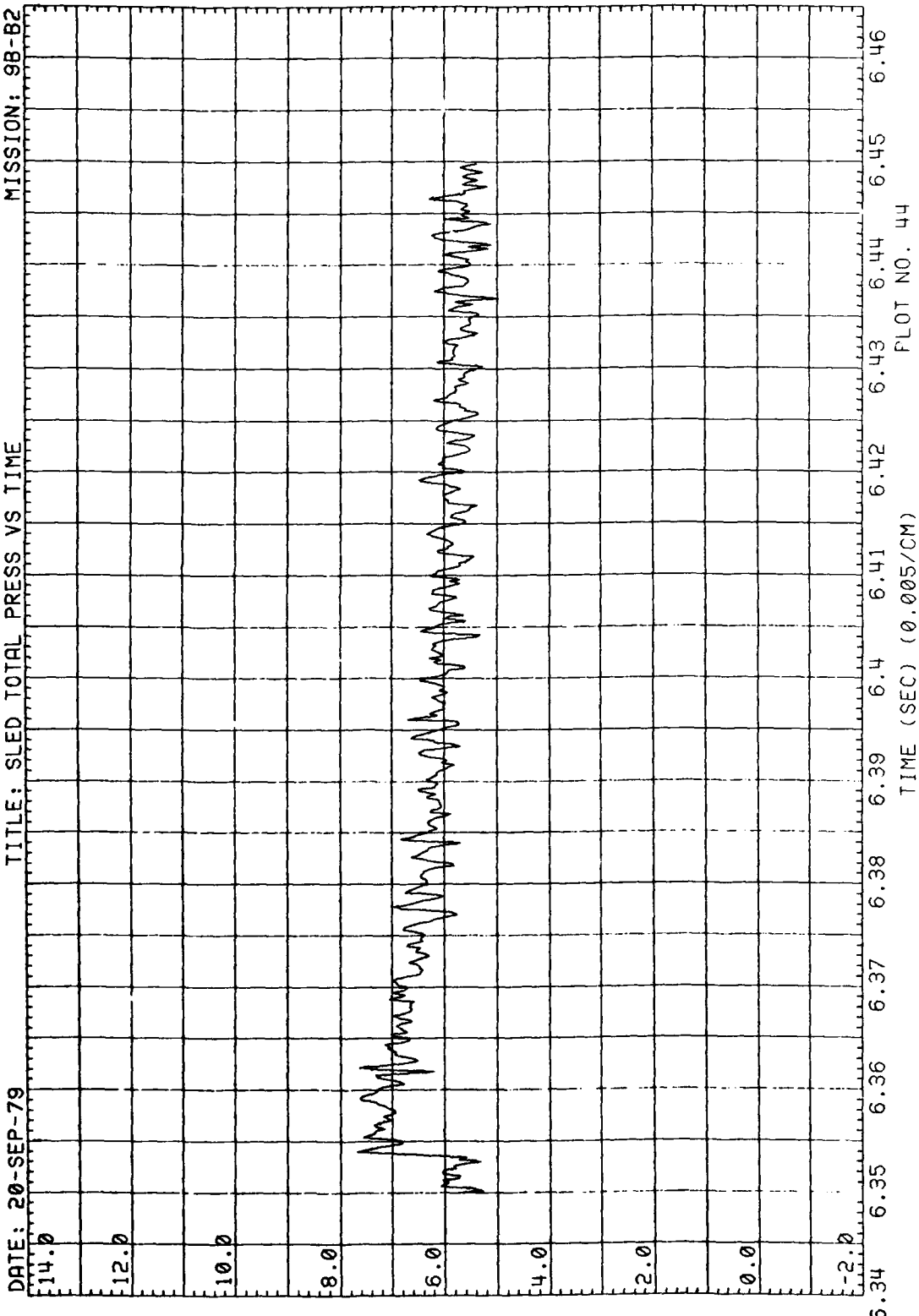

Figure 83. (Concluded)

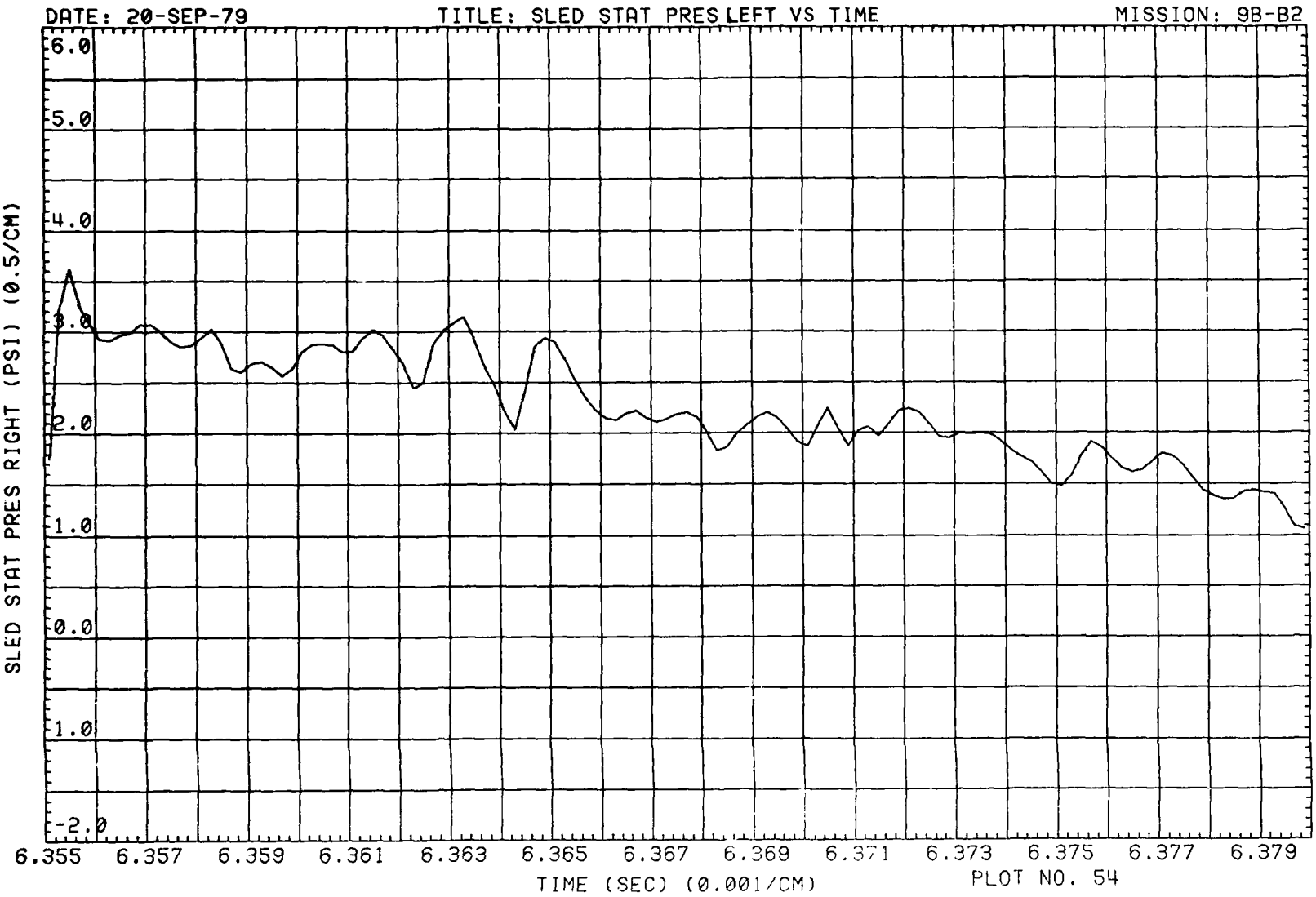

Figure 84. Left Side Static Pressure at Sled, Run 9B-B2, Intercept 3

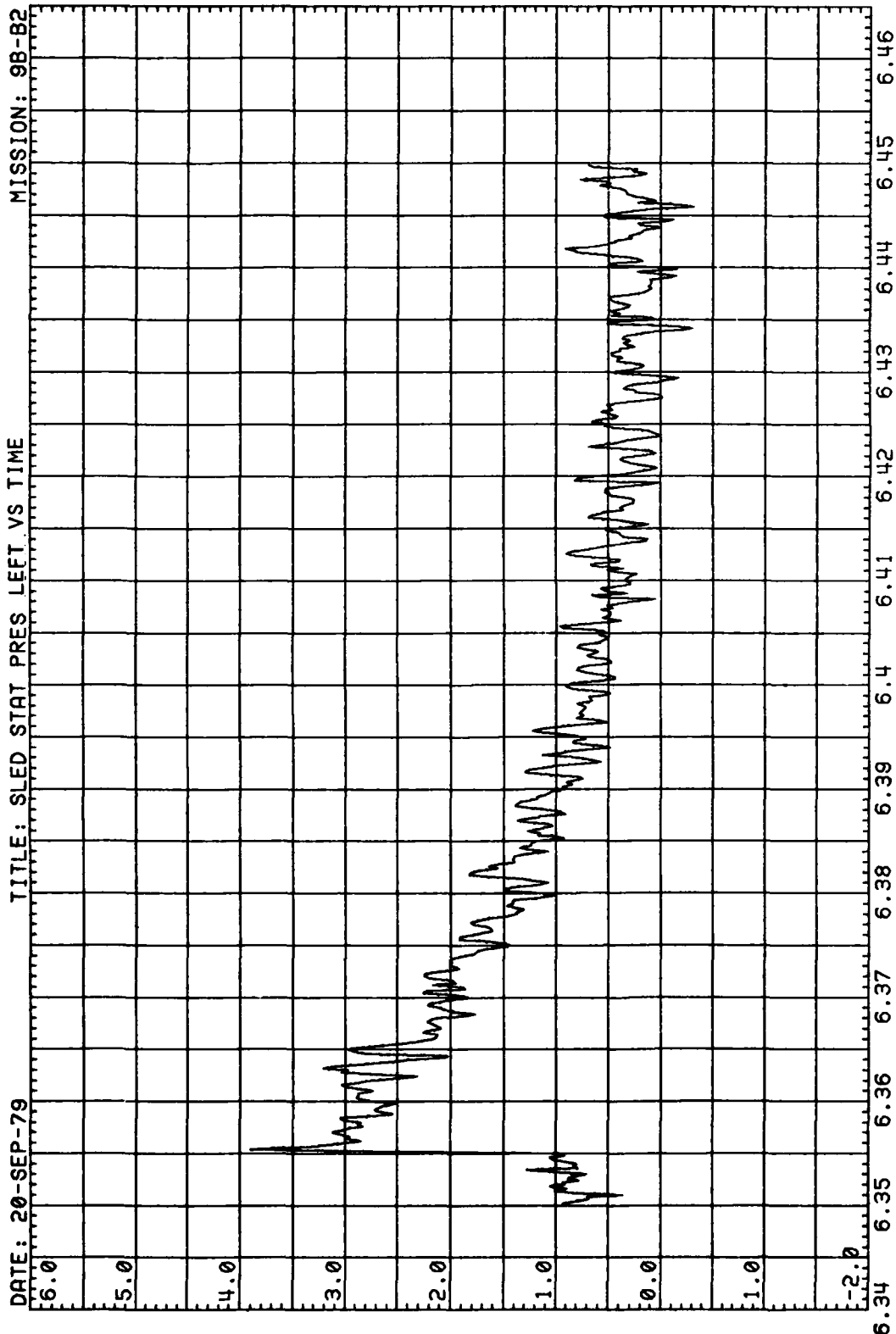

Figure 84. (Concluded)

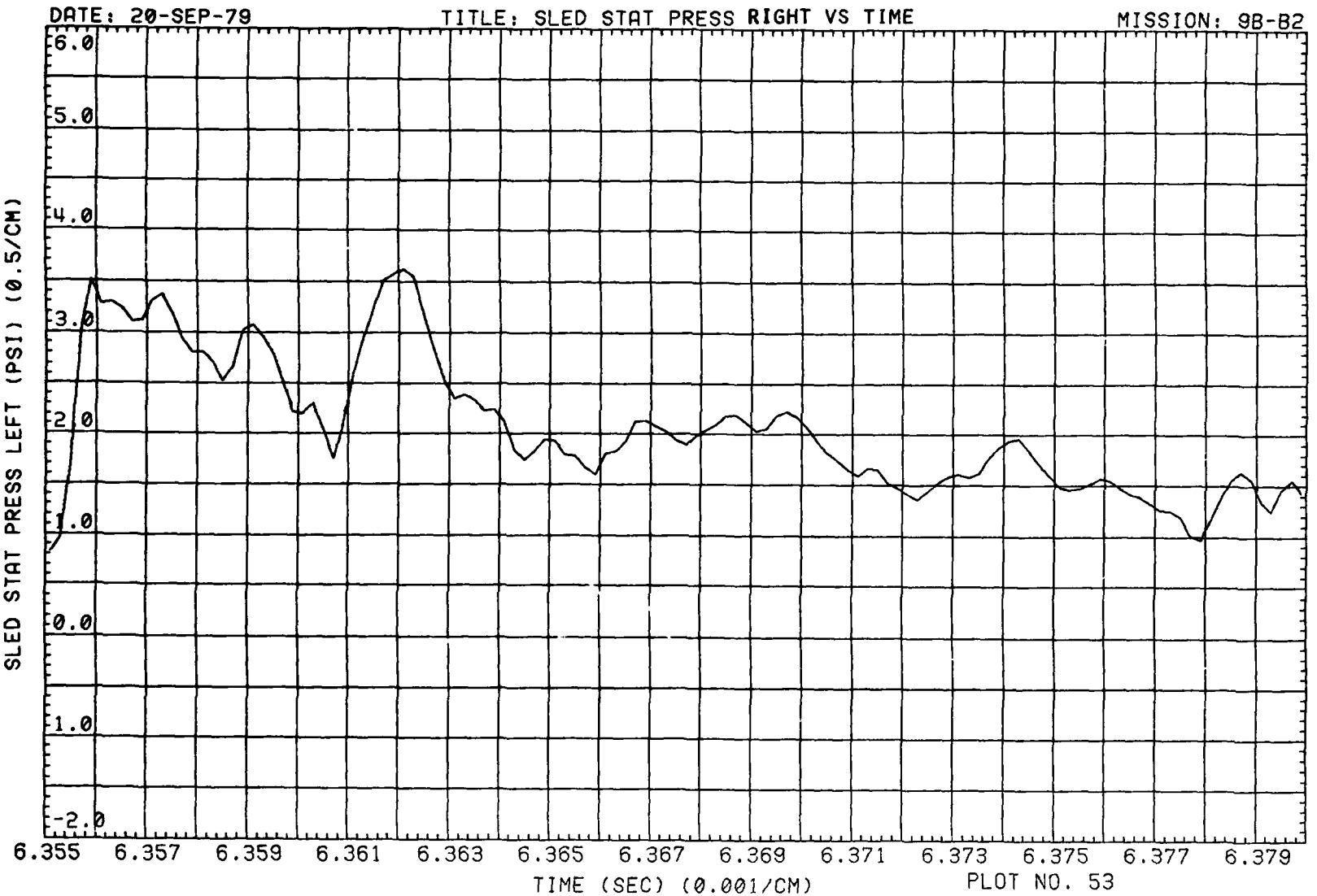

Figure 85. Right Side Static Pressure at Sled, Run 9B-B2, Intercept 3

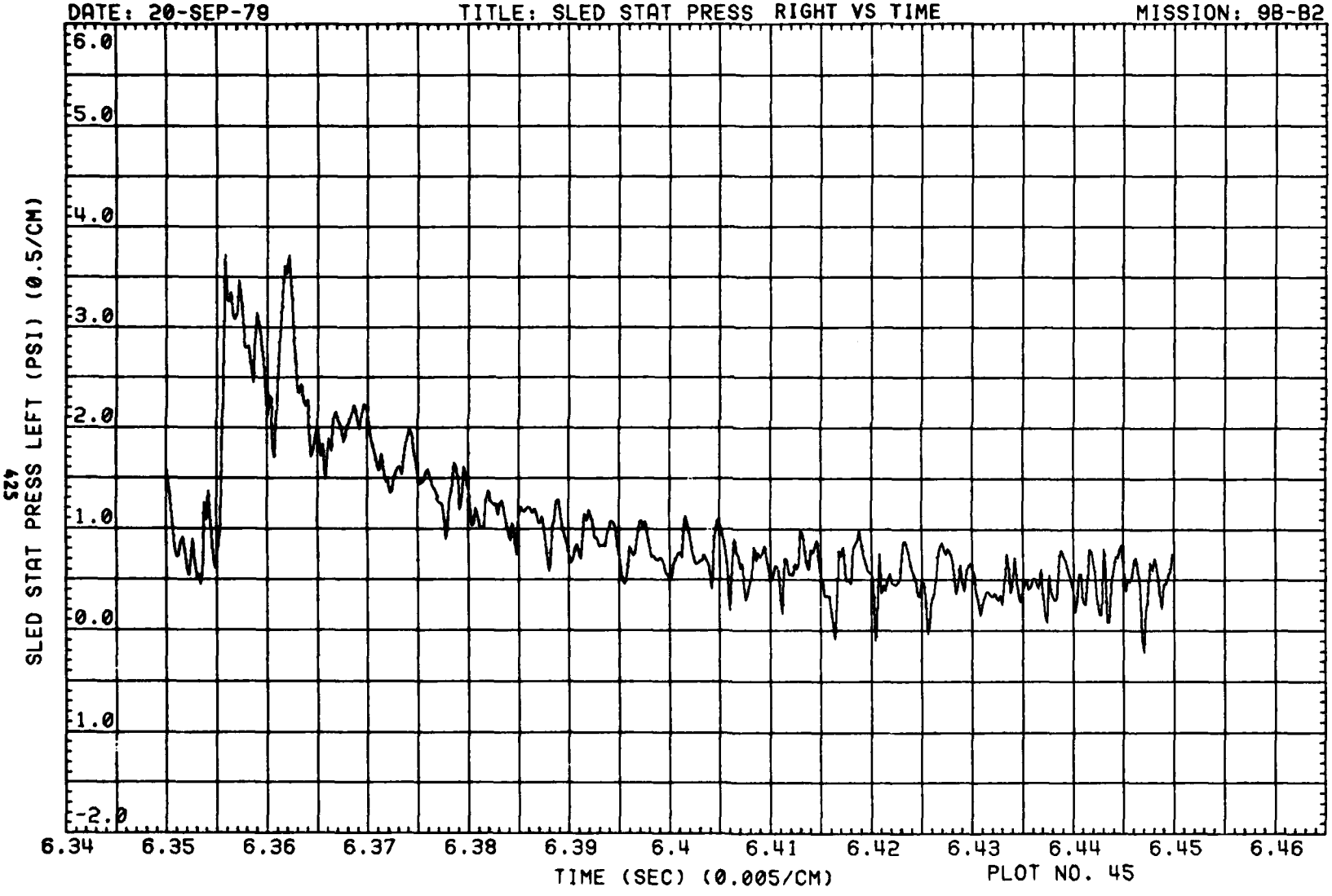

Figure 85. (Concluded)

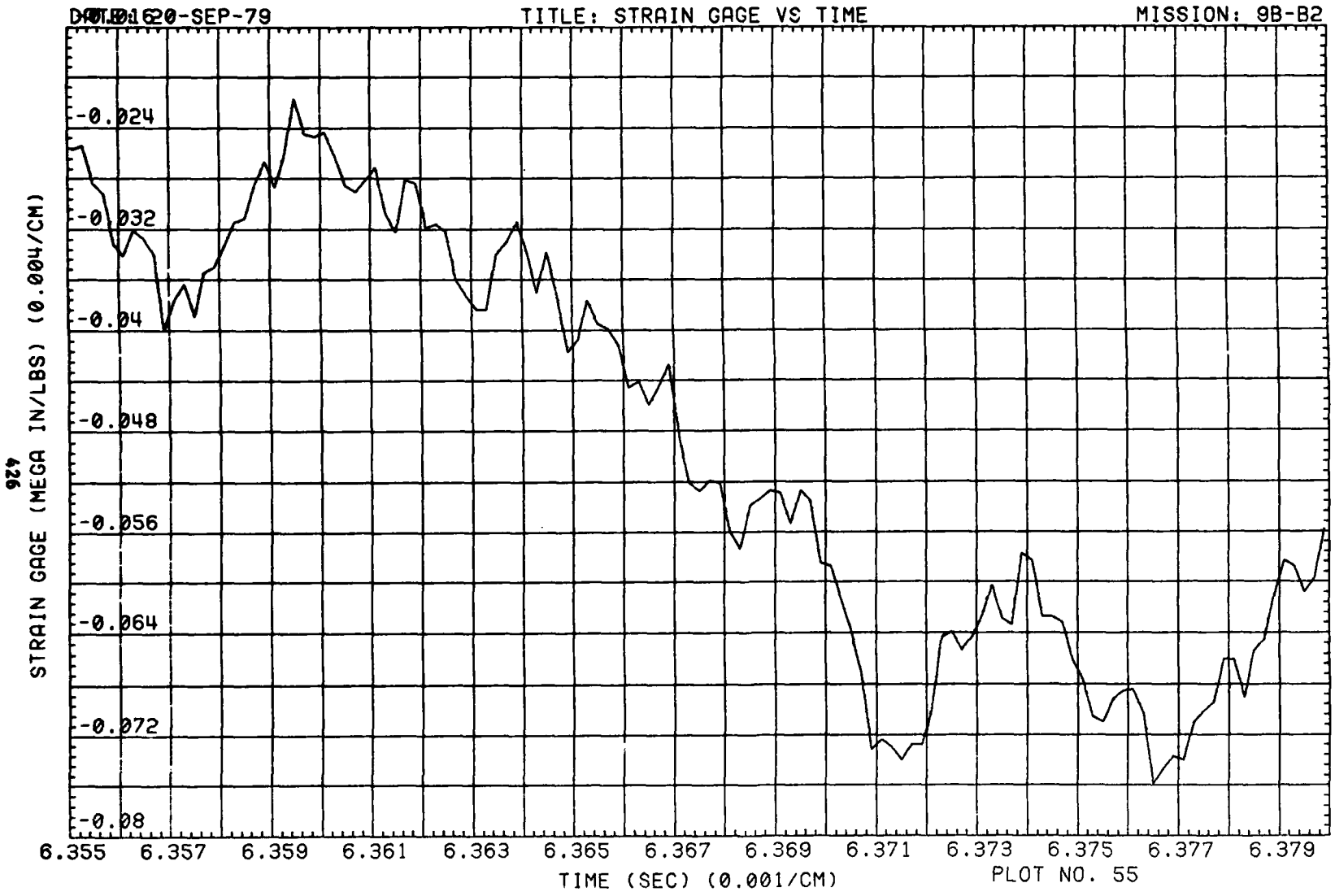

Figure 86. Strain at Model Support, Run 9B-B2, Intercept 3

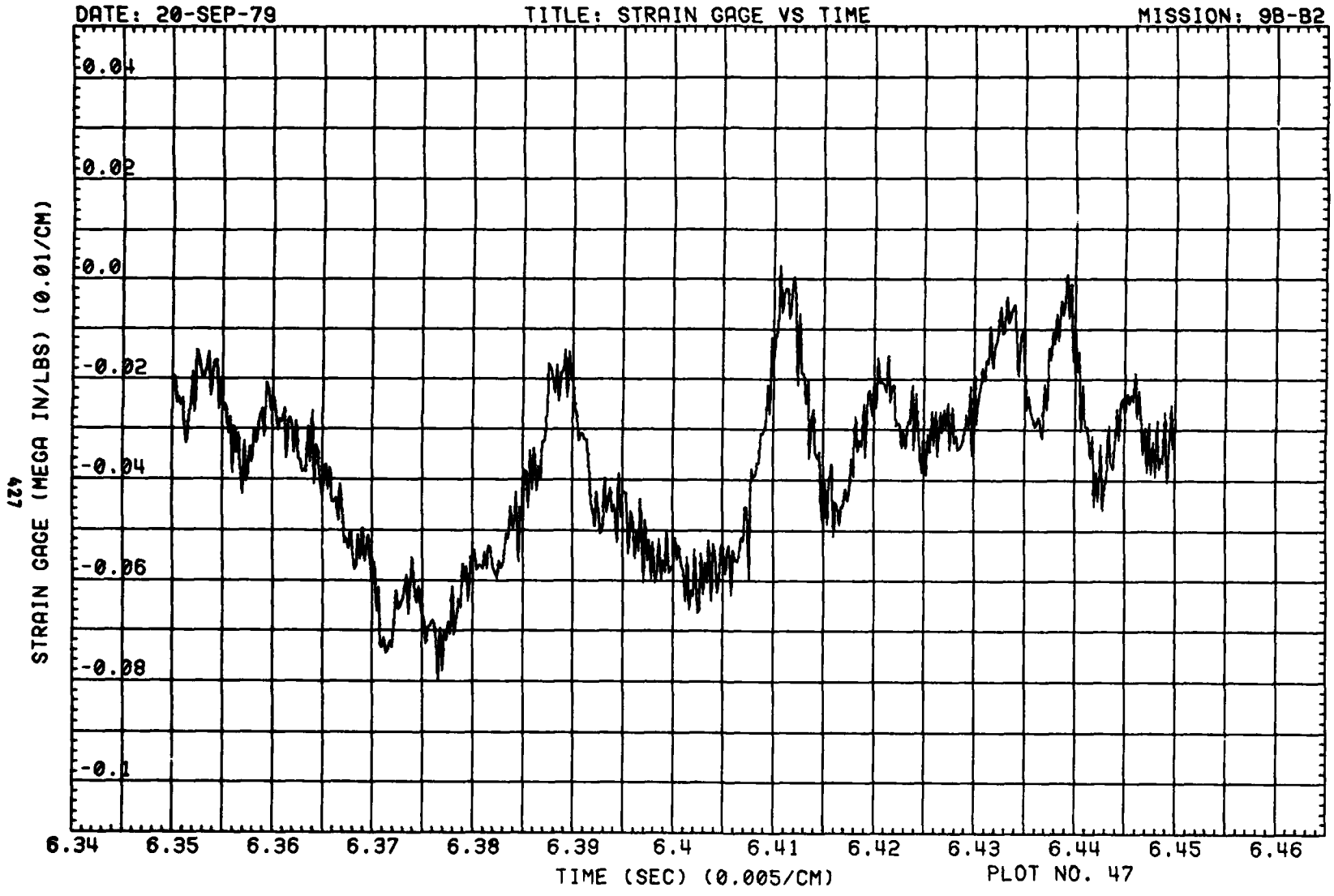

Figure 86. (Concluded)

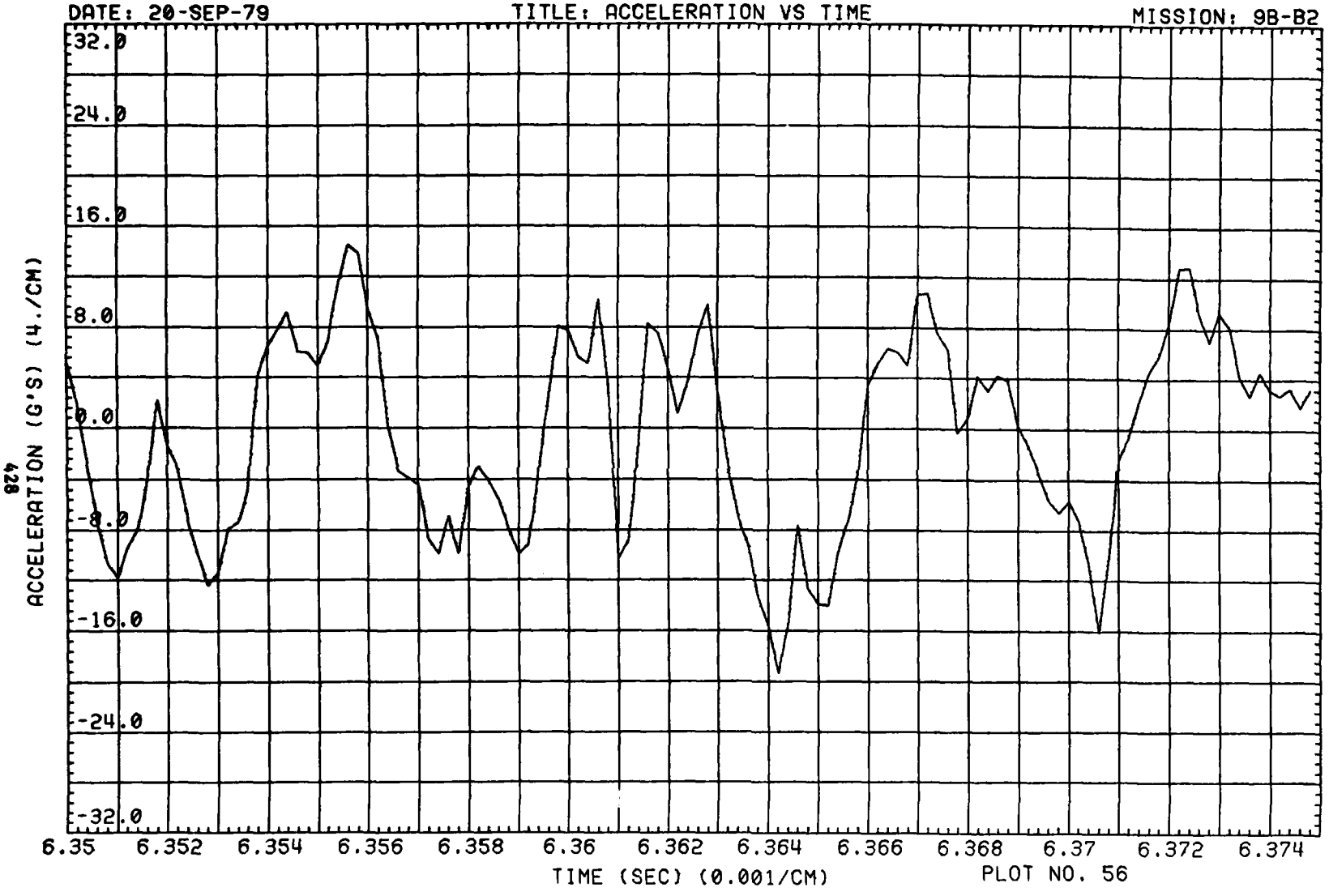

Figure 87. Wing Acceleration, Run 9B-B2, Intercept 3

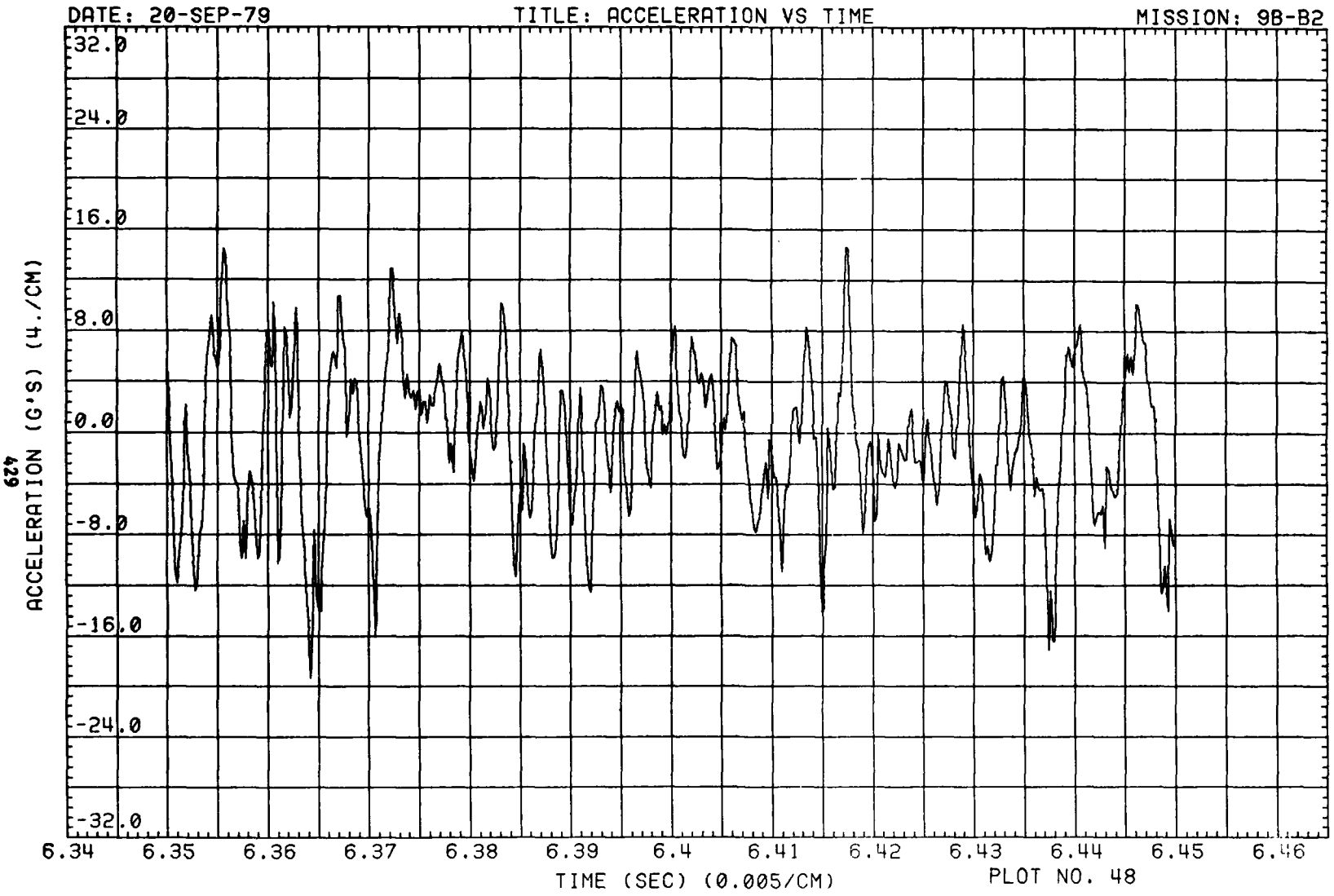

Figure 87. (Concluded)

DISTRIBUTION LIST

DEPARTMENT OF DEFENSE

Assistant to the Secretary of Defense
Atomic Energy
ATTN: Executive Assistant

Defense Intelligence Agency
ATTN: DB-4C, V. Fratzke

Defense Nuclear Agency
ATTN: SPAS
ATTN: STSP
4 cy ATTN: TITL

Defense Technical Information Center
12 cy ATTN: DD

Field Command
Defense Nuclear Agency
ATTN: FCPR
ATTN: FCT, W. Tyler

Field Command
Defense Nuclear Agency
ATTN: FCPRL

Undersecretary of Def for Rsch & Engrg
ATTN: Strategic & Space Systems (OS)

DEPARTMENT OF THE ARMY

Harry Diamond Laboratories
Department of the Army
ATTN: DELHD-N-P, J. Gwaltney

U.S. Army Ballistic Research Labs
ATTN: DRDAR-BLT, W. Taylor
ATTN: DRDAR-BLT, J. Keefer

U.S. Army Materiel Dev & Readiness Cmd
ATTN: DRCDE-D, L. Flynn

U.S. Army Nuclear & Chemical Agency
ATTN: Library

DEPARTMENT OF THE NAVY

Naval Material Command
ATTN: MAT 08T-22

Naval Research Laboratory
ATTN: Code 2627

Naval Surface Weapons Center
ATTN: Code F31, K. Caudle

Naval Weapons Evaluation Facility
ATTN: L. Oliver

Office of Naval Research
ATTN: Code 465

Strategic Systems Project Office
Department of the Navy
ATTN: NSP-272

DEPARTMENT OF THE AIR FORCE

Aeronautical Systems Division
Air Force Systems Command
ATTN: ASD/ENFT, R. Bachman
4 cy ATTN: ASD/ENFTV, D. Ward

Air Force Aero-Propulsion Laboratory
ATTN: TBC, M. Stibich

Air Force Materials Laboratory
ATTN: MBE, G. Schmitt

Air Force Weapons Laboratory
Air Force Systems Command
ATTN: NTV, G. Campbell
ATTN: NTV, A. Sharp
ATTN: NTV, D. Payton
ATTN: SUL

Assistant Chief of Staff
Studies & Analyses
Department of the Air Force
ATTN: AF/SASC, B. Adams
ATTN: AF/SASB, R. Mathis

Deputy Chief of Staff
Research, Development, & Acq
Department of the Air Force
ATTN: AFRDQI, N. Alexandrow

Foreign Technology Division
Air Force Systems Command
ATTN: SDBF, S. Spring

Strategic Air Command
Department of the Air Force
2 cy ATTN: XPFS, F. Tedesco

DEPARTMENT OF ENERGY CONTRACTORS

Sandia National Laboratories
ATTN: A. Lieber

OTHER GOVERNMENT

Central Intelligence Agency
ATTN: OSWR/NED

DEPARTMENT OF DEFENSE CONTRACTORS

APTEK
ATTN: T. Meagher

Boeing Co.
ATTN: M/S 85/20, E. York

Boeing Wichita Co
ATTN: R. Syring

Calspan Corp
ATTN: M. Dunn

DEPARTMENT OF DEFENSE CONTRACTORS (Continued)

University of Dayton
Industrial Security Super KL-505
ATTN: B. Wilt

Effects Technology, Inc
ATTN: R. Globus
ATTN: R. Parisse
ATTN: E. Bick

General Electric Company—TEMPO
ATTN: DASIAC

General Electric Company—TEMPO
ATTN: J. Moulton

General Research Corp
ATTN: T. Stathacopoulos
ATTN: J. Cunningham

Kaman AviDyne
ATTN: N. Hobbs
ATTN: E. Criscione
ATTN: R. Ruetenik
ATTN: B. Lee

DEPARTMENT OF DEFENSE CONTRACTORS (Continued)

Kaman Sciences Corp
ATTN: D. Sachs

Los Alamos Technical Associates, Inc
ATTN: B. Myers
ATTN: C. Sparling
ATTN: P. Hughes

Prototype Development Associates, Inc
ATTN: C. Thacker
ATTN: J. McDonald
ATTN: H. Moody

R & D Associates
ATTN: F. Field
ATTN: C. MacDonald
ATTN: A. Kuhl
ATTN: P. Roust
ATTN: P. Haas

Science Applications, Inc
ATTN: W. Layson